ORAL MUCOSA-NANOPARTICLE INTERACTIONS AND UPTAKE PATHWAYS IN FORMULATION EXCIPIENT PROFILING

MARK BEST

A Thesis Submitted in partial fulfilment for the degree of Doctor of Philosophy

March 2014

The School of Pharmacy & Biomolecular Sciences

The University of Brighton

ABSTRACT

Nanomaterials are generally defined as chemical substances or materials that contain particles with one or more dimensions less than 100 nanometres in size. They may be either engineered or naturally occurring, but have unique properties due to a vastly increased surface area to volume ratio when compared to non-nano (bulk) materials. This provides the potential for the development of a wide range of enhanced formulations with superior efficacy including applications in oral healthcare. As the properties of a material change at the nano-scale, there are concerns that the toxicological profile of these materials may also change. Size is only one factor; changes in shape, surface chemistry, chemical composition, porosity and solubility all contribute to the overall biological toxicity profile of a nano-scale ingredient. Established links between the specific properties of a nanomaterial and toxicity are not well understood, leaving an important data gap in the literature. The purpose of this work was to utilise *in vitro* oral epithelial models for the assessment of safety profiles of nanomaterials for applications in next generation oral care products.

Four commercially sourced nanomaterials were analysed, alongside respective bulk counterparts already found within oral care product formulations. These nanomaterials comprised of two nano-zinc oxides (ZnO), silicon dioxide (SiO_2), titanium dioxide (TiO_2) and hydroxyapatite ($Ca_5(OH)(PO_4)_3$). Comprehensive characterisation of each material was carried out using a range of analytical techniques to identify any structure-function relationships *in vitro*. Initial toxicity screening experiments were conducted using a non-keratinised oral epithelial cell monolayer (H376 cell line) with both cell viability and lysis analysed using MTT and LDH assays respectively. Materials were investigated further using two 3-dimensional tissue models representative of the main tissue types constituting the human oral mucosa: non-keratinised buccal (RHO) and keratinised gingival (GIN-100) models. Nanomaterial uptake in the models was investigated using confocal microscopy with a styrl dye (FM 1-43). This led to the development of a novel, high throughput fluorescent assay as a potential method for screening nanoparticle-uptake.

Results highlighted the complexities involved with nano-characterisation in biological media using current techniques. A wide variety of particle shapes and sizes were recorded between different nanomaterials, with results being dependent upon the sample preparation steps and specific methods of analyses used. These disparities represent the current challenges experienced by both researchers and regulators of nanotechnology at the present time. ZnO was observed to be the most cytotoxic material during monolayer screening, at concentrations exceeding 0.3125% w/v when delivered in protein-free media. Differences between bulk and nanomaterial properties were recorded for all the materials, except for TiO_2, but these did not necessarily transfer to effects seen in the more representative 3-D models. Cytotoxicity results from both RHO and GIN-100 models exemplified the disparity between sensitivity of monolayer and the natural stratified tissue structure of human oral mucosa. Keratinised gingival tissue models showed significantly greater durability over the less robust buccal model, in both cytotoxicity assays and IL-1α cytokine response. Of all materials examined, cellular uptake was only observed for nano-SiO_2. This was the only material detected trafficking inside the cell using the FM 1-43 styryl dye assay, with confocal data serving to verify the analysis of nanoparticle internalisation using fluorescence.

In conclusion, nanomaterials pose considerable difficulties during formulation and analysis in healthcare products. The risk of potential uptake and bioaccumulation or translocation to particularly sensitive areas of the body also requires further investigation. Nanomaterials have to be assessed on a case by case basis, and robust/consistent regulatory strategies developed to enable industry to produce and market novel but safe nanoparticle containing formulations. Risks to human health may be less of a hazard when applied to fully functioning healthy human tissue, especially in comparison to existing bulk material effects and current, accepted irritant ingredients (*e.g.* Sodium lauryl sulphate).

CONTENTS

ABSTRACT i
LIST OF TABLES v
LIST OF FIGURES vi
ACKNOWLEDGEMENTS xiv
AUTHORS DECLARATION xv
ABBREVIATIONS AND DEFINITIONS xvi
1 INTRODUCTION 1
1.1 Nanotechnology and nanomaterials 1
1.1.1 Nano-scale properties 2
1.2 Nanotoxicology 4
1.2.1 Exposure routes 6
1.2.2 Nanomaterial capacity for systemic toxicity 9
1.2.3 Dose metrics 10
1.2.4 Nanomaterial toxicity testing strategy 13
1.2.5 Nanomaterial cytotoxicity mechanisms 16
1.2.6 Uptake pathways 24
1.2.7 Endocytosis 27
1.2.8 Carrier mediated transport 31
1.2.9 Paracellular transport routes 32
1.3 The human oral mucosa 36
1.3.1 Keratinisation 38
1.3.2 Physical barriers in the human oral mucosa 46
1.4 Nanomaterials in industry 47
1.4.1 Nanomaterials in Oral Healthcare 49
1.5 Aims and objectives of the thesis 53
2 GENERAL METHODS 57
2.1 Materials 57
2.2 Methods 61
2.2.1 Characterisation of materials 61
2.2.2 Cell culture 76
2.2.3 Biochemical assays 82
2.2.4 Cell imagaing 92

2.2.5 Statistical analysis 96
3 CHARACTERISATION OF MATERIALS 97
3.1 Results 99
3.1.1 SEM analysis of particle size and morphology 99
3.1.2 TEM analysis of particle size and morphology 106
3.1.3 EDS analysis of chemical composition 112
3.1.4 DLS nanoparticle hydrodynamic diameter measurements and material polydispersity 117
3.1.5 NanoSight nanoparticle tracking analysis (NTA) of nanomaterial size distribution 134
3.1.6 Nanomaterial zeta potential measurements 143
3.2 Discussion 149
3.2.1 Size determination 150
3.2.2 Colloidal stability 163
3.2.3 Temperature effects on nanomaterial characteristics 167
3.2.4 Evaluation of nanomaterial characterisation 167
4 IN VITRO MONOLAYER SCREENING OF MATERIALS 170
4.1 Cytotoxicity screening results 172
4.1.1 LDH assay results 172
4.1.2 MTT assay results 177
4.1.3 SEM visual analysis of material particle-H376 cell interactions 182
4.2 Discussion 190
4.2.1 Evaluation of nanoparticle cytotoxicity by colorimetric assays 191
4.2.2 Cytotoxicity assessed through cell imaging 197
5 NANOMATERIAL CYTOTOXICTY TESTING USING 3-DIMENSIONAL IN VITRO MODELS 203
5.1 Results 205
5.1.1 Cytotoxicity testing using the RHO model of non-keratinised oral mucosal tissue 205
5.1.2 Cytotoxicity testing using the EpiGingiva™ keratinised oral mucosal tissue model 210
5.1.3 ICP-OES measure zinc ion concentration 216
5.2 Discussion 220
5.2.1 Assessment of in vitro toxicity testing 220
5.2.2 Comparisons of 3-D keratinisation models 223

5.2.3 Further investigation of potential cytotoxic mechanisms 226
5.2.4 Inflammatory response 229
5.2.5 Risk implications of nanomaterial exposure on the oral mucosa 233
6 UPTAKE POTENTIAL OF NANOMATERIALS IN VITRO 235
6.1 Results 237
6.1.1 SynaptoGreen™ uptake assay results 237
6.1.2 Confocal laser scanning microscopy imaging of particle uptake 242
6.1.3 TEM-EDX analysis of nanoparticle uptake in 3-D tissue models 252
6.2 Discussion 258
6.2.1 Nanomaterial uptake routes 260
6.2.2 Endocytosis as a transcellular uptake pathway for nanomaterials putative of interest in future oral healthcare applications 264
6.2.3 Paracellular transport of nanoparticles 269
6.2.4 Nanomaterial uptake potential summary 273
7 GENERAL DISCUSSIONS AND CONCLUSIONS 275
7.1 Study conclusions 275
7.2 Experimental limitations of the study 277
7.2.1 Difficulties associated with accurate nanoparticle characterisation 277
7.2.2 In vitro models and the current limitations of toxicity testing 279
7.3 Future study 284
7.4 Original contribution to research 286
8 REFERENCES 287
9 APPENDICIES 333
9.1 H376 cell loss of cell adhesion in response to SDS cytotoxicity 333
9.2 SiO_2-ACROS-Bulk material characterisation 334

LIST OF TABLES

Table 1.1. A table to demonstrate the details of key keratinised proteins found in oral epithelial keratinocytes. *Compiled from data within (Dale et al., 1990).*

Table 2.1. Parameters used for automatic optimised particle size analysis using Malvern Zetasizer ZS90 (Zetasizer v6.1). Information obtained from experimental data and (Malvern, 1996).

Table 3.1. Nanomaterial particle diameter results analysed at 22°C and 37°C using the DLS based particle sizing instrument (ZetaSizer Nano ZS90).

Table 3.2. Nanomaterial particle diameter results analysed at ambient temperature using the NTA based particle sizing instrument (NanoSight LM10). All measurements are the average of 6 runs (n=6) with standard deviation reported.

Table 3.3. Zeta potential of nanoparticles measured in three different solvent dispersions at both 22°C and 37°C. The Smoluchowski's theory was used for calculations of electrophoretic mobility of the particles based on laser doppling and M3-PALS in the Malvern ZetaSizer NS90. [a] *All results stated are the average of 6 runs (n=6) averaged from at least 4 measurements per run.*

Table 3.4. pH measurement of nanomaterials diluted to a 0.001% w/v concentration in either dH2O or PRF medium prior to Zeta Potential analysis. All measurements carried out at room temperature, with results an average of 3 different readings carried out on different days (n=3) with standard deviation reported.

Table 3.5. A summary of the particle size analysis for all current materials tested in all methodologies reported within this chapter*. All results included are taken from analysis carried out at 22°C.

LIST OF FIGURES

Figure 1.1. Schematic of human body with pathways of exposure to nanoparticles, affected organs, and associated diseases from epidemiological, *in vivo* and *in vitro* studies. *Taken from (Buzea et al., 2007).*

Figure 1.2. Flowchart outlining the current best strategy approach for the risk assessment of nanomaterials. *Adapted from ((SCENIHR), 2006).*

Figure 1.3. Hypothetical cellular interactions of nanoparticles causing inflammatory effects on lung epithelium. *Adapted from (Oberdorster et al., 2005b).*

Figure 1.4. The hierarchal oxidative stress model. *Adapted from (Nel* et al.*, 2006).*

Figure 1.5. A model showing the simplified NF-kB signalling pathway that is activated by oxidative stress in response to nanoparticle generated ROS in keratinocytes. *Adapted from (Huang et al., 2010b).*

Figure 1.6. The main transport pathways associated with nanoparticle internalisation through cell layers and membranes in the human body. *Adapted from (Forth et al., 1987).*

Figure 1.7. The main types of endocytosis. *Taken from Mariana Ruiz Villarreal (free of copyright), 2007.*

Figure 1.8. Outline of the main events in receptor-mediated endocytosis. *Figure taken from* (Grant & Donaldson, 2009).

Figure 1.9. A diagram showing the tight cell to cell adhesion in keratinised epithelium. *Adapted from (Cooper, 2000).*

Figure 1.10. A schematic to show a to non-keratinised epithelial cell tight junction, at the apical surface of stratified tissue structures. *Taken from Mariana Ruiz, 2006.*

Figure 1.11. A diagram showing the epithelial tissues of the oral mucosa, with its four epidermal layers. *Adapted from (Wertz & Squier, 1991).*

Figure 2.1. A schematic representation of Zeta potential. *Taken from (Kaszuba et al., 2010).*

Figure 2.2. The chemical structure of (a) SynaptoGreen™ and (b) FM®1-43X both variants of N-(3-triethylammoniumpropyl)-4-(4-(dibutylamino)styryl)pyridinium

dibromide, styryl dyes. Taken from: www.lifetechnologies.com/order/catalog/product/T3163

Figure 3.1. SEM images 1,000X magnification of particles (bulk and nano) in typical agglomerates, as observed by imaging their distribution spread across the aluminium specimen stub.

Figure 3.2. SEM images 100,000 X magnification of all particles (bulk and nano) investigated for their interest within oral healthcare.

Figure 3.3. SEM images 300,000X magnification of all particles (bulk and nano) investigated for their interest within oral healthcare.

Figure 3.4. Mean particle sizes of both nano and bulk materials measured from SEM images taken between 1,000 and 100,000 times magnification.

Figure 3.5. TEM images 80,000X magnification of particles (bulk and nano) in typical agglomerates, spread across the formvar coating on the copper grid.

Figure 3.6. TEM images at 75,000X magnification of bulk-sized particles included as control materials for comparisons of nano-sepcific properties of nanoparticles of the same chemicals.

Figure 3.7. TEM images at 350,000X magnification of nanoparticles investigated for potential use within oral healthcare formulations.

Figure 3.8. Mean particle sizes of both nano and bulk materials measured from TEM images taken between 3,000 and 180,000 times magnification.

Figure 3.9. EDS spectra of Hydroxyapatite ($Ca_5(OH)(PO_4)_3$) material (top) bulk, (bottom) nanoparticle.

Figure 3.10. EDS spectra of Silicon dioxide (SiO_2) material (top) bulk, (bottom) nanoparticle.

Figure 3.11. EDS spectra of Titanium dioxide (TiO_2) material (top) bulk, (bottom) nanoparticle.

Figure 3.12. EDS spectra of Zinc oxide (ZnO) nanomaterial solutions (top) ZnO-45009, (bottom) ZnO-45408.

Figure 3.13. EDS spectra of Zinc oxide (ZnO) bulk powder .

Figure 3.14. DLS particle size distributions by intensity polystyrene standards dispersed in dH_2O at 22°C (top) and 37°C (bottom).

Figure 3.15. Demonstration of the difficulty in accurate measurement of DLS particle size distributions by intensity of back scattered light by hydroxyapatite nanomaterial dispersed in three different solvents at 22°C (a) dispersed in dH_2O, (b) PRF media, (c) ethanol and (d) n = 6 mean values.

Figure 3.16. DLS particle size distributions by intensity of SiO_2 nanomaterial dispersed in three different solvents at both 22°C (top) and 37°C (bottom).

Figure 3.17. DLS particle size distributions by intensity of TiO_2 nanomaterial dispersed in three different solvents at both 22°C (top) and 37°C (bottom).

Figure 3.18. DLS particle size distributions by intensity of ZnO-45009 nanomaterial dispersed in three different solvents at both 22°C (top) and 37°C (bottom).

Figure 3.19. DLS particle size distributions by intensity of ZnO-45408 nanomaterial dispersed in three different solvents at both 22°C (top) and 37°C (bottom).

Figure 3.20. DLS ZetaSizer data showing the polydispersity index (y axis) versus the averaged actual polydispersity width of particle diameters recorded during size measurements (x axis), for all nanomaterials dispersed in each of three different solvents at 22°C.

Figure 3.21. DLS ZetaSizer data showing the polydispersity index (y axis) versus the averaged actual polydispersity width of particle diameters recorded during size measurements (x axis), for all nanomaterials dispersed in each of three different solvents at 37°C.

Figure 3.22. NTA size distribution expressed as number of particles of hydroxyapatite nanomaterial dispersed in: dH_2O (blue), PRF media (red) or ethanol (green). Analysed at room temperature (n = 6).

Figure 3.23. NTA size distribution expressed as number of particles of SiO_2 nanomaterial dispersed in: dH_2O (blue), PRF media (red) or ethanol (green). Analysed at room temperature (n = 6).

Figure 3.24. NTA size distribution expressed as number of particles of TiO_2 nanomaterial dispersed in: dH_2O (blue), PRF media (red) or ethanol (green). Analysed at room temperature (n = 6).

Figure 3.25. NTA size distribution expressed as number of particles of ZnO-45009 nanomaterial dispersed in: dH_2O (blue), PRF media (red) or ethanol (green). Analysed at room temperature (n = 6).

Figure 3.26. NTA size distribution expressed as number of particles of ZnO-45408 nanomaterial dispersed in: dH_2O (blue), PRF media (red) or ethanol (green). Analysed at room temperature (n = 6).

Figure 3.27. The general classification of colloid stability in solution based on zeta potential (ζ) measurements, negating charge on particle. *Adapted from* (Vallar *et al.*, 1999).

Figure 3.28. Zeta potential measurements of nanoparticle surface charge, taken from the data in Table 3.4.

Figure 4.1. A graph comparing the cytotoxic effects of bulk versus nano material exposure to H376 monolayers at concentrations ranging from 0 to 0.25% w/v in serum free growth media, for 5 minutes at 37°C/5% CO_2.

Figure 4.2. A graph comparing the cytotoxic effects of nanomaterial exposure to H376 monolayers at concentrations ranging from 0 to 0.25% w/v when delivered in different media, incubated at 37°C/5% CO_2 for 5 minutes.

Figure 4.3. A graph comparing the cytotoxic effects of bulk particle sized material exposure to H376 monolayers at concentrations ranging from 0 to 0.25% w/v when delivered in different media, incubated at 37°C/5% CO_2 for 5 minutes.

Figure 4.4. A graph comparing the cytotoxic effects of additional control materials exposed to H376 monolayers at concentrations ranging from 0 to 0.25% w/v when delivered in different media, incubated at 37°C/5% CO_2 for 5 minutes.

Figure 4.5. A graph comparing the cytotoxic effects of bulk versus nanomaterial exposure, to H376 monolayers, in terms of cell viability calculated from MTT metabolism at concentrations ranging from 0 to 0.25% w/v in serum free growth media for 5 minutes at 37°C/5% CO_2.

Figure 4.6. A graph comparing the cytotoxic effects of nanomaterials exposed to H376 monolayers at concentrations ranging from 0 to 0.25% w/v when delivered in different media, incubated at 37°C/5% CO_2 for 5 minutes.

Figure 4.7. A graph comparing the cytotoxic effects of bulk particle sized materials exposed to H376 monolayers at concentrations ranging from 0 to 0.25% w/v when delivered in different media, incubated at 37°C/5% CO_2 for 5 minutes.

Figure 4.8. A graph comparing the cytotoxic of additional control materials exposed to H376 monolayers at concentrations ranging from 0 to 0.25% w/v when delivered in different media, incubated at 37°C/5% CO_2 for 5 minutes.

Figure 4.9. SEM images of H376 cells exposed to control substances for 5 minutes incubation at 37°C and 5% CO_2 in serum-free DMEM-Ham's F12 without *L*-Glutamine. (Top) Negative control cells treated with just serum free media. (Bottom) Positive control cells treated with 1% Triton-X100. *(a) = 1K X magnification with scale bar = 25μm, (b) 5K X magnification with scale bar = 5μm, (c) 10K X magnification with scale bar = 2.5μm and (d) enlarged 10K X magnification with scale bar = 2.5μm. All samples are indicative of n=3 samples.*

Figure 4.10. SEM images of H376 cells exposed to hydroxyapatite materials for 5 minutes incubation at 37°C and 5% CO_2 in serum-free media. (Top) 0.125% w/v Hydroxyapatite-nanomaterial. (Bottom) 0.125% w/v Hydroxyapatite bulk material. *(a) = 1K X magnification with scale bar = 25μm, (b) 5K X magnification with scale bar = 5μm, (c) 10K X magnification with scale bar = 2.5μm and (d) enlarged 100K X magnification with scale bar = 250nm. All samples are indicative of n=3 samples.*

Figure 4.11. SEM images of H376 cells exposed to SiO_2 materials for 5 minutes incubation at 37°C and 5% CO_2 in serum-free media. (Top) 0.125% w/v SiO_2-nanomaterial. (Bottom) 0.125% w/v SiO_2 bulk material. *(a) = 1K X magnification with scale bar = 25μm, (b) 5K X magnification with scale bar = 5μm, (c) 10K X magnification with scale bar = 2.5μm and (d) enlarged 100K X magnification with scale bar = 250nm. All samples are indicative of n=3 samples.*

Figure 4.12. SEM images of H376 cells exposed to TiO_2 materials for 5 minutes incubation at 37°C and 5% CO_2 in serum-free media. (Top) 0.125% w/v TiO_2-nanomaterial (Bottom) 0.125% w/v TiO_2 bulk material. *(a) = 1K X magnification with scale*

bar = 25μm, (b) 5K X magnification with scale bar = 5μm, (c) 10K X magnification with scale bar = 2.5μm and (d) enlarged 100K X magnification with scale bar = 250nm. All samples are indicative of n=3 samples.

Figure 4.13. SEM images of H376 cells exposed to ZnO materials for 5 minutes incubation at 37°C and 5% CO_2 in serum-free media. (Top) 0.125% w/v ZnO-45009 nanomaterial. (Middle) 0.125% w/v ZnO-45408 nanomaterial.(Bottom) 0.125% w/v ZnO bulk material. *(a) = 1K X magnification with scale bar = 25μm, (b) 5K X magnification with scale bar = 5μm, (c) 10K X magnification with scale bar = 2.5μm and (d) enlarged 75K X magnification with scale bar = 250nm. All samples are indicative of n=3 samples.*

Figure 5.1. A graph comparing the cytotoxic effects of bulk versus nano material exposure to RHO tissue models at a 1% w/v concentration dispersed in serum free growth media for 1 hour exposure at 37°C/5% CO_2.

Figure 5.2. A graph comparing the cytotoxic effects of bulk versus nanomaterial exposure, to RHO tissue models, in terms of cell viability calculated from MTT metabolism.

Figure 5.3. IL-1α cytokine release in RHO tissue models following 1 hour exposure to treatments applied apically, dispersed in serum free growth media at a 1% w/v concentration.

Figure 5.4. A graph comparing the cytotoxic effects of bulk versus nano material exposure to GIN-100 tissue models at a 1% w/v concentration dispersed in serum free growth media for 1 hour exposure at 37°C/5% CO_2.

Figure 5.5. A graph comparing the cytotoxic effects of bulk versus nanomaterial exposure, to GIN-100 tissue models, in terms of cell viability calculated from MTT metabolism at a 1% w/v concentration dispersed in serum free growth media for 1 hour of exposure at 37°C/5% CO_2.

Figure 5.6. A graph comparing the cytotoxic effects of bulk versus nanomaterial exposure, to GIN-100 tissue models that had been lysed before extracting formazan formed during MTT metabolism. at a 1% w/v concentration dispersed in serum free growth media for 1 hour of exposure at 37°C/5% CO_2.

Figure 5.7. IL-1α cytokine release in GIN-100 tissue models following 1 hour exposure to treatments applied apically, dispersed in serum free growth media at a 1% w/v concentration.

Figure 5.8. Zn^{2+} concentration of zinc materials analysed with ICP-OES, without a nitric acid digestion.

Figure 5.9. Zn^{2+} concentration of zinc materials analysed with ICP-OES, after a 24 hour nitric acid digestion.

Figure 6.1. SynaptoGreen™ fluorescence measured following uptake into H376 cells during 5 minute exposure to test materials.

Figure 6.2. SynaptoGreen™ fluorescence comparing ACROS SiO_2 bulk particle uptake into H376 cells to 5 minute exposure of SiO_2 nanomaterial.

Figure 6.3. SynaptoGreen™ fluorescence measured following uptake into Caco-2 cells during 5 minute exposure to test materials.

Figure 6.4. SynaptoGreen™ fluorescence comparing ACROS SiO_2 bulk particle uptake into Caco-2 cells to 5 minute exposure of SiO_2 nanomaterial.

Figure 6.5. Confocal laser scanning microscope images taken at 126X magnification of H376 cells treated for 5 minutes with 0.125% w/v of materials diluted in 50μM FM®1-43FX.

Figure 6.6. Enlarged Confocal laser scanning microscope images to highlight increased uptake of nanoparticle containing SiO2 material, into 50μM FM®1-43FX fluorescent vesicles (green) within the cytoplasm of H376 cells.

Figure 6.7. Confocal laser scanning microscope images taken at 64 X magnification of Caco-2 cells treated for 5 minutes with 0.125% w/v of materials diluted in 50μM FM®1-43FX.

Figure 6.8. Enlarged Confocal laser scanning microscope images (63X magnification) demonstrating increased uptake of nanoparticle containing SiO_2 material, into 50μM FM®1-43FX fluorescent vesicles (green) over the baseline vesicle formation demonstrated in the negative control.

Figure 6.9. Zoomed in 256X magnification images to show the spherical shape of suspected vesicles loaded with FM®1-43FX dye (as indicated by arrows) within (a) H376 cells and (b) Caco-2 cells.

Figure 6.10. Confocal laser scanning microscope images taken at 64 X magnification of test materials without cells.

Figure 6.11. Confocal microscope images overlaid on light microscopy images at 20X magnification to depict internalised FM®1-43FX dye in Caco-2 cells.

Figure 6.12. TEM images of SkinEthic RHO tissue sections taken at 1,000 times magnification using the Hitachi-7100 TEM.

Figure 6.13. TEM images of EpiGingiva™ GIN-100 tissue sections taken at 1,000 times magnification using the Hitachi-7100 TEM.

Figure 6.14. Enlarged TEM micrographs to highlight ZnO nanoparticle internalisation into 3-D tissue model sections.

Appendix Figure 9.1. Light microscopy images taken of H376 cells using a Nikon Eclipse TE2000-U Light-Fluorescence Microscope with Digital SLR Camera, at 40X magnification.

Appendix Figure 9.2. SEM micrographs demonstrating the micron size of SiO_2 – ACROS-Bulk material. (a) 100X magnification and (b) 1,000X magnification with scale bar shown respectively.

ACKNOWLEDGEMENTS

So many people have contributed to help me make this Thesis possible. It is truly hard to know where to start thanking everyone. So perhaps I should start at the beginning and move through in chronological order…

This project would not have been possible where it not for the generous funding of the BBSRC and GSK consumer healthcare. In particular, I would like to thank both Dr Joanna Rowland and Dr Christabel Fowler who, as part of GSK supervisory team, have always provided excellent advice and enthusiastic encouragement in equal measures. Your warm receptions in our regular discussions have always been enjoyable. The great help, support and direction you have both provided throughout my PhD has been much appreciated. Thank you both.

On to my academic supervisors from the University of Brighton, Dr Jacqui Elsom and Dr Gary Phillips, or 'Mum' and 'Dad' over the course of this project! Not only have you provided the awe inspiring scientific knowledge to direct this project so effectively, you have done this with friendly, fun and infectious enthusiasm that has been a great help and inspiration at all times. Without your reassurances at various stages of the project, I would be a trembling wreck. And without all the joking and fun, I would not have enjoyed it as half as much as I have. You really are the best supervisors I could ever have hoped for!

Throughout my time completing this PhD, I have had the privilege to have shared the post-grad office with an amazingly fun and supportive network of colleagues. Everyone in H404 has been a pleasure to have known, bounced ideas against and enjoyed so many numerous good times. I did not expect to make such a unique and great set of friends. Lads like Joe, James, Lubinda, Jonathan, Kush, Ben, Gee & Sandeep, and of course the girls Michelle, Meenal and Nina (also keen to get Laddy). You've all been a hoot and I'll never forget all the good times and banter.

There are so many other people that have also been a real help to me during my time at Brighton, and I'd especially like to mention Dr Angie Sheerin for keeping me on the straight and narrow in the lab, Steve Jones for all the IT support, Dr Jon Salvage and Mike Helias for trusting me with the FEG-STEM. Additionally, Pete Lyons, Chris English, Dr Guy Standen, Dr Julian Thorpe, Chris Morris, Maurizo and Joe Hawthorne have all unselfishness given their time to help me in at various stages in a great variety of ways.

I also feel I should mention the impact colleagues from previous jobs have had on me, shaping my science skills. Particularly the guys from Ludger, and especially Dr Daniel Spencer who I appreciate now has had a profound impact on me, as the scientist I am today. A belated (whilst you waited for me to mature) and heartfelt "thank you" Daniel.

Of course, I would not have attempted such a feat as this Thesis, if it were not for the loving support of my family and close friends, who are always encouraging, whilst somehow simultaneously always maintaining that I still keep my feet firmly on the ground. There are too many to individually name, but thank you to my Dad, sisters, brother, grandparents, auntie and uncles, including Laura's side of the family too. Carmel & Doug, you both deserve acknowledgement for your support by way of a roof over my head when I first started.

Finally, I would like to dedicate this work to my beautiful Fiancé, Laura McLean (soon to be Mrs Best). Without you in my life, I would never have had the ambition and drive to carry out something like this. With your support I have achieved something I never thought possible, and it has only ever been to prepare for our future together. With thanks and love, **Mark Best**.

AUTHORS DECLARATION

Declaration

I declare that the research contained in this thesis, unless otherwise formally indicated within the text, is the original work of the author. The thesis has not been previously submitted to this or any other university for a degree, and does not incorporate any material already submitted for a degree.

Signed

Dated

ABBREVIATIONS AND DEFINITIONS

Analysis of variance	ANOVA
Activator protein-1 transcription factor	AP-1
Antioxidant response element	ARE
Adenosine triphosphate	ATP
Calcium ions	Ca^{2+}
Calmodulin Kinase-Kinase	CaMKK
4'6,-Diamidino-2-phenylindole dihydrochloride	DAPI
Dynamic light scattering	DLS
Dimethyl sulfoxide	DMSO
Deoxyribose nucleic acid	DNA
European Commission	EC
The half maximal effective concentration	EC_{50}
Extacellular matrix	ECM
Electrical double layer	EDL
Energy dispersive X-Ray spectroscopy	EDS
Epidermal growth factor receptor	EGFR
Extracellular Lipid	EL
Enzyme linked immunosorbent assay	ELISA
Electron microscopy	EM
European Union	EU
European centre for the validation of alternative methods	EVCAM
Fetal Bovine Serum	FBS
Food and Drug Administration (USA)	FDA
Fourier transform infrared spectroscopy	FTIR
Friends of the Earth	FoE
Granulocyte macrophage colony stimulating factor	GM-CF
Glutathione	GSH
GlaxoSmithKline Consumer Healthcare division	GSK CH
Hydrochloric acid	HCl
Health and safety executive (UK)	HSE
Hydrogen peroxide	H_2O_2
Human beta defensins	hBD
Inhibitor of apoptosis proteins	IAPs
The half maximal inhibitory concentration	IC_{50}
Inductively coupled plasma optical emission spectroscopy	ICP-OES
Interferon-γ	IFN-γ
Interleukin	IL-
Intracellular lipid	IL
Lactate dehydrogenase assay	LDH
Light emitting diode	LED
Mitogen-activated protein Kinase	MAPKinase
Membrane coating granule	MCG
(3-(4,5-dimethylthiazol-2-yl)-2,5-diphenyltetrozolium bromide)	MTT

Nicotinamide adenine dinucleotide hydrogenase	NADH
Nicotinamide adenine dinucleotide phosphate oxidase	NADPH
Nuclear factor Kappa-B	NF-$\varkappa$B
National Institute of Standards and Technology™	NIST™
Nuclear magnetic resonance	NMR
Nanoparticle tracking analysis	NTA
Nuclear factor (erythiod-derived 2)	Nrf-2
Hydroxide	OH
Oral squamous cell carcinoma	OSCC
Phase analysis light scattering	PALS
Polymerase chain reaction	PCR
Phosphate buffered saline	PBS
Polyethylene glycol	PEG
Phenazine ethosulfate	PES
Protein Kinase B	PKB
Parts per million	ppm
Registration Evaluation and Authorisation of CHemicals	REACH
Reconstructed human oral epithelium	RHO
Refractive index	RI
Reactive oxygen species	ROS
Standard deviation	SD
Standard error	SE
Sodium dodecyl / lauryl sulphate	SDS / SLS
Scanning electron microscopy	SEM
Second mitochondria-derived activator of caspases	SMACs
Trans epithelial electrical resistance	TEER
Transmission electron microscopy	TEM
Tumour necrosis factor	TNF
Ultra violet	UV
Volume per volume dosage	v/v
Weight per volume dosage	w/v
X-Ray diffraction	XRD

Agglomerate: Collection of weakly-bound particles or aggregates or mixtures of the two where the resulting external surface area is similar to the sum of the surface areas of the individual components.

Aggregate: Particle comprising strongly-bonded or fused particles where the resulting external surface area may be significantly smaller than the sum of calculated surface areas of the individual components.

Nanomaterial: A natural, incidental or manufactured structure containing particles, in an unbound state or as an aggregate or as an agglomerate and where, for 50 % or more of the particles in the number size distribution, one or more external dimensions is in the size range 1 nm - 100 nm.

1 INTRODUCTION

1.1 Nanotechnology and nanomaterials

Nanotechnology is an ever popularised current term that is multi-encompassing across many areas in science. The term is most often used to describe techniques, materials and technologies that are able to design, produce or utilise tiny structures (Maynard *et al.*, 2006). These technologies now encompass applications as vast as: computing, cosmetics, electronics, energy production, medicine, optics, pharmaceutics, and robotics; with the term now applied across the entire spectrum of sciences (physics, chemistry, biotechnology and the environment). Because of this level of interest it represents one of the most promising areas of the 21st century for technological development.

Nanotechnologies include the development and production of nanosized particles, fibres, tubes, composite materials and surfaces or coatings (Bleeker *et al.*, 2013), collectively referred to as nanomaterials. They can be both engineered and naturally occurring (Handy *et al.*, 2008). Hence, nanomaterials are a very varied population of different materials. Despite the diversity of nanomaterial types, common to all is their small size, defined by consensus as a single particle with a diameter in the range of 1 – 100nm ((SCENIHR), 2009, Borm *et al.*, 2006, Nel *et al.*, 2006, Oberdorster *et al.*, 2005b, Stone *et al.*, 2010). Nanofibres are a sub-class of nanoparticles, which have two dimensions less than 100nm, but the third dimension (axial) can be much larger (Stone *et al.*, 2010). For the purpose of this study, the focus remains on metal oxide nanomaterials.

Today, metal oxide nanomaterials can be increasingly seen utilised in sporting goods, tyres, catalysts, electronic components, window sprays, paints, varnishes, coatings, foods, sunscreens, cosmetics, and antimicrobial and antifungal preparations; and are expected to be increasingly applied to the medical field in diagnosis, imaging, and drug delivery (Scientific Committee on Consumer Products (SCCP), 2007, Borm *et al.*, 2006, Buzea *et al.*, 2007, Kimbrell, 2006, Nel *et al.*, 2006). As technological advancement races ahead of legislation (Choi *et al.*, 2009), recently the definition used to confer nano-status on a small particle is subject to ongoing debate. Andrew Maynard argues that we are better off without a 'one-size-fits-all' definition of engineered nanomaterials for regulatory purposes (Maynard, 2011), a result of the inherent difficulties in grouping

together such a diverse population of materials, that all exhibit a wide range of different properties. This opinion would seem to hold weight, through the ambiguous, fractured nanomaterial identification that currently exists between the different regulatory bodies. Currently, organisations have restricted nanomaterial definitions to working guidelines, recommendations that are not legally binding (Bleeker *et al.*, 2013). For the purposes of this study, we have defined nanomaterials according to the current European Union published recommendation, which states:

"*A natural, incidental or manufactured material containing particles, in an unbound state or as an aggregate or as an agglomerate and where, for 50 % or more of the particles in the number size distribution, one or more external dimensions is in the size range 1 nm - 100 nm.* ((EU), 2011).

1.1.1 Nano-scale properties

The intense interest and excitement in the nanoscale can be explained by the unique behaviour of particles when their size falls between 1 and 100nm. In this range, their physiochemical behaviour changes from classical to quantum physics, predominantly due to the vastly increased ratio of surface area to volume, present in many nanomaterials (Aitken *et al.*, 2006). For particles smaller than 100nm in diameter, the number of surface atoms or molecules is inversely related to particle size, and because the number of atoms or molecules on the surface of the particle may determine the material reactivity, this ratio is key to defining the chemical and biological properties of the nanomaterial (Nel *et al.*, 2006). For materials greater than 1μm in size (>1000nm), the percentage of atoms at the surface is insignificant in relation to the number of atoms in the total bulk of the material. This allows it to exhibit the constant physical properties characteristic to its particular chemical species, regardless of how big (in terms of aggregation) the particle becomes (Borm *et al.*, 2006).

The unique behaviour of nanomaterials has been of great scientific interest because it introduces individual size-dependent properties to the chemical species. These have been manipulated to develop a range of observed performances that differ from the 'bulk' (non-nano) material. New, nano-specific characteristics that have been exploited include substances that are opaque at ordinary scales becoming transparent, stable materials turning combustible and inert substances that can become catalysts, as well as having increased electrical, magnetic and optical properties (Borm *et al.*, 2006, Buzea *et al.*, 2007, Community Research and Development Information Service (CORDIS),

2009, US Environment Protection Agency (EPA), 2005, Maynard, 2007b, Nohynek *et al.*, 2007, Whitesides, 2005).

Small particle size is not the only characteristic attributed to the unique and unpredictable properties exhibited in nanomaterials. Other characteristics thought important, include:

(i) Shape
(ii) Solubility
(iii) Structure (including crystallinity)
(iv) Chemical composition
(v) Porosity
(vi) Surface topology
(vii) Particle charge
(viii) Agglomeration/aggregation state

(From (Scientific Committee on Emerging and Newley Identified Health Risks (SCENIHR), 2009)).

Whilst nanoparticles come in many shapes and sizes, agglomeration/aggregation tendency is particular common for nanomaterials without pre-designed surface function. Due to highly energetic adhesive forces close to the surface, the nanoparticles are either agglomerated with their neighbours, glued to the next available surface or work like an activated charcoal filter towards other small molecules (Borm *et al.*, 2006). It is useful to note the difficulty in the consistent definition of a nanomaterial when aggregation into a bigger complex (that commonly exceeds the nano-scale (>100nm)) is frequent, especially in terms of official legislation/regulation. Despite this, their consideration is thought important enough to have been incorporated into the most recent EU definition ((EU), 2011):

"Agglomerate: Collection of weakly-bound particles or aggregates or mixtures of the two where the resulting external surface area is similar to the sum of the surface areas of the individual components.

Aggregate: Particle comprising strongly-bonded or fused particles where the resulting external surface area may be significantly smaller than the sum of calculated surface areas of the individual components". (((ISO), 2008)).

Clusters of nanoparticles are still considered nanomaterials due to the possibility of resulting nano-pores conferring functionality within the agglomerate. In addition, it

reflects the difficulties associated with accurate characterisation of nano-scale properties (Nel *et al.*, 2009, Oberdorster *et al.*, 2005a, Stone *et al.*, 2010). Currently, the best recommended approach remains unstandardized (Stone *et al.*, 2010), and involves utilisation of multiple complex analyses to cover the range of the aforementioned characteristics ((SCENIHR), 2009, Borm *et al.*, 2006, Nel *et al.*, 2009, Oberdorster *et al.*, 2005a, Powers *et al.*, 2006). A recent report by the EU has looked to address the challenges of nanomaterial characterisation, and has recommended the application of 8 selective methods for measuring nano-size alone (Linsinger *et al.*, 2012b).

The need for thorough characterisation of nanomaterials emanates from the lack of understanding with regards to properties exerted through interactions with their environment (Borm *et al.*, 2006, Murdock *et al.*, 2008, Powers *et al.*, 2006, Stone *et al.*, 2010). This is important for those wishing to develop novel nanomaterial properties into new technologies, but equally too in understanding the safety of nanomaterials (Boverhof & David, 2010, Nyström & Fadeel, 2012, Oberdörster, 2010, Oberdorster *et al.*, 2005b, Tsuji *et al.*, 2006). The properties of nanomaterials are likely to differ from their more established, conventional chemical counterparts, and this applies to their behaviour in the environment including reaction kinetics and toxic properties (Bleeker *et al.*, 2013). Currently, very little is known on how nanomaterials interact with biological systems, meaning that their impact on both the environment and human health is not yet fully elucidated (Jennifer, 2013). At the rate of expansion currently experienced by nanotechnology, it is impossible to predict the possible future exposures and interactions, but their presence within a wide-variety of industries at present, poses an immediate challenge to regulators of health and safety (Aitken *et al.*, 2006, Borm *et al.*, 2006, Maynard *et al.*, 2006, Nyström & Fadeel, 2012, Oberdorster *et al.*, 2005b, Stone *et al.*, 2010). Attempts to remove the uncertainty regarding nanomaterial risk assessment have given rise to a new discipline: nanotoxicology.

1.2 Nanotoxicology

Classical chemical compounds are routinely subject to well established toxicity tests prior to release to the public (Oberdorster *et al.*, 2005a, Tsuji *et al.*, 2006, Warheit *et al.*, 2007). No such procedures currently exist to specifically combat the unique properties that may arise in a material upon reduction in particle size (<100nm). Yet nanomaterials

must be classed as new chemical entities, and undergo thorough risk assessment prior to safe application ((SCENIHR), 2009). The burden in testing the same parameters for bulk materials on a case by case basis for nanotoxicity studies, is both slow and costly (Murdock *et al.*, 2008). In addition, the appropriateness of existing toxicology testing methods, and the extent to which they may be applied to nanomaterials, remains a highly contentious area (Kimbrell, 2006), acknowledged as requiring improvement (Stone *et al.*, 2010). Therefore, characterisation remains important, in attempting to identify common features in nanomaterials that may pose a risk to human health under certain environmental conditions, linked to exposure (Oberdorster *et al.*, 2005a, Thomas *et al.*, 2006). Currently, there are many gaps in the knowledge of the fate of nanomaterials used increasingly new technologies. Subsequently, concern for toxicological testing is based on the current lack of understanding and predictability observed between interactions of different individual nanoparticles and cells, and/or subcellular structures; with their biokinetics and full biological effects likely to be very different from those of both larger-sized particles and other nanoparticle species (Landsiedel *et al.*, 2010). The large relative surface areas of nanoparticles creates active surface chemistries that can result in increased reactivity that may be intrinsically toxic (Nel *et al.*, 2006). Furthermore, their small size causes them to fall within the same scale as many organic biomolecules used in the human body (US Food and Drug Administration (FDA), 2009). It is presumed this characteristic provides them with unprecedented mobility, across biological membranes, cells, tissues and organs, more effectively than larger materials (Oberdorster *et al.*, 2005b). The increased uptake potential of nanomaterials has led to concern for unregulated access to sites that are not linked with intended applications or routes of exposure (where nanoparticle translocation reaches systemic circulation (Hoet *et al.*, 2004, Tsuji *et al.*, 2006)). Nanomaterials circulating within the blood stream have been reported to experience secondary uptake and bioaccumulation in the brain, liver, heart, kidneys, spleen, bone marrow and nervous system (Kreyling *et al.*, 2009).

Nanotoxicity studies aim to evaluate the structure-function properties of nanomaterials, and their effects to human health and impact towards the environment (Stone *et al.*, 2010). Charged primarily with reducing the lack of toxicology testing data specifically for individual nanomaterial species, it is hoped a common consensus on the exact health implications, relative to specific nanomaterial characteristics, can eventually be realised.

1.2.1 Exposure routes

As an emerging discipline, nanotoxicology has had to rely upon building data extrapolated from existing toxicology studies of traditional substances as its starting base ((SCENIHR), 2009, Crane *et al.*, 2008, Klaine *et al.*, 2008). Existing work carried out investigating airborne particulate toxicity, has led to inhalation being identified as the primary route of human exposure to nanoparticles (Borm *et al.*, 2006, Hoet *et al.*, 2004). As such, it is currently the most intensely studied site for nanomaterial toxicology (Buzea *et al.*, 2007). The different compartments of the respiratory tract (nose, larynx, airway and lungs) all act as a filter for inhalation of airborne particles. However, smaller particles are more likely to reach the lung, and demonstrate increased efficiency in depositing in all regions of the respiratory tract (Hackenberg *et al.*, 2011b, Oberdorster *et al.*, 2005b). As Figure 1.1 shows, this has led to the implication of nanomaterials in respiratory diseases such as asthma, bronchitis, emphysema, lung cancer, and through subsequent translocation from lung epithelial tissue. Even neurodegenerative diseases such as Parkinson's and Alzheimer's diseases have been linked to nanomaterials (Buzea *et al.*, 2007).

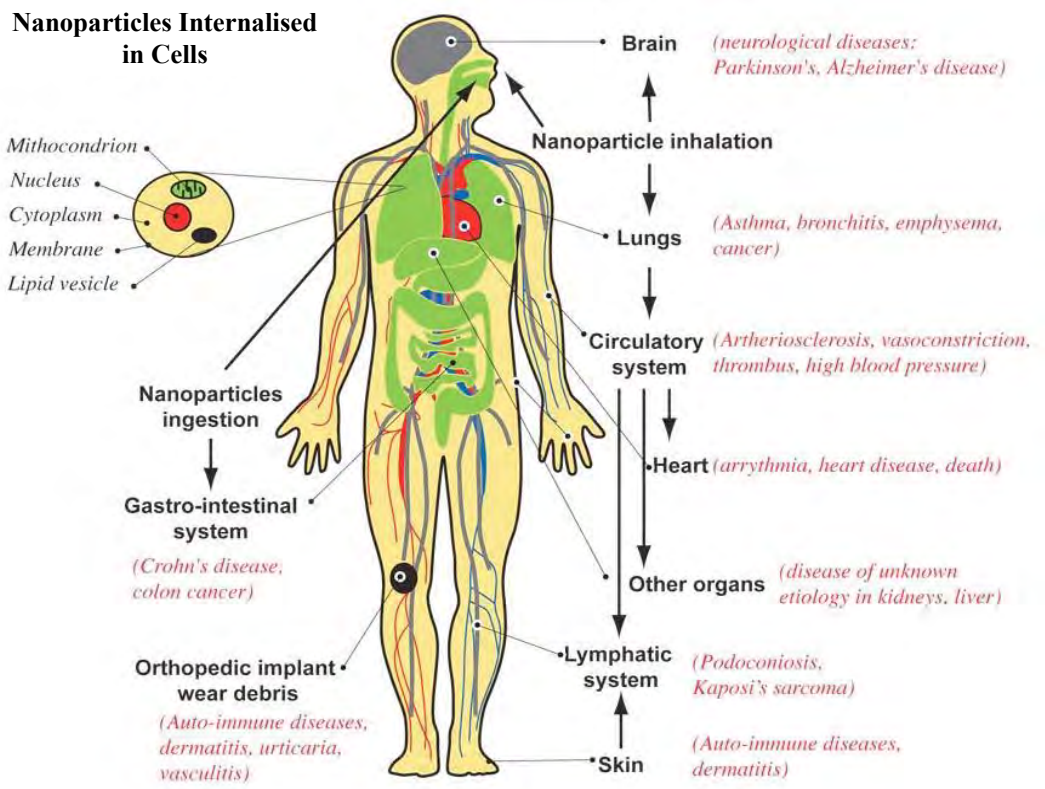

Figure 1.1. Schematic of human body with pathways of exposure to nanoparticles, affected organs, and associated diseases from epidemiological, *in vivo* and *in vitro* studies. *Taken from (Buzea et al., 2007).*

In addition, the facilitative uptake environment present in the gut also provides an alternate systemic exposure route, should nanoparticles become ingested (Borm *et al.*, 2006). Dust, soil, food additives, toothpaste and excipients for pharmaceuticals or nutraceuticals, all provide exposure of many billions of sub-micron sized particles on a daily basis, to the average Western person's gut (Powell *et al.*, 2010). Particulate induced inflammation has been demonstrated to play a role in the immune response linked to Crohn's disease (Lomer *et al.*, 2002). Titanium dioxide (TiO_2) and silicon dioxide (SiO_2) are widely utilised as formulation enhancers within both food and cosmetic products, and are increasingly present as nanomaterials (Martin, 2007, Weir *et al.*, 2012). The gastrointestinal tract has already been demonstrated to provide a risk of systemic toxicity by the translocation of bulk TiO_2 particles (50nm-500nm), that eventually reside in the liver and spleen (Jani *et al.*, 1994).

The subject of nanomaterial penetration occurring through the layers of the dermal epithelial cells in skin provides perhaps the most controversial and intensely debated aspect of the perceived potential dangers to exposure. It holds particular significance due to the existing availability of nanomaterial formulation sunscreens ((SCCP), 2007, Morabito *et al.*, 2011, Weir *et al.*, 2012) and in being a primary site of exposure alongside inhalation during their manufacture (Aitken *et al.*, 2008). The evidence related to nanomaterial penetration in skin remains highly debated ((FoE), 2006, Borm *et al.*, 2006, Maynard, 2007a, Nohynek *et al.*, 2010, Schilling *et al.*, 2010). Many studies have reported nanoparticle internalisation into the apical cell surface layers (Lademann *et al.*, 1999, Lin *et al.*, 2011, Schilling *et al.*, 2010, Schulz *et al.*, 2002), yet not fully translocated deeper into the tissue with only limited reports of them reaching systemic circulation (Gulson *et al.*, 2012). However, the fate of nanoparticles after application to human skin is not completely understood. Studies utilising *in vitro* keratinocyte cell models have demonstrated, to some extent, resultant nanoparticle linked oxidative stress responses (Nel *et al.*, 2006, Park *et al.*, 2011, Samberg *et al.*, 2009, Shvedova *et al.*, 2003). Some have even found more severe consequences to the tissue, such as DNA damage in dermal cells (Dunford *et al.*, 1997, Patlolla *et al.*, 2010, Sharma *et al.*, 2011). But these cytotoxic responses have mainly occurred under specific conditions, which often isolate the study from natural scenarios, either through excessive exposure times or exaggerated dose levels (Elder *et al.*, 2009).

The majority of nanomaterial toxicology data has been generated through the investigation of TiO_2 and zinc oxide (ZnO) nanoparticles, due to their inclusion as the leading UVA/UVB defensive component in sunscreen lotions ((SCCP), 2007, Gulson *et al.*, 2010, Lademann *et al.*, 1999, Lewicka *et al.*, 2013, Monteiro-Riviere *et al.*, 2011, Morabito *et al.*, 2011, Nohynek *et al.*, 2010, Schilling *et al.*, 2010, Schulz *et al.*, 2002, Tan *et al.*, 1996). Different experiments using *in situ* animal studies of rat and rabbit models, as well as *ex vivo* experiments with intact human and pig skin, have demonstrated the passage of these particles through tissue (Alvarez-Román *et al.*, 2004, Elder *et al.*, 2009, Moran *et al.*, 1991, Tan *et al.*, 1996). However, most studies have only reported significant penetration of the tissue via hair follicles and flexed or damaged skin (Meidan *et al.*, 2005, Oberdorster *et al.*, 2005a, Toll *et al.*, 2003). With reference to nanoparticles, various metal oxide nanomaterials have been used in studies demonstrating increased accumulation and retention time at hair follicles, due to the mechanical flexion of skin (Baroli *et al.*, 2007, Lademann *et al.*, 2006, Tan *et al.*, 1996, Tinkle *et al.*, 2003, Toll *et al.*, 2003). Langerhans cells recovered from human skin and exposed to nanoparticles have shown uptake of 40nm polymers in 24% of the cells, indicating transport through the tissue, although not by larger particles (Vogt *et al.*, 2006). Broken skin is thought to provide an even greater risk for selective particles reaching the systemic circulation, offering a less restricted barrier to the penetration of skin for a wide range of materials, including large particle sizes up to 7μm in diameter (Oberdorster *et al.*, 2005b).

Uptake of particles may not prove cytotoxic, due to the protective mechanisms available to the keratinised tissue of the epidermis. These include rapid proliferation of cells that enable tissue integrity to be maintained during increased rates of desquamation (Presland & Dale, 2000, Squier & Kremer, 2001). The risk to health posed by unregulated uptake persist, with reports of chronic inflammation occurring where repeated exposure of metal oxide material has led to internalisation and subsequent accumulation over time (Oberdorster *et al.*, 2005a, Park *et al.*, 2009, Wang *et al.*, 2008a, Yang *et al.*, 2008). As yet, nobody has conclusively linked nanomaterial inclusion in sunscreen products as being detrimental to human health, and it has even be argued that the harmful effects of the sun's rays will always constitute a larger risk to health (Schilling *et al.*, 2010).

1.2.2 Nanomaterial capacity for systemic toxicity

Figure 1.1 also shows how the ultra small size of a nanoparticle facilitates uptake into cells and can transcytosis across epithelial and endothelial tissues into blood and lymph circulation where they then have the opportunity to reach potentially sensitive target sites (Kreyling *et al.*, 2009, Oberdorster *et al.*, 2005b). It is this potential, for translocation into other parts of the body that makes airborne nanomaterials a particularly prospective danger. However, like most research into nanomaterial toxicity, conflicting evidence can be presented, in particular towards the extent of translocation ((SCENIHR), 2009, Borm *et al.*, 2006).

Kreyling *et al.*, 2002 report the use of highly insoluble iridium nanoparticles, with differences in size between 15nm and 80nm. They found that these nanoparticles were cleared from the lungs via the airways into the gastrointestinal tract. Less than 1% were found to be translocated into secondary organs like the liver, spleen, heart and brain. The study found that the 80nm sized particles were translocated an order of magnitude less than the 15nm sized particles, indicating the importance of size even within the nano-scale (Kreyling *et al.*, 2002). Despite only a small fraction of the iridium particles being seen to be translocated, the actual amount was significant, when exposure times where increased through intravenous administration. Being a dense, inorganic metallic substance, it is unsurprising that iridium nanoparticles were not metabolised and subsequently absorbed from the gut. Instead, they accumulated and were retained in the liver and spleen which caused hepatotoxicity: with the inability of the body to clear toxic agents from its system. This example supports the speculation that nanomaterials are able to cause long-term toxicity (Kreyling *et al.*, 2006a, Oberdorster *et al.*, 2005b). The extent of uptake is an important consideration and whilst translocation of nanomaterials has been demonstrated to occur, systemic availability of inhaled nanoparticles outside the lung remains limited to such exaggerated exposure conditions (Kreyling, 2013). It remains possible however, that continued or repeated exposure may result in greater toxicity through increased accumulation and translocation of significant quantities of nanoparticles to the circulation (Card *et al.*, 2008).

Bioaccumulation has been demonstrated through multiple-dosing of nanoparticles delivered intravenously. Consistently these studies have revealed preferential agglomeration located within phagocytotic cells in the liver and spleen, including gold (Balasubramanian *et al.*, 2010, Lipka *et al.*, 2010), carbon-iron oxide nanotube hybrids

(Wu *et al.*, 2011), SiO_2 (Hasezaki *et al.*, 2011, Liu *et al.*, 2012, Nishimori *et al.*, 2009) and silver nanoparticles (De Jong *et al.*, 2013, Johnston *et al.*, 2010a). In most cases, acute toxicity was not reported, with only exposure to nanomaterial silver linked to possible immunotoxic signals (De Jong *et al.*, 2013).

Deliberate intravenous administration has alluded to a particularly concerning prospect related to the ability of nanoparticles to cross the blood brain barrier, demonstrated through their applications as permeation enhancers optimised to facilitate pharmaceuticals acting within the brain (Koffie *et al.*, 2011, Wohlfart *et al.*, 2012, Zensi *et al.*, 2010). This ability raises a need for caution for systemic administration of nanoparticles, in terms of the potential for unregulated brain toxicity (Bulcke *et al.*, 2013, Sharma *et al.*, 2009a). Such uptake and subsequent passage was suggested to be possible by the toxic effect of small particles (approximately 200nm) on cerebral endothelial cells (Koziara *et al.*, 2003, Olivier *et al.*, 1999). However, in similar studies, other small particles (about 300nm) contradicted the research and blood-brain barrier translocation for a different type of nanoparticle was not found (Kreuter, 2013, Lockman *et al.*, 2003). An alternative route to the brain has also been demonstrated for nanoparticles exposed via nasal inhalation, with both magnesium and ZnO particulates observed within the olfactory bulb of rodents (Elder *et al.*, 2006, Kao *et al.*, 2012).

In studies where nanoparticles with different surface characteristics were evaluated, neutral nanoparticles and low concentrations of anionic nanoparticles were found to have no effect on blood brain barrier integrity (Lockman *et al.*, 2003); whereas high concentrations of anionic nanoparticles and cationic nanoparticles were observed to be toxic to the endothelial cells that line and protect the blood brain barrier (Kreuter, 2013). Similar to drug delivery, surface charge is an important parameter linked to the uptake potential of nanoparticles (Zolnik *et al.*, 2010), and must also be considered alongside size characteristics when investigating toxicity (Nel *et al.*, 2009).

1.2.3 Dose metrics

Investigations into the toxicity of nanoparticles in the respiratory system highlight complications with regard to accurate quantification of uptake rates. Roughly 25% of inhaled particles have been found to settle in the lung tissue, whilst a similar amount are exhaled, with the remaining 50% diverted to the pharynx where they are ingested orally (Oberdorster *et al.*, 2005b, Soto *et al.*, 2007). This can provide a discrepancy over quantification on distinct toxic dose levels for diseases implicated with specific

nanoparticles. For skin, this is equally as controversial, with some studies reporting no nanoparticle passage through the epidermis (Alvarez-Román *et al.*, 2004, Baroli *et al.*, 2007, Gamer *et al.*, 2006, Squier & Hall, 1985) and some showing only partial internalisation into the top epithelial cell layers (Schulz *et al.*, 2002, Tan *et al.*, 1996, Vogt *et al.*, 2006), while others report their passage into systemic circulation (Gulson *et al.*, 2012, Schilling *et al.*, 2010). Consistent across all studies, is the disparity between the amount and rates of absorption. This has led to one of the key questions related to nanomaterial exposure, which is 'how to most accurately report dose' (Borm *et al.*, 2006, Oberdorster *et al.*, 2007), important in quantifying toxicity levels in different systems (Bleeker *et al.*, 2013).

Nanoparticles can settle, diffuse, and aggregate differentially according to their size, density, and surface physicochemistry, all of which may change over time due to the dynamic nature of nanomaterial dispersions (Teeguarden *et al.*, 2007). As discussed, these include influences via interactions with constituent parameters from the environment (viscosity, density, presence of proteins in solution, *etc.*) (Murdock *et al.*, 2008, Powers *et al.*, 2006, Stone *et al.*, 2010). Of course, these difficulties may also be experienced by insoluble bulk particles; however, due to the increased surface reactivity of nanoparticles, the effects are likely to be more pronounced at the nano-scale. The definition of dose for nanoparticles in an *in vitro* system is therefore more dynamic, more complicated, and less comparable across material types, than it is for soluble or bulk chemicals (Teeguarden *et al.*, 2007). The complexities involved in accurate dose-metrics for nanomaterial exposure currently generate intense discussion and debate. Solutions to the problems have looked towards building collaborative databases (Marvin *et al.*, 2013, Schug *et al.*, 2013) that can help with tiered testing strategies (Choi *et al.*, 2009, McCall *et al.*, 2013) and development of *in silica* methods (Nel *et al.*, 2013). Currently, best practice remains to carry out toxicity testing on a case by case basis, alongside careful descriptions of the test system including media constituents, media depth and volume, dimensions of the wells, as well as a thorough characterisation of the nanomaterial, specifically relating to conditions of exposure (Teeguarden *et al.*, 2007). In addition, comparison with reference materials (such as a bulk material control) is imperative to determine the significance of nano-size over other nano-specific properties (Kroll *et al.*, 2009, Stefaniak *et al.*, 2013, Stone *et al.*, 2010) and crucial for reporting the distinguished characteristics responsible for a nanomaterials possible enhanced risk to health. Currently, nanomaterial standards remain limited in both

choice and validation (Stone *et al.*, 2010). Development has focused solely on the most commonly produced and exploited nanomaterials such as polystyrene, TiO_2, carbon black, SiO_2, silver and gold (Stefaniak *et al.*, 2013, Linsinger *et al.*, 2012a). Therefore, the majority of studies rely on physical metric comparisons to comparative bulk materials, used as a control for quantifying nanomaterial effects. These include mass, surface area and particle number, but are highly dependent upon the techniques applied during characterisation and the compatibility in extrapolating analysis conditions to match the environment of exposure (Oberdorster *et al.*, 2005a).

Issues of dose metrics are further complicated, as demonstrated by the inconsistencies that have arisen from inhalation study outcomes. Emissions generated from motor vehicle combustion of fossil fuels accounts for the most significant source of nanoparticulates in the atmosphere, and this area of toxicity is well studied with respect to pollutants such as diesel exhaust fumes (BeruBe *et al.*, 2007, Muller *et al.*, 2010, Wallace *et al.*, 2007). Although researchers can accurately reproduce reasonably pure specimens of pollutant nanoparticles for investigation, synthetic compounds may differ considerably from representative fractions present in ambient air. The greater surface area to volume ratio of nano-air particulate pollutants means they frequently absorb other chemicals on their surface, including biological compounds such as endotoxins (Kreyling *et al.*, 2006b, Schins *et al.*, 2004). This ability demonstrates a heightened toxic effect exerted by nanoparticle pollutants (over their micro-sized compatriots) and has been demonstrated through various *in vitro* studies (Xia *et al.*, 2004). Such examples serve to highlight implications for nanotoxicology investigated *in vitro*, with the effects of biological environments and delivery vehicles also thought likely to impact upon nano-properties (Nel *et al.*, 2009). A consideration now common to many biological *in vitro* studies, involves the formation of a protein-corona and the impact that this has on governing cytotoxicity (Dominguez-Medina *et al.*, 2013, Landsiedel *et al.*, 2010, Merhi *et al.*, 2012, Prasad *et al.*, 2013b, Tedja *et al.*, 2012, Xia *et al.*, 2008) and uptake potential (Cedervall *et al.*, 2007a, Cedervall *et al.*, 2007b, Dominguez-Medina *et al.*, 2013, Lynch *et al.*, 2007, Tedja *et al.*, 2012). Both size and surface properties have been found to play a significant role in determining the nanoparticle-protein coronas on the different particles of the same material (Lundqvist *et al.*, 2008). However, our current knowledge about conformational changes of the proteins upon adsorption onto nanoparticle surfaces remains limited, in part due the complexity in accurately mapping the epitopic structures of the protein layer (Cedervall *et al.*, 2007a), association/dissociation rates

between peptide species (Cedervall *et al.*, 2007b) and exploration outcomes directed towards modelling nanoparticle-protein corona interactions (Lynch *et al.*, 2007). Novel methodologies are increasingly being developed and utilised to measure nanoparticle-protein corona interactions at equilibrium (Boulos *et al.*, 2013, Cedervall *et al.*, 2007a, Montes-Burgos *et al.*, 2010, Svensson *et al.*, 2013, Tenzer *et al.*, 2013), but to fully elucidate understanding of their interactions in biological systems will require huge collaborative efforts by nano, colloidal specialist, biochemist, cell and molecular biology groups (Faunce *et al.*, 2008, Lynch *et al.*, 2007).

1.2.4 Nanomaterial toxicity testing strategy

Exposure to nanomaterials, whether at the primary site or as the consequence of translocation, has been reported to cause cytotoxicity, through a variety of different mechanisms. Until recently, animal studies have routinely been used to reveal physiological effects of nanoparticle induced toxicology. Increases in pulmonary inflammation, oxidative stress, and distal organ involvement have been demonstrated upon respiratory exposure to inhaled or implanted nanoparticulate matter (Oberdörster, 2010). However, limitations remain in the extrapolation of animal study outcomes applied to the risk assessment in humans. The majority of *in vivo* studies are carried out on mice or rat animal models that are not always compatible to human cell systems. Complications relate to the inherent differences between animal and human *in vitro* models. Examples from the literature of specific differences, include variations in alveolar architecture and epithelial fluid transport disparities between mice and human lungs (Ware, 2008). Of particular relevance to this study is the fact that rodent oral mucosal tissue follows entirely the keratinised differentiation process and is therefore not comparable to the non-keratinised areas in the human mouth (the importance of which is discussed in detail below).

These examples identify potential problematic incompatibilities for a toxicological model system, which could be applicable to most studies that utilise animal model as representatives of the human body. Coupled with the unpredictable and often completely individual properties exhibited by a nanomaterial, this highlights the complexity of nanotoxicology and the challenges required to study and accurately assess the risk of a nanomaterial to human health. The need to treat nanomaterials as new chemical entities ((SCENIHR), 2009) means this is expected to increase the burden of outstanding and outdated list of substances the EU is currently in the process of re-

evaluating as part of the Regulation on Registration, Evaluation, Authorisation and Restriction of Chemicals initiative (REACH) ((EC), 2006). Ambitiously, this programme looks to review the safety of over 30,000 chemicals (including nanomaterials) within 15 years of its implementation, that started back in 2006 (Williams *et al.*, 2009). Using traditional toxicity testing methods, wide ranging estimates were made as to the number of animals required for toxicity testing on this scale. Common to all are the extreme costs and ethical considerations that challenge the validity of such a programme of work without the development of new toxicity testing strategies (Rovida & Hartung, 2009). In its wake, integrated testing strategies have been utilised alongside a weight of evidence approach to speed up and more intelligently categorise the risk assessment, and subsequent toxicology testing strategy for different substances (Jaworska *et al.*, 2010). Crucial to the efficiency of these systems has been the promotion, development, validation and implementation of *in vitro* models to replace animal studies where possible (Grindon *et al.*, 2007).

In vitro tissue and cell culture analysis has supported the physiological response seen in whole animal models, whilst also providing more detailed mechanisms for increased incidence of oxidative stress leading to inflammatory cytokine production and apoptosis, in response to exposure to nanoparticles (Nel *et al.*, 2006). They are now heavily integrated in nanotoxiciology testing strategy, that relies on the accumulation of data generated through intelligently designed, diverse 'batteries' of *in vitro* assays (as outlined in Figure 1.2, below). For cosmetics, *in vitro* assay importance can be described as crucial, since the ban on animal testing became EU legislation through updates to the Cosmetic Directive (76/768/EEC) that became effective in March 2013 ((EU), 2013).

The integrated tiered testing strategy relies on a group of assays conducted together, or as part of a sequential assessment (where a result at one tier is used to determine the next step), to provide a prediction for a toxicity endpoint (Jaworska *et al.*, 2010). They are vitally required to address the unknowns in hazard assessment that arise through the unpredictable transition of properties, for a material reduced in particle size, from bulk to nanoscale form.

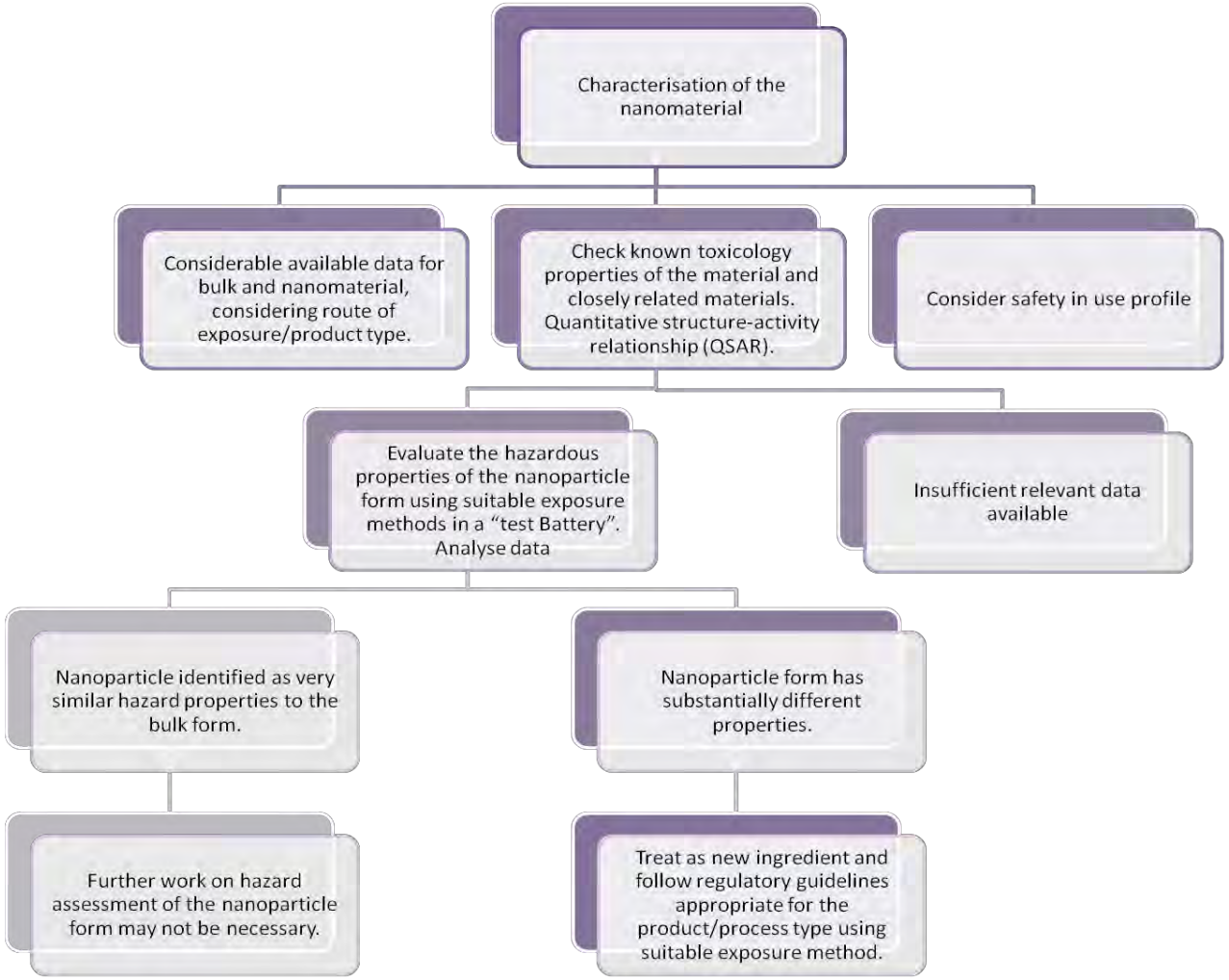

Figure 1.2. Flowchart outlining the current best strategy approach for the risk assessment of nanomaterials. *Adapted from ((SCENIHR), 2006).*

1.2.5 Nanomaterial cytotoxicity mechanisms

In vitro studies have shown that the risk associated with nanoparticulate toxicity initiates with localised damage through interactions with exposed cells. Whilst small quantities of metals, such as zinc, iron, sodium, calcium, potassium, copper and magnesium are essential for proper functioning of biological systems, both exposure at high levels and indeed low level deficiency often result in adverse health conditions to humans (Buzea *et al.*, 2007, Ho & Ames, 2002). For metallic nanomaterials specifically, including metal ions and metal oxides, two main actions are able to manifest cell damage in eukaryotes. Firstly, the large surface area to volume ratio indicative of the nanoscale, allows them to have increased catalytic activity (Huang *et al.*, 2010b, Kroll *et al.*, 2009, Park *et al.*, 2011). This makes them more likely to interfere with intracellular biochemical processes, or react with external toxic agents to become chemically modified, thereby differing from their bulk material form. Secondly, as with free metal ions, nano-metal decomposition from the nanoparticle and subsequent ion leakage, may result in formation of free radicals which can interfere with the existing metal ion homeostasis within the cell (Dick *et al.*, 2003, Donaldson *et al.*, 1998, Shvedova *et al.*, 2003). Nanoparticles have been shown to generate more free radicals and reactive oxygen species (ROS) than larger particles, which is likely due to their higher surface area (Buzea *et al.*, 2007). It is this mechanism of inducing oxidative stress that is now widely regarded as the main marker of nano-toxic cellular injury pathways. Mechanisms of ROS generation are well established (Proctor & Reynolds, 1984) and under conditions of environmental stress, the levels of ROS increase dramatically. Due to their role in cell redox signalling, imbalances in ROS levels cause disruption to the immune system (the release of cytokines), cell replication (through damage to DNA) and transport systems (by destroying cell membranes and inactivating important enzymes in metabolic processes). ROS can oxidise amino acids in proteins and lipids (peroxidation)) and ultimately promote apoptosis: programmed cell death (Rada & Leto, 2008).

The exceptionally small size, and reactivity, of some nanoparticles means they have the potential to cause oxidative stress by mimicking the ways in which ROS, and other free radicals, affect the cell. However, even on the nanoscale these types of nanoparticles would be very small (<10nm), and so far, this mechanism of cytotoxicity has mainly been demonstrated by quantum dots (Hardman, 2006, Hoshino *et al.*, 2004, Yang *et al.*, 2007). Nanoparticles that are larger than 10nm in size produce toxic effects by their reactive surface properties interacting with the cells membrane. This can either be an

isolated effect that causes toxicity through a cascade of oxidative stress mechanisms spiralling out of control within the exposed cell (thought to be due to direct nanoparticle-cell interaction); or the cell membrane might be damaged to the extent that nanoparticles become internalised in sufficient quantities to induce an oxidative stress environment from within the cell.

Calcium ions (Ca^{2+}) are of such vital importance to many physiological processes that their concentration homeostasis ranks alongside the most crucial physiological variables in the human body (Salido *et al.*, 2009). Intracellular calcium also plays an important role in the oxidative stress mechanism (Conrad, 2008) with levels temporarily increased in response to stimuli, through the opening of calcium channels in the cell membrane that allows extracellular calcium to be transported into the cell with the aid of calcium-binding proteins, such as calmodulin, calcinerium, S-100 and troponin-C (Conrad, 2008). Stimuli leading to accumulation of Ca^{2+} ions in the cell include the binding of cytokines and chemokines to cell surface receptors, in times of oxidative stress (Salido *et al.*, 2009). These conditions have been observed as occurring during nanoparticle-cell interactions, including acute increases in ROS generation that result in a sustained oxidative stress environment on the cell. In this environment, any prolonged or severe alterations in the delicate calcium ion homeostasis can also cause a range of other cellular dysfunctions (Salido *et al.*, 2009). These can include mitochondrial depolarisation, abnormal electrical activity and disruption of the entire signalling transduction, with excessive intracellular calcium levels heavily linked to apoptosis and necrosis (Conrad, 2008, Donaldson & Tran, 2002, Mattson & Chan, 2003, Oberdorster *et al.*, 2005b, Salido *et al.*, 2009) for example, and all these events have been observed through exposure of cells to cytotoxic ZnO nanoparticles (Huang *et al.*, 2010a).

Internalised nanoparticles are known to promote even greater levels of ROS, leading to the production of inflammatory cytokines and cytotoxic cellular responses that cause cell damage and often apoptosis (George *et al.*, 2010, Nel *et al.*, 2006, Rada & Leto, 2008, Shvedova *et al.*, 2003). The primary pathways of nanoparticle-cell interactions are summarised in Figure 1.3, but are thought to include:

(i) The particle surface causing oxidative stress, resulting in increased intracellular calcium and gene activation *e.g.* nuclear factor kappa-light-chain enhancment of activated B cells (NF-κB), a protein complex that controls the transcription of DNA (Donaldson & Tran, 2002).

(ii) Transition metals released from particles resulting in oxidative stress, increased intracellular calcium and gene activation, as reported for ZnO nanoparticles (Huang *et al.*, 2010a).

(iii) Cell surface receptors, such as the epidermal growth factor receptor (EGFR), becoming activated by transition metals released from nanoparticles, resulting in subsequent gene activation (Donaldson & Tran, 2002).

(iv) Intracellular distribution of nanoparticles in mitochondria generating oxidative stress (Oberdorster *et al.*, 2005b, Xiao *et al.*, 2003).

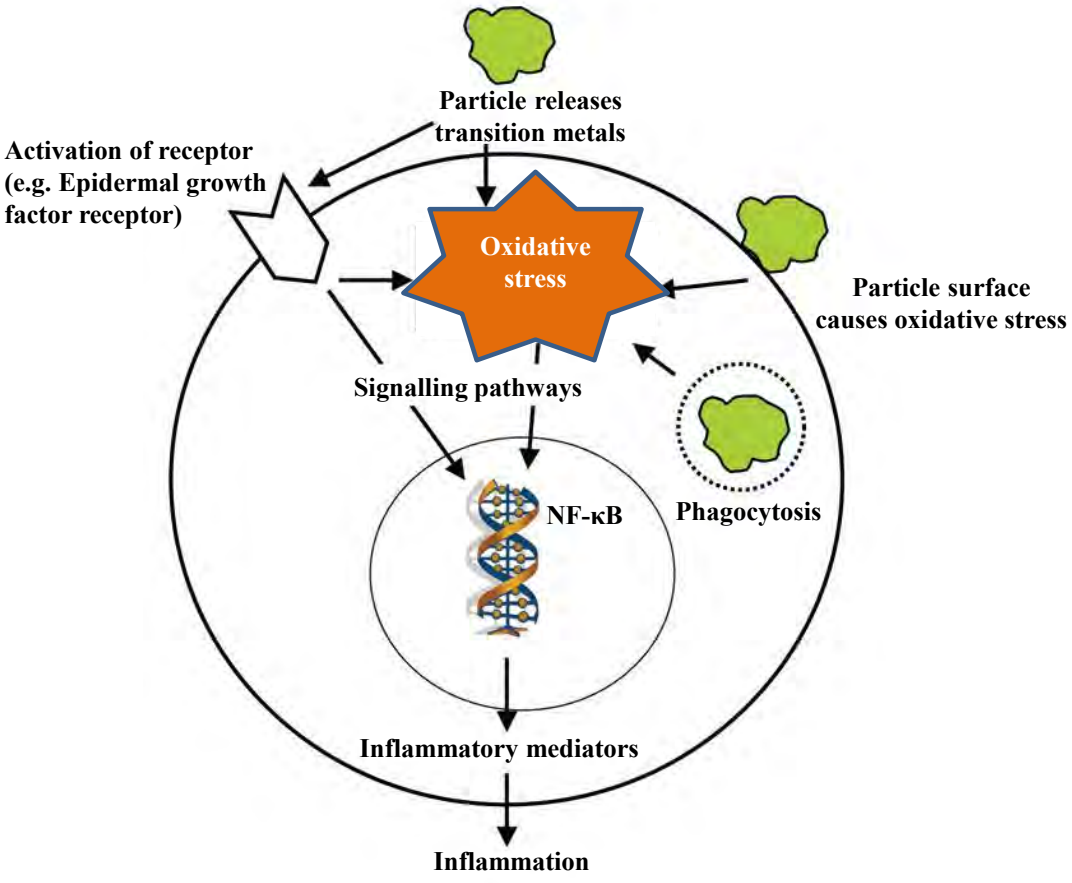

Figure 1.3. Hypothetical cellular interactions of nanoparticles causing inflammatory effects on lung epithelium. *Adapted from (Oberdorster et al., 2005b).*

To date, most reports have shown how the cytotoxicity of nanoparticles is likely to be caused by an inflammatory response upon contact with the cell. Inflammation is a protective response by the organism or cell, and is controlled by a complex series of many intracellular and extracellular events (Buzea *et al.*, 2007). Nanoparticles have been proven to induce oxidative stress in cells, which triggers the inflammatory response mechanism, resulting in the release of pro-inflammatory mediators or cytokines. These are the intercellular chemical messages alerting the immune system to the threat created by nanoparticles exposure, with their ability in forming ROS that contribute to the heightened oxidative stress in the cellular environment. Pro-inflammatory mediators are numerous in variety, depending on tissue or cell type and the specific interactions with the inflammatory causing agents, as well as the level or severity of inflammation (Goodman *et al.*, 2001). The oxidative stress response for a eukaryote cell can be split into three distinct phases, marked by the specific inflammatory signalling pathway activated, and these are highlighted in Figure 1.4.

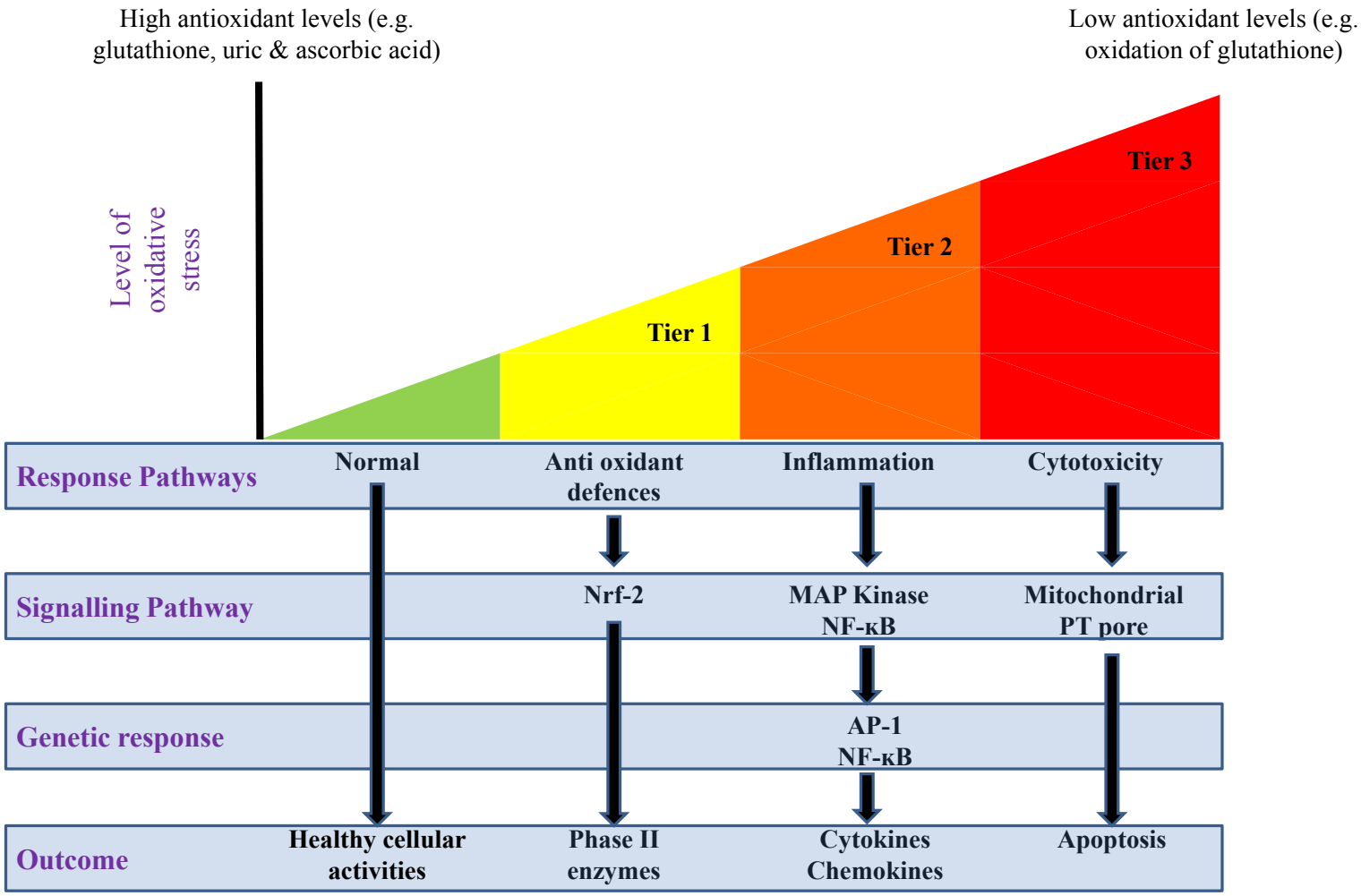

Figure 1.4. The hierarchal oxidative stress model. *Adapted from (Nel* et al.*, 2006).*

At the lowest level of oxidative stress (tier 1 of Figure 1.4), phase II antioxidant enzymes are induced via transcriptional activation of the antioxidant response element (ARE) by nuclear factor (erythroid-derived2) like-2, also known as NFE2L2 or Nrf-2 or the master regulator of antioxidant response (Xiao *et al.*, 2003). This mechanism aims to restore cellular redox homeostasis (Li & Kong, 2009). If the actions of tier 1 oxidative stress response fail, then an intermediate amount of oxidative stress prevails (tier 2). This stimulates activation of mitogen-activated protein kinases (MAPK) and NF-ϰB cascades, inducing pro-inflammatory responses. This includes the secretion of small soluble signalling proteins, known as cytokines and chemokines. These are released in response to specific feedback mechanisms related the cellular environment, and transmit signals to change the cells' behaviour accordingly. They interact only with specific target cells through high affinity binding with a target cell surface receptor, and for this reason, are a very large and diverse family produced by many cell types, throughout the body (Balkwill & Burke, 1989). In response to a pro-inflammatory situation, important cytokine and chemokine species secreted from macrophage cells, include: interleukin (IL) 1, IL-6, IL-8 and IL-11, as well as: tumour necrosis factor alpha (TNF-α) and transforming growth factor beta (TGF-β) (Cannon, 2000). In the skin, ROS generation results in excess TNF-α activating the NF-ϰB pathway through degradation of its inhibitor, IϰB, and this increases the expression of mRNA for similar cytokines IL-6, IL-8 and TNF-α itself (Young *et al.*, 2008), alongside unbalancing IL-1 family expression levels (Bernhofer *et al.*, 1999, Coquette *et al.*, 2003, Schroder, 1995). With respect to this study, oral mucosal epithelial cytokines are expected to follow similar networks to that of the skin (Rhodus *et al.*, 2005, Schmalz *et al.*, 2000). This mechanism is shown in Figure 1.5 (below).

If pro-inflammatory signalling is unable to deal with the overload in oxidative stress inducing agents formed through nanoparticle-cell interactions, *e.g.* excess ROS inside the cell, then a higher level of oxidative stress prevails. Figure 1.4 shows how tier 3 cellular mechanisms are the most severe action a cell can take in response to cytotoxic stress. The result is apoptosis: cell suicide in an attempt to send further pro-inflammatory signals to the organism's immune system that is under attack. Positive induction initiating programmed cell death is achieved via apoptotic proteins targeting mitochondria functionally (Cotran *et al.*, 1999).

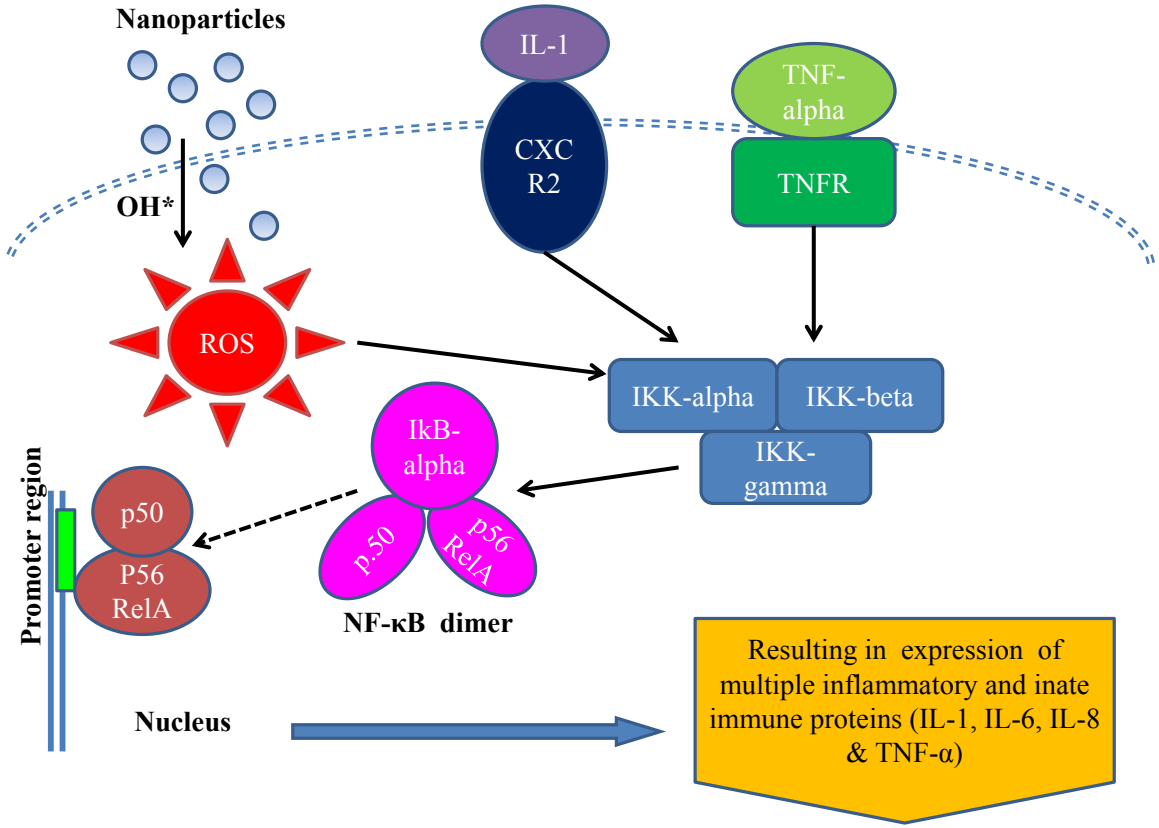

Figure 1.5. A model showing the simplified NF-kB signalling pathway that is activated by oxidative stress in response to nanoparticle generated ROS in keratinocytes. *Adapted from (Huang et al., 2010b).*

In response to oxidative stress mechanisms, TNF-α has been linked in inducing apoptosis by one of two main ways. TNF-α binding to the receptor activates transcription of proteins that cause the formation of mitochondrial pores and swelling of the organelle, or increasing permeability of the mitochondrial membrane. This allows apoptotic effectors, such as secondary mitochondria-derived activator of caspases (SMACs), to leak out into the cytosol, and bind with inhibitor of apoptosis proteins (IAPs), deactivating them (Fesik & Shi, 2001). Alternatively, perturbation of the mitochondrial permeability transition pore causes disruption of electron transfer, and without fully functioning mitochondria, cellular apoptosis or necrosis occurs rapidly (Nel *et al.*, 2006).

Nanoparticle cytotoxicity has also been implicated with inhibiting the effective workings of the immune system, by impairing macrophage phagocytosis (Barlow *et al.*, 2008, Renwick *et al.*, 2001). This effect has been implicated in Crohn's disease, when nanomaterials have been ingested into the gastrointestinal tract (Lomer *et al.*, 2002, Powell *et al.*, 2010). Another study found nanoparticles took on free radical and ROS specific roles, mediating inflammation that was enhanced by blocking actions of antioxidants in the release of TNF-α from alveolar macrophages (Dick *et al.*, 2003). One study likened the nanoparticle ROS induced DNA damage, observed in alveolar-like cell exposure to a selection of common airborne nanoparticulates, to the effects seen during irradiation related carcinogenesis (Mroz *et al.*, 2008). Other studies, using nano-metal oxides, have demonstrated oxidative damage to DNA (Bhattacharya *et al.*, 2009, Hackenberg *et al.*, 2011b, Xia *et al.*, 2006, Yang *et al.*, 2009); whilst TiO_2 and ZnO ROS have caused damage to DNA resulting in micronucleus formation and apoptosis (Dunford *et al.*, 1997, Huang *et al.*, 2010a, Rahman, 2002).

Despite the relative abundance of established research into cellular oxidative stress mechanisms, studies have only just begun unravelling the functional properties unique to nanoparticles that can be linked to instances of cytotoxicity. Whilst a number of *in vitro* studies may have detected nanoparticles enhanced capability for increasing ROS to a greater extent over bulk forms of the same material (Jeong *et al.*, 2013, Han *et al.*, 2013, Sharma *et al.*, 2012, Shukla *et al.*, 2011, Xia *et al.*, 2008, Papageorgiou *et al.*, 2007, Xia *et al.*, 2006), few have provided conclusive and in depth detail into the exact effects the ROS has on the subsequent oxidative stress mechanisms observed in the model. As alluded to previously, attributing cytotoxic effects solely to the nano-size characteristic

dramatically over-simplifies the interactions responsible for oxidative stress generation. It is also important to consider that the subsequent cellular damage that results from ROS is not uniquely confined to nanomaterial interactions. Many other stimuli have been observed causing similar cytotoxic mechanisms *e.g.* alcohol (Axford *et al.*, 1999, Robinson *et al.*, 2010), cigarette smoke (Jeong *et al.*, 2010) and UV exposure (Köck *et al.*, 1990) *etc.* However, the potential for nanoparticle internalisation into the cell carries with it the possibility for heightened oxidative stress through direct involvement with intracellular processes, and this is thought to be a unique risk attributed to the specific size of nanoparticles (Cho *et al.*, 2010). These cellular responses are now easily detectable and the extent of cytotoxicity (if not the exact mechanism) can be quantified using well established assay technology, such as the assessment of cytokines using enzyme-linked immunosorbent assays (ELISA); extracellular lactase dehydrogenase assessment (LDH), that detects intracellular enzymes released into supernatant following cell lysis (Wacker *et al.*, 1956); MTT (that requires the healthy functioning of a mitochondria to convert a chemical derivative to a coloured by-product that can be detected to assess cell viability (Mosmann, 1983)) and the comet assay, for the detection of DNA strand breakages (McKelvey-Martin *et al.*, 1993).

1.2.6 Uptake pathways

The primary function of any epithelial tissue is to protect the underlying cell layer, and this includes unpermitted access by foreign, potentially toxic substances. However, the human body is not self-sufficient; it requires external agents for energy and growth, and to remove waste products. These transport requirements emanate from the overall need to maintain tissue homeostasis (Marchiando *et al.*, 2010). Epithelial membranes (such as the oral mucosa), by nature, are involved in both the secretion and absorption of substances. The selective movement of substances implies the acceptance of certain molecules to traverse the tissue (Squier *et al.*, 1991). The main transport pathways that exist within human epithelial cell layers are shown in Figure 1.6. Each has been investigated to differing extents, particularly in relation to drug delivery; where studies increasingly investigate optimised delivery and release of pharmaceutical compounds to different areas of the body (Hearnden *et al.*, 2012, Medina-Kauwe, 2007, Wadia & Dowdy, 2005). Drug delivery is linked to specific uptake pathways of the pharmaceutical agent. The mechanism of internalisation within the targeted area of the body must be identified to comply with strict safety legislation that governs drug application in humans (Zhao *et al.*, 2010). For nanomaterials, less is known about the

specific uptake mechanisms, due to the wide variety of nano-specific characteristics that exist, conferring many preferential properties that have been observed to increase their potential for successful internalisation (Asati *et al.*, 2010, Cho *et al.*, 2010, Holpuch *et al.*, 2010, Lin *et al.*, 2010, Vranic *et al.*, 2013a, Yu & et al., 2011). These properties have been exploited, as nanoparticles themselves have been developed as permeation enhancers to facilitate the uptake of larger compounds across different membranes in the body (Card *et al.*, 2008, Gaumet *et al.*, 2008, Kipp, 2004, Rahimnejad *et al.*, 2006, Sarin *et al.*, 2008, Sun *et al.*, 2008a).

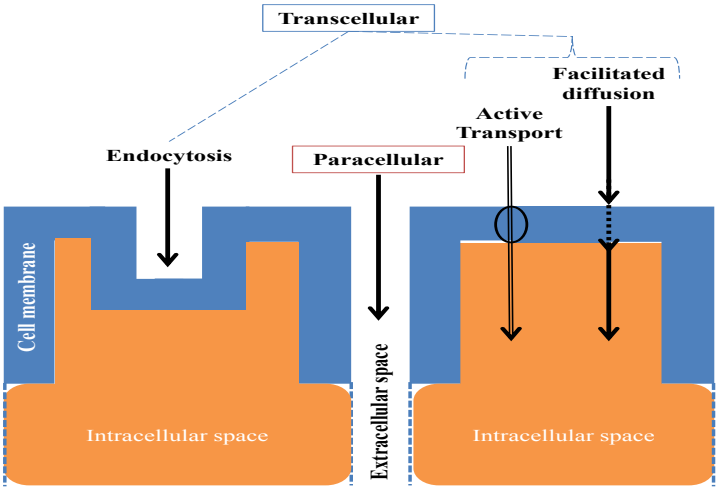

Figure 1.6. The main transport pathways associated with nanoparticle internalisation through cell layers and membranes in the human body. *Adapted from (Forth et al., 1987).*

Particle size remains the most obvious nano-characteristic that embodies disparity between a nanomaterial and its bulk comparator. Nano-size affords nanomaterials with routes through tissues and entry into cells unavailable to other larger, particles. In addition, characteristics attributed to the nano-scale include high surface area and reactivity, and in the case of ZnO, rod-like shapes; all properties that facilitate an increased risk of uptake (Barillet *et al.*, 2010, Elder *et al.*, 2009, Hsiao & Huang, 2011). Nanomaterial characteristics are thought to afford numerous transport routes into the body, both through tissues (paracellular transport), and across cell membranes into the cytoplasm (transcellular) (Campisi *et al.*, 2010). Many transport mechanisms exist in the body and nearly all of these may be exploited by nanomaterials that match or mimic the specific properties designated for native molecules under normal transport conditions (Cho *et al.*, 2010, Gupta *et al.*, 2004, Soenen *et al.*, 2009). Unregulated uptake remains a

primarily safety concern in the risk of nanomaterial exposure, to many areas in the body (Oberdorster *et al.*, 2005a).

It has been suggested that some nanoparticles may be able to bypass the protective inflammatory mechanisms of the body, if they are small enough to be transported into individual cells, by being mistaken as normal molecular components *e.g.* lipid vesicles (Penn *et al.*, 2005). The properties available to nanomaterials that contribute to their ease of absorption, penetration, circulation and distribution in biosystems are a direct consequence of their unique nano-characteristics (Borm *et al.*, 2006, Buzea *et al.*, 2007, Nel *et al.*, 2006). As discussed during monolayer cytotoxicity, this often manifests through their greater surface reactivity and ability to generate ROS that contribute to an environment of high oxidative stress on the cells. This mechanism of cytotoxicity can result from interactions at the cell surface, or more severely following internalisation (Asati *et al.*, 2010, Barillet *et al.*, 2010, Berg *et al.*, 2010, Huang *et al.*, 2010b, Limbach *et al.*, 2007, Maurer-Jones *et al.*, 2010, Sharma *et al.*, 2011, Xia *et al.*, 2006, Xia *et al.*, 2007).

In a similar way to the transport pathway exploited by nanoparticles gaining entry into the cell, size and charge are both linked to their localisation once inside the cell, and consequently their cytotoxic potential, dependent upon interactions with different cellular machinery (Buzea *et al.*, 2007). Intracellular nanoparticles have been determined as a cause of cytotoxicity through interactions with various components of the cell, including actin cytoskeleton architecture and subsequent inhibition of focal adhesion complexes (Soenen *et al.*, 2009); lipid membrane disruption (Leroueil *et al.*, 2008, Lin *et al.*, 2010, Verma & Stellacci, 2010), mitochondria (Hussain *et al.*, 2005, Jeng & Swanson, 2006, Liu & Sun, 2010, Moos *et al.*, 2010) and even within the nucleus, causing genotoxicity through interaction with DNA (Bhattacharya *et al.*, 2009, Hackenberg *et al.*, 2011b, Papageorgiou *et al.*, 2007, Patlolla *et al.*, 2010, Prasad *et al.*, 2013b, Sharma *et al.*, 2011, Shukla *et al.*, 2011). In exceptional cases, both the mitochondria and nucleus have been observed to partake in nanoparticle uptake (AshaRani *et al.*, 2008, Faunce *et al.*, 2008, Hackenberg *et al.*, 2011a, Johnston *et al.*, 2010b, Mao *et al.*, 2010), including hydroxyapatite into the nucleus (Motskin *et al.*, 2009). The type of nanoparticles that preferentially localise to mitochondria proceed to disrupt the electron transport chain, resulting in excess O_2 production and further oxidative stress placed on the cell (AshaRani *et al.*, 2008, Jaeger *et al.*, 2012, Moos *et al.*, 2010, Oberdorster *et al.*, 2005b, Xia *et al.*, 2007). This scenario causes major structural damage by perturbing mitochondrial

transition pores, which leads to an increase in severity of the cytotoxic state, and often results in the release of pro-apoptotic factors responsible for programmed cell death (Nel *et al.*, 2006, Oberdorster *et al.*, 2005b), as shown in Figure 1.3. Therefore, elucidating the uptake pathways available to nanomaterials that exhibit specific characteristics linked to increased internalisation remains key in determining their risk to human health.

1.2.7 Endocytosis

Endocytosis is an umbrella term for a variety of mechanisms that internalise substances into vesicles during transcellular uptake, by which cells absorb exogenous molecules by engulfing them within their cell membrane. It is a constitutive process of most eukaryotic cells (Innes & Ogden, 1999), and for this reason, is thought a likely mechanism of unregulated nanoparticle internalisation. The process is divided into three main types: phagocytosis, pinocytosis and receptor-mediated, as shown in Figure 1.7. Each specific mechanism is carried out with differing degrees of application between cell types.

Phagocytosis is only carried out by certain cells, such as macrophages, that are able to engulf larger particles as part of an immune response to pathogens, bacteria and in removal of cell debris in a process called efferocytosis (Kodali *et al.*, 2013). These cell types are present in healthy oral mucosal cells, increasing in number in response to inflammatory stimuli (Merry *et al.*, 2012). Phagocytosis is a ligand-induced process triggered only through the homologous binding between the phagocyte surface receptors and corresponding particles (Watts & Marsh, 1992). Although not constrained to the nano-size, this selective binding adds specificity to this method which has been reported to experience impairment through phagocytosis of cytotoxic nanomaterials (Lundborg *et al.*, 2006), including zinc (Schlesinger *et al.*, 1993, Wilson *et al.*, 2007).

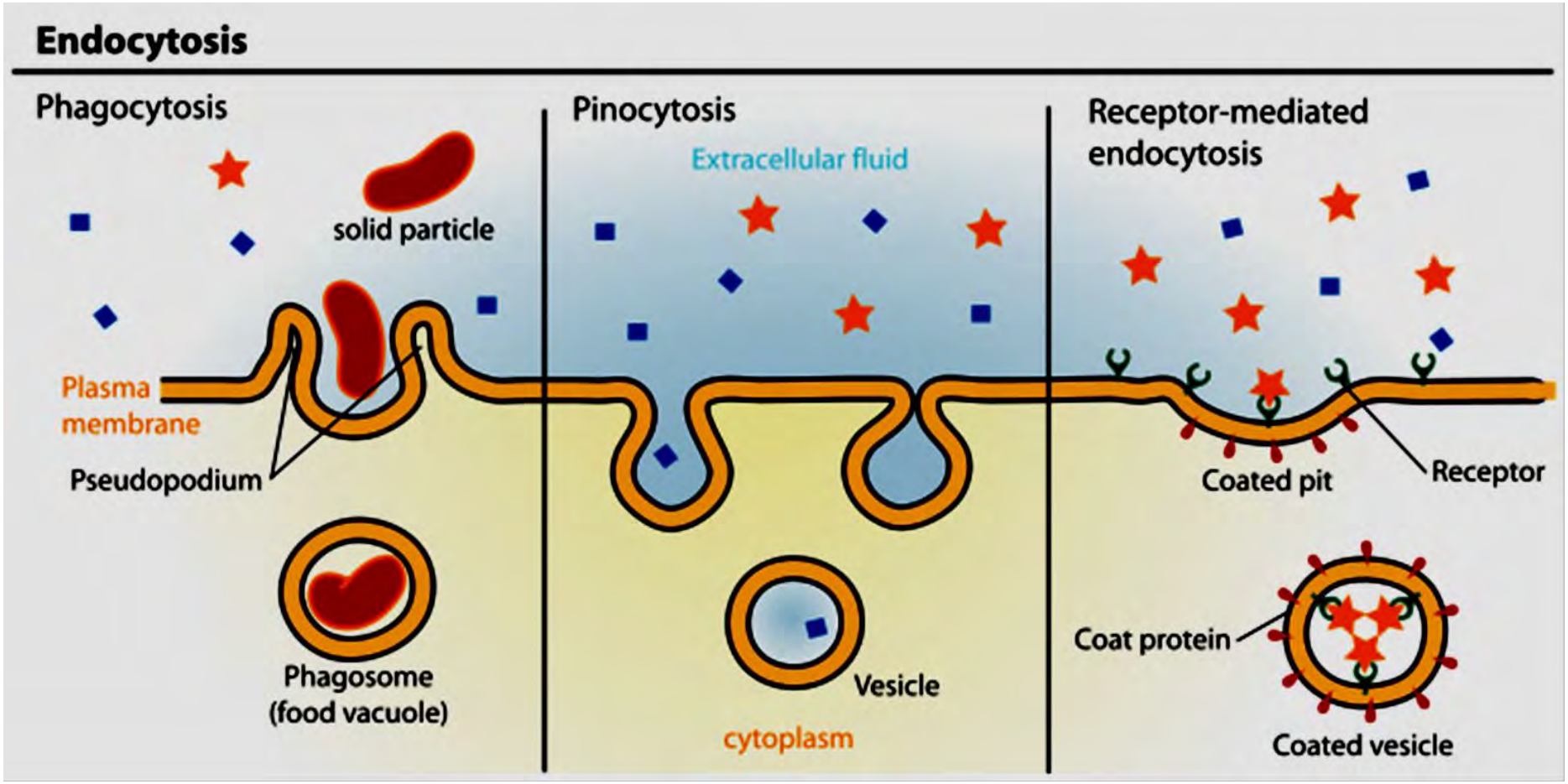

Figure 1.7. The main types of endocytosis. *Taken from Mariana Ruiz Villarreal (free of copyright), 2007.*

Pinocytosis and receptor-mediated endocytosis were considered the most likely uptake mechanisms within this study, being available for nanoparticle transcellular transport in nearly all cells (Treuel *et al.*, 2013). Both processes share a similar enodcytotic process for engulfing fluids and small materials (with discrepancies in size reported between 0.5-10μm) found in the extracellular environment: a process known as membrane invagination. This involves the inwards folding of the plasma membrane, trapping internalised material in pits that bud off, forming vesicles. These can then be transported through the cytoplasm for subsequent hydrolysis, and as such, offers a cellular pathway of transport into cells and across tissues (Okamoto, 1998). By far the most common receptor-mediated enodcytotic transport system available in eukaryotic cells is the clathrin dependent pathway. As such, a relatively well-established characterisation of the mechanistic details of the process exists. Other receptor-mediated transport systems are often referred to as clathrin-independent, and include flotillin-dependent, caveolar type and CLIC/GEEC[1]-type endocytosis (Doherty & McMahon, 2009). Studies elucidating these clathrin-independent endocytotic pathways remain limited in comparison to clathrin-mediated endocytosis, especially in relation to epithelial cells. In addition, it has been suggested that the best studied of the clathrin-independent pathways (caveolar-type endocytosis) may be restricted to 80nm in size of the invagination that can form (Iversen *et al.*, 2011). This threshold would likely act as size exclusion to agglomerates expected to form during the nanomaterial interactions within biological systems. Figure 1.8 describes the mechanism followed during clathrin-mediated endocytosis. It depicts the main processes involved in uptake of a molecule following recognition to the clathrin receptor at the membrane surface, and the cascade of intercellular signalling this sets in motion to form clathrin pits. This is a complex process involving a number of different receptors, proteins and lipids, and for further information, the reader is directed towards an excellent review of the process by Doherty & McMahon, 2009 (Doherty & McMahon, 2009). Whilst the diagram demonstrates the invagination process for capturing exogenous material, the notable barrier to entry for nanomaterials involves initial interaction with a receptor protein present at the cell surface. Transmembrane receptor proteins punctuate the cell membrane at numerous sites. They exist in numerous forms and chemistries to cater for the wide array of binding to different molecules required by the cell under different

[1] CLIC, clathrin-independent carrier; GEEC, GPI-AP (glycosyl-phosphatidylinositol-anchored proteins) enriched early endosomal compartment

conditions. They sense molecules in the extracellular environment and activate signal transaction pathways that govern receptor-mediated endocytosis upon binding. The specificity of binding reduces the probability of it as a viable uptake mechanism for uncoated, inorganic nanomaterials. However, unregulated protein coatings adhered to the surface of nanoparticles would likely lead to receptor recognition and incidental internalisation (Nel *et al.*, 2009).

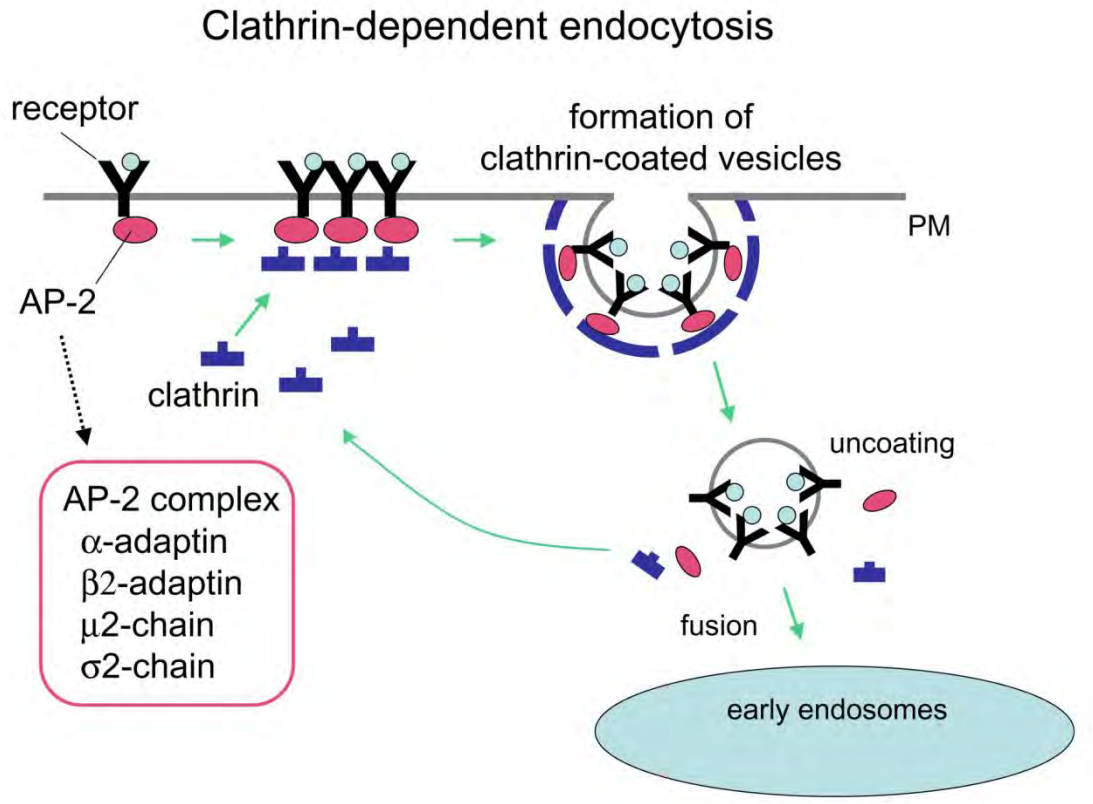

Figure 1.8. Outline of the main events in receptor-mediated endocytosis. The clathrin triskelia assemble into a polygonal lattice at the plasma membrane to form coated pits that bud and pinch off from the membrane in a dynamin-dependent manner and give rise to clathrin-coated vesicles. Clathrin-binding adaptors, such as adaptor protein-2 (AP2), bind to clathrin directly to initiate this process, and they also bind to cargo proteins and thereby mediate their endocytosis. In addition, phospholipids, such as phosphatidylinositol-4,5-bisphosphate, are also found in coated pits and they facilitate vesicle formation and budding by binding to clathrin adaptors such as epsins. Clathrin-coated vesicles are uncoated after endocytosis and then fuse with the early endosome. *Figure taken from* (Grant & Donaldson, 2009).

Pinocytosis differs from receptor-mediated endocytosis only through the lack of selectivity of substances it transports into the cell. It is commonly known as *cell drinking*, or fluid endocytosis, due to the engulfing action predominantly capturing surrounding fluids; however, this process also traps small particles and solutes contained within the extracellular environment. The non-specific nature of this uptake mechanism makes it a highly probable route for nanomaterial entry into the cell, based on their nano-size conferring the ability to fit inside the invagination of even micropinosomes less than 100nm in diameter (Buono *et al.*, 2009). Gold (Lund *et al.*, 2011, Shukla *et al.*, 2005); quantum dots (Ryman-Rasmussen *et al.*, 2007) and hydroxyapatite (Cai *et al.*, 2007) nanoparticles have all been demonstrated as passing through different cell membranes using incidental pinocytosis because of their small size. However, recent studies have also demonstrated the important influence of surface chemistries, in governing uptake through the indiscriminate pinocytotic pathway (Saha *et al.*, 2013).

1.2.8 Carrier mediated transport

Whilst nano-size does confer potential for incidental uptake via endocytosis, it is doubtful whether the mechanism could account for complete transit to systemic penetration. This is because the transcellular route, involves having to pass through a number of different membranes in stratified epithelial tissue structures; such as the nature of the oral mucosa architecture (Sudhakar *et al.*, 2006). Therefore, nanomaterial transport through tissue structures has often been linked to energy expenditure, with endocytosis mechanisms commonly observed alongside carrier mediated transport (Campisi *et al.*, 2010).

The two common forms of carrier mediated transport include active transport and facilitated diffusion (Puckett *et al.*, 2010). Active transport works against a concentration gradient, and therefore requires chemical energy (usually in the form of ATP) whereas facilitated diffusion involves the movement of a molecule through a membrane in the absence of energy. Both may use a transporter protein to move the molecule along a concentration gradient. In each case, both mechanisms rely on specific interactions between the molecules to be transported being recognised by a transmembrane integral protein. This acts as the 'gate' and under specific conditions, such as a localised increase in concentration either from within the cell or outside the extracellular environment; or through the presence of certain stimuli, these proteins then act as mediators to carry or force molecules through a channel in the membrane, it

could not otherwise pass. Examples of nanoparticle uptake via facilitated diffusion remain limited to those within the very small range of the nanoscale, such as quantum dots and engineered carbon nanostructures (Buzea *et al.*, 2007, Dobson & Kell, 2008, Sugano *et al.*, 2010, Wang *et al.*, 2012b). These are thought able to penetrate cell membranes through ion channels or polar pores that open in response to other (non-size related) characteristics of the nanomaterial.

Carrier mediated transport mechanisms are available for macromolecules far exceeding the size defined as the nano-range, to become internalised in the cell. Glucose, amino acids, sodium and potassium ions are just a few examples of very small molecules (≤1nm) frequently utilising active transport as a means for crossing the cell membrane. This mechanism has been relatively well established in studies involving oral drug delivery, modelled by Caco-2 cell *in vitro* (Grandvuinet *et al.*, 2013, Grès *et al.*, 1998, Hubatsch *et al.*, 2007, Neuhoff *et al.*, 2005). When size is not the principle property governing uptake, other physiochemical factors must take precedent. It was already discussed how charge and surface properties play a major role in nanomaterial interactions at the cell membrane. These properties are being explored with regard to surface coatings applied or formed in nanoparticles, used as penetration enhancers for larger molecules (Gaumet *et al.*, 2008, Holpuch *et al.*, 2010, Kipp, 2004, Kreuter *et al.*, 2003, Lockman *et al.*, 2002, Veerapandian *et al.*, 2009, Yin Win & Feng, 2005). For example, polymeric surface coatings have been designed and applied to allow higher doses of less toxic, targeted drug delivery, via specific cell receptors, such as those used to cross the blood brain barrier (Agarwal *et al.*, 2009) and intestinal mucosa (Yun *et al.*, 2012).

1.2.9 Paracellular transport routes

Paracellular, or intercellular transport, involves the transfer of a substance through the intercellular lipid based barrier between the cells of an epithelium. Since the paracellular spaces contribute less than 1% of the mucosal surface area, significant paracellular transport of macromolecules and particles is considered an unlikely event (Jung *et al.*, 2000), ions aside (Turner, 2009). Yet it is important for consideration of cytotoxicity to note that this can occur over time, through repeated dosage ((SCENIHR), 2009). The small size of nanomaterials can be thought to increase their chances of penetration, albeit only in combination with favourable surface charge modifications (Kreuter, 2012). Permeability is also dependent upon exposure to the different regions of the

body, with different epithelial tissue linings containg different anatomy (dependent upon required function). Common to all epithelia are the presence of cell junctions that form structural connections between the neighbouring cells of a tissue. These are protein complexes that anchor cells in position within the extracellular space, thus providing the different barrier qualities for paracellular transport in different parts of the body (Van Itallie & Anderson, 2006). Five main types are found in human tissues: tight junctions, adheren junctions, desmosomes, hemidesmosomes, and gap junctions (Yan *et al.*, 2009). With respect to the oral mucosa, two tissue varieties are present within the lining epithelium, and each forms different cell junctions types, dependent upon the keratinisation differentiation process followed by prevalence of apical migratory cells (Wertz & Squier, 1991) (discussed within the next section).

Keratinised tissues, such as the *gingiva* and hard palate are routinely exposed to the high shearing forces during mastication (Squier & Kremer, 2001). Consequently, the tissue structure is required to be firm and rigid. Anchoring cells in such tightly packed, squamous stratified structures is attained by desmosome complexes, the structure of which is depicted in Figure 1.9. Desmosomes are multi-molecular complexes composed of transmembrane glycoproteins and cytosolic plaque proteins connected to the keratin cytoskeleton. These anchoring junctions are essential in maintaining keratinocyte cohesion and integrity, as well as the epidermal architecture and functions, and so represent the main adhesive structures expressed by keratinocytes (Sandjeu & Haftek, 2009). The transmembrane desmosomal cadherins of neighbouring cells interact in the extracellular space to provide further adhesion. This extracellular central region, comprising the space between the two plasma membranes, is termed the desmoglea, and is 30 nm-thick (Cozzani *et al.*, 2000).

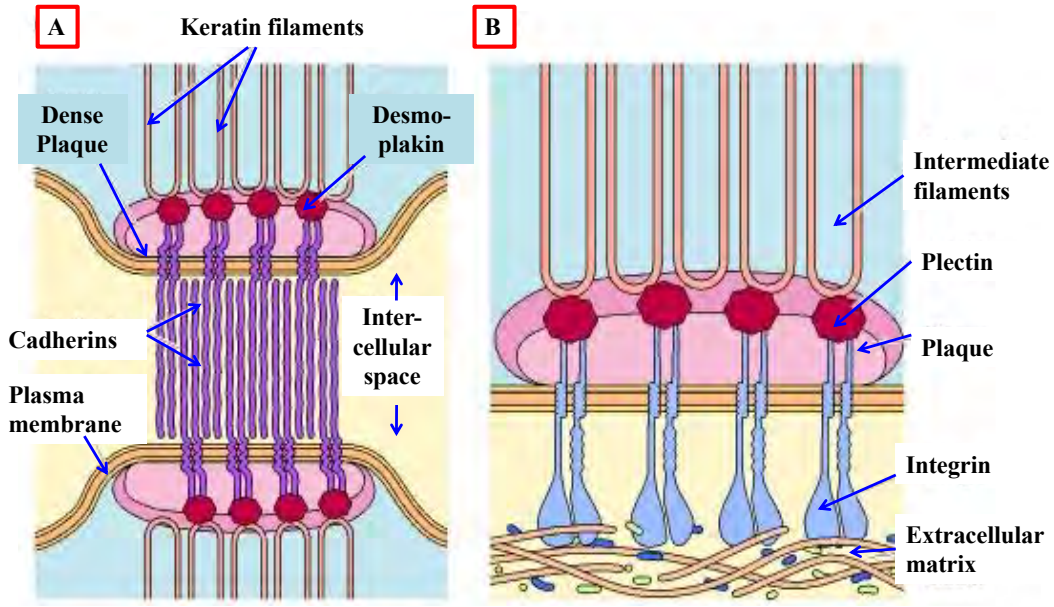

Figure 1.9. A diagram showing the tight cell to cell adhesion in keratinised epithelium. (**A**) Schematic of a desmosome. Intermediate filaments are anchored to sites of cell-cell adhesion by desmoplaskin. (**B**) Schematic of a hemidesmosome. Intermediate filaments are anchored to an integrin by plectin. *Adapted from (Cooper, 2000).*

On the cytoplasmic sides of each junction, the C-terminal regions of cadherins are rooted in the desmosomal plaques composed of proteins, such as desmoplakins and plectin. Plaque proteins bind, in turn, to the intermediate keratin filaments (Garrod & Chidgey, 2008). In this way numerous desmosomes associate with an individual cells' cytoskeleton, to form a mechanically resistant trans-epithelial structure. The 30nm desmoglea restricts the passage for very small molecules, even on the nano-scale. However, the paracellular pathway has been exploited for the permeation of hydrophilic molecules that are not able to permeate through the lipid membrane using transcellular uptake mechanisms (van der Lubben *et al.*, 2001). Absorption remains difficult to control, however; and paracellular transport has been mainly limited to chitosan and polymer surface coatings. These have proved to be useful when engineered as nanoparticle penetration enhancers, exploiting the net negative charge of tight junctions to increase the absorption through mucosal epithelial layers (van der Lubben *et al.*, 2001).

The application of nanomaterial penetration enhancers has led to non-keratinised epithelial layers of the buccal mucosa being identified as more permeable structures, better suited for paracellular drug delivery (Campisi *et al.*, 2010, Nicolazzo *et al.*, 2003,

Rossi *et al.*, 2005, Sudhakar *et al.*, 2006). The *buccal* and sub-lingual regions of the oral mucosa are involved in processes that require greater flexibility for the associated tissue, such as swallowing and speech (Squier & Kremer, 2001). Cells are held together less rigidly by tight-junctions that are lower in number than the desmosome complexes of keratinised tissue (Wertz *et al.*, 1993). Figure 1.10 shows the typical structure of a non-keratinised epithelia surface cell adhesion complex. These have been well studied with regard to the oral administration of drugs that come into contact with the intestinal epithelial lining (Ward *et al.*, 2000). Evidence in the literature suggests that most compounds penetrate the buccal mucosa tissues via the paracellular route, as it fits more closely with the mechanisms of true passive diffusion: by requiring no external energy (Campisi *et al.*, 2010). Substances are able to move more freely through the less dense, liquid-like intercellular spaces around cells, avoiding the resistance offered up by the lipid molecules present as the major barrier function through epithelia cell membranes (Hoogstraate & Wertz, 1998, Nicolazzo *et al.*, 2005), as discussed in greater detail below (1.3.1). However, with reference to this study, even the (nano) size of nanomaterials may prove secondary to the influences of surface properties, such as charge (des Rieux *et al.*, 2006). This is demonstrated by the majority of paracellular nanoparticle penetration enhancers being either coated or produced using polymeric materials that modulate their physicochemical characteristics *e.g.* hydrophobicity, zeta potential *etc.* (Jung *et al.*, 2000).

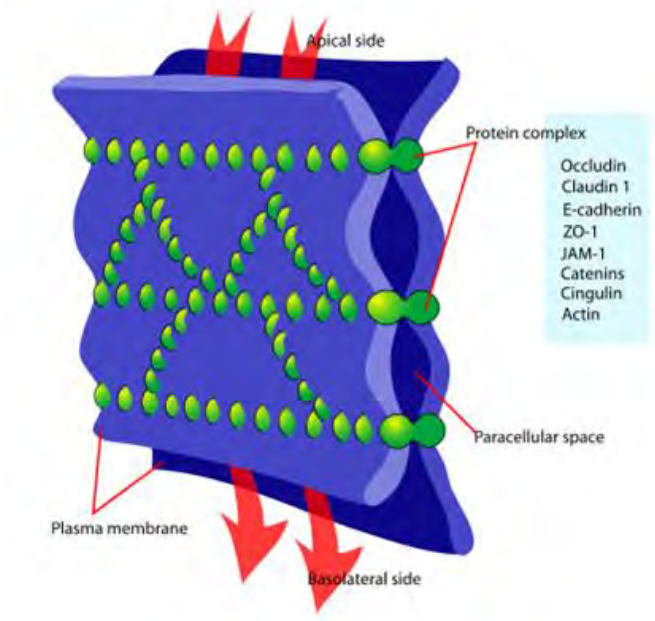

Figure 1.10. A schematic to show a to non-keratinised epithelial cell tight junction, at the apical surface of stratified tissue structures. *Taken from Mariana Ruiz, 2006.*

1.3 The human oral mucosa

As previously touched upon, certain key characteristics govern the properties of a nanomaterial, but only with respect to interactions within the particular environment in which they are located. Different environments can cause disparity into the types, rates and extent of nano-specific properties reported. With the project aiming to investigate nanoparticle reactions within the human oral mucosa, it is pertinent to introduce in more detail, the different tissues present at this site of the body.

The human oral cavity is comprised of multiple, complex structures and varied cellular materials, all with specific functions, situated in close proximity together in the mouth. One common feature is the mucosal surface epithelial lining that coats the entire oral cavity, totalling approximately 100cm^2 surface area of tissue (Rossi *et al.*, 2005). The oral mucosa starts at the opening of the mouth (the orifice) and comprosises the vermillion border (where the external skin at the face meets with the inside of the lips (*labial mucosa*)), the entire vestibule *i.e.* the lining of the cheeks (*buccal mucosa*) and gums (*gingiva*) coating the alveolar arch and joining to the teeth via the epithelial tissue of the mucogingivial junctional. The oral mucosa continues all the way through to the back of the mouth and down the oesophagus. Here it differentiates into the oesophageal mucosa, then again further down into the gastric mucosa of the digestive system and epithelial mucosa of the lungs. The remaining part of the mouth: oral cavity proper (*cavis oris proprium*), also contours the oral mucous membrane enclosed laterally and in front by the alveolar arches, roofed by the hard and soft palate, and continuing along underneath on the floor of the mouth and also onto the surface of the tongue (*lingua*) (Stranding, 2008).

The oral mucosa is a specialised lining that displays a high level of differentiation with respect to function morphology of the tissue type. Each tissue has developed to become responsible for the functional demands of the location, within the oral cavity, and can be classified into three main types:

(i) Keratinised masticatory mucosa of the *gingiva* and hard palate.
(ii) Non-keratinised lining, or *buccal* mucosa, of the cheek, lips, floor of mouth and ventral surface of the tongue.
(iii) Specialised or mixed mucosa (partially keratinised and non-keratinised) of the dorsum of the tongue and vermilion border of the lip (Dale *et al.*, 1990).

All three oral mucosal linings have evolved to protect the underlying tissue; including, principally for the oral mucosa against mechanical damage associated with mastication, as well as penetration of the epithelia of exogeneous noxious or therapeutic substances (Dale *et al.*, 1990). These may include potentially harmful environmental agents, such as; microbial toxins, enzymes, antigens and carcinogens from foods and beverages ((Squier & Kremer, 2001). The differences in how they give protection manifests most obviously in the considerable variation of thickness, histology and differentiation of each oral mucosae epithelia cell type and their respective, underlying connective tissue layers.

The term 'keratinocyte' describes the cell categories that constitute the differentiated stratified epithelium of the outer layer of human skin (or epidermis), and oral mucosal tissues. Keratinocytes form the four layers that make up two distinct epithelial structures, as illustrated in Figure 1.11. These include cells of the basal, spinous, granular and superficial layers. Proliferation occurs in the deepest layer of epithelium, the basal cells that rest above the basement membrane. These elongated cuboid (columnar) looking cells are bound with a plasma membrane and possess a full complement of normal intracellular organelles, making them capable of mitotic division. In this layer also reside the progenitor cells, separated into two distinct sub-populations (Squier & Kremer, 2001). A small portion follow a very slow cell growth cycle and are considered stem cells that function to produce basal cells, sustaining the layer; albeit only for a limited/finite number of divisions (unlike "true" embryonic stem cells that can replicate infinitely (Hume, 1985, Watt, 1998)). The second, more abundant population are known as amplifier cells. These enter into mitosis to increase the amount of cells ready for maturation, differentiating as they migrate up through the other epidermal layers to replenish the surface epithelial cells. Switching between proliferation and differentiation of the basal epithelial layer, *in vivo*, is mediated by peptide growth factors (collectively known as cytokines), extracellular calcium (Sacks *et al.*, 1985), phorbol esters (Dale *et al.*, 1990), retinoic acid (Presland & Dale, 2000) and vitamin D (Dale *et al.*, 1990), amongst other substances. The condition of the membrane *e.g.* age or health also play an important role, as well as the interaction between keratinocytes and the supportive connective tissue. The combination of all these changes is reflected in the composition of intracellular proteins, termed cytokeratins that can be of use in research to measure and observe differentiation rates (Squier & Kremer, 2001).

For the keratinocytes of the oral mucosa, amplifier cells initially pass into the polyhedral shaped prickle layer (or stratum spinosum); which is the maturation compartment where keratin protein production and the differentiation pattern begin (Alberts, 2002). They proceed to migrate up into the two apical layers is pre-determined by the programmed differentiation course. The outcome of a number of complex precursors and biochemical mechanisms leads to the formation of the outer layer of the oral mucosa, being either keratinised or non-keratinised. These processes are widely referred to as keratinisation.

1.3.1 Keratinisation

Keratinisation is the name given to the mechanism of protein expression for the production of keratin, found in stratified squamous epithelium. It describes the various morphological and biochemical changes that occur to the progenitor amplifier cells as they migrate up through the suprabasal layers, towards the apical surface. Epithelial cells of the mucosa (like all epithelial cells) contain keratin intermediate filaments as the major component of the cytoskeleton (constituting as much as 85% of the total cellular protein present (Presland & Dale, 2000)). These filaments help to maintain both the shape of the cell, and inter-cell tissue relationship via the cell junction connections (discussed previously), as well as anchoring organelles in the cytoplasm.

Keratin is a fibrous structural protein, coming from a multi-gene family of approximately 30 proteins with differing molecular weights. All keratins share a common structure of: a central alpha-helical portion, approximately 310 amino acids long (Presland & Dale, 2000) flanked by non-helical branched amino-carboxyl termini (Dale *et al.*, 1990), as a coiled coil dimer. They differ depending on the amino-acid sequence lending to a charge. As Table 1.1 shows, keratins found in oral epithelium, are divided into one of two further keratin sub-families: the acidic Type I (keratin numbers 9 to 20) and the relatively basic or neutral Type II (comprised of keratins 1 to 8). The fibrous intermediate filament constructing the cytoskeleton in epithelial cells is formed by the fusion of two of each type, into a four chain heteropolymer.

The keratinisation process that follows, dictates the morphology of the apical cells of the tissue. Differences in the keratin proteins expressed, result in the markedly different permeability of substances between keratinised and non-keratinised tissue regions, brought about by cell structures present, tissue thickness and tissue structure. However, the permeability of the intercellular lipid barrier is thought to constitute the greatest

restrictive force to paracellular transport (Senel & Hincal, 2001, Sudhakar *et al.*, 2006), a consequence of the disparity in lipid content expelled by membrane coating granules in the upper third of epithelium. Proof that these intercellular lipids constitute the main barrier has been demonstrated in various studies that result in a freely permeable tissue upon their extraction (Hoogstraate & Wertz, 1998). The degree of permeability is least in keratinised gingiva followed by the buccal mucosa with the most easily permeated area of the oral mucosa being the sublingual mucosa (Squier & Hall, 1985).

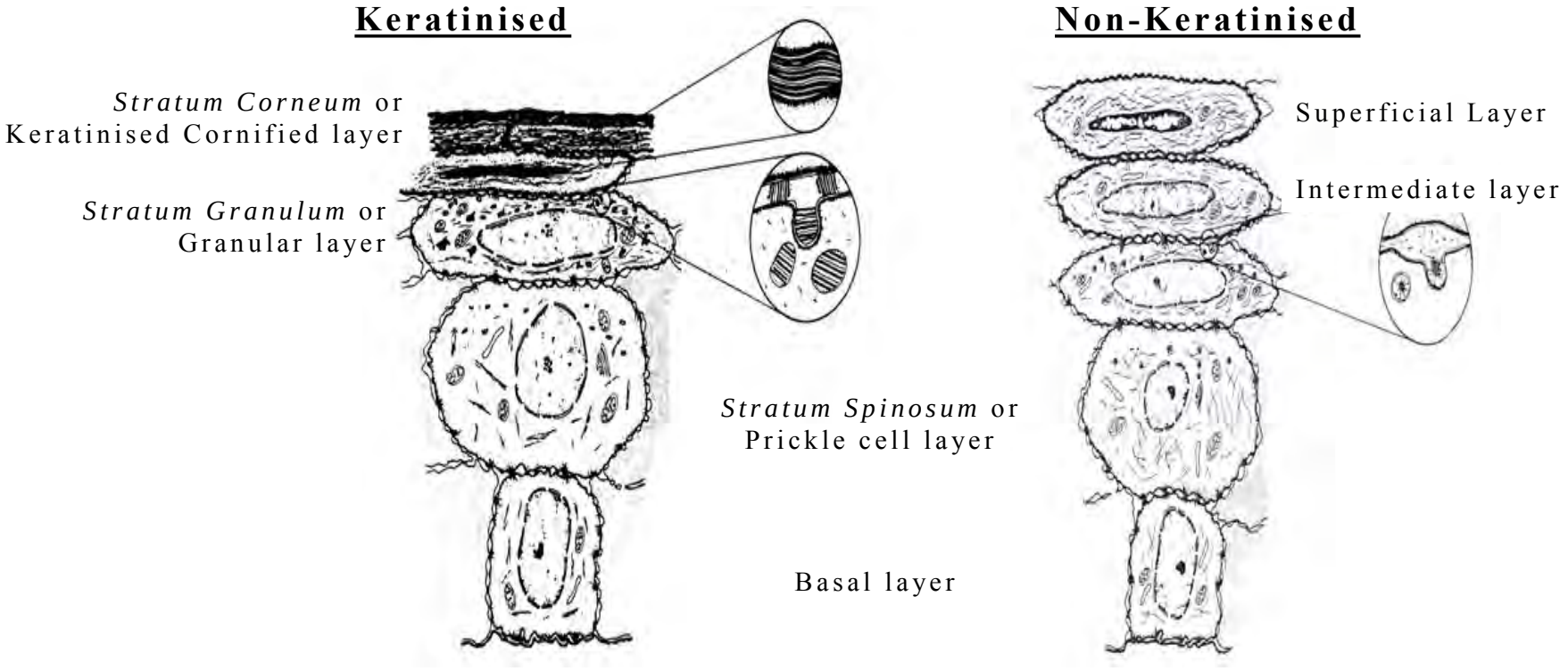

Figure 1.11. A diagram showing the epithelial tissues of the oral mucosa, with its four epidermal layers. *Adapted from (Wertz & Squier, 1991).*

Table 1.1. A table to demonstrate the details of key keratinised proteins found in oral epithelial keratinocytes. *Compiled from data within (Dale et al., 1990).*

Keratin protein classification number	Molecular weight (kDa)	Keratin Type	Differentiation pattern
K 1	65	Type I - BASIC	Keratinised
K 4	59	Type I	Non-keratinised
K 5	58	Type I	Both
K 10	56.5	Type II - ACIDIC	Keratinised
K 13	52	Type II	Non-keratinised
K 14	50	Type II	Both
K 19	40	Type II	Non-keratinised

1.3.1.1 Keratinised tissue

Keratinised tissues of the oral mucosa are naturally thinner tissues (than non-keratinised), located in regions that are routinely subjected to the highest degree of abrasion (Shojaei, 1998, Squier & Kremer, 2001). To maintain tissue integrity, they constantly renew the tough apical cell populations (Squier & Kremer, 2001, Walker *et al.*, 1973, Wertz & Squier, 1991). The robust cell morphology is most obviously manifested in the development of the cornified envelope at the *stratum corneum* of keratinised epithelium (Figure 1.11). As the mature basal cells enter into differentiation in the prickle cell layer, the keratin protein expression and subsequent intracellular matrix modifies. The cells become larger and start to flatten as the larger keratin filaments accumulate into dense, fibrous bundles that pack the cytoplasm. This leads to the complete degradation of normal organelles in orthakeratinised cells of the hard palate, including the nucleus along with all the genetic material (Winning & Townsend, 2000).

Approaching the granular layer, small intermediate filament-associated proteins are produced, as precursors for a cornified envelope. These include important differentiation markers, such as involucrin, profilaggrin and loricin. Involucrin is a soluble proten precursor that becomes cross-linked to membrane proteins on the inner plasma membrane of the cornified envelope upon transglutaminase metabolism. Profilaggrin is the precursor to filaggrin (after phosphorylation of various protein kinases) that aids in the packing of keratin at the cornified envelope. Loricin is a highly insoluble, glycine and cysteine rich protein that accounts for 75% of the overall protein total in the cornified envelope (Presland & Jurevic, 2002). From the granular layer, these are deposited to the inner aspect of the plasma membrane, forming a relatively thick (approximately 15nm) band of protein that cross links with the keratin filaments inside the cell (Squier & Kremer, 2001). The formation of the cornified layer in 'dead' apoptic cells at the apical surfaces reduces the chances of substances traversing the membrane using transcellular pathways.

Paracellular transport is also reduced in keratinised tissues, due to the greater number, of larger and rougher membrane coating granules (MCG). At the boundary between the granular and cornified layers, these migrate towards the apical aspect of the keratinocytes where they fuse with the plasma membrane. The lipid lamelle cargo is expelled, via exocytosis, into the extracellular spaces around desmosome complexes (up

to 50% of their intercellular space may be desmosomes, required to fix the cells to a rigid, stratified tissue structure (Garrod & Chidgey, 2008)). The lipid composition of the MCG present in keratinised tissue accounts for the increased resistance, especially to hydrophilic materials.

The major lipid constituents have been determined as neutral lipids, with the most abundant types including ceramides, cholesterol and saturated fatty acids (Gandhi & Robinson, 1994). In the epidermis of the skin, all phospholipids get catabolised resulting in the preferred synthesis of sphingolipids to produce the hydrophobic ceramide derivatives (Wertz *et al.*, 1993). Ceramides in particular are associated with lipid barrier function (Gunstone, 1996), with a high ceramide content inversely correlated to water permeability in the tissue (Campisi *et al.*, 2010). Keratinised oral mucosal tissue has lesser amounts of these lipids than skin; and in non-keratinised tissue, sphingolipid content is almost negligible (Wertz *et al.*, 1993).

Characterisation of lipid content also revealed MCG cargo expulsion alongside a number of hydrolytic enzymes. Those identified included, acid-phosphatase, carboxy-peptidase, acid lipase, sphingomyelinase and phospholipase (Gandhi & Robinson, 1994). These have been implicated in the partial breakdown, or deglycosylation, of glycolipids upon expulsion. Deglycosylation is thought to allow stronger interactions between the different lipids, producing larger lamellae ('blocking' molecules) that result in the strong gel like structure accredited with being more able to restrict the transport of exogenous material between cells (Campisi *et al.*, 2010, Shojaei, 1998). Lamallae have been observed to be packed more solidly in skin, which reduces penetration by hydrophilic substances to a greater extent over keratinised oral mucosal tissue, which has more liquid-like non-keratinised lamellae (Nicolazzo *et al.*, 2005).

1.3.1.2 Non-keratinised tissue

The buccal, or lining mucosa, provides the principal example of non-keratinised differentiation. This is something of a contradicting statement due to tissue areas it encompasses (the lining of the cheeks, floor of the mouth, underside of the tongue and soft palate) sharing a common basal layer with keratinised epithelium. The basal cells of all epithelia express keratin 5 and 14, and so even the buccal mucosal cells are considered keratinocytes (Sun *et al.*, 1985).

The principal differentiation pattern for non-keratinised epithelium manifests morphological changes in the prickle cells that express different keratin proteins with distinctly smaller molecular weights (see Table 1.1); perhaps due to the extra presence of keratin 19 in the preceding basal layer. (Dale *et al.*, 1990) But the biochemical pathway still programmes a mechanism for the cells to flatten with an accumulation of keratin filaments in the intermediate layer of cells, and a subsequent thickening of the plasma membrane as they migrate towards the superficial layer. Notable, however, is the continued presence of organelles and a complete nucleus in non-keratinised superficial cells, making the pattern of differentiation less evident with the change in morphology. The described events result in the formation of a stratified squamous epithelium (Winning & Townsend, 2000), albeit distinguished as non-keratinised due to the discrete mechanism of differentiation.

The exposed superficial layer of non-keratinised epithelium does not rely on a tough, dead coating to protect it. It has a thickened plasma membrane, due to loricin and involucrin cross linking to the loose bundles of keratin built up in the flattened squamous cells. Without the expression of filaggrin it cannot facilitate the dense packing of a proteinaceous cornified envelope (Dale *et al.*, 1990). To protect against the shearing forces involved in the oral cavity environment, the epithelium of the buccal mucosa has developed as a considerably thick tissue layer: measured as between 500 to 800μm thick and comprising between 40 to 50 cell layers in total (Rossi *et al.*, 2005, Shojaei, 1998). This allows a certain level of superficial damage to be endured, matching the durability the cornified envelope exhibits in keratinised epithelium.

To sustain the thick non-keratinised epithelium, the lamina propria and submucosa contain numerous blood vessels connecting back to the maxillary artery. This allows for a fast (2.4mL/min/cm^2), rich, nourishing supply of blood, containing all the constituents to maintain the tissue (Sudhakar *et al.*, 2006), as well as enabling efficient removal of cell metabolic waste products (Wertz *et al.*, 1993). At this premium level of support, the epithelial cell layers can proliferate successfully and rapidly to match the loss at the superficial layer; thus maintaining homeostasis. This view is supported by the faster turnover of whole epithelial layers in regions of non-keratinised differentiation, compared with keratinisation layers (Walker *et al.*, 1973). There is some discrepancy on exact values but the general consensus follows median calculations, that for healthy human adults, there is a 14 day turnover of non-keratinised tissue regions compared

with 24 days in the hard palate (Wertz *et al.*, 1993). Despite the discrepancies between the course of differentiation on tissue turnover time, it is generally accepted that the rate in the oral mucosa is much faster than on skin (Dover & Wright, 1991, Xia *et al.*, 1997). This leaves little doubt that tissue homeostasis plays a major role in the protection of the entire oral mucosa to the physicality of the environment in which it exists, for both types of keratinisation process *e.g.* mechanical and chemical insult (Wertz *et al.*, 1993).

The subtle changes observed in non-keratinisation maybe caused by a difference in keratin proteins expressed in the suprabasal layer (compared to keratinised cells), but it is thought that the underlying connective tissue retains an overall influence over differentiation (Presland & Dale, 2000). This can be appreciated by the differences of buccal connective tissue when compared with the skeletal, inflexible lamina propria of keratinised regions lacking a deep submucosa (Squier & Kremer, 2001). The adaptations in differentiation of the connective tissue may allow the non-keratinised epithelium to protect the tissue system in the absence of a tough cornified layer, whilst also being observed providing some resistance to lipophilic materials, due to high level of hydration (Kulkarni *et al.*, 2009).

Although the non-keratinised regions do not form a distinct *stratum granulosum* above the prickle cell layer, they do develop what is most commonly termed an intermediate layer. The cells here also develop MCGs, albeit smaller (0.2μm in diameter) and smoother than the keratinised cell equivalent (Squier, 1977). The MCGs are particularly important vessels involved in providing the main barrier to permeation for non-keratinised cells (Hoogstraate & Wertz, 1998) that lack the compact structure of the masticatory mucosa. The non-keratinised mucosa lipid barrier is predominantly produced from polar lipids: of phospholipids, cholesterol sulphate and monohexosylceramides. Crucially, they contain no acylceramides and only a small number of ceramides (Gandhi & Robinson, 1994, Wertz *et al.*, 1993). This is thought to be due to the very low content of hydrolytic enzymes present within non-keratinised extracellular space. This suggests non-keratinised regions lack the mechanism for converting the glycoceramide to ceramide (Squier *et al.*, 1991), and consequently, the lower number of lamellae present within the extracellular space are less efficient at packing into tight, solid structures. Lacking the solid blocking lamellae structures causes a more liquid-like lipid permeability barrier that, along with a reduced number of cell junctions, aids in the function of the more flexible tissue structure required for speech and swallowing. However, it has also caused

non-keratinised regions of the oral mucosa to be considered easier to exploit for the transport of drugs into systemic circulation (Campisi *et al.*, 2010, Hoogstraate & Wertz, 1998, Junginger *et al.*, 1999, Rossi *et al.*, 2005, Shojaei, 1998, Sudhakar *et al.*, 2006). Some of the advantages realised by the use of the buccal mucosa as a drug delivery site include (i) ease of accessibility to a relatively immobile surface (ii) rapid recovery time of the tissue, and (iii) an abundance of vascularisation with low immune activity (Hoogstraate & Wertz, 1998, Junginger *et al.*, 1999, Rossi *et al.*, 2005, Senel & Hincal, 2001, Sudhakar *et al.*, 2006). Consequently, the non-keratinised areas lining the oral cavity are thought more permeable for nanomaterial uptake, in comparison to keratinised tissues of the *gingiva* and hard *palate* (Wertz & Squier, 1991).

1.3.2 Physical barriers in the human oral mucosa

Despite researchers considering non-keratinised regions of the oral mucosa to be more permeable as a route for alternate drug transport, the application of drug delivery at this site has remained low. Common to all areas of the oral mucosa are the physical barrier properties that further protect the underlying tissue, to prevent exogenous and endogenous materials from entering the body. These include the flow of saliva and the formation of the salivary pellicle in conjunction with mucus layer (Lendenmann *et al.*, 2000).

Produced in lobules of cells, sites called parotids are found near the upper teeth, submandibular region under the tongue, and the sublingual area on the floor of the mouth. Saliva is a 70μm coating that flows over the epithelium (Collins & Dawes, 1987). Composed of 95% water (Silvers & Som, 1998), saliva constantly flows over the surface of the oral mucosa at 1.2mL/min, accounting for between 0.5 and 2.0 litres in total that can be produced under normal stimulation in one day (Mattes, 1997). Apart from water, saliva contains many other active components. These include: electrolytes, epidermal growth factors, mucus, proteins, various enzymes and other antimicrobial compounds. Consequently, both the physical washing effect and multiple constituent of saliva, provide complications for researchers looking to deliver drugs via the oral mucosa (Rossi *et al.*, 2005).

Substances looking to penetrate into the oral mucosa have to negotiate a further layer lying beyond the flowing obstruction provided by saliva. An intercellular ground substance 40 to 300μm thick, known as mucus, surrounds the epithelial cells of the buccal mucosa (Sudhakar *et al.*, 2006). Mucus can be described as a viscous colloid,

produced in the sublingual and minor salivary glands. The chief components of mucus are mucins, alongside inorganic salts suspended in water. Mucins are a family of large, heavily glycosylated proteins that range in molecular weight from 1 to 10 million Daltons in size (Slomiany *et al.*, 1996). The common structural arrangement of the family is a protein core to which many oligosaccharide chains are attached. This confers on them chemical properties to carry out functions in lubricating mucosal cell-to-cell movement, epithelial surface hydration and as an inhibitory chemical barrier (Marin *et al.*, 2008). At oral pH it forms a strong, cohesive gel-like structure that binds to the epithelial surface providing an additional, extended three-dimensional barrier that offers flexible movement and concentration. This contributes to a robust barrier that can trap and immobilise invasive materials and pathogens (Cone, 2009). It is heavily speculated that this mechanism is the most probable defence, and challenge, when nanomaterials are applied to the oral mucosa.

1.4 Nanomaterials in industry

Nanomaterial use in industry may be reflected by the staggering 103 tonnes currently produced annually ((CORDIS), 2009). The total world output is only expected to increase, and it is speculated to reach 58,000 tonnes by the year 2020 (Lewinski *et al.*, 2008), equating to approximately 10% of all chemicals produced globally belonging to the nanomaterial subset, by then (Borm *et al.*, 2006). Today, metal oxide nanomaterials can be increasingly found utilised in a huge variety of products and industries ((SCCP), 2007, Borm *et al.*, 2006, Buzea *et al.*, 2007, Kimbrell, 2006, Nel *et al.*, 2006). However, it is the consumer healthcare industry (also known as the cosmetics industry) that is leading the way in implementing nanomaterials into widespread consumable products (Kimbrell, 2006, Sharma *et al.*, 2009b), with nano-metal oxides already contributing heavily in product formulations. With the global consumer healthcare industry estimated to have had an annual turnover of between $170 and $200 billion in 2007 ((FoE), 2006, Berger, 2006, Boulanger, 2009) increasing to $2.6 trillion by 2015 (Raj *et al.*, 2012), utilising nanomaterials in new, superior products is perceived to be a very lucrative and viable business strategy. This view is backed by the healthcare and cosmetics industries holding the largest number of patents for nanoparticles, ready for use in toothpaste, mouthwash, shampoo, various make-up formulations, after-shave, moisturiser and deodorant technology (Woodrow-Wilson., 2010); with L'Oreal alone

accounting for the sixth highest nanoparticle based patents in the US (Raj *et al.*, 2012). In Japan, nanomaterials have already been developed by Sangi Co., Ltd, using nano-hydroxyapatite in their Apagard® toothpaste brand since the 1980's (Itthagarun *et al.*, 2010).

The EU Cosmetic Regulation 1223/2009 defines a cosmetic product as:

"any substance or preparation intended to be placed in contact with the various external parts of the human body (skin, hair and/or hair follicles, nails, lips, and genitals) or with the teeth and the mucous membranes of the oral cavity, with a view exclusively or mainly to clean them, perfume them, change their appearance, and/or correct body odours, and/or protect them or keep them in good condition." ((EU), 2010).

Nanotechnology is currently employed in the development of essentially three areas of the cosmetics production process: formulation, packaging, and manufacturing equipment; with the largest fraction of ongoing nano-related research and development concerning the formulation aspects (Mihranyan *et al.*, 2012). The direction of research for nanomaterial formulations has been driven by a conservative policy based on the legacy inclusion of existing bulk constituents in personal care products (Seaton *et al.*, 2010). This is expected to simplify the safety review of new ingredients, restricted by the ban on animal testing ((EU), 2013), with the onus on manufacturers to compile comprehensive information files on safety assessment ((EU), 2010).

Nanomaterial formulated cosmetics mainly constitute the active ingredient, the delivery vehicle (or nanocarrier) or act as a formulation aid (Mihranyan *et al.*, 2012). As active ingredients, nanomaterials have been increasingly included into cosmetic formulations due to the unique properties available following a reduction in particle size (Borm *et al.*, 2006, Buzea *et al.*, 2007, Maynard, 2007b, Nohynek *et al.*, 2010, Whitesides, 2005). Novel nano-scale properties can often be unpredictable and very different from the bulk constituent or much enhanced in terms of efficacy (Thomas *et al.*, 2006). Metal oxides account for the greatest degree of interest, with nanoparticles of carbon, gold, silver, silica, titanium and zinc present in currently marketed cosmetic products ((SCCP), 2007, Aitken *et al.*, 2006, Mihranyan *et al.*, 2012, Nohynek *et al.*, 2010, Raj *et al.*, 2012, Thomas *et al.*, 2006). Examples include both silver and ZnO demonstrating improved antimicrobial action through a reduction in particle size (Cho *et al.*, 2005, Li *et al.*, 2008, Liu *et al.*, 2009, Nagarajan & Rajagopalan, 2008). The mechanism of action is thought to

include the same generation of ROS through increased surface reactivity and release of metal ions, as observed in eukaryote cytotoxicity (Zhang *et al.*, 2010). Nanomaterials are also utilised to improve formulations, offering superior efficacy in rheology profiles, transparency, reflectivity and colour, in novel ways that are not possible for bulk sized composites (Mihranyan *et al.*, 2012). This has been claimed for gold and silver nanoparticles of differing shapes, to enhance the colour perception of skin (Alfano *et al.*, 2007), with different compositions used to create different lipstick, emulsion foundation and face powder pigments (Mihranyan *et al.*, 2012). TiO_2 and iron oxide nanoparticles developed into an opaque gel have proven more successful (following consumer testing) in blurring the appearance of skin imperfections than bulk particles (Dingley *et al.*, 2008). SiO_2 and aluminium nanoparticles have proven to fill wrinkles more consistently than could be achieved under bulk particle packing (Maitra *et al.*, 2008). As previously mentioned, TiO_2 and ZnO nanomaterials have been found to filter UV light more efficiently then micron-sized particles, but have the additional benefit of proving colourless on the nano-scale, resulting in transparent formulations (Nohynek *et al.*, 2010). These nanomaterials have been formulated as a 25% w/v component of sunscreen products (Schilling *et al.*, 2010)

Similar to their applications in drug delivery, the small size and surface characteristics of nanomaterials has been exploited in their use as nanocarriers for vitamins, antioxidants, chemical UV filters, anti-acne or anti-aging substances, normally delivered via the skin (Wu & Guy, 2009). Many other uses may already be in diverse, commercially available products ((SCCP), 2007), providing a challenge for governments' and regulators alike, in keeping track of their inclusion and potential risk to the consumer (Kessler, 2011).

1.4.1 Nanomaterials in Oral Healthcare

Across Europe, oral diseases constitute a major public health burden attributed principally to dental caries, periodontal diseases and oral cancers. Oral diseases do not only impact on the individual through pain and discomfort, they also affect the wider community through the health system and wider economic costs (Patel, 2012). Frequent exposure to fluoride, regular brushing, a healthy diet and routine oral care regimes all contribute to improved oral healthcare outcomes and a reduction in oral care inequality (Petersen, 2003). Personal oral healthcare products form an important part of any oral hygiene routine and include the use of toothpastes, flossing agents and mouthwash

products that can help conditions, such as dentine hypersensitivity, tooth decay, gum disease, halitosis and xerostomia.

Dentine hypersensitivity is the response of pulp nerves to stimuli that results in sharp pain or dull aching at the site of the dentine surface (Addy, 2002). Desensitising toothpastes often act to deliver tubule-occluding formulations that block the opening at the dentine surface (Addy & Smith, 2010), as well as changing the balance of potassium ions across the nerve cell membrane to calm the nerve (Markowitz, 2012). Recently, the greater solubility of nanomaterials has been exploited, using nano-SiO_2 and hydroxyapatite formulations in toothpastes that have been determined to improve dentin permeability (Chiang *et al.*, 2010). SiO_2 in particular has many desirable qualities involved in improving formulation textures, viscosity and in controlling fouling or foaming, all of which are speculated to be improved through a reduction in particle size (Mihranyan *et al.*, 2012). At the nano-scale it has been demonstrated that such materials improve filling efficiency in exposed tubules (Rybachuk *et al.*, 2009). The effects of dentine-hypersensitivity are reduced further when nano-SiO_2 was formulated alongside hydroxyapatite nanomaterial (Gupta, 2011). As previously mentioned, the Sangi Company in Japan has been using nanoparticle hydroxyapatite in their Apagard® brand since the 1980's (Itthagarun *et al.*, 2010), due to the established the "remineralisation" properties of hydroxyapatite nanomaterial that is only attained through nanoparticle size (Tschoppe *et al.*, 2011). This has gained more attention recently, due the biocompatibility and bioactivity of hydroxyapatite being well established in medicine with regard to bone replacement technologies (Hannig & Hannig, 2010).

Demineralisation of enamel at the tooth surface can be a result of a number of factors, including acid erosion, mechanical abrasion, accidental abfraction and attrition (Attin *et al.*, 2001, Lussi *et al.*, 2011). It is of particular clinical relevance, as loss of the enamel can expose the underlying features of the tooth leading to dentine hypersensitivity (Addy & Smith, 2010). Traditionally, enhanced calcium and fluoride concentrations have been used to promote remineralisation, with bulk scale hydroxyapatite proving relatively unsuccessful (Tschoppe *et al.*, 2011). Recently, nano-hydroxyapatite formulations have been developed that demonstrate greater affinity to enamel surfaces (Hannig & Hannig, 2010), whilst allegedly proving equally as proficient to fluoride remineralisation (Tschoppe *et al.*, 2011).

Tooth loss through decay and acid erosion can also be caused by both a sugary or acidic diet respectively, that results in acidic demineralisation and weakening of surface enamel of the teeth (Lussi *et al.*, 2011). These factors are degenerative conditions that cannot easily be reversed, and ultimately may result in tooth extraction (Lussi *et al.*, 2006). However, intensive fluoride treatments and remineralisation agents can be incorporated into oral healthcare regimes to manage and limit these conditions (Lagerweij & Ten Cate, 2010, Schemehorn *et al.*, 1999), with research continuing in new dental materials to offer improved restoration of the appearance and function of teeth (Burke *et al.*, 2005). New nanomaterial dentifrices are increasingly being explored as both nano-ceramics and resins (Jevnikar *et al.*, 2010), with nano-SiO_2 again proving advantageous due to improved rheology properties (Rybachuk *et al.*, 2009).

At the bulk-scale, SiO_2 is a well-established additive in the food industry (Hansen *et al.*, 2008) and has been widely employed throughout the cosmetic industry for its use as an anti-caking, bulking and opacifying agent, amongst other uses (Martin, 2007). In oral healthcare, it is already employed at the bulk scale as a polishing, or abrasive agent in toothpastes, with its inclusion in formulations involved in physically removing bacterial adhesion to the surface of teeth (Allaker, 2010, Newby *et al.*, 2011). At the nano-scale, SiO_2 polishing has proved more successful on human teeth *ex vivo*, with considerably lower roughness observed on the tooth surfaces when compared to bulk material (Gaikwad & Sokolov, 2008). It has also been explored as a nanoparticle coating for target delivery and controlled release of other anti-bacterial agents (*e.g.* nitric oxide), demonstrating improved efficacy in the removal of biofilm embedded bacteria (Allaker, 2010), and in its development as a bioactive glass (Waltimo *et al.*, 2007). These properties are expected to improve gum health maintenance and help combat gum disease. Poor oral hygiene can result in plaque bacterial colonisation on the teeth with established biofilms known to cause inflammation of gingival tissues (Pihlstrom *et al.*, 2005). Mechanical abrasion, such as that generated through regular flossing, has been found the best way to remove adhered plaque organisms (Ong, 1990), with nano-carriers for chlorhexidine mouth rinses employed to combat mild gingivitis that may result from advanced biofilm formation (Jones, 1997).

ZnO too is a well-established antibacterial agent (Lorenz *et al.*, 2011, Zhang *et al.*, 2010), second only to silver as a metal oxide ingredient included across the personal care and home care products (Cho *et al.*, 2005, De Jong *et al.*, 2013). It is widely formulated in,

toothpastes, mouthwashes, deodorant, sanitary ware coatings, nappy rash creams and textile fibre coatings ((SCCP), 2007).

In toothpastes and mouthwashes, zinc has been formulated in a number of different forms *e.g.* zinc citrate, zinc acetate and ZnO (Allaker, 2010). Each zinc compound has normally exploited the release of Zn^{2+} for its antibacterial action (Giertsen, 2004). The mechanism of antibacterial action has been demonstrated across a broad spectrum of organisms, and is thought to cause oxidative stress through the generation of ROS in much the same way as reported in eukaryote cytotoxicity (Zhang *et al.*, 2007). For insoluble materials, the efficacy has been well reported to improve in relation to a reduction in particle size, within the nano-scale (Liu *et al.*, 2009, Nagarajan & Rajagopalan, 2008, Zhao *et al.*, 2005), and is far less likely to evolve into bacterial resistance unlike the conventional narrow-target antibiotics (Pal *et al.*, 2007) that may be used to contain gingivitis (Cuesta *et al.*, 2011). Furthermore, nanomaterial ZnO has received increasing attention because it is stable under harsh processing conditions (Allaker & Memarzadeh, 2013), is insoluble/water resistant, becomes transparent and is generally regarded biocompatible (Monteiro-Riviere *et al.*, 2011). These qualities would help improve efficacy of mouthwashes, targeted at alleviating halitosis, or oral malodour. This condition has been defined as an unpleasant odour that emanates from the oral cavity with intra-oral and or extra-oral origins (Armstrong *et al.*, 2010). Up to 90% of breath odour is thought to emanate from within the mouth, and is associated with volatile sulphur compounds, methyl mercaptan and hydrogen sulphide that are a by-product of bacterial putrefaction of amino acids derived from food, cells, saliva and blood (Scully & Felix, 2005). Therefore, similar to regular maintenance of gum health, a regular oral hygiene routine is essential to limit the colonisation of bacteria in the oral cavity (Newby *et al.*, 2011).

In line with the competitive commercial environment that exists in the cosmetic industry, personal care products for oral healthcare are also looking to nanomaterials to increase efficacy of product formulations (Mihranyan *et al.*, 2012). The nanomaterials investigated within this study, were chosen due to the inclusion of hydroxyapatite, SiO_2, TiO_2 and ZnO in existing oral healthcare formulations, as non-nano constituents. In each case, a reduction in particle size is of putative interest for future oral healthcare formulations, due to enhanced efficacy in their respective inclusion properties. Within the EU, oral healthcare products are typically regulated as cosmetics, requiring a

comprehensive safety assessment to ensure safety under reasonable and foreseeable use ((EU), 2010).

TiO_2 nanomaterial was included within the investigation as a necessary comparison to assess cytotoxic effects of other nanomaterials, due to its consideration as a relatively inert and non-toxic nanomaterial, found in many current consumer healthcare products ((SCCP), 2007, Hansen *et al.*, 2008, Weir *et al.*, 2012). It is one of the most widely produced nanomaterials globally, with the broadest spectrum of uses (Aitken *et al.*, 2006): from paints to sunscreen, with latter use receiving the greatest attention in nanotoxicology studies (Gamer *et al.*, 2006, Schilling *et al.*, 2010, Schulz *et al.*, 2002). It is also a component of some dental implants (Subramani *et al.*, 2009), of which the subject of nanomaterial induced inflammation has emerged as a consequence of the degradation that occurs over the lifetime of its use (Lalor *et al.*, 1991).

In oral healthcare, TiO_2 is utilised in low-end bulk particle sizes that mean some may already be nanomaterials within toothpaste products. It is primarily formulated as a pigment used for imparting whiteness, brightness and opacity (Khataee & Kasiri, 2010). The optical properties that differentiate the nanomaterial from bulk TiO_2 are being explored as a photocatalytic antibacterial agent (Allaker & Memarzadeh, 2013, Mihranyan *et al.*, 2012) and photocatalytic bleaching agent (Mihranyan *et al.*, 2012), are thought to demonstrate superior rheology profiles when formulated from a nanopowder (Allaker, 2010, Mihranyan *et al.*, 2012).

1.5 Aims and objectives of the thesis

With the increasing application of nanomaterials across all technologies, human exposure will become more common. Advantageous nano-scale properties hold great potential for reputedly improving the efficacy of putative oral healthcare formulations, but require thorough risk assessment to comply with new EU cosmetic ingredient legislation. This study aims to address the lack of research into nanomaterial toxicity and uptake potential in the oral mucosa. To address the current gap in knowledge as to the fate of nanomaterials in this area of the body; this will be accomplished through risk assessing all factors relating to potential cytotoxicity, in both keratinised and non-keratinised tissues.

Three specific research questions emerge regarding the potential risk associated with the use of nanoparticles in oral health care preparations and their assessment. The aim of the thesis will be to answer these main questions:

1) Do nanomaterials pose a higher degree of risk to the human oral mucosae over bulk versions of the same material, if exposed as a potential oral healthcare ingredient? Currently nanomaterial exposure to the oral mucosa remains devoid of research specifically concerning toxicity, and this adds weight to the original contribution to knowledge of this study.

If so,

2) How do they pose this (greater) risk? Is it through increased cytotoxicity, potential uptake or a combination of both? What mechanisms are available to each nanomaterial and do any particular properties link to specific nano-characteristics *e.g.* purely nano-size, particle shape or is it another surface property? Outcomes will add to the ongoing, collaborative impetus aimed at profiling new chemical ingredients to build currently missing or inadequate safety data. This will help with the ultimate goal in toxicology, to one day reliably predict nanomaterial properties and the level of risk exposure to certain types poses.

3) Do they warrant further risk assessment in relation to the health of other areas in the body? For example, cytotoxicity may be different depending upon tissue type between non-keratinised and keratinised regions. It can be expected that exposure to the oral mucosa will likely have implications for the gut and stomach epithelia if swallowed. The kidneys, heart and spleen may also be at risk if nanoparticles are found to be internalised and transported through tissues, where they may be able to access the systemic circulation. The application of nanomaterials as excipients in oral healthcare products poses questions regarding the risks associated with repeated exposure, and the impact this may have on cumulative effects, both in the oral mucosa and elsewhere.

In answering these key research questions, this study will seek to address the following objectives:

(i) Fully characterise each nanomaterial in relation to bulk composites, to identify any nano-specific physiochemical characteristics that may change the toxicity profile in the oral mucosa.

Measurements of particle size will be assessed in the context of polydispersity, changes from starting state as supplied by commercially relevant manufacturers towards more representative *in situ* environments an oral healthcare excipient may be exposed to within the oral mucosa. Multiple techniques will be employed to investigate particle morphology, surface properties (such as appearance, charge, stability in solution), chemical composition and agglomeration state.

(ii) Link any nano-specific properties to effects resulting from nanomaterial-cell/tissue interactions.

These will be analysed using a mix of biochemical assays and imaging techniques in combination, to build a picture of cell health under different parameters of exposure. Studies will be designed to mimic likely scenarios of nanomaterial delivery to the oral mucosa as part of an oral healthcare formulation.

(iii) As the nanomaterials chosen for investigation are reputed to be of interest in future oral healthcare formulations, risk assessment will have to be carried out following the regulations stated in the cosmetic regulation ((EU), 2013). Specifically, this regards the imposition of a ban on marketing and testing cosmetic products that have had ingredients tested on animals.

To accomplish this, studies will not utilise in animal models, instead following a tiered, integrated testing strategy utilising a battery of *in vitro* models. These will range from monolayer cell lines, to more representative commercially available 3-D tissue models. Information will be built following a tiered-testing strategy, with the direction of investigation provided through data accumulated from the previous set of experiments.

(iv) Ascertain the risk pathway in relation to cytotoxicity, inflammatory response or particle uptake and potential translocation.

This will employ the culmination of multiple assessments to elucidate the most probable potential risks for each of a range of nanomaterials tested. It is perhaps an ambitious aim to provide a fully comprehensive risk assessment for each nanomaterial of interest, especially with regards to exposure to the oral mucosa (an area of the body currently devoid of study relating to nanomaterial toxicity). Therefore, by identifying the main causes of concern regarding nanomaterial safety in oral healthcare products, this is anticipated to aid future study direction: an important objective for early stage exploratory scientific investigation. This remains the current situation regarding new applications of nanomaterials (as oral healthcare excipients) without established safety profiling.

2 GENERAL METHODS

Reported here are all the materials used and methods carried out to underpin the experiments included within this research.

2.1 Materials

Acetic acid glacial 99+%. Specified by Fisher Scientific, Loughborough, UK. Catalogue number A/0360/PB08

Adenosine 5'-triphosphate disodium salt hydrate (ATP) microbial, BioReagent, suitable for cell culture, ≥99%. Sigma-Aldrich, Gillingham, Dorset, UK. Catalogue number: A6419

Blotting paper. Fisher Scientific UK. Catalogue number: SDE1

Cover glasses (22 x 22mm). Menzel Gläser® Thermo Fisher Scientific UK. Catalogue number: MNJ-450-020-W

CryoTube™ Vials from Nunc®. Fisher Scientific UK. Catalogue number: CRY-960-070B

CytoTox 96® Non-Radioactive Cytotoxicity (LDH) Assay. Promega, Southamption, UK. Catalogue number: G1780

Dimethylsulfoxide (DMSO) Hybri-Max®. Sigma-Aldrich UK. Catalogue number: D2650

Dulbecco's MEM/Ham's F12 basic medium, phenol-red free. Gibco, Fisher Scientific UK. Catalogue number: 21041

Dulbecco's MEM/Ham's F12 basic medium, without *L*-Glutamine. PAA Laboratories Ltd., Yeovil, UK. Catalogue number: E15-012

Eagles's MEM with Earle's salt without *L*-glutamine. PAA Laboratories Ltd., UK. Catalogue number: E15-024

EpiGingival™ tissue model (0.6cm^2). MatTek Corporation, Ashland MA, USA. Catalogue number: GIN-100

Ethanol (200 proof). Sigma-Aldrich UK. Catalogue number: 493456-1L

Ethylenediaminetetraacetic acid EDTA Disodium Salt: Dihydrate FW 372.2. Sigma-Aldrich UK. Catalogue number: ED2SS

Falcon™ 6-well Multiwell plate. Becton-Dickson, Oxford, UK. Catalogue number: 353046

Falcon™ 12-well Multiwell plate. Becton-Dickson UK. Catalogue number 351143

Falcon™ 24-well Multiwell plate. Becton-Dickson UK. Catalogue number 351147

Fetal Bovine Serum (FBS), heat inactivated, EU approved. PAA Laboratories Ltd., UK. Catalogue number: A15-104, University of Brighton reserved batch number: A10408-1516

Fisherbrand™ conical centrifuge tubes (15mL). Fisher Scientific. Catalogue number: 11879640

FisherBrand® 4 mL single use UV curvette. Fisher Scientific UK. Catalogue number: FB55923

Fluoroshield™ with 4',6-diamidino-2-phenylindole (DAPI). Sigma-Aldrich UK. Catalogue number: F6057

FM® 1-43FX, fixable analogue of FM® 1-43 membrane stain. Life Technologies™, Fisher Scientific UK. Catalogue number: F-35355

Formalin solution, 10% v/v (approximately 4% w/v formaldehyde), neutral buffered for histological tissue fixative. Sigma-Aldrich UK. Catalogue number: HT501128

Formvar /Carbon on 100 Mesh Nickel TEM sample grids. Agar scientific Ltd., Stanstead, UK. Catalogue number: AGS162N1

Formvar coated 3 mm copper mesh TEM grids. Agar Scientific Ltd., UK. Catalogue number: S138

GIN-100 maintenance medium. MatTek Corporation. Catalogue number: GIN-100-ASY

25% Glutaraldehyde Solution – Grade I especially purified for use as an electron microscopy fixative. Sigma-Aldrich UK. Catalogue number: G5882-50ML

***L*-Glutamine**. Sigma-Aldrich UK. Catalogue number: G-8540

Hanks' Balanced Salt solution (HBSS) modified, with sodium bicarbonate, without phenol red, calcium chloride and magnesium sulfate, liquid, sterile-filtered, suitable for cell culture. Sigma-Aldrich UK. Catalogue number: H6648

High purity 12.5mm aluminium SEM stub. Agar Scientific Ltd., UK. Catalogue number: G301P

Hydrochloric acid solution (1N). Sigma-Aldrich UK. Catalogue number: H9892

Hydrocortisone 21-hemisuccinate. Sigma-Aldrich UK. Catalogue number H2270-100MG

Hydroxyapatite (bulk) powder. Sigma-Aldrich UK. Catalogue number: 289396-25G

Hydroxyapatite nanopowder. Sigma-Aldrich UK. Catalogue number: 677418-5G

Isopropanol (propan-2-ol 99.5%). Fisher Scientific. Catalogue number: P/7507/17

Lead citrate (electron microscopy grade). Agar Scientific Ltd., UK. Catalogue number: AGR1210

Microlance™ disposable syringe needle (50mm, 21 gauge). Becton Dickinson, UK. Catalogue number: 301155

Microcentrifuge tubes (1.5 mL). Fisher Scientific UK. Catalogue number: FB74075

Microplates (96-well, black and PS surface treated for cell culture). PAA Laboratories Ltd., UK. Catalogue number: PAA-30296X

Microscope slides Superfrost® Plus(76 x 26mm) Menzel Gläser® Thermo Fisher Scientific UK. Catalogue number: MNJ-700-020-K

1-(4,5-Dimethylthiazol-2-yl)-3,5-diphenylformazan, Thiazolyl blue formazan (MTT). Signma-Aldrich. Catalogue number: M2003-1G

Nitric acid ≥ 68% and ≤70% (Specified analytical reagent). Fisher Scientific, UK. Catalogue number: N/2300

Osmium tetroxide 2% w/v Solution. Agar Scientific Ltd., UK. Catalogue number: AGR1019

Penicillin/Streptomycin (100X). PAA Laboratories Ltd., UK. Catalogue number: P11-010

Phalloidin – tetramethylrhodamine B isothiocyanate conjugate from *Amanita phalloides*. Fluka™ Analytical UK. Catalogue number: 77418

Phosphate buffered saline (PBS) tablets, from Oxoid. Fisher Scientific UK. Catalogue number: BR014G

Polyethylene glycol 300. Fluka by Sigma Aldrich UK. Catalogue number: 81162

Polystyrene polymer spheres in aqueous suspension (21nm) - NIST™ traceable size standard. Brookhaven Instruments Ltd. Worcester, UK. Catalogue number 3020A

Polystyrene polymer spheres in aqueous suspension (70nm) - NIST™ traceable size standard. Brookhaven Instruments Ltd., Catalogue number 3070A

Propylene oxide ReagentPlus®. Sigma-Aldrich UK. Catalogue number: 110205

Quantikine® Human IL-1α ELISA kit. R&D Systems Europe Ltd.. Abingdon, UK Catalogue number: DLA50

Reconstructed human oral (RHO) epithelium models (0.5cm^2). SkinEthic Laboratories, Lyon, France. Catalogue number: RHO/S/5

Saran® wrap (cling film). Fisher Scientific UK. Catalogue number: SEL-360-500Q

Scalpel. Swann-Morton® Ltd., Sheffield, UK. Catalogue number: 3991.

Silicon dioxide powder (ACROS organics). Fisher Scientific UK. Catalogue number: 11944121

Silicon dioxide (bulk) powder. Sigma-Aldrich UK. Catalogue number: 381276

Silicon dioxide nanopowder. Sigma-Aldrich UK. Catalogue number: 718483

SkinEthic maintenance cell culture media. SkinEthic Laboratories. Catalogue number: SMM/L

Sodium cacodylate. Agar Scientifc Ltd., UK. Catalogue number: R1104-100g

Sodium dodecyl sulphate (SDS). Sigma-Aldrich UK. Catalogue number: L-4390

Sodium pyruvate solution (100mM) sterile-filtered, BioReagent, suitable for cell culture. Sigma-Aldrich UK. Catalogue number: S8636

Sticky tabs for SEM specimen stubs (12.5mm). Agar scientific Ltd., UK. Catalogue number: G3109

SynaptoGreen™ C4 (FM 1-43 dye). Sigma-Aldrich UK. Catalogue number: S6814

Syringe (2ml, disposable) Plastipak™. Becton Dickinson UK. Catalogue number: 300185

Syringe (10ml, disposable) Discardit™II. Becton Dickinson UK. Catalogue number: 309110

Syringe end filter (0.2µm) MiniStart Plus® from Sartorius. Fisher Scientific UK. Catalogue number: FDP-635-010M

T-25 Thermo Scientific Nunc® tissue culture flask. Fisher Scientific UK. Catalogue number: TKT-130-050P

T-75 Thermo Scientific Nunc® tissue culture flask. Fisher Scientific UK. Catalogue number: TKT-130-370U

TAAB Low Viscosity resin. TAAB Laboratories Ltd., Reading, UK. Catalogue number: T049

Thermo Scientific Nunc® 96 Microwell™. Fisher Scientific UK. Catalogue number: TKT-180-070U

Thermanox™ cover slips (13 mm). Agar Scientific Ltd. Catalogue number: L4350

Titanium(IV) oxide, mixture of rutile and anatase – nanoparticles in dispersion, 33-37 wt. % in H2O, 99.9% trace metals basis. Sigma-Aldrich UK. Catalogue number: 700347-25G

Titanium(IV) oxide puriss (bulk) powder. Sigma-Aldrich UK. Catalogue number: 14027

Triton™ X-100 surfactant (1% solution in PBS). MatTek Corporation. Catalogue number: TC-TRI

Trypsin 0.05% w/v EDTA (1X), from Invitrogen. Fisher Scientific. Catalogue number: VX25300054

Universal tube (30mL). Appleton woods Ltd., Birmingham, UK. Catalogue number: AB304

Uranyl acetate (electron microscopy grade). Agar Scientific Ltd., UK. Catalogue number: AGR1260A

Zeta potential disposable capillary zeta cell. Malvern Instruments Ltd, Malvern, UK. Catalogue number: DTS1061

Zeta potential transfer standard (-68mV). Malvern Instruments Ltd, UK. Catalogue number: DTS1230

Zinc acetate 99.99% powder. Sigma-Aldrich UK. Catalogue number: 383317

Zinc oxide (bulk) powder. Sigma-Aldrich UK. Catalogue number 96479

Zinc oxide 45408 nanomaterial, NanoArc® ZN-2210, 50% in H2O, colloidal dispersion with dispersant. Alfa-Aesar (a Johnson Matthey Company), Heysham, UK. Catalogue number: 4545408

Zinc oxide 45009 nanomaeterial NanoShield® ZN-3008C, 50% in H2O, colloidal dispersion with cationic dispersant. Alfa-Aesar. Catalogue number: 45009

Zinc standard for ICP TraceCERT® (Fluka). Sigma-Aldrich UK. Catalogue number: 18562-100ML-F

2.2 Methods

2.2.1 Characterisation of materials

2.2.1.1 Scanning Electron Microscopy (SEM)

Scanning electron microscopy (SEM) produces pseudo 3-dimensional topographical images by scanning the surface of a sample with a focused beam of electrons. Electron interactions with the sample (which also needs to be electrically conductive, at least at the surface) produce energy exchanges that result in the back scattering of electrons via three main ways: reflection of high energy electrons from the SEM ion beam by the sample (known as elastic scattering), inelastic back scattering through the emission of secondary electrons after collisions between incident beam electrons from the SEM and atoms in the sample surface region, and emission of electromagnetic radiation through incident beam-sample interactions (Reed, 2005, Yao & Wang, 2006). Each type of energy exchange can be detected through specialised detectors installed within the SEM instrument.

The instrument utilised in this study was a Zeiss sigma field emission gun scanning transmission electron microscope (FEG-STEM), operating in SEM mode. It utilises secondary electron detection, reconfigured as a distribution map showing the intensity of the electron signal emitted from scanning the sample surface topography. The image is formed by mapping pixels to the position and intensity of detected signal (Williams & Carter, 2009b).

The inclusion of a field emission gun (FEG) to generate the electron beam allows for a smaller, sharper and more concentrated incident beam when compared to traditional thermoionic emitters/filaments found in older instruments. This allowed for a lower accelerating voltage to be used to generate images, resulting in a significantly improved signal-to-noise ratio that produces shaper, more defined images (Kuypers, 2002).

SEM analysis was primarily carried out to determine the morphology of materials to be used in later cell work. The images provide insight into particle shape, surface structure and extent of aggregation. Single particle sizing was also carried out to contribute to the overall particle size analysis, and allow direct comparisons between bulk and nano forms of each material.

Nanomaterial dispersions were analysed directly as supplied by the manufacturers. Approximately 2μL aliquots were deposited onto an aluminium SEM stub. A pipette tip was used to streak material across the surface, forming a thin smeared layer. SEM stubs were left to dry at room temperature in a fume hood overnight before analysis.

Nanomaterials in powder form were fixed to an aluminium SEM stub with the addition of an adhesive patch onto the surface. Approximately 25mg was fixed to the stub before excess powder was removed via a burst of sterile air from a pressurised can (Dust-off® Plus, Agar Scientific UK Ltd.).

SEM imaging was performed using the Zeiss sigma FEG-STEM (Carl Zeiss Ltd., Cambridge, UK) at a extra-high accelerating voltage (EHT) of 2kV combined with a working distance of 3mm (between detector and sample) to acquire images ranging from 1K and 500K times magnification. These were configured as Carl Zeiss Tiff files.

Micrographs were also used to accurately determine individual particle sizes present within each sample. This was carried out by measurements of 30 different particles using the Carl Zeiss Tiff Annotation Editor (Carl Zeiss Ltd. UK). Particles measured were selected by dividing micrographs taken at 3 different magnifications (1K X, 50K X and 100K X) into sectors into sectors and choosing the most prominent particle within a randomly generated sector. This was repeated 3 times from micrographs imaged at 3 different areas of each sample.

2.2.1.1.1 SiO_2 alternate bulk control material.

A true 'bulk' SiO_2 was sourced from Acros Organics (Fisher Scientific UK) later into the prokect, and checked for particle size using SEM (Appendix Figure 9.2), as described for characterisation of other materials in the above section. This was measured as having an average particle size of 214.7μm (±49.0μm) and provided a control against the nano-sized particles measured within SigmaAldrich sourced SiO_2 powder, in the SynaptoGreen™ FM1-43 assay.

2.2.1.2 Transmission Electron Microscopy (TEM)

Transmission electron microscopy (TEM) produces a magnified image focused on a single thin cross-section of a plane through the sample. Here, a high energy electron beam is transmitted through an ultrathin sample (in this case, nanoparticles suspended

on formvar grids). It is the complex interaction between electrons and sample, specifically their path through thin sections or conversely scattering by materials, that allows for the formation of sharp, resolved images at magnifications over thousands of times greater than light microscopy (Buseck *et al.*, 1988).

Transmission electron microscopes are able to exploit three main interactions between the electron beam and sample: un-scattered electrons (transmitted beam), elastically scattered electrons and in-elastically scattered electrons (diffracted beams) (Williams & Carter, 2009a) and each of these principles can be analysed in distinct detectors to form different types of images. The latter two interactions involve the redistribution of electrons post contact with a sample: a 'scattering' effect, but this technique was not employed using these studies. Instead, TEM micrographs were generated through the detection of un-scattered electrons, to characterise material size and shape, from a 2-dimensional micrograph constructed via incident beam detection at 180° *i.e.* below the sample. An image was then formed in a similar way to light microscopy, by occlusion and absorption of signal (in this case electrons), where transmission is inversely proportional to sample thickness (Flegler *et al.*, 1993).

The instrument utilised in this study was the same Zeiss sigma field emission gun scanning transmission electron microscope (Carl Zeiss Ltd. UK) as described for SEM. Again, the inclusion of a FEG allowed for a lower accelerating voltage to be used to capture sharper images at higher magnifications.

TEM analysis was carried out to consolidate size and morphological information generated from other characterisation methods. Principally, the technique was considered as a comparative method to SEM when analysing particle morphology. A secondary consequence, from sample preparation involving dispersion in ethanol, is that size data was considered directly comparable against results of similar samples using Dynamic Light Scattering (DLS) and Nanoparticle Tracking Analysis (NTA).

All solvents used for diluting samples were first filtered using a 0.2µm syringe filter.

For the nanomaterials supplied dispersed in aqueous based solutions (ZnO-45009, ZnO-45408 and TiO_2), a one in twenty dilution was performed in absolute (200 proof) ethanol (Sigma-Aldrich, UK). For all other materials supplied as solids, a 5% w/v working solution was made up in ethanol before further dilution to one in twenty as above. All diluted materials were sonicated (Ultrawave U50H Sonic bath, Ultrawave

Ltd., UK) at 400 watts in three bursts of 90 seconds. A further one in twenty dilution was carried out in ethanol, again with sonication as before. This resulted in a 400 fold final dilution for sample analysis. TEM sample preparation was completed with addition of approximately 2μL sample onto a formvar coated copper TEM grid. These were left to dry overnight at room temperature prior to analysis.

TEM imaging was performed on the Zeiss sigma FEG-STEM (Carl Zeiss Ltd. UK) at a EHT voltage of 20kV and a working distance of 4mm (between detector and sample), to acquire images ranging from 3.5K to 450K times magnification. Analysis was again configured as a Carl Zeiss TIFF image. Particle sizing was carried out using the micrographs generated, as described in the previous section (2.2.1.1) for SEM analysis.

2.2.1.3 Energy Dispersive X-ray Spectroscopy (EDS)

EDS identifies the elements present in a sample by exploiting the fundamental principles of each element having a unique atomic structure. In this analysis, an 80mm^2 X-max silicon drift detector (Oxford instruments, UK) integrated with the Zeiss STEM system was used. The apparatus works by using a high energy electron beam, known as the incident beam, to be directed at a region of the sample. This excites electrons within the inner shell of the atom(s) causing them to be ejected from that energy region, leaving behind an electron hole that is filled by a higher-energy shell electron. The difference in energy required for this to happen is emitted as an X-ray and can be measured with an energy dispersive spectrometer (Goldstein, 2003).

EDS was carried out on samples alongside SEM analysis, and so samples were prepared as described previously in section 2.2.1.1. Samples were focused to a high quality image using the Zeiss sigma FEG-STEM (Carl Zeiss Ltd. UK) before subjecting areas of interest on the image to high intensity X-rays, using the 80mm^2 X-max silicon drift detector (Oxford instruments, UK).

An EHT voltage of 20kV was used with a working distance of 8.5mm to 10.0mm (depending on image quality) between detector and sample, to acquire the images at 1,000 times magnification which proved sufficient for EDS analysis. The results were reported in spectra using AZtec software v2.0 (Oxford instruments, UK).

2.2.1.4 Nanoparticle size analysis using the Dynamic Light Scattering (DLS) principal

Particle size analysis of each material was undertaken using a Malvern Zetasizer Nano ZS90 (Malvern instruments LTD., UK). This relies upon the principles of dynamic light scattering (DLS) to calculate the average particle diameter of a test material. It measures the Brownian motion of particle diffusion when in dispersion, through the back-scattering of light at a 90° angle to a photo-multiplying detector that occurs as a particle moves through the laser beam. Measurement is based on Rayleigh scattering principles of particle movement through the laser light, with the intensity fluctuations recorded by a digital correlator and applied to a computer algorithm known as the autocorrelation function (Malvern, 2011). Large particles move slowly and therefore the intensity of scattered light also fluctuates slowly (with the reverse holding true for smaller particles). This is the fundamental property exploited by the Stokes-Einstein equation (Einstein, 1905), used to calculate the hydrodynamic diameter of the particle.

Equation 2.1. Stokes-Einstein equation:

$$d(H) = \frac{kT}{3\pi\eta D}$$

Where:

d(H) = hydrodynamic diameter (of the particle)

D = transitional diffusion coefficient (between the particle and surrounding medium)

k = Boltzmann's constant

T = absolute temperature

η = viscosity (of the medium)

The hydrodynamic diameter is reported as a Z-average: expressed as the intensity based harmonic mean (Thomas, 1987). This is calculated from analysis of DLS data by the use of the technique of cumulants (Koppel, 1972). Since this technique relies on numerically stable least squares fitting, it is relatively insensitive to experimental noise.

Due to the analytical design of the instrument, only nanomaterial samples underwent analysis; (particles > 5μm would be expected to dominate the light scattering signal as they pass through the laser beam). Nanomaterials were dispersed in each of three

solvents to investigate the effects that different chemical environments would exert upon hydrodynamic diameter:

- **Phenol-red free Dulbecco's MEM/Ham's F12 basic medium (PRF media)**, to closely mimic the formulations used for cell treatments
- **Deionised water (dH_2O)**, to act as a control against the presence of salts in cell culture medium.
- **Ethanol**, due to reports in the literature of its consistent dispersion property constant through effects of dilution (Hackenberg *et al.*, 2011b, Krebs *et al.*, 2008).

2.2.1.4.1 Zetasizer sample preparation

All solvents used were syringe filtered using a 0.2μm cellulose acetate membrane (Sartorius Stedim UK Ltd), except PRF media. This was not deemed appropriate because interactions with biological molecules were desired for the investigation. No samples were filtered, so that the true state of the material particle sizes could be analysed.

NIST™ [2] traceable polystyrene standards (21nm and 70nm) (Brookhaven Instruments Ltd., Worcester, UK) were used as a control for DLS sample analysis. Preparation involved the addition of a single drop from the standard from stock solution, into 1mL dH_2O pre-pipetted into a UV grade plastic curvette (Fisher scientific UK). This was allowed to stand for 2 minutes before analysis, to allow sufficient diffusion for an even distribution of particles within the sample (Malvern, 1996).

For each nanomaterial analysed, 6mL of a 0.001% w/v solution was freshly prepared in each of the respective solvents (dH_2O, ethanol or PRF media). These were vigorously vortexed for approximately 30 seconds, left for 5 minutes at room temperature before sonicating (Ultrawave U50H Sonicator, Ultrawave Ltd., UK) for 10 minutes prior to DLS measurement following the protocol in 2.2.1.4.2 (below).

[2] The National Institute of Standards and Technology is an agency of the U.S. Department of Commerce tasked with improving measurement accuracy of standards in technology.

To avoid any variations due to sample dilution, the same samples were then re-suspended through sonication and re-analysed by either/or:

- NanoSight analysis for direct particle size analysis with particle tracking analysis.
- Transferring to a capillary flow cell for Zeta potential measurement.
- Heating to 37°C and analysed again in the Zetasizer to mimic physiological conditions.

2.2.1.4.2 Zetasizer particle size measurements

Samples were re-sonicated for 3 minutes immediately prior to analysis, by pipetting 0.001% w/v sample solutions into disposable, UV grade cuvettes, before loading into the Malvern Zetasizer Nano ZS90 (Malvern instruments Ltd., UK). Samples were left to diffuse/equilibrate for 2 minutes prior to analysis. Instrument settings for sample particle size analysis using DLS are shown in Table 2.1. All samples were measured five times at both 22°C and 37°C during a single size analysis, with a mean value calculated at each temperature (± standard deviation). These experiments were repeated six times for each nanomaterial, to report an overall average particle diameter size using n=6 (± standard deviation).

Size distributions of the materials were calculated using the polydispersity index. The lower the value, the more mono-dispersed or uniform the particles are in suspension. Polydispersity widths were calculated to show the range of particle sizes in that measurement.

Table 2.1. Parameters used for automatic optimised particle size analysis using Malvern Zetasizer ZS90 (Zetasizer v6.1). Information obtained from experimental data and (Malvern, 1996).

Nanomaterial / Solvent	Manufacturer particle size specification (nm)	Material refractive index (RI)	Number of runs for size measurement	Mean Count rate (Kcps)	Solvent viscosity	Solvent RI
Polystyrene standard	21	1.590	11 to 13	243.72		
Polystyrene standard	70	1.590	11 to 13	347.94		
ZnO-45408	~ 20-30	2.008	13 to 15	280.54		
ZnO-45009	~ 70	2.008	13 to 16	293.19		
nano TiO2	< 30	2.600	15 to 21	287.68		
nano SiO2	12	1.480	15 to 18	245.92		
nano hydroxyapatite	< 200	1.651	13 to 19	232.67		
dH2O					0.954	1.333
PRF media					0.954	1.540
Ethanol					1.074	1.360

2.2.1.5 Nanoparticle Tracking Analysis

Nanoparticle tracking analysis (NTA) with the NanoSight LM10 instrument uses a 640nm class-1 laser to detect light scattering of nanoparticle movement through the laser beam by Brownian motion, similar to traditional DLS. Where this technique differs, is in the capture of detection and analysis of the scattered light. Where DLS relies upon time dependent scattering intensity fluctuations calculated using data from a digital correlator input into an autocorrelation function algorithm, NTA uses real-time filming at a resolved part of the laser beam to detect scattered light through a charge couple device (CCD) camera. This produces data in the form of recorded video files, for subsequent analysis using known sample variables. The NTA tracking software is able to individually track each and every scattered light movement simultaneously. The speed and distance travelled, in relation to the field of view detected by the camera, is linked to the Stokes-Einstein equation stated in Equation 2.1 (Einstein, 1905), from which particle size can be calculated as a direct number/frequency distribution. Advantages in this detection over DLS include, size determination that is not overly influenced by intensity weighted z-average distributions, increasing the ability to resolve heterogeneous/polydisperse particle mixtures, and direct particle counting that can reveal information on particle concentrations (Filipe *et al.*, 2010). In these respects, NTA proves to be superior to conventional ensemble methods of particle sizing *e.g.*, DLS and photon correlation spectroscopy (PCS). However, it is limited by the refractive index of the sample material. Highly refractive materials (such as metals) scatter more light and combined with larger particles, this may result in saturation of the relatively narrow field of view used to film their Brownian movement. In this regard, NTA is truly a measure of nanoparticle sizes, with the upper limit restricted to sub-micron particle sizes (NanoSight, 2009).

2.2.1.5.1 NTA sample preparation

NIST™ traceable polystyrene standards were again used as controls for the instrument. Due to the low RI of polystyrene, sizing the 21nm standard proved difficult as the non-metallic particle characteristics did not scatter enough light. Therefore only the 70nm was, used. This was not expected to be a problem for the more light reflective metal oxide nanomaterial samples.

The standard was prepared by adding 100µL of the standard from stock solution, into 6mL deionised and pre-filtered (0.2µm) H_2O in a sterile universal tube. This was

allowed to stand for 5 minutes before analysis. Standards were analysed on the instrument pre- and post-sample analysis.

The nanomaterial dispersions analysed were prepared according to details in section 2.2.1.4.1. Sonication was used to re-suspend any sedimenting particles, or to break up aggregates that may have formed during the course of DLS analysis (Siddiqui *et al.*, 2009).

Approximately 2mL of 0.001% w/v suspension was injected into the sample chamber of the NanoSight insturment. The 20X magnification lens was focused manually, to show clear particles moving in the laser beam pathway. Particle movement under Brownian motion was recorded for 100 seconds and particle size calculated using the NanoSight NTA software (version 2.2) to give mean particle diameters (± standard deviation). Each nanomaterial was analysed six times on different days to account for small fluctuations in room temperature (n=6).

2.2.1.6 Zeta potential measurement of colloidal stability

Zeta potential (ζ) is a measurement of the electrostatic charge differential at the interfacial layer between particle surfaces in dispersed medium. This measurement relies upon the Derjaguin and Landau, Verwey and Overbeek (DLVO) theory that describes the electrostatic force between charged particles interacting in solution (as shown in Figure 2.1). It assumes there to be an electrical double layer (EDL) that exists around each particle, which is the product of two parallel ionic layers interfacing between the particle surface and liquid molecules in solution. The inner layer, known as the Stern layer, is comprised of strongly bound ions directly on the particle surface. The outer, or diffuse layer, is formed through free ions in solution of opposite charge, being attracted to the stern layer and electrically shielding the particles from affecting other molecules in the solution (Sze *et al.*, 2003). As a particle moves in solution, the diffuse layer can be seen as dynamic depending upon the net charge exerted by the Stern layer. Some ions remain fixed to the Stern layer and move with the particle, whilst others remain fixed in solution. This dynamic frontier is known as the slipping plane, and the ionic potential at this point is the zeta potential (Delgado *et al.*, 2007, Lyklema, 2005).

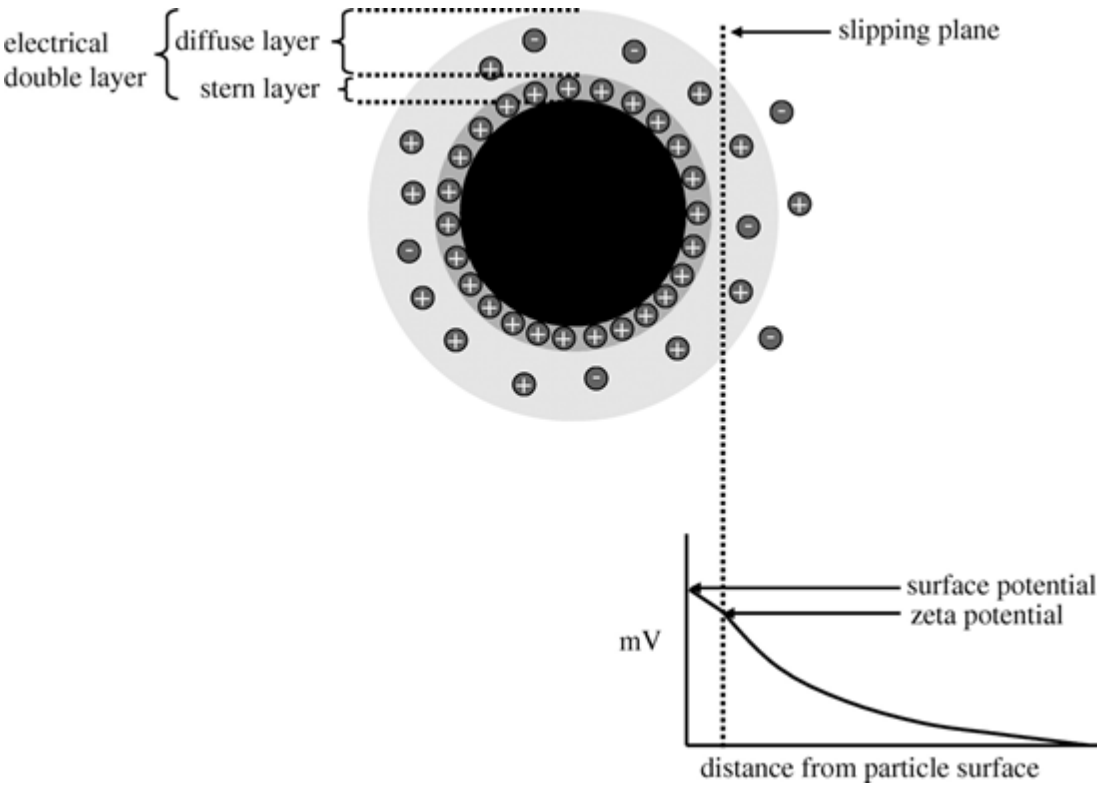

Figure 2.1. A schematic representation of Zeta potential. *Taken from (Kaszuba et al., 2010).*

Zeta potential measurement allows for assessment of the stability of nanoparticle colloidal suspension in fluid environments, and subsequently the degree of aggregation, sedimentation, or flocculation of particles (Everett, 2007, Hunter, 1993). It is not measurable directly, but is calculated using theoretical models from experimentally determined electrophoretic mobility obtained with the Malvern Zetasizer Nano ZS instrument (Malvern Instruments, UK). This utilises a combination of laser Doppler velocimetry and phase analysis light scattering (PALS) in a patented technique called M3-PALS to measure the particle electrophoretic mobility (Kaszuba *et al.*, 2010, Malvern, 2001) (in essence, this involves passing a rapid, alternating negative-positive charge through the sample solution to 'sway' particle movement between the two electrodes). The same fundamentals of particle movement under Brownian motion can then be used to determine the light scattered as the particle is pulled and pushed in the direction of current. This information contributes towards the calculation of zeta potential (based upon DLVO theory) using Henry's law and involving the Smoluchowski's approximation (Equation 2.2):

Equation 2.2. The Henry equation.

$$U_E = \frac{2\varepsilon\zeta f(Ka)}{3\eta}$$

Where:

U_E = Electrophoretic mobility (of the particle in the medium)

ε = Dielectric constant (of the medium)

ζ = Zeta potential (of the complete colloidal system)

f(Ka) = Smoluchowski's approximation

η = Viscosity (of the medium)

DLVO theory suggests that the sum of van der Waal's forces of attraction between particles, and the repulsion from particles EDL, can be used to calculate the energy barrier between particles in the solution. A high zeta potential, with either a positive or negative reading, indicates a large charge within the dispersion with many repulsive interactions stopping adherence between particles. This is generally accepted to correspond with stability in a colloidal dispersion. In contrast, low zeta potential values, correspond to greater imbalances between the electrostatic potential at the interfacial EDL. With this scenario, less kinetic energy is required by particles moving in solution to overcome the repulsive barrier of opposing electrostatic forces at the EDL. This results in strong adherence or irreversible binding of particles, and hence low zeta potential measurements are associated with aggregation and flocculation as the dispersant breaks down (Kirby, 2010).

At the beginning of each analysis, the instrument was checked for calibration using a known -68mV zeta potential standard (Malvern Instruments, UK. Catalogue number: DTS1230). Three measurements were taken, with calibration accepted by a mean reading remaining within 10% of the stated value of each standard.

Samples were those prepared as described in section 2.2.1.4.1. Samples were used to flush the zeta cell (Malvern Instruments Ltd, UK. Catalogue number: DTS1061) using a 2mL syringe, leaving approximately 500µL of sample within the chamber for analysis (the sample was then loaded *in situ* ready for analysis).

Laser attenuation and number of runs constituting a single measurement were optimised against the particle RI, count rate and solvent viscosity (stated in Table 2.1) using the instruments Zetasizer software (version 6.20). Zeta potential was calculated using Smoluchowski's approximation, averaged over four different measurements per analysis. This experiment was carried out six times (on different days), with results expressed as a mean value (± SD) of the readings (n=6).

2.2.1.7 pH measurements of nanomaterial dispersions in aqueous media

pH is an important parameter for controlling particle sizes of colloids because it affects the stability of surface charge and particle interactions (Berg *et al.*, 2009, Vallar *et al.*, 1999, Vane & Zang, 1997). It is strongly linked with zeta potential theory, and as such pH values were recorded in this study to provide the context for zeta potential measurements. Whilst manipulation of pH could have been investigated to determine optimal dispersion conditions, to improve stability of nanomaterials in solution, the aim here was to ascertain actual nanoparticle state in relation to characteristics that could affect nanomaterials properties *in vitro*. Therefore, the same dispersions that were prepared according to the method described in 2.2.1.4.1, were also analysed here (*e.g.* dH_2O, PRF medium and ethanol).

pH measurements were taken using a Mettler Toledo Seven easy™ pH meter (Mettler-Toledo Ltd., UK). The instrument was calibrated against Thermo pH solutions at 7.01, 4.01 and 10.01 respectively (Fisher Scientific, UK. Catalogue number 910199).

This technique was not appropriate for nanomaterials dispersed in ethanol. But other dispersions results presented are the average of 3 readings across 6 different samples produced on different days (n=6).

2.2.1.8 ICP-OES determination of zinc ion content in ZnO material

Inductively coupled plasma optical emission spectroscopy (ICP-OES) is an analytical characterisation technique that detects chemical composition on a quantitative scale. It utilises electromagnetic induction (fluctuating the polarity of magnetic fields) to generate an electrical current that ionises gas into a high energy plasma. This is used to convert samples from a liquid solution into a gaseous, excited state. Atoms and ions are

then able to emit electromagnetic radiation at characteristic wavelengths specific to a particular element. The colours of the emitted light and their intensity can be measured to identify sample elemental compositions and respective concentrations present within a sample.

The ICP-OES instrument used was the PerkinElmer Optima 2100 DV (PerkinElmer, UK). Liquid sample is pumped into a nebuliser where it is converted to a fine aerosol that becomes desolvated, vaporised and ionised in argon plasma. This causes atoms of the sample to emit electromagnetic radiation preceding the energy decay from a reduction in excited state during plasma ionisation (Fredeen, 1997). The wavelengths of electromagnetic radiation were detected from an axial orientation (with the normal analytical zone in the plasma rotated to a horizontal position) using a high-speed, high-resolution double monochromator, and converted to electronic signal by the instruments CCD array detector. Analysis was carried out using WinLab 32 software for ICP (version 3.3.1.0210).

The instrument required all samples to be in liquid form, compatible for vaporisation. The nanomaterials investigated were considered insoluble from previous characterisation, as observed forming a colloidal system of particles in suspension. Therefore, a wet acid digest was carried out to fully dissolve solid material into fully recoverable analytes. This technique was carried out to investigate reports in the literature of free zinc ions being linked to cytotoxicity in cells (Deng & et al., 2009, George *et al.*, 2010, Hackenberg *et al.*, 2011b, Xia *et al.*, 2008, Yeh *et al.*, 2011). Therefore, the following methodology was only carried out for zinc materials, based upon the British Standards Institute EN ISO11885:2009 (BSI, 2009) methodology. Comparisons to known concentrations of elemental standards were required to calibrate the system thereby confirming sample elemental composition and respective concentrations.

All samples were prepared from a 1% w/v solution, including calibration standards: Zinc TraceCERT® (Fluka, UK. Catalogue number: 18562-100ML-F). Zinc materials were diluted in three different solvents for analysis: ultra-pure dH_2O, phenol-red free Dulbecco's MEM/Ham's F12 basic media (PRF media) or PRF media with the addition of 10% fetal bovine serum (FBS media). The protective effects of FBS inclusion in media has been observed in the literature, thought to contribute ion adsorption properties (Auffan *et al.*, 2009, Hugh J. Byrne, 2010, Kim *et al.*, 2000, Nel *et al.*, 2009,

Okeson *et al.*, 2004). These studies correlate with the protective effect of FBS, observed following delivery alongside cytotoxic materials to H376 cells (section 4.1), and so this nanomaterial delivery was also investigated.

Zinc TraceCERT® calibration standards were prepared fresh for each run, at concentrations of 1.0, 0.8, 0.6, 0.4, 0.2 and 0.0% w/v diluted in each of the three solvents. From these results, internal calibration of the instrument was carried out to enable accurate quantification of Zn^{2+} in samples.

Sample solutions (1% w/v) were mixed thoroughly using a vortex-mixer, before sonication (Ultrawave U50H Sonicator (Ultrawave Ltd., UK)) for 10 minutes. Samples were then diluted 1:4 with either ultra-pure dH_2O or underwent an acid digest in 16N nitric acid (Fisher Scientific UK. Catalogue number: N/2300). Both sets of solutions were left to react in a fume hood for 24 hours; so that digested samples would release all available Zn^{2+}. The reaction was quenched by the addition of 2/3rds total volume of respective solvent, before undergoing ultra-centrifugation (Sorvall® RC Plus with SS-34 rotor (Thermo Fisher Scientific, UK)) at 20,000rpm for 30 minutes. This was carried out three times to remove any solid precipitate, including nanoparticles. Samples were diluted 100 fold in respective solvents, to produce a 0.001% w/v final concentration. Analysis was carried out using the PerkinElmer Optima 2100 DV ICP-OES instrument.

Results were processed using PerkinElmer WinLab software; with Zn^{2+} concentrations calculated from the internal calibration of optical emissions produced from the zinc TraceCERT® standards results. Results were carried out in triplicate with the mean calculated from three repeats (n=3).

2.2.2 Cell culture

2.2.2.1 H376 monolayer tissue culture

The H376 cell line is derived from a human oral squamous cell carcinoma (OSCC) derived from a non-keratinised sublingual tissue site. Cells were originally investigated for their integrin expression and metastatic potential (Patel *et al.*, 1993) and have since been characterised in full by Elsom, 2004.

The line was developed after spontaneous immortalisation of the keratinocytes due to a p53 mutation and was donated by Professor S. S. Prime (Department of Oral Medicine, Pathology and Microbiology, University of Bristol). The cells were maintained in culture for no longer than 10 passages, between the total numbers of passage 30 to 40. This was to ensure that their metastatic/neoplastic phenotype would not change as a result of prolonged passage *in vitro* (Sacks, 1996).

2.2.2.1.1 H376 culture medium

Dulbecco's MEM/Ham's F12 (without *L*-glutamine) was supplemented by the addition of 10% v/v heat inactivated fetal bovine serum (FBS), 2mM *L*-glutamine, 0.5µg/mL hydrocortisone and 2,500IU/mL Penicillin/Streptomycin (all as final concentrations), and used as H376 cell growth medium for routine culture conditions.

2.2.2.2 H376 routine cell culture and passage

H376 cell stocks were maintained by routinely culturing as monolayers at a seeding density of 3.0 x 10^3 cells/cm^2 in T-75, surface treated polystyrene flasks for cell culture. Cells were incubated at 37°C in a humidified, 5% CO_2 atmosphere (Sanyo-MCO715). Medium was changed every two days after passage. The cell populations were left to grow to approximately 75-85% confluence before passage.

Passage was carried out by standard trypsinisation (0.05% w/v trypsin/EDTA (1X) for 10 minutes at 37°C/5% CO_2). Cell suspensions were removed from the flask and centrifuged at 500 x *g* for 5 minutes (Sigma/Phillips-Harris 2K15). Cell pellets were re-suspended in fresh medium and cells counted using a haemocytometer.

2.2.2.2.1 Freezing and storage of H376 cell stocks

Cells were cryopreserved at a density of 1.0 x 10^6 cells/mL under liquid nitrogen in a solution containing the cryoprotectant dimethyl sulfoxide (DMSO). Freezing solution was prepared containing 70% v/v culture medium, 20% v/v FBS and 10% v/v DMSO and filter sterilised (0.45μm). Aliquots of cells were suspended in a mixture of fresh medium and freezing solution (50:50) in sterile cryovials (CryoTube™ Vials from Nunc®, Fisher scientific UK). Cells were frozen slowly (approximately 1°C per minute, to -70°C) and then transferred to liquid nitrogen for long term storage.

2.2.2.2.2 Thawing H376 cells from cold storage

Frozen cells were thawed rapidly by incubating at 37°C. Cells were washed once in fresh medium to remove cryoprotectant before seeding into a T-25 surface treated polystyrene flask at a seeding density of 1.0 x 10^6/25cm^2. Cells were washed daily to remove unrecovered cell debris and grown to 75% confluence prior to routine passage.

2.2.2.3 Ninety-six well plate growth for assays

H376 cells were cultured in 96 well plates (Thermo Scientific Nunc® 96 Microwell™, Fisher Scientific UK) for cytotoxicity experiments. The seeding density was increased to 8.0 x 10^3 cells/cm^2 so cells would provide 70% confluent growth surface areas within 48 hours of culture post-passage[3]. Previous seeding density experiments had identified 70% confluence to produce a cell surface coverage able to provide reproducible response in assay detection whilst ensuring that an ample growth surface availability was maintained for the duration of the assay.

[3] An indirect mechanism of nanoparticle toxicity has been reported which suggests their large surface area to volume ratio, responsible for molecular interactions, causes adsorption of medium constituents to the particle surfaces resulting in subsequent cytotoxicity associated with cell starvation Casey, A., Herzog, E., Lyng, F. M., Byrne, H. J., Chambers, G. & Davoren, M. (2008). Single walled carbon nanotubes induce indirect cytotoxicity by medium depletion in A549 lung cells. *Toxicology Letters,* **179,** 78-84.. Reduced cell confluence used here was a precautionary step to ensure sufficient nutrition was available to cells prior to addition of nanomaterials in the assay (as greater cell numbers would consume medium constituents at a greater rate during growth).

2.2.2.3.1 H376 cell treatment in 96 well plate assays

Whilst many studies have reported cytotoxicity in cell lines exposed to similar nanoparticles for longer durations (Hackenberg *et al.*, 2011b, Lison *et al.*, 2008, Motskin *et al.*, 2009, Sharma *et al.*, 2011, Shukla *et al.*, 2011, Xiong *et al.*, 2013, Yu *et al.*, 2009), a shorter time period was considered more representative of interactions between the human oral mucosa and nanomaterials subjected to model exposure with a typical oral healthcare formulation *e.g.* toothpaste. Currently, the NHS in conjunction with the British Dental Health Foundation recommend normal oral hygiene routine to involve brushing teeth with fluoride containing toothpaste for a minimum of 2 minutes, followed by a rinse with a mouthwash for 30 seconds; both occurring twice daily ((BDHF), 2013, NHS, 2013). In practice however, accurate assessment reflecting actual patient oral hygiene practices often differ between studies, demographics and healthcare product (Al-Dlaigan *et al.*, 2002, Al-Otaibi & Angmar-Månsson, 2004, Blinkhorn, 1978, Gallagher *et al.*, 2009, Kambhu & Levy, 1993). The average exposure time of a single application of a typical oral healthcare product was not thought to exceed 5 minutes daily, and this was reflected in the study design ((ISO), 2010)).

Cell media was removed prior to washing cells twice with PBS before the addition of 30μL of test material suspension. Each treatment was incubated with the cells for 5 minutes at 37°C/5% CO_2. After exposure, treatment solutions were removed before washing cells thrice in PBS, followed by replacing with culture medium. Cells were incubated for a further 24 hours at 37°C/5% CO_2 before cytotoxicity assays were performed.

2.2.2.4 Caco-2 cell tissue culture

The human epithelial cell line: Caco-2 is a colorectal adenocarcinoma derived from the large intestines. The cells were grown in monolayer as a positive control model for uptake of behaviour, widely reported for investigating adsorption of drugs administered orally (Sun *et al.*, 2008b). The Caco-2 cell line was purchased from the ATCC catalogue (LGC Standards, Queens Road, Teddington, Middlesex, TW11 0LY, UK). The cells (p.39) were maintained in culture for no longer than 10 passages as a protective step, taken to ensure that their metastatic/neoplastic phenotype would not change as a result of prolonged passage *in vitro* (Sacks, 1996).

2.2.2.5 Caco-2 culture media

Caco-2 culturing media was prepared by the addition of 10% fetal bovine serum (FBS), 2mM *L*-glutamine and 1mM sodium pyruvate (all as final concentrations) to Eagles's MEM with Earle's salt without *L*-glutamine.

2.2.2.6 Routine Caco-2 cell culture and passage

A working population of Caco-2 cells were maintained by routine growth in the same way as described for H376 cells, including freezing and thawing methods (section 2.2.2.1). The main difference between cell lines was the growth media, and seeding density. For monolayer growth in 80cm^2 plastic flasks (T-75 Thermo Scientific Nunc®, Fisher Scientific UK), Caco-2 cells were serially cultured at plating densities of 1.0 x 10^4 cells/cm^2.

2.2.2.7 Caco-2 cell growth in 96-well plates for the FM 1-43 assay

Caco-2 cells were seeded into black 96-well plates at a seeding density of 8.0 x 10^3 cells/cm^2 and incubated in culture media for 72 hours at 37°C/5% CO_2 (Sanyo-MCO715), until cells reached approximately 70% confluence.

2.2.2.8 Reconstructed Human Oral epithelium tissue model (RHO)

Matching the phenotype of the H376 cells used in monolayer screening, the non-keratinised 3-dimensional reconstructed human oral epithelium tissue model (RHO) was sourced from SkinEthic Laboratories (Lyon, France). Cultivated from the human TR146 cell line, this model is a well-differentiated keratinised carcinoma cell derived from the buccal mucosa (Rupniak *et al.*, 1985). These cells are grown on permeable membranes at the air/liquid interface, facilitate the formation of multiple layers. After 5 days (the age at which the tissues were dispatched) the RHO tissue model was expected to have 6 distinct, non-keratinised cell layers, resembling the histology of the buccal mucosa in humans (Kazmi *et al.*, 2011). Since the cells were derived from carcinoma cells, the model is then at least 10 times thinner than native healthy tissue (Rossi *et al.*, 2005, Shojaei, 1998), and not considered fully representative of the buccal mucosa. However, the multiple layers and non-keratinised morphology are expected to allow a more comprehensive and representative study into the assessment of nanomaterials (when compared against monolayer models).

2.2.2.9 EpiGingival™ tissue model (GIN-100)

Purchased from MatTek Corporation (Ashland, MA, USA), the EpiGingival™ tissue model (GIN-100) was identified as a viable, reliable commercial *in vitro* 3-D model representative of native human gingival tissue. It consists of normal human derived oral keratinocytes cultured to form 8-10 cell layers of highly differentiated tissue, with a keratinised gingival phenotype (Klausner *et al.*, 2007). Models were derived from primary epithelial tissue, sourced from non-diseased, human oral tissues obtained from patients undergoing tooth extractions. These were seeded onto collagen coated Millicell™ CM microporous membrane tissue culture inserts (Millipore Corporation, Bedford, MA) and cultured at 37 °C, 5% CO_2, 98% relative humidity for 4 days submerged in media. The cell seeded inserts were then elevated to the air-liquid interface and cultured for 7 days to promote differentiation (Klausner *et al.*, 2007). This change in growth condition mimics the environment *in situ*, and causes stratification of the apical surface that result in a fully differentiated *stratum corneum*. The cell models were shipped at 4°C, within 48 hours from MatTek laboratories USA, ready to use as a fully-differentiated human gingival 3-D tissue representative.

2.2.2.9.1 Tissue construct post-transport reception

Tissue models were delivered secured in agarose gel within 24-well plates and maintained at 4°C during shipping. The sub-optimal physiological conditions experienced during transportation were expected to cause a temporary negative impact on the health of each tissue. It was therefore recommended to allow a recovery period, for the leaching of stress products associated with the transportation process, to return the tissue models back to optimal health before use in studies (Kidd *et al.*, 2007).

Under sterile cell culture conditions, respective maintenance media for each tissue construct was pipetted into wells of a 6-well plate (Falcon™ 6-well Multiwell plate, Becton-Dickson UK) and equilibrated to 37°C/5% CO_2 (Sanyo-MCO715 incubator). The agarose gel was removed from the tissue model inserts, before transferring models into the pre-warmed media (0.9mL) and incubating for 24 hours in humidified atmosphere at 37°C / 5% CO_2.

2.2.2.9.2 Apical dosing of tissue models with materials in suspensions

Maintenance media was aspirated before washing each tissue model twice in sterile PBS and blotting dry on sterile blotting paper.

Fresh media was pre-incubated in a new 6-well plate before the addition of tissue models. These were then incubated in the fresh media at 37°C / 5% CO_2, for 1 hour prior to treatment.

Material treatment solutions (nano and bulk) were prepared as described in section below. The highest concentration of 1% w/v was used to treat the tissues, in serum-free Dulbecco's MEM/Ham's F12 basic media, without *L*-Glutamine. 5% w/v SDS was included as a cytotoxic comparison. The higher concentration was used to ensure that a severe cytotoxic response was observed in each tissue, with the concentration reflective of the current upper limit for what is accepted as an irritant but safe in existing commercially available cosmetic formulations ((CIR), 2008, Robinson *et al.*, 2010).

Treatment suspension (100µL) was applied to the apical surface of each tissue construct. Serum free Dulbecco's MEM/Ham's F12 basic media, without *L*-Glutamine was used as a negative control and Triton™-X100 (1% v/v in PBS) as the positive control (to induce cell lysis). Tissue models were incubated at 37°C / 5% CO_2 for 1 hour of exposure with the treatment solution.

Following treatment, the tissue models were rinsed in PBS by washing and inverting continuously for 20 seconds. They were then dried by dabbing insets on blotting paper and placed in new 6-well plates prefilled with 0.9mL of maintenance media. Tissues were then left to incubate at 37°C in 5% CO_2 humidified atmosphere, for 24 hours.

2.2.3 Biochemical assays

2.2.3.1 Preperation of material suspensions to test on cell models

All treatments were applied to cell models at equal concentrations to determine the effect of their interactions *in vitro*. In all experiments, nanomaterial exposures were carried out alongside non-nano (bulk) equivalent materials. These were prepared for cell work as follows.

All dilutions were prepared under aseptic conditions to ensure sterility. A stock solution was made for each test material (bulk and nano) to a concentration of 1% weight per volume (w/v) by diluting in either:

(i) Dulbecco's MEM/Ham's F12 medium, without *L*-Glutamine, termed serum free (SF) medium, due to the absence of protein.

(ii) Dulbecco's MEM/Ham's F12 medium, without *L*-Glutamine supplemented with 10% FBS v/v[4].

TiO_2-nano and the two ZnO nanomaterials (45009 and 45408) were supplied as nanoparticles in unknown liquid dispersion. These were diluted from manufacturer concentrations of 35%, 50% and 40% w/v for TiO_2, ZnO-45009 and ZnO 45408 respectively. Hydroxyapatite and SiO_2 were supplied as anhydrous nanopowders from Sigma-Aldrich, UK, as were all bulk materials, sourced commercially as powders.

All 1% w/v nanomaterial dispersions in cell culture media were vortex mixed (Fisons WhirlMixer™) before sonicating (Ultrawave U50H Sonicator) at 400watts for 10 minutes to break up any nanomaterial aggregates. Solutions were sonicated again, immediately prior to use when required for dilution to final treatment concentrations. All suspensions were stored at 4°C when not in use. When solutions were stored for an extended period of time (in excess of 5 days), sonication and vortex steps were repeated prior to further dilution.

For bulk materials, the sonication step carried out for the nanomaterials was not repeated, in an effort to avoid possible disintegration of particle sizes in solution.

[4] FBS addition was carried out immediately after sonication only. This step aims to reduce the agglomeration of proteins expected to act as biological dispersants to the nanoparticles, as reported by Bihari, P., Vippola, M., Schultes, S., Praetner, M., Khandoga, A. G., Reichel, C. A., Coester, C., Tuomi, T., Rehberg, M. & Krombach, F. (2008). Optimized dispersion of nanoparticles for biological in vitro and in vivo studies. *Particle and Fibre Toxicology,* **5,** 14.

Instead, 1% w/v suspensions were vortexed for approximately 30 seconds prior to use when required to dilute into final treatment concentrations.

Additional control substances included:

- Sodium lauryl sulphate, or sodium dodecyl sulphate (SDS). This was included in cytotoxicity studies as a well-established contact irritant that was expected to cause cytotoxicity in the *in vitro* models (Barkvoll, 1989, Coquette *et al.*, 2003, di Nardo *et al.*, 1996, Healy *et al.*, 2000). Included in oral healthcare formulations at low concentrations, it was used as a control or benchmark for currently accepted inclusion limits for irritant formulation constituents.

- Polyethylene glycol (PEG) 300 and acetic acid were also tested to evaluate their possible toxicity as both are known constituents in the dispersion formulae used by manufacturers/supplier of TiO_2 and ZnO nanomaterial products. Analysis was carried out using Fourier transform infrared spectroscopy (FTIR) and nuclear magnetic resonance (NMR). Unfortunately, the exact composition was not made available by the manufacturers, so analysis constituted the use of speculative standards against dispersive fluid separated from nanoparticles using ultracentrifugation. This crude approach did match acetic acid inclusion in TiO_2 dispersion, and a variety of PEGs in both ZnO nanomaterial products. To guard against any dispersion constituent cytotoxicity, acetic acid and PEG-300 were assessed at concentrations representative to their respective nanomaterials. Comparative analysis of these in results would ascertain whether any cytotoxicity observed was a consequence of the nanoparticles themselves, or the combined effect with dispersive constituents. This was considered an important test in relation to reporting any nano-specific cytotoxicity against their bulk counterparts.

- Zinc acetate was included to assess zinc ion release between differing forms of the metal.

For each of the additional control samples, these were treated as bulk materials and prepared in solution accordingly.

2.2.3.2 LDH assay evaluation of cytotoxicity

The Lactate dehydrogenase (LDH) assay is based on the work of Wacker *et al.*, in 1956 (Wacker *et al.*, 1956). LDH, a stable cytosolic enzyme, is found across many different cell species and is responsible for the catalysis of lactate to pyruvate with simultaneous reduction of NAD^+ to NADH. LDH is an intracellular enzyme and can only be measured upon its release following cell lysis and as such, gives an indication of loss of cell membrane integrity (Yang *et al.*, 2009). The LDH leakage into cell supernatant is measured in conjunction with a coupled enzymatic assay which results in the conversion of a tetrazolium salt (INT) into a red formazan product (Nachlas *et al.*, 1960). The amount of colour formed through this reaction can be analysed spectrophotometrically, and is proportional to the number of lysed cells. Released LDH in culture supernatants is measured using the Promega CytoTox96® Non-Radioactive Cytotoxicity Assay (Promega UK). The kit was used following an adapted method from the Promega technical bulletin (Promega, 2010).

Lysis solution (1% v/v Triton™-X100) was used to initiate lysis and provide a positive control to determine 100% LDH release from the standard number of cells in each sample. In each experiment at least one sample was not exposed to any treatment, and was instead used as a control to determine the absorbance of LDH release following full cell lysis. This was carried out by the addition of lysis solution to the control sample 45 minutes prior to the assaying of other wells, with cells maintained at 37°C/5% CO_2 in an incubator. A media only 'blank' sample (containing no cells) was also incubated to control against all background absorbance.

LDH substrate mix was prepared according to manufacturer instructions. This was added to equal volumes of cell supernatant from the respective sample of cells previously exposed to treatments 24 hours before. The reaction was carried out at room temperature away from light for 30 minutes before halting with of an equal volume of stop solution (1M acetic acid, supplied with the kit). Absorbance was read at 492nm using a spectrophotometer (Thermo Multiskan Ascent 354). Absorption was converted to a measurement of toxicity based upon the per cent total LDH released from the cell, using the following equation.

Equation 2.3 . Calculation of percent cytotoxcity from LDH release.

$$\left(\frac{((S-mean\ CF)-(\ mean\ NC-mean\ CF)\ )}{((mean\ PC-mean\ CF)-(mean\ NC-mean\ CF))}\right) \text{x } 100$$

Where: S = sample absorption

CF = average cell free blank absorbance

NC = average negative control, or non-treated healthy population absorbance value

PC = average positive control, or fully lysed cell population absorbance value.

Values greater than 50% were generally considered to be indicative of a toxic response. This equates to the median lethal dose (LD_{50}), a crude measure of acute toxicity based on the dose or concentration (LC_{50}) required to kill half the members of tested population over the given treatment time (Zbinden & Flury-Roversi, 1981).

2.2.3.3 MTT assessment of cell viability

The (3-(4,5-dimethylthiazol-2-yl)-2,5-diphenyltetrozolium bromide) (MTT) assay is a measure of cell viability. It relies upon mitochondrial reductases, present in healthy cell populations, to reduce a tetrozolium salt. In this case, MTT (3-(4,5-Dimethylthiazol-2-yl)2-5-diphenyltetrozolium bromide), a yellow compound that is reduced to a purple formazan product (Mosmann, 1983), was used. This conversion is accomplished by nicotinamide adenine dinucleotide phosphate (NADP) or NADhydrogenase (NADH), co-factors to the dehydrogenase enzymes in metabolically active cells (Berridge & Tan, 1993), with the quantity of formazan product as measured by absorbance, directly proportional to the number of living cells. MTT requires a solubilising solution to extract the formazan crystal product from inside the cells *e.g.* isopropanol.

MTT solution was prepared at a 1mg/mL concentration in supplemented culture medium without FBS, and filter sterilised at 0.2µm prior to use. It was added to samples following the removal of growth medium, 24 hours after treatment exposure. The reaction was carried out at 37°C/5% CO_2 in a dark incubator for 4 hours.

Following incubation, the MTT solution was aspirated and formazan crystals were solubilised by the addition of isopropanol to each sample. The plate was sealed with cling film, to avoid loss of solution through evaporation, and stored at 4°C overnight. Again, a sample of containing no cells was also incubated as a control against background absorption (in practice, this lane contained only extracting solution (isopropanol)).

Absorbance was read at 540nm, in a spectrophotometer (Thermo Multiskan Ascent 354). MTT absorption values were converted into cell viability percentages using the following equation:

Equation 2.4. Percent cell viability from MTT absorption.

$$\left(\frac{(S-mean\ CF)}{(mean\ NC-mean\ CF)}\right) \text{x } 100$$

Where: S = sample absorption

CF = average cell free blank absorbance

NC = average negative control, or non-treated healthy population absorbance value.

For these measurements, values lower than 50% were considered to be indicative of a toxic response (through loss of cell viability). This equates to the half maximal inhibitory concentration (IC_{50}) accepted as showing a drug or toxins ability to inhibit biological function.

2.2.3.4 MTT cell viability assay on 3-dimensional tissue constructs

Due to the more comprehensive 3-dimensional structure of the tissue models compared against monolayers, the previous method described above had to be adapted. But the fundamental assessment, linking mitochondrial metabolism of MTT to a formazan product as measure cell viability, remained the same.

A 1mg/mL syringe-filter sterilised MTT solution (300µL) was added into wells of a fresh 24-well plate (Falcon™ 24-well Multiwell plate, Becton-Dickson UK). Following the 24 hour time period after treatment exposure, tissue models were removed from the 6-well plate, dabbed on sterilised blotting paper (Fisher Scientific, UK) to remove excess liquid, before placing into the wells containing MTT solution. The 24-well plate

containing tissue samples was then incubated for 3 hours at 37°C in 5% CO_2 in a humidified atmosphere.

Tissue models were removed from each well, dried on blotting paper, before being placed into a corresponding well of a fresh 24-well plate. The wells were then filled with 2mL isopropanol to extract the formazan from the cells. The 24-well plate was covered in cling film (Fisher Scientific, UK) and sealed within a zipliock bag to reduce volume distortion by evaporation. This was then kept at 4°C overnight before colorimetric analysis of each solution at 540nm.

Over the course of the cell viability investigations, concerns arose as to the effectiveness of formazan extraction in 3-D models, especially regarding the method used with EpiGingiva™ GIN-100 tissues.

A hypothesis was proposed that either the stratified nature of the tissue models, and/or the stratum coreneum in apical cell layers; may have trapped formazan product, within the cells. Hence it was decided to investigate this further by repeating the experiment on n=2 GIN-100 models with the inclusion of an additional step following the 3 hour incubation with MTT solution (before extraction using isopropanol). Tissue models were lysed through the addition of 100μL Triton™X-100 (1% v/v) to their apical surface. Lysis was left to occur at 4°C overnight, before extracting formazan by the addition of a further aliquot of 2mL isopropanol, as carried out previously.

To determine cell viability, the formazan dissolved in isopropanol was decanted from each sample back into the well. The extracting solution was then mixed and 200μL was added to wells of a 96-well plate (Thermo Scientific Nunc® 96 Microwell™. Fisher Scientific UK) in triplicate. Results were determined after, again reading the plate at 540nm in a spectrophotometer (Thermo Multiskan Ascent 354). Cell viability was calculated as previously described, using Equation 2.4.

2.2.3.5 IL-1a enzyme linked immunosorbent assay (ELISA)

IL-1α was chosen as the initial cytokine to assess inflammation in this study. This is based on its principal role as the instigator within the oxidative stress paradigm, as described in Figure 1.4. It has also been detected effectively following tissue model response of both MatTek and SkinEthic 3-D models to different toxic stimuli (Kazmi

et al., 2011, MatTek, 2010, Moharamzadeh *et al.*, 2007, Spielmann *et al.*, 2007). Investigating IL-1α cytokine levels in both of the models used was thought to contribute towards the novelty of research, as the comparison of keratinised and non-keratinised tissue model responses to these nanomaterials has not been investigated to date.

2.2.3.5.1 Human IL-1a quantification from GIN-100 and RHO cell media supernatant

Detection of human IL-1α cytokine release using enzyme linked immunosorbent assay (ELISA) technology allowed for the rapid and reliable relative quantification in cell culture supernatant. The principals of the Quantikine® human IL-1α ELISA Quantikine® is consistent with all other ELISA tests that employ the quantitative sandwich enzyme immunoassay technique. Briefly, this involved the binding of a monoclonal antibody to IL-1α present within the samples, before the addition of a polycolonal antibody conjugated to a enzyme that would react during detection. In this case, hydrogen peroxidase was conjugated to the polyclonal antibody that yielded chromogenic conversion in colour pigment upon oxidisation. The ELISA was sensitive to the lower limit of 1pg/mL (R&D Systems Quantikine® human IL-1α ELISA kit instruction manual). Levels of IL-1α cytokine were expected to increase in response to cell injury and tissue inflammation, stimulated through cytotoxic treatments.

Cytokine levels were measured in supernatant collected from tissue models following the 1 hour treatment period *and* a 24 hour recovery incubation, carried out to as stated in the kit protocol. Analysis of both samples enabled the assessment of inflammatory response that may have occurred instantly (during 1 hour treatment exposure), or alternatively over a post-treatment period (24 hours), Samples were centrifuged to separate any cellular material, at a speed of 4000rpm/1000 x *g* (Thermo IEC Micromax) for 10 minutes.

The microplate provided in the Quantikine® human IL-1α ELISA kit was prepared by blocking any non-specific binding sites with 50µL of the assay diluent before the addition of 200µL of neat sample supernatant. Samples were run in duplicate for each experiment. Sample and assay diluent was incubated for 2 hours at room temperature, before washing all wells with 4 x 400µL volumes of wash buffer. IL-1α polyclonal antibody conjugated horseradish peroxidase (200µL) was added to each well and left to react at room temperature for 1 hour, before removal and repetition of the wash step

(for a total of 5 rinses in this instance). The substrate solution was reconstituted from two reagents in a 1:1 ratio immediately on completion of the final wash step. Substrate (200µL) was then added to all wells and left to react away from light for 20 minutes at room temperature. The reaction was stopped with 50µL of acidic 'stop solution'.

The optical density of each well was determined within 30 minutes of completing the ELISA using a spectrophotometer (Thermo Multiskan Ascent 354). Absorbance was calculated following wavelength correction of the microplate by subtracting measurements at 540nm from those at 450nm, with quantified IL-1α cytokine release of each sample calculated from the standard curve regression output of IL-1α standards (run alongside the sample in the ELISA) between 0 and 250pg/mL.

2.2.3.6 SynaptoGreen™ (FM1-43) 96-well assay for the analysis of nanoparticle uptake

SynaptoGreen™ is the trademark of Biotium Incorperated (Hayward, California USA). It is a member of the group of fluorescent dyes known as lipophillic styryl compounds. These have been utilised in a wide array of studies investigating plasma membrane trafficking, including vesicle recycling, endocytosis, exocytosis and has been widely employed by studies investigating synaptic activity (Amaral *et al.*, 2011, Betz & Angleson, 1998, Brager *et al.*, 2003, Murthy & Stevens, 1998, Rea *et al.*, 2004).

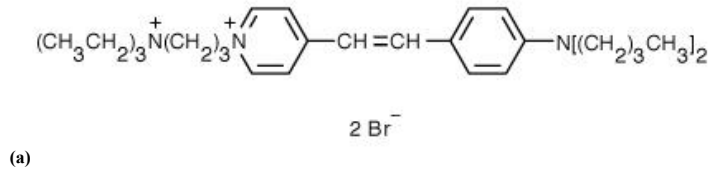

(a)

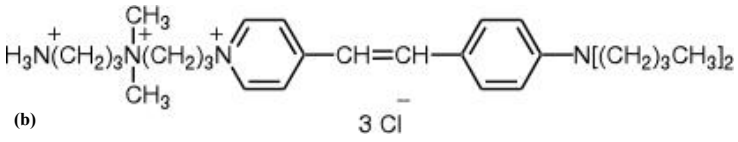

(b)

Figure 2.2. The chemical structure of (a) SynaptoGreen™ and (b) FM®1-43X both variants of N-(3-triethylammoniumpropyl)-4-(4-(dibutylamino)styryl)pyridinium dibromide, styryl dyes. *Taken from:* http://www.lifetechnologies.com/order/catalog/product/T3163

Styryl dyes are amphiphilic molecules constituting three different parts to their function. They possess a lipophilic electron-donating dialkylaminophenyl group as the tail to enable partition into cellular membranes. This is linked to a catonically charged electron withdrawing pyridinium group (the 'head'), and this stops complete molecule penetration into the cell. Both parts are joined by the body of the molecule, or the nucleus, consisting of multiple double bonds and aromatic rings that determine the dyes specific spectral properties (Betz *et al.*, 1996). The length of the styryl hydrocarbon tail determines the dissociation constant for membrane insertion. Short tails have a high dissociation constant and move fast in and out of lipids (this equates to lower staining brightness), while longer tails have a lower dissociation constant which can lead to irreversible staining. Figure 2.2 shows the structure of FM1-43 dye, with the number of hydrocarbons constituting the lipophilic tail, thought to strike a good balance between bright fluorophore signal and reversible staining that would easily washed away from non-specific cell-surface membrane attachment.

FM®1-43 is a water-soluble dye and nontoxic to cells with virtually no fluorescence in aqueous medium. Fluorescent occurs at the point of insertion of the lipophilic tail into the cell membrane. Application to the cell causes the entire outer membrane to be labelled through the lipophilic dialkylaminophenyl group interaction with the cell membrane. When internalised, quantum yield increases enormously, speculated to be attributed due to the differential qualities of solvent properties (Betz *et al.*, 1996) and vesicle pH (Simon *et al.*, 2000) between the intra- and extracellular environments. This property has resulted in the majority of studies in literature, reporting endocytosis as the preferential uptake mechanism and driven the dye to be predominantly applied as a tool in neurology, for investigations imaging synaptic vesicle recycling (Simon *et al.*, 2000). However, it is important to report studies that have also observed FM 1-43 uptake through nonspecific cation channels (Nishikawa, 2011) and even via the sodium pump (Mazzone *et al.*, 2009). }.

It was hypothesised that utilising this dye with nanoparticles to investigate uptake, would result in greater fluorescent signal for incidences of increased particle uptake. Nanoparticles uptake was anticipated to coincidentally permit entry of previously non-fluorescing FM1-43 dye, through the membrane, where it would fluoresce. Any residual dye that did not pass through the cell membrane would be washed away, together with nanomaterial particulates that were not internalised. This method is thought to be the

first application of these dyes used for detecting nanomaterial internalisation within an assay format. It was developed in both H376 and Caco-2 cell monolayers models.

2.2.3.6.1 SynaptoGreen™ reconstitution

SynaptoGreen™ powder was reconstituted to a 10mM working stock solution by dissolving in 0.2µm syringe-filtered distilled water. This was aliquoted into smaller volumes and stored at -20°C.

Aliquots were defrosted and diluted in Dulbecco's MEM/Ham's F12 basic media (phenol-red and L-glutamine free) to a final concentration of 50µM. This solution was then used to dilute the treatment material solutions to final concentrations, from the 1% w/v solutions prepared as described in section 2.2.3.1.

2.2.3.6.2 Adenosine-5'-triphosphate (ATP)

Adenosine-5'-triphosphate (ATP) has been used for its critical role in the transport of macromolecules across the cell membrane (Puckett *et al.*, 2010). It was included as a positive control substance to promote SynaptoGreen™ FM1-43 into epithelial cells because extracellular ATP has previously been demonstrated to increase incidence of macromolecule uptake in different cell types (Kao *et al.*, 2012, Sanches *et al.*, 2002), including oral and intestinal epithelium (Bertrand *et al.*, 2006, Bourke *et al.*, 1999, Bours *et al.*, 2007, Campisi *et al.*, 2010, Shojaei, 1998). These supported its use with the H376 and Caco-2 cell lines utilised here.

ATP was purchased as a crystalline solid (Sigma-Aldrich, UK) and reconstituted in 0.2µm syringe filtered dH_2O to a concentration of 100mM. It was further diluted to a stock concentration of 1mM in sterile PBS, before splitting into aliquots suitable for storage at -20°C. Aliquots were defrosted at 4°C immediately prior to use, diluted to final working concentrations from 0.25mM in FM1-43 dye/PRF cell culture media for use in the *in vitro* experiments.

2.2.3.6.3 SynaptoGreen™ FM 1-43 assay

Cultured cells were washed in ice cold HBSS before the addition of test material suspension (50µL). Bulk and nanomaterials were delivered in serum and phenol-red free culture media at room temperature, as described previously in section 2.2.3.1, with the addition of 50µM SynaptoGreen™/FM 1-43 dye. Cells were exposed to the materials for

5 minutes before the treatment solution was removed by aspiration, and washed three times with ice-cold HBSS. Serum and phenol red-free media was added to wells before fluorescence was measured using 485 ± 20nm excitation and 590 ± 35nm emission filters in a microplate reader (BioTek® Synergy™ HT).

2.2.4 Cell imagaing

2.2.4.1 H376 cell-nanomaterial interaction as observed using SEM

H376 cells incubated with nanomaterials were investigated using SEM to identify changes in cell morphology as a result of nanoparticle-cell interaction. In addition, this method was used to compare nanoparticle characteristics when in a biological environment to the observations concluded from the previous chapter.

2.2.4.1.1 Growth on Thermanox™ cover slips for SEM

H376 cells were grown on 13mm diameter, circular Thermanox™ cover slips (Agar Scientific Ltd) within 6 well plates (Falcon™ 6-well Multiwell plate, Becton-Dickson UK). These were sterile cell culture treated polyolefin polymer cover slips, used for direct attachment (post treatment and post fixing of cells) to high purity aluminium SEM stub (Agar Scientific Ltd., UK) ready for SEM analysis.

Cells were seeded at a density of 8.0 x 10^3 cells/cm^2 and maintained in culture as before (2.2.2.2). Culture medium was changed daily until the cell population adhered to each coverslip was observed at 70% confluence. Cells were exposed to 0.125% w/v concentrations of treatments, delivered as described above in 2.2.2.3.1.

2.2.4.1.2 H376 sample fixation

Post treatment and incubation, cell coated Thermanox™ cover slips were rinsed twice in PBS then fixed in 5% v/v glutaraldehyde in 0.1M sodium cacodylate buffer (pH 7.4) by immersion at 4°C for 2.5 hours. Excess glutaraldehyde solution was removed via washing coverslips three times in 0.1M sodium cacodylate buffer at pH 7.4. This washing step was continued with 5 further rinses of coverslips immersed into fresh aliquots of 0.1M sodium cacodylate buffer pH 7.4 (changed every 15 minutes) maintained at 4°C. Preceding the final rinse, samples were left in 0.1M sodium cacodylate buffer at pH 7.4 for 48 hours at 4°C.

Samples were dehydrated prior to SEM analysis, by 60 second immersions into a graded ethanol series (5%, 10%, 20%, 50%, 80% and 100% v/v).

Prior to imaging, samples were freeze-dried (Christ® Alpha labs 2-4) under vacuum (0.42mbar) for 2-3 hours; then coated with a 4nm layer of platinum using the Q150T ES Turbo pumped sputter coater (Quorum Technologies Ltd., UK). Platinum was used to increase the ability of the biological material in the sample to emit secondary electrons from the microscope beam, thus reducing the accumulation of charge at the surface which distorts image quality (Brunk *et al.*, 1981).

2.2.4.1.3 Image analysis using SEM

SEM imaging was performed using a Zeiss sigma field emission gun scanning electron microscope (Carl Zeiss Ltd. UK). An EHT voltage of 5kV was used with a working distance of 8mm to acquire images between 5K and 250K times magnification.

2.2.4.2 FM®1-43FX confocal laser scanning microscopy

FM®1-43FX membrane probe is a derivative of the SynaptoGreen™ FM1-43 membrane probe that has been modified to contain an aliphatic amine (Figure 2.2). This makes it more compatible with aldehyde-based fixatives used in histology, such as 4% formaldehyde used to preserve the cell monolayers in this study.

2.2.4.2.1 Monolayer cell culture on coverslips

Coverslips were sterilised using an autoclave at 121°C for 15-20 minutes (Prestige™ Medical 2100 Classic). Once cooled, they were placed inside a 6-well plate and coated with FBS before incubation at 37°C for 2 hours to pre-treat their surface ready for cell culture. FBS was removed by aspiration, before seeding H376 cells at 8.0 x 10^3 cells/cm^2 and Caco-2's at 1.0 x 10^4 cells/cm^2. Plates were incubated at 37°C/5% CO_2 for 48 hours, or until 70% confluence was reached.

2.2.4.2.2 FM® 1-43FX measured particle uptake in cell monolayers

Media was removed and wells washed twice in HBSS. 1mL of bulk or nanomaterial was suspended at a concentration of 0.125% (w/v) in 50μM FM®1-43FX/serum and phenol red-free culture media. Exposure to cells was carried out for 5 minutes and samples incubated at 37°C/5% CO_2. Treatment solution was removed from wells before

carrying out three washes with ice-cold HBSS. Cells were fixed with 500µL 10% formalin for 30 minutes at room temperature. Samples were then rinsed with PBS to remove excess formalin. 25µL of 1µg/mL tetramethyl-rhodamine B isothiocyanate (TRITC) conjugated phalloidin diluted in PBS was used to stain the cellular cytoskeleton, for 1 hour in the dark before rinsing in PBS. Coverslips were mounted on microscope slides using Fluoroshield™ with the nuclear stain DAPI.

2.2.4.2.3 Confocal laser scanning microscopy

Confocal images were obtained using a Leica TCS SP5 confocal laser scanning microscope system. Samples were viewed using a 63 times magnification oil immersion lens with zoom factor 2 to form combined sequential images at 126 times magnification. The 405 diode excited DAPI at 405 nm with emissions collected from 415-485nm; the argon laser excited FM1-43 dye at 458nm, with emissions collected from 487-540nm before a helium-neon laser was used to detect TRITC-phalloidin by excitation at 543nm and emissions between 556-653nm.

2.2.4.3 3-D tissue model preparation heavy metal staining for TEM imaging

Nanomaterial internalisation was assessed using both the SkinEthic RHO and EpiGingiva™ GIN-100 3-D models. This involved treating the tissues as stated in section 2.2.2.9.2, before preparing thin sections suitable for TEM anlysis that allowed cross-sectional observation through the tissue cell layers.

2.2.4.3.1 3-D tissue treatment

Both MatTek EpiGingiva™ GIN-100 keratinised tissue models, and SkinEthic RHO non-keratinised models were treated with test ZnO materials as described in section 2.2.2.9.2. Following the 24 hour post-treatment exposure period, tissues were carefully removed from the insert by hand, using a scalpel. Each tissue model was sliced in half vertically, to expose the inner cells of the tissue, before fixing in 5% glutaraldehyde dissolved in 0.2M sodium cacodylate buffer at pH 7.4.

2.2.4.3.2 Heavy metal staining

After fixing in 5% glutaraldehyde for 2.5 hours, the following procedure was kindly carried out by Dr Julian Thorpe at The University of Sussex (Sussex Centre for

Advanced Microscopy, John Maynard Smith Building, Falmer, Brighton, BN1 9QG). Epithelial tissue models were initially post-fixed in 1% osmium tetroxide dissolved in 0.2M sodium cacodylate buffer at pH 7.4, for 4 hours. They were subsequently dehydrated in an ethanol series, passed through the transition solvent propylene oxide and embedded in TAAB Low Viscosity resin (TAAB Laboratories Ltd., Aldermaston, UK). Thin (100nm) sections were cut on a Leica Ultracut ultramicrotome (Leica Microsystems Ltd., Milton Keynes UK), collected on nickel support grids and post-stained in 2% aqueous, 0.22μm-filtered uranyl acetate for 1 hour and subsequently lead citrate for 20 minutes.

2.2.4.3.3 TEM analysis of nanoparticle uptake

In attempt to locate instances of nanoparticle uptake TEM was carried using a Hitachi-7100 (Hitachi High-Technologies Europe GmbH) TEM at 100kV and images acquired digitally with an axially-mounted (2K X 2K pixel) Gatan Ultrascan 1000 CCD camera (Gatan UK, Oxford, UK).

2.2.5 Statistical analysis

Any significant difference in values were reported after checking data for normality, and carrying out a one-way ANOVA with Tukey's post-hoc test, using the PASW 18 (v.18.0.0) statistics package (IBM SPSS software, USA).

Significance was identified by a *P* value lower than 0.050, and the degree of significance are also indicated on figures where appropriate.

Non normalised data were improved by logging data, and accepted for two-way ANOVA with Tukey's post-hoc test, using the PASW 18 (v.18.0.0) statistics package (IBM SPSS software, USA). This was chosen over non-parametric tests when certain criteria were fulfilled:

- The majority of other results in the comparison set were normal (indicated by Kolmogorov-Smirnov *P* values greater than 0.050).
- The data set was large with only a few outliers.
- No left or right skews were observed on normal Q-Q plots of standard residuals.

To guard against improper reporting of marginal significance in results with non-normalised data, *P* values were adjusted using the Bonferroni Correction (the significance level / n).

3 CHARACTERISATION OF MATERIALS

The metal oxides investigated in this study are all currently utilised in oral healthcare products in bulk form (Allaker, 2010, Khataee & Kasiri, 2010, Tschoppe *et al.*, 2011). Whilst regulation dictates the stringent grade and purity necessitated for ingredients utilised in these formulations, industry often requires large volumes of chemical materials to mass produce products for commercial markets. Therefore, the materials investigated here have been sourced from industrially relevant commercial suppliers. Specific nanomaterial characteristics are known to be governed by the level of control exerted on certain parameters during their production (Skapin *et al.*, 2007) *e.g.* particle size linked to temperature and pH of reaction during synthesis (Choo *et al.*, 2002, Dixon *et al.*, 2012). As manufacturing conditions were unknown for the commercially sourced materials used in this study, characterisation was thought a necessity, to provide some level of quality control and to determine the exact starting state of each nanomaterial. In addition, characterisation was carried out to fully evaluate the interaction between the structure-function properties of a nanomaterial and any effects these might have in biological environments. This was important, both for understanding the change in properties as particle size moves away from that of the bulk material, and in identifying individual characteristics responsible for any specific nano-scale effects exerted in the cellular environment. Therefore, characterisation methods should ideally be designed to replicate *in situ* conditions as closely as experimentally possible.

The aim of this chapter is then to accurately determine the characteristics of each of the nanomaterials, investigated for putative improved properties in future healthcare formulations. Where possible, characteristics were compared directly to bulk composites, to identify and assess the potential novel properties that may arise from differences in the nanoparticle form. Identification of specific attributes are compared to the literature, in an attempt to extrapolate potential effects exerted by the nanomaterial *in vitro*. Characterisation can be achieved through the utilisation of an array of different techniques that encompass multiple analyses. These were combined to generate data that could be critically reviewed. The appropriateness of this method of application with these materials is used to establish profiles of each nanomaterials individual characteristics. Moving forward, these can be used to better understand their behaviour in cell culture media formulations and effects of exposure to *in vitro* models, representative of cell and tissue types relating to the human oral mucosa.

Through the application of analytical (dynamic light scattering, nanoparticle tracking analysis) and visual imaging techniques (electron microcopy) the size, shape, crystallinity and surface composition of each nanomaterial can be observed in direct comparison to bulk (non-nano) counterparts. It was anticipated that imaging techniques, at low magnification, would also show the natural aggregation behaviour of each material to compliment additional data generated from nanoparticle size analysis. Utilising multiple sizing techniques, alongside zeta potential and pH measurement enables investigation into nanoparticle size across a range of environments: from distinct nanoparticle chemical compounds to their formulation in biocompatible dispersions, both at room and physiological temperatures.

3.1 Results

The following results were determined from the methods described previously. Results encompass multiple techniques used to comprehensively characterise each material, from starting state, to changes that may have occurred under conditions representative of the human oral mucosa.

3.1.1 SEM analysis of particle size and morphology

This section utilised the high power detailed imaging of SEM to enable individual particle size, morphology and surface appearance to be distinguished.

Figure 3.1 shows low magnification micrographs that provide an overview of the natural particle state in agglomerates, to contextualise observations drawn from individual particles imaged at higher magnification. At this magnification, hydroxyapatite displayed the most notable disparity between bulk and nanomaterial particle-particle interactions. The bulk material formed groups of particles in distinct domes with a rough mottled surface appearance measuring between 4μm and 30μm in diameter. Nanomaterial hydroxyapatite, however, formed flatter, more irregular shaped particle groupings very much on the micron scale of size measurement (the largest measuring in excess of 60μm). Both forms of hydroxyapatite material displayed relatively tight clusters of particles together; suggesting that particle-particle attraction was favoured over a loose distribution of particles that otherwise would have more evenly covered the surface of the SEM sample stub. These nanomaterials were therefore considered as agglomerates[5].

SiO_2 material was very similar in appearance to the nano-hydroxyapatite with regard to bulk and nanomaterial particle agglomeration. It was difficult to draw comparisons between both TiO_2 and ZnO respective bulk and nanomaterial compositions at this scale. This was in part due to the smooth surface after drying that had formed in nanomaterial samples prepared from dispersions being different to bulk powders.

[5] The term 'agglomerates' is used here to differentiate between the term 'aggregate' which is used in incidence of a permanent change to the material. As the degree of permanency was currently unknown, agglomerate was deemed more appropriate.

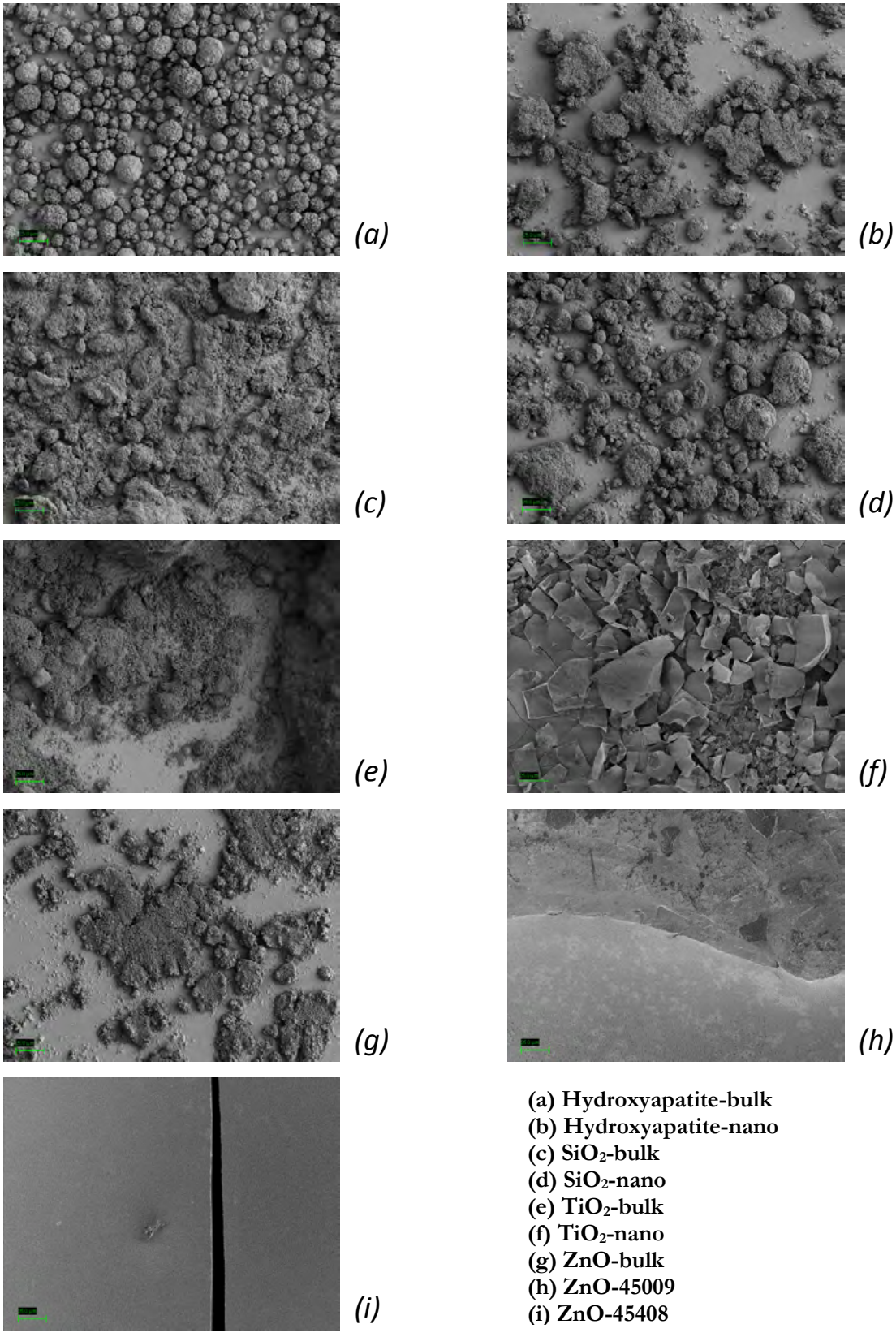

Figure 3.1. SEM images 1,000X magnification of particles (bulk and nano) in typical agglomerates, as observed by imaging their distribution spread across the aluminium specimen stub. *Scale bar = 25μm.*

Scanning electon micrographs taken at 100,000X magnification better displayed the morphology and sizes of individual particles in each sample. This enabled identification of specific nano-characteristics when comparing bulk and nano particles. Figure 3.2 shows hydroxyapatite material demonstrating the greatest disparity between bulk and nanomaterial, with the bulk having a heterogeneous population of different shaped and sized particles, all with sharp angular edges producing a crystal-like appearance. The irregular shapes and sizes demonstrated rod-like particles alongside those of a more spherical nature, comprising a wide range of sizes to be measured dependent upon the dimension orientation that was sized. The majority of particles measured in excess of 100nm, but the presence of a secondary population, observed as nanoparticle, was also noted. Conversely, the hydroxyapatite nanomaterial sample was mainly formed by uniformly-shaped nanoparticle spheres interjected by the presence of much larger 'bulk-scale' spheres. The regularity of both particle-types within the nanomaterial sample, gave rise to a distinctly bi-modal particle population, different from the bulk material.

In contrast, both forms of SiO_2 material were observed to be very similar in appearance, with no major difference between bulk and nanomaterial. Individual particle morphology was difficult to interpret due to the small size of particles at this magnification, with both bulk and nanomaterial samples comprised solely from nanoparticles (<100nm).

Figure 3.2 enabled a good comparison between the scale differences observed for TiO_2 bulk materials over the much smaller nanoparticles observed in the nanomaterial sample. Particle morphology was uniformly spherical in both materials, with size of particle providing the sole difference between samples (mean values of 28.5nm $\pm$ 9.8nm and 183.2nm $\pm$ 73.9nm were recorded for nano and bulk TiO_2 particles, respectively).

Size differences between bulk and nanomaterial samples were also evident for ZnO, which shared similarly diverse particle morphologies across all three forms of the material imaged. ZnO particles, whether in bulk or nano-form, were very different from spherical entities observed for other materials. Formed partially of short, flat-faceted granular particles, these were interspersed alongside long, thin, spindle-like rods to produce a highly non-uniform, polydispersed sample. In the heterogeneity displayed, the only common characteristic between ZnO materials was the predominantly flat, straight edges of their particles. The main difference between bulk and nano forms of ZnO was deemed to be the greater frequency of much larger particles present in bulk

samples only. However, small particles were present within bulk ZnO material, with at least one or more dimension measuring less than 100nm in length and so conforming to nanoparticle definition. The majority of particles present within the samples of ZnO-45009 and 45408 conformed to the same nano-size range. However, no notable difference could be observed between the two nanomaterials, from micrographs taken at this magnification.

The further increased resolution at greater magnification (300,000X) used in Figure 3.3 (below), allowed for even greater dissemination between individual particles of bulk and nanomaterials. They confirmed the observations of particle morphologies reported at 100,000X magnification (Figure 3.2), including disparity between bulk and nanomaterial particle sizes, for all materials except SiO_2. At 300,000X magnification, individual SiO_2 nanoparticles could be depicted. Observations support size measurements made at lower magnification, whilst also depicting the similarities shared by both bulk and nanomaterial particle morphology: roughly spherical, granular nanoparticles.

In addition, the increased resolution enabled accurate observational analysis of surface properties, such as relative surface areas and porosity. These are important characteristics that govern increased particle surface reactivity, reported for nanomaterials. No nano-pores were visible on the surface of particles for any material, but, sub-100nm gaps were noted between hydroxyapatite and TiO_2 nanoparticle agglomerates, as well as both SiO_2 composites.

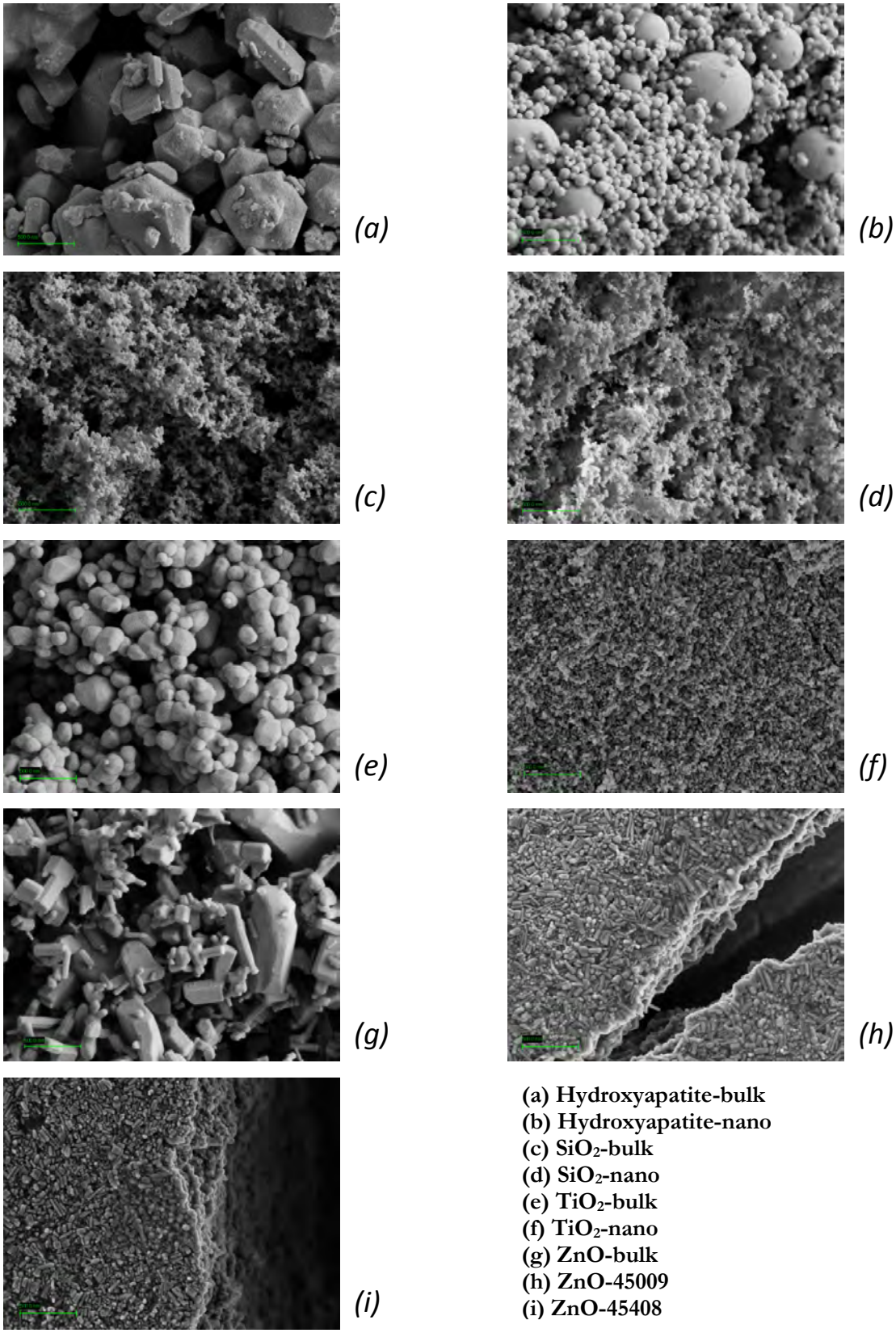

Figure 3.2. SEM images 100,000 X magnification of all particles (bulk and nano) investigated for their interest within oral healthcare. Size, shape, surface appearance and to some extent, particle-particle interaction' can all be observed at this magnification. *Scale bar = 500nm.*

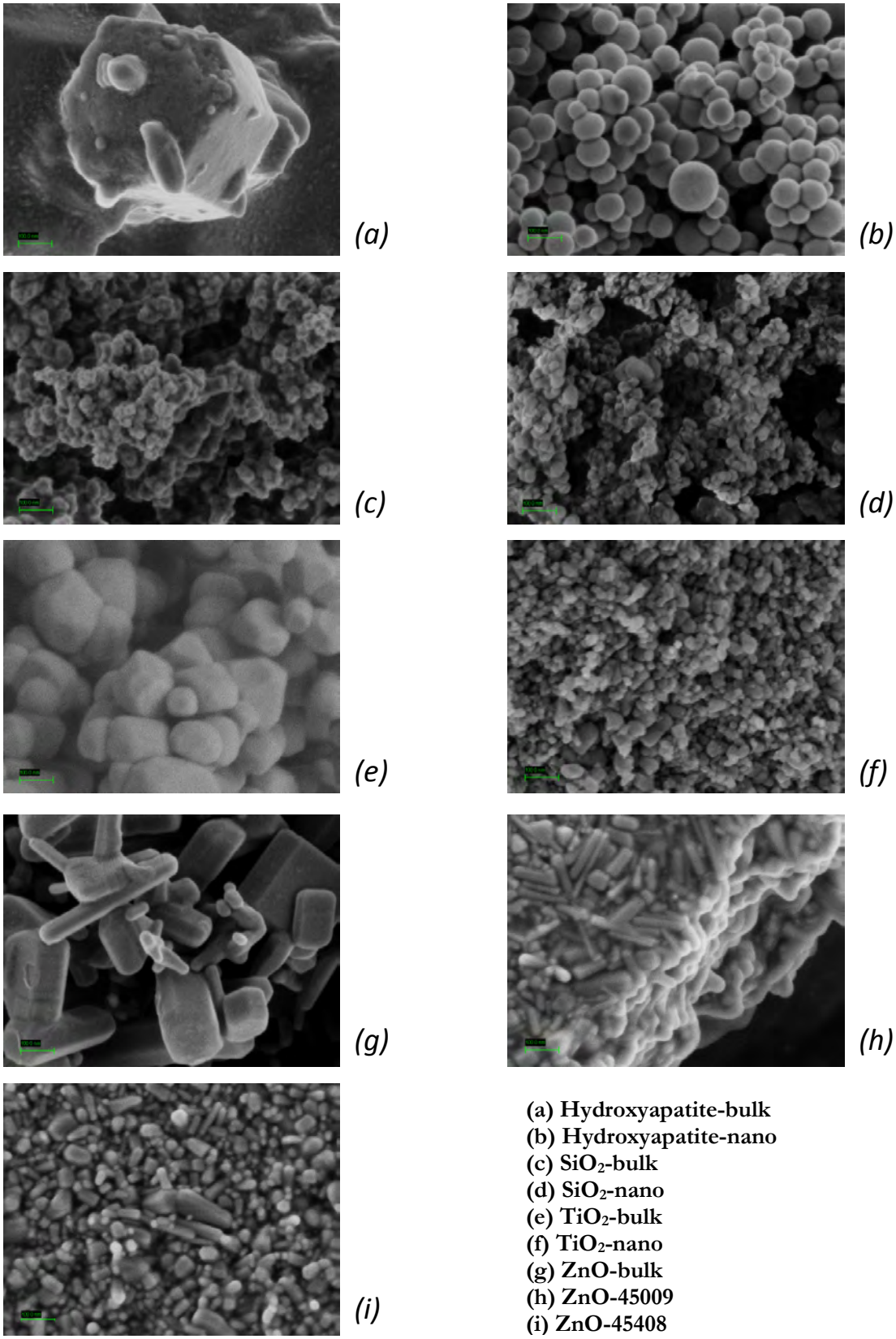

Figure 3.3. SEM images 300,000X magnification of all particles (bulk and nano) investigated for their interest within oral healthcare. The precise dimensions and surface characteristics of each particle can be observed at this high magnification. *Scale bar = 100nm.*

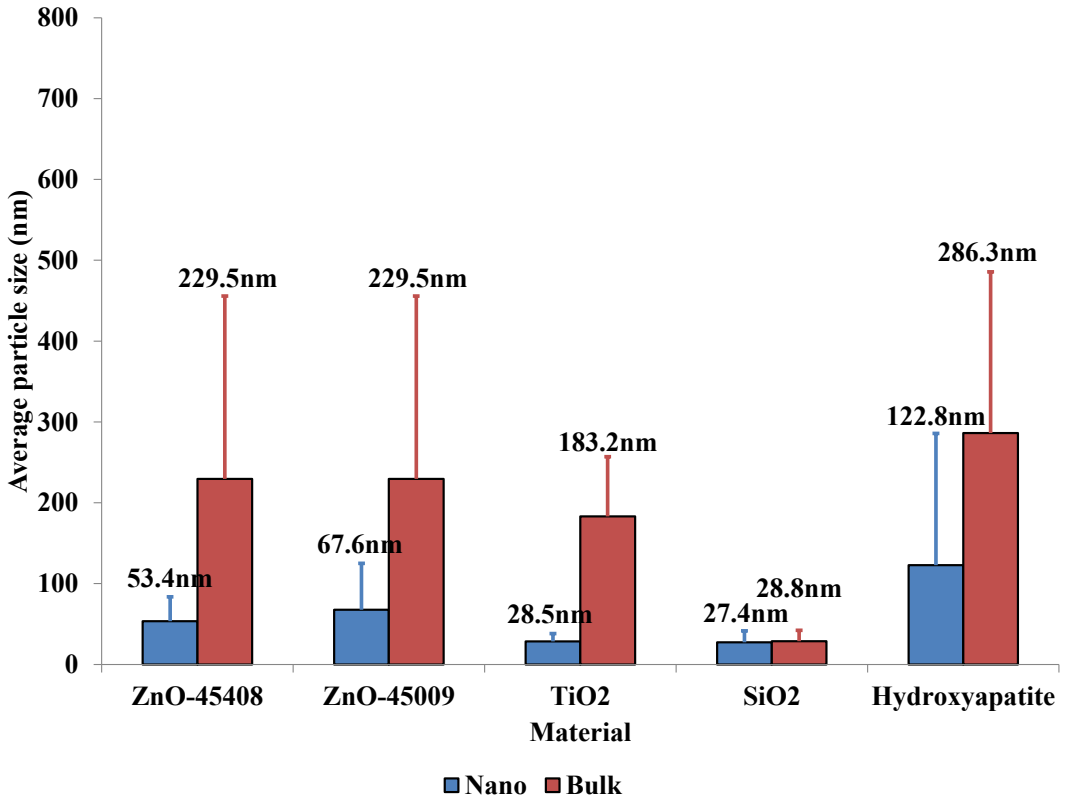

Figure 3.4. Mean particle sizes of both nano and bulk materials measured from SEM images taken between 1,000 and 100,000 times magnification. Particle size was calculated by averaging the measurements of 30 different particles, selected at random by dividing images from 3 different magnifications into sectors, taken from 3 different areas of sample (n=3). *Error bars show the standard deviation (S.D.).*

Observations described for the SEM images in Figure 3.2 and Figure 3.3 supported trends measured through particle-by-particle sizing using the SEM micrographs collected and recorded in Figure 3.4. All bulk materials had a larger mean particle size when compared to their nanomaterial equivalents. SiO_2 material was the only exception, with a mean particle size measured from bulk form, as less than 100nm. At 28.76nm (± 13.5nm), this material cannot be considered a true bulk variation, due to the similarity in average size closer to the distinct nanomaterial product (measured at 27.36nm ± 14.1nm) than above the 100nm nano-threshold cut off.

It was noted that both ZnO and hydroxyapatite bulk materials exhibited a high standard deviation in particle measurements. This was explained by the presence of very large (>500nm) and nano-scale dimensions (<100nm) particles, measured in the respective SEM images.

The hydroxyapatite nanomaterial sample has a large standard deviation in particle sizes of ± 163.1nm, with the mean particle size measured exceeding the 100nm definition of a nanoparticle. The disparity in size between the larger spheres and the nanoparticles observed in Figure 3.2 (b), perhaps explains the standard deviation exhibited by nanoparticle sizing here. However, it was still considered a nanomaterial based upon the total number of particles, measuring less than 100nm exceeding 50% of the total sample population ((EU), 2011, (SCENIHR), 2009).

Overall, the mean measurement in nanomaterial particle sizes recorded using SEM were ranked, and closely followed the order expected from manufacturer information (Table 2.1):

Hydroxyapatite > ZnO-45009 > ZnO-45408 > TiO_2 > SiO_2.

3.1.2 TEM analysis of particle size and morphology

Similarly to SEM, TEM enabled analysis of shape and size of particles. In addition, it provided verification to other particle sizing methods employed during characterisation through comparisons with SEM, including the potential for agglomeration behaviour that may result from sample preparation in solvent (ethanol). This is shown below, in Figure 3.5. Combined with information from low magnification SEM, these micrograhs weres expected to aid explanations in results observed through DLS and NTA size analysis (also carried out on dilutions of sample dispersed in solutions, including ethanol).

At increased magnification individual particle morphology was more evident amongst the structure of agglomerates that formed (Figure 3.6 and Figure 3.7). In all samples, TEM analysis of particle morphology supported the observations described from SEM micrographs. Disparity was observed between the crystal-like hydroxyapatite bulk particles and the obviously spherical nanomaterial hydroxyapatite. A similar granular appearance was seen in both forms of TiO_2 material that only differed in particle diameter and number of particles. ZnO materials displayed heterogeneous particles across all forms, which were observed agglomerating in different ways across the different samples.

Particle morphology of SiO_2 bulk material proved difficult to accurately observe at 75,000X magnification (Figure 3.6) due to the small size and lack of contrast evidenced in TEM micrographs. At a similar magnification, the nanomaterial form also proved difficult to observe in terms of individual nanoparticle structures. But evidence of their branched, chain-like agglomeration was noted from the high magnification (350,000X) micrographs (Figure 3.7).

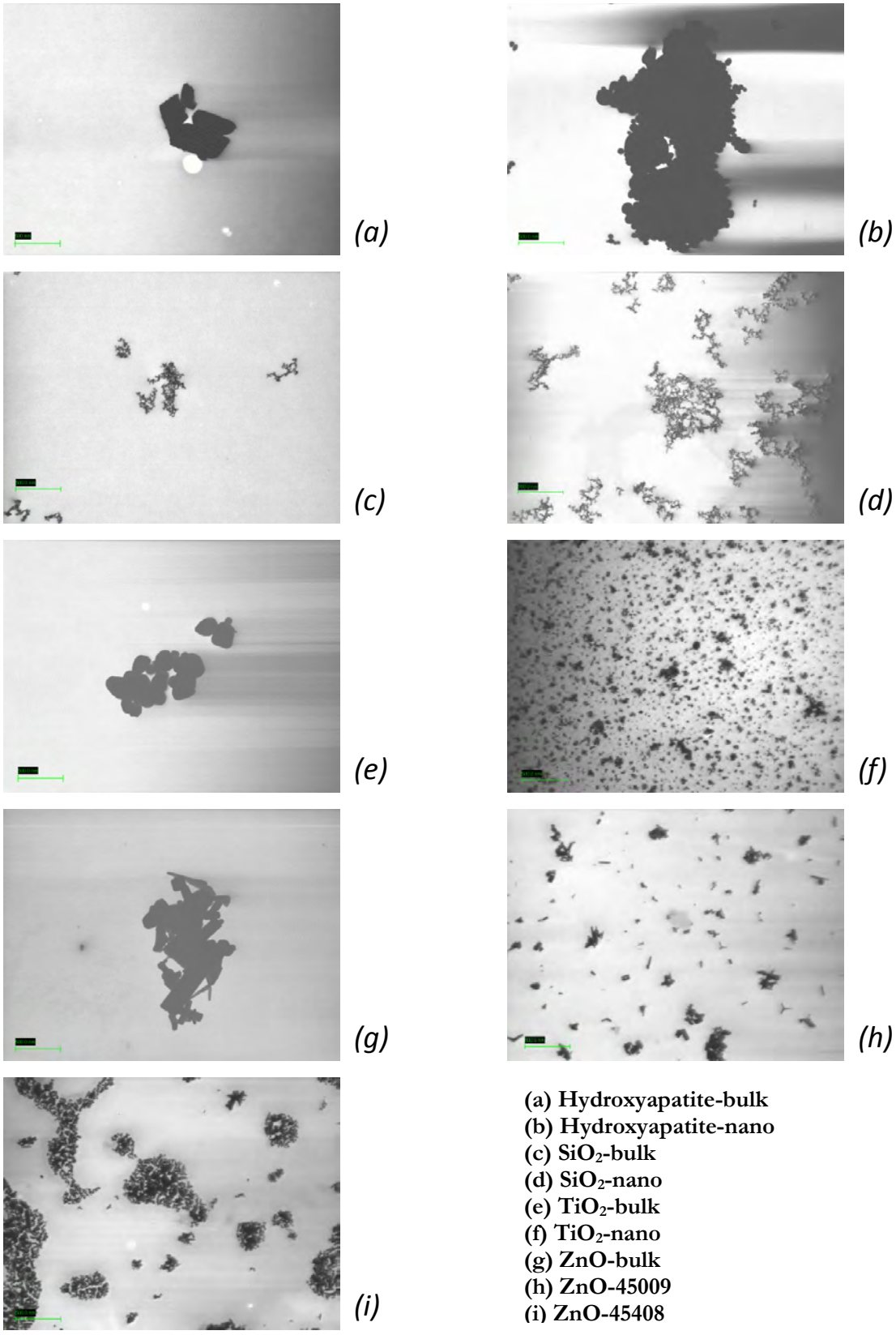

Figure 3.5. TEM images 80,000X magnification of particles (bulk and nano) in typical agglomerates, spread across the formvar coating on the copper grid. *Scale bar = 500nm.*

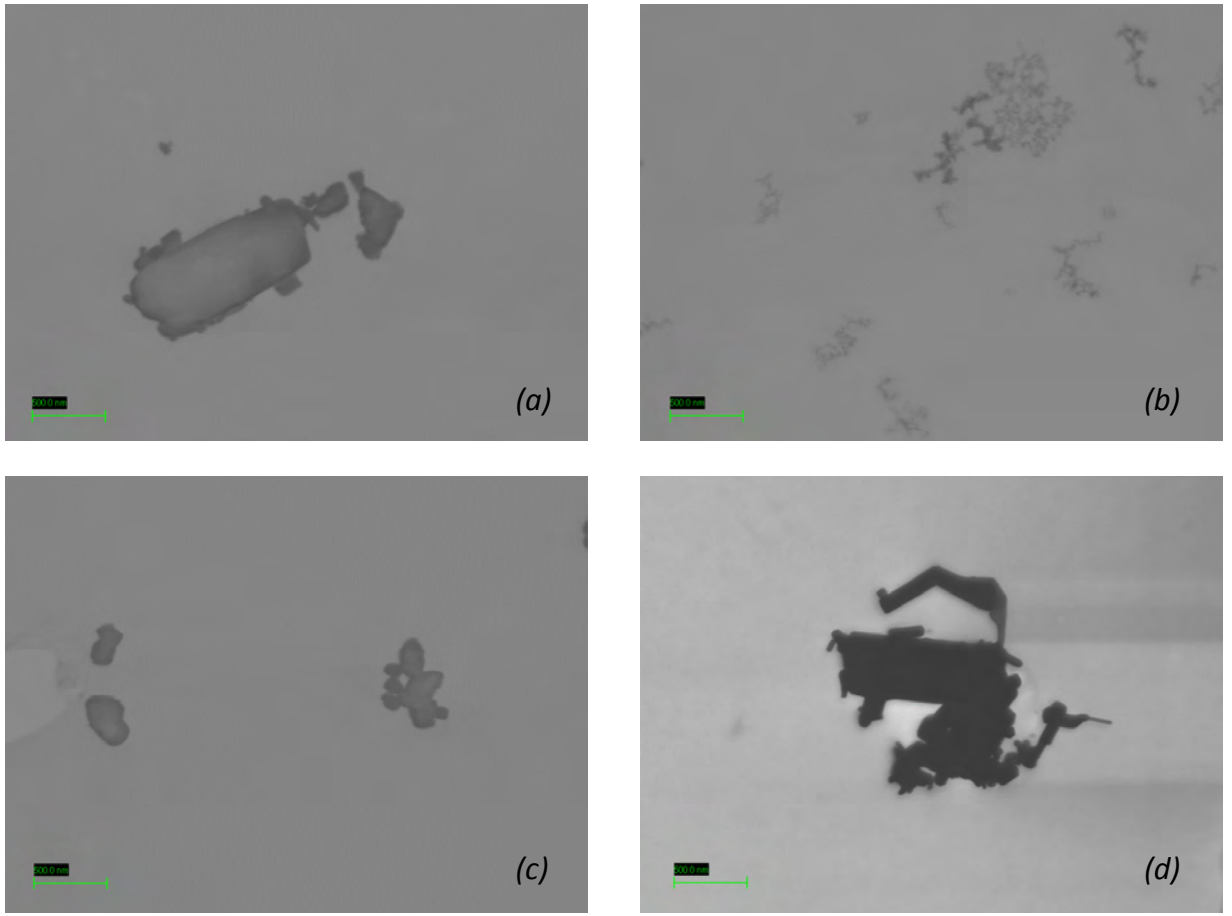

Figure 3.6. TEM images at 75,000X magnification of bulk-sized particles included as control materials for comparisons of nano-sepcific properties of nanoparticles of the same chemicals. Size and shape can be made out at this magnification, along with agglomeration tendency of the material and approximate particle concentration when dispersed in ethanol. *Scale bar = 500nm.* ***(a) Hydroxyapatite-bulk, (b) SiO_2-bulk, (c) TiO_2-bulk and (d) ZnO-bulk.***

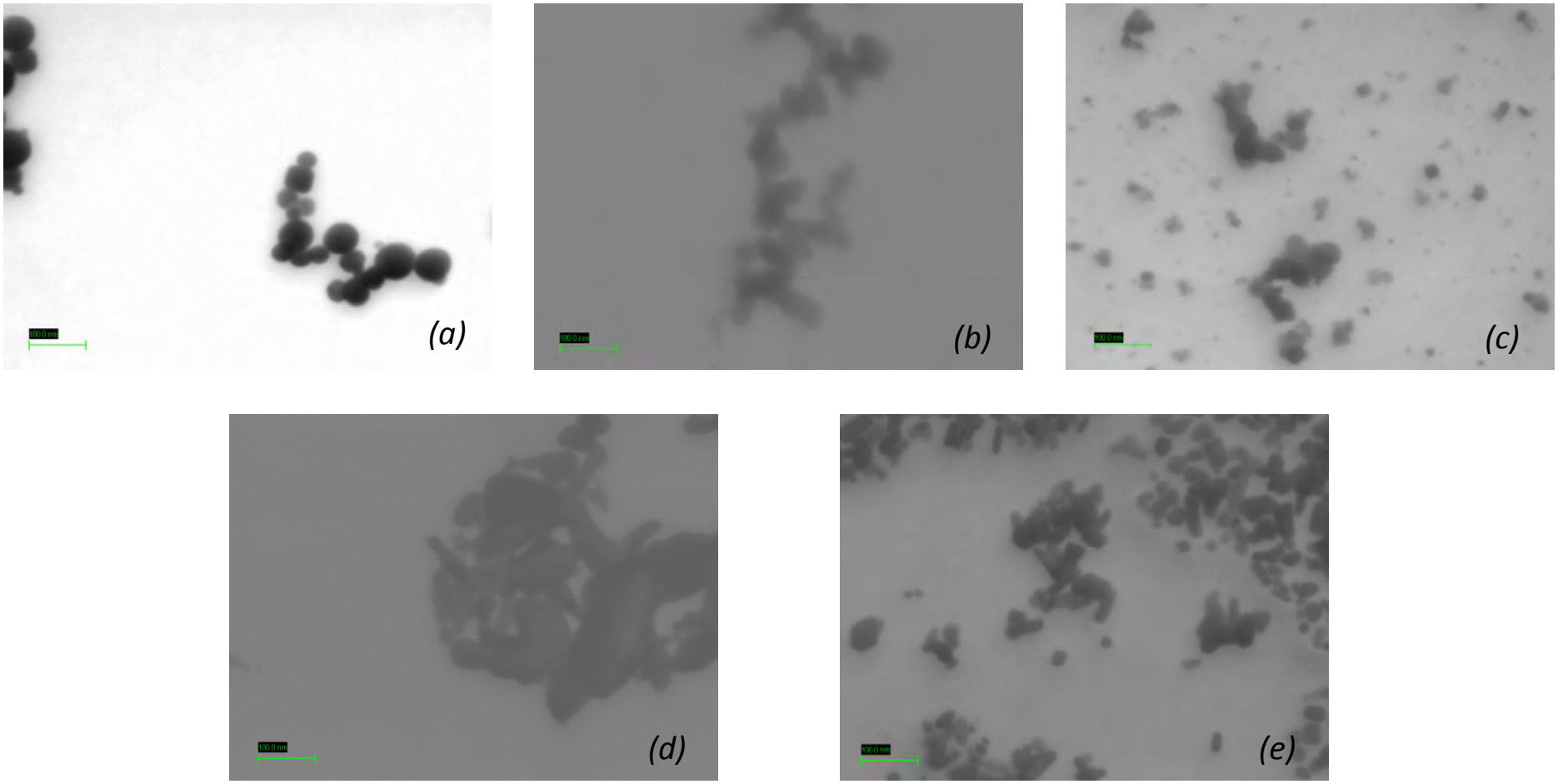

Figure 3.7. TEM images at 350,000X magnification of nanoparticles investigated for potential use within oral healthcare formulations. Size and shape can be made out at this magnification, along with agglomeration tendency of the nanomaterial and approximate particle concentration when dispersed in ethanol. *Scale bar = 100nm.* ***(a) Hydroxyapatite-nano, (b) SiO_2-nano, (c) TiO_2-nano, (d) ZnO-45009 and (e) ZnO-45408.***

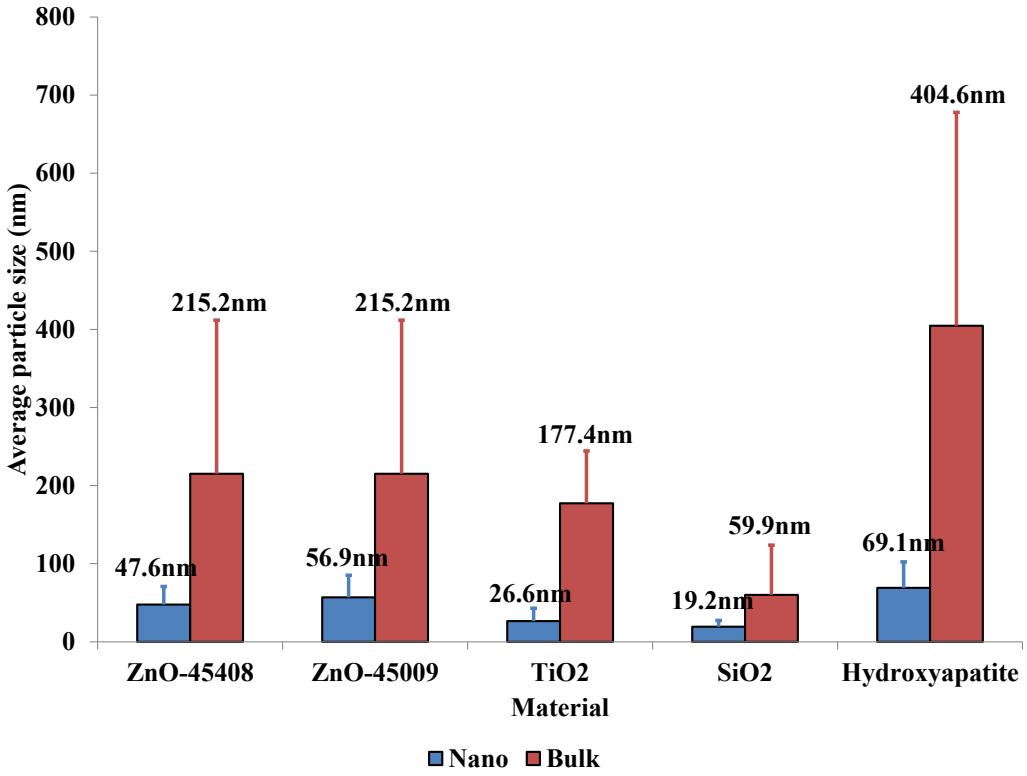

Figure 3.8. Mean particle sizes of both nano and bulk materials measured from TEM images taken between 3,000 and 180,000 times magnification. Particle size was calculated by averaging the measurements of 30 different particles, selected at random by dividing images from 3 different magnifications into sectors, taken from 3 different areas of sample (n=3). *Error bars show the standard deviation (S.D.).*

Size measurements from TEM recorded in Figure 3.8 differ from those calculated by SEM. Most notable was the increase in mean particle size for SiO_2 bulk material. This result was larger and recorded a greater standard deviation (59.9nm ± 63.8nm) when measured from TEM micrographs. Despite the increase, the mean particle size was not large enough to exceed the 100nm threshold used to define a nanomaterial. Thus, SiO_2 bulk particles were again considered within the nanoscale size range.

Hydroxyapatite nanomaterial particle size (69.1nm ± 33.3nm), indicates more evidently the sample being formed of 'nanoparticles' when measurements were taken from TEM micrographs (compared against SEM analysis). Hydroxyapatite material showed the greatest disparity between bulk and nanomaterial particles sizes.

ZnO-45009, ZnO-45408 and TiO_2 nanomaterials, were all measured to be within the nano-scale and with smaller standard deviations recorded from TEM micrographs when compared against SEM. This reflects the disparity in particle sizes recorded in

Figure 3.8, between nanomaterial and bulk particle mean sizes. However, overall results of particle sizes measured across both electron microscopy techniques were similar. This included the ranking of nanomaterial particle sizes from TEM micrographs to match that recorded from SEM analysis (from largest to smallest):

Hydroxyapatite > ZnO-45009 >ZnO-45408 > TiO_2 > SiO_2.

3.1.3 EDS analysis of chemical composition

EDS was carried out to confirm the elemental composition of the materials, thereby acting as a quality control check against the manufacturer specifications given for each material. The X-ray signal was measured as number of counts per second in electron volts (cps/eV) detected, and configured as peak area by the AZtec (version 2.0) software (Oxford Instruments, UK). This allowed semi-quantitative comparisons to indicate the quantity of a particular element in relation to other constituents in the same sample, although not in terms of a definitive mass.

Elemental analysis results confirmed the expected chemical composition for each of the materials, in both bulk and nano forms. Constituent peak intensities relating to elemental signal were higher for bulk materials over nano forms, likely linked to the greater abundance of sample (as was visible in the corresponding SEM image).

Carbon and platinum were detected in all samples in small amounts. These elements were considered contaminants from previous sample analysis. Platinum, due to sputter coating commonly carried out to prevent accumulation of charge on some sample surfaces, and carbon from the adhesive used to attach the sample to SEM stub.

Aluminium was detected as background from nanomaterial dispersions dried directly on the SEM sample stub (Figure 3.11 and Figure 3.12). Trace levels of sulphur (Figure 3.10), potassium (Figure 3.11) and sodium (Figure 3.10 and Figure 3.12) were also noted which may be residual artefacts from particle production processes or nanomaterial dispersants.

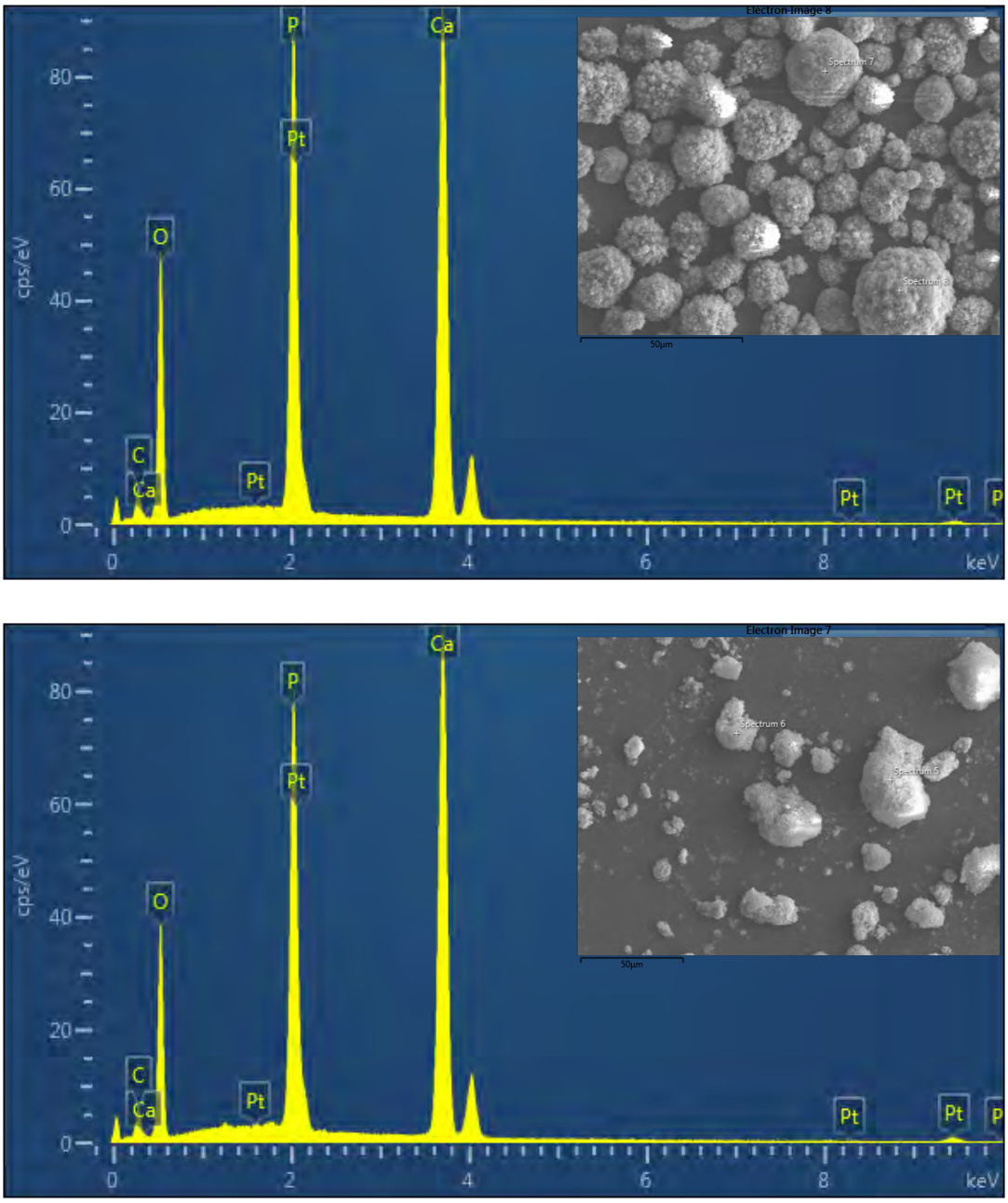

Figure 3.9. EDS spectra of Hydroxyapatite ($Ca_5(OH)(PO_4)_3$) material (top) bulk, (bottom) nanoparticle using the 80mm² X-max silicon drift detector (Oxford instruments, UK) integrated with the Carl Zeiss FEG-STEM system, set-up to take SEM images (shown).

C = Carbon, Ca = Calcium, O = Oxygen, P = Phosphorus and Pt = Platinum.

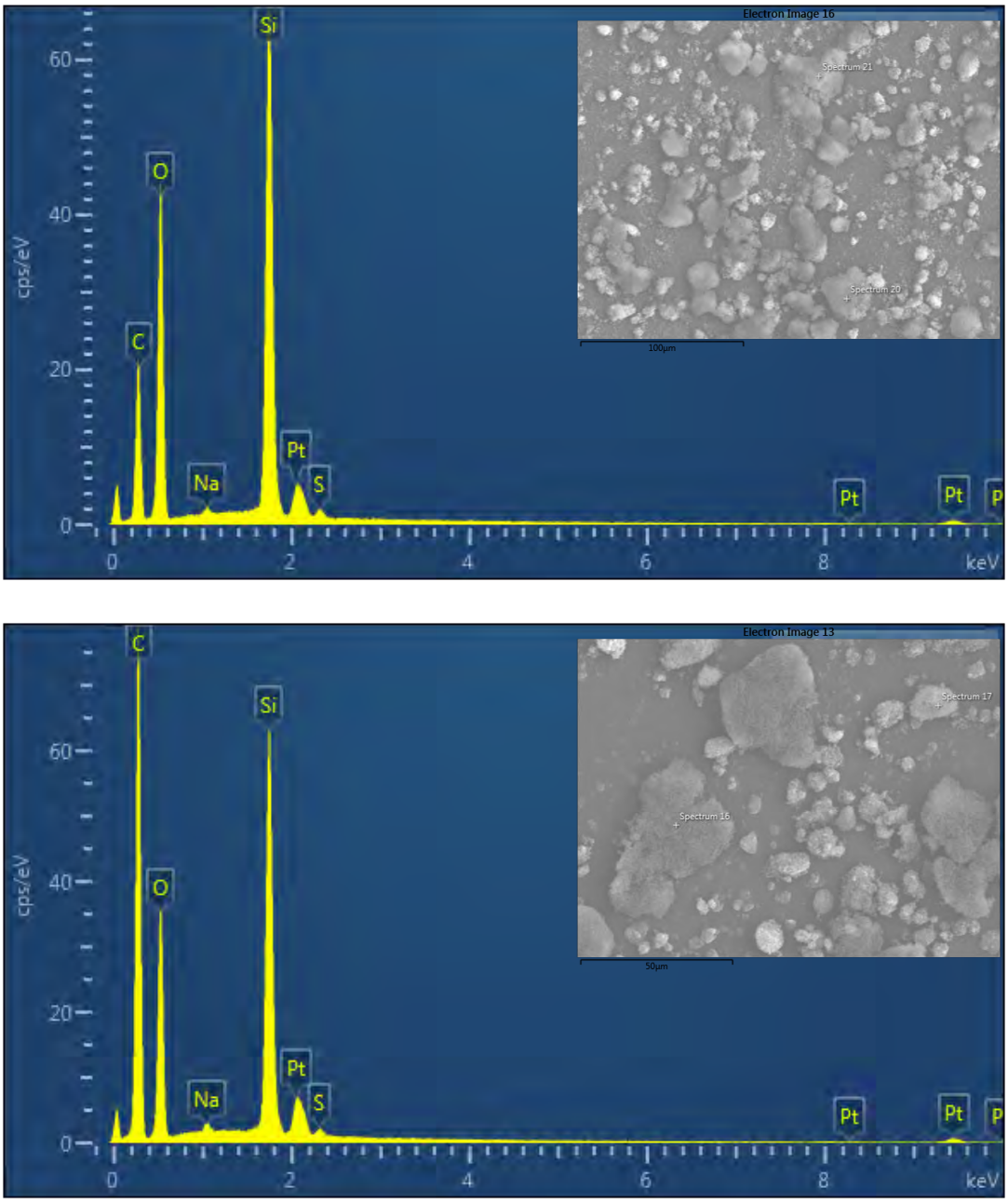

Figure 3.10. EDS spectra of Silicon dioxide (SiO_2) material (top) bulk, (bottom) nanoparticle using the 80mm² X-max silicon drift detector (Oxford instruments, UK) integrated with the Carl Zeiss FEG-STEM system, set-up to take SEM images (shown).

C = Carbon, O = Oxygen, Na = Sodium, Pt = Platinum, S = Sulphur and Si =Silicon.

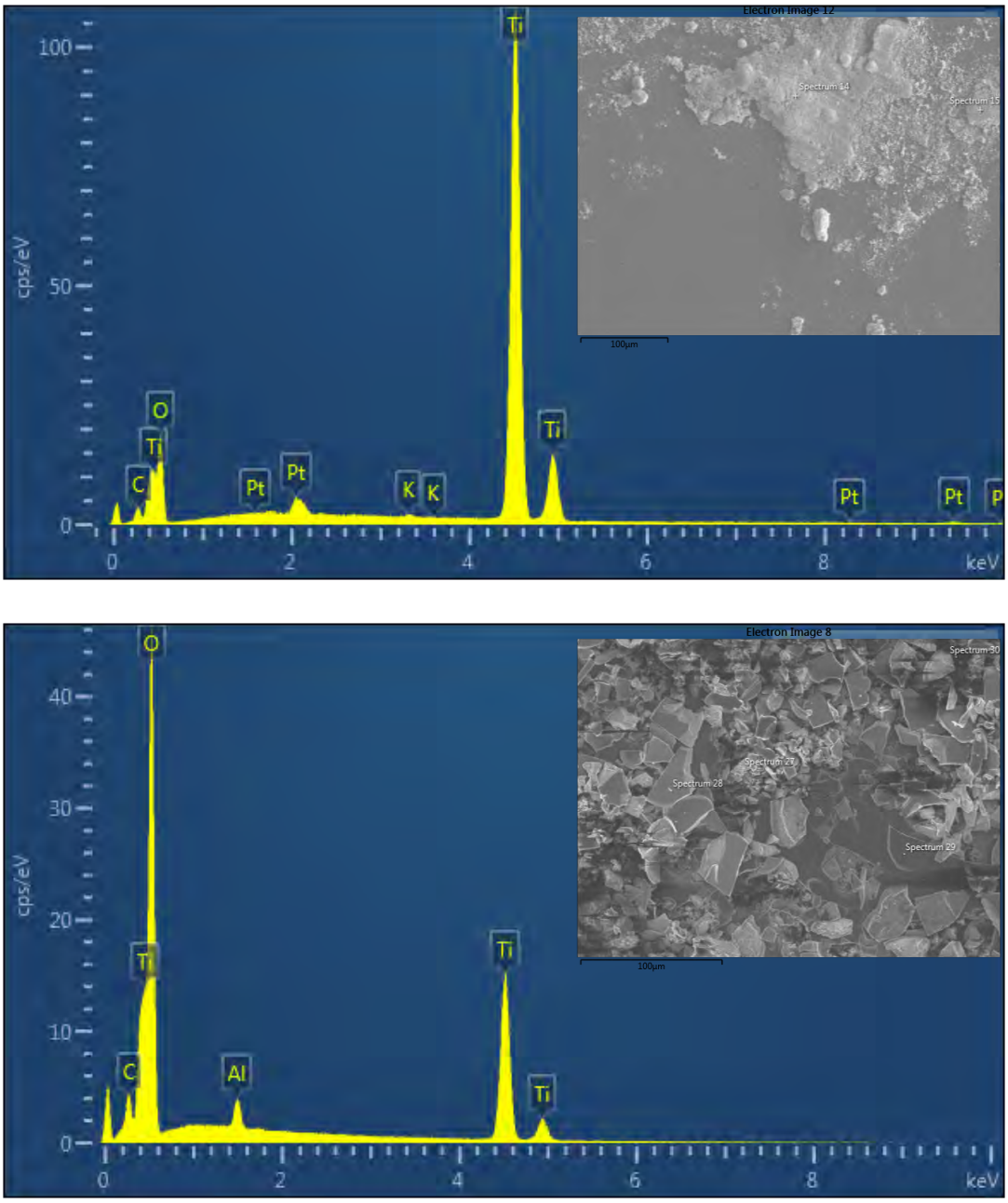

Figure 3.11. EDS spectra of Titanium dioxide (TiO_2) material (top) bulk, (bottom) nanoparticle using the 80mm² X-max silicon drift detector (Oxford instruments, UK) integrated with the Carl Zeiss FEG-STEM system, set-up to take SEM images (shown).

Al = Aluminium, C = Carbon, K = Potassium, O = Oxygen, Pt = Platinum and Ti = Titanium.

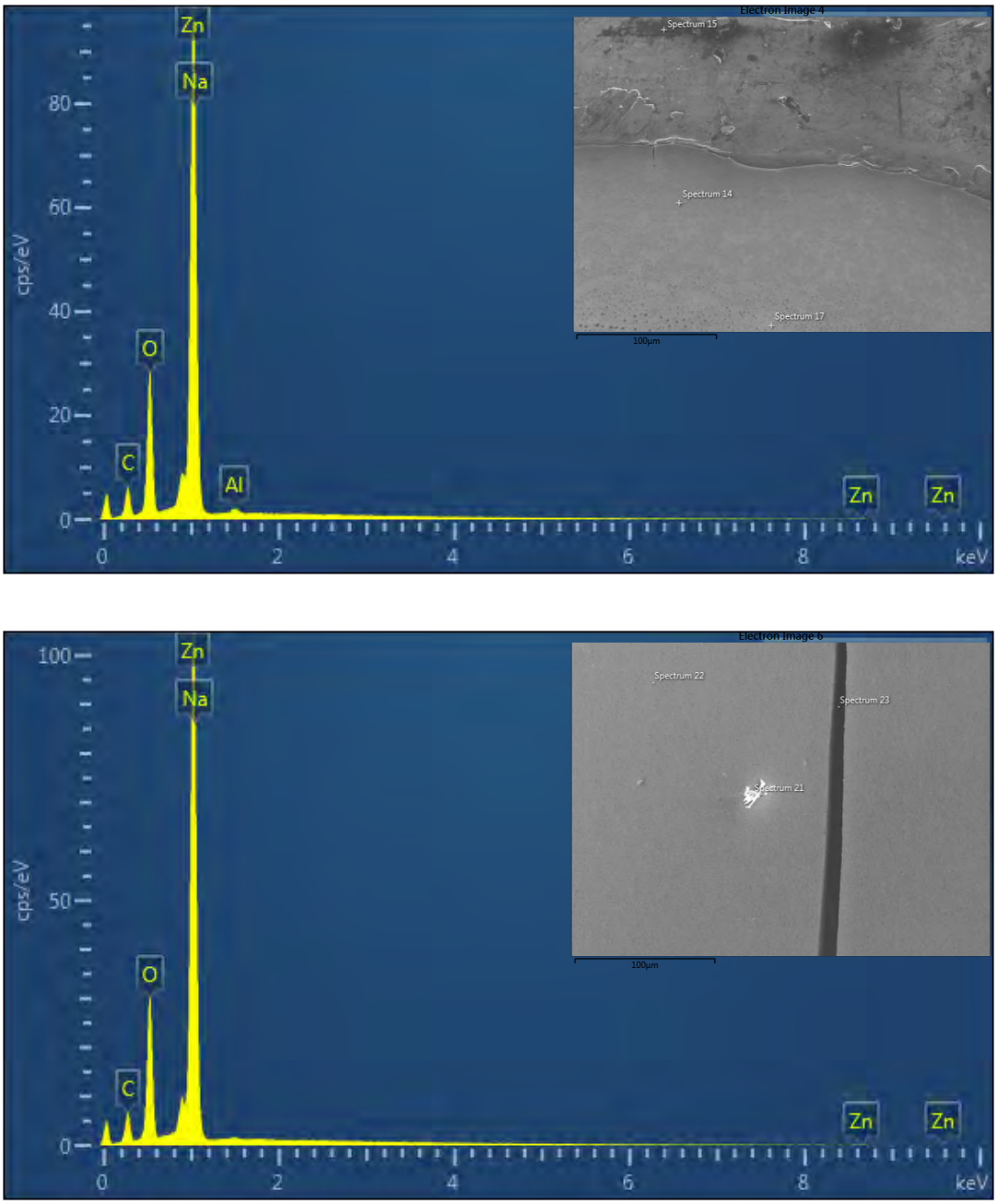

Figure 3.12. EDS spectra of Zinc oxide (ZnO) nanomaterial solutions (top) ZnO-45009, (bottom) ZnO-45408 using the 80mm² X-max silicon drift detector (Oxford instruments, UK) integrated with the Carl Zeiss FEG-STEM system, set-up to take SEM images (shown).

Al = Aluminium, C = Carbon Na = Sodium, O = Oxygen and Zn = Zinc.

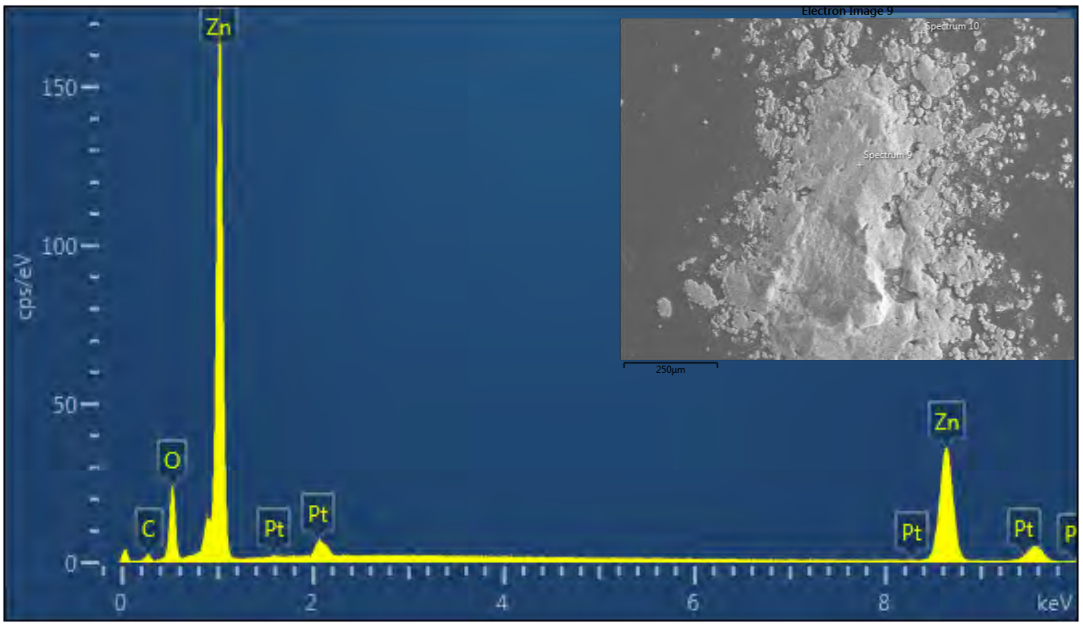

Figure 3.13. EDS spectra of Zinc oxide (ZnO) bulk powder using the 80mm² X-max silicon drift detector (Oxford instruments, UK) integrated with the Carl Zeiss FEG-STEM system, set-up to take SEM image (shown).

C = Carbon, O = Oxygen, Pt = Platinum and Zn = Zinc.

3.1.4 DLS nanoparticle hydrodynamic diameter measurements and material polydispersity

The reporting of particle size distributions and polydispersity alongside Z-average hydrodynamic diameter enabled nanomaterial particle size to be investigated in the context of their behaviour in suspension at physiological temperature (37°C). DLS results were compared against nanomaterial particle size measurements from alternative techniques, enabling assessment towards the effect each solvent environment had on the particle dispersions. This formed the basis for evaluation into those nano-characteristics that may be present for each particular nanomaterial, when in later chapters, particles are to be delivered under conditions more representative of the human oral mucosa *in vitro*. The effects of dilution, increased temperature and chemical composition of media were all speculated to cause increased agglomeration in nanomaterials (Kaszuba *et al.*, 2010).

Understanding the relationship between nanoparticle characteristics and the effect of biological environments remains challenging due to the numerous complex interactions that govern nanoparticle properties. There remains little information specifically focused on the behaviour of nanoparticle dispersion at physiological temperature. It was

thought essential, in modelling the impact that environmental conditions play on nanoparticle effects in biological systems, to investigate any potential differences that may arise from particle behaviour of analysis, and upon exposure *in vitro* at 37°C.

3.1.4.1 Nanoparticle size measurements by DLS

Table 3.1 reports the Z-average particle sizes recorded from DLS analysis carried out at room temperature (22°C) and physiological temperature (37°C), for each nanomaterial dispersed in dH_2O, phenol-red free media (PRF) and (a non-aqueous comparison) in ethanol. Overall, analysis using DLS recorded particle size measurements produced far larger sizes than those specified by the manufacturers of each nanomaterial. In all samples, the particle size reported exceeded the 100nm nano-size threshold used to define a nanomaterial.

Results from 21nm and 70nm polystyrene standards were considered within specification at 22°C (set at ± 2nm and ± 3nm, respectively), but slightly exceeded standard deviations when the temperature of analysis was increased to 37°C. However, its increase may be attributed to thermo-expansion properties of polystyrene (Patnode & Scheiber, 1939), and was not deemed significantly outside the expected results for the standards not to serve as controls in assessing other nanomaterial Z-average hydrodynamic diameters.

Based on the accuracy of DLS to measure polystyrene standards, and in the context of previous particle sizing data from electron micrographs, Z-averages reported in Table 3.1 were thought to be influenced by agglomeration. Complex, dynamic colloidal systems were speculated to have developed in each of the nanomaterial dispersions, with the rate and extent of agglomeration differing in respect to nanomaterial sample, dispersion solvent and temperature of analysis. This was displayed best by the re-ordering of materials when ranked in size order (large to small):

Manufacturer Expected → Hydroxyapatite > ZnO-45009 > ZnO-45408> TiO_2 > SiO_2.

dH_2O → Hydroxyapatite > TiO_2 > SiO_2 > ZnO-45009 > ZnO-45408.

PRF media → TiO_2 > SiO_2 > Hydroxyapatite > ZnO-45009 > ZnO-45408.

Ethanol → TiO_2 > SiO_2 > ZnO-45009 > ZnO-45408 > Hydroxyapatite.

The order changed again when analysis took place at 37°C:

dH_2O → Hydroxyapatite > SiO_2 > ZnO-45009 > ZnO-45408 > TiO_2.

PRF media → Hydroxyapatite > TiO_2 > SiO_2 > ZnO-45009 > ZnO-45408.

Ethanol → TiO_2 > SiO_2 > hydroxyapatite > ZnO-45009 > ZnO-45408.

The large variation observed in the particle size data (constituting the Z-average), meant statistical significance could not be accurately reported from DLS data. Results suggested all nanomaterials were present within a dynamic colloidal system, particularly so when dispersed in PRF medium. As a solvent, this led to the largest Z-average for all nanomaterials across both temperatures, in addition to the largest standard deviation in measurements. Hydroxyapatite nanomaterial was the exception, with dH_2O dispersion recording the largest Z-average for this material (1535.7nm ± 648.8nm (22°C) and 1241.5nm ± 850.4nm (37°C)), and ethanol the smallest (153.8nm ± 149.2nm (22°C) and 292.0nm ± 114.6nm (37°C)).

ZnO nanomaterials were seen as the most stable samples, consistently ranking amongst the smallest in terms of Z-average values recorded and standard deviation in the measurement. No notable difference in Z-average hydrodynamic diameter was observed during analysis at both temperatures, with ethanol and dH_2O dispersions recorded as comparable for each respective ZnO nanomaterials. In all dispersions, ZnO-45408 nanomaterial recorded smaller Z-averages when compared against ZnO-45009, which is consistent with trends observed in earlier particle sizing work.

TiO_2 was consistently ranked larger than SiO_2 (except for analysis at 37°C in dH_2O) and both nanomaterials were amongst the larger Z-averages recorded. However, an incidence of decreased hydrodynamic diameter was recorded when both materials were analysed at 37°C (consistent across all dispersions). This was also linked to large standard deviation values that were speculated to imply that increased agglomeration, flocculation and sedimentation may have occurred during the analysis.

3.1.4.2 Nanoparticle size distributions of samples analysed in dispersions using DLS

Z-averages in Table 3.1 reported the intensity weighted mean hydrodynamic size of the particles. Since nanomaterial sizing in solution had resulted in the measurement of significantly larger particle sizes (than electron microscopy), the data contributing to Z-average hydrodynamic diameters was investigated further, to scrutinise the precise

particle sizes within each sample. The aim was to determine the effects that different dispersions had on the nanomaterial, and to establish why the particle sizes recorded using DLS (unexpectedly) constituted sizes outside the 100nm threshold. In addition, reviewing the particle distributions served to verify the reliability of averaging size values (and standard deviations) recorded for nanomaterial particle sizing assessed by DLS.

Figure 3.14 through to Figure 3.19, report the particle size distribution graphs for each nanomaterial dispersed in all three solvents. Comparisons can be made between particle size distribution analyses carried out at 22°C and 37°C. The distribution results were considered to be a more complete representation of the nanomaterial particle sizes in solution, constituting precise and comprehensive inclusion of all particle sizes present within the sample. This was speculated to include large agglomerates up to the instruments limit in detection (5μm), that may have skewed the Z-average hydrodynamic diameter (Bootz *et al.*, 2004, Filipe *et al.*, 2010, Kato *et al.*, 2009).

Table 3.1. Nanomaterial particle diameter results analysed at 22°C and 37°C using the DLS based particle sizing instrument (ZetaSizer Nano ZS90).

All measurements are the mean of 6 runs (n=6) averaged from at least 5 analyses per measurement, with standard deviation reported.

Nanoparticle size* (nm) *Manufacturer details	Material	Solvent	ZetaSize Z-average **at 22 C** hydrodynamic diameter (nm)	S.D. (nm)	ZetaSize Z-average **at 37 C** hydrodynamic diameter (nm)	S.D. (nm)
21	Polystyrene standard	dH_2O	21.5	0.2	22.2	0.6
70	Polystyrene standard	dH_2O	73.2	1.3	76.2	2.3
~ 30	ZnO-45408	dH_2O	177.1	4.8	180.7	6.7
		PRF media	376.0	167.4	348.0	155.4
		ethanol	184.1	10.6	161.7	10.0
~ 70	ZnO-45009	dH_2O	231.6	12.4	243.1	50.8
		PRF media	522.2	467.7	591.8	400.0
		ethanol	212.0	13.6	180.8	12.0
<30	TiO_2	dH_2O	345.8	539.8	145.6	93.6
		PRF media	3352.7	795.1	956.2	364.7
		ethanol	1890.6	770.6	711.8	519.8
~ 12	SiO_2	dH_2O	334.3	119.1	254.2	101.4
		PRF media	1417.7	577.4	777.5	655.2
		ethanol	637.3	153.8	499.1	333.1
< 200	Hydroxyapatite	dH_2O	1535.7	648.8	1241.5	850.4
		PRF media	577.4	228.0	1452.9	520.7
		ethanol	153.8	149.2	292.0	114.6

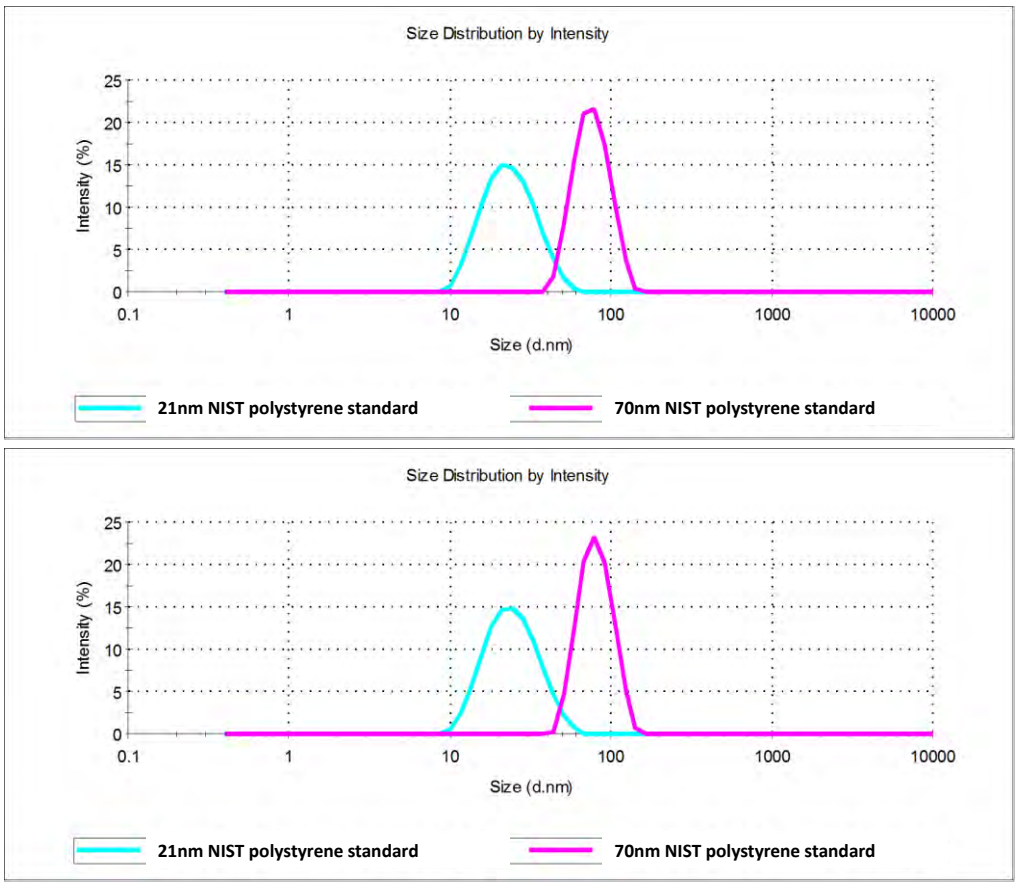

Figure 3.14. DLS particle size distributions by intensity polystyrene standards dispersed in dH_2O at 22°C (top) and 37°C (bottom): *turquoise line indicates particle distribution of 21nm standard and pink line indicates particle distribution of 70nm standard.* All results report the mean of n = 6 from a minimum of 5 readings per n.

Figure 3.14 shows the particle size distribution for polystyrene nanosphere control samples. The distributions for both 21nm and 70nm standards depict highly stable monodispersed nanoparticle populations that were not altered despite analysis occurring at 22°C and 37°C. These results served to successfully report accuracy of the DLS instrumentation, in replicating the average particle sizes stated in Table 3.1.

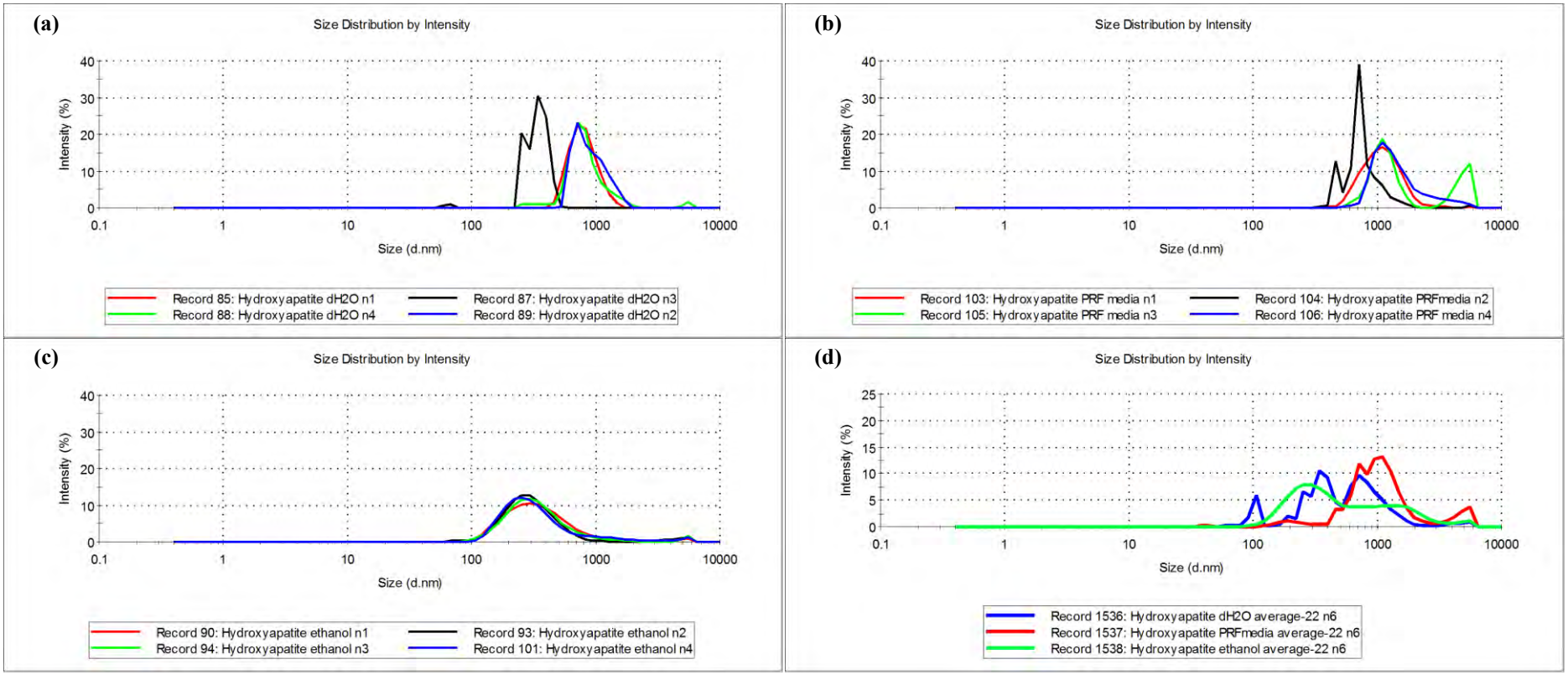

Figure 3.15. Demonstration of the difficulty in accurate measurement of DLS particle size distributions by intensity of back scattered light by hydroxyapatite nanomaterial dispersed in three different solvents at 22°C (a) dispersed in dH_2O, **(b)** PRF media, **(c)** ethanol and **(d)** n = 6 mean values.

Figure 3.15 has been included to demonstrate the typical size distribution of hydroxyapatite nanomaterial in each of the different solvent dispersions, and the difficulties that arise in reporting the average size distribution for this nanomaterial. Hydroxyapatite nanoparticles were only stable when dispersed in ethanol, with reproducible traces observed for each analysis. In this dispersion, nanoparticles were monodispersed, with a single peak, constituting all particle sizes detected between 100nm and 1μm.

In aqueous media (dH_2O and PRF media), different particle size distributions were observed for each analysis, with little relation to the average distribution reported (d). This disparity was speculated as being an indication of a dynamic, unstable dispersion that formed different sized agglomerates at different rates for each analysis.

Hydroxyapatite was observed as the most difficult nanomaterial to analyse in dispersion using this method, and this has been demonstrated here in the way results were reported for this sample. All of nanomaterials displayed in the figures below, were thought more stable during DLS analyses, hence averages are reported. Unstable dispersions have been noted from observations of their size distributions in descriptions of the results, but included: SiO_2 nanomaterial dispersed in PRF media (Figure 3.16) and TiO_2 nanomaterial dispersed in both PRF media and ethanol (Figure 3.17).

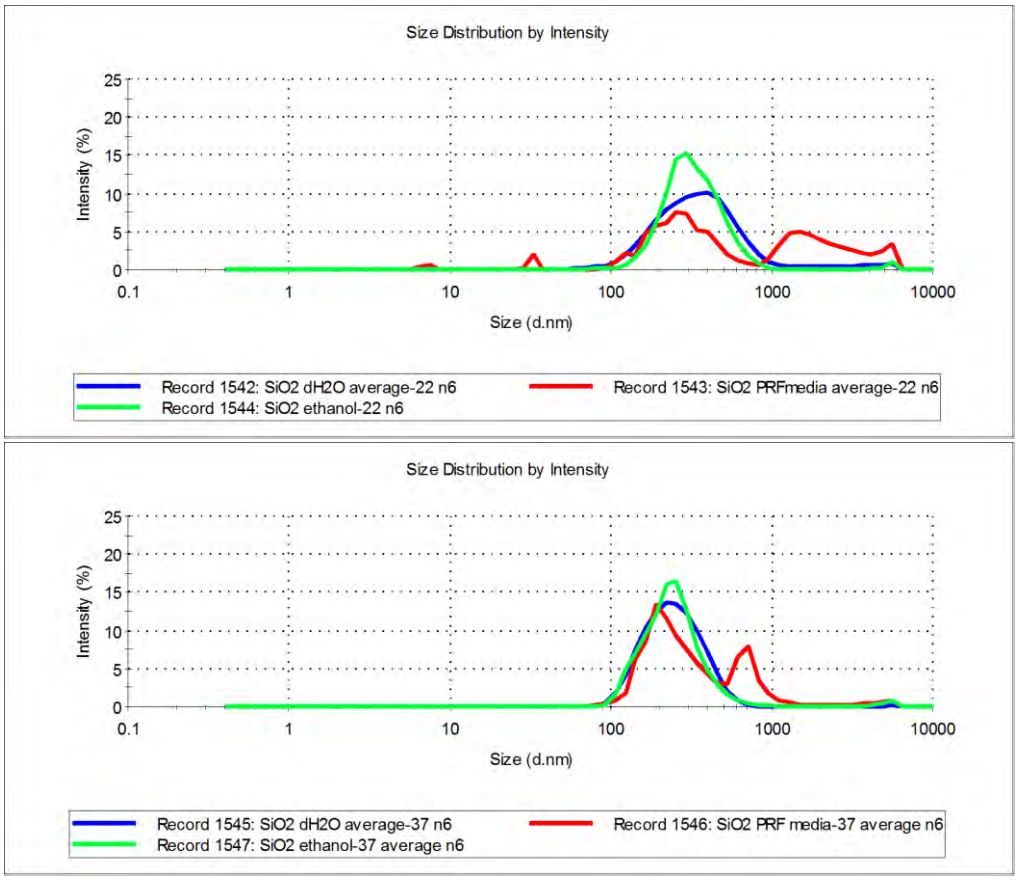

Figure 3.16. DLS particle size distributions by intensity of SiO_2 nanomaterial dispersed in three different solvents at both 22°C (top) and 37°C (bottom): *blue line indicates particle distribution in dH_2O, red line indicates particle distribution in PRF media and green line indicates particle distribution in ethanol.* All results report the mean of n = 6 from a minimum of 5 readings per n.

Figure 3.16 shows SiO_2 nanomaterial dispersed in dH_2O and ethanol to form a more stable colloidal system (than PRF media). This was observed by the wide, but monomodal particle size distribution. At 37°C analysis, the particle size distribution narrowed in both dispersions, shifting peak intensity towards the smaller hydrodynamic diameters. For dH_2O dispersion, the peak in intensity correlated closely with the Z-average, in Table 3.1, but was observed to be smaller than the SiO_2-ethanol Z-average.

The more unstable PRF media dispersion recorded a multimodal particle size distribution when analysis was carried out at 22°C. This was formed by varied particle sizes, all recorded at low intensities, due to the irreproducible analyses. Within the average distribution was a distinct population measuring below 30nm in size, whereas the majority of particles measured between 100nm to 1µm in size. This sample also produced large agglomerates, indicated by a separate distribution of particles measuring in excess of 1µm. The analysis of the SiO_2-PRF media sample at 37°C produced a

narrowed distribution in the particle sizes recorded, constituting a bi-modal distribution at smaller hydrodynamic diameters. This was sized with the highest intensity peaking at 200nm with a secondary shoulder recorded at half the intensity around 700nm in size. In relation to the Z-average (777.5nm ± 655.2nm), the distribution implied more bias towards the larger particle sizes recorded, but correlated closely with the standard deviation in the measurement calculated for this sample.

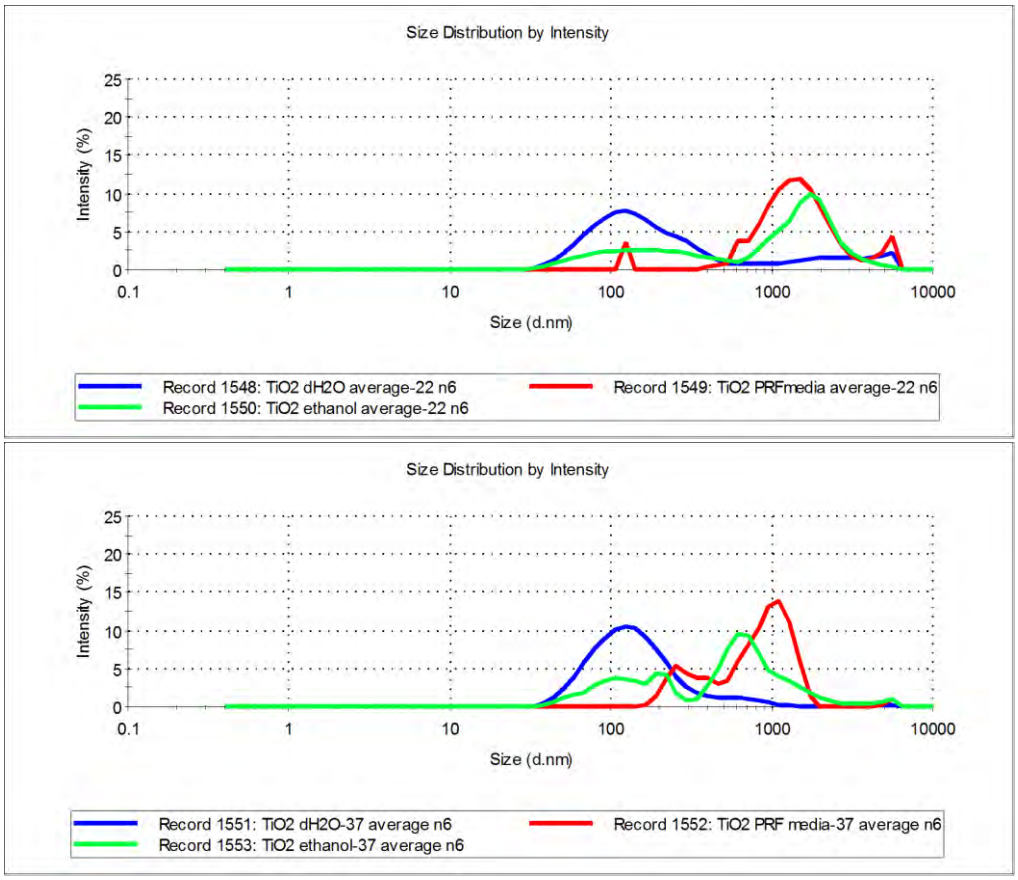

Figure 3.17. DLS particle size distributions by intensity of TiO_2 nanomaterial dispersed in three different solvents at both 22°C (top) and 37°C (bottom): *blue line indicates particle distribution in dH_2O, red line indicates particle distribution in PRF media and green line indicates particle distribution in ethanol.* All results report the mean of n = 6 from a minimum of 5 readings per n.

Figure 3.17 is the analysis of TiO_2 nanomaterial and shows wide particle size distributions recorded for all dispersions at 22°C analysis. The greatest intensity of particles were measured peaking in excess of 1μm for both PRF and ethanol dispersions, and did not correspond closely with the Z-averages recorded in Table 3.1. The Z-average may have been skewed by the presence of larger particle size populations observed in the tail of the distribution curves. This was also observed for dH_2O dispersed TiO_2 nanomaterial, although this peaked with the highest intensity of particles measuring closer to 100nm in size. The particle size distributions were observed to have similar size ranges when analysis was carried out at 37°C; however, there was an absence in the larger particle sizes recorded as tails in the relative peaks in intensities at 22°C analysis. This caused each particle distribution to narrow, with peaks recorded being more closely aligned with the respective Z-averages recorded in Table 3.1.

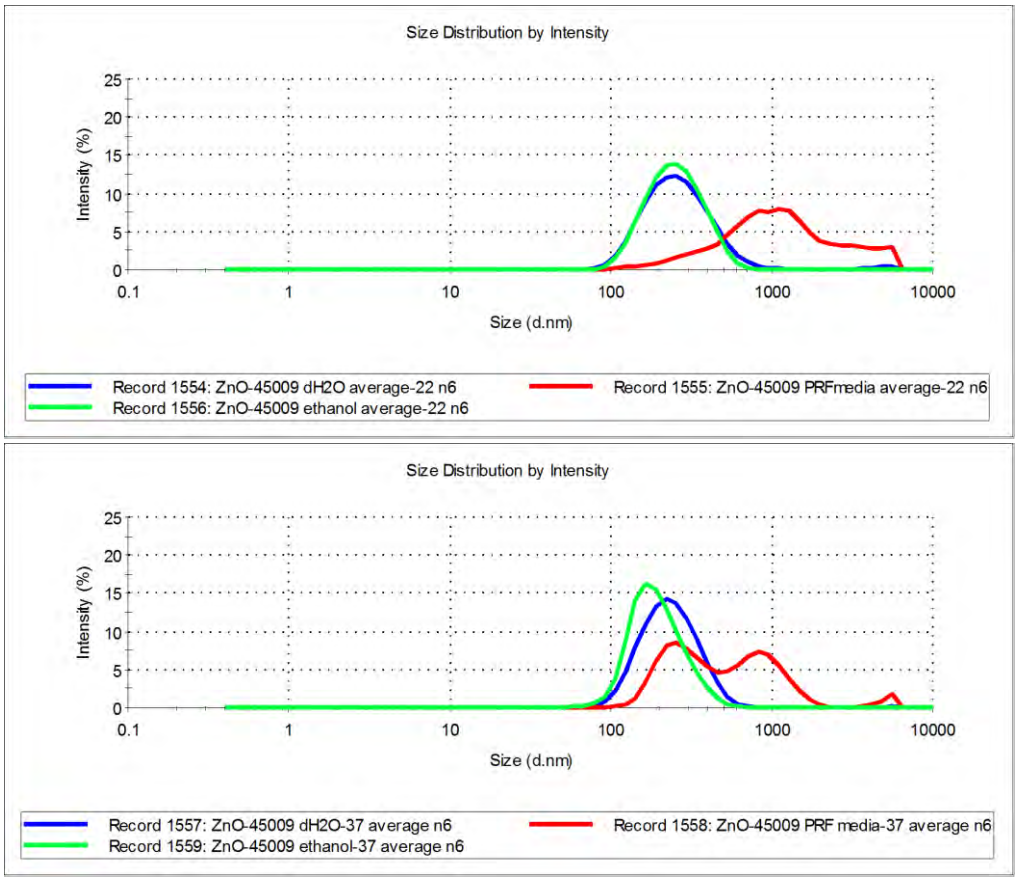

Figure 3.18. DLS particle size distributions by intensity of ZnO-45009 nanomaterial dispersed in three different solvents at both 22°C (top) and 37°C (bottom): *blue line indicates particle distribution in dH_2O, red line indicates particle distribution in PRF media and green line indicates particle distribution in ethanol.* All results report the mean of n = 6 from a minimum of 5 readings per n.

ZnO-45009 nanomaterial distribution curves are shown in Figure 3.18 and were observed to be similar at the two temperatures tested, for nanomaterials dispersed in dH_2O and ethanol. The intensity of the peaks from the particle size distributions corresponded closely with those stated in Table 3.1, with narrow peaks relating to smaller standard deviations (in dH_2O at 22°C and ethanol at 37°C). No large particle sizes were detected in either of these two dispersions (outside the main distribution curve) indicating a more stable monomodal colloidal system of ZnO nanoparticles in these solvents. This was not the case in PRF media, where the distribution was skewed to a higher average particle diameter, over a broad range with some very large sizes detected at 22°C. Particle sizes around the 1μm size were measured, with a lower intensity recorded exceeding the sensitivity of the Zetasizer instrument. Narrowing of the particle size distribution was observed in this sample, when analysed at 37°C. The peak intensity was positioned exceeding 100nm and had a relatively broad distribution (between 100nm and 400nm) with a shoulder on the main peak covering particle size ranging in excess of 1μm. This broad particle size distribution for ZnO-45009 nanomaterial dispersed in PRF media was suspected to contribute the high standard deviation values calculated in Table 3.1. However, these data do not correlate with the Z-average size, which was more heavily weighted towards the larger sized particles / agglomerates.

Particle size distributions recorded in Figure 3.19, showed similarities to the previous ZnO-45009 nanomaterial analysis. The ZnO-45408 nanomaterial dispersed in both dH_2O and ethanol had size distributions that corresponded closely with each other. This was consistent under analysis at both temperatures, and the intensity of the peaks matched closely the Z-averages stated in Table 3.1. Compared with the results for ZnO-45009, size distribution curves for ZnO-45408 were shifted towards the smaller nanoparticle sizes (validating manufacturing specifications given in Table 2.1). PRF media was considered the dispersion solvent that experienced the greatest agglomeration, observed by the shift in particle population intensities towards an increased measurement of larger particle sizes. These peaked at intensity levels correlating to hydrodynamic sizes comparable with those stated in Table 3.1.

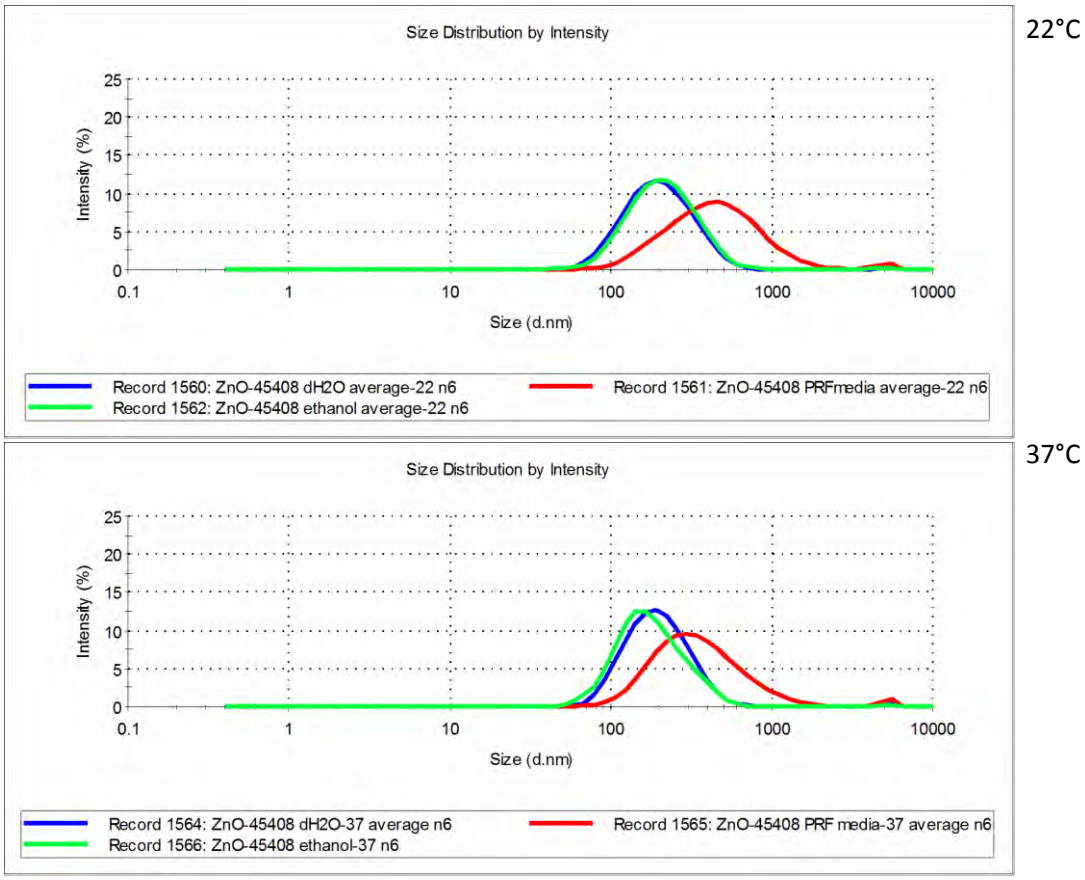

Figure 3.19. DLS particle size distributions by intensity of ZnO-45408 nanomaterial dispersed in three different solvents at both 22°C (top) and 37°C (bottom): *blue line indicates particle distribution in dH_2O, red line indicates particle distribution in PRF media and green line indicates particle distribution in ethanol.* All results report the mean of n = 6 from a minimum of 5 readings per n.

3.1.4.3 Polydispersity calculations of nanoparticle dispersions using analysis by DLS

In addition to size measurements of hydrodynamic diameter for each nanomaterial, the Malvern ZetaSizer instrument was able to generate a polydispersity index (PDI) measurement. This utilised the Cumulants analysis algorithm from the DLS measured autocorrelation function (Malvern, 2011), to report a number that signifies the width of particle size distribution that was detected within a single sample. This number can be between 0 and 1, with values closer to 0 symbolising monodisperse samples containing particles of similar size. Conversely, samples are described as polydisperse the nearer they approach 1.

In Figure 3.20 and Figure 3.21, this value was plotted against the absolute polydispersity width to provide comparison between actual particle size distributions recorded, allowing the disparity in particle sizes measured to be put in context against the sample.

Data points closer to the 0 value for both axes were expected to relate to particles similar in size, which are recorded as sharp peaks in distribution curves. Using comparisons from both of the polystyrene standards at either temperature, it was clear to see the correlation. Therefore, comparisons between Figure 3.20 and Figure 3.21 allowed for trends of particle behaviour at each temperature to be easily noticed, which added towards the explanation of particle sizes recorded in Table 3.1.

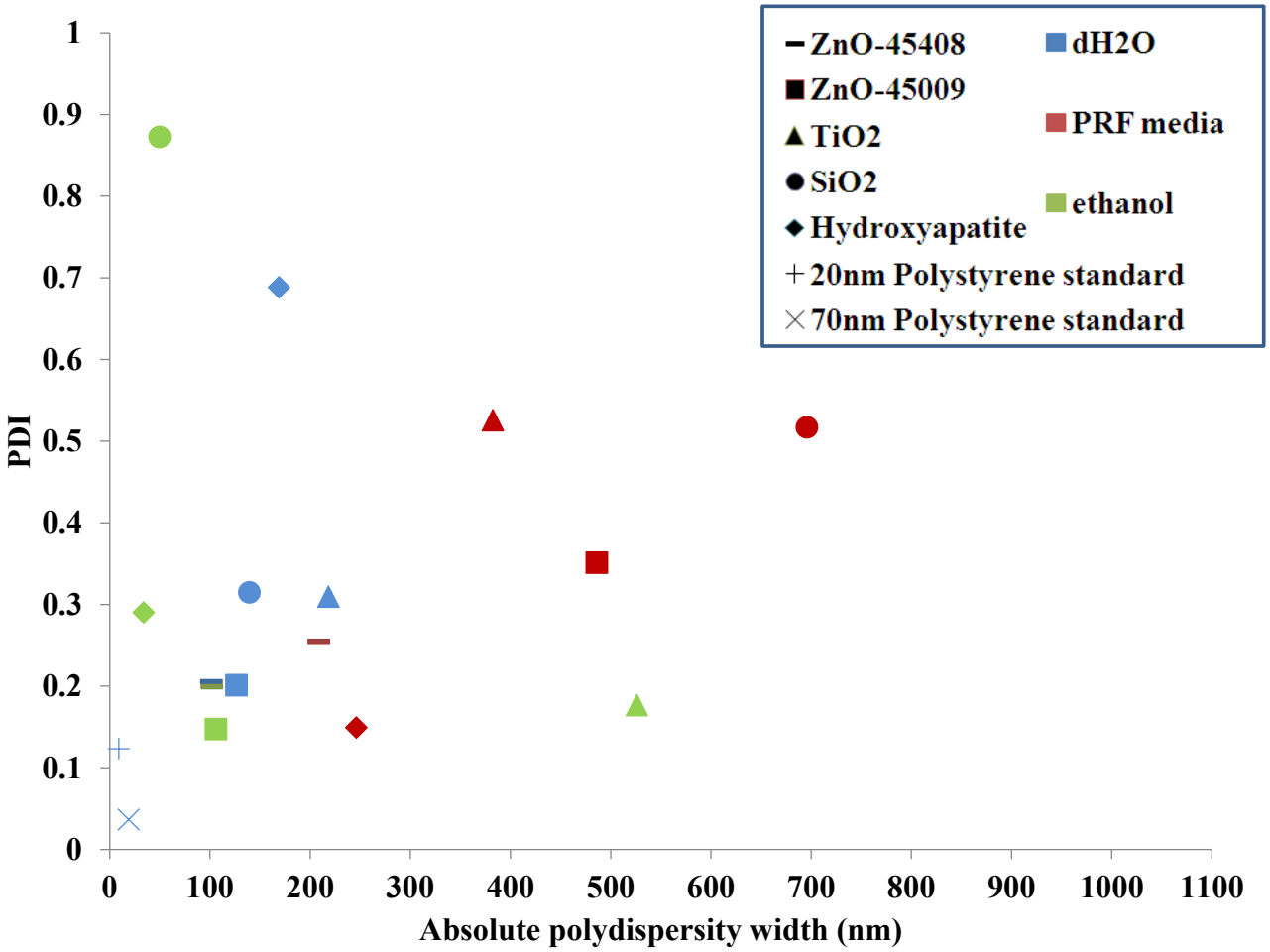

Figure 3.20. DLS ZetaSizer data showing the polydispersity index (y axis) versus the averaged actual polydispersity width of particle diameters recorded during size measurements (x axis), for all nanomaterials dispersed in each of three different solvents at 22°C.

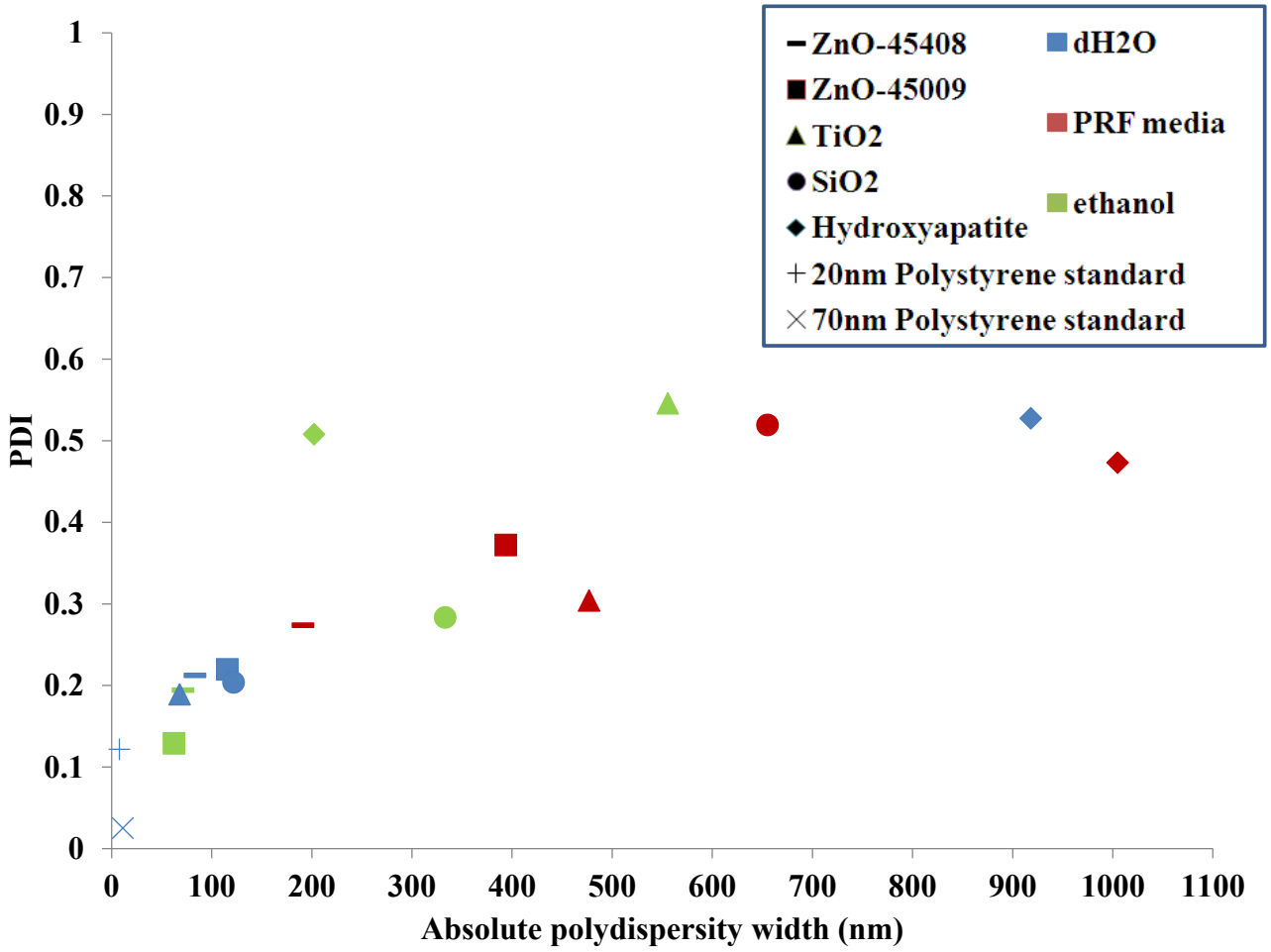

Figure 3.21. DLS ZetaSizer data showing the polydispersity index (y axis) versus the averaged actual polydispersity width of particle diameters recorded during size measurements (x axis), for all nanomaterials dispersed in each of three different solvents at 37°C.

The results showed dH_2O to be the most stable and monodisperse solutions for all nanomaterials across both temperatures, except for nano-hydroxyapatite. This was indicated by the cluster of '*blue*' points seen closer to the 0 value on both axes (Figure 3.20 and Figure 3.21). PRF media was observed to produce the least stable dispersions, with a greater scatter of points showing more variability in particle distributions and polydispersity, indicated by points spread out further from the bottom left corner of PDI figures.

Nanomaterials that recorded large Z-average hydrodynamic diameters (Table 3.1) were determined as aggregates when data points were located closer to the *y* axis of the PDI figures (and considering the size ranges recorded through electron microscopy). At this position in the graph, large average particle sizes were detected within a sample of otherwise similarly sized particulates (low PDI) and within a low absolute PDI width. Using this hypothesis, regularly sized aggregates were thought to form when hydroxyapatite nanomaterials were dispersed in dH_2O and ethanol, as well as SiO_2 nanoparticles in dH_2O (when analysis occurred at 22°C).

Dispersions were considered unstable when data points were aligned further to the right on the absolute PDI width (*x)* axis and higher up the PDI (*y)* axis. This indicated a particle size that was dynamic and changing as the analysis occurred. This situation was observed for all nanomaterials dispersed in PRF media, analysed at 37°C, as well as SiO_2, TiO_2 and hydroxyapatite nanomaterials analysed at 22°C, and hydroxyapatite-nanomaterial dispersed in dH_2O. All of these samples corresponded to wide particle size distribution curves in the respective DLS analysis figures.

Nanomaterial dispersions that recorded a low PDI value but high absolute PDI were linked to larger Z-average measurements speculated to have been skewed by the presence of large agglomerates during DLS analysis. These corresponded to Zetasizer software sample reports, warning of sedimentation or contamination relating to the presence of large agglomerates forming. Incidence of PDI-PDI interactions corresponding to sample warnings was noted for both hydroxyapatite and ZnO-45009 nanomaterials in PRF media, TiO_2 nanomaterial dispersed in ethanol (all at 22°C) and at 37°C: both TiO_2 and SiO_2 nanomaterials dispersed in PRF media and ethanol respectively.

3.1.5 NanoSight nanoparticle tracking analysis (NTA) of nanomaterial size distribution

As a complementary technique to DLS, NTA was used to support findings from nanomaterial sizing in solution. Furthermore, NTA has been shown to be advantageous (over DLS) for resolving polydisperse samples due to its ability to measure individual nanoparticles (Filipe *et al.*, 2010). DLS results have already suggested that the majority of nanomaterial samples investigated in this study are of polydisperse nature.

3.1.5.1 Average particle size measurement by NTA

The following data in Table 3.2 show the mean particle diameters recorded during NTA from 100 second video clips of nanomaterial particles scattering light, when dispersed in each of the three solvents.

The 20nm polystyrene standard did not have a high enough refractive index to visibly refract the light required to record particle Brownian movement necessary for NTA. It was therefore not included in this study.

The 70nm polystyrene standard was measured to have an average diameter of 71.7nm (± 44.0nm). The mean value was acceptable within the limits verified by NIST™ authentication (± 3.0nm), but the high standard deviation exceeded the expected range in particle sizes measured. As this sample was a traceable standard control, these values suggested limitations with the reliability of sample size results recorded. A critical review into the accuracy in size measurements recorded by NTA, was further prompted by the close proximity of the mean particle diameter measured for each nanomaterial in different dispersions; a conflicting outcome in comparison to DLS data. Major discrepancies between the two techniques were revealed through viewing the average nanomaterial particle size measured by NTA in rank order:

Manufacturer Expected → Hydroxyapatite>ZnO-45009 >ZnO-45408>TiO_2> SiO_2.

SEM/TEM Expected → Hydroxyapatite> ZnO-45009> ZnO-45408> TiO_2> SiO_2.

dH_2O → Hydroxyapatite > ZnO-45009 > SiO_2 > TiO_2 > ZnO-45408.

PRF media → SiO_2 > Hydroxyapatite > TiO_2 > ZnO-45009 > ZnO-45408.

Ethanol → Hydroxyapatite > ZnO-45009 > SiO_2 > ZnO-45408 > TiO_2.

Hence the trends observed for NTA were different to those following DLS analysis, and from what was expected based on manufacturer information. This prompted further investigation into the data used to report mean particle diameters measured by NTA.

Table 3.2. Nanomaterial particle diameter results analysed at ambient temperature using the NTA based particle sizing instrument (NanoSight LM10). All measurements are the average of 6 runs (n=6) with standard deviation reported.

Manufacturer Stated size (nm)	Material	Solvent	NanoSight NTA **mean average particle diameter** (nm)	S.D. (nm)
70	70nm Polystyrene standard	dH_2O	71.7	44.0
~30	ZnO-45408	dH_2O	68.6	39.5
		PRF media	68.5	41.2
		ethanol	75.2	40.8
~70	ZnO-45009	dH_2O	101.4	52.7
		PRF media	95.6	54.0
		ethanol	92.9	47.5
<30	TiO_2	dH_2O	94.8	51.3
		PRF media	99.0	57.6
		ethanol	62.7	38.4
~12	SiO_2	dH_2O	98.4	44.0
		PRF media	104.8	55.3
		ethanol	82.0	44.8
<200	Hydroxyapatite	dH_2O	109.0	54.3
		PRF media	102.8	57.1
		ethanol	105.3	55.7

3.1.5.2 Nanomaterial particle size distribution measured by NTA

In the following Figure 3.22 through to Figure 3.26, nanomaterial particle size distributions were reported as direct particle number counts measured at specific sizes ranging between 1nm and 200nm. Detection limits were restricted by the refractive index (RI) of each nanomaterial in reference to the sensitivity and field of view available to record light scattering of particles using the CCD camera.

Nanomaterial sample distributions were compared to results of the NIST™ traceable 70nm polystyrene standard (shown in yellow within each figure), with the aim to provide assessment of reliability in the mean particle sizes reported in Table 3.2. In addition, the manufacturer stated sizes as a guide to any differences that may have occurred from alterations between dry and nanoparticle size distributions in solution.

Consideration of results obtained for the 70nm polystyrene standard dispersed in dH_2O, shown across Figure 3.22 to Figure 3.26, constituted a homogenous particle distribution across the size range, forming an obvious peak in particle concentration at 47nm. This did not correlate with the mean particle size reported in Table 3.2, measured as 71.7nm ± 18.0nm. The known particle size monodisperisty in polystyrene spheres (NIST™ traceable) caused this broad distribution to be considered unrepresentative. Observation of peak concentration of particles recorded at sizes below what was present within the 70nm standards inferred false reporting of nanoparticle sizes and increased scepticism towards the lack of accurate representation in particle size distributions recorded using the NTA technique. The particle distribution reported using NTA of 70nm standard, reduced confidence in the reliability of mean sizes stated in Table 3.2. Nanomaterial samples in dispersion were analysed with reference to the observations noted from particle distribution results of the 70nm polystyrene standard. Figure 3.22 shows hydroxyapatite nanomaterial having the largest number of nanoparticles when dispersed in ethanol. In both dH_2O and PRF media, hydroxyapatite nanomaterial particles were sized over a wide distribution (from 29nm to the upper limit of detection 200nm) but at low concentrations and no obvious peak. It was difficult to compare these particle sizes with reference to the manufacturer details, as all data recorded during NTA falls within stated particle sizes (<200nm). In comparison to electron microscopy sizing, NTA measurements would be consistent with the range of nanoparticle sizes, if not the calculated average. Despite the difference in particle distribution observed for hydroxyapatite nanomaterial dispersed in each solvent, the mean size of particles was

calculated to be similar across all three samples. This was consistent with the outcome observed in the standard, and attributed to the larger numbers of particles detected in the tail of NTA analysis. These may have indicated the formation of an agglomerated nanomaterial, consistent with behaviour experienced in DLS analysis (Figure 3.15), but which fell outside the upper limit of detection for NTA.

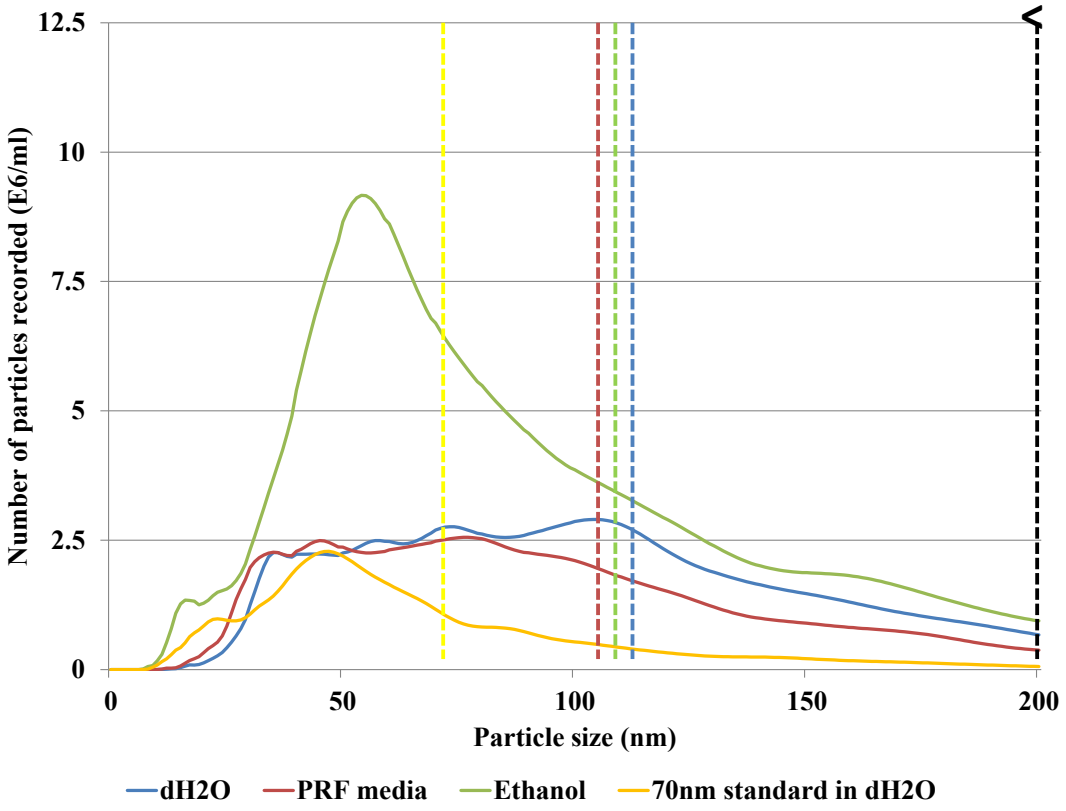

Figure 3.22. NTA size distribution expressed as number of particles of hydroxyapatite nanomaterial dispersed in: dH_2O (blue), PRF media (red) or ethanol (green). The 70nm polystyrene standard results are shown in yellow. *The dotted lines indicate the position of mean particle size calculated from distribution data for each dispersion with the black line indicating manufacturer stated size.* Analysed at room temperature (n = 6).

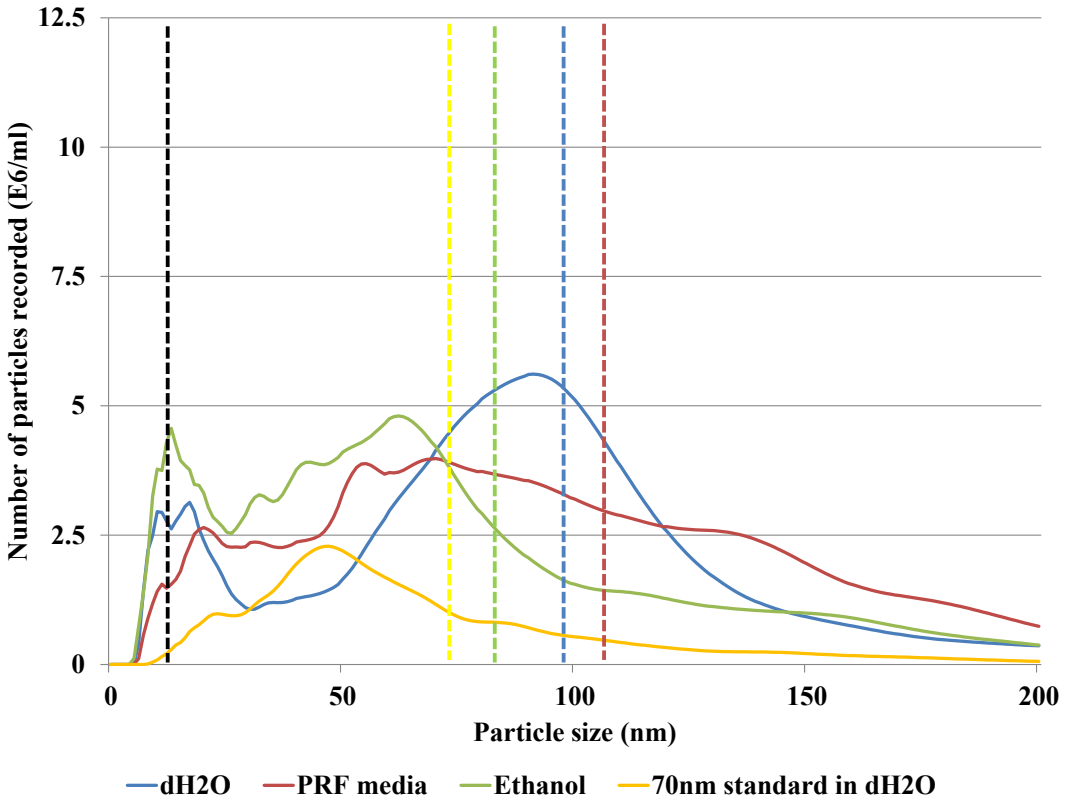

Figure 3.23. NTA size distribution expressed as number of particles of SiO_2 nanomaterial dispersed in: dH_2O (blue), PRF media (red) or ethanol (green). The 70nm polystyrene standard results are shown in yellow. *The dotted lines indicate the position of mean particle size calculated from distribution data for each dispersion with the black line indicating manufacturer stated size.* Analysed at room temperature (n = 6).

Figure 3.23 shows SiO_2 nanomaterial particle size distributions as being multimodal, recording a wide range of particle sizes over the 100seconds of analysis. In all dispersions, SiO_2 nanomaterial was measured between 10nm and 21nm as an initial peak in number of particles detected, similar to the stated size expected from manufacturer data. However, the average for PRF media and ethanol dispersions were likely to be skewed by larger particle sizes peaking in a wider distribution between 25nm to 71nm before slowly tailing off towards the upper limit of detection. SiO_2 nanomaterial dispersed in dH_2O recorded particle concentrations forming a secondary peak close to the 98.4nm ± 44.0nm mean reported by the manufacturer (at approximately 92nm). All results would imply likely agglomeration in comparison to the initial peak of particle numbers, expected from close compatibility with manufacturer description.

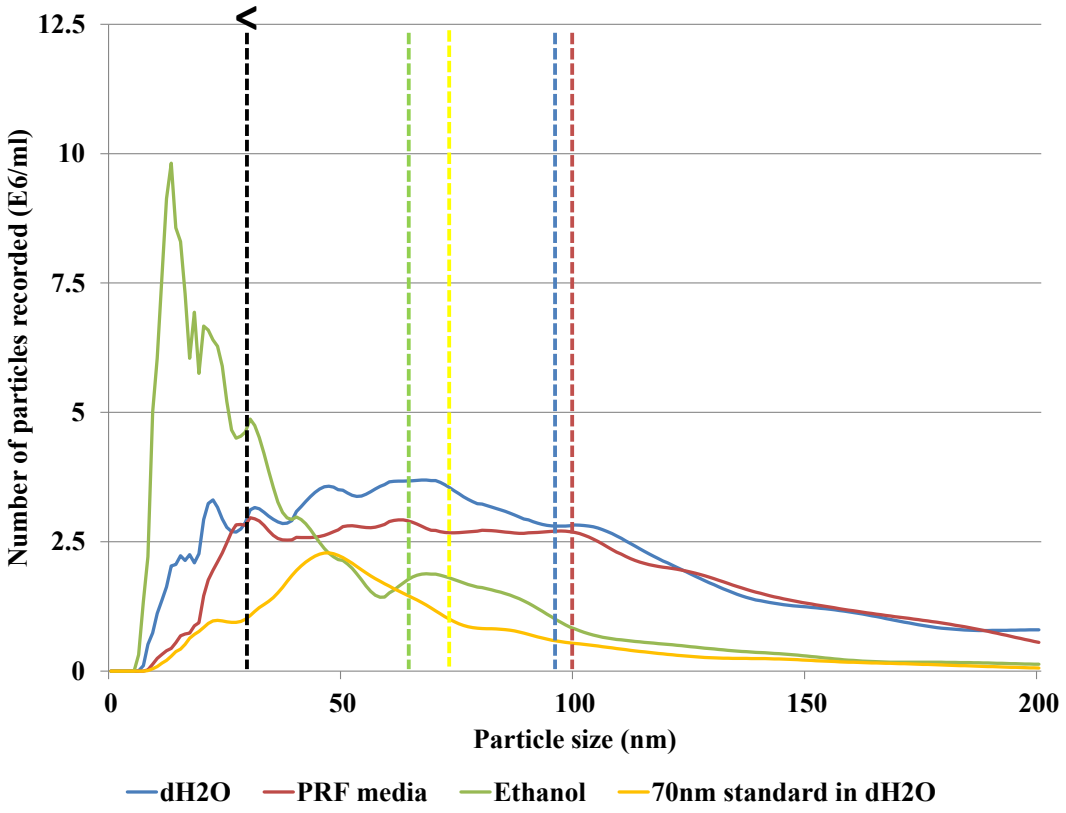

Figure 3.24. NTA size distribution expressed as number of particles of TiO_2 nanomaterial dispersed in: dH_2O (blue), PRF media (red) or ethanol (green). The 70nm polystyrene standard results are shown in yellow. *The dotted lines indicate the position of mean particle size calculated from distribution data for each dispersion with the black line indicating manufacturer stated size.* Analysed at room temperature (n = 6).

Figure 3.24 shows TiO_2 nanomaterial particle size measurements in both dH_2O and PRF media, which follow wide and flat distribution with no obvious peak in concentration, and no obvious relationship with regard to mean values reported. This follows the discrepancies noted in the 70nm polystyrene standard, implying data lacked reliability.

When dispersed in ethanol, TiO_2 nanomaterial particle size was observed through a distinct population peaking at 13nm with two shoulder peaks measured at 20nm and 31nm. The distribution then tailed off before the upper limit in detection (200nm). This produced the smallest mean particle diameter recorded, closer to the manufacturer stated size range (<30nm).

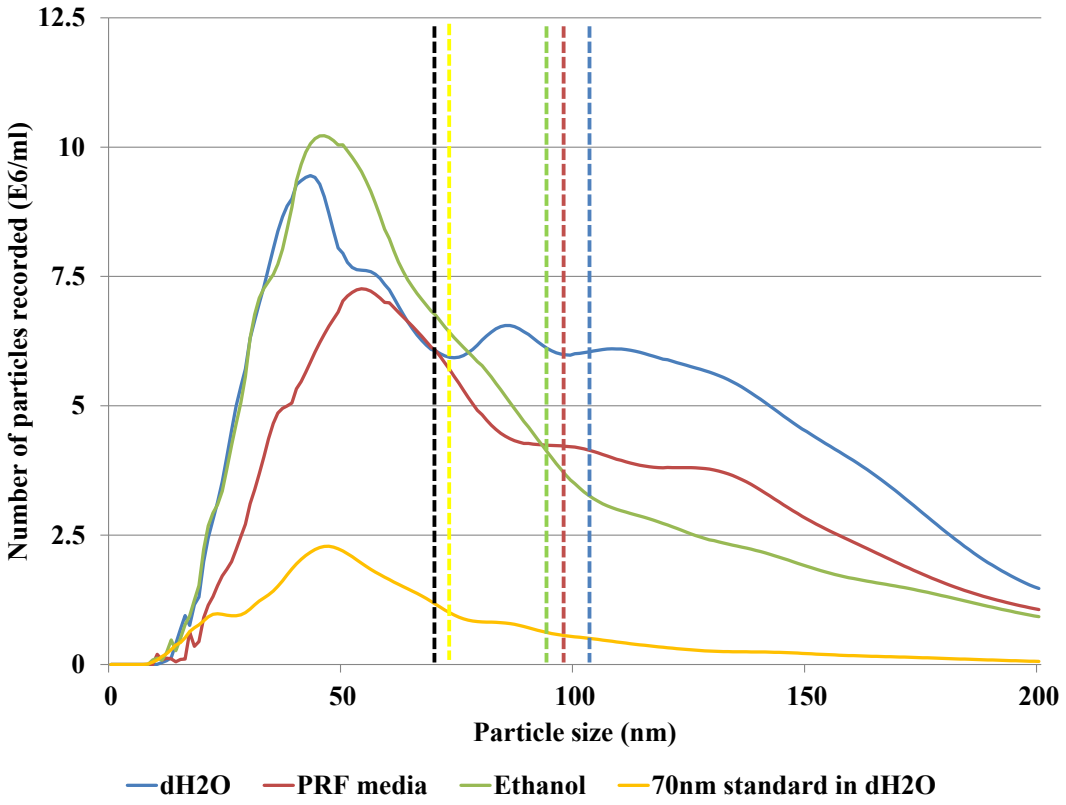

Figure 3.25. NTA size distribution expressed as number of particles of ZnO-45009 nanomaterial dispersed in: dH_2O (blue), PRF media (red) or ethanol (green). The 70nm polystyrene standard results are shown in yellow. *The dotted lines indicate the position of mean particle size calculated from distribution data for each dispersion with the black line indicating manufacturer stated size.* Analysed at room temperature (n = 6).

The particle size distributions in Figure 3.25 show ZnO-45009 nanomaterial dispersed in all solvents peaking with the highest concentration of particles at a similar size to those recorded for the 70nm polystyrene nanosphere standard (43nm, 54nm, 46nm and 47nm for dH_2O, PRF media, ethanol and the standard, respectively). These were smaller than the manufacturer particle size indication (~70nm).

There was an obvious skew noted in the calculation of the averages reported, due to larger particles in the tail of distribution curves. This was consistent with the result from NTA analysis of the polystyrene standard. For ZnO-45009 nanomaterial dispersions, this was likely a consequence of the high number of particles recorded across the entire size range in all dispersions. The dH_2O and PRF media dispersions in particular displayed high concentrations of particles above 100nm, corresponding to the largest mean diameters.

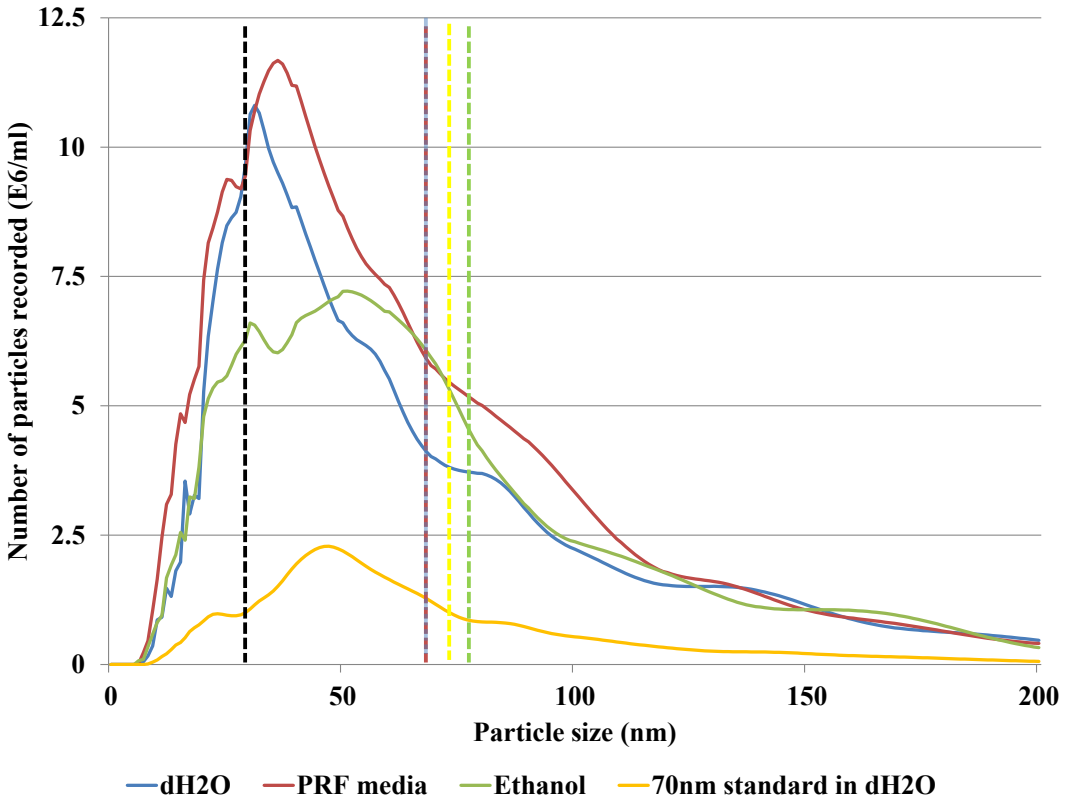

Figure 3.26. NTA size distribution expressed as number of particles of ZnO-45408 nanomaterial dispersed in: dH_2O (blue), PRF media (red) or ethanol (green). The 70nm polystyrene standard results are shown in yellow. *The dotted lines indicate the position of mean particle size calculated from distribution data for each dispersion with the black line indicating manufacturer stated size.* Analysed at room temperature (n = 6).

Figure 3.26 shows the particle sizes recorded for dH_2O and PRF media dispersions of ZnO-45408 nanomaterial, displaying a sharp peak in particle size distribution curve corresponding well with manufacturer details. However, it is evident that the mean is skewed due to the presence of particle numbers measuring in excess of 100nm, as explained by the 'tail' in size distribution. The 'tails' were lesser in extent to those for the previous ZnO-45009 nanomatetial, resulting in a smaller average across all dispersions. In ethanol, a lower number of particles was recorded across the size range of detection, as this dispersant contributed a broad peak stretching between particle size measurements of 20nm-85nm.

The effects of solvent on nanomaterials were hypothesised to have contributed these 'real' measurements, speculated as agglomerates formed in unstable colloidal systems that were thought dynamic and in the process of flocculation. This was tested by evaluating colloidal stability as inferred by measuring nanomaterial zeta potential.

3.1.6 Nanomaterial zeta potential measurements

Zeta potential measurements allowed for assessment of the stability of nanoparticles in each of the three dispersions used for DLS and NTA size measurements. To present the zeta potential measurement in the correct context, pH values of the solutions analysed were also included.

Results are reported below, and refer to data in Table 3.3 and Table 3.4 with zeta potential stated graphically in Figure 3.28 with respect to the generally accepted assessment of colloidal stability depicted within the Figure 3.27 below.

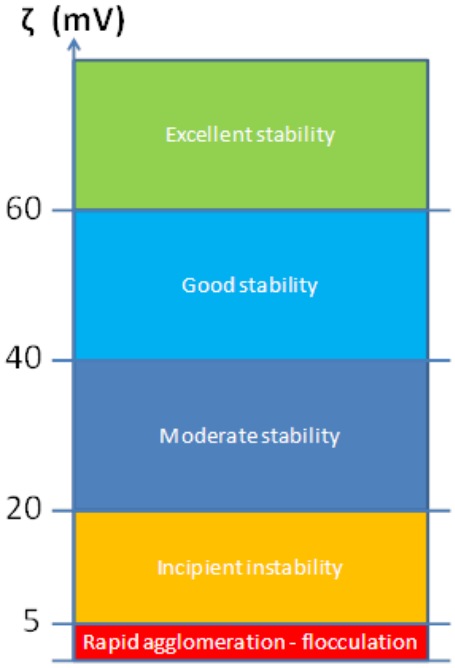

Figure 3.27. The general classification of colloid stability in solution based on zeta potential (ζ) measurements, negating charge on particle. *Adapted from* (Vallar *et al.*, 1999).

Table 3.3. Zeta potential of nanoparticles measured in three different solvent dispersions at both 22°C and 37°C. The Smoluchowski's theory was used for calculations of electrophoretic mobility of the particles based on laser doppling and M3-PALS in the Malvern ZetaSizer NS90. [a] *All results stated are the average of 6 runs (n=6) averaged from at least 4 measurements per run.*

Material	Solvent	Zeta potential **at 22°C** (mV)	± S.D. (nm)	Zeta potential **at 37°C** (mV)	± S.D. (nm)
ZnO-45408	dH_2O	-18.0	1.0	-18.8	0.9
	PRF media	-3.5	2.2	-4.6	1.7
	ethanol	+19.4	5.3	+15.6	8.5
ZnO-45009	dH_2O	+18.2	8.0	+16.9	10.4
	PRF media	+7.9	1.2	+5.5	0.8
	ethanol	+31.4	9.5	+40.2	3.9
TiO_2	dH_2O	-4.5	26.0	+5.3	21.6
	PRF media	-7.7	7.4	-9.4	2.2
	ethanol	+8.4	8.5	+15.9	15.3
SiO_2	dH_2O	-27.5	18.8	-24.8	4.0
	PRF media	-17.8	13.7	-23.2	4.8
	ethanol	-17.5	6.5	-20.8	8.2
Hydroxyapatite	dH_2O	-12.4	7.7	-8.9	7.5
	PRF media	-11.1	5.0	-7.2	2.4
	ethanol	+28.6	24.8	+46.8	13.4

Table 3.4. pH measurement of nanomaterials diluted to a 0.001% w/v concentration in either dH2O or PRF medium prior to Zeta Potential analysis. All measurements carried out at room temperature, with results an average of 3 different readings carried out on different days (n=3) with standard deviation reported.

Nanomaterial	Solution	Temperature °C	Mean average of results pH	Standard deviation
BLANK	dH_2O	24.3	5.99	0.16
	PRF media	25.1	5.54	0.01
	Ethanol	25.4	N/A	N/A
ZnO-45408	dH_2O	26.4	7.18	0.17
	PRF media	25	7.19	0.09
	Ethanol	24.8	N/A	N/A
ZnO-45009	dH_2O	25.1	7.41	0.12
	PRF media	25	8.11	0.72
	Ethanol	25.1	N/A	N/A
TiO_2	dH_2O	25.5	6.27	0.56
	PRF media	24.1	6.70	1.17
	Ethanol	24.9	N/A	N/A
SiO_2	dH_2O	24.4	6.88	0.06
	PRF media	24.6	7.42	0.94
	Ethanol	25	N/A	N/A
Hydroxyapatite	dH_2O	24.4	7.25	0.34
	PRF media	24.4	7.05	0.52
	Ethanol	24.8	N/A	N/A

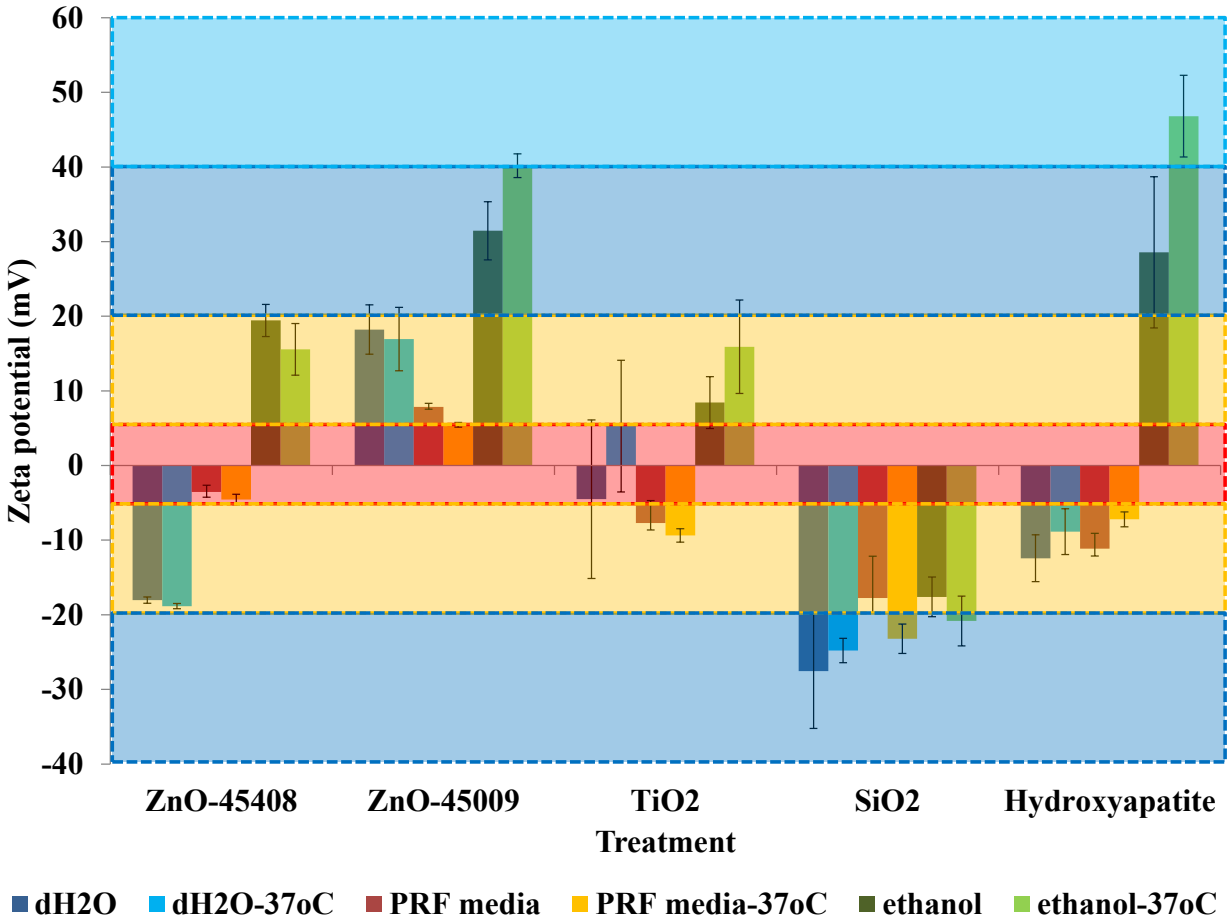

Figure 3.28. Zeta potential measurements of nanoparticle surface charge, taken from the data in Table 3.4. Coloured zones indicate the generally accepted levels of colloidal stability: **RED** = Flocculation, **AMBER** = instability, **DARK BLUE** = Moderate stability and **LIGHT BLUE** = Good stability.

Table 3.3 highlights the range of zeta potential measurements of the various nanomaterials and also the differences exerted by the solvent environment they were dispersed in. Both positive and negative charges were observed, ranging from +46.8mV (hydroxyapatite nanomaterial dispersed in ethanol (37°C)) to -27.5mV (SiO_2 nanomaterial dispersed in dH_2O (22°C)). Results remained consistent for the majority of nanomaterials in each of the dispersions, despite the 15°C temperature difference between the two analyses. These data suggested physiological temperature had little impact on colloidal stability, with no statistical significance noted. The sole exception was TiO_2 nanomaterial in dH_2O, where the validity of the measurement was questioned due to large standard deviations at both 22°C and 37°C. This was thought to contribute an assessment of colloidal instability for this nanomaterial when dispersed in dH_2O.

The pH values recorded in Table 3.4 showed elevated H^+ levels in both aqueous solutions through the presence of nanomaterials in dispersion. However, the values reported do not exceed human physiological pH ranges and would not be expected to cause harm to cells, except for ZnO-45009 in PRF media. ZnO-45009 was the only sample to record a positive zeta potential measurement in PRF media, and this was observed alongside increased the pH of solution (by nearly 50% from the original control value). This dispersion was more alkaline, with pH value exceeding that of most living systems in the human body (Boron & Boulpaep, 2008). Whilst the remaining nanomaterials also increased the alkalinity of the dispersions, none of the values were considered extreme, with respect to other physiological conditions found in the human body.

During nanomaterial sizing in solution (DLS and NTA results), most particle distributions had inferred nanomaterial instability in each of the disperions tested, to differing extents. This hypothesis was supported by the zeta potential data, as can be visualised in Figure 3.28. The graph plots zeta potential for each nanomaterial-dispersion, measured at both 22°C and 37°C, in the context the value implies to colloidal stability with reference to the generally accepted classification shown in Figure 3.27 (Berg *et al.*, 2009, Kaszuba *et al.*, 2010, Vallar *et al.*, 1999).

Figure 3.28 shows zeta potential measurement of TiO_2 nanomaterial in dH_2O analysed, at both temperatures (to correspond with the red zone) indicating the likely occurrence of flocculation or agglomeration. Flocculation was also indicated for the ZnO-45408

nanomaterial dispersed in PRF media. Zeta potential values corresponding with the highest incidents of instability (the amber zone) were recorded in this dispersant.

Temperature of analysis was not considered a significant factor relating to nanomaterial stability in dispersion, with only hydroxyapatite and SiO_2 nanomaterials dispersed in ethanol (and the example of SiO_2 in PRF media) observed to change the stability label of the suspension. However, in all examples, analysis at 37°C corresponded with improved stability, but only marginal differences were observed in the actual zeta potential measurement when compared to the results at 22°C. Dispersion solvent was considered to have a greater influence on zeta potential. In aqueous solutions (dH_2O and PRF media), all zeta potential measurements recorded a net negative charge (ZnO-45009 being the exception), and for all nanomaterials this was reversed to a net positive charge in ethanol (except for SiO_2 nanomaterial).

Due to the relative ionic neutrality of the three solvents, both ZnO-45009 and SiO_2 nanomaterials were thought to express the strongest ionic charges (positive and negative, respectively) at their particle surfaces. The polarity of their strong ionic net charge prevailed despite the effects of solvent molecules, and this corresponded to some of the largest zeta potential values measured across all samples (Table 3.3). ZnO-45009 and SiO_2 nanomaterials were observed to form the most stable dispersions, along with hydroxyapatite nanomaterial-ethanol dispersions.

3.2 Discussion

It has been documented previously that nano-scale confers new and often unique properties to a nanomaterial over its bulk counterpart. These are increasingly being exploited in new technologies, with safety assessment and legislation struggling to keep pace with nano-technological developments (Choi *et al.*, 2010). This is complicated by governments, regulators and industry adopting a cautious approach in definitively specifying the criteria required for new chemical entities to trigger a 'nano' tag. This is most obvious through mapping the European Commissions' (EC) progress towards a regulatory framework tasked to deal with the growing presence of nanomaterials ((SCCP), 2007, (SCENIHR), 2006, (SCENIHR), 2009). On the 18th October 2011, the EC adopted the recommendation of the current definition of a nanomaterial ((EU), 2011). This states':

"*A natural, incidental or manufactured material containing particles, in an unbound state or as an aggregate or as an agglomerate and where, for 50 % or more of the particles in the number size distribution, one or more external dimensions is in the size range 1 nm - 100 nm.*

In specific cases and where warranted by concerns for the environment, health, safety or competitiveness the number size distribution threshold of 50 % may be replaced by a threshold between 1 and 50 %."

Whilst not legally binding, this legislation gives both those working towards exploiting nano-properties or investigating their safety a guideline to work to so that research can start to employ these conditions when investigating nanomaterials. This project seeks to comply with these conditions, and so initial characterisation work in this chapter was chiefly concerned with identifying nano-characteristics in each commercially sourced nanomaterial. Through comprehensive utilisation of as many techniques available, comparisons back to bulk and between the different chemical materials, any nano-specific findings were to be linked with explanations for potential cytotoxic effects observed later, using *in vitro* models. This constituted the initial stage of the risk assessment of hydroxyapatite, SiO_2, TiO_2 and ZnO nanomaterials for use in formulations putatively advantageous in future oral healthcare products.

The slow progress in arriving at a consensus on a clear and full nano definition has in part been due to legal ramifications for commercial products and industrial processing working with nanomaterials, with their risk assessment not fully complete. But it has also been complicated due to the intrinsic complexities manifested at the nano-scale

when traditional materials are reduced in size. These were experienced during the course of this investigation, and will now be discussed in detail.

3.2.1 Size determination

Working within the EC recommended definition of a nanomaterial, measuring the particle size was considered the most fundamental characteristic to determine. However, from the results presented in this chapter, the average particle size of each material characterised was different dependent on the technique used for analysis. Table 3.5 summarises the average particle diameters recorded for each material, measured using the different sizing techniques. Average particle size values recorded were generally outside those reported by the manufactures for each material. However, it is important to accept how crude a single size value may be when not reported alongside the conditions of analysis to provide appropriate context. No one value recorded using any one of the different methods was considered more or less accurate than another. These points highlight the difficulty in simply determining a characteristic considered a fundamental attribute of a material being defined as "nano" ((HSE), 2010, Borm *et al.*, 2006).

When we consider the term "particle size", it projects an assumption towards a definitive, fundamental characteristic. However, in reality this view is too simplistic. For example, particle size can be expressed in many different ways (*e.g.* average particle size, primary particle size, agglomerate, surface area *etc.*) depending upon a number of factors ((SCENIHR), 2009). It can be affected by particle shape, uniformity of shape in the sample, uniformity of size within a sample (known as polydispersity) and from these, the size distribution must be considered which in turn can influence the terminology by which the average particle size data is reported (Domingos *et al.*, 2009). To make the situation even more complicated, many of these factors can change with regard to experimental conditions, nanomaterial manufacturing processes, sample preparation and even method of reporting size analysis (Stone *et al.*, 2010).

Determining the morphology of particles using electron microscopy was perhaps the most straight forward characterisation process. It relied upon visual inspection to determine the size, shape and with SEM, surface appearance. Both SEM and TEM micrographs showed clear nanoparticle morphologies which allowed direct measurement of individual particle sizes. Figure 3.4 and Figure 3.8 were deemed to be the most representative assessment of size due to the close proximity of the mean

values of size measurements recorded with those stated by nanomaterial suppliers (Table 3.5). Electron microscopy had the additional benefit of being the only technique employed that allowed for direct comparison with the bulk counterparts, over a range of magnifications. However, this technique of measuring size also relied most heavily on operator intervention and interpretation in identifying the most appropriate magnification, image quality and manual measurement to generate reliable sample populations. By dividing each image using a grid and randomly selecting particles to measure, it was hoped subjectivity in size measurement would be avoided. However, in reality subjectivity was impossible to circumvent completely. For example, the greater value for bulk SiO_2 mean particle size recorded from TEM micrographs, in comparison to SEM may have been a consequence of particle morphology being harder to observe from the TEM micrographs. The size measured may have also been dependent upon geometry of the particles. For example, the size of a regular sphere is measured in terms of a radius, or diameter. A cuboid, by its height, width and depth. This simplicity breaks down dramatically as structures move further away from these regular shapes, and this has implications for the vast majority of current particle sizing techniques that are inadequate in dealing with particle geometry and orientation (Mathaes *et al.*, 2013). For example, particular difficulties have arisen in characterising dispersed carbon nanotubes (Krause *et al.*, 2010), nano-rods and fibres (Oberdorster *et al.*, 2005a) (such as ZnO), with length and width dependent upon sample orientation. Even more difficult is the accurate measurement of surface modifications with relation to particle diameter, that considerations such as the thickness a protein corona may contribute (Lynch *et al.*, 2007). Non-spherical particles are difficult to characterise over mono-modal spheres in terms of sizing techniques, but all nanoparticles are subject to increased agglomeration in biological media, which often creates non-uniform and unpredictable structures (Landsiedel *et al.*, 2010). This was definitely the situation experienced with the nanomaterials characterised in this study, with an array of particle shapes and sizes observed, sometimes all within the same sample.

Heterogeneity was likely to be a factor that contributes to the high standard deviations recorded for particle sizing carried out from micrographs (Figure 3.4 and Figure 3.8). The particle size measurements for hydroxyapatite bulk material and all three ZnO materials were noted as particularly troublesome; each sample exhibited highly heterogeneous particle morphologies. Morphology was not the sole contributor towards increased error in particle size measurement: particle orientation when fixed during

sample preparation and and non-symmetrical particle morphologies were also problematic. In addition to the difficulties these posed towards accurate particle sizing, they also had important connotations for other areas of this study. Reports in the literature have long linked particle shape with cytotoxic properties (Borm *et al.*, 2006, Buzea *et al.*, 2007, Nel *et al.*, 2006, Oberdorster *et al.*, 2000):, particularly with regards to rod-like fibres (the classical example being that of asbestos fibres causing chronic diseases in humans (Mossman *et al.*, 1983, Oberdorster *et al.*, 2005a)). Furthermore, shape of particle has an important bearing on the theory of DLS. A fundamental assumption used in the calculations of a particle size assumes Brownian movement of *spherical* particles. Rod-like shapes as observed in some ZnO material morphologies can still follow Brownian motion at the right concentrations. However, their movement is likely to involve a tumbling motion that during lengthways rotation scatters light from the surface at a greater intensity than reflection from the alternative axis surface momentum. This results in the detection of more scattered light, transpiring as a larger average particle diameter. The degree to which this situation influences results was difficult to accurately assess because of the unpredictable movement of nanoparticles, which is by nature random when moving by Brownian motion. In practice, most regular shapes, devoid of one or more extreme dimension in relation to the majority of the particle surfaces (*e.g.* long thin fibres) fit the algorithm with only a small percentage of error occurring when they form some symmetry in rotation (Pabst & Gregorová, 2007). This makes DLS particle sizing a popular nanoparticle characterisation tool.

Table 3.5 displays the low standard deviations for values recorded for average particle diameters of both bulk and nano forms of SiO_2 and TiO_2. Electron microscopy imaging depicted the more uniform nature of these particle structures and sizes, but this did not necessarily correspond to a low polydispersity index values from DLS analysis (Figure 3.20 and Figure 3.21). The explanation behind this again refers back to subjectivity in that operator expertise is required to interpret particles morphology observed through electron microscopy imaging. Through manual interpretation of micrographs, it was possible to identify nanomaterial agglomerates, distinguishable from individual nanoparticles. In doing so, this limited the extent of large agglomerates contributing to the average measurements by excluding them from particle size calculations. This may be a subjective decision, but it was also a deliberate action to measure the primary particle size, in an attempt to gain some baseline towards unmodified, individual particle size. It is therefore difficult to compare electron microscopy particle size measurements

with more automated techniques, which lack effective direct agglomeration/aggregation identification.

Modern software packages often possess complex computational analysis programmes able to flag up warnings of heavy agglomeration and sedimentation during sample analysis, but these are still relatively insensitive. DLS analysis using the ZetaSizer software (version 6.1) reported these warnings for hydroxyapatite nanomaterial dispersed in dH_2O (22°C) and PRF media (37°C); SiO_2 nanomaterial dispersed in PRF media (22°C and 37°C); and TiO_2 nanomaterial dispersed in both PRF media (22°C) and ethanol (37°C). In all cases, except SiO_2 nanomaterial in PRF media at 37°C, these indications were confirmed by zeta potential values that corresponded to the red and amber zones used to indicate flocculation and dispersion instability (Figure 3.28). Other nanomaterial dispersions also fell within these regions on the graph, and yet were not detected by the instrument software. Automated, algorithm-based size determination software serves these warnings, which can prove useful when reporting the data, but they do not actively manipulate the data to aid single particle size measurements. Therefore, other nanomaterials in dispersion may have sizing data skewed by the measurement of agglomerates as large single particles. This was speculated to have major consequences in the average particle sizes measured, specifically those reliant upon DLS. Since the intensity of the scattered light is inversely proportional to the sixth power of the radius of the nanoparticle, a 50nm particle will scatter a million times as much light as a 5nm particle. As such, average particle size values determined by DLS are likely to be heavily biased in the presence of large particulates (Filipe *et al.*, 2010, Linsinger *et al.*, 2012a). It is not only the larger size of agglomerates over individual particles, but the irregular shapes formed by uncontrolled, complex particle-particle interactions that can lead to increased skewing in size averages (again connected with their random orientation as they move through the laser beam to scatter light) (Landsiedel *et al.*, 2010). Both of these effects were considered as occurring during DLS analysis of the nanomaterials investigated here. This was observed through the much greater particle sizes recorded when using this technique in comparison to all others (Table 3.5), and consolidated by zeta potential values falling within the range considered unstable. Results reported in this study correlate closely with Domingos *et al.*, findings; notably the increased particle sizing of TiO_2 and ZnO nanoparticles by DLS, due to agglomerates, in a multi-method sizing comparative study (Domingos *et al.*, 2009). This

rationale was used to exclude the results from DLS analysis when size measurements were applied to display the overall ranking of size between the nanomaterials.

Conversely, very large agglomerates may also skew results in the opposing direction, producing smaller particle size measurements that are different from the real particle size distributions. Large agglomerates may become dense enough to sediment to the bottom of the solution (Allouni *et al.*, 2009, Bootz *et al.*, 2004, Murdock *et al.*, 2008, Provder, 1997), a process termed flocculation. Large masses of agglomerates can then be negated from the size measurement and cause the detection of larger numbers of smaller particles than actually present. This occurs through falsely recording fast sedimentation as Brownian movement (with fast light scattering correlating to smaller particles), or alternatively, real detection of nanoparticles still suspended and present within the dispersion. Both of these effects may have been present within the DLS data reported, where small average particle sizes calculated correspond with zeta potential measurements below 20mV. This effect was highly probable to have occurred within the relatively unstable TiO_2 nanomaterial dispersion in dH_2O, as both DLS and zeta potential results corresponded to visual flocculation in the sample tube. This view was backed up by Meiβner *et al.*, who also experienced the high agglomeration rates of mixed anatase:rutile TiO_2 that was dispersed in serum-free media (Meißner *et al.*, 2009).

Throughout the characterisation of these nanomaterials in dispersion, many of the problems associated with DLS particle size analysis can be attributed to the high heterogeneity between the particle size and morphology of each sample, as observed in Figure 3.20, Figure 3.21 and through observations with electron microscopy. These were deemed a consequence of utilising commercially sourced, bulk manufactured nanomaterial products. Whilst the particle size variation added complexity to the characterisation process, especially in regard to determining common characteristics that may have implications in future cytotoxicity studies, these outcomes reflect real life scenarios. Large-scale industrial manufacturing of nanomaterials is currently unlikely to result in strictly uniform, monodisperse nanoparticles (Schulze *et al.*, 2008), as was highlighted during this study. These remain difficult to produce on the analytical scale, due to the high level of environmental control required to produce nanoparticles (Skapin *et al.*, 2007), that maintain their characteristics *in situ* (Borm *et al.*, 2006). Heterogeneity has implications for the cosmetic industry, where it is likely to require bulk scale masses of nanomaterials in the formulation of commercial scale product

manufacturing (Aitken *et al.*, 2006). Outcomes from characterisation fully reflected the challenges facing nanomaterial formulation in future oral healthcare products, in fulfilment towards stringent regulation and legislation to protect the consumer ((SCCP), 2007).

Despite its well documented problems, particle size measurements recorded by DLS were thought to be fully vindicated for inclusion as a characterisation technique. DLS was the only technique able to detect the likely occurrence of a change in nanoparticle state with regards to agglomeration or aggregation, when dispersed in different solutions (Domingos *et al.*, 2009). It was important to consider agglomerates, as they are likely to exist or manifest in real life nano-samples. The EC has accepted this, and incorporated into the nanomaterial definition the terms agglomerate and aggregate. The ISO Technical Specification (TS) 27687 defines particles clustered in agglomerates and aggregates separately:

"Agglomerate: Collection of weakly-bound particles or aggregates or mixtures of the two where the resulting external surface area is similar to the sum of the surface areas of the individual components.

Aggregate: Particle comprising strongly-bonded or fused particles where the resulting external surface area may be significantly smaller than the sum of calculated surface areas of the individual components". ((ISO), 2008).

Their consideration as nanomaterials is due to the possibility of nano-pores conferring functionality within the agglomerated nanoparticles. Low magnification images of the samples studied here showed large agglomerates in some of the powdered starting materials. The term agglomerates is preferred here, due to the unknown reversibility of material back to nano-form. When magnification was increased, gaps in particles were measured and deemed to meet the criteria constituting a nanoparticle definition. However these were not included in the measurements that constituted the mean size of nanoparticles at this stage of initial characterisation. This was due to the primary interest directed towards the raw nanomaterial properties, and no nano-pores were observed through SEM analysis of particle surfaces.

The NTA method has also been reported to suffer from similar inaccuracies associated with nanoparticle agglomeration tendencies (Domingos *et al.*, 2009). This was not considered such a problem with the NanoSight instrument, as results using this method reported lower particle size distributions for all nanomaterials dispersed in solutions. As

the same samples were analysed for both DLS and NTA instrumentation, the latter measurements were thought to be restricted by a lower upper limit of particle size. The reason is due to the small field of view used to video the nanoparticle movements which can easily become saturated by materials that have high refractive indexes, a property indicative of metal oxides (such as those of the nanoamaterials investigated in this project). This method could be interpreted so as to distort the mean particle size, away from the 'real' average of the sample, present within a wide mix of nanoparticle sizes and agglomerates.

This behaviour of the nanomaterials may have contributed to these 'real' measurements, indicated by the initial peaks in number of particles detected, for SiO_2, TiO_2 and ZnO-45408 nanomaterial sizes by NTA, which match well with the manufacturer stated particle sizes (Figure 3.23, Figure 3.24 and Figure 3.26 respectively). Alternatively, the remaining distribution may have been skewed by agglomerates forming in unstable, dynamic colloidal systems that may have been in the process of flocculation, as observed by DLS. However, an alternate explanation may be that the origin is similar to the problems associated with polystyrene standards, in respect to RI values of the material. Polystyrene, hydroxyapatite and SiO_2 were known to have lower RI in comparison to the other nanomaterials (Table 2.1), and would have scattered light less prominently. NTA using the NanoSight LM10 instrument relies upon visualised light scattering through the CCD camera. Changes in these parameters govern image quality in the video files. Where inadequate light scattering resolution was observed, changes in these parameters (such as increased gain), may have caused NTA software to detect background interference as small particles. Noise from data capture may not entirely be a result of low RI, as Montes-Burgos *et al.*, experienced similarly broad peaks as reported for the 70nm polystyrene here, with their study using a NIST™ traceable 60nm gold standard (known to scatter light well (Jans *et al.*, 2009) for evaluating DLS versus NTA for nanotoxicology related characterisation (Montes-Burgos *et al.*, 2010). Therefore, low and high RI values may heavily influence the respective lower and upper limits of particle detection for this technique (Gardiner *et al.*, 2013, Malloy & Carr, 2006).

Despite the limitations, NTA analysis was thought beneficial to this study, utilising the greater sensitivity reported for this technique in analysing highly polydisperse samples (like these nanomaterials investigated in this research) (Filipe *et al.*, 2010). NTA was able

to avoid the influence of larger particulates within a polydisperse sample, by sizing on a particle by particle basis, using video tracking of the light refracted by a single moving particle. It then followed similar theoretical assumptions as DLS, where smaller particles move faster and larger ones migrate more slowly when in Brownian motion. NTA particle size distributions peaked before the nanosize definition of 100nm particle size was reached for the majority of samples analysed. Only the NIST™ traceable standards recorded a comparable average size result to DLS analysis. This suggests that whilst NTA sizing data might fail to show the true picture of average particle sizes for the overall sample, it is more sensitive at the nanoscale. This was important information to collate within the research, as it enabled a more accurate assessment of just how small the particles in each nanomaterial might be. It is expected that like most nanomaterials dispersed sub-optimally in culture media (mimicking conditions of delivery when applied to treat cells *in vitro*), hydroxyapatite and the metal oxides investigated here, would also agglomerate (Allouni *et al.*, 2009, Murdock *et al.*, 2008, Teeguarden *et al.*, 2007). But it remains important to fully characterise the entire population of nanoparticles, some of which may remain nano in size and in doing so, able to exert a nano-specific cytotoxic effect (Jaeger *et al.*, 2012, Moos *et al.*, 2010, Patri *et al.*, 2009, Yang *et al.*, 2009, Yuan *et al.*, 2010). Through identification of the smallest sizes of nanoparticle in each sample, potential nanomaterial toxicity could be considered, assessing the full risk of nanotoxicity from the worst case scenario.

Problems experienced by both DLS and NTA include relating particle size distributions to the average values within each sample. This was especially pertinent considering the positioning of the mean in relation to NTA size. DLS in contrast, reports quantitative intensity-size distributions, which are direct representations of the 'raw' signals and use a minimum of additional assumptions about the particles. From this, the hydrodynamic diameter was calculated as the mean effective size within the population. Conversion of DLS data to a number-weighted result requires assumptions about nanomaterial shape and dispersity, which are usually much different in real samples. It can therefore be prone to errors that are exponential in their influence as the calculations are applied. Therefore, direct comparison between particle distributions achieved through DLS and NTA analysis cannot be made.

A particle size distribution can be characterised by various parameters. Traditionally, as was the case here, means are often reported (Mathaes *et al.*, 2013). However, there are

compelling arguments towards including the modal size value and/or the median average (Roebben *et al.*, 2011). In perfect monomodal nanoparticle dispersions, the mean, modal and median values would all be equal, located at the centre of a symmetric particle size distribution curve. As observed over the course of characterisation with these nanomaterials, this was not the case. Similarly, it would be viewed as uncommon for most nanomaterials in the real world. Reporting the modal average constitutes the particle size measurement corresponding to the highest peak in respective size distributions. This may be appropriate under comparable bi- or multimodal distributions, where particle size distributions concisely fits into separate populations of equal intensity/concentration (Montes-Burgos *et al.*, 2010). In a similar way to Montes-Burgos *et al.*, 2010, who reported modal average of gold nanoparticles dispersed with protein, this may also have been effective in DLS reporting of hydroxyapatite nanomaterial dispersed in dH_2O (Figure 3.15) or SiO_2-nanomaterial analysed in PRF media (Figure 3.16). However, it was not considered appropriate for the other samples, viewed during analysis as (presenting a dynamic, turbulent environment) many of which were suspected to experience un-quantified but significant flocculation. During repetitive measurements (n=6), individual distributions were viewed differently between analysis, as indicated by relatively high standard deviations in hydroxyapatite sizing. Whilst the mode may have been acceptable for an individual run, the variation in sample distributions experienced between results may have produced a wildly inaccurate averaged modal value, constituted from the data of multiple analysis (n). The lack of reducibility between runs raises serious questions as to the appropriateness of particle sizing this material without first stabilising particles in the dispersant. Whilst this could have been done, through the use of biocompatible surface coatings such as polyethylene glycol (Wang *et al.*, 2010) or FBS proteins (Dominguez-Medina *et al.*, 2013), this was considered a modification which would have invalidated the study investigating the natural effect hydroxyapatite nanomaterial has on the human oral mucosa. Both PEG and FBS protein coatings applied to nanoparticles surfaces to aid dispersion, have been subsequently found to increase uptake into cells (Prasad *et al.*, 2013b, Shah *et al.*, 2012, Walkey *et al.*, 2011).

The median particle size reports the middle value in the sample distribution. This has proved useful for nanomaterials specifically, when the wording of the current recommended definition is considered. This states a nanomaterial to be defined as such:

"…where 50 % or more of the particles in the number size distribution, one or more external dimensions is in the size range 1 nm - 100 nm." ((EU), 2011).

Therefore, in most cases where there exists no large population of nanoparticles (less than 1nm in size), materials with a median particle size between 1nm and 100nm can be considered as meeting the requirements to be defined as a nanomaterial. Reporting this average may have worked well for NTA particle distributions, where the upper limit of detection was below 200nm. However, the upper limits of DLS detection was stated to be on the μm scale (5μm), and so agglomerate size measurements were as significant in the particle distributions as nanoparticles. The bias towards light scattering from larger particles, as reported by the median from these data would likely skew the average size towards a larger value then actually present in the distribution. Therefore, whilst median arithmetic values may strike a good balance between extremes of small and large sizes on the nano-scale, the mean was reported for the data known to constitute micron sized agglomerate, which is consistent in multiple analyses. This was a compromise to allow for comparison between the different sizing techniques, but was only deemed accurate when reporting values in the context of how the particle size distribution was configured: a strategy currently deemed most appropriate for the reporting of polydisperse nanomaterial sizes (Bootz *et al.*, 2004, Gaumet *et al.*, 2008, Kato *et al.*, 2009, Murdock *et al.*, 2008).

In the context of the multiple techniques used to assess the nanomaterial particle sizes investigated within this study, the best approach to compare size disparity was via their rank position, from smallest to largest (Domingos *et al.*, 2009). All data was pooled in Table 3.5 to allow direct comparisons between the materials investigated. The general trend indicated from the manufacturer particle size information was considered accurate in comparison to the relative ranking position of each material. The exception was unexpectedly the SiO_2 bulk material, positioned first with the smallest particles (measured using electron microscopy). Key to the study research goal was particle disparity between nano and bulk materials, to highlight any nanomaterial differences observed during *in vitro* cytotoxicity testing. Bulk materials remain the best available reference or control to nano-investigation in the face of few limited standardised

nanomaterial controls (Stefaniak *et al.*, 2013). Attempts are being made to establish a catalogue of traceable nanomaterial standards that measure reproducible characteristics between different labs (Aitken *et al.*, 2008), but the variety of these systems currently remains limited. Slow progress has perhaps been in part due to the difficulties in handling nanoparticles. As characterisation has proved here, identifying clear attributes is highly dependent upon the environment they are in (Nel *et al.*, 2009, Oberdorster *et al.*, 2005a) and the technique and sample preparation steps carried out during analysis (Linsinger *et al.*, 2012a). SiO_2 size results may have proved to be a surprise, and prompt caution in reporting any nano-specific effects as the investigation moves forward into their use as treatments in the *in vitro* studies, but they actually serve to highlight the importance and need for thorough characterisation of materials. Understanding what the characteristics mean related to raw properties is crucial in the context of cosmetic ingredient regulation ((SCCP), 2007, (EU), 2010, Faunce, 2008), and important in establishing the background for ascertaining the full risk assessment of their inclusion in future healthcare formulations.

SEM and TEM imaging techniques provided the greatest insight into nanomaterial characteristics such as the shape, surface appearance and overall morphology of each material. Hydroxyapatite appeared the most different when comparing bulk and nano forms, however it was impossible to determine the similarity of material composition in terms of crystalline structure, specific isoform or other stereochemistry's without other analytical investigation. This may be crucial in attempting to explain effects of a material through interaction with biological structures, with toxicity studies plentiful with reports of specific isoforms of a material causing a different reaction over the same chemical in alternative forms (Brunner *et al.*, 2006, Gulson *et al.*, 2012, Maurer-Jones *et al.*, 2010, Park *et al.*, 2011, Xia *et al.*, 2008, Zhang *et al.*, 2003). The generation of a polydispersity index in DLS analysis was a particularly useful calculation and enabled numerical attributes to be used to compare the differences in particle sizes and appearance observed for SEM and TEM.

Bulk hydroxyapatite was noted as lacking uniformity between particle to particle morphologies in SEM micrographs. Whilst polydispersity was also present in bi-modal sizes of the nanoparticles constituting the nanomaterial, overall it remained more likely to find two particles dissimilar in size and appearance for bulk hydroxyapatite material. This was not considered a major issue as bulk materials are expected to be cruder in size

and appearance, due to the less strict controls exerted over particle formation during manufacturing. In contrast nanomaterials are relatively difficult to manufacture. Their complex chemistry's require accurate and precise control over temperature, pH, pressure, precipitation rates as well as the milling, recovery and classification processes, which are all intertwined to produce nano-sized materials (Applerot *et al.*, 2009, Skapin *et al.*, 2007). ZnO nanoparticles (ZnO-45009 and ZnO-45408) emphasised this, with some particulates that are long and spindly mixed in with shorter, wider, relatively more spherical particles.

EDS was carried out to confirm the composition of materials were what were stated by the manufacturers: a level of quality control validated in the light of SiO_2 bulk particles measuring nano in size (<100nm). Spectra confirmed the composition of the materials contained elements expected from chemical structure of each material. Spectra were consistent between bulk and nanomaterial comparison for each distinct material, including hydroxyapatite despite the clear differences in particle morphology. Unexpected elements were largely accounted for by background from the FEG-STEM instrument (aluminium, carbon and platinum). However, some additional peaks were observed for elements speculated to account as remnants from sample preparation.

The EDS samples were prepared for initial SEM analysis, with dispersions not diluted from stock solution. These were highly concentrated and contained elements of the manufacturers original dispersant. Evidence of this was seen by the presence of unexpected elements following EDS analysis of SEM samples, particularly sodium present alongside both ZnO nanomaterials (Figure 3.12). This was speculated to belong to the dispersant, with sodium based salts commonly formulated alongside polyethylene glycol[6] (Chen *et al.*, 2011, Shah *et al.*, 2012, Zhang *et al.*, 2007). The presence of these artefacts from EDS may have inferred the presence of residual coatings on nanoparticle surfaces, used to avoid particle-particle interaction, much like what is possible when engineering nanoparticles as drug delivery permeation enhancers (Andrews *et al.*, 2009, Kipp, 2004, Kreuter *et al.*, 2003, Lockman *et al.*, 2003, Lockman *et al.*, 2002, Rahimnejad *et al.*, 2006, Senel *et al.*, 2000, Yin Win & Feng, 2005).

[6] Polyethylene glycol (PEG) was determined to be a prominent constituent of both ZnO-45009 and ZnO-45408 nanomaterial dispersions (see appendix data). PEG is a widely employed coating to reduce particle-particle interactions between nanomaterials, and was likely utilised with ZnO nanomaterial products to maintain the nano-size range of their particles in solution.

Table 3.5. A summary of the particle size analysis for all current materials tested in all methodologies reported within this chapter*. All results included are taken from analysis carried out at 22°C.

Material	Supplier information	Solvent	ZetaSize	± S.D	NanoSight	± S.D	SEM	± S.D	TEM	± S.D	Overall mean particle diameter *	Particle size ranking
			Mean particle diameter (nm)								(nm)	(1-9)
ZnO-45408	Alfa Aeasar	dH_2O	177.1	4.8	68.6	39.5	53.4	30.2				
nanomaterial	Aqueous suspension	PRF media	376.0	167.4	68.5	41.2					**62.7**	**3rd**
	~ 30nm particle size	ethanol	184.1	10.6	75.2	40.8			47.6	23.1		
ZnO-45009	Alfa Aeasar	dH_2O	231.6	12.4	101.4	52.7	67.6	57.5				
nanomaterial	Aqueous suspension	PRF media	522.2	467.7	95.6	54					**82.9**	**5th**
	~ 70nm particle size	ethanol	212.0	13.6	92.9	47.5			56.9	28.4		
Bulk ZnO	Sigma-Aldrich bulk scale powder	dry powder					229.5	226.3			**222.4**	**8th**
		ethanol							215.2	196.6		
TiO_2	Sigma-Aldrich	dH_2O	345.8	539.8	94.8	51.3	28.5	9.8				
nanomaterial	Aqueous suspension	PRF media	3352.7	795.1	99.0	57.6					**62.3**	**2nd**
	~21nm particle size	ethanol	1890.6	770.6	62.7	38.4			26.6	16.3		
Bulk TiO_2	Sigma-Aldrich bulk scale powder	dry powder					183.2	73.9			**180.3**	**7th**
		ethanol							177.4	67.1		
SiO_2	Sigma-Aldrich	dH_2O	334.3	119.1	98.4	44	27.4	14.1				
nanomaterial	nanopowder	PRF media	1417.7	577.4	104.8	55.3					**66.3**	**4th**
	~10-20nm particle size	ethanol	637.3	153.8	82.0	44.8			19.2	8.2		
Bulk SiO_2	Sigma-Aldrich	dry powder					28.8	13.5			**44.3**	**1st**
	bulk scale powder	ethanol							59.9	63.8		
Hydroxyapatite	Sigma-Aldrich	dH_2O	1535.7	648.8	109.0	54.3	122.8	163.1				
nanomaterial	nanopowder	PRF media	577.4	228	102.8	57.1					**101.8**	**6th**
	<200nm particle size	ethanol	153.8	149.2	105.3	55.7			69.1	33.3		
Bulk hydroxyapatite	Sigma-Aldrich bulk scale powder	dry powder					286.3	199.4			**345.4**	**9th**
		ethanol							404.6	273.3		

***** Zetasizer measurements were negated from the overall mean due to questions upon the reliability of the method to assess nanomaterial particle size accurately.

3.2.2 Colloidal stability

Leading on from difficulties experienced attempting to measure the size of each nanomaterial, much of the explanation can be attributed to their instability in solution. Nanoparticle behaviour was particularly dynamic when dispersed in cell culture media, a crucial characterisation environment to consider when wanting to understand the condition of nanomaterials applied *in vitro*. In determining the risk assessment of test nanomaterials it was important to determine their characteristics, not only as a primary particle, but also their interactions between other particles and environmental constituents. These were investigated under a simplified protein containing model of the human oral mucosal environment. Many issues arose, especially size measurement carried out in PRF media, with flocculation encountered as described earlier. This has implications for cell based cytotoxicity assays, with nanomaterial delivery in culture media. It also had important implications for accurate characterisation of nanomaterials, with some of the methods used. In particular, the uniformity in sample preparation, required for direct comparison with nanomaterials investigated at the same dilution in a non-aqueous environment which they may not universally be stable in. The dispersion of nanomaterials governs their behaviour with respect to particle-particle interactions (agglomeration and more permanent aggregation) and particle-solvent interactions that control colloidal stability (Chowdhury *et al.*, 2010, Murdock *et al.*, 2008).

Total protein content in DMEM-Ham's F-12 PRF cell culture media was calculated as 0.75g/L, including essential amino acids such as histidine, isoleucine, lysine, methionine, phenylalanine, threonine, tryptophan and valine, amongst many others (noted from the formulation sheet). As previously discussed, these may affect interactions at the 'naked' nanoparticle surface, due to their reputed high surface area and reactivity (Borm *et al.*, 2006, Hussain, 2009). The protein corona has proved difficult to accurately model and measure (Cedervall *et al.*, 2007b, Faunce *et al.*, 2008, Lynch *et al.*, 2007), but has been implicated in driving interactions at the cell surface with implications on cytotoxicity (Prasad *et al.*, 2013b, Treuel *et al.*, 2013). More applicable to colloidal stability with regard to characterisation difficulties, is the composition of various salts in cell culture media, calculated to contain 7.6g/L, including important elemental salts from ferric, manganese, magnesium, potassium, sodium and zinc derivatives (amongst many others). The variety promotes a highly complex ionic environment that results in interactions that affect the electrokinetic potential measured by the zeta potential (Chowdhury *et al.*, 2010). This measurement has been attributed to reflecting the stability of nanoparticles

in solution, depending upon the value corresponding to Figure 2.1. The difference in ionic environment was most evident between ethanol and aqueous dispersion of nanomaterials, as indicated by the larger zeta potential values in ethanol.

For all size investigation analysis, a successful method of dispersing the nanomaterials was using ethanol. It was chosen to compare the effects of ionic composition in a non-aqueous environment, in part due to preliminary investigations highlighting problems with sedimentation of particles, following dilution (required for accurate analysis) carried out in water or PBS (due to the complex ionic interactions that govern metal oxide nanomaterials dispersion). It is important to note that ethanol is not compatible with cell culture, and so whilst it provided preliminary starting sizes of the nanomaterials, it is unlikely to be an accurate reflection of the state of nanomaterials subjected as solution utilised *in vitro*.

Changes in nanomaterial concentration may have an effect on the behaviour, and in turn the solubility and flocculation tendencies, of each material in dispersion. This related back to views that nanomaterials have individual and unpredictable properties specific to the nano-scale which often different to the bulk scale chemical counterpart (Nel *et al.*, 2006). In particular, it is thought this impacts on their ability to form agglomerates/aggregates with each other and/or other biological material (Kreyling *et al.*, 2006b, Schins *et al.*, 2004, Xia *et al.*, 2004), due to the increased surface area available for particles at the nanoscale resulting in increased surface reactivity (Borm *et al.*, 2006). Whilst dilution can cause agglomeration, it was not observed as a major problem that occurred for the sample preparation carried out using the nanomaterial investigated here. At each characterisation analyses, solutions underwent de-aggregation using a sonicator, as has proven successful in other studies (Siddiqui *et al.*, 2009). This was visibly seen to re-suspend particulates, where during post-cold storage (4°C) agglomeration and sedimentation were both observed. Considering the EC definition of the terms, agglomeration was therefore considered a more probable definition to use throughout this study, due to the reversibility of dispersing nanoparticles back into solution. Alternatively, dispersion can be achieved through a change of the chemical environment in which the agglomerates are kept (pH, concentration of dispersants, *etc.*) (Meißner *et al.*, 2009). However, biological systems work hard to maintain equilibrium under set physiological environments, and this was considered the least controllable

factor, and less compatible with nanomaterial interactions to be studied on cell models under *in vitro* conditions (Schulze *et al.*, 2008).

The science behind colloidal dispersions (such as nanomaterials in solution) is very much governed by particle surface charge interactions at the boundary with solvent molecules (Delgado *et al.*, 2007). As demonstrated in Figure 3.27, zeta potential measurements allude to the solubility of nanoparticles under specific pH interactions (Berg *et al.*, 2009). These results showed that most nanomaterials investigated were unstable or liable to flocculate under the dispersive conditions of analysis. The exceptions included hydroxyapatite and ZnO-45009 nanomaterial (both in ethanol), as well as SiO_2-nanomaterial in dH_2O and PRF media (37°C). These zeta potential measurements were deemed of good or moderate stability, respectively (Figure 3.28).

As touched upon, zeta potential measurement is not only useful in supporting assessment of particle stability/instability state, but has important implications for the future study involving exposure to cells in the *in vitro* models. In particular, with regards to the interaction of nanomateirals with cell membranes, their proteins and constituents within the delivery vehicle, and importantly, the link between nano-surface properties and cytotoxicity (Berg *et al.*, 2009, He *et al.*, 2010, Yin Win & Feng, 2005). Charge in relation to cytotoxic effect of nanoparticle properties was discussed in detail earlier, specifically relating to the release of ions that generate an oxidative stress environment inside the cell (section 1.2.5). Example studies prompted the analysis of two different nanomaterials from the same chemical material, hence the inclusion of both ZnO-45009 and ZnO-45408 in this study.

From what is known of the ZnO nanomaterial production, ZnO-45009 is supposedly drawn from a cationic dispersant and is likely to have a different surface charge to that of ZnO-45408 (prepared from an uncharged dispersant) (AlfaAesar, 2012). Charge is a complicated property with regards to the current nanotoxicity landscape. The majority of studies find cationic nanoparticles to be the most toxic (Xia *et al.*, 2006, Yu & et al., 2011). Conversely, a negative surface charges has also been demonstrated to confer toxicity, particularly in gold nanoparticles (Schaeublin *et al.*, 2011) and across the blood brain barrier (Kreuter *et al.*, 2003, Lockman *et al.*, 2003, Nel *et al.*, 2006). Furthermore, it has proved preferential in cytotoxicity towards tumours (He *et al.*, 2010).Yet the surface charge has also been speculated to account for protein adsorption interactions to the nanoparticle surface in biological media, neutralising the effect of negative surface

charges, but increasing intracellular uptake that can result in increased cytotoxicity (Alkilany & Murphy, 2010, Chithrani *et al.*, 2006, Horie *et al.*, 2009).

Zeta potential measurement, although not strictly a direct assessment of particle charge, is related to the surface ionic properties (surface charge) in relation to interactions within the ionic environment (dispersant). Results here displayed a difference in the surface properties between the two ZnO nanomaterials analysed under the same conditions. ZnO-45009 differed from all other nanomaterials, with a positive zeta potential measurement when dispersed in aqueous solutions. This re-enforces the hypothesis that there may have been some modification to its nanoparticles' surface chemistry, by the dispersant. In terms of the cytotoxic effect, the difference in availability of polar opposite surface charge may hold importance to the properties exerted by the nanoparticles on cell interactions.

The relationship between surface charge, zeta potential and colloidal stability is highly dependent upon ionic composition of the dispersant, therefore, pH is always required to provide the context of a zeta potential measurement (Berg *et al.*, 2009, Cosgrove, 2010). Under physiological conditions, the nanomaterials were reported to exhibit agglomeration and flocculation tendencies, as discussed. The relationship between pH and zeta potential governs the stability with a solid, and relates to the disparity in net double layer charge; between the solvent molecules interacting at particle surface and the boundary called the slipping plane, saturated by solvent and further away from the influence of the molecules at the particles surface. Considering nanoparticle surface reactivity has been well documented to be enhanced over bulk composites of the material (Dick *et al.*, 2003, Donaldson & Tran, 2002, Duffin *et al.*, 2007, Nel *et al.*, 2006, Oberdorster *et al.*, 2005b, Zhang *et al.*, 2003), it is possible that the relationship between particle and dispersion medium is more sensitive for nanomaterials than bulk (Navrotsky *et al.*, 2008). This scenario would cause nanoparticles to more readily flocculate out of dispersion when conditions are sub-optimal, as was the case for the all nanomaterials investigated here in biologically compatible PRF media. Alternatively, it could be assumed that they may also form a closer relationship with the dispersion medium when conditions are more suitable, improving solution stability. This might explain the behaviour of hydroxyapatite nanomaterial in ethanol having good stability, thought a consequence of the free OH^- groups in solution that could act to stabilise the ionic balance of hydroxyapatite ($Ca_5(PO_4)_3OH$) chemical structure (Kuriakose *et al.*,

2004). Unfortunately, the ZetaSizer instrumentation detection sensitivity was not suitable for comparison with bulk material, which may have proved useful to help explain morphological differences observed in low magnification SEM images of aggregated material (Figure 3.1).

3.2.3 Temperature effects on nanomaterial characteristics

Through size comparisons carried out using the ZetaSizer instrument, temperature was investigated to determine if this parameter influences the properties of nanoparticles, specifically when increased to physiological body temperature. Whilst the results reported that TiO_2 nanomaterial in PRF media having a smaller average particle diameter at 37°C, in general there is a lack of statistical significance for this trend. The materials investigated in this study were metal oxides not expected to, in terms of hydrodynamic diameter, experience expansion or contraction of individual particle size across the moderate 15°C temperature swing (between ambient and physiological temperatures). Therefore, changes in nanoparticle sizes recorded were more likely observations of a dynamic colloidal environment that involved all, or none, of agglomeration, aggregation or sedimentation of the material, at different rates in solution. The extra reaction kinetics of increased temperature were speculated to account for any disparity (Freitas & Müller, 1998, Sawai *et al.*, 1996), but that the effect of a 15°C increase would be minimal.

Results suggested that temperature was the least influential parameter that governs the nanomaterial properties investigated during this study. The consequence of this result means nanomaterial treatments carried out *in vitro*, at physiological temperatures, are unlikely to experience any difference from the sample preparation carried out at ambient laboratory temperature (22°C).

3.2.4 Evaluation of nanomaterial characterisation

Overall, most of the characteristics currently available to nanotechnology have been explored through the employment of one or multiple techniques within this chapter. It should be stressed, that the purpose of this section was not to critically examine the strengths and weakness of one method of analysis over another; but rather to assess the measurement given in a context that allows for the best possible understanding of particle characteristics for each nanomaterial. This is important to determine extent *nano*-size specific characteristics will contribute to the properties of the nanomaterial,

and how these could influence what type of interactions are available at biological membranes encountered in the human oral mucosae.

Whilst some techniques revealed greater depth of information over others, all must be employed in a multifaceted approach to accurately determine the characteristics of each material as it changes from a stable chemical entity, to a dynamic colloidal system with implications to the environment in terms of aggregated size, surface area, ion release, charge and of course toxicity when interfacing with biological membranes. In that respect, size results reported here may be best utilised as ranges for each nanomaterial, purposely stated as being dependent upon the conditions they are measured in (Bootz *et al.*, 2004, Kato *et al.*, 2009, Murdock *et al.*, 2008, Gaumet *et al.*, 2008), with nano-characteristics investigated through comparisons with bulk equivalent materials and/or other varieties of the same species of nanomaterial. The size ranges gain further clarity when linked with information from polydisperisty and zeta measurements, as well as visual inspection of particle appearance that hint at agglomeration/aggregation behaviour. All this combined, helped build a profile of particle behaviour in relation to its size, at first in native chemical form, right through to when found in physiological representative environments used to model conditions of nanoparticle interaction with tissue of the oral mucosa.

Hydroxyapatite-nanomaterial can be described as a nanomaterial produced from a bi-modal mix of spherical nanoparticles that are likely to produce varied sized agglomerates in cell culture media (577.4nm ± 228.0nm (DLS)). These are still likely to remain smaller than the bulk material (101.8nm (nanomaterial) and 354.4nm (bulk) (Table 3.5)), of differing particle morphology. Therefore, it would be expected that any differences observed during *in vitro* effects may not solely be attributed to nano-characteristics, but also morphology.

SiO_2-nanomaterial was observed to have the smallest nanoparticles of all nanomaterials investigated within this study (27.4nm ± 14.1nm and 19.2nm ± 8.2nm for SEM and TEM analysis respectively), with nanoparticles roughly spherical in appearance but no different to the 'bulk' control material. Dispersion in cell culture media resulted in rapid agglomeration (1417.7nm ± 577.4nm (DLS)) that was not expected to sediment. Therefore, nano-sized effects are likely to be less prominent *in vitro*, with SiO_2-nanoparticles more likely to get delivered as larger agglomerates. Properties may prove indistinguishable between bulk effects that were measured of

similar diameter when sized using electron microscope techniques (28.8nm ± 13.5nm and 59.9nm ± 63.8nm for SEM and TEM respectively).

TiO_2-nanomaterial can be described as a monodisperse nanomaterial made from roughly spherical and uniformly distributed nanoparticles (at starting state). These measured 28.5nm ± 9.8nm for SEM, and 26.6nm ± 16.3nm using TEM, but were likely to flocculate rapidly into large agglomerates that are liable sediment in cell culture media solutions (3352.7nm ± 795.1nm (DLS)). Morphologically, it differed from bulk material solely on reduced particle sizes, therefore any disparity exerted *in vitro* would likely be attributed to nano-specific characteristics.

ZnO nanomaterials were both considered very similar to each other in terms of morphology, and this can be linked to common ancestry with bulk material. All versions of the material constituted particles considered less spherical in shape with the presence of spindly rod-like fibres evident. EDS elemental composition matches both expected chemical composition (zinc and oxygen) and ratio in comparison to bulk material. The major difference occurred from disparity in zeta potential measurements between the two nanomaterials in cell culture media. Size was the major differentiating factor between the ZnO materials, with bulk significantly larger in average particle size to both nanomaterials (>200nm (Table 3.5)), and nanomaterials both loosely following the manufacturer stated ranking: ZnO-45408 being the smaller of the two, with particles ranging from 23.2nm to 83.6nm in size (SEM), with agglomeration tendencies that increased the size measurement most severely when dispersed in PRF media (376.0nm ± 167.4nm). In comparison, ZnO-45009 nanoparticles ranged from 10.1nm to 125.1nm in size (SEM), again increasing dramatically when dispersed in PRF media, to average agglomerate measuring 522.2nm (± 467.7nm).

The profiles generated from the characterisation experiments carried out in this chapter, will be used to explain effects observed through studying the response in cell models *in vitro*. Any cytotoxic effects will then be related back to individual characteristics of the nanomaterial that may differ from bulk composite. These will be used to explain interactions with oral mucosal cells, linking unique attributes to specific effects observed.

4 IN VITRO MONOLAYER SCREENING OF MATERIALS

The initial stage of investigation concerned screening nanomaterials to identify any cytotoxic effects. Cytotoxicity testing was carried out with a variety of nano-formulations alongside bulk (non-nano) counterpart controls. Bulk material inclusion was thought important in providing the context for any nanotoxicity, due to the absence of established nanomaterial standards that could act as controls to the nanomaterials investigated (Nyström & Fadeel, 2012, Stone *et al.*, 2010). It was hoped that any nanomaterial cytotoxicity, could be linked to specific nanoparticle characteristics, or conditions relating to their exposure (*e.g.* doses, exposure times or composition of delivery vehicle).

A targeted approach to risk assessment was carried out using a tier based system (or decision tree (Figure 1.2)), following a strategy devised from current best practice in toxicology (Hansson & Rudén, 2007). It has been adopted by the EC to fill gaps in data that currently exist regarding nanotoxicity ((SCENIHR), 2009), whilst simultaneously attempting to reduce the use of animals in toxicity testing by increasing the reliability and sophistication of *in vitro* models. These were important considerations for this study, as oral healthcare regulation typically falls under the EC Cosmetics Regulation that now completely prohibits the use of animals in the safety assessment of cosmetic ingredients and cosmetic products ((EU), 2013). Current toxicological assessment uses a multi-endpoint approach that generates data through a battery of *in vitro* tests. The results of this chapter constitute the top tier of initial risk assessment for nanomaterials, requiring investigation as new chemical entities.

Studies in this area are currently limited for toxicology risk assessment in the human oral mucosa, therefore it was thought important to test a wide variety of nanomaterials under differing conditions to provide a comprehensive exploratory study. This led to the development and subsequent optimisation of an *in vitro* screening model that could investigate interactions between nanoparticles and the human oral mucosa. H376 monolayers had been previously characterised in full, and were considered a representative model of non-keratinised oral epithelium (Elsom, 2004). The non-keratinised tissue type, expressed in buccal mucosa, covers the largest surface area of epithelium within the human oral cavity (Rossi *et al.*, 2005). It has been proven to demonstrate a high sensitivity to cytotoxic and permeable stimuli populations (Squier &

Kremer, 2001, Walker *et al.*, 1973, Wertz & Squier, 1991), and both these properties were expected to prove advantageous in a model required for detection of cytotoxicity exhibited by nanomaterials. In representing the worst-case scenario, this cautionary approach was thought useful for preliminary risk assessment. Development and optimisation of H376 cell use in 96 well plates would enable basic cytotoxic evaluation, investigating a number of experimental variables relating to modelling nanomaterial exposure *in vitro* (such as concentration). Establishing the conditions that may result in cytotoxicity (assessed using the LDH assay) and loss in cell viability (using MTT to assess the mitochondrial activity), constituted initial risk assessment.

In addition, the successful identification of nanomaterial cytotoxicity using H376 cells would validate the model as a sensitive screening tool for substances exposed to the human oral mucosa. Scanning electron microscopy (SEM) was utilised to consolidate cytotoxic assay assessment, provided through surface interactions. Observations in cell and nanoparticle morphology were speculated to provide insight into the health of cells exposed to each nanomaterial, consolidating results from LDH and MTT assays, as well as identification of common characteristics that may link to cytotoxic properties.

4.1 Cytotoxicity screening results

4.1.1 LDH assay results

Figure 4.1 to Figure 4.4 report LDH release by H376 cells 24 hours post treatment (5 minutes exposure) incubated at 37°C and in a 5% CO_2 humidified atmosphere. Results were reported as a % cytotoxicity measurement in the context of normal LDH release (negative control) and a fully lysed population, indicating the maximal amount of cellular LDH available for release. Cytotoxicity was defined using the LD_{50} threshold, where a material dose was considered cytotoxic when LDH release (indicating cell death) exceeded 50%.

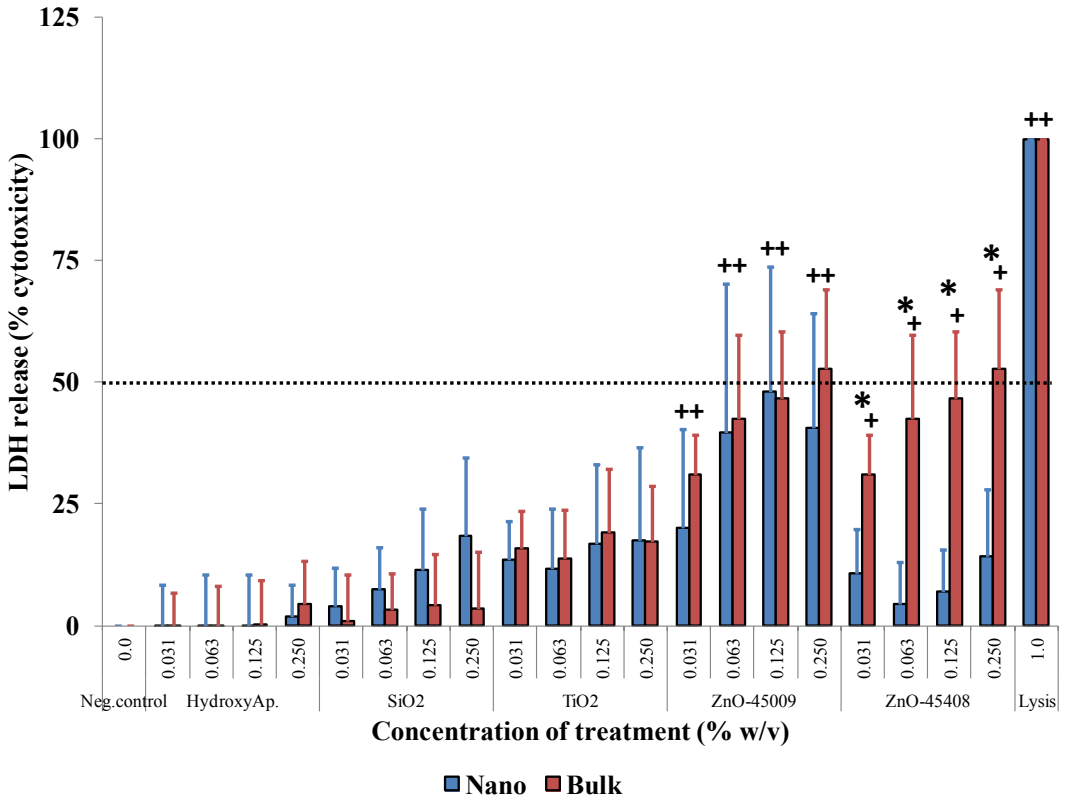

Figure 4.1. A graph comparing the cytotoxic effects of bulk versus nano material exposure to H376 monolayers at concentrations ranging from 0 to 0.25% w/v in serum free growth media, for 5 minutes at 37°C/5% CO_2. *Results are the average of six experiments (n = 6) with standard deviation reported.* ***** indicates statistical significance using one-way ANOVA with Tukey's post-hoc test to highlight a difference between results when nano cytotoxicity was compared to bulk results at the same concentration. **+** indicate significant cytotoxicity when compared against negative control (P<0.050). The dotted line represents the LD_{50} threshold.

Figure 4.1 compares nano versus bulk effects on cytotoxicity when cells were exposed to treatments delivered in serum-free media. All nanomaterial treatments tested under these conditions were deemed non-cytotoxic when compared to LD_{50}. In addition, all test materials, even at the highest doses, had statistically lower values compared to the positive control (with all *P* values < 0.001 when compared against lysis result).

Comparisons to the negative control, did show statistically significant increases in LDH released, for cells treated with ZnO-bulk and ZnO-45009 materials ($P < 0.001$ at all concentrations, bar ZnO-45009 at 0.031% w/v ($P = 0.017$)). In contrast, low levels recorded for cells treated with all concentrations of ZnO-45408 nanomaterial meant bulk versus nano comparison resulted in an obvious distinction in the effects observed with statistical significance across all concentrations (bulk more cytotoxic than ZnO-45408 nanomaterial at 0.250, 0.125, 0.063% ($P < 0.001$) and 0.031% ($P = 0.020$)).

Despite the low percentage of cytotoxicity in cells exposed to SiO_2 nanomaterial, a dose dependent trend was exhibited that was different to the bulk material. No other difference between nano and bulk effects were observed, because all materials except ZnO-bulk and ZnO-45009 were considered well tolerated by the H376 cell model, with <20% cytotoxicity recorded.

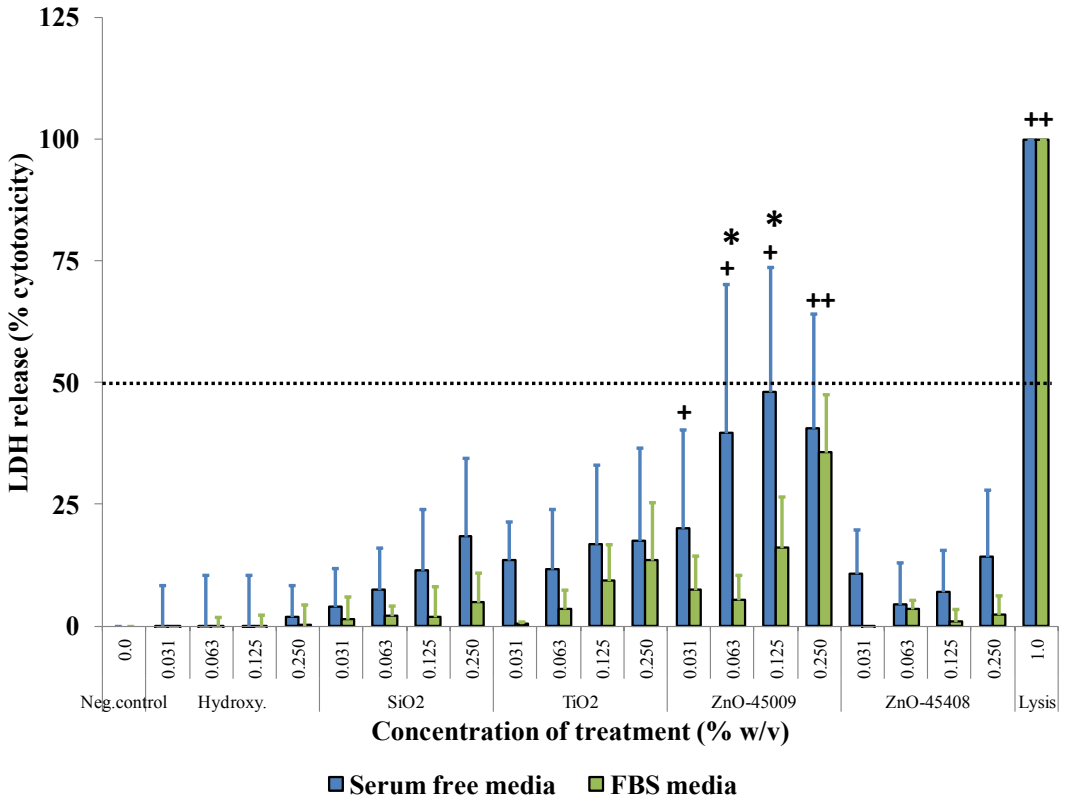

Figure 4.2. A graph comparing the cytotoxic effects of nanomaterial exposure to H376 monolayers at concentrations ranging from 0 to 0.25% w/v when delivered in different media, incubated at 37°C/5% CO_2 for 5 minutes. *Results are the average of six experiments (n = 6) with standard deviation reported.* ***** indicates statistical significance using one-way ANOVA with Tukey's post-hoc test to highlight a difference between results when serum free delivery was compared to FBS media results at the same concentration. **+** indicate significant cytotoxicity when compared against negative control (P<0.050). The dotted line represents the LD_{50} threshold.

Figure 4.2 shows results that compare the effect of FBS proteins present in nanomaterial delivery vehicles to serum-free delivery results. No difference was observed for hydroxyapatite nanomaterial exposure, as evidenced by the lack of LDH release reported across all concentrations. There was a reduction in SiO_2 nanomaterial cytotoxicity in the presence of FBS proteins, although not statistically different. This trend was also observed with TiO_2 nanomaterial exposure (although less marked) and also for ZnO-45408 nanomaterial, across all concentrations tested. Cell exposure to ZnO-45009 recorded statistically significant difference in the protective effect of FBS protein nanomaterial delivery at doses of 0.125 and 0.063% w/v (P = 0.008 and 0.004 respectively).

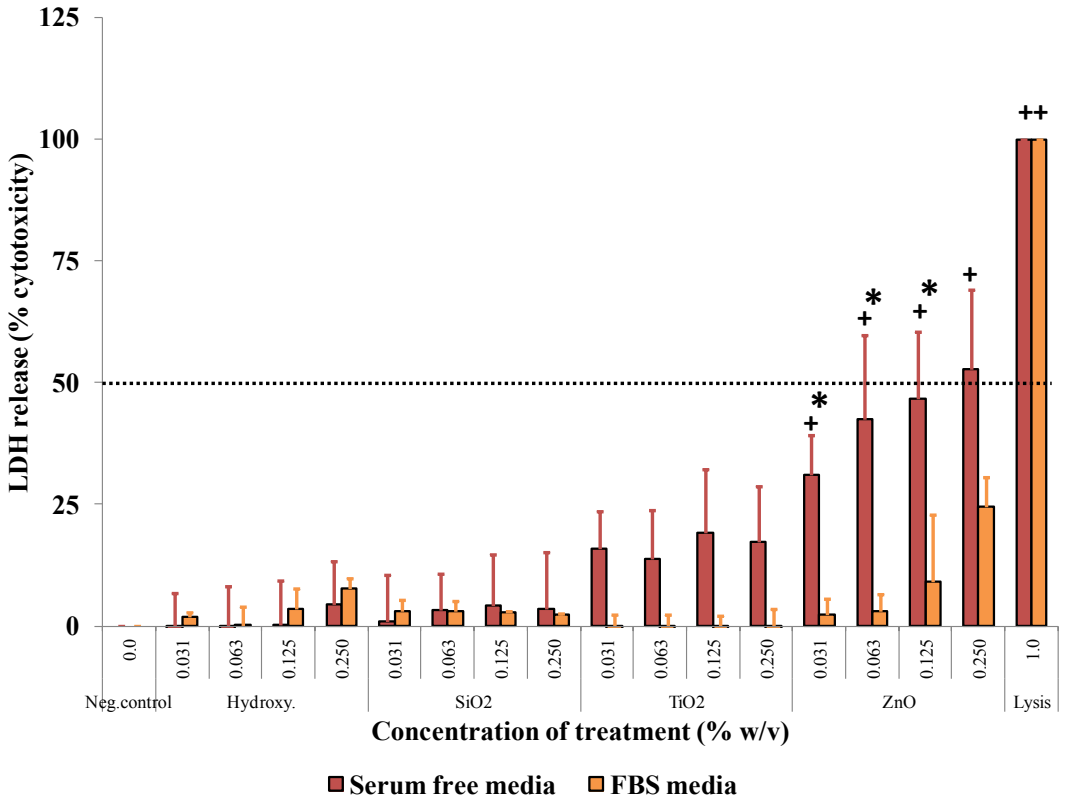

Figure 4.3. A graph comparing the cytotoxic effects of bulk particle sized material exposure to H376 monolayers at concentrations ranging from 0 to 0.25% w/v when delivered in different media, incubated at 37°C/5% CO_2 for 5 minutes. *Results are the average of six experiments (n = 6) with standard deviation reported.* * indicates statistical significance using one-way ANOVA with Tukey's post-hoc test to highlight a difference between results when serum free delivery was compared to FBS media results at the same concentration. + indicate significant cytotoxicity when compared against negative control (P<0.050). The dotted line represents the LD_{50} threshold.

Similarly to the trend observed for FBS delivery of nanomaterials, Figure 4.3 shows reduced LDH release following H376 cell exposure to bulk materials in presence of FBS supplemented media. As expected, this effect was most pronounced with exposure of cytotoxic ZnO bulk material, with a statistically significant decrease in LDH release observed across all concentrations less than 0.250% w/v (P<0.002). In the TiO_2 bulk material results, no LDH release was recorded when the material was delivered in FBS supplemented media, although the effect on cytotoxicity was limited due to the relatively low levels recorded for serum-free exposure (<20% at all concentrations).

The effect that FBS proteins had on LDH release was not as obvious for evaluations of SiO_2 and hydroxyapatite bulk materials, due to their respective low cytotoxicity at the concentrations tested in both delivery vehicles.

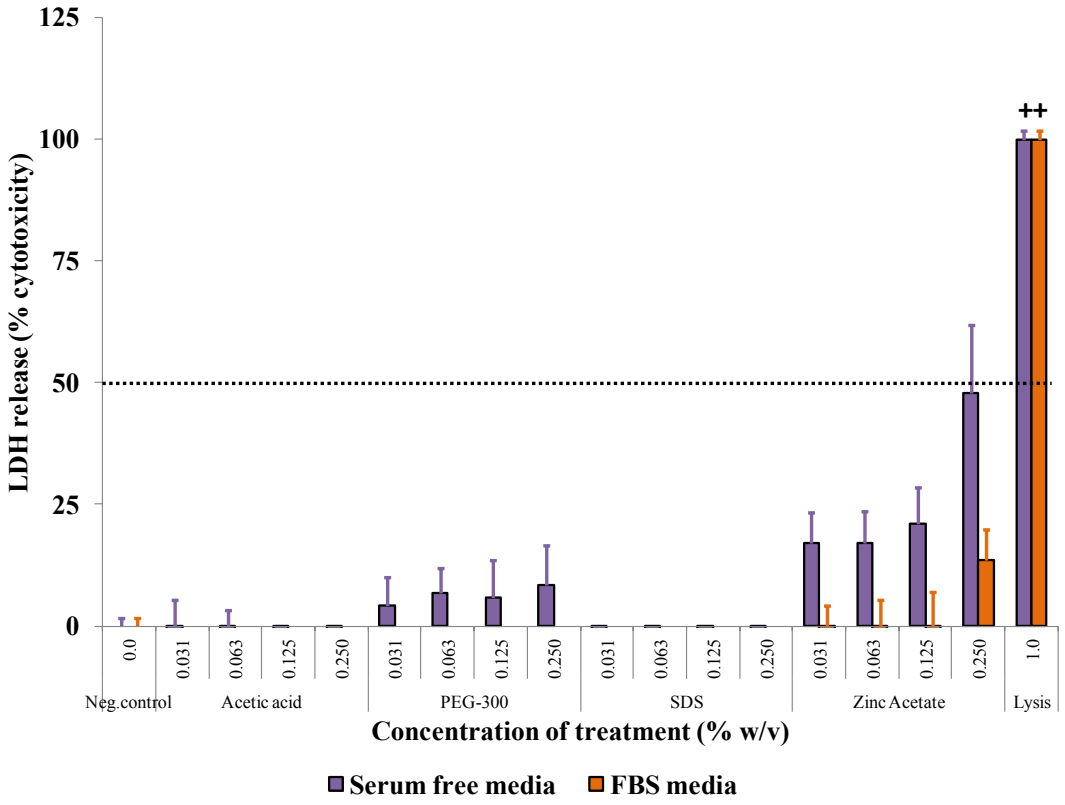

Figure 4.4. A graph comparing the cytotoxic effects of additional control materials exposed to H376 monolayers at concentrations ranging from 0 to 0.25% w/v when delivered in different media, incubated at 37°C/5% CO_2 for 5 minutes. *Results are the average of six experiments (n = 3) with standard deviation reported.* ***** indicates statistical significance using one-way ANOVA with Tukey's post-hoc test to highlight a difference between results when serum free delivery was compared to FBS media results at the same concentration. **+** indicate significant cytotoxicity when compared against negative control (P<0.050). The dotted line represents the LD_{50} threshold.

As demonstrated in Figure 4.4, cytotoxicity (LD_{50}) was not observed in cells exposed to the additional control materials included in this study (*i.e.* agents used for nanoparticle colloidal suspensions, SDS and an alternate form of zinc (zinc acetate)) exposed to cells under the same experimental conditions as that used for screening nanomaterials and bulk metal oxides. Differences were observed however, following exposure with zinc acetate, which recorded a high, but non-cytotoxic reading for LDH release at 0.250% w/v dose (48.0% ± 12.2%). The cytotoxic effect was again reduced by exposure following delivery in presence of FBS proteins (13.6% ± 4.5%). This trend was observed at all other concentrations. PEG-300 was the only other material to register a low level cytotoxic response as measured by LDH release (8.4% ± 6.5% was the highest cytotoxicity measurement, following serum-free exposure at 0.250% w/v).

4.1.2 MTT assay results

The MTT assay results reported below in Figure 4.5 to Figure 4.8 show cell viability for the same H376 cell populations assayed for LDH, 24 hours after treatment exposure (of 5 minutes duration) incubated at 37°C and in a 5% CO_2 humidified atmosphere. LDH values inversely correlated to MTT results with the latter reported as cell viability in the context of % MTT metabolised to formazan by a healthy cell population (negative control).

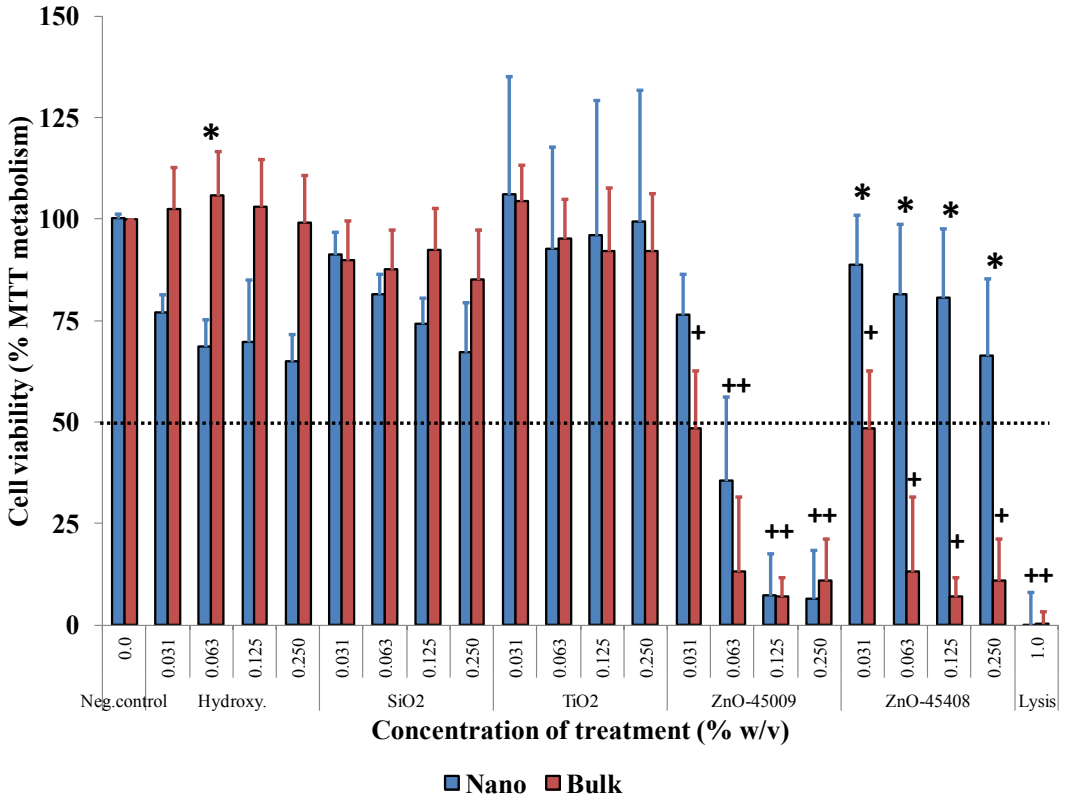

Figure 4.5. A graph comparing the cytotoxic effects of bulk versus nanomaterial exposure, to H376 monolayers, in terms of cell viability calculated from MTT metabolism at concentrations ranging from 0 to 0.25% w/v in serum free growth media for 5 minutes at 37°C/5% CO_2. *Results are the average of six experiments (n = 6) with standard deviation reported.* ***** indicates statistical significance using one-way ANOVA with Tukey's post-hoc test to highlight a difference between results when nano cytotoxicity was compared to bulk results at the same concentration. **+** indicates significantly reduced cell viability when compared against negative control (P<0.050). The dotted line represents the IC_{50} threshold.

Figure 4.5 shows that both ZnO-bulk and ZnO-45009 nanomaterial exposure caused a pronounced effect on H376 cells under the conditions tested. The loss in cell viability after exposure to these treatments, constituted a cytotoxic response (as defined using the IC_{50} threshold) for concentrations greater than 0.031% w/v. At doses exceeding

0.063% w/v, ZnO-bulk and ZnO-45009 nanomaterial had no statistical difference in cell response comparison to the fully lysed H376 cell population that constituted a positive control. Alternate statistical comparisons against the negative control cell viability result, reported a significant difference for both ZnO-45009 and the bulk material at concentrations above 0.031% w/v ($P < 0.001$).

No statistically significant nano-specific effect was observed, until comparisons were made between ZnO-bulk and the well tolerated ZnO-45408 nanomaterial. This comparison was significantly different at all concentrations ($P < 0.001$), despite the dose-dependent reduction in cell viability observed following cell exposure to the nanomaterial (ZnO-45408). This dose-dependent decrease was observed for both hydroxyapatite and SiO_2 nanomaterials, however, it was only statistically significant when compared against bulk composite for hydroxyapatite at 0.063% w/v concentration ($P = 0.022$). A rationale for this result was explained through a general tolerance of H376 cells to all materials exposed under the conditions for this investigation (when assessed using MTT), with only ZnO bulk and ZnO-45009 nanomaterials having any significant cytotoxic effect on cell viability.

Overall, the trends observed here correlate closely with those obtained using the LDH assay.

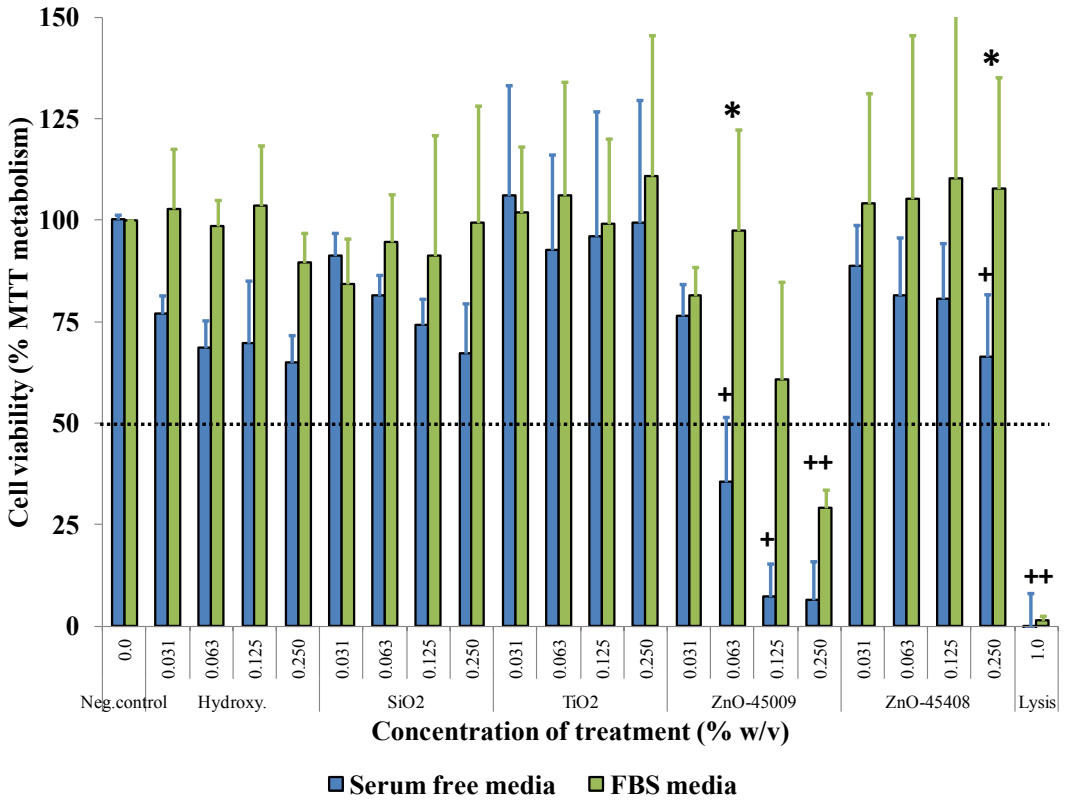

Figure 4.6. A graph comparing the cytotoxic effects of nanomaterials exposed to H376 monolayers at concentrations ranging from 0 to 0.25% w/v when delivered in different media, incubated at 37°C/5% CO_2 for 5 minutes. *Results are the average of six experiments (n = 6) with standard deviation reported.* ***** indicates statistical significance using one-way ANOVA with Tukey's post-hoc test to highlight a difference between results when serum free delivery was compared to FBS media results at the same concentration. **+** indicates significantly reduced cell viability when compared against negative control (P<0.050). The dotted line represents the IC_{50} threshold.

Figure 4.6 shows that cell exposure to all treatments did not produce losses in mitochondrial function, as indicated by high cell viability measurements. This shows that most nanomaterial treatments were non-cytotoxic, with respect to the IC_{50} definition. ZnO-45009 nanomaterial was the exception, at concentrations exceeding 0.063% w/v in serum-free media and at the top concentration, and cells showed higher viability only when delivered in FBS supplemented media. All nanomaterial treatments across the concentrations tested showed a marked increase in cell viability when delivered in FBS media compared against the results from serum-free media. The exceptions were SiO_2 and TiO_2 nanomaterials at 0.031% w/v, where only small changes in cell viability were observed.

Statistically significant impacts of the FBS proteins resulting in greater cell viability (when compared against the serum-free media delivery vehicle for nanomaterials) was only observed for treatments of ZnO-45009 at 0.063% w/v concentration, and ZnO-45408 at 0.250% w/v (P <0.001 and P =0.022, respectively).

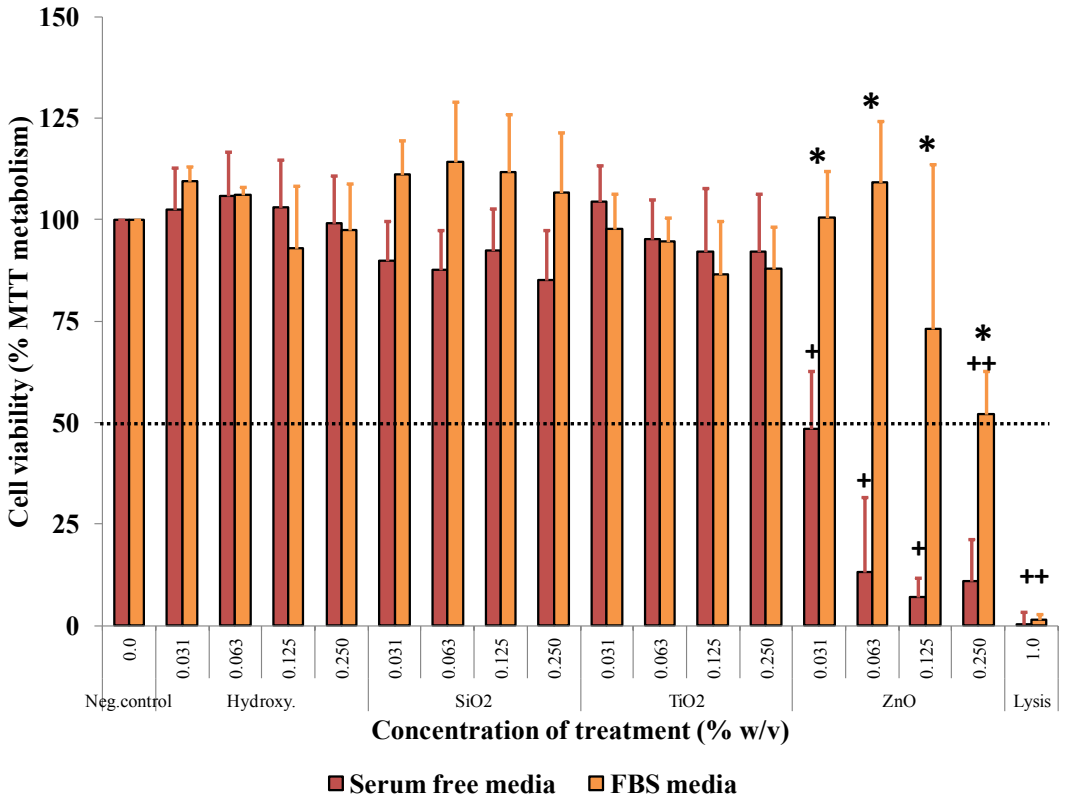

Figure 4.7. A graph comparing the cytotoxic effects of bulk particle sized materials exposed to H376 monolayers at concentrations ranging from 0 to 0.25% w/v when delivered in different media, incubated at 37°C/5% CO_2 for 5 minutes. *Results are the average of three experiments (n = 3) with standard deviation reported.* * indicates statistical significance using one-way ANOVA with Tukey's post-hoc test to highlight a difference between results when serum free delivery was compared to FBS media results at the same concentration. + indicates significantly reduced cell viability when compared against negative control (P<0.050). The dotted line represents the IC_{50} threshold.

Figure 4.7 results show how, hydroxyapatite, SiO_2 and TiO_2 bulk materials have been well tolerated by the H376 cell model at all concentrations tested. There was no obvious effect on cell viability by the inclusion of FBS in their delivery media. ZnO bulk material exhibited cytotoxicity at all concentrations when exposed in serum-free media, but displayed statistically significant increases in cell viability when cells were exposed

using FBS supplemented delivery vehicle ($P < 0.001$ for all concentrations except 0.250% w/v ($P = 0.011$)). The protective effect of FBS proteins increased most notably with cell viability above the IC_{50} threshold when ZnO-bulk was delivered in FBS media at top concentration (52.2% ± 5.3%). In serum-free media, this treatment had been observed cytotoxic (cell viability recorded as 10.9% ± 4.0%).

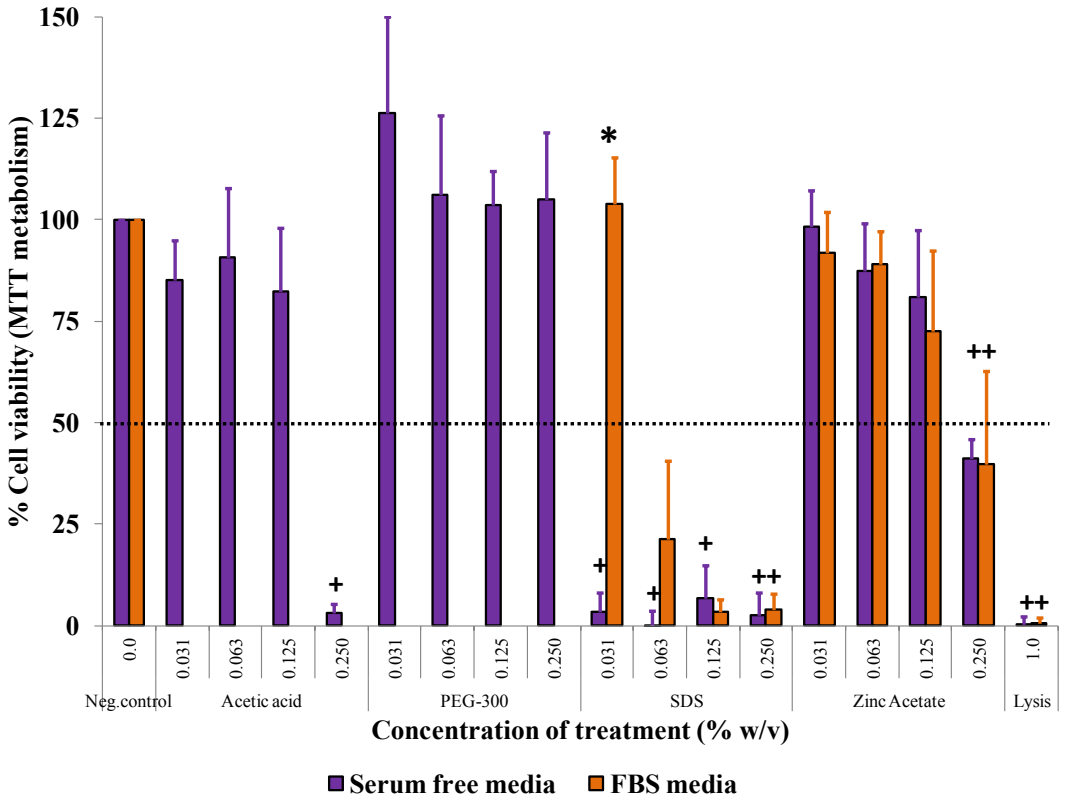

Figure 4.8. A graph comparing the cytotoxic of additional control materials exposed to H376 monolayers at concentrations ranging from 0 to 0.25% w/v when delivered in different media, incubated at 37°C/5% CO_2 for 5 minutes. *Results are the average of three experiments (n = 3) with standard deviation reported.* ***** indicates statistical significance using one-way ANOVA with Tukey's post-hoc test to highlight a difference between results when serum free delivery was compared to FBS media results at the same concentration. **+** indicates significantly reduced cell viability when compared against negative control ($P<0.050$). The dotted line represents the IC_{50} threshold. **Acetic acid and PEG-300 were not assessed alongside FBS delivery due to LDH data reporting no cytotoxicity.**

The cell viability results in Figure 4.8 show that the additional control materials screened using the H376 monolayer model are inconsistent with trends observed for nanomaterials and their bulk constituents. The lack of cytotoxicity observed through measuring LDH release (Figure 4.4) did not always correspond to high cell viability, as

indicated by 0.250% w/v acetic acid and all concentrations of SDS delivered in serum-free media, exhibiting a statistically significant decrease when compared to the negative control ($P < 0.001$). These results were consistent with the levels for the lysed positive control.

For acetic acid, this reduction in cell viability was not considered a problem regarding its application in TiO_2 nanomaterial as a dispersant; as this nanomaterial itself had been well tolerated in the H376 cell model, using the same LDH and MTT assay assessment towards cytotoxicity. PEG-300 was also well tolerated in the cell model, inferring ZnO mediated cytotoxic effect to be a consequence of cell interaction with particles and not the dispersant constituents. This tolerance was used as a rationale for not completing studies alongside FBS delivery that would be expected to decrease cytotoxicity in line with results observed for nanomaterials.

FBS inclusion in zinc acetate delivery did not result in notably different cell viability responses. This was an exception to trends observed for other ZnO containing materials (in Figure 4.1 through to Figure 4.7), and the cytotoxic SDS. At the lowest concentration (0.031% w/v) FBS supplemented media delivery of SDS significantly increased cell viability when compared against serum-free media ($P < 0.001$).

4.1.3 SEM visual analysis of material particle-H376 cell interactions

The SEM images presented in the following figures depicted both cell and particle morphologies, representing the H376 cell response to nanomaterial and bulk treatment exposure. The micrographs obtained over a range of magnifications, were aimed at identifying specific particle characteristics that could be linked to cytotoxic properties observed during assay screening.

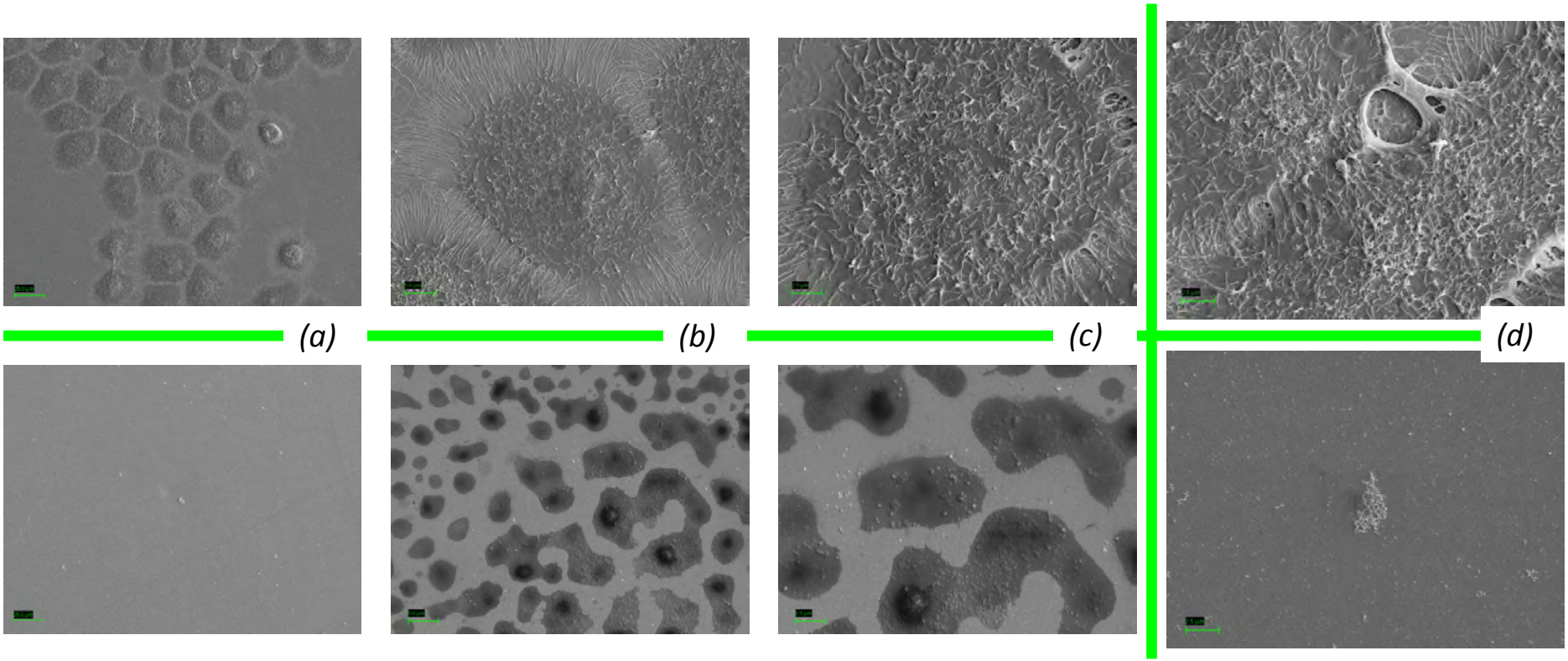

Figure 4.9. SEM images of H376 cells exposed to control substances for 5 minutes incubation at 37°C and 5% CO_2 in serum-free DMEM-Ham's F12 without *L*-Glutamine. (**Top**) Negative control cells treated with just serum free media. Colonies of cells are uniform in size with clear evidence of membrane structure and extrusions promoting cell-cell contact and communication. (**Bottom**) Positive control cells treated with 1% Triton-X100. There is notable absence of cell structures with only remnants of surface modification where cellular integrins would leave interacted components of extra cellular matrixes (ECM). *(**a**) = 1K X magnification with scale bar = 25μm, (**b**) 5K X magnification with scale bar = 5μm, (**c**) 10K X magnification with scale bar = 2.5μm and (**d**) enlarged 10K X magnification with scale bar = 2.5μm. All samples are indicative of n=3 samples.*

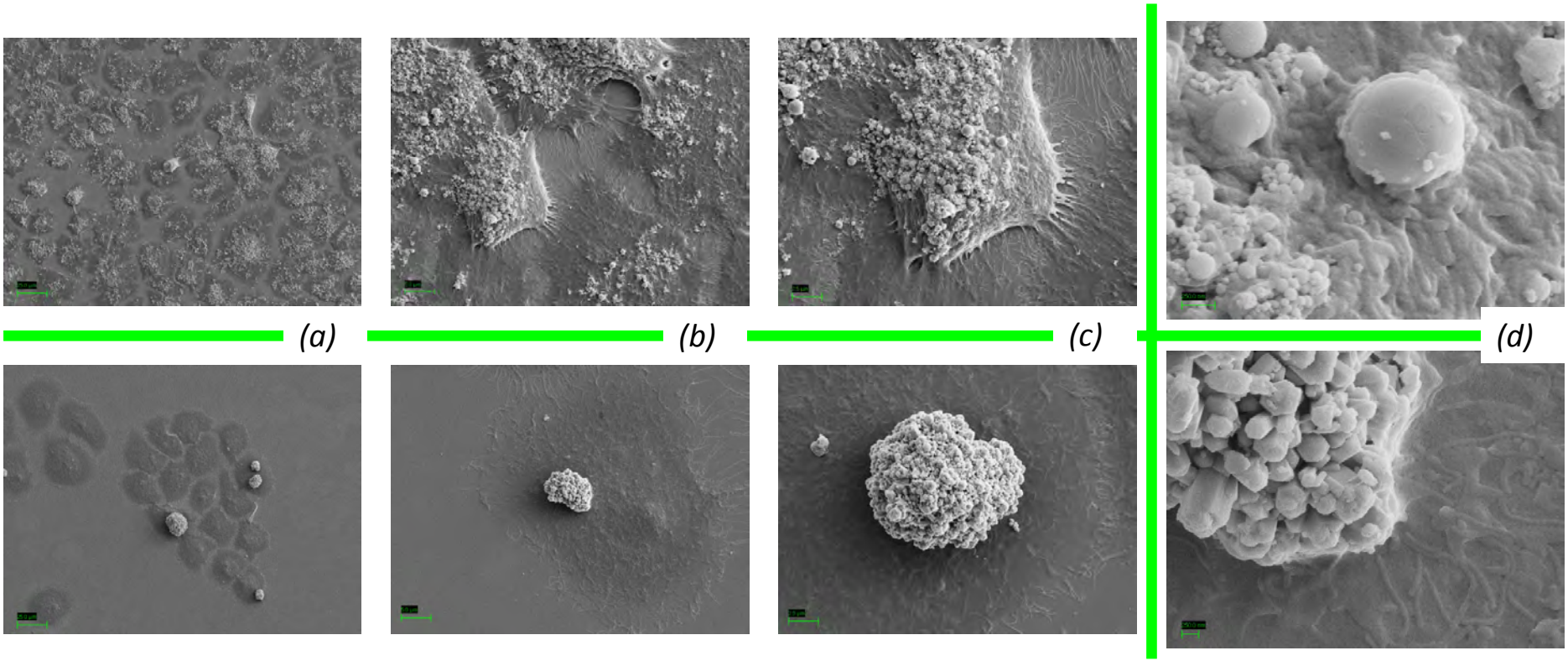

Figure 4.10. SEM images of H376 cells exposed to hydroxyapatite materials for 5 minutes incubation at 37°C and 5% CO_2 in serum-free media. (**Top**) 0.125% w/v Hydroxyapatite-nanomaterial. Cells appeared smaller than healthy control populations with irregular squamous shapes and reduced membrane extrusions in the presence of hydroxyapatite nanomaterial clearly observed as distinguishable particles in contact with the cell apical membrane. At the higher magnification, cell-nanoparticle interaction seems confined to the apical surface, with little evidence of particle penetration deep within the cell structure observed. (**Bottom**) 0.125% w/v Hydroxyapatite bulk material. Sparse interaction of bulk material was observed with cell membranes with material forming large aggregates few in number. This suggested a more limited interaction of the material with the cell surface when compared against nanomaterial. *(**a**) = 1K X magnification with scale bar = 25µm, (**b**) 5K X magnification with scale bar = 5µm, (**c**) 10K X magnification with scale bar = 2.5µm and (**d**) enlarged 100K X magnification with scale bar = 250nm. All samples are indicative of n=3 samples.*

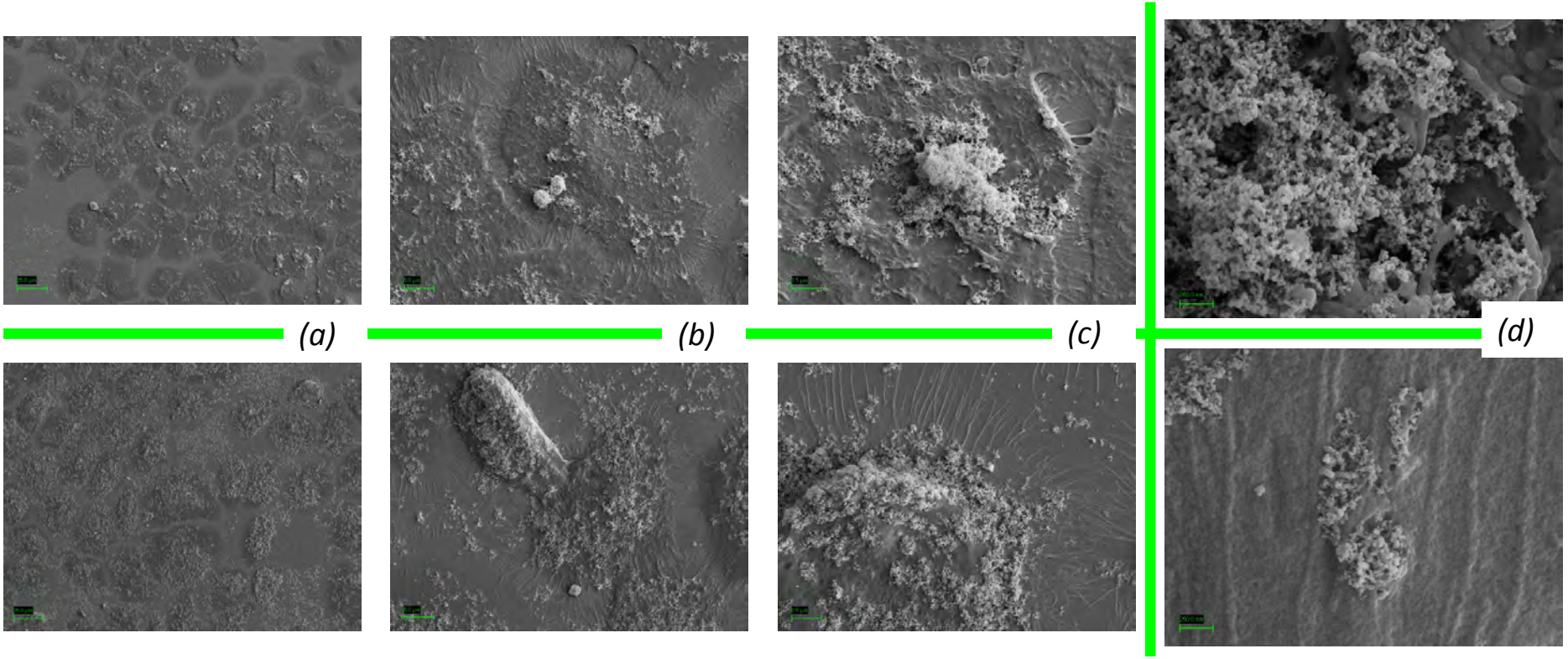

Figure 4.11 SEM images of H376 cells exposed to SiO_2 materials for 5 minutes incubation at 37°C and 5% CO_2 in serum-free media. (**Top**) 0.125% w/v SiO_2-nanomaterial. Cells remained consistent in membrane appearance and size despite clear evidence of SiO_2-nanomaterial at the cell surfaces which form agglomerates in places. Limited material interactions were observed with non-cellular areas of the surface *i.e.* protein coated Thermanox support. (**Bottom**) 0.125% w/v SiO_2 bulk material. Similar observations to the nanomaterial were observed for the bulk material here, with no apparent size difference between the particles, or obvious changes in cell morphology noted. *(**a**) = 1K X magnification with scale bar = 25µm, (**b**) 5K X magnification with scale bar = 5µm, (**c**) 10K X magnification with scale bar = 2.5µm and (**d**) enlarged 100K X magnification with scale bar = 250nm. All samples are indicative of n=3 samples.*

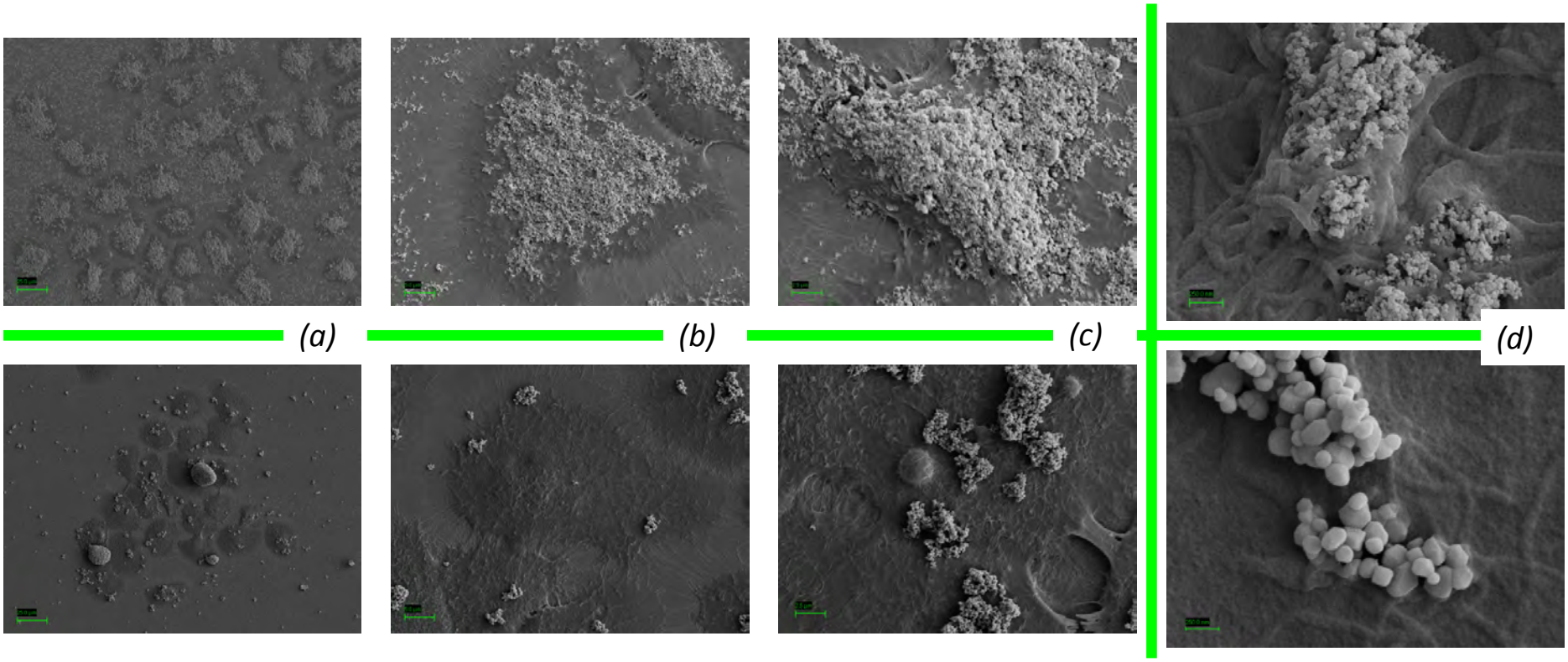

Figure 4.12 SEM images of H376 cells exposed to TiO_2 materials for 5 minutes incubation at 37°C and 5% CO_2 in serum-free media. (**Top**) 0.125% w/v TiO_2-nanomaterial particles were observed interacting at the apical surface of the cells, however, particles are also observed across the protein coated Thermanox support suggesting non-specific affiliation towards a particular surface. Individual particles were nano in scale but showed evidence of agglomeration. These were observed within structures apparent at the apical membrane. (**Bottom**) 0.125% w/v TiO_2 bulk material. A greater particle size was observed for bulk material, which may be attributed to a sparser interaction with cell membranes. These again, readily formed agglomerates and seemed to sit on top of the cell surface membrane with no obvious effect on H376 cell appearance. *(**a**) = 1K X magnification with scale bar = 25μm, (**b**) 5K X magnification with scale bar = 5μm, (**c**) 10K X magnification with scale bar = 2.5μm and (**d**) enlarged 100K X magnification with scale bar = 250nm. All samples are indicative of n=3 samples.*

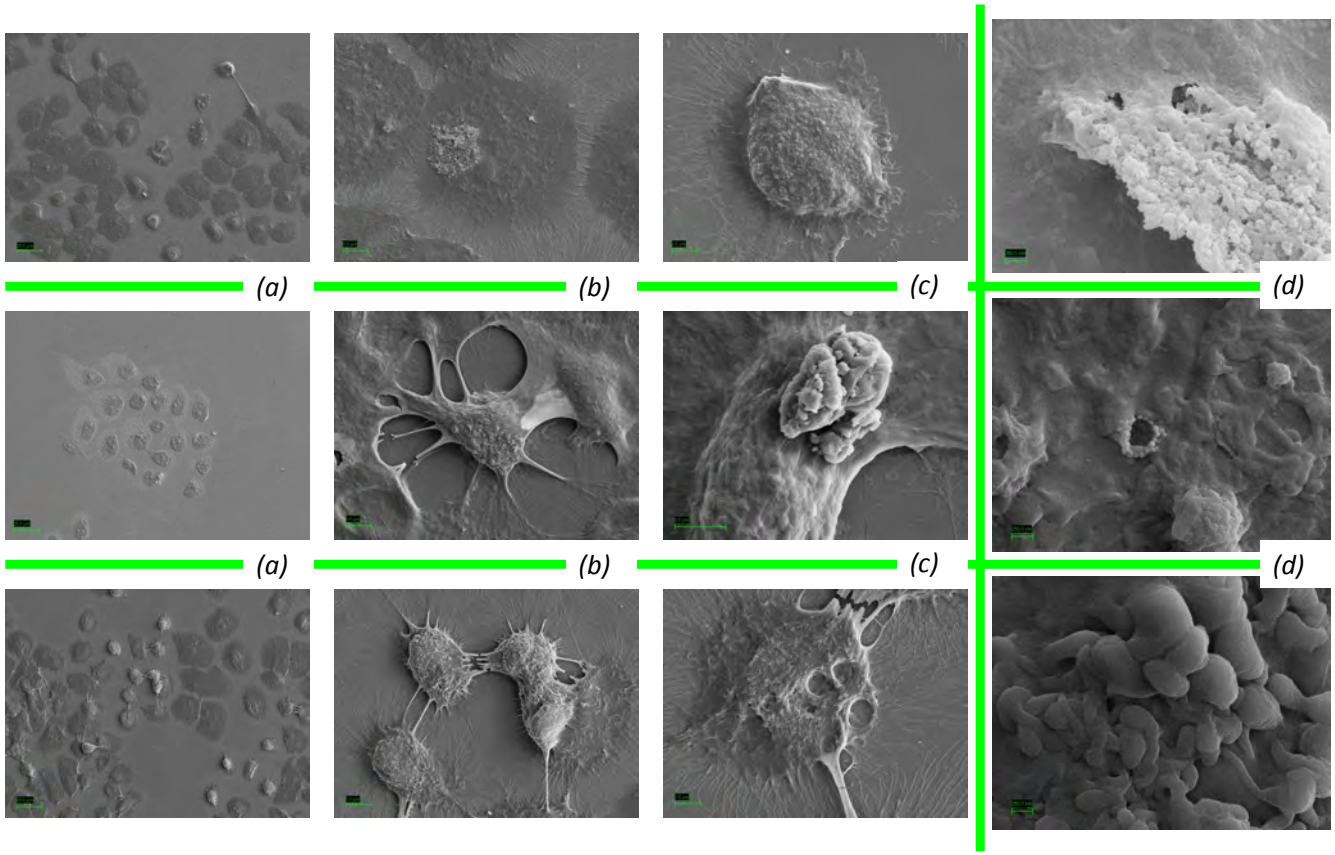

Figure 4.13. SEM images of H376 cells exposed to ZnO materials for 5 minutes incubation at 37°C and 5% CO_2 in serum-free media. (**Top**) 0.125% w/v ZnO-45009 nanomaterial. (**Middle**) 0.125% w/v ZnO-45408 nanomaterial.(**Bottom**) 0.125% w/v ZnO bulk material. Across all ZnO materials, there was evidence of morphological changes associated with cell cytotoxicity observed through cell appearance (*i.e.* cell shrinkage, blebbing and deconstruction of normal ECM and cell extrusions). These were combined with changes in surface topography in the absence of defined ZnO material. *(**a**) = 1K X magnification with scale bar = 25μm, (**b**) 5K X magnification with scale bar = 5μm, (**c**) 10K X magnification with scale bar = 2.5μm and (**d**) enlarged 75K X magnification with scale bar = 250nm. All samples are indicative of n=3 samples.*

SEM micrographs for H376 cells exposed to control treatments (serum-free media (negative) and 1% Triton™X-100 (positive)) served as references to the extremes in cell appearance. A typical healthy population is shown for the negative control sample (Figure 4.9 (top)), and the effects of 100% full lysis is depicted in the positive control (Figure 4.9 (bottom)). Healthy cells appeared roughly spherical, approximately 45μm in diameter and flat. They were grouped together in clusters, each with long microfilaments over their surfaces and extruding from the cell body in all directions. These seemed to contact with other cells in the surrounding space to form networks between neighbouring cells. As expected, H376 cells were completely absent following treatment with Triton-X100. All that remained of cellular adherence were dark areas on the SEM stub with undefined remnants of biological material that implied smaller, irregular shaped bodies had once been present.

Hydroxyapatite treatments showed disparity between the two forms of the material, both in terms of cell and particle appearances (Figure 4.10). H376 cells exposed to hydroxyapatite nanomaterial exhibited typical morphological signs of cell stress, such as a raised, domed surface that seemed to be recoiling away from neighbouring cells. Examples this was can be observed in Figure 4.10-top (*c*), showing obvious interaction of particles at the apical surface. The particulate material was spherical and correlates with the appearance noted from SEM characterisation (Figure 3.2). In contrast, the H376 cells exposed to the bulk form of hydroxyapatite were observed to be flatter in appearance. This was despite the presence of a large agglomerate of particles resting on their surface, observed as having little interaction with any cellular material (Figure 4.10-top (*d*)). Clear disparity observed between nanoparticle and bulk material appearance with H376 cells, supports results recorded from LDH and MTT assays.

Similarly to hydroxyapatite bulk material, neither bulk nor nanoparticle distributions of SiO_2 material exposure were seen to cause any notable changes in H376 cell morphological appearance (Figure 4.11), with little deviation from cell morphology observed from negative control. Subtle differences in material distributions and interaction between particle and cell included greater agglomeration of SiO_2-nanoparticles leading to a reduction in the number of particles interfacing with each cell (Figure 4.11 (*c*)). In comparison, bulk material remained distributed more evenly across cell membrane surfaces, and in smaller numbers of particles per agglomerate. Despite these close interactions, no obvious signs of cell stress were observed and particle

morphology resembled closely that observed during characterisation, including the similarity between bulk and nanomaterial particle sizes (Figure 3.3).

Observations of H376 cells interacting with TiO_2-nanomaterial differed from that observed in exposure to bulk material (Figure 4.12). The cells exposed to TiO_2 nanoparticles were densely coated with agglomerated material that covered the majority of the apical surface through close interactions. The presence of particulates corresponded with symptoms of cell stress that were observed, similarly, to cells exposed with hydroxyapatite nanomaterial. These samples dislayed cell surfaces that seemed to be raised as its total surface area shrank, with cells observed moving away from their neighbours. These effects contradict the results of cytotoxicity analysis for this nanomaterial, using LDH and MTT assays. There was an abundance of agglomerated TiO_2 nanoparticulates, distributed widely across the sample. In contrast, the bulk material was observed in clusters seemingly less connected with the underlying, healthy appearing H376 cells they were in contact with.

ZnO material interaction with cells provided the most unique set of observations, in comparison to the negative control and the other materials used to treat H376 cells. Exposure to all ZnO material treatments exhibited clear visual signs of cytotoxicity observed through cell stress markers that included a reduced or complete lack of filament networks on the cell surface, reduced cell diameter and blebbing combined with "doming" as the stressed cell lost flatness (Figure 4.13). There were similarities between cells exposed to both nanomaterials and the bulk ZnO treatments, however, cytotoxic effects were more obvious in cells exposed to ZnO bulk particles, which generally follows outcomes observed in results from cytotoxic screening (Figure 4.1 and Figure 4.5). Common to all ZnO treated cell samples (but different to the other nanoparticle exposed cells) was the absence any particles interfacing at the apical surface. Therefore, no comparison could be made to the elongated, rod-like particle morphologies observed from characterisation micrographs.

4.2 Discussion

Most toxicity testing begins with an investigation into the dose dependent effect of cytotoxicity *in vitro* (Choi et al., 2010, Hillegass et al., 2010, Rabolli et al., 2010, Soenen & De Cuyper, 2010). These initial studies are aimed at ascertaining the concentration or dose of a material that will instigate a toxic response on the cellular level. If the cytotoxic dose administered correlates with a plausible level for *in natura* exposure, the material will warrant concern and require further investigation. Three main conditions were investigated here, comparing i) nano versus bulk material results (to determine nano-specific cytotoxicity of each material), ii) nanomaterial versus nanomaterial, to establish what nano-characteristics relate to cytotoxic properties and iii) protein free versus protein containing delivery systems. The latter explored comparisons between the environments the cells are cultured in FBS containing media and a serum-free media solution, representative of a low protein containing delivery vehicle *e.g.* saliva. The purpose was to determine if the presence of protein in media had any significant bearing on cytotoxicity of the nanomaterials used to treat H376 cells *in vitro*.

Combining cytotoxicity assay results with observations from SEM imaging was a strategy designed to complement biochemical responses (detected using LDH and MTT) with observations from cell-particle interactions. The micrographs revealed information augmenting basic cytotoxicity results, linking with material properties determined in the previous characterisation chapter. Notable changes in cell morphology were linked with assay results to speculate the likely hypotheses towards each nanomaterials specific cytotoxic mechanism of action.

It is important to consider that the monolayer cell model differs significantly in representing the full permeability and protective properties of native tissue, lacking even the barriers of protection more accurately afforded by artificial 3-D tissue constructs. However, this limitation was actually considered an important and beneficial property for preliminary toxicity screening. Exposure to an overly sensitive model in comparison to *in-situ* or *in vivo* conditions, allowed low level cell damage to be detected. The outcomes from screening nanomaterial effects on H376 cells enabled identification of any potential harmful interactions in a model representing the most sensitive area of the human oral mucosa epithelium. The use of H376 OSCC in monolayer *in vitro* experiments, served as initial tier testing to assess the risk posed by nanomaterials in

oral healthcare products. Cytotoxic 'hits', or established conditions resulting in cytotoxicity, would then undergo further investigation.

4.2.1 Evaluation of nanoparticle cytotoxicity by colorimetric assays

There currently exists an abundance of well-established tests that can determine cell health, with many optimised for use with 96 well plates and other high-throughput formats, as required to assay drug or compound cytotoxicities *in vitro* (Weyermann *et al.*, 2005). All have their own particular merits and limitations, which can make choosing the correct assay challenging, particularly when screening a range of treatments that may act upon the model via differing cytotoxic mechanisms. Additionally, each assay exploits conditions relating to the parameters of the biochemical components used within the cytotoxicity test *e.g.* LDH assay linked to cell membrane damage and MTT with mitochondrial function. The culmination from all of these consequential variations has meant standardisation between assays is difficult, often with different cytotoxicity results generated for a specific material, dependent upon the assay employed (Weyermann *et al.*, 2005). Therefore, nanotoxicity, like traditional toxicological screening, has recommended the adoption towards a multi-faceted, multi-tiered strategy to assess potential nanomaterial dangers towards human safety (Borm *et al.*, 2006, Fotakis & Timbrell, 2006, Monteiro-Riviere *et al.*, 2009, Nel *et al.*, 2006, Oberdorster *et al.*, 2005a). Here, two common assays were chosen to screen nanomaterial responses on the H376 cell line, in the context of control substances. These were the LDH and MTT assays.

Potential future excipients containing nanomaterials were compared to bulk constituents currently formulated in oral healthcare products (Allaker & Memarzadeh, 2013, Khataee & Kasiri, 2010, Mihranyan *et al.*, 2012, Tschoppe *et al.*, 2011). These non-nano controls represented the established biochemical response in the cell model, to compare against potential nano-specific properties. They were utilised in each assay alongside traditional experimental controls that included a healthy H376 cell population (negative control), SDS as a known irritant but accepted in oral healthcare formulations and Triton™ X-100: a non-ionic surfactant used to permeablise cell membranes. This causes rapid cell death through necrosis (Jones, 1999) and was considered suitable as a cytotoxic positive control. Selection of appropriate controls is an important consideration for studies investigating nanoparticle behaviour, due to the lack of standardisation that exists in both nanomaterial composition (as demonstrated by

characterisation of heterogeneity in particle morphologies in a specific sample) and study parameters. Currently, only a very limited range of nanoparticle reference standards exist (Nelson *et al.*, 2013). With outcomes from nanomaterial characterisation suggesting nanoparticle characteristics may change dependent upon the environment, comparisons between studies may be heavily dependent upon the conditions of exposure. In this work, cytotoxic properties of each nanomaterial were described in comparison against a bulk composite, with the context provided by cytotoxic positive controls.

The screening method employed here allowed the assessment of cytotoxicity to be carried out from two different endpoints on the exact same H376 cell population. The LDH assay was chosen pragmatically, due to its speed and relative ease of use, a decision supported by its widespread application in other, similar nanotoxicity studies (Eun *et al.*, 1994, Hussain *et al.*, 2005, Li *et al.*, 1999, Liu & Sun, 2010, Yu *et al.*, 2009). The choice of which assay to utilise for initial cytotoxicity screening also considered the mechanism of cell death expected. Loss of intracellular LDH is widely accepted as an indicator of irreversible cell death (Fotakis & Timbrell, 2006). This corresponded with reports of cell membrane damage in a variety cell types, following exposure with zinc materials (Gerloff *et al.*, 2009, Lin *et al.*, 2009, Liu *et al.*, 2009, Nair *et al.*, 2009, Nel *et al.*, 2006, Yeh *et al.*, 2011, Zhang *et al.*, 2007). MTT was employed to assess the effect of nanomaterials from the inverse perspective of cell viability in addition to the provision of checking against mechanisms of cell injury that do not result in cell lysis and/or LDH detection. This avoided false safety reporting. These two complimentary measurements of cytotoxicity mirrored their application together across many *in vitro* toxicology studies (Fotakis & Timbrell, 2006, Hillegass *et al.*, 2010, Monteiro-Riviere *et al.*, 2009, (NIEHS), 2001, Oberdorster *et al.*, 2005a, Weyermann *et al.*, 2005).

Overall LDH assay results showed all nanomaterial treatments were non-cytotoxic, even at the highest concentrations. ZnO-bulk was the only exception, releasing 52.8% ± 6.1% of the total LDH available in the H376 cell population at the 0.25% w/v top concentration. Hydroxyapatite and ZnO-45408 nanomaterials were particularly well tolerated, alongside both SiO_2-bulk and even SDS. SiO_2-nanomaterial exposure was observed to lyse more cells at the higher concentration, but no more so than TiO_2 material: well established as relatively inert and non-toxic in work supported by many studies (Hsiao & Huang, 2011, Hussain *et al.*, 2005, Jeng & Swanson, 2006, Lewicka *et*

al., 2013, Simon-Deckers *et al.*, 2008). Common to many of the examples, is the use of LDH-assessed cytotoxicity, showed the reduced effects of TiO_2 nanoparticles (in cell lines to model lung epithelium, primary and carcinoma derived liver cells and human skin) in comparison to many other metal oxide nanomaterials, including aluminium, carbon nanotubes, iron, silver and ZnO. In this work, ZnO-45009 was the only nanomaterial to release significantly more LDH into supernatant, when compared against the negative control (but not the positive lysed population). Both assay results were clear in the reporting of a protective effect of a protein supplemented delivery vehicle for all the treatments tested. These results also included the IC_{50} evaluation reporting no cytotoxicity observed for hydroxyapatite, SiO_2, TiO_2 and ZnO-45408 materials. However, the associated MTT assay did display cytotoxicity (not detected in LDH results), for all but the lowest 0.03125% w/v concentration of both ZnO-bulk and ZnO-45009 and SDS at all concentrations tested. In addition, a more severe loss of cell viability was observed for hydroxyapatite nanomaterial over its bulk counterpart, indicating a nano-specific effect that was not recorded using the LDH assay.

Therefore, whilst it was evident that there exists some close correlation between the IC_{50} and LD_{50} values, results of which were used to confer evaluations of cytotoxicity for each nanomaterial in the context of the H376 model, there were also some discrepancies. In particular, towards correlation of the exact dose and levels cytotoxicity measured by each of the materials. These discrepancies implied greater sensitivity of the MTT assay results over LDH, observations shared by many other studies into nanotoxicity (Fotakis & Timbrell, 2006, Kroll *et al.*, 2009, Monteiro-Riviere *et al.*, 2009, Weyermann *et al.*, 2005). Specific examples include: cadium particles, smaller than 50μm in size. These particles were observed to impair respiration in rat hepatocytes prior to any membrane breakdown being visualised (Koizumi *et al.*, 1996). Cadium chloride nanoparticles have been observed to manipulate internal cell structures without destroying cell membrane in a porcine renal epithelial model (Gennari *et al.*, 2003). Additionally, colbolt-chronium nanoparticles have been observed showing cytotoxicity in terms of reduced formazan conversion (MTT) a full 3 days before cytotoxic results were observed by LDH in human fibroblasts (Papageorgiou *et al.*, 2007). Disparity may exist between all comparative methodologies, and care should be exercised relating to specific parameters used for each particular study. The examples in literature demonstrate differential assay sensitivity that may in part be attributed to extremes in

exposure models when considering the highly toxic nature of such metals, reported even on the bulk scale (Basketter *et al.*, 2003, Maret & Moulis, 2013).

Experimental outcomes reported within this chapter have resulted in the suggested explanation that extremely toxic and fast acting treatments were responsible for interference with cell adhesion, causing a loss of cells from the population (and thus with less cells left to contribute LDH supernatant levels). The reduced sensitivity of the LDH assay suggests interference with adhesion proteins, likely as a cytotoxic mechanism of action for SDS treatment on the H376 cell model. Evidence towards this hypothesis was provided in light microscope images, detailing loss of cells following 5 minutes exposure to SDS (Figure 9.1). This phenomenon was perhaps not surprising given SDS's well-defined role in protein denaturation through disruption of covalent bonds that can lead to the removal of proteins from tissue culture plastic ware (Ostuni *et al.*, 2001). It is this property that accounts for its widespread inclusion in cosmetic formulations, as a chemical penetration enhancer able to increase the skins permeability (James-Smith *et al.*, 2011). Just as nano-structured surfaces are being used to develop more specificity in cell-type adhesion (Popat, 2010), so too is it reasonable to assume that alternate nanomaterials may interfere with the permeability process, and thereby with cell adhesion. Cell adhesion disruption been reported for gold nanoparticles (Comfort *et al.*, 2011, Wei *et al.*, 2007), and is now an area currently under investigation using other nanomaterials.

Equally, numerous studies exist to support the application of LDH in conjunction with MTT, including those related to the materials investigated within this work. Motskin *et al.*,(2009) prepared and screened nano-hydroxyapatite on human monocyte derived macrophages. They found the data between LDH and MTT results followed similar experimental outcomes experienced in this work, with assay sensitivity weighted in favour of MTT assessed cytotoxicity, evident at lower concentrations than detected using LDH (Motskin *et al.*, 2009). The same trend was observed through nano-silica exposure on the human hepatic cell line: L-02 (Ye *et al.*, 2010) and ZnO nanoparticles on a human epidermal cell line (Sharma *et al.*, 2009b). Comparative studies investigating TiO_2 nanoparticles are harder to report, mainly due to conclusions that the material is generally non-toxic (Borm *et al.*, 2006, Heinlaan *et al.*, 2008, Hussain *et al.*, 2005, Schilling *et al.*, 2010, Suska *et al.*, 2005, Xia *et al.*, 2006). This consensus fits well with results reported here for TiO_2 effects on H376 cultures. Similar observations were repeated by

Dumetrescu *et al.*, (2010), when human gingival cell line HGF-1 was exposed to TiO_2-nanorods 120nm in diameter and found to be non-cytotoxic by MTT and LDH assays, despite there being small increases in LDH signal (Demetrescu *et al.*, 2010).

Conversely, it should be noted that a lack of sensitivity has been reported in cell viability assays following exposure with TiO_2 nanomaterial due to the materials ability to produce free oxidative species. This can affect the rate of tetrazolium salt metabolism to formazan (Valant *et al.*, 2012, Wang *et al.*, 2011). Other comparative studies can be found reporting problems associated with nanoparticle assessment of cell viability using MTT. These consistently link the colorimetric output of MTT assay results (a common design of many traditional high-throughput methodologies) with a susceptibility to optical interference by both light absorbing and scattering abilities reported to specific nanoparticles (Díaz *et al.*, 2008, Gonzales *et al.*, 2010, Kroll *et al.*, 2012, Kroll *et al.*, 2009, Oostingh *et al.*, 2011, Simon-Deckers *et al.*, 2008). This may also be expected through LDH application, which may suffer additional interference by the fundamental catalysis of the assay reaction preceding enzyme release into cell media supernatant (outside of the intracellular environment). This increases the probability that LDH enzyme will likely encounter direct contact with nanoparticles. Their small size has been reported to interact at the binding site of other enzymes, causing conformational change, partial efficiency or complete inhibition of catalytic action ((SCENIHR), 2006, Cheng *et al.*, 1999, Hainfeld & Powell, 2000, Penn *et al.*, 2003). These effects have been linked to the large surface area and subsequent increased reactivity afforded to a nanoparticles' surface, with literature reporting nanoparticle adherence to the protein make-up of macromolecules (including enzymes), reducing functionality (Cedervall *et al.*, 2007b, Klein, 2007, Lynch *et al.*, 2007, Schrand *et al.*, 2010, Soenen *et al.*, 2010, Xiong *et al.*, 2013).

In the absence of direct nanoparticle-macromolecule contact, nanotoxicology consequences may bring about inhibition of LDH in the assay through changing the environmental conditions. This can include both acidic and alkaline pH moving in a negative direction for optimal enzymatic catalysis (Babson & Phillips, 1965, Nachlas *et al.*, 1960), as well as ionic potential through the leeching of ions in cell culture (Kroll *et al.*, 2009). The latter is especially relevant for nanotoxcity, considering the abundance of reports related to metal oxide nanoparticle ion release causing damage through the generation of ROS. This can occur at the interface with macromolecules (such as LDH)

in much the same way as reported for nanotoxicity (Kroll *et al.*, 2009). With respect to this study, this mechanism of LDH inhibition has been observed by copper nanomaterial ions (Han *et al.*, 2011, Suska *et al.*, 2005), silver nanoparticles (Comfort *et al.*, 2011, Wei *et al.*, 2007) and carbon nanotubes (Wang *et al.*, 2012a). A number of these scenarios are reported to have similar cytotoxic effects in the whole cells, detected using the MTT assay. But with the LDH assay reliant upon the release of an internal enzyme into an extracellular environment compared against direct nanoparticle inference with MTT dependent upon uptake into the cell, the mechanism of LDH assay was seen to be more susceptible to breakdown.

Despite this, critical evaluations that report nano-induced problems with LDH, MTT or other colorimetric assays, all seem to concern the application of engineered nanomaterials with highly refractive, extremely small nanoparticles, or those with large surface areas (<50nm particle sized nano-gold and silver in particular, posing problems associated with optical interference with colorimetric assays). The main examples include carbon nanotubes, quantum dots and gold nanomaterials (Alkilany & Murphy, 2010, AshaRani *et al.*, 2008, Dhawan & Sharma, 2010, Han *et al.*, 2011, Kroll *et al.*, 2012, Monteiro-Riviere *et al.*, 2009, Oostingh *et al.*, 2011, Wörle-Knirsch *et al.*, 2006). In all cases, the characteristics that mark them as problematic in colorimetric assays are also beneficial to the desirable nano-specific properties that researchers are looking to exploit in technology: a common dilemma posing the further expansion of nanotechnology. But equally, the individual characteristics of the nanomaterial are noted in many a study as specific towards effects observed under very distinct environmental parameters. This unfortunately contributes towards the great controversy surrounding nanomaterial safety that must now be determined definitively by researchers, on a case by case basis, due to limitations in current technology.

In all examples, nanoparticle interference within assay mechanistic relies upon the interaction of the nanoparticle being present within the assay. Every effort was made to avoid this during the washing steps employed immediately following treatment and before the addition of assay reagents (2.2.2.3.1). Unfortunately, from the data reported, it is impossible to determine the effectiveness of these steps in ensuring the complete removal of every nanoparticle from contact with the cell. But reproducibility of results and cytotoxicity outcomes that fit well within trends described within the literature promoted confidence. In addition, consideration of the challenges reflected by unique

nanoparticle properties in traditional cytotoxic evaluation consolidated the requirement for multi-endpoint risk assessment, employing multiple assays ((SCENIHR), 2009, Borm *et al.*, 2006).

4.2.2 Cytotoxicity assessed through cell imaging

The previous chapter characterised key microstructural properties of the nanomaterials investigated in this study, with outcomes showing each of them having none of the extreme characteristics associated with engineered nanomaterials (such as carbon nanotubes, graphene or quantum dots), in terms of the particle size-surface area ratio. The smallest particles analysed were bulk-SiO_2 (44.3nm mean from Table 3.5) sourced commercially in amorphous form. This measurement was considered an anomaly with regards to the non-nano size expected of bulk particles. Most nanomaterials were characterised with particle sizes in excess of 60nm (Table 3.5). During analysis of nanoparticle properties it became evident that accurate and definitive sizing of particles would be difficult, especially in biological media due to the formation of agglomerates and aggregates. This scenario was thought likely to occur under the cell culture conditions necessitated for H376 growth. This behaviour was observed for all materials, except ZnO, which was imaged on the surface of H376 cells by SEM (Figure 4.10 to Figure 4.12), and is consistent with outcomes from many studies working with uncoated nanoparticles *in vitro* (Albanese & Chan, 2011, Allouni *et al.*, 2009, Chowdhury *et al.*, 2010, Kendall, 2004, Limbach *et al.*, 2007, Oberdorster *et al.*, 2005a, Pickrell *et al.*, 2010). One study reported agglomeration in different carbon nanomaterials used to treat human epidermal keratinocytes as part of an evaluative study investigating the suitability of nine common *in vitro* cytotoxicity methods with engineered nanoparticles (Monteiro-Riviere *et al.*, 2009). They concluded active discrimination against the use of direct cell counting assays (such as live/dead cell count, trypan blue exclusion assay and calcein AM) due to the inaccuracies in reporting data obscured by the shielding of visual cytotoxic indicators by agglomerate sedimentation and adherence to monolayer surfaces. These are considered some of the main alternative methodologies to both LDH and MTT assays.

With bulk materials comprising much larger sized particles, at any equal weight (in comparisons to nanomaterials) there is likely to be an increased number of nanomaterial particles, over the bulk. Assuming direct particle contact is related to increased incidents of cell cytotoxicity, then the higher number of nanoparticles to bulk would likely lead to

greater levels of cell death within a sample population. Conversely, bulk particle interactions would occur less frequently and be limited to affecting 'hot spots' of cell damage that result in an overall reduced level of cellular damage across the sample population (Balásházy *et al.*, 2008). This is clearly evident in both Figure 4.10 and Figure 4.12, for the hydroxyapatite and TiO_2 materials respectively. They demonstrate how the difference in both the size and number of particles between bulk and nanomaterial, led to a large differential in the ability of each to directly contact and exert influence on the H376 cell population. Whilst this only manifested using MTT to compare the effects between hydroxyapatite bulk and nanomaterial exposure (Figure 4.5), it would be expected to have implications on the accurate dosing of nanoparticles.

SEM images depicted morphological signs of cell stress, including nuclear condensation, blebbing and obvious cell shrinkage (Friis *et al.*, 2005, Green & John C. Reed, 1998, Green, 2011, Strasser *et al.*, 2000, Taatjes *et al.*, 2008, Wyllie *et al.*, 1980, Ziegler & Groscurth, 2004). Where cell morphology was thought to exhibit symptoms of cytotoxicity, these were seen to correspond closely to assay results in Figure 4.5. For example, ZnO-bulk and ZnO-45009 materials were shown to be the most cytotoxic, and this is evident from the greater abundance of H376 cells showing morphological signs of cell death in the SEM images (treated with a 0.125% w/v concentration). In contrast to the assay results, cell morphologies indicative of cell death were also observed through H376 cell interaction with ZnO-45408 nanoparticles. The high cytotoxicity of bulk ZnO, even at low concentrations, reduces the likelihood of 'nano' properties being solely attributable to greater cell death for this material, a view consolidated by the sensitivity of the H376 model to zinc acetate exposure (Figure 4.4 and Figure 4.8). An alternative explanation may come from considerations of ion release, an area well established regarding nano-uptake through their application in drug delivery design (Cho *et al.*, 2009, Yin Win & Feng, 2005, Yu & et al., 2011).

The incorporation of two different dispersions of ZnO nanomaterial proved crucial in determining the importance of charge on material behaviour and potential toxicity. Whilst ZnO-bulk charge could not be characterised and compared to zeta potential measurements of the ZnO-nanomaterials, the characterisation results reported in Figure 3.28, highlighted the opposing charges of ZnO-45009 and ZnO-45408 nanomaterials. The revelation that ZnO-45009 was the only nanomaterial from all studied, to possess a positive zeta potential in biological media, would seem to infer the importance of this

property when investigating cytotoxicity. Evidence from literature enhances this hypothesis, with numerous studies able to demonstrate the large surface areas (characteristically niche to nanoparticles) linked to their ability to generate oxidative stress in cells through ion release and surface reactivity (Asati *et al.*, 2010, Berg *et al.*, 2010, Kroll *et al.*, 2009, Oberdorster *et al.*, 2005a). Whilst this connection cannot be concluded from results given in this study, and in part due to the high cytotoxicity caused by ZnO-bulk on this cell model, it does serve as verification to explore this property further.

The SEM images presented within this chapter provide additional validation of particle behaviour that was hypothesised from the characterisation chapter. Examples include the inherent instability of nanomaterial dispersions in biological media, as observed from EM and particle size data determined by DLS in addition to zeta potential measurements. All suggested agglomeration and sedimentation would be highly probable. This is evident in distributions of many nanoparticles interacting at the surface of cells. ZnO material was the exception and it was hypothesised that the particles may be interacting with cellular material present at the surface of the H376 cells, causing them to be less easily seen elsewhere in the images. This was speculated as a route/mechanism for uptake, even by the bulk materials which were characterised as containing low numbers of small and nanoparticles (Figure 3.3). The other nanomaterials particles were obvious at the higher magnifications, observed interacting in groups or agglomerates at the cell surface. Combined with evidence from the literature, this suggested a probable explanation for the unanimously reduced cytotoxicity seen when nanomaterials were delivered in protein supplemented media. The large surface area afforded specifically to nanoparticles over their bulk counterparts is well established as contributing their high surface reactivity (Borm *et al.*, 2006, Nel *et al.*, 2006, Oberdörster, 2010). This same property associated with cytotoxicity, is also thought to protect against nanoparticle-cellular injury, where macromolecules may form a barrier, neutralising the direct interaction between nanoparticle surface and cell structures. Biocompatiable surface coatings have been exploited for nanoparticle drug delivery (Andrews *et al.*, 2009, Kreuter, 2001, Kreuter *et al.*, 2003, Lockman *et al.*, 2002, Rahimnejad *et al.*, 2006, Yin Win & Feng, 2005) and surface functionality in product formulation (*e.g.* sunscreens (Lewicka *et al.*, 2013, Morabito *et al.*, 2011, Schulz *et al.*, 2002, Tsuji *et al.*, 2006)). The surface coatings used to deter agglomeration in dispersion solutions were expected to be diluted following nanomaterial preparation described in

2.2.3.1, and this was indicated by the agglomerates observed in SEM micrographs. To determine whether cytotoxicity observed during screening was definitively a result of nanoparticle action, it was considered important to screen dispersant constituents. Whilst the exact constitution and composition of nanomaterial dispersants remained confidential as the intellectual property (IP) of the manufacturers, preliminary assessment had revealed acetic acid and PEGs present in TiO_2 and ZnO nanomaterial solutions respectively. These are common chemical additions that act as stabilisers in nanoparticle dispersions (Trung *et al.*, 2003). Low cytotoxicity was observed for PEG-300 in terms of LDH release, with 8.4% ± 6.5% recorded at the top concentration of 0.25% w/v dose. This was just over half the total of the comparative low cytotoxicity recorded for ZnO-45408 nanomaterial (14.1% ± 4.7% LDH release), and approximately a fifth in comparison to the levels reported for ZnO-45009 at the same concentration (40.7% ± 7.4%). Assessment using MTT resulted in negligible losses in cell viability following all exposure limits of PEG-300. As such, the risk assessment exerted by ZnO dispersant was deemed negligible in comparison to the effects of ZnO nanoparticles. Acetic acid had more impact on cell viability, exhibiting a statistically significant decrease in cell viability at 0.250% w/v concentration ($P < 0.001$). However, this was not matched by TiO_2 nanomaterial cytotoxicity, and so the effects were thought to have been diluted during nanomaterial exposure treatment preparation.

Equally, nanoparticle surface coating has also been found to occur non-specifically by the formation of a protein corona (Cedervall *et al.*, 2007b, Faunce *et al.*, 2008, Lynch *et al.*, 2007). Many different protein and peptide species have been observed forming a layer over a nanoparticle surface, both through uncontrolled interactions in a biological environment (Cedervall *et al.*, 2007a, Horie *et al.*, 2009, Klein, 2007, Lynch *et al.*, 2007, Merhi *et al.*, 2012) and during a controlled surface modification of nanoparticles during formulation for drug delivery (Rahimnejad *et al.*, 2006, Senel *et al.*, 2000, Soppimath *et al.*, 2001, Yin Win & Feng, 2005). Many examples also report this alongside a similarly marked decrease in cytotoxicity (Dominguez-Medina *et al.*, 2013, Landsiedel *et al.*, 2010, Merhi *et al.*, 2012, Prasad *et al.*, 2013b, Tedja *et al.*, 2012, Xia *et al.*, 2008), was also observed in the assay results reported here (Figure 4.2 and Figure 4.6). How exactly this protein layer affords protection to the cell is currently not fully understood. Current theories encompass a wide range of different scenarios. These include neutralisation of direct contact between a highly reactive 'naked' nanoparticle surface, reported to form and release ROS that can inflict an oxidative stress reaction on the cell (Dominguez-

Medina *et al.*, 2013, Hardman, 2006, Merhi *et al.*, 2012). This has been speculated to halt an immune-reaction that may otherwise occur in response to a foreign body (such as a 'naked' chemical nanoparticle surface) if substituted by a biocompatiable 'native' protein as seen in *in vivo* studies (Johnston *et al.*, 2010b, Scheel & Hermann, 2011, Walkey *et al.*, 2011). The formation of a protein corona is also linked with the modification of nano-characteristics, by overruling particle-particle forces that may govern solubility in dispersions, especially as a protein corona has been seen to be affiliated with greater aggregation of random large agglomerates. The protein adhered agglomerated nanoparticles may subsequently be too large to gain entry into cells, reducing cytotoxicity, when the mechanism of cell injury is dependent upon nanoparticle internalisation (Díaz *et al.*, 2008, Tedja *et al.*, 2012). However, this explanation is complicated by reports of genotoxicity caused after long exposure times with TiO_2 nanoparticles that led to increased particle uptake and bioaccuimulation without significant cytotoxicity (Prasad *et al.*, 2013b, Shukla *et al.*, 2011). Results presented within this chapter did not investigate genotoxic effect, but due to the short term exposure and single dose of nanomaterial treatment to the cells they were not expected to observe similar effects. These results reported FBS protection observed here, consistent with the majority of literature.

For zinc acetate (bulk) material, no protective effect was observed through delivery in FBS supplemented media. This was surprising considering the presence of ligands in the media aimed at regulating zinc ion levels, which are a required nutrient, but known to be toxic in elevated concentrations (Bozym *et al.*, 2010). Albumin protein too, present in FBS was expected to have a high affinity with zinc ions (Masuoka & Saltman, 1994), essentially binding with the free ions to stop their cytotoxic action in cells (as observed for ZnO material). It was therefore speculated that the increased solubility of this form of zinc (over metal oxide), may have led to the increased dissolution of zinc ions in solution, irrespective of protein content, to levels sufficient to overwhelm the H376 cells used in the model. This hypothesis was based on the ability of zinc acetate to deliver high amounts of free Zn^{2+} ions at physiological pH when applied as a common cold remedy (Eby, 2008) and through its use in supplements to combat in zinc deficiency (Stefanidou *et al.*, 2006). The link between zinc ion release and cytotoxicity will be explored further in the proceeding chapter, to determine mechanisms of action for the material that exhibited the highest cytotoxic response during H376 cell screening.

The experimental parameters investigated here will be used for further investigation with the more comprehensive models in the next chapter. This includes the use of both assays (LDH and MTT), and nanomaterial treatment delivery in serum-free culture media. It could be argued that the inclusion of protein might more accurately represent the complex mix of proteins that contribute to the physiological barrier of the oral mucosa (section 1.3.2 of the introduction). But the significantly increased protection afforded across delivery of all materials in this model may screen against any potential cytotoxic effects of exposure to nanomaterials investigated here. Therefore, to consider a worse-case-scenario for initial investigation, serum-free delivery will used in 3-D tissue models. This will be employed alongside greater exposure times and increased doses of nanomaterials, to guard against the expected increase in durability of 3-D models over the sensitivity of H376 monolayers. The application of nanomaterials to the 3-D models of the oral mucosa remains a novel study in reference to contributing the advancement of research for nanotoxicology *in vitro*. The use of more complex models will more realistically replicate conditions of exposure to assess the risk these nanomaterials pose to an area of the body currently devoid of examination: the human oral mucosa.

5 NANOMATERIAL CYTOTOXICTY TESTING USING 3-DIMENSIONAL IN VITRO MODELS

The European Union has long strived for a reduction in animal testing and this has culminated in the recent amendment to the Cosmetics Directive that now prohibits the testing of ingredients on animal models ((EU), 2013). Improved *in vitro* 3-dimensional models are now available to more accurately represent native tissue. The development and complexity of models has advanced as a direct consequence of the EU ban on animal testing in cosmetics (Daston & McNamee, 2005, Hartung, 2009). A lucrative commercial market has subsequently emerged for such models. In toxicology, these are being utilised for studies investigating new materials and pharmaceuticals across all areas of the body (Alépée *et al.*, 2013, Dhiman *et al.*, 2005, Härmä *et al.*, 2010, Loessner *et al.*, 2010, Lu *et al.*, 2012, Ren & Daines, 2011, Subramanian *et al.*, 2010). Some of the more advanced models that have been developed include epithelial layers, such as those representative of human skin (Berthiaume *et al.*, 2011, Group, 1999, Meyer *et al.*, 2009). The close relationship shared by keratinocytes in human skin and the two tissues of the oral mucosa, have seen both keratinised and non-keratinised tissue constructs developed as commercially available oral mucosal models. Artificial 3-D tissue constructs allow more comprehensive *in vitro* testing, through the use of models that more accurately represent the thickness and differentiated strata of native tissue (Mazzoleni *et al.*, 2009). Two such constructs have been utilised here, to investigate the effects of nanomaterial interactions on more representative models of the oral mucosa (both keratinised and non-keratinised tissues).The added sophisitication of 3-D models builds upon the exploratory data gained from simplified monolayer cell screening studies. This approach to toxicity testing aligns closely with the multiple tiered-testing approach adopted by nanotoxicologists, in determining the effects on health of nanoparticle exposure in the body (Oberdorster *et al.*, 2005a).

Cytotoxicity of all nanomaterials was again analysed in comparison against bulk and traditional controls, using the LDH and MTT assays. The lack of cytotoxicity experienced in H376 monolayers for all but ZnO nanomaterial (45009 only) and the bulk ZnO material warranted the investigation into early inflammatory response, which may have indicated only mild irritation to preceed a cytotoxic response. Interleukin-1 alpha (IL-1α) will be used to monitor this response.

The reported cytotoxic mechanisms of zinc materials were discussed in the previous chapter. The outcomes led to the hypothesis that Zn^{2+} ions may have been responsible for the cytotoxic effects of zinc material, observed on H376 cells during screening, similarly to other studies reporting zinc material cytotoxicity (Applerot *et al.*, 2009, George *et al.*, 2010, Huang *et al.*, 2010a, Lin *et al.*, 2009, Sharma *et al.*, 2009b, Wong *et al.*, 2010, Xia *et al.*, 2008). The role of free Zn^{2+} ion concentration related cytotoxicity was investigated further by quantifying ion concentrations of each zinc material.

5.1 Results

5.1.1 Cytotoxicity testing using the RHO model of non-keratinised oral mucosal tissue

5.1.1.1 LDH assay results reporting cytotoxicity in the RHO non-keratinised model

Figure 5.1 reports the results of LDH release when RHO models were exposed to 1% w/v concentration of the material solutions delivered in serum free media. No cytotoxicity was observed for any of the tissue model samples at a 0.1% w/v concentration (not reported) using exposures comparable with H376 dose investigations. LDH results reported are those generated 24 hours after treatment, as preliminary results identified that no LDH release was detected when assayed immediately preceding the 1 hour treatment exposure period.

Results report a % cytotoxicity measurement in the context of normal LDH release (negative control) and a fully lysed population, indicating the maximal amount of cellular LDH available in the tissue models. As before, cytotoxicity was defined using the LD_{50} threshold, where a material dose was considered cytotoxic when LDH release (indicating cell death) exceeded 50%.

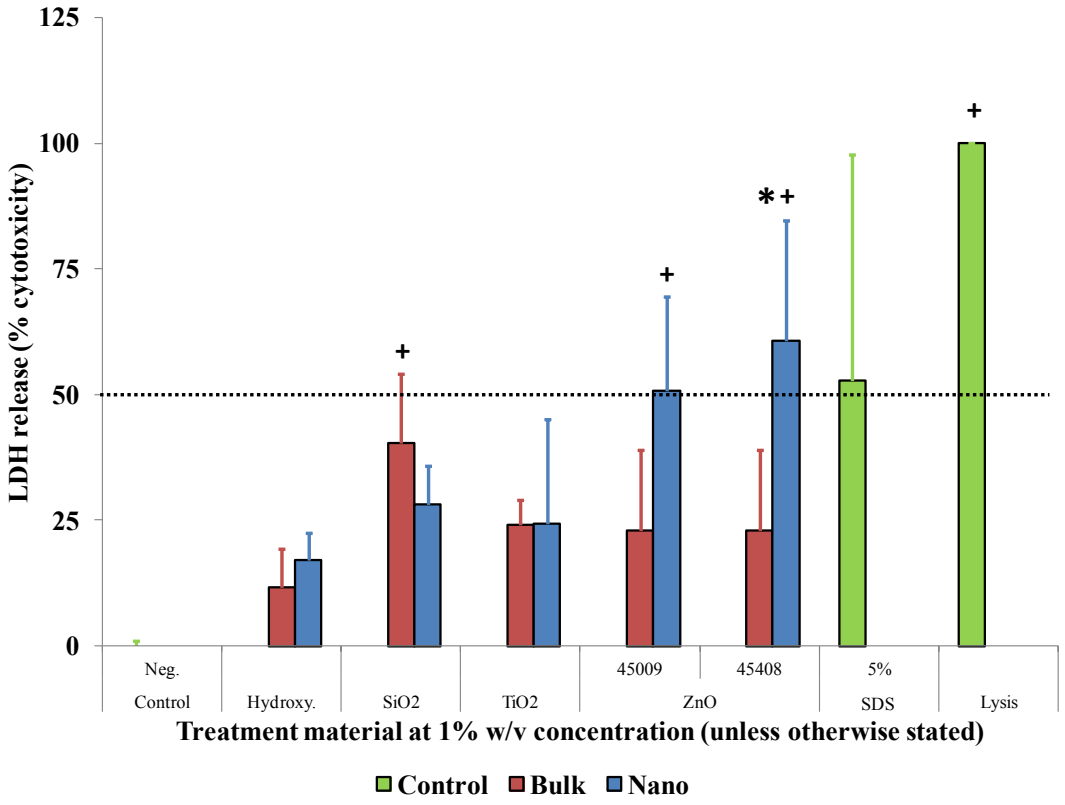

Figure 5.1. A graph comparing the cytotoxic effects of bulk versus nano material exposure to RHO tissue models at a 1% w/v concentration dispersed in serum free growth media for 1 hour exposure at 37°C/5% CO_2. *Results are the average of three experiments (n = 3) with standard deviation reported.* ***** indicates statistical significance using one-way ANOVA with Tukey's post-hoc test to highlight a difference between results when nano cytotoxicity was compared to bulk results at the same concentration. **+** indicate significant cytotoxicity when compared against negative control (P<0.050). The dotted line represents the LD_{50} threshold.

The results presented in Figure 5.1 demonstrated detectable levels of LDH were released from RHO tissue models in response to 1 hour exposure to all test materials (apart from negative control), under the conditions tested. SiO_2 bulk and the two ZnO nanomaterials (45009 and 45408) showed a statistically significant increase in amount of LDH released when compared to the negative control (P = 0.004 and <0.001, respectively). However, this was not to the same extent as the more cytotoxic Triton™X-100 lysed tissue models (P = <0.001 over SiO_2 bulk and ZnO-45009, and P = 0.003 over ZnO-45408). Along with positive controls (SDS and lysis), the ZnO nanomaterials were observed as being cytotoxic, as assessed using the LD_{50} definition. However, the ZnO-45408 nanomaterial was the sole treatement observed to cause a statistically greater cytotoxic effect than the ZnO bulk material equivalent (P = 0.005).

5.1.1.2 MTT assay results of cell viability using the RHO non-keratinised model

The MTT assay results show cell viability for the same RHO tissue models, 24 hours after treatment exposure (1 hour duration) incubated at 37°C and in a 5% CO_2 humidified atmosphere. LDH values were therefore inversely correlated to MTT results with the latter reported as cell viability in the context of % MTT metabolised to formazan by a healthy cell population (negative control).

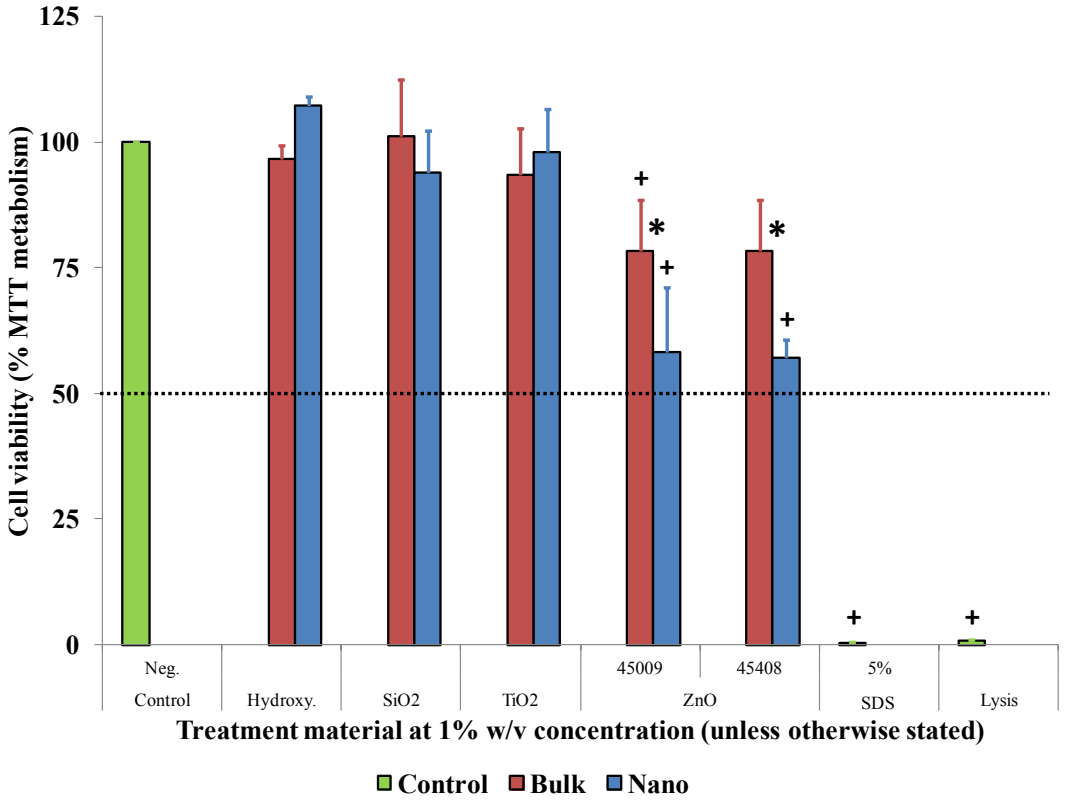

Figure 5.2. A graph comparing the cytotoxic effects of bulk versus nanomaterial exposure, to RHO tissue models, in terms of cell viability calculated from MTT metabolism. *Results are the average of three experiments (n = 3)* at a 1% w/v concentration dispersed in serum free growth media for 1 hour of exposure at 37°C/5% CO_2. *Error bars shown report standard deviation.* ***** indicates statistical significance using one-way ANOVA with Tukey's post-hoc test to highlight a difference between results when nano cytotoxicity was compared to bulk results. **+** indicates significantly reduced cell viability when compared against negative control (P<0.050). The dotted line represents the IC_{50} threshold.

Figure 5.2 shows MTT results corresponded closely to outcomes observed using LDH assay for cytotoxic assessment. Both ZnO nanomaterials reported a statistically significant decrease in cell viability compared to the negative control (P <0.001), although not to the same severity as SDS and full lysis (P <0.001 when compared against nanomaterials).

Unlike the results obtained using the LDH assay, ZnO bulk material exposure to RHO models did not exhibit a decrease in cell viability (as compared to the negative control). Instead, ZnO bulk particles caused a reduction in cell viability (P <0.001) in comparison to negative control values under the conditions investigated here. Despite the bulk effect on cell viability, both ZnO-45009 and ZnO-45408 nanomaterials were observed to have decreased cell viability to a statistically significant level (P <0.001) in comparison: a result displaying the only nano-specific effect of treatmens, experienced by RHO tissue model cell viability examinations.

5.1.1.3 IL-1a release in RHO non-keratinised models.

IL-1α cytokine release was measured at two time points, as described in the methods. ELISA results were amalgamated to report the total amounts of IL-1α detected, but split into a ratio of levels released during both the 1 hour incubated exposure time period, and 24 hours after treatment with each material. These were quantified values (in pg/mL) extrapolated from the calibration curve of a known concentration of IL-1α (as measured from the 250pg/mL standard supplied with the kit).

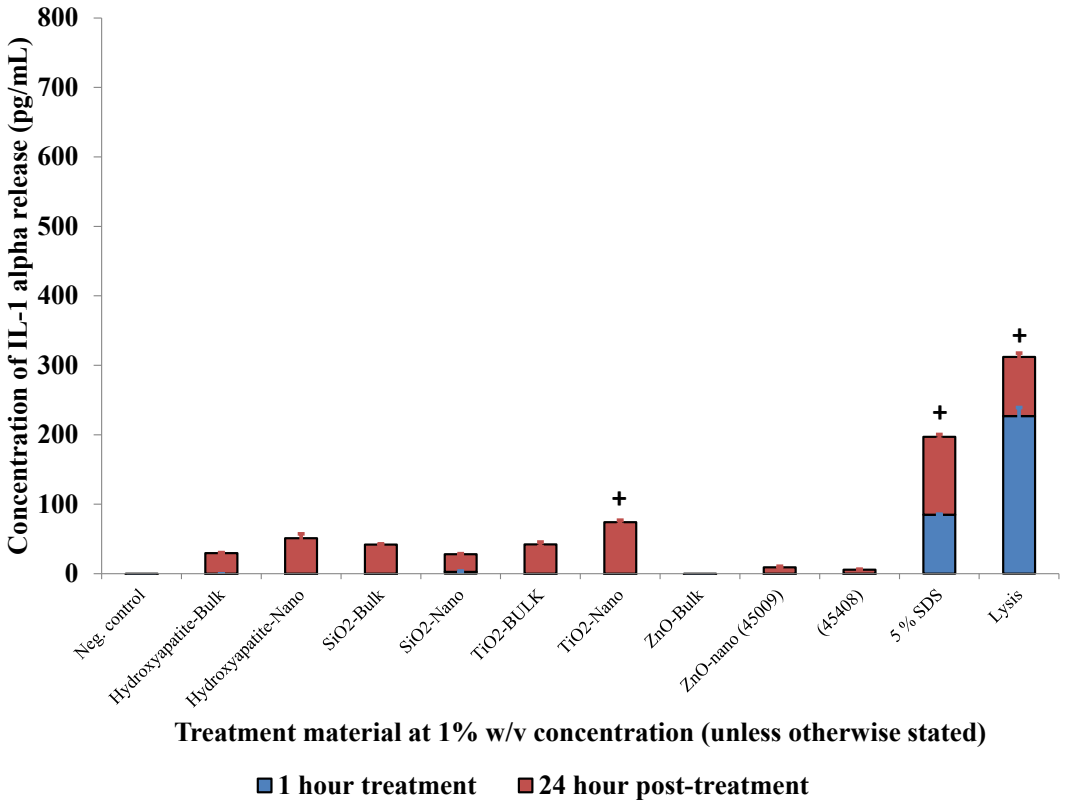

Figure 5.3. IL-1α cytokine release in RHO tissue models following 1 hour exposure to treatments applied apically, dispersed in serum free growth media at a 1% w/v concentration. *Results are the average of three experiments (n = 3) with standard deviation reported.* ***** indicates statistical significance using one-way ANOVA with Tukey's post-hoc test to highlight a difference between results when nano cytotoxicity was compared to bulk results. + indicate significant cytotoxicity when compared against no treatment /negative control (0% w/v). *P* = <0.050.

Figure 5.3 shows the cytokine release by the RHO models after exposure to all test material treatments, delivered under conditions described previously. Measurements were carried out for supernatant corresponding to the 1 hour and the post treatment recovery period (24 hours). Only the cytotoxic positive controls (SDS and Triton™X-100 induced lysis) were observed to cause statistically significant levels of IL-1α detected (*P* = 0.018 and <0.001 respectively), during what was considered rapid release phase of the cytokine, detected in supernatant collected from the 1 hour treatment exposure period. Levels were also statistically significant in the supernatant collected 24 hours post-treatment (*P* <0.001 for SDS and 0.004 following full lysis).

RHO model exposure to 1% w/v TiO_2 nanomaterial was the only other treatment to display a statistically significant increase in IL-1α release compared to the negative

control, when ELISA was carried out on 24 hour post-treatment supernatants (P = 0.016).

It was noted that ZnO bulk material exposure recorded no detection of the IL-1α cytokine, and both ZnO nanomaterials (45009 and 45408) also displayed low levels across supernatants tested at 1 hour and 24 hours post exposure. This result was in contrast to the increased cytotoxicity observed following tissue treatment, as assessed using the LDH and MTT assays (Figure 5.1 and Figure 5.2).

5.1.2 Cytotoxicity testing using the EpiGingiva™ keratinised oral mucosal tissue model

5.1.2.1 LDH assay results reporting cytotoxicity in the EpiGinigiva™ keratinised tissue model

Figure 5.4 reports the results of LDH release from MatTek's EpiGinigiva™ keratinised tissue model (GIN-100), presented in the same way as that described for the study using RHO models. Again, no cytotoxicity was observed for any of the materials tested, when exposed to the tissue model at a 0.1% w/v concentration (not reported). LDH results reported are those generated 24 hours after 1% w/v treatment, as no LDH release was detected when assayed immediately preceding the 1 hour treatment exposure period.

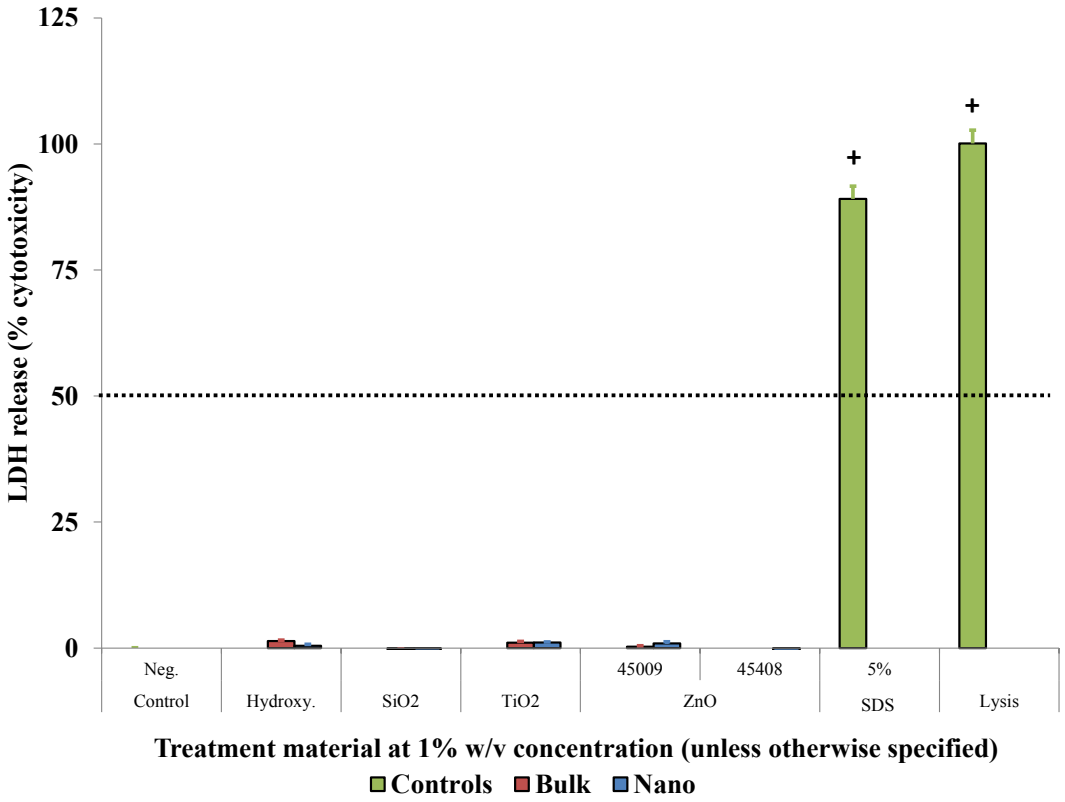

Figure 5.4. A graph comparing the cytotoxic effects of bulk versus nano material exposure to GIN-100 tissue models at a 1% w/v concentration dispersed in serum free growth media for 1 hour exposure at 37°C/5% CO_2. *Results are the average of three experiments (n = 3) with standard deviation reported.* ***** indicates statistical significance using one-way ANOVA with Tukey's post-hoc test to highlight a difference between results when nano cytotoxicity was compared to bulk results at the same concentration. **+** indicate significant cytotoxicity when compared against negative control (P<0.050). The dotted line represents the LD_{50} threshold.

Figure 5.4 shows that negligible detection of LDH levels were released in the keratinised tissue model, following exposure to all nano and bulk materials (< 1% cytotoxicity). Only the results of positive controls (SDS and lysis solution) instigated a cytotoxic effect that was statistically significant in comparison to the negative control (P <0.001 in both instances).

5.1.2.2 MTT assays results of cell viability using the EpiGinigiva™ keratinised tissue model

The MTT assay results show cell viability for GIN-100 tissues exposed to treatments in exactly the same way as reported for RHO tissues. This includes cell viability assessment carried out on the same models assayed by LDH *i.e.*, 24 hours after treatment exposure (1 hour duration) incubated at 37°C and in a 5% CO_2 humidified atmosphere. These were therefore expected to show an inverse correlation to results demonstrating no cytotoxicity.

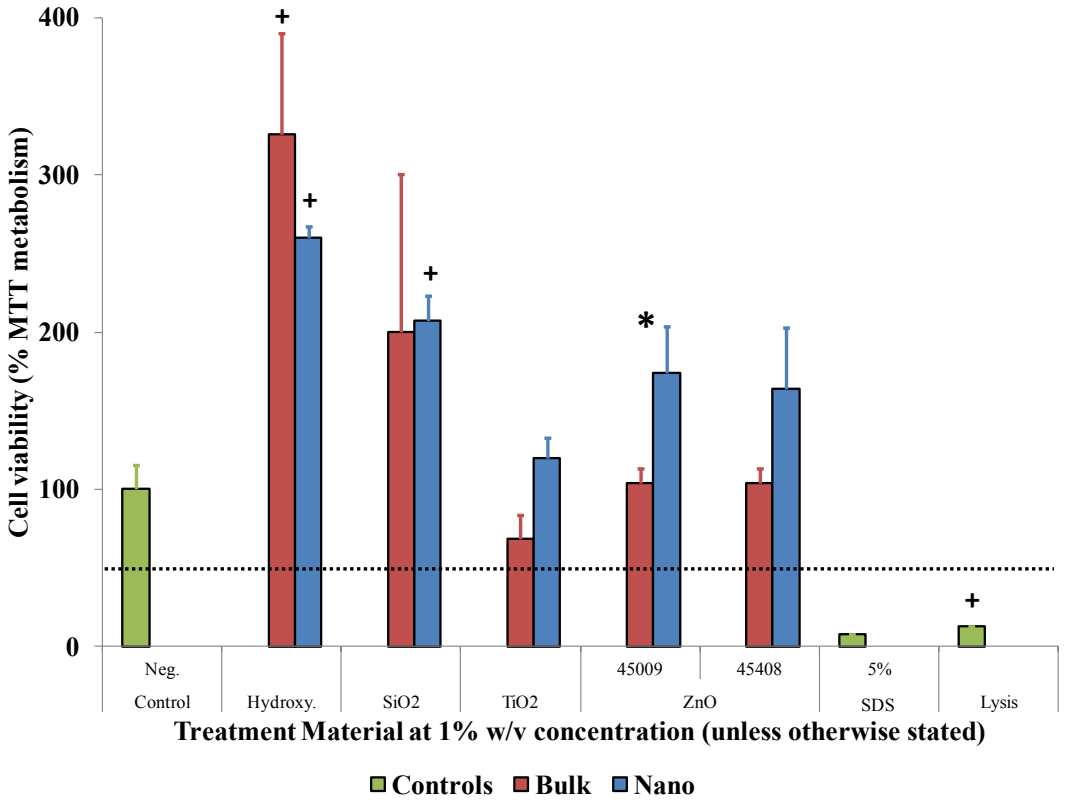

Figure 5.5. A graph comparing the cytotoxic effects of bulk versus nanomaterial exposure, to GIN-100 tissue models, in terms of cell viability calculated from MTT metabolism at a 1% w/v concentration dispersed in serum free growth media for 1 hour of exposure at 37°C/5% CO_2. *Results are the average of three experiments (n = 3) with standard deviation reported.* ***** indicates statistical significance using one-way ANOVA with Tukey's post-hoc test to highlight a difference between results when nano cytotoxicity was compared to bulk results. **+** indicates significantly reduced cell viability when compared against negative control (P<0.050). The dotted line represents the IC_{50} threshold.

Figure 5.5 demonstrates the increased cell viability experienced by the GIN-100 models, following treatment with both bulk and nanomaterials. This was observed through comparison with the negative control, which reported a reduced cell viability measurement to all models treated with bulk and nanomaterial hydroxyapatite, SiO_2 and ZnO. The differences were statistically significant in comparison to hydroxyapatite bulk and nanomaterial (P <0.001), and SiO_2 nanomaterial (P <0.001). The standard deviation bars reported for the bulk material SiO_2 may have reduced the reporting towards a statistical significance increase in cell viability, observed at 200.1% (± 70.9%). Increase in cell viability was also observed for GIN-100 exposure to previously cytotoxic nanomaterials, ZnO-45009 (173.9% ± 14.1%) and ZnO-45408 (163.9% ± 19.6%).

The data presented in Figure 5.5 correspond well with those from LDH assay assessment values, which reported no cytotoxicity in the GIN-100 models. However, the increase in cell viability was unexpected and required further investigation. Two hypotheses were considered:

(i) The materials investigated may promote increased cell proliferation, not previously reported for keratinised tissues.

Or, based upon characterisation outcomes from chapter 3:

(ii) Insoluble materials precipitate upon delivery, resulting in hard particles that may mechanically disrupt tissue structure, or promote desquamation (known to contribute a protective mechanism for gingiva tissue) and rapid renewal of the cells that comprise the tissue model. In both instances, it was speculated that increased levels of formazan may have been present in solution, more so than amounts that may have been locked within the cornified cells of the negative control.

Therefore, the experiment was repeated on additional GIN-100 tissue models, but with lysis occurring following their incubation with MTT solution (as previously described in section 2.2.3.4). This additional step was intended to release all available formazan crystals from cells, prior to solubility with isopropanol and calculation of cell viability as normal.

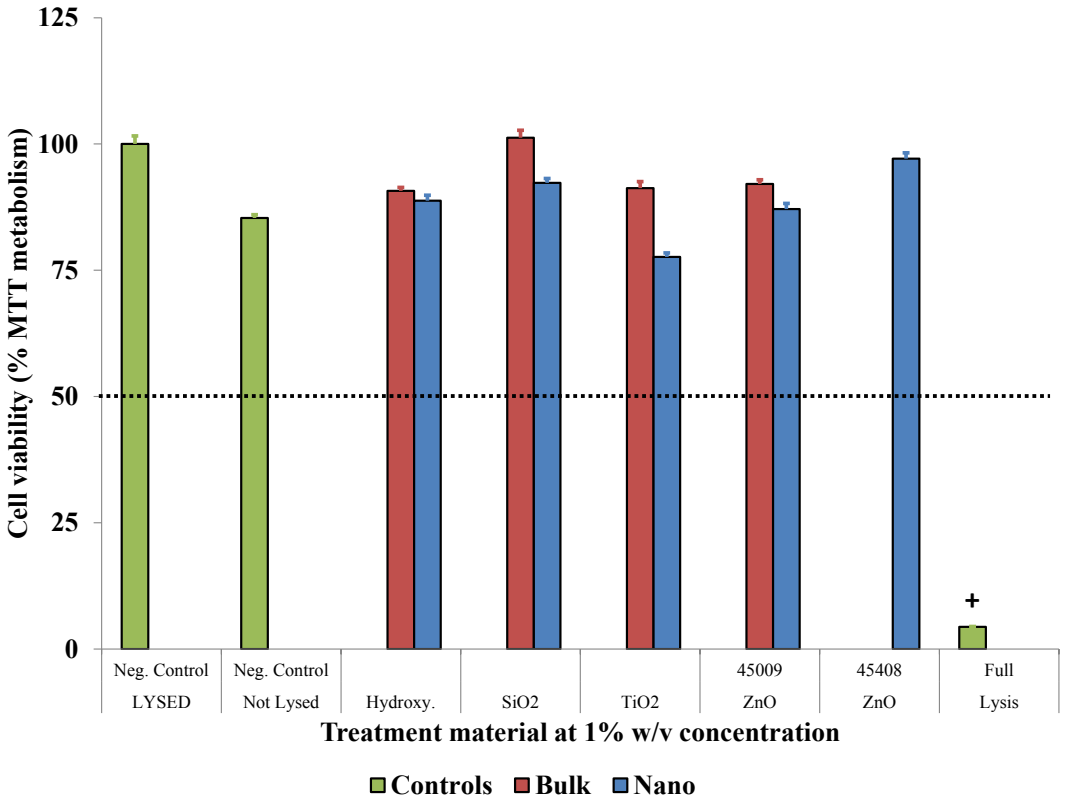

Figure 5.6. A graph comparing the cytotoxic effects of bulk versus nanomaterial exposure, to GIN-100 tissue models that had been lysed before extracting formazan formed during MTT metabolism. at a 1% w/v concentration dispersed in serum free growth media for 1 hour of exposure at 37°C/5% CO_2. *Results are the average of three experiments (n = 2) with error bars reporting standard deviation.* ***** indicates statistical significance using one-way ANOVA with Tukey's post-hoc test to highlight a difference between results when nano cytotoxicity was compared to bulk results. **+** indicates significantly reduced cell viability when compared against negative control (P<0.050). The dotted line represents the IC_{50} threshold.

Figure 5.6 shows the results of the experiment investigating lysis to release all available formazan from tissue models. When the negative control samples underwent lysis before isopropanol extraction, cell viability was calculated to show effects of material treatments anticipated from previous data. No cytotoxicity was observed, as assessed using IC_{50} with only full lysis by Triton™X-100 inducing a statistically significant reduction in cell viability.

Lysis following MTT incubation released 15% more formazan than that from the tissue models that did not undergo the step (unlysed). There was also a reduction in variability between results, expressed as smaller standard deviations, when samples exposed to treatments had been lysed before extracting formazan in isopropanol.

5.1.2.3 IL-1a release in the EpiGinigiva™ keratinised tissue models.

The following results report the quantified levels of IL-1α released in cell supernatant from EpiGingiva™ GIN-100 models, exposed to treatments in exactly the same way as reported previously in the RHO non-keratinised models.

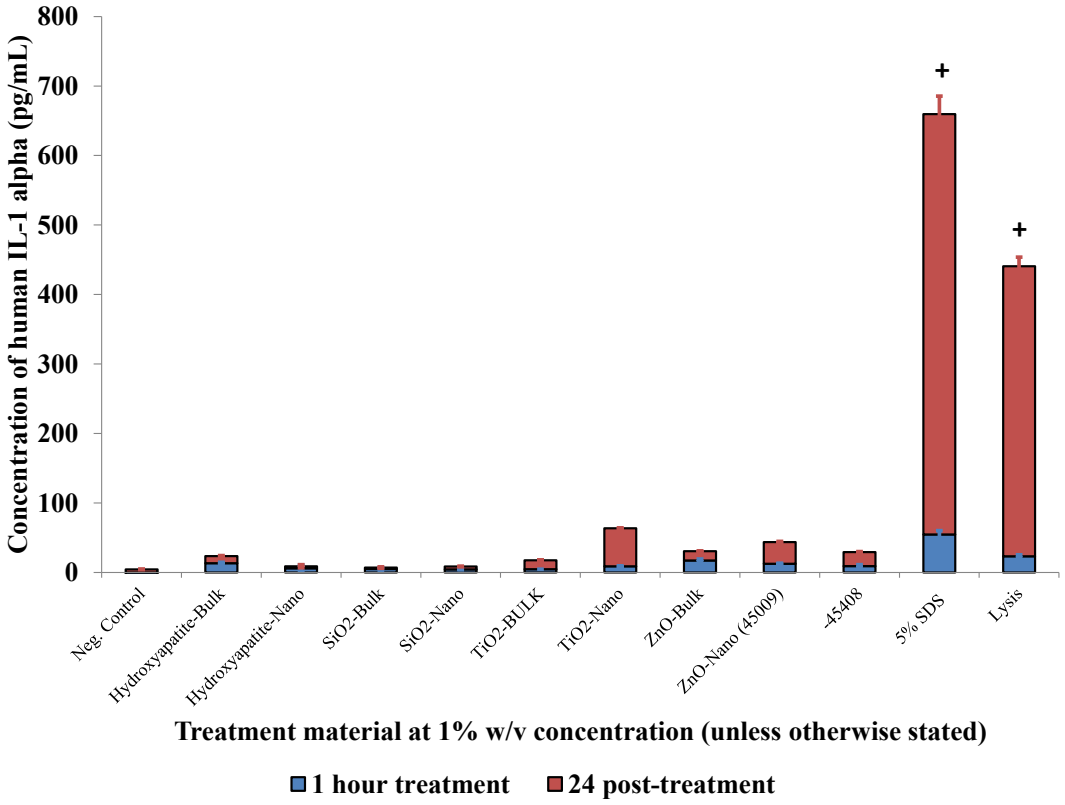

Figure 5.7. IL-1α cytokine release in GIN-100 tissue models following 1 hour exposure to treatments applied apically, dispersed in serum free growth media at a 1% w/v concentration. *Results are the average of three experiments (n = 3) with standard deviation reported.* ***** indicates statistical significance using one-way ANOVA with Tukey's post-hoc test to highlight a difference between results when nano cytotoxicity was compared to bulk results. + indicate significant cytotoxicity when compared against no treatment /negative control (0% w/v). *P* = <0.050.

Figure 5.7 reports the levels of IL-1α cytokine released from GIN-100 tissue models, following exposure to all treatments tested under the conditions studied. Only cytotoxic positive controls (SDS and lysis) induced a statistically significant increase in the release of IL-1α (*P* = 0.008 and 0.011 respectively). The concentrations detected from the release by GIN-100 positive control tissues, emphasised the low levels observed following treatment by the other materials. This was considered in relation to the total amount available for release (659.5 ± 31.6pg/mL and 440.7 ± 15.3pg/mL for SDS and

lysis positive controls) in GIN-100 tissue models, significantly greater than that detected for non-keratinised RHO models (196.9 ± 4.4pg/mL and 312.2 ± 17.8pg/mL respectively).

The other notable result observed in Figure 5.7 was the detection of IL-1α after exposure to ZnO materials (bulk and nano) that was the negligible following exposure to the RHO model. This included low concentrations released during the initial 1 hour of exposure.

5.1.3 ICP-OES measure zinc ion concentration

This experiment was carried out in an attempt to determine any difference between the concentrations of zinc ions present in the different forms of the material. Alongside the three forms of ZnO (bulk, nano-45009 and nano-45408), zinc acetate was analysed to provide a control for zinc chemical structure. The following figures show results quantifying the concentration of Zn^{2+} ions released either natively, or following a nitric acid digest, for the different forms of ZnO material used in this study.

Figure 5.8 shows the zinc ion concentration for each undigested zinc material. An inverse trend was noted relating to high zinc ion concentrations corresponding with small average particle sizes recorded during characterisation (Table 3.5). Bulk ZnO recorded less free Zn^{2+} content in comparison to the two nanomaterials, with the larger ZnO-45009 nanoparticles having less free ions than ZnO-45408 nanomaterial. Zinc acetate also measured significantly lower concentration of Zn^{2+} in comparison to the nanomaterials (P <0.001).

No difference was noted between Zn^{2+} concentrations measured across the different solvents used to disperse the zinc particles. This highlighted how the dispersion media had little effect on the concentration of Zn^{2+} recorded. Only ZnO-45009 dispersion in PRF media recorded a statistically significant difference in concentration of 10.8ppm Zn^{2+} ions (± 0.7 standard deviation), which was larger than the measurement taken from the material dispersed in other solvents (P <0.001). The result was not thought a direct consequence of the dispersion media, with Zn^{2+} ion concentration measured as negligible in the control (blank) results.

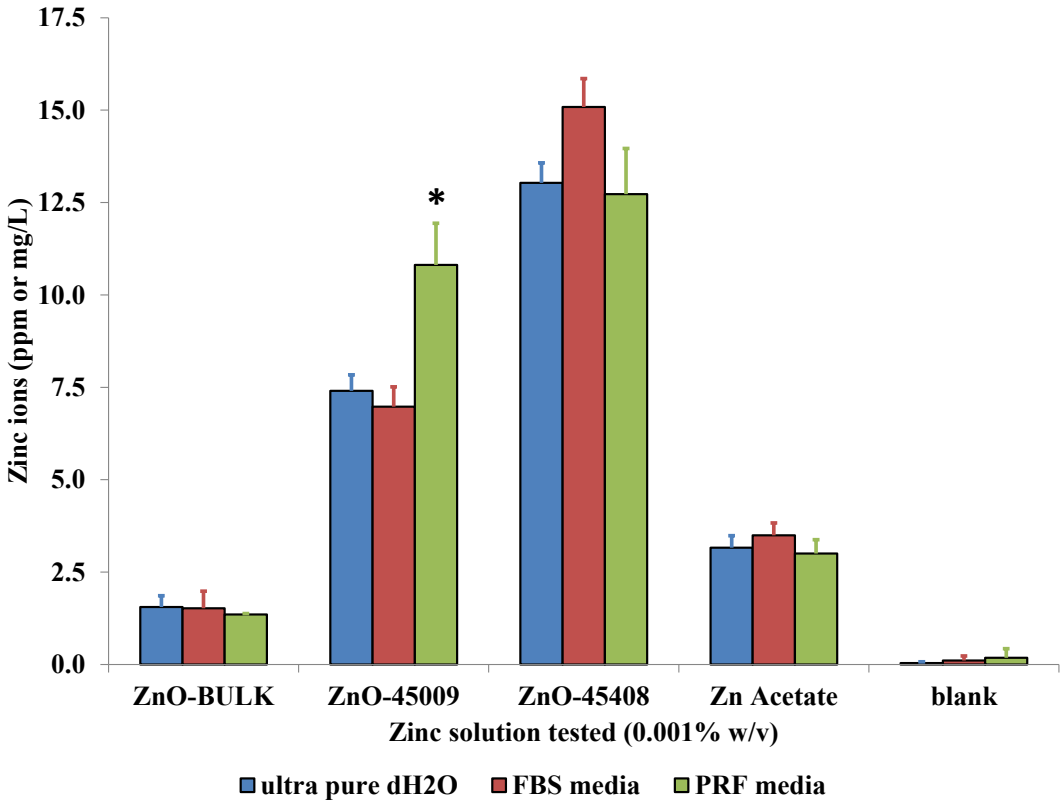

Figure 5.8. Zn^{2+} concentration of zinc materials analysed with ICP-OES, without a nitric acid digestion. *Results are the average of three experiments (n = 3) with standard deviation bars shown.* ***** indicates statistical significance using one-way ANOVA with Tukey's post-hoc test to highlight a difference between (comparisons of each material in the three solvents used for dispersion ($P < 0.050$).

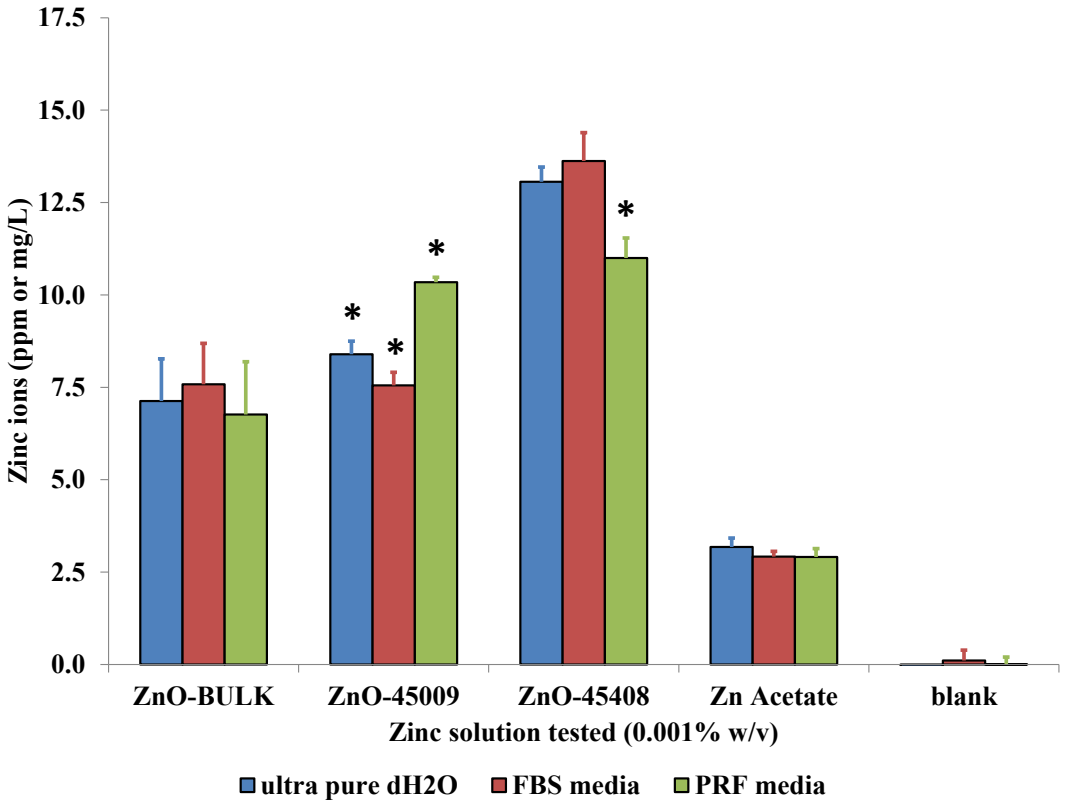

Figure 5.9. Zn^{2+} concentration of zinc materials analysed with ICP-OES, after a 24 hour nitric acid digestion. *Results are the average of three experiments (n = 3) with standard deviation bars shown.* ***** indicates statistical significance using one-way ANOVA with Tukey's post-hoc test to highlight a difference between (comparisons of each material in the three solvents used for dispersion ($P < 0.050$).

Figure 5.9 shows the effect digestion by nitric acid had on the concentration of zinc ions released from each of the materials investigated. Overall, the digestion was observed to have only a limited effect on the concentration of Zn^{2+} released from the respective materials. Statistically significant differences were detected between the different dispersions of ZnO-45009 and ZnO-45408 nanomaterials in PRF media (all P <0.001). However, the actual values recorded following the digest compared to the undigested materials, showed little difference. This was displayed best when comparing zinc acetate Zn^{2+} concentration in dH_2O dispersion, averaging 3.2ppm in both undigested and nitric acid digested sample (± 0.1ppm and 0.2ppm standard deviation, respectively).

Only ZnO bulk material exhibited a statistically significant difference in levels of Zn^{2+} detected, being between undigested sample and that following oxidisation by nitric acid. Across all dispersions, the nitric acid digest increased Zn^{2+} concentration (P <0.001), to similar levels observed for ZnO-45009 nanomaterial dispersion in dH_2O and FBS media.

ZnO-45408 nanomaterial samples were again observed measuring the greatest concentration of Zn^{2+} ions.

The results of ICP-OES analysis of different zinc materials imply the ready availability of free Zn^{2+} ions from particles is related to the surface area, and chemistry of the material. This was demonstrated by the use of nitric acid digestion to release all potential ions from each material into solution with only ZnO bulk recording a significant difference between sample preparation methods. In comparison, dissolution of ions was complete without the aid of digestion in nanomaterials, with measurements related to their average particle size, characterised previously (Table 3.5). Zinc acetate is a more soluble form of the zinc (Yang *et al.*, 2004), and the compound is made up of particle sizes measuring in excess of the nano-scale (>100nm). It is therefore suggested that zinc ions were released in solution without the need of an acid digestion, but were still not recorded at equivalent concentrations as the two ZnO nanomaterials (with greater surface areas linked to higher free ion release).

5.2 Discussion

The results presented here form an integral part of the tiered strategy approach recommended for both skin irritancy testing and nanotoxicology. They build upon the previous results and outcomes determined using the H376 monolayer model, but allow for a more sophisticated representation of the fate of nanomaterials applied to human oral mucosae. By investigating cytotoxicity, cell viability and the primary cytokine switch responsible for keratinocyte inflammation (IL-1α release), in comparison to both a known irritant used in cosmetics (SDS) and respective bulk constituents, a more comprehensive assessment of the impact of potential nanomaterial formulations in oral healthcare was established.

5.2.1 Assessment of in vitro toxicity testing

The differences in outcomes between H376 screening compared to the non-keratinised RHO model, demonstrate the increased sensitivity of monolayer cell growth, thought to reduce representation of nanomaterial interactions with the oral mucosa. For over thirty years studies have indicated the significant limitations of 2-D monolayers in closely mimicking natural tissues and organs (Eisenbrand *et al.*, 2002, Mazzoleni *et al.*, 2009). In 2-D cell culture, cells are grown and adhere to synthetic surfaces *e.g.* treated polystyrene plastics. Cell monolayers disperse across the growth surface in stiff, flat, very unnatural structures that are anchored by proteins that are deposited and denatured on the synthetic surface (Sackmann & Tanaka, 2000). In this regard, monolayer growth cannot adequately capture the relevant complexity of the *in vivo* microenvironment, including the loss of tissue-specific architecture, mechanical and biochemical signals, and cell–cell communication (Eisenbrand *et al.*, 2002). Furthermore, this disparity may cause misrepresentation in resultant outcomes to some extent, by forcing cells to adapt to an artificial, flat and rigid surface, moving them away from normalised functioning (Mazzoleni *et al.*, 2009). An example of this effect in this work was thought to be demonstrated by the lack of LDH release detected from H376 cells following exposure to otherwise cell viability reducing SDS concentrations (Figure 4.4).

In contrast, 3-D cell culture *ex vivo* models better simulate the composition of extracellular matrix by using collagen or hyaluronic acid based scaffolds (Chen *et al.*, 2012, Pescosolido *et al.*, 2011), with selective incorporation of signalling factors, adhesion factors, and proteins (Rimann & Graf-Hausner, 2012). Central to constituting representative *ex vivo* structure is the direct cell-cell attachment that interacts with the

extracellular matrix to form stratified cell layers. Consequently, the complex structural proteins remain in their native configuration and so provide important biological instructions to other cells. This includes inducing force on one another, directing the migration of cells during differentiation (Friedl & Gilmour, 2009). Differentiation and more accurate depiction of direct cell-cell interactions are demonstrated by the greater prevalence of gap junctions in 3-D tissue models (Debnath & Brugge, 2005, McNeilly *et al.*, 1996, Radisic *et al.*, 2004). These enable more natural cellular communications through the exchange of ions, small molecules and electrical currents (Grellier *et al.*, 2009, Griffith & Swartz, 2006, Radisic *et al.*, 2004), which is thought to be a better model of cell-cell communication and signalling that is critical for cell function. The closer development of 3-D models into tissue-like structures, produces greater similarity in morphology to *ex vivo* tissue (Carlson *et al.*, 2001, Griffith & Swartz, 2006, Moharamzadeh *et al.*, 2012), which in turn enables a better representative model to investigate function in living organisms (Rimann & Graf-Hausner, 2012). This has been observed most successfully in studies comparing 3-D technology to monolayer cell models of the liver (Gunness *et al.*, 2013, Mueller *et al.*, 2013, Yip & Cho, 2013), gut (Cencič & Langerholc, 2010b), various epithelial tissue (including, lung epithelium (Balharry *et al.*, 2008, Carterson *et al.*, 2005, Rothen-Rutishauser *et al.*, 2008) and human skin (Junginger *et al.*, 1999, Moharamzadeh *et al.*, 2012, Sun *et al.*, 2006)) and cancer studies (Härmä *et al.*, 2010, Loessner *et al.*, 2010).

The development of increasingly sophisticated and representative *in vitro* and *ex vivo* models is reflected by the growth in application of such 3-D tissue models in research. There is strong demand in toxicology studies, as scientists look to move away from traditional animal models that suffer from ethical issues, high costs and interspecies variation (Piersma, 2006), with the latter limiting the extent to which extrapolation of results outcomes may apply to humans (Hartung, 2009). Regarding the oral mucosa, many common laboratory animal models would suffer major limitations due to the high frequency of predominantly keratinised epithelium lining their oral cavity (Harris & Robinson, 1992, Wertz *et al.*, 1993). Driven by the principals of the 3 R's: replace, reduce and refine (Russell *et al.*, 1959), the EU is particular keen to employ validated alternate models to minimise the extent of animal studies. Urgency can perhaps be attributed to the current EU initiative, for Registration, Evaluation, and Authorisation of CHemicals (REACH) (Pedersen *et al.*, 2003), which is aimed at completing a minimal toxicity database for thousands of existing chemicals during the coming decade. In

current guise, REACH assessments will have to intensify animal testing dramatically, a process estimated to consume over half the total resources attributed to the initiative (Piersma, 2006), and clearly not sustainable as more and more new materials, drugs and chemicals are developed. In applications investigating the internalisation of nanoparticles, the scientific committee on emerging and newly identified health risks (SCENIHR) promotes the use of *in vitro* and *ex vivo* models, due to scepticism of the suitability in whole animal models working to assess cellular uptake ((SCENIHR), 2009).

It is the cosmetic industry that currently leads the way in validating alternative models to replace laboratory animals in testing (Rimann & Graf-Hausner, 2012). The skin can be considered a relatively simple organ in comparison to others that function within the body (*i.e.* the liver, kidneys, heart *etc.*), and limitations in organotypic 3-D models for other human tissues need to be overcome before widespread replacement of animal models can occur in alternate industries. Currently, 3-D culture is often more time-consuming than monolayer growth, and this has kept costs high, reducing their viability for widespread or large studies. In addition, many 3-D models remain novel, with very niche and specific applications as of a consequence of their design to model a particular scenario *e.g.* keratinocyte and melanocyte co-culture models for research into melanogenesis (Iriyama *et al.*, 2011). Whilst batch to batch variability between models has largely been overcome through substitution of animal derived scaffold components to synthetic chemical materials (Kim & Mooney, 1998), the artificial construction of many models may not demonstrate the full range of biological functions representative of native tissue. These issues are at odds to the properties desired by industrial pharma companies, reliant upon efficient, universally standardised but versatile high-throughput screening technology.

Versatility is an important consideration in the replacement of *in vivo* studies by artificial 3-D models. In particular regarding tissue areas of the body prone to mechanical or biomechanical stresses *i.e.* the epithelial layers of the oral mucosa, exposed to mechanical insult during mastication. More sophisticated 3-D tissue models are still currently limited in only representing static conditions (Mathes *et al.*, 2010). The impact in comparison to *in vivo* studies, is the necessity of multiple tissue models to mimic a range of scenarios (*e.g.* damaged or diseased skin alongside healthy models), and the subsequently increased volume of analysis required to enable accurate extrapolation and

interpretation of results. The analysis itself can be complicated through study of 3-D models, in particular regarding conventional imaging techniques. 3-D samples are typically highly light scattering and several hundreds of micrometres thick, prone to photobleaching and light-induced damage (Pampaloni *et al.*, 2007).

Problematic for many *in vitro* studies, not solely attributed to 3-D models, are the limitations placed on simplified models of complex biological systems. For *ex vivo*, there remains a lack of validated non-animal models for the evaluation of systems available to study systemic or long-term toxicity (Bhanushali *et al.*, 2010). The level of validation required for a regulatory framework means this is a long process and by no means assured to succeed in gaining acceptance by the regulators. For the foreseeable future, toxicity testing conforming to the 3 R's is likely to have to rely on a battery of different assays and models (Jaworska *et al.*, 2010). However, limitation in the use of 3-D studies can only be considered in the context of comparisons to *in vivo* models. Cost and efficiency aside, nearly all applications of 3-D cell culture will provide a more sophisticated and representative model when compared against cells grown in monolayer. Utilisation of the 3-D tissue models representative of human oral mucosae, allowed for cytotoxic effects to be analysed in models closer to an *in vivo* situation than H376 cell monolayers used previously.

5.2.2 Comparisons of 3-D keratinisation models

By testing nanomaterials on two different tissue models, a more realistic evaluation of both types of distinct tissues that encompass the human oral mucosa was fulfilled (kertainised and non-keratinised). In addition, cytotoxicity testing contributed towards the novel impact on knowledge: at the time of writing, no nanomaterials reputed of interest to oral healthcare formulations have been assessed for nanotoxicity with either MatTek EpiGingiva™ or SkinEthic RHO tissue models. These well characterised 3-D tissue constructs formed multilayer, stratified non-keratinised and keratinised oral epithelium, respectively, which exhibit *ex vivo*-like properties and growth characteristics (Moharamzadeh *et al.*, 2007). Keratinised tissue has already proved important in the development of mouthwashes and oral healthcare technology; particularly toothpastes, denture implants and denture adhesives that are either applied in close proximity to, or more vigorously on, keratinised regions of the oral mucosa (De Clement & Wheater, 2009, Koschier *et al.*, 2011, Sullivan *et al.*, 2011, Yang *et al.*, 2011). The use of such

models in this study, allowed for the cytotoxic assessment of potential nanoparticle excipients for next generation oral healthcare products.

It was hypothesised here that the additional cell layers afforded to 3-D tissue constructs would manifest an increased robustness towards the cytotoxic effects of treatments observed during monolayer screening. This was expected to be enhanced in the EpiGingiva™ GIN-100 model, due to the differentiation process forming a tough, cornified *stratum corneum* at the apical surface, representative of *in vivo* keratinised tissue of the gingiva and hard palate (Wertz & Squier, 1991). Preliminary data (not included) had confirmed this effect in the models, enhancing their credential to more accurately mimic nanomaterial effects on human oral mucosae *in situ*. Therefore, both dosage and exposure times were increased when using the 3-D models, continuing the investigation from the 'worst case scenario' perspective. A 1 hour exposure time with nanomaterials was considered well within the period expected for residual contact reported for compounds formulated in some oral care products (Creeth *et al.*, 1993, Cummins & Creeth, 1992, Gilbert & Williams, 1987, Saxton *et al.*, 1986, Zero *et al.*, 1992). After 1 hour exposure, results still showed no cytotoxicity in response to exposure of any test material on the GIN-100 model, and only low levels of IL-1α inflammatory cytokine release were observed. In comparison, cytotoxicity was observed for ZnO material exposed to the RHO models. In the non-keratinised tissue models, this was observed more prominently using LDH assay, as defined using the LD_{50}. Furthermore, moderate levels of cell lysis were observed, following exposure to all other materials (Figure 5.1). Whilst different to H376 results, which reported ZnO bulk and ZnO-45009 nanomaterial cytotoxicity as a loss in cell viability, (with the MTT assay proving more sensitive than LDH on monolayer cells), these results were attributed to the accurate reflection of greater durability indicative of native keratinised tissue (Squier & Kremer, 2001). This was exemplified by the requirement of lysis following MTT incubation to fully release formazan locked within GIN-100 tissue models.

However, the superior robustness may also have been in part, due to difference in tissue models. Whilst neither 3-D model reflected the true, full thickness expected of native tissue (Rossi *et al.*, 2005, Shojaei, 1998, Winning & Townsend, 2000), there was a difference in the number of cell layers between the two models. GIN-100 samples were validated to encompass 8-10 fully differentiated cell layers, consistent with keratinised tissue morphology. These were considered thicker than RHO tissue models, comprised

of just 6, non-keratinised cell layers. Considering the increased doses required to instigate only a mild cytotoxic response for most materials, following exposure to RHO, comparison to the more sensitive H376 monolayer models necessitated consideration of the impact of increased cell layers on cytotoxicity. Similar trends were observed during the cytotoxicity testing of hydrogen peroxide and silver nitrate in three different human skin keratinocyte cell types (both normal and the transformed keratinocyte cell line, HaCaTs), fibroblasts and endothelial cells, all demonstrating superior robustness in 3-D models over 2-D monolayers (Sun *et al.*, 2006). RHO models were considered less representative of normal human oral mucosae tissues, cultured exclusively from the transformed TR146 cell line. Compared with normal oral keratinocytes, these do not form a fully differentiated oral epithelium (Yadev *et al.*, 2011), solely recreating the structural and functional features present at the superficial layer of the human buccal mucosa (Vande Vannet *et al.*, 2007). For example, Langerhans cells play a critical role in cutaneous immune response and cytokine production, but are absent from the RHO model used (Cumberbatch *et al.*, 1996, Srivastava *et al.*, 1994). However, these are now close to becoming available commercially, in more sophisticated, full thickness buccal mucosal models (Chang *et al.*, 2007).

Whilst cell line use may have reduced batch-to-batch variability (Moharamzadeh *et al.*, 2012), 3-D models based on normal oral keratinocytes (seeded onto fibroblast-populated bovine collagen matrices (Mostefaoui *et al.*, 2004)) have been observed as more accurately representing the complex interactions that govern keratinocyte differentiation, basal cell proliferation and cytokine expression similar to normal oral mucosa (Yadev *et al.*, 2011). The EpiGingiva™ GIN-100 models were derived from normal human oral keratinocytes, isolated from non-diseased, human oral tissues that were obtained from patients or cadavers (Klausner *et al.*, 2007). K*eratinised p*rimary cells are considered more readily available via "off cuts" from routine dental surgery that does not require invasive biopsies *i.e.* unlike the punch biopsy employed to collect specimens from the buccal mucosa (Sasaki *et al.*, 2012). They are and considered to better represent normal cell functioning, that can deviate as cell lines acquire a molecular phenotype quite different from cells *in vivo (Cencič & Langerholc, 2010a, Pan et al., 2009).* Traditionally, culturing primary cells has been linked to short culture periods and batch-to-batch variation as a consequence of dissimilarity between donors (van der Valk *et al.*, 2010). These issues seem to have been addressed during manufacturing methodologies, perhaps as a result of keratinised tissue sharing close alignment to

human skin, and the development of well-established and fully validated skin models that are widely commercially available (Groeber *et al.*, 2011, Macfarlane *et al.*, 2009, Spielmann *et al.*, 2007, Vinardell & Mitjans, 2008). Consequently, the GIN-100 model has been successfully utilised in assessing the response of alcohol based mouthwashes (Moharamzadeh *et al.*, 2009), SDS (Klausner *et al.*, 2007, Moharamzadeh *et al.*, 2012) and other dental materials (Yang *et al.*, 2011), to mimic outcomes representative of native tissue.

In summary, whilst limitations exist in the use of 3-D *in vitro* models, they can still be considered more representative towards modelling the interactions that would be expected for short-term exposure of nanomaterials on the human oral mucosa. Both keratinised and non-keratinised tissue types represent the first cells in contact with test products, and have been widely embraced as alternates to animal testing for initial stages of cellular irritation. From these results, ZnO nanomaterials pose the greatest risk of cytotoxicity, but were well tolerated by the EpiGingiva™ GIN-100 models, mimicking the anticipated greater robust of native gingiva tissue. Caution must be observed, however, in extrapolating comparisons between the two models. In particular the mild cytotoxicity and inflammation observed in RHO tissue studies, which will now be discussed.

5.2.3 Further investigation of potential cytotoxic mechanisms

Cytotoxicity was only observed in the RHO non-keratinised tissue models exposed to ZnO material treatments (bulk and nano), consistent with outcomes from screening materials using the H376 model. However, in the RHO model, both nanomaterial samples studied were observed as causing cell lysis and loss in cell viability, more so than the bulk material. This reflected outcomes of ICP-OES analysis for quantification of free Zn^{2+} ion concentrations, which showed the smaller nanomaterials to have significantly greater Zn^{2+} dissolution over larger particulates (ZnO-45408 > ZnO-45009 > ZnO bulk). In this respect, the RHO results were thought to align more closely with reports in the literature obtained using other *ex vivo* models, that demonstrate similar increases in cytotoxicity of ZnO nanoparticles over bulk composites (Hackenberg *et al.*, 2011b, Hsiao & Huang, 2011, Sharma *et al.*, 2011, Xia *et al.*, 2008, Yu & et al., 2011).

As previously discussed, zinc ion release has been heavily reported to cause oxidative stress and is considered the main mechanism of action resulting in cytotoxicity ftom the material (Rabani, 2001, Ross *et al.*, 1997, Wong *et al.*, 2010, Wu *et al.*, 2012, Xia *et al.*,

2008, Yeh *et al.*, 2011). Whilst needed in small quantities for regular cell function, an environment overloaded with Zn^{2+} can contribute to the initiation of an inflamed reaction by the cell. In an effort to consolidate the link between zinc ions and cytotoxicity exerted by non-keratinised oral epithelia, the use of ICP-OES was employed to quantify Zn^{2+} concentrations, specifically for those that may be available as free ions during *in vitro* exposure. These results (Figure 5.8) indicate the ready availability of free ions relating to all zinc nanomaterials (not bulk), as demonstrated by no significant change occurring upon nitric acid digestion of the nanomaterials (Figure 5.9). Relating these findings to the increased cytotoxicity reported for nanomaterials (over bulk particulate material), the Zn^{2+} concentrations detected were noted as being inversely correlated to average particle size. The smaller ZnO-45408 nanomaterial was observed to have the highest concentration of Zn^{2+} in all dispersions, readily available without the need for a nitric digest. This was then followed by the slightly larger nanomaterial, ZnO-45009. Free ion content may be linked to their increased surface reactivity, reported for nanoparticles due to the greater proportion of their atoms being present at the surface of the particle (Borm *et al.*, 2006). Silver nanoparticles, also investigated for their reputed antimicrobial activity, show ion release kinetics linked to both particle characteristics and the environmental factors they are dispersed in (Alissawi *et al.*, 2012). Dissolved oxygen, pH, temperature and complex interaction with organic constituents were found to have the greatest influence (Liu & Hurt, 2010). No obvious trend was observed with respect to dispersion media impacting upon zinc ion concentration in these studies. The low concentrations recorded for each respective media controls (both undigested and nitric acid digested) inferred a negligible effect by the solvents.

For ZnO-45009 nanomaterial results, significant differences were observed between the zinc ion concentrations observed for each type of media (the more so following digestion). This was also observed for digested ZnO-45408 nanomaterial in PRF media (measured to have lower concentrations to both dH_2O and FBS media dispersion). An explanation for these results proved difficult, leading to the consideration and critical review of sample preparation. The method utilised followed an ISO standardised protocol to detect zinc (ISO11885:2009), but in traditional bulk form. It is possible that measurements for nanoparticle specific characteristics may require further investigation, or optimisation of the methodology. The small particle size of nanoparticles was thought likely to contribute a decreased density when compared against bulk composite

(Jeong *et al.*, 2005). Centrifugation was used to separate any remaining solid present within the sample prior to analysis, however, this may not have been sufficient to remove the smallest particles. The presence of ZnO nanoparticles may have contributed spikes in zinc ion detection, if they were small and light enough to remain suspended following desolvation, prior to ionisation within the ICP-OES instrument. However, this was considered unlikely for samples digested using the wet acid preparation (BSI, 2009). Strong nitric acid was used to oxidise the ZnO environment, degrading all zinc material to soluble Zn^{2+} analytes in each of the aqueous media. Digestion for 24 hours at room temperature was deemed sufficient to produce reproducible results for each experiment (n=3), as shown in Figure 5.9. Further optimisation could have involved increasing the strength of the nitric acid digestion, through the addition of a complexing acid *e.g.* HCl, or another oxidiser e.g. hydrogen peroxide (Gleyzes *et al.*, 2002, Silva *et al.*, 2006). Reaction kinetics can also be increased through the use of a closed system, which permits the digestion to occur safely at higher temperatures and pressures than the atmospheric pressure and room temperature conditions used here (Araújo *et al.*, 2002, Bettinelli *et al.*, 2000). These modifications in methodology may ensure a more comprehensive digestion of solid material, combating concerns of potential particulate spiking (through nanoparticle ambient suspension during vaporisation, prior to detection following ionisation). However, no evidence was observed in the data suggesting unreliability in the results presented, related to sample preparation. The similarity in zinc ion concentrations detected for nanomaterials actually consolidated the method, for successfully reporting maximal available ion concentration for each material, regardless of digestion.

The different concentrations of zinc ions detected for each sample, were more likely influenced by particle size characteristics than properties related to the media they were dispersed/analysed in. Increased reaction kinetics have been reported for nanoparticle surfaces, corresponding to studies linking smaller particle sizes with increased ion release rates and concentrations (Sotiriou & Pratsinis, 2010, Zhang *et al.*, 2011b). From size characterisation of the materials investigated previously, the smallest average particle size was confirmed for ZnO-45408, followed by ZnO-45009 nanomaterial and then bulk material and is linked the role of increased nano-reactivity, related to greater zinc ion concentrations detected. Alternatively, the smaller size of particles may also relate to increased ion concentrations in the samples, simply through the greater number of particles and larger surface areas involved, when different samples were at

comparable w/v concentrations In addition to zinc ion detection disparity, this may have a major consequence associated with cytotoxicity and dose relationships.

5.2.4 Inflammatory response

LDH results from the RHO models exposed to cytotoxic ZnO nanomaterials, corresponded to significant decreases in cell viability. Evaluation of these results implied ZnO nanomaterial effect on RHO tissue health may bypass the IL-1α cytokine controlled inflammatory pathway. Instead, perhaps a more severe or rapid cytotoxic response by the non-keratinised cells was initiated in the presence of ZnO material. Similar results have been observed with the RHO model, supplemented by the addition of polymorphonuclear leukocytes, to investigate the immune response to *Candida albicans* infection (Schaller *et al.*, 2004). Schaller *et al.*, observed a stronger expression of interleukin-8 (IL-8) and the cytokine granulocyte-macrophages colony-stimulating factor (GM-CSF), over a mild IL-1α response. In addition, the modification of the 3-D model accurately mimicked the *in vivo* reaction through the up-regulated Th-1 immune response. The Th-1type cytokines interferon *γ* (IFN-*γ*) and tumour necrosis factor alpha (TNF-*α*), are pro-inflammatory and are up-regulated as part of an autoimmune response to kill intracellular parasites (Berger, 2000). The inflammatory response is controlled by the expression of Th-2 neutralising cytokines, and where the imbalances in equilibrium exist, this has been implicated with contact allergies to metals (Minang *et al.*, 2006).

Inflammation remains an intricate process, delicately controlled by a number of complex pathways. Keratinocytes produce and are able to release a number of different inflammatory cytokines that rapidly generate cutaneous inflammation in response to a number of different materials. These can be grouped as irritants and/or sensitizers, but no specific marker has clearly been identified able to distinguish one effect from another (Coquette *et al.*, 2003).

Interleukin-1 alpha (IL-1α) is an important signalling protein amongst the 11 cytokines that constitute the interleukin-1 family. It is one of the most widely studied members of the IL-1 family alongside interleukin-1 beta (IL-1β), due to their critical role in immune and inflammatory responses. Both are structurally related polypeptides that share 25% homology at the amino acid level. Synthesised in cells as 31kDa precursors, they are subsequently cleaved into proteins with molecular weights of approximately 17.5kDa (Dinarello, 1998). The precursor and mature form, are both biologically active. More importantly, both exert their effects through recognition and binding to the same cell

surface receptors, identified as IL-1 receptor type 1 and 2 (RI and RII) (O'Neill & Greene, 1998). IL-1 RI has been isolated from T-cells, fibroblasts, keratinocytes, endothelial cells, synovial lining cells, chondrocytes and hepatocytes, with IL-1 RII found on B cells, neutrophils and bone marrow cells. Furthermore, IL-1 possesses a wide variety of biological activities, from specific cell type responses to targeting entire systems. This has led to it being described as 'prototypic "multifunctional" cytokine' affecting nearly every cell type in the human body (Dinarello, 1998, O'Neill & Greene, 1998).

Normal production of IL-1 is critical to the mediation of normal host responses to injury and infection, and as such, IL-1 is expressed constitutively in keratinocytes, some epithelial cells and specific cells of the central nervous system. These experience a dramatic increase in levels in response to stimulation by inflammatory agents, infections or toxins (Dinarello, 1998). In keratinocytes, the majority of IL-1α stays in its precursor form, accumulating in the cytoplasm when there are no inflammatory stimuli. A smaller portion interacts with the cell membrane where it has been linked to acting in a paracrine fashion on neighbouring cells that contain IL-1 receptors (Sims *et al.*, 1993). Under normal conditions, IL-1α has no hydrophobic leader in its polypeptide sequence, and so is not a candidate for transmembrane secretion (Welss *et al.*, 2004). IL-1α can only be released from lysed cells that have experienced injury or membrane perturbation. Upon release, it is believed to be the main 'switch' in the initiation of inflammation identified for it its principal role as an important controller of inflammatory mediation in keratinocytes (Coquette *et al.*, 2003). In this capacity, IL-1α acts as the primary response towards inflammation in keratinocytes (Williams & Kupper, 1996), and is the stimulant responsible for inducing the release of other markers of inflammation, including TNF-α, IL-6 and IL-8 (Coquette *et al.*, 2003, Welss *et al.*, 2004).

Commercially available non-keratinised 3-D models, similar to the models used here, have been reported to have elevated IL-1α release in response to SDS exposure, indicating its use as a toxicity biomarker (Klausner *et al.*, 2007, Ponec & Kempenaar, 1995). Therefore, analysis using a human IL-1α ELISA was carried out to constitute an initial assessment towards the mechanism of nanotoxicity responsible for any cytotoxic manifestation in the RHO 3-D model, in an effort to correlate results from the other assays used. Hydroxyapatite, SiO_2 and TiO_2 materials (both bulk and nano) were noted

as having very mild inflammatory responses, correlating with low levels of IL-1α and cell viability reductions with non-significant detection of LDH release. IL-1α inflammatory response correlated well with the non-cytotoxic outcomes observed through exposure to monolayers. Explanation towards the lack of IL-1α release in response to ZnO material exposure would require future study into a more comprehensive cytokine analysis.

The RHO model only recreates the structural and functional features of the epidermis in non-keratinised oral mucosa epithelium, and suffers from the absence of blood-derived and resident leukocytes, along with Langerhans cells, this may reduce the complexity of the cytokine network *ex vivo* (Vande Vannet *et al.*, 2007). Commercially available 3-D models are a relatively new development, and are associated with high cost. Hence, full exploration into the inflammatory response expressed through cytokine release, remains in the infancy with regard to only a limited number of studies and materials tested. To determine how far down the inflammatory cascade (Figure 1.4) RHO models are able to replicate *in vivo* responses, future work could involve 'chasing' the cascade of cytokine release that initiates inflammation following exposure to the nanomaterials while tested using this model. The central role IL-1α plays in initiating inflammatory response (Williams & Kupper, 1996), means that it is considered a potent inducer of IL-8 and important for controlling the recruitment of leukocytes in inflammatory skin disorders (Schroder, 1995). This may be the next cytokine to investigate, consistent with elevated release of IL-8 in the SkinEthic RHO model, in response to common dental materials: nickel chloride and cobalt chloride (Schmalz *et al.*, 2000).

TNFα also governs IL-8 release, and an ELISA analysis for TNFα was attempted during preliminary experiments with the GIN-100 model, but none was detected (results not shown). It was carried out due to reports of its release in the tissue models utilised during this study (Moharamzadeh *et al.*, 2012), corresponding to release following stimulation in other keratinocyte cell models (Köck *et al.*, 1990), independent to the release of IL-1α (Corsini *et al.*, 1996). However, similar to the use of other skin equivalent models, other studies have concluded that not all chemicals, which have the potential to cause skin irritation and cutaneous inflammation, will elicit detectable TNF-alpha responses (Bernhofer *et al.*, 1999, Heylings *et al.*, 2003). These studies serve to demonstrate the limitation in cytokine analysis using ELISA due to either the tissue

model restraints in representing real *in vivo* function, or in a challenge to the sensitivity of ELISA detection. As discussed, the RHO model only partially represents full thickness tissue, with limited immune function (Vande Vannet *et al.*, 2007). Limitations in cytokine analysis have been demonstrated by the feasibility of IL-6 as a marker of skin irritation, but only in co-culture models of fibroblasts and keratinocytes (Ponec & Kempenaar, 1995, Welss *et al.*, 2004). Yet IL-6 induction has been observed in the RHO model, in response to non-toxic dental materials (Schmalz *et al.*, 2000).

The sensitivity of ELISA is dependent upon the fluorescent signal of the conjugate, in turn governed by the amount of cytokine able to bind to the monoclonal capture antibody (Crowther, 2000). In typical kits, the lower limits of sensitivity remain on the pg scale (manufacturer data). Yet on the cellular scale, smaller amounts may be released, especially in cases of subtle or slow release that may be linked to low-grade inflammation, associated with a wide variety of chronic human diseases (Cancello & Clément, 2006, Kolb & Mandrup-Poulsen, 2010, Monteleone *et al.*, 2014, Moutsopoulos & Madianos, 2006). Analysis of IL-1β levels was considered for investigation following exposure to non-cytotoxic nanomaterials (hydroxyapatite, SiO_2 and TiO_2) to determine if more subtle changes were occurring in tissue homeostasis (Dinarello, 1998). This may have implications for studying nanomaterial damage associated with long term or multiple exposures (Gui *et al.*, 2013, Liu *et al.*, 2012, Park *et al.*, 2009, Sang *et al.*, 2012, Yang *et al.*, 2008). However, the role of IL-1β in homeostasis makes it difficult to study, due to the sensitivity in differences thought likely to occur on a cellular level. Human skin keratinocytes produce significant amounts of the IL-1β precursor protein constitutively, but fail to convert it to the bioactive form unless stimulated by a suitable irritant (Zepter *et al.*, 1997). Release into cell supernatant, and subsequent ELISA analysis may prove too insensitive to accurately determine disparity in cytokine signal.

Mechanistic investigation of intracellular changes can be more sensitive indicators of immune response. Various molecular biology techniques, including western blotting, immunostaining and polymerase chain reaction (PCR) have been widely employed to investigate inflammatory pathways initiated in response to nanoparticle exposure, similar to the hydroxyapatite, SiO_2, TiO_2 and ZnO nanomaterials investigated here (Ahmad *et al.*, 2012, Han *et al.*, 2013, Jaeger *et al.*, 2012, Jeong *et al.*, 2010, Márquez-Ramírez *et al.*, 2012, Park *et al.*, 2013, Romoser *et al.*, 2012, Sharma *et al.*, 2012, Yin *et al.*, 2012). Referring back to the hierarchal oxidative stress model (Figure 1.4) thought to

contribute nanoparticle cytotoxic actions, NF-$\varkappa$B and activating protein (AP-1) were considered likely transcription factors that could have been investigated as early indicators of IL-1α directed inflammatory response (Welss *et al.*, 2004). Molecular expression of these would have served to consolidate results from IL-1α release detected in cell supernatant (O'Neill & Greene, 1998, Stylianou & Saklatvala, 1998).

5.2.5 Risk implications of nanomaterial exposure on the oral mucosa

The correlation between greater zinc ion concentration and increased cytotoxicity in cell models does enhance the link between free ion induced oxidative stress as the cytotoxic mechanism of ZnO nanomaterials. However, the exact mechanism of action cannot be conclusively deduced from the data reported here. Caution would have to be exercised when considering these nanomaterials for use in future oral healthcare formulations. This is despite the significantly greater effect observed in the 3-D models following exposure to the cytotoxic SDS, which was similar to results observed in other studies using models of the oral mucosa (Healy *et al.*, 2000), and the more robust skin epidermis (Coquette *et al.*, 2003). Based on the cytotoxicity results, the nanomaterials, hydroxyapatite, SiO_2 and TiO_2 would be considered to constitute less risk. The only adverse effects they exhibited were in the RHO model, with LDH release related to a mild inflammatory response. It is important to consider the physiological relevance of these concentrations (Hiroshima *et al.*, 2011), with persistent mild inflammation constituting gingivitis that can develop into the more serious periodontal disease (Pihlstrom *et al.*, 2005). However, IL-1α ELISA has also been demonstrated to lack the same sensitivity as MTT results in the RHO model (Kazmi *et al.*, 2011). The low inflammatory response coupled with no significant losses in cell viability in either 3-D cell model, and during monolayer screening, would support the safe application of all nanomaterials bar ZnO in future oral healthcare formulations at this stage of the investigation. Furthermore, the data reported has been carried out through investigations negating the stabilising effects of other formulation constituents that may offer surface coating on nanoparticles to reduce their reactivity (Ryman-Rasmussen *et al.*, 2007, Tsuji *et al.*, 2006, Yin Win & Feng, 2005) and also without representation of the physiological barriers of saliva and mucus (Lendenmann *et al.*, 2000).

For ZnO nanomaterials, further risk analysis could include an extension of the battery test approach, to encompass assays specifically assessing oxidative stress. This could be carried out either through depletion of a cellular antioxidant known as glutathione

(GSH) (Berg *et al.*, 2012, Prasad *et al.*, 2013a, Zhang *et al.*, 2011a), quantified in ratio to its oxidised state (GSSG) (Betha *et al.*, 2012, Brown *et al.*, 2013), or conversely, the increase in hydrogen peroxide detection (AshaRani *et al.*, 2008, Limbach *et al.*, 2007, Musa *et al.*, 2012). Each of the approaches to quantify levels of oxidative stress can easily be performed thanks to commercially available assay technology. Similarly, genotoxicity may also easily be performed *in vitro* using commercial assay technology (Barillet *et al.*, 2010, Hackenberg *et al.*, 2011a, Hackenberg *et al.*, 2011b, Sharma *et al.*, 2009b, Shukla *et al.*, 2011, Yang *et al.*, 2009). The comet assay has already been widely employed in studies demonstrating the potential for nanoparticles to cause harmful DNA damage on a cellular level. Long term exposure studies, likely involving animal models, would therefore be necessary to elucidate the full extent and severity. However, this remains beyond the remit of this work, and would not prove compatible with research contributing new cosmetic ingredient testing ((EU), 2013). Continuing investigation into the cytotoxic mechanism would instead follow existing reports of ZnO nanomaterial toxicity in other studies using similar assays for *in vitro* toxicity testing (Ho & Ames, 2002, Huang *et al.*, 2010a, Lin *et al.*, 2009, Sharma *et al.*, 2012, Xia *et al.*, 2008, Yang *et al.*, 2009).

For 3-D tissue models, the MTT assay can be used as an indirect measurement of the barrier function afforded to tissue structure (Klausner *et al.*, 2007). The MTT assay depends on the reduction of MTT by mitochondrial dehydrogenases (Mosmann, 1983), with activity predominantly occurring deeper in the tissue cell layers (Ayehunie *et al.*, 2006). For a test material to affect the MTT response, as seen for ZnO nanomaterial exposure in RHO models of the non-keratinised tissue, the material must permeate into the tissue and interact with, or damage the basal cell layers. Therefore it is important to understand whether and how nanoparticles were taken up into the cells used in this investigation. This will be explored in the proceeding chapter.

6 UPTAKE POTENTIAL OF NANOMATERIALS IN VITRO

This chapter investigates the uptake of the materials using cell-based *in vitro* models due to the small particle size affords nanomaterials the capacity for uncontrolled uptake, and possible translocation to more sensitive areas ((SCCP), 2007, Borm *et al.*, 2006, Florence *et al.*, 1995, Kreyling *et al.*, 2002, Oberdorster *et al.*, 2000, Oberdorster *et al.*, 2005a, Tay *et al.*, 2013). Subsequent bioaccumulation is thought to contribute the greatest safety concern following metal oxide nanomaterial exposure, likely to induce severe toxicity and considerable threat to the health of an organism ((SCENIHR), 2009). However, nanoparticle internalisation into cells has been linked to increased cytotoxic action (introduction section 1.2.6). Out of the nanomaterials investigated here, it is speculated that ZnO nanomaterials may pose the greatest risk of nanoparticle internalisation. This hypothesis is consistent with reports in the literature demonstrating ZnO nanoparticle uptake into cells (Sharma *et al.*, 2011, Xia *et al.*, 2008, Yu & et al., 2011), passage through tissues relating to the use of ZnO and TiO_2 nanomaterials formulated in sunscreen products (Gulson *et al.*, 2012, Lewicka *et al.*, 2013, Monteiro-Riviere *et al.*, 2011, Schulz *et al.*, 2002) and importantly within the context of this study, that results from previous chapters that have shown ZnO nanomaterial exposure resulting in greater cytotoxicity and losses in cell viability. It is therefore important to evaluate, as part of a risk assessment towards safe levels of exposure in the oral mucosa, whether this is a consequence of either nanoparticle internalisation into the cell or uptake through the tissue.

To determine ZnO nanomaterial uptake potential for inducing increased cytotoxicity in the 3-D models, TEM was used to search for evidence of nanoparticle internalisation in fixed EpiGingiva™ and RHO model samples. Locations of nanomaterial within the tissue were speculated to contribute to assessment towards which transport pathway may have been used (para- or transcellular transport). Furthermore, micrographs were expected to reveal morphological indication related to cytotoxicity of ZnO exposure, and any differences between the keratinised and non-keratinised protective mechanisms (*e.g.* cell junctions, stratum corenum structure and desquamation *etc.*) Analysis was only carried out for ZnO materials, due to the limited number of tissue models available.

Using the H376 monolayer cell model, transcellular uptake pathways were investigated for all nanomaterials. Specifically, this related to endocytosis associated nanoparticle

internalisation, as a non-receptor mediated form of endocytosis was considered the most likely mechanism of internalisation for the inorganic nanomaterials used here (Treuel *et al.*, 2013). In this respect, it was considered important to maintain *in vitro* conditions relating to those previously characterised for the nanomaterials, as evidence has linked changes (*i.e.* through changing environment *etc.*) to altered nanomaterial behaviour in solutions and cytotoxicity properties (Meißner *et al.*, 2009, Montes-Burgos *et al.*, 2010, Nel *et al.*, 2009). The commercially sourced nanomaterials possessed no optical properties that could naturally be exploited to enable cellular localisation mapping, resulting from potential uptake. Therefore, a non-toxic, water soluble fluorescent membrane probe, more usually associated with studying synaptic vesicle cycling (Amaral *et al.*, 2011, Betz & Bewick, 1992, Rea *et al.*, 2004, Richards *et al.*, 2005), was applied to correlate internalised membrane invaginations with speculated nanoparticle intercellular locations. This was achieved through the development of an assay and consolidated using confocal microscopy study.

As the mechanisms of uptake are currently unestablished for the H376 cell line, Caco-2 cells were utilised as a positive control for uptake capacity of the nanomaterials. The Caco-2 monolayer model is well-established within pharmacokinetic studies, and has proven uptake capacity in facilitating the transport of many different molecules across its membrane (Grès *et al.*, 1998, Hubatsch *et al.*, 2007, Sambuy *et al.*, 2005, Sun *et al.*, 2008b), including nanoparticles (Fröhlich & Roblegg, 2012, Gaiser *et al.*, 2012, Jahn *et al.*, 2012, Kenzaoui *et al.*, 2012).

6.1 Results

6.1.1 SynaptoGreen™ uptake assay results

Figure 6.1 to Figure 6.4 show results from the fluorescent emissions of 50µM SynaptoGreen™ FM1-43 dye that was internalised in each of the epithelial cell monolayer models. Fluorescence was compared against background levels from the negative control cell population undergoing natural vesicle recycling. Increased fluorescence in the presence of nanomaterial exposure was taken to indicate uptake into the cell. ATP was used as a positive control to validate the capacity of the cell lines to increase uptake above background vesicle recycling rates.

6.1.1.1 H376 cellular uptake of nanomaterials

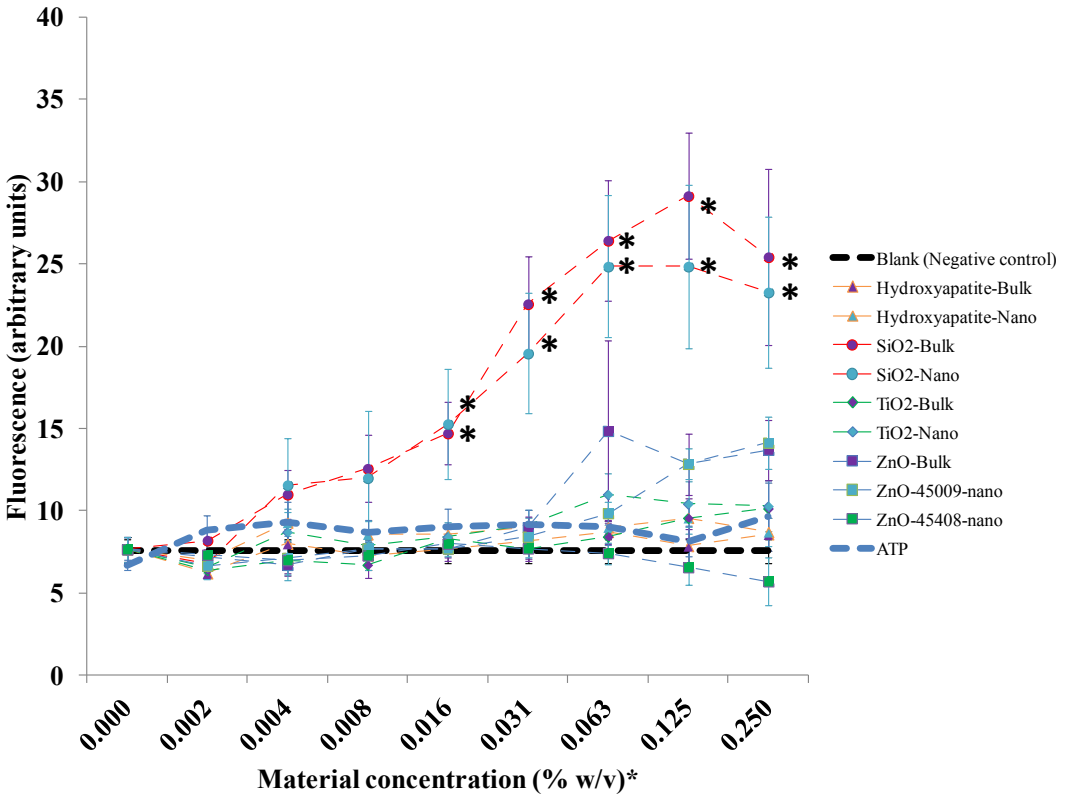

Figure 6.1. SynaptoGreen™ fluorescence measured following uptake into H376 cells during 5 minute exposure to test materials. *Results are the average of n = 8 with standard deviation bars reported.* Statistical significance was calculated using one-way ANOVA with Tukey's post-hoc test ($P<0.050$) comparing results with negative control (*****) and nanomaterial difference to respective bulk (**+**).

*** ATP concentration relates to mM at the same values as other materials diluted from a % w/v unit of measurement.**

Figure 6.1 shows the results of SynaptoGreen™ fluorescence detected in response to the test materials exposed to H376 cells for 5 minutes. SiO_2 materials (bulk and nano) were the only treatments to result in increased measurement, which followed a dose dependent response of increasing fluorescence, up to 0.125% w/v concentration. Both bulk and nanomaterial SiO_2 caused similar readings that were significantly different (P<0.020) above 0.008% doses, in comparison to the background vesicle cycling of H376 cells (negative control) and the negligible increased in fluorescence observed following exposure to all other materials. This also included ATP 'positive control' treatment, which did not exhibit an increase in fluorescence in the H376 cell model.

SiO_2 nanomaterials had previously been characterised as measuring the smallest starting particle sizes (Table 3.5). To determine if SiO_2 associated uptake was due to the nano-size of particles, this assay was repeated with an alternative bulk control. The results of this experiment are shown in Figure 6.2 below, comparing the SigmaAldrich sourced SiO_2 nanomaterial, to a newly sourced SiO_2-bulk material (ACROS), verified as a true 'bulk' control (Figure 9.2).

The repeated assay showed only SiO_2 nanomaterial, sourced from SigmaAldrich, to elicit an increase in SynaptoGreen™ fluorescent in the H376 cells, similarl to the results determined previously. This was statistically significant at concentrations delivered at 0.016% w/v or above (P <0.001), when compared against the ACROS-bulk and the negative control. Like the ACROS-bulk, ATP again displayed no propensity to increase fluorescence in the cell model, following 5 minute of exposure.

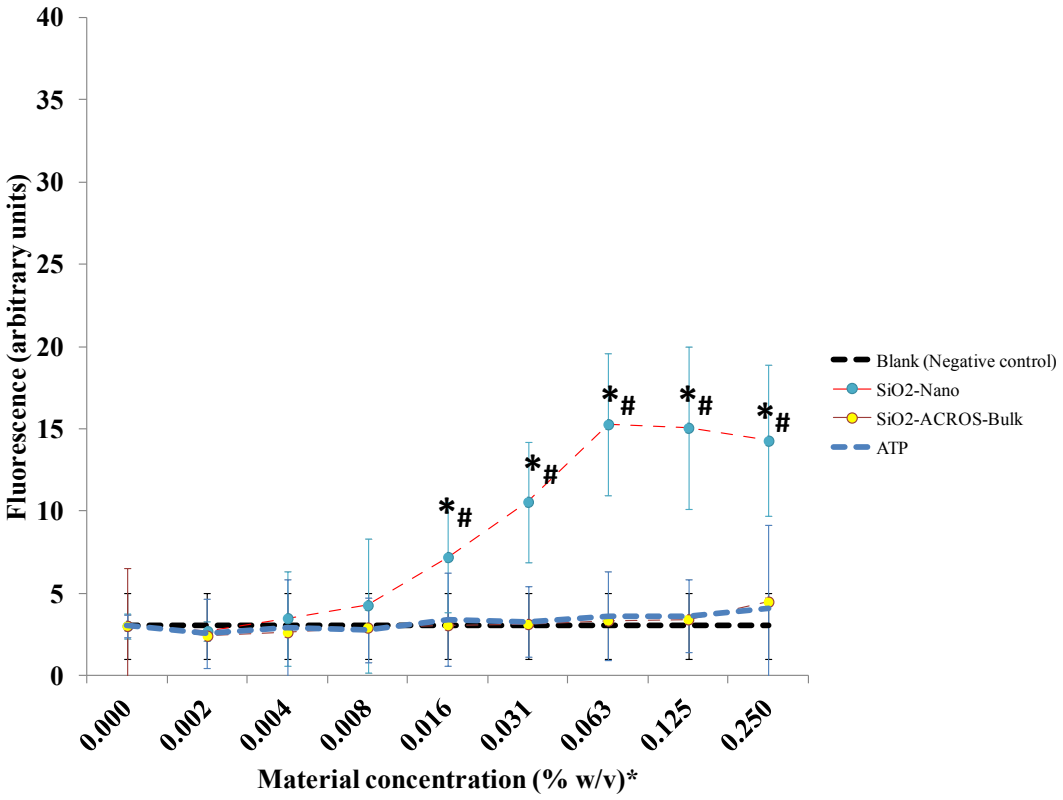

Figure 6.2. SynaptoGreen™ fluorescence comparing ACROS SiO_2 bulk particle uptake into H376 cells to 5 minute exposure of SiO_2 nanomaterial. *Results are the average of n = 7 with standard deviation bars reported.* Statistical significance was calculated using one-way ANOVA with Tukey's post-hoc test ($P<0.050$) comparing results with negative control (*****) and comparison to SiO_2-ACROS-Bulk (**#**).

*** ATP concentration relates to mM at the same values as other materials diluted from a % w/v unit of measurement.**

6.1.1.2 Caco-2 cellular uptake of nanomaterials

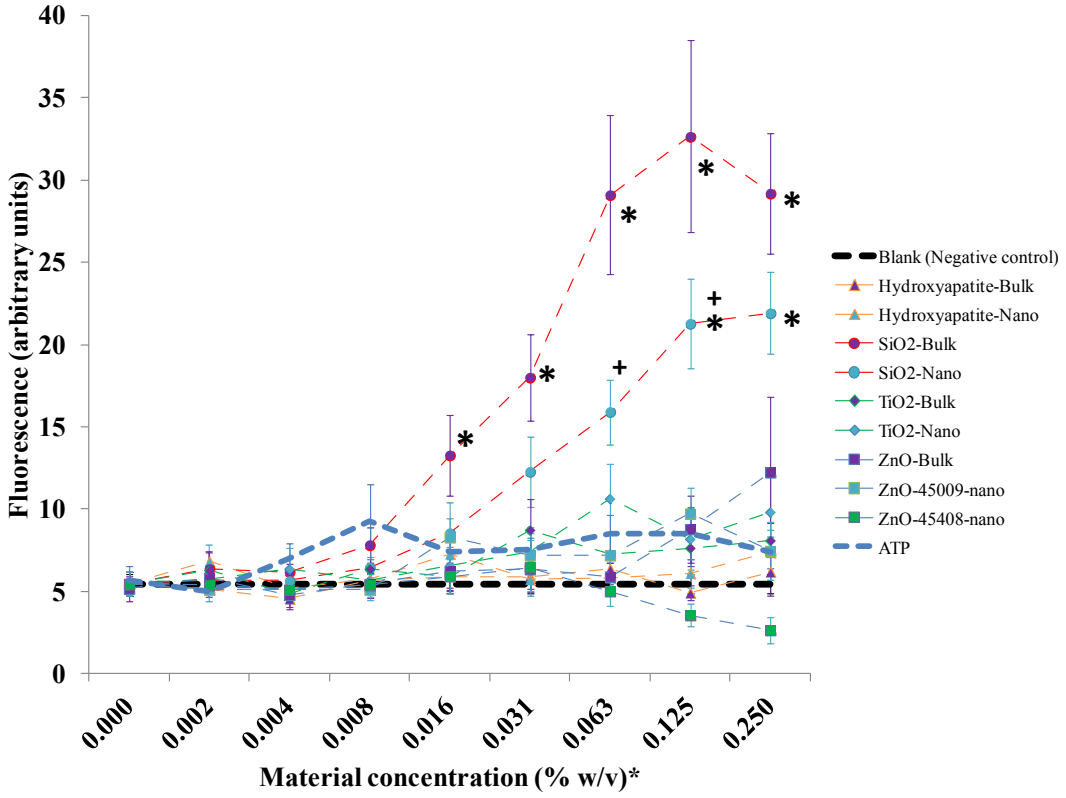

Figure 6.3. SynaptoGreen™ fluorescence measured following uptake into Caco-2 cells during 5 minute exposure to test materials. *Results are the average of n = 11with standard deviation bars reported.* Statistical significance was calculated using one-way ANOVA with Tukey's post-hoc test (P<0.050) comparing results with negative control (*****) and nanomaterial difference to respective Bulk (**+**).

*** ATP concentration relates to mM at the same values as other materials diluted from a % w/v unit of measurement.**

Figure 6.3 shows the results obtained using Caco-2 cell uptake in response to the materials tested. The results showed similar trends to those observed in the H376 model. This confirms that the H376 cell assay works, in respect to uptake potential for SynaptoGreen™ associated internalisation alongside nanoparticles with characteristics affording them entry into cells. Caco-2 uptake of SigmaAldrich sourced SiO_2 materials, bulk and nano, confirmed the heightened ability of these particles to become internalised into cells. Similarly with H376 cell assays, a dose dependent relationship was observed for SiO_2 materials, but was only significant at concentrations exceeding 0.016% w/v for bulk (P <0.001), and in the top two concentrations of nanomaterial exposure (P <0.001). The disparity noted between the two forms of SiO_2 material

related to fluorescent signal of internalised SynaptoGreen™ produced a statistically significant difference at 0.063% and 0.031% w/v respectively (P <0.001 and P = 0.007 respectively).

The Caco-2 baseline SynaptoGreen™ fluorescence was marginally lower than that observed in the H376 cells, and this meant ATP stimulated uptake was statistically greater than negative control treated Caco-2 cells, and so was considered a more effective control, in this model, increasing uptake.

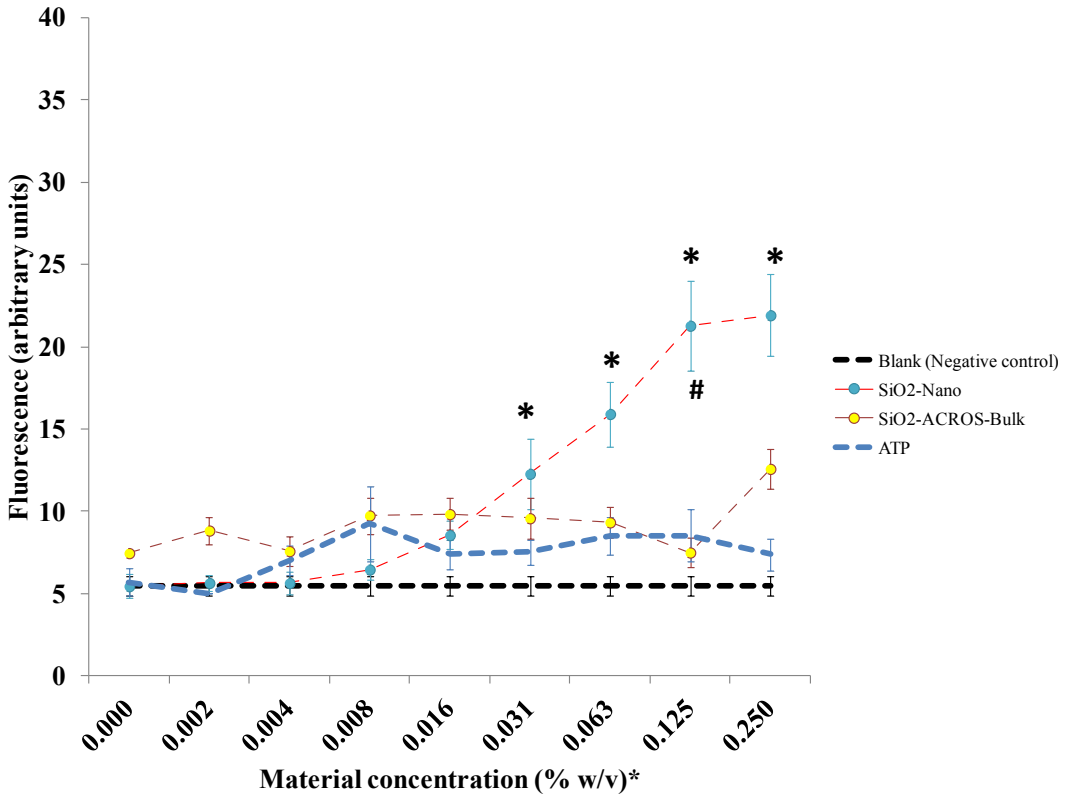

Figure 6.4. SynaptoGreen™ fluorescence comparing ACROS SiO_2 bulk particle uptake into Caco-2 cells to 5 minute exposure of SiO_2 nanomaterial. *Results are the average of n = 6 with standard deviation bars reported.* Statistical significance was calculated using one-way ANOVA with Tukey's post-hoc test (P<0.050) comparing results with negative control (*****) and comparison to SiO_2-ACROS-Bulk (**#**).

*** ATP concentration relates to mM at the same values as other materials diluted from a % w/v unit of measurement.**

The experiment with SiO_2-ACROS bulk material was repeated in the Caco-2 cell models, to compare against the suspected nano-specific effect of SiO_2 uptake. Results shown in Figure 6.4 supported those obtained using the H376 model. This noted the lack of SynaptoGreen™ fluorescence associated with SiO_2-ACROS bulk exposure, which resulted in a statistical difference between SiO_2 nanomaterial dosed at 0.125% w/v concentration (P <0.001).

6.1.2 Confocal laser scanning microscopy imaging of particle uptake

Confocal microscopy was used to validate the findings from the previous studies with images displaying increased fluorescence, for both cell lines, exposed to the two SiO_2 materials sourced from SigmaAldrich (Figure 6.1 to Figure 6.4). The use of cytoskeletal and nuclear labelling allows co-localisation of the internal cellular structures in conjunction with the fluorescing vesicles, associated with nanoparticle uptake. Furthermore, cell cytoskeleton and nuclear morphology would contribute visual information that could be used to interpret the health of each cell imaged *i.e.* determining if high vesicle internalisation related to apoptotic nuclear distortion or loss of regular cell structure.

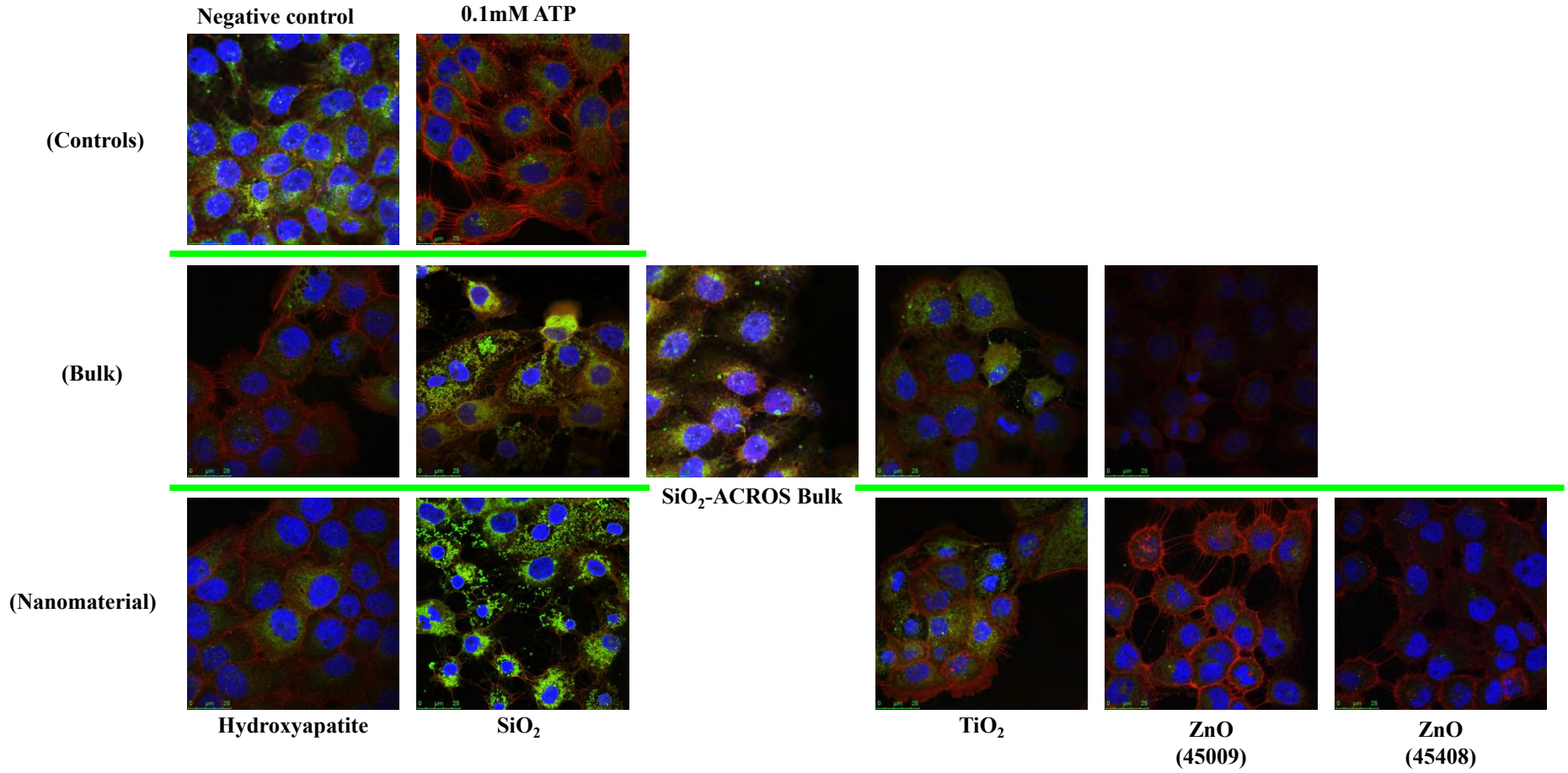

Figure 6.5. Confocal laser scanning microscope images taken at 126X magnification of H376 cells treated for 5 minutes with 0.125% w/v of materials diluted in 50µM FM®1-43FX. Using sequential scans internalised FM®1-43FX dye can be observed fluorescing (**green**) alongside DAPI stained cell nuclei (**blue**) and TRITC-phalloidin fixed actin cytoskeleton (**red**). *Scale bar = 25µm.*

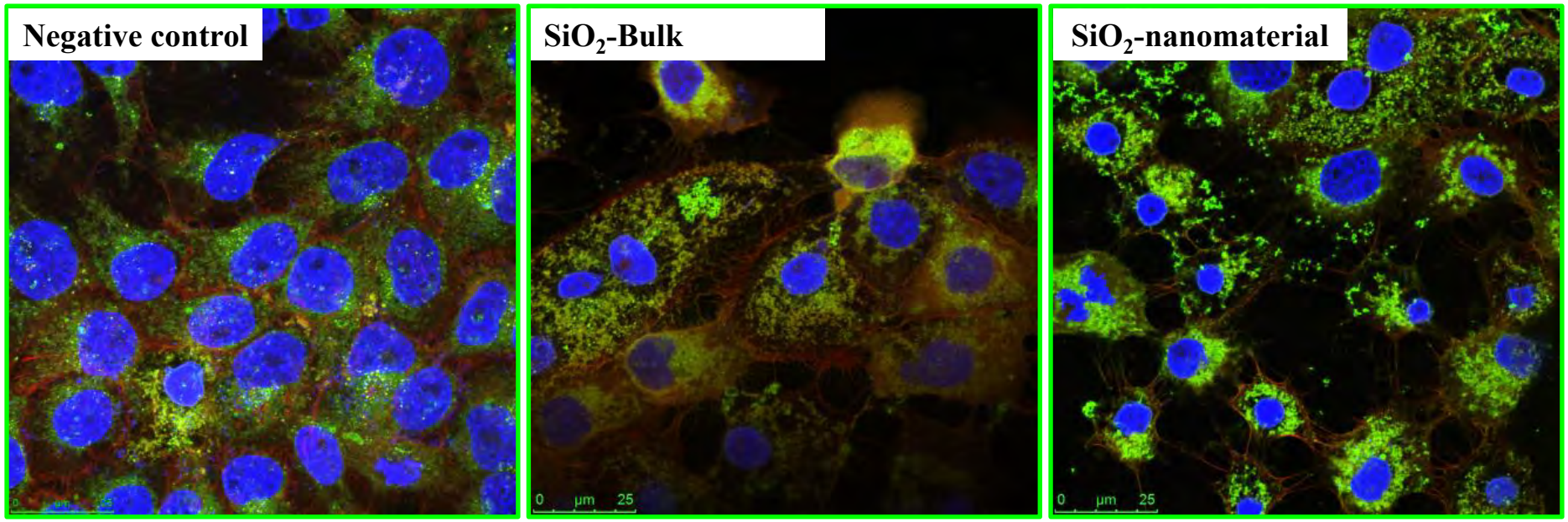

Figure 6.6. Enlarged Confocal laser scanning microscope images to highlight increased uptake of nanoparticle containing SiO2 material, into 50µM FM®1-43FX fluorescent vesicles (green) within the cytoplasm of H376 cells. DAPI stained cell nuclei (blue) and TRITC-phalloidin fixed actin cytoskeleton (red). *Scale bar = 25µm.*

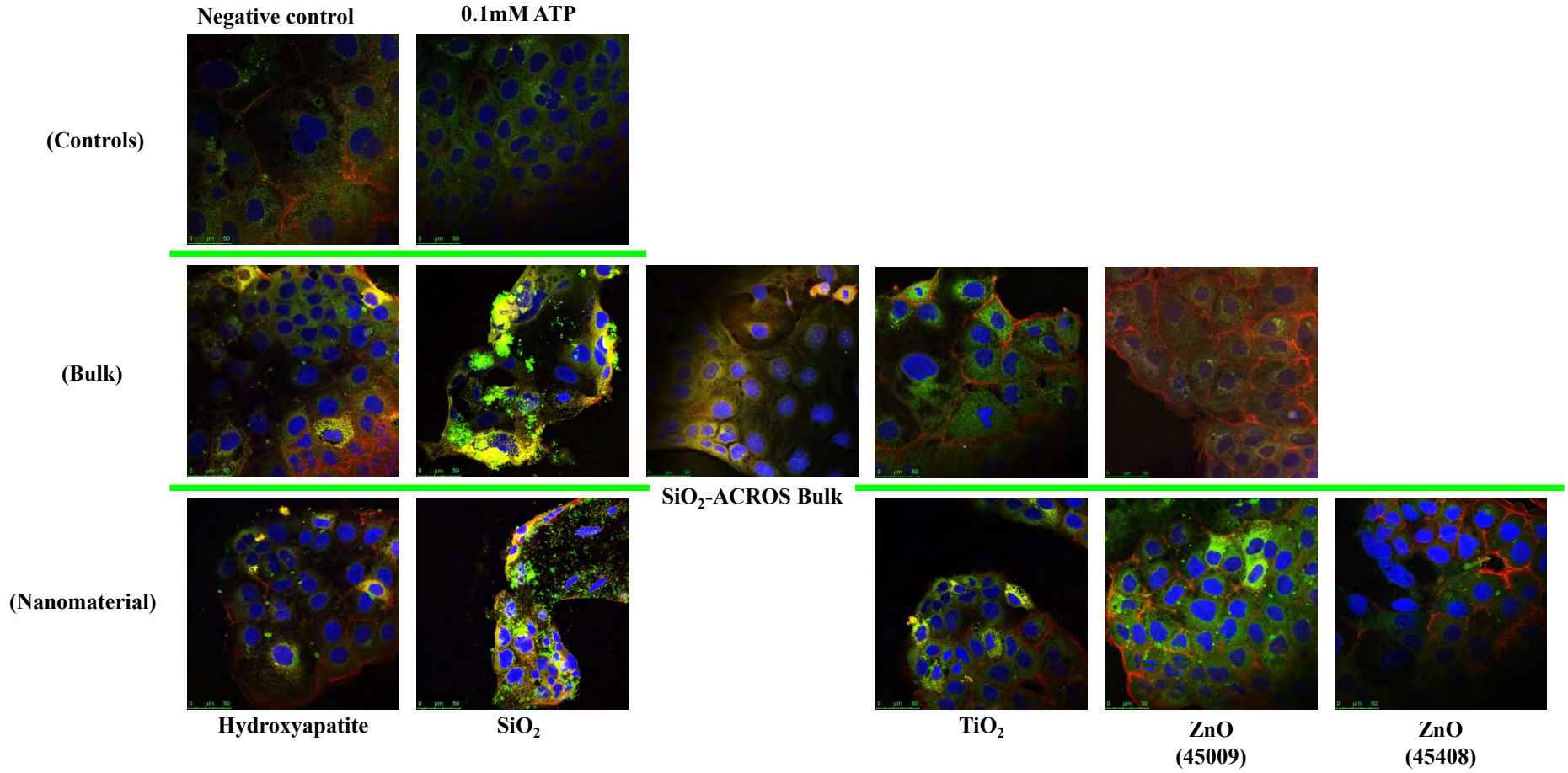

Figure 6.7. Confocal laser scanning microscope images taken at 64 X magnification of Caco-2 cells treated for 5 minutes with 0.125% w/v of materials diluted in 50µM FM®1-43FX. Using sequential scans internalised FM®1-43FX dye can be observed fluorescing (**green**) alongside DAPI stained cell nuclei (**blue**) and TRITC-phalloidin fixed actin cytoskeleton (**red**). *Scale bar = 50µm.*

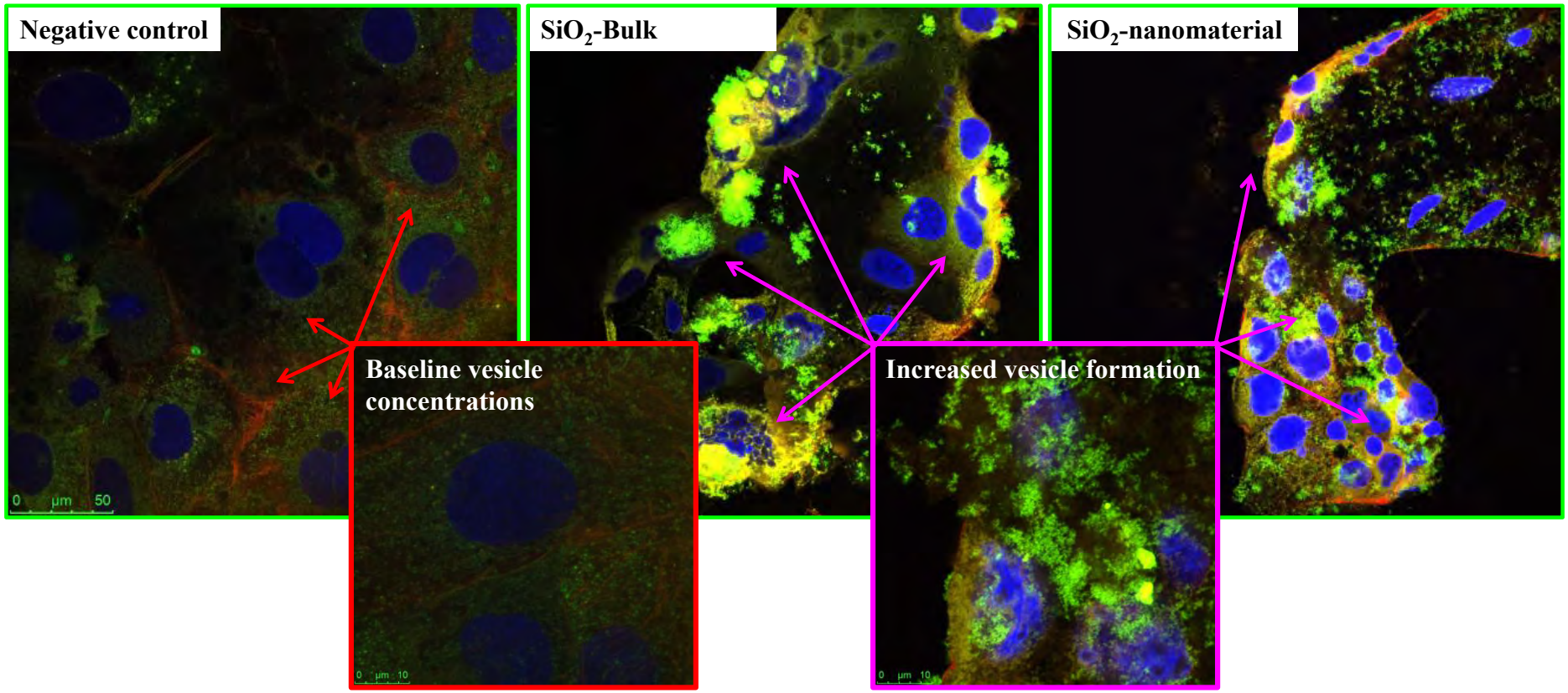

Figure 6.8. Enlarged Confocal laser scanning microscope images (63X magnification) demonstrating increased uptake of nanoparticle containing SiO_2 material, into 50µM FM®1-43FX fluorescent vesicles (green) over the baseline vesicle formation demonstrated in the negative control. DAPI stained cell nuclei (blue) and TRITC-phalloidin fixed actin cytoskeleton (red). *Scale bar = 50µm.* Images taken at 252X magnification have been included to highlight evidence of the increased number of vesicles internalised within the cytoplasm of cells following exposure to the two SiO_2 materials that contain nanoparticles (*scale bar = 10µm).*

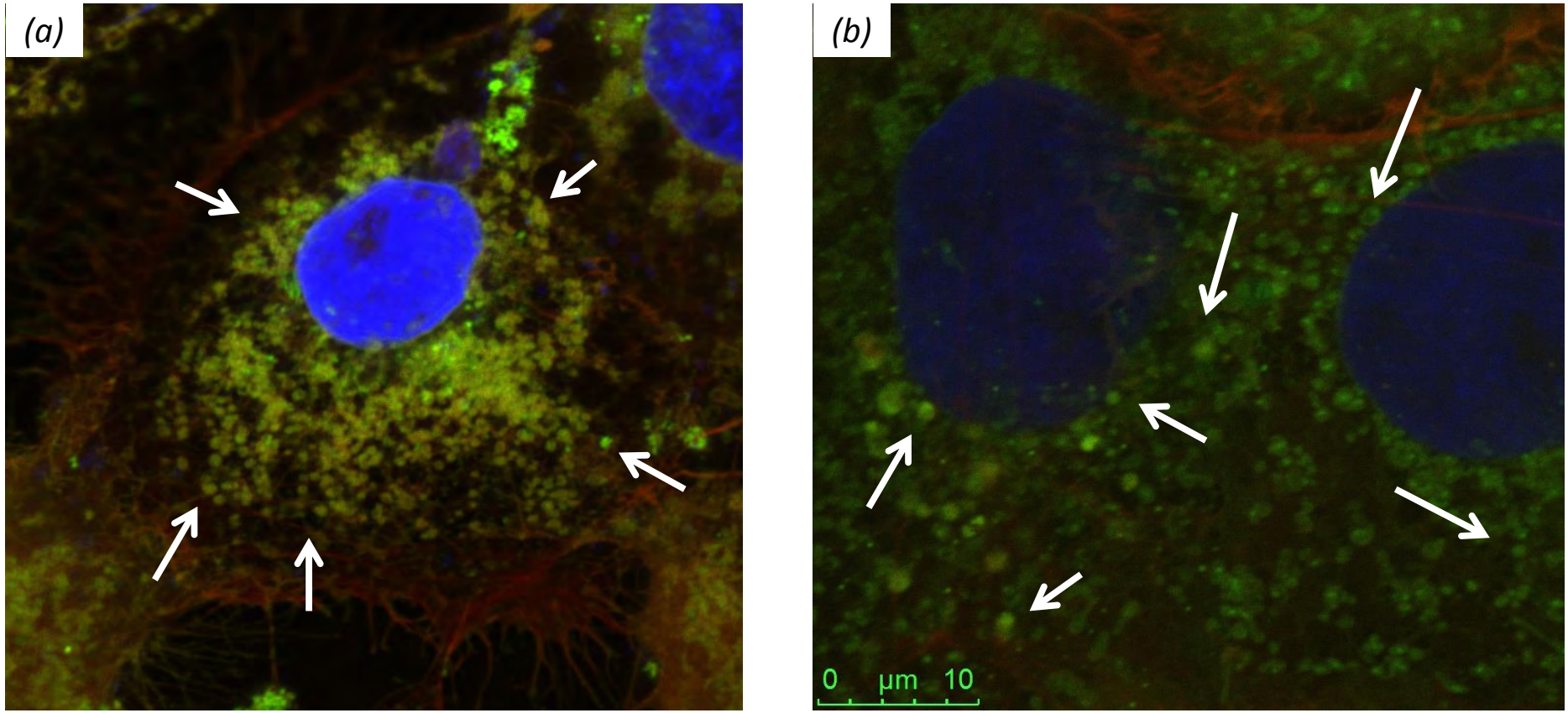

Figure 6.9. Zoomed in 256X magnification images to show the spherical shape of suspected vesicles loaded with FM®1-43FX dye (as indicated by arrows) within (a) H376 cells and (b) Caco-2 cells. These images support the previous set of figures that demonstrate exposure to SiO2 nanoparticles correlated to increased endocytotic uptake into the cytoplasm. *Scale bar = 10µm.*

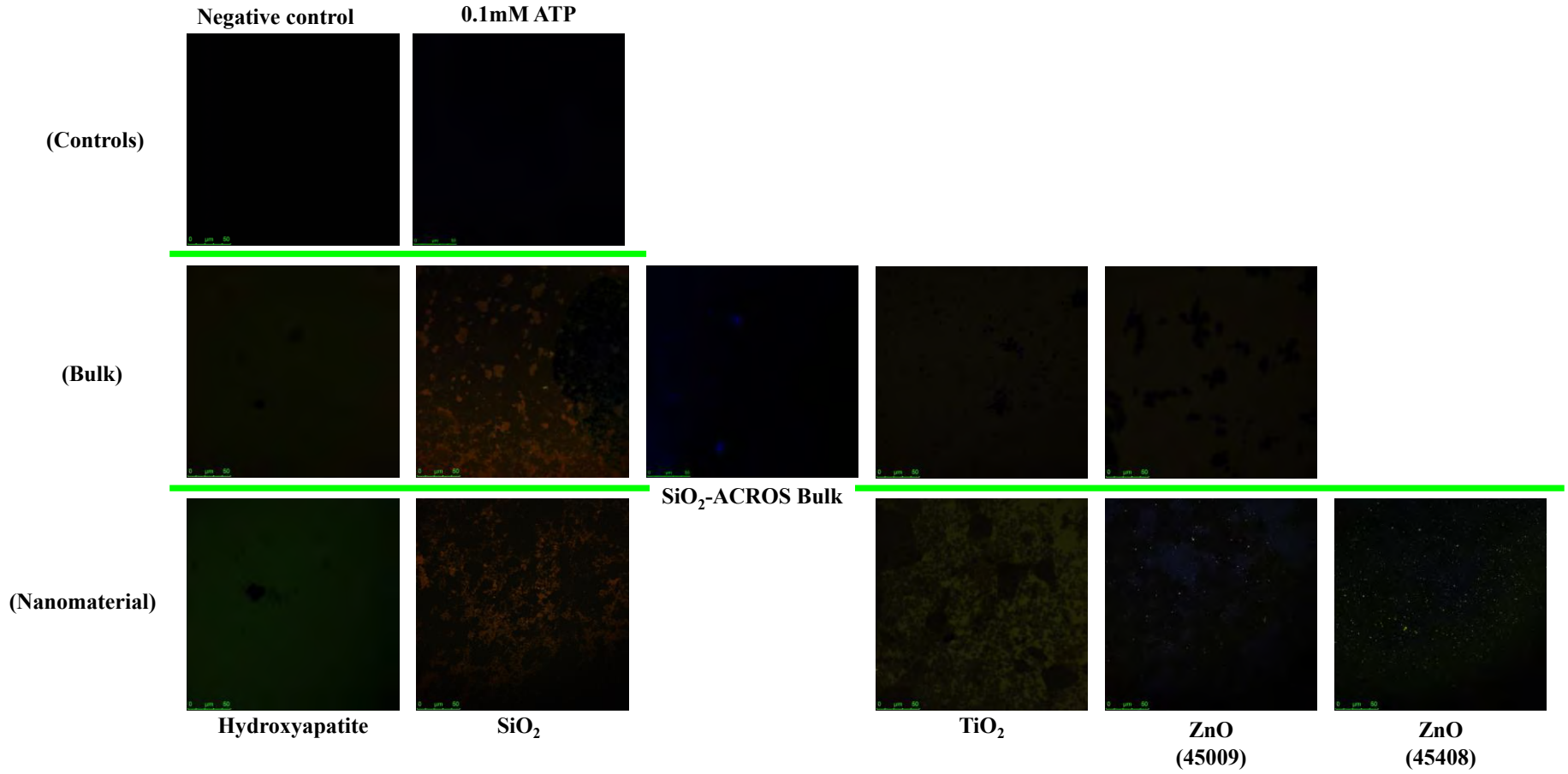

Figure 6.10. Confocal laser scanning microscope images taken at 64 X magnification of test materials without cells. Using sequential scans background fluorescence of materials was checked as a control to guard against cross fluorescence from particulates that may have resulted in false positives incurred as FM®1-43FX dye uptake. The confocal set up remained the same as previous figures for cell work, with FM®1-43FX emissions (**green**) alongside DAPI stain (**blue**) and TRITC-phalloidin emission (**red**). *Scale bar = 50µm.*

Confocal images seen in Figure 6.5 and Figure 6.10 correspond closely with the SynaptoGreen™ assay results (Figure 6.1 to Figure 6.4). The brightest FM®1-43FX fluorescence signal was observed following exposure to nanoparticle containing SiO_2 materials (sourced from SigmaAldrich) and was consistent in both H376 and Caco-2 cell lines, as highlighted in the enlarged images shown in Figure 6.6 and Figure 6.8, respectively. Fluorescence remained localised within the cytoplasm of cells, with no FM®1-43FX signal observed overlapping with that of DAPI stained nuclei.

SiO_2 material with larger, micron sized particles (ACROS-bulk) only caused low intercellular fluorescence, no greater than the negative control (in H376 and Caco-2 cells). All other materials, including 0.1mM ATP positive control, exhibited fluorescence levels similar to that of normal vesicle recycling, demonstrated by the negative control.

ZnO material exposure to H376 cells showed disparity, with a lack of FM®1-43FX corresponding to indications of cell stress extrapolated from observations of cell morphology (Figure 6.5). These include cell shrinking, observed by the TRITC-phalloidin stained actin filaments outlining the cytoskeleton; and nuclear fragmentation and chromatin condensation, indicated by the shape and brightness of DAPI interactions with adenine and thiamine present in the nuclei. To some extent, high incidents of internalised vesicle fluorescence following SiO_2 nanoparticle exposure which also displayed some similar examples of cell stress, especially following SiO_2 nanomaterial to H376 cells (Figure 6.5).

In all samples, FM®1-43FX fluorescence was linked to fluorescing dye internalised in vesicles (as demonstrated in Figure 6.9) and not particle auto-fluorescence, as demonstrated by the lack of 'green' signal in Figure 6.10. ZnO nanomaterials (45009 and 45408) registered some background fluorescence of particles (under the wavelengths used in the sequential scan for DAPI and FM®1-43FX settings), but this did not correspond to greater FM1-43FX fluorescence in the cell samples.

To determine that FM®1-43FX fluorescence was associated with internalisation of the dye within the membrane forming vesicle that envelopes nanomaterials during transcellular transport mechanisms, Z-stack images were taken for 4.99μm horizontal slices through Caco-2 monolayer.

Figure 6.11 confirmed the increased fluorescence recorded with SiO_2 nanoparticle exposure was associated with uptake of FM®1-43FX dye into the cell, and was not

accumulation of fluorescence at the surface of the cell where exposure occurred. The majority of FM®1-43FX associated fluorescence emanated from within the Caco-2 cells, with the fluorescent intensity peaking within the middle sections of the cell monolayer: Z4 to Z7.

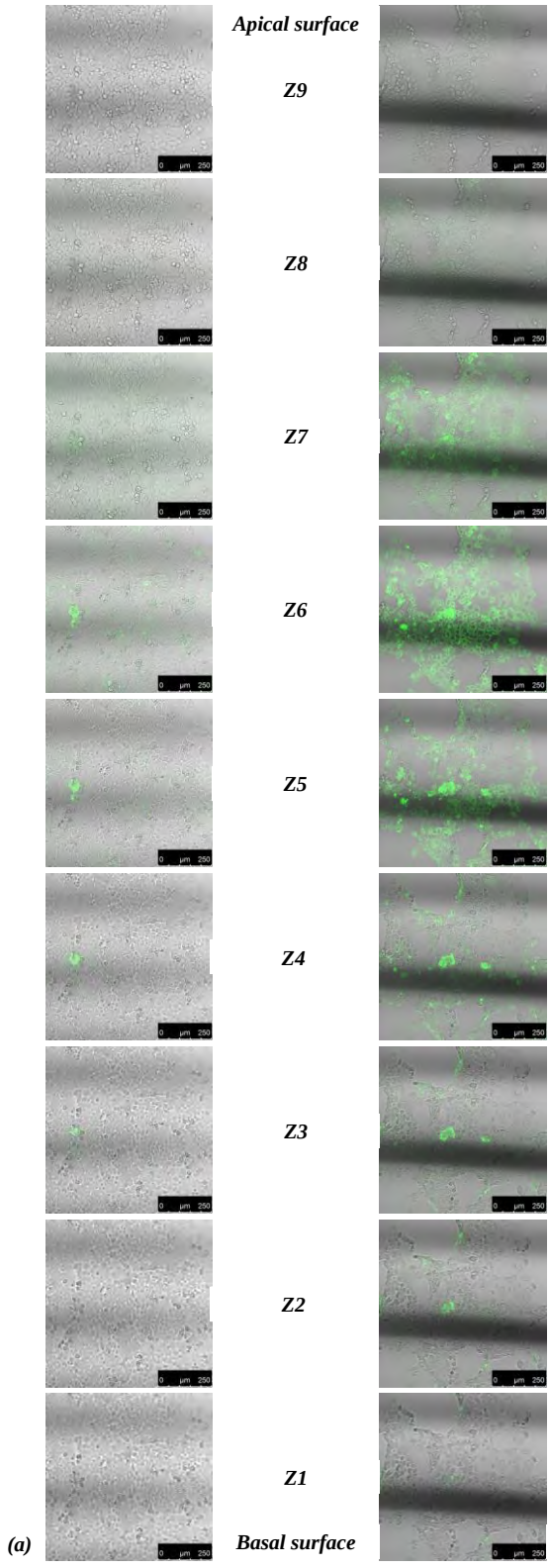

Figure 6.11. Confocal microscope images overlaid on light microscopy images at 20X magnification to depict internalised FM®1-43FX dye in Caco-2 cells. Z-stack images taken at 4.99μm intervals were used to visualise Caco-2 cell sections after 5 minutes exposure to ***(a) 50μM FM®1-43FX/PRF media and (b) 0.125% $^{w}/_{v}$ SiO_2 nanomaterial dispersed 50μM FM®1-43FX/PRF media***. Light microscopy images were overlaid with FM®1-43FX fluorescent signal collected from emissions between 487-540nm after excitation by argon laser at 458nm. *Scale bar =250μm.*

6.1.3 TEM-EDX analysis of nanoparticle uptake in 3-D tissue models

SEM micrographs presented earlier had alluded to ZnO nanomaterials as the prime candidates for internalisation into the cell. Yet this remained unproven as a mechanism of cytotoxicity (as has been demonstrated in the literature) following study using the fluorescent SynaptoGreen™/FM1-43 internalisation method. It was considered that the cytotoxicity of ZnO material may have contributed to the break down in the dye fluorescence, through disruption of the cell membrane. This provided rationale for the preferential study of ZnO materials with the limited number of 3-D tissue constructs (left over from cytotoxicity work (chapter 5)).

Following treatment with ZnO bulk and both nanomaterials (45009 and 45408), tissue models were fixed and stained to identify cellular structures observed using TEM. This approach is a common method that has been used in other studies to locate nanoparticle internalisation within individual cells (Kasper *et al.*, 2013b, Ben-Dov & Korenstein, 2012, Hackenberg *et al.*, 2011b, Simon-Deckers *et al.*, 2008). Using both the keratinised and non-keratinised tissue models, signs of ZnO uptake were investigated either within cell structures, implying transcellular uptake; or alternatively, within the extracellular spaces that would demonstrate their penetration using paracellular transport.

6.1.3.1 RHO non-keratinised tissue model analysis of nanomaterial uptake using TEM imaging

The TEM micrographs in Figure 6.12 show 100nm tissue sections of the SkinEthic RHO tissue models that were treated with 1% w/v of each ZnO material (for 1 hour of exposure). Particle penetration was assessed through comparison to a negative control (serum free culture media), and in comparison to the bulk ZnO material.

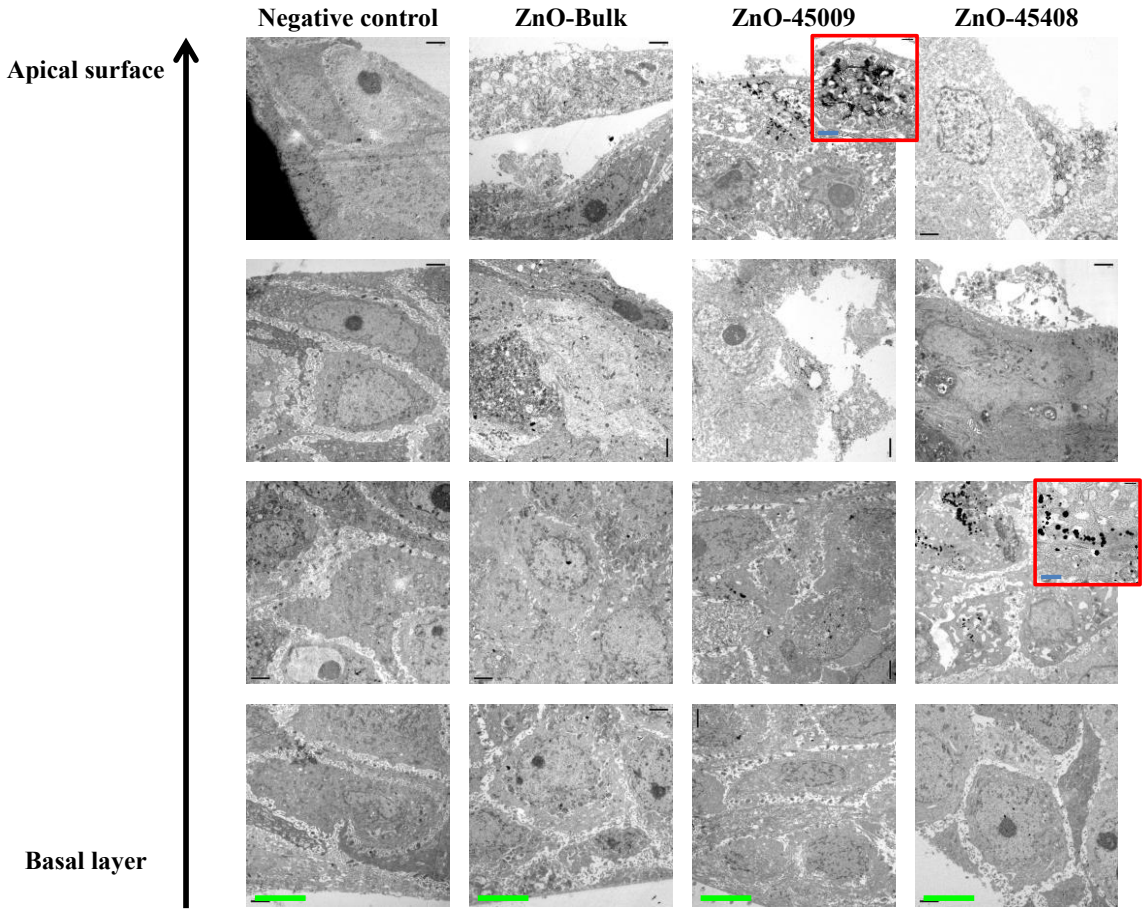

Figure 6.12. TEM images of SkinEthic RHO tissue sections taken at 1,000 times magnification using the Hitachi-7100 TEM. Samples were treated for 1 hour with serum free culture media (Negative control), ZnO-bulk, ZnO-45009 nanomaterial and ZnO-45408-nanomaterial all at 1% w/v in serum free culture media before fixing. *Green scale bar = 5μm*. In general, from bottom to top images are representative coming from the base of the tissue to the apical surface, but are not scaled to accurate depths within the tissue. *Areas of suspected nanoparticle uptake have been magnified to 5,000X and are shown with red borders. Blue scale bar = 1μm.*

Figure 6.12 shows signs of nanomaterial internalisation as uncharacteristic non-organic shaped electron dense material, within the cells of RHO tissue (these have been enlarged in Figure 6.14, below). The positioning of electron dense material suggested ZnO material internalisation was limited to transcellular uptake pathways, with none of the particles observed located with the extracellular spaces. Nano-size may also have played a role, with little evidence of ZnO particles in bulk treated tissue, and increased depth of penetration for the smaller ZnO-45408 nanomaterial over ZnO-45009. Measuring the size of the electron dense regions, and considering the inorganic morphology of suspected of ZnO nanomaterials, revealed the likelihood of them forming agglomerates that were confined within vacuole-like structures in the cytoplasm of individual cells, but there was no incidence of them entering nuclear envelope.

Cell morphology showed signs of cytotoxicity evident in all the tissue models exposed to ZnO materials, including bulk and nanomaterial forms. Comparisons with the apical cells of the negative control revealed ZnO exposure to result in severe vacuolisation, with surface cells appearing ruptured, alongside the loss of apical cells structure. In contrast, the negative control tissue sample has intact apical cells with a full complement of organelles. The respective observations correspond well with results from cytotoxicity testing using the RHO models (Figure 5.1 and Figure 5.2), with ZnO-45408 cell damage considered more severe than ZnO-45009 and bulk material treated sample limited to the top cell layer.

6.1.3.2 EpiGingiva keratinised tissue model analysis of nanomaterial uptake using TEM imaging

TEM micrographs enable comparisons to be drawn between the two tissue models treated with 1% w/v of each ZnO material (for 1 hour). Here, Figure 6.13 shows EpiGingiva™ GIN-100 tissue structure following ZnO bulk and nanomaterial exposure.

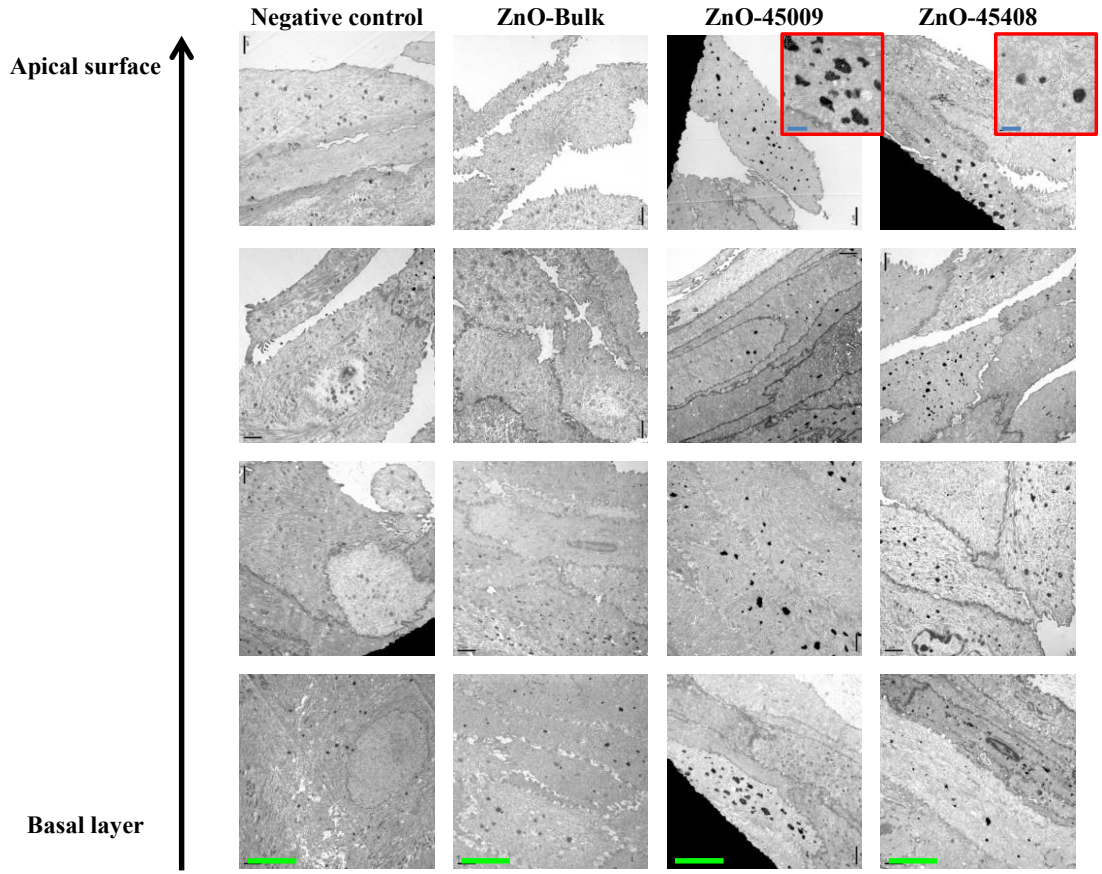

Figure 6.13. TEM images of EpiGingiva™ GIN-100 tissue sections taken at 1,000 times magnification using the Hitachi-7100 TEM. Samples were treated for 1 hour with serum free culture media (Negative control), ZnO-bulk, ZnO-45009 nanomaterial and ZnO-45408-nanomaterial all at 1% w/v in serum free culture media before fixing. *Green scale bar = 5μm.* In general, from bottom to top images are representative coming from the base of the tissue to the apical surface, but are not scaled to accurate depths within the tissue. *Areas of suspected nanoparticle uptake have been magnified to 5,000X and are shown with red borders. Blue scale bar = 1μm.*

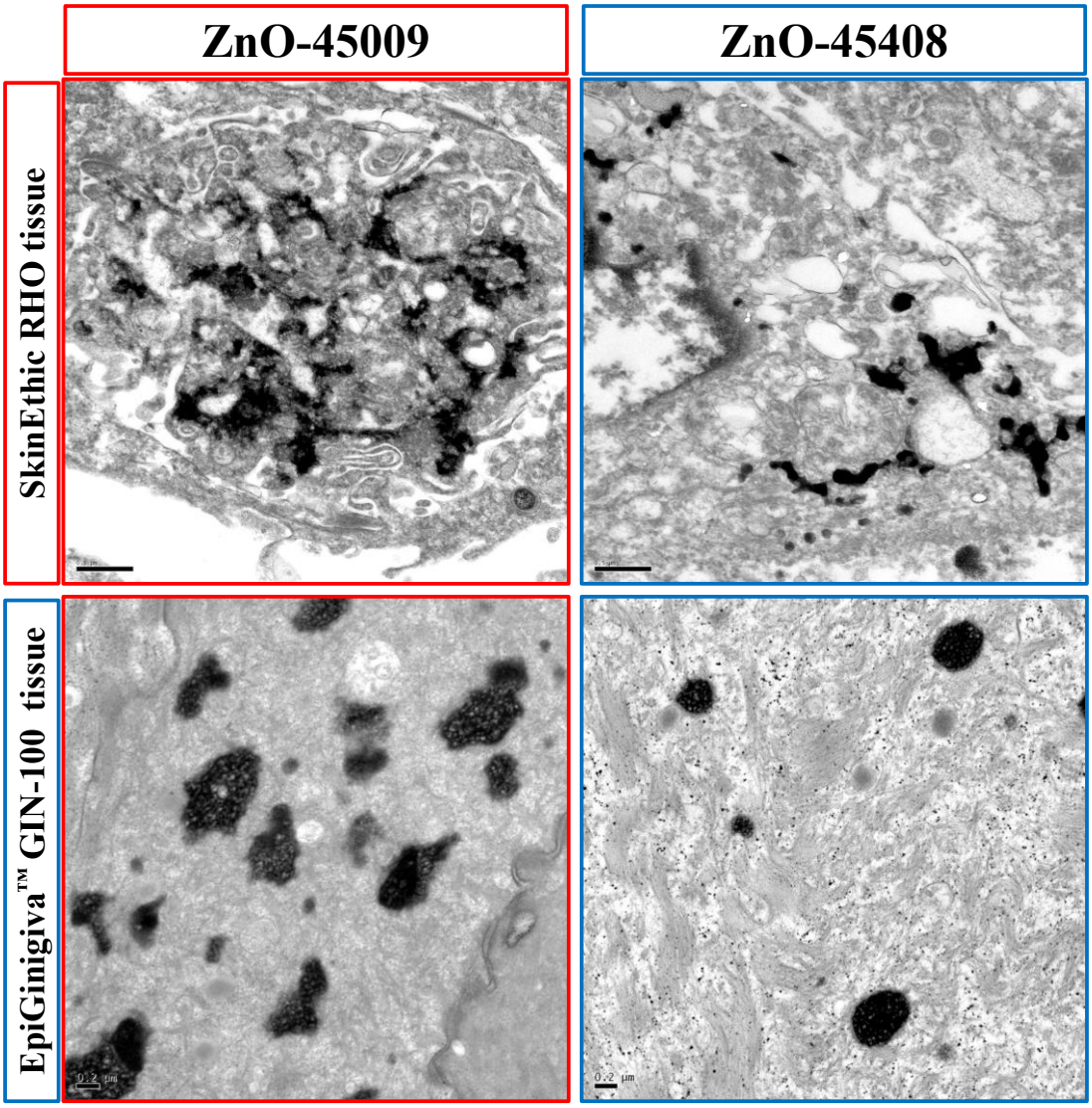

Figure 6.14. Enlarged TEM micrographs to highlight ZnO nanoparticle internalisation into 3-D tissue model sections. *Scale bar = 0.5µm* and *0.2µm* for SkinEthic RHO (non-keratinised tissue) model and the EpiGinigiva™ GIN-100 (keratinised tissue) model, respectively.

As anticipated, micrographs in Figure 6.13 show the MatTek GIN-100 keratinised models with morphology considerably different to the RHO non-keratinsed tissue constructs. In the keratinised models, cell layers were less well differentiated, dense with stained biological material and had no obvious organelle structures, including nuclei. Cell membranes that partitioned the cell layers were also difficult to interpret due to the dense cell structure. Clearly evident was the squamatisation of the cells towards the apical surface. These were stacked in stratified structures thicker than the RHO model, consisting of 8-11 cell layers.

Evidence of ZnO material internalisation was again confined to nanomaterials, with electron dense areas observed within the cells (Figure 6.14). Differently to RHO models, was the depth of penetration, with suspected nanomaterial agglomerates (>500nm) observed throughout all cell layers. However, the lack of cellular structure distinction makes it difficult to determine their positioning within the cells.

Common to all samples was the disheveled appearance of their apical cells in the keratinised model, with no other signs of cell stress observed. This perhaps indicated evidence towards the desquamation defence, known to occur in native keratinised epithelium of the oral mucosa *e.g.* gingiva. The occurrence of apical layers being lost in response to cytotoxic stimulation may help to explain the lack of cytotoxicity experienced in this tissue model, with no loss in cell viability or elevation in LDH levels above that of the negative control (Figure 5.4 and Figure 5.6).

6.2 Discussion

As a consequence of the novel properties exhibited by a material reduced in particle size to the nano-scale, it is important to assess the potential health and environmental risks of exposure (Oberdörster, 2010). Hydroxyapatite, SiO_2, TiO_2 and ZnO have all been safely incorporated into existing oral healthcare formulations for a number of years, as bulk-scale particles (Allaker, 2010, Khataee & Kasiri, 2010, Tschoppe *et al.*, 2011). The data generated within this thesis has contributed towards the compilation of a safety assessment, in terms of the risks involved through exposure of the oral tissues, to nano-forms of the materials. Whilst ZnO has demonstrated incidents of cytotoxicity in previous chapters, the accepted use of SDS[7] in oral healthcare (Newby *et al.*, 2011) provides context, suggesting the low risk of cytotoxicity posed by ZnO materials on oral mucosal tissues. With hydroxyapatite, SiO_2 and TiO_2 nanomaterials all demonstrating lower cytotoxicity than ZnO, these too would be considered to constitute a low risk based on the cytotoxicity hazard assessed *in vitro* in this study.

However, a unique attribute of nanomaterials widely exploited in drug delivery, is related to their small size facilitating increased uptake into cells and penetrating tissues (Elder *et al.*, 2009), including permeation through the buccal mucosa (Campisi *et al.*, 2010, Harris & Robinson, 1992, Rossi *et al.*, 2005, Shojaei, 1998). The cytotoxicity exhibited by ZnO would subsequently constitute a more serious hazard to health, when uptake risks are considered in comparison to localised cytotoxicity. Nanomaterial uptake manifests the potential to reach systemic circulation and cause cytotoxicity in more sensitive, secondary exposure sites within the body (Holsapple *et al.*, 2005, Oberdorster *et al.*, 2005a). Furthermore, the lack of degradation that would be expected for metal oxide nanomaterials in the body, could manifest a risk of bioaccumulation more serious than initial cytotoxic action ((SCENIHR), 2009). Both TiO_2 and ZnO nanoparticle internalisation has been observed to cause genotoxicity in epidermal keratinocytes (Prasad *et al.*, 2013b, Shukla *et al.*, 2011, Sharma *et al.*, 2011), which could pose increased risk of carcinoma following long term or multiple exposure (Bercu *et al.*, 2008).

[7] an existing and widely formulated surfactant agent in oral healthcare products, known to cause localised inflammation following exposure (EU) (2013). Cosmetics Directive 76/768/EEC. *Official Journal (OJ) of the European Union,* **L 262,** p. 169, di Nardo, A., Sugino, K., Wertz, P., Ademola, J. & Maibach, H. I. (1996). Sodium lauryl sulfate (SLS) induced irritant contact dermatitis: a correlation study between ceramides and in vivo parameters of irritation. *Contact Dermatitis,* **35,** 86-91., but considered an acceptably low hazard for inclusion in cosmetics

Nanomaterial uptake has been investigated relating to the skin as a primary exposure site (Borm *et al.*, 2006, Oberdorster *et al.*, 2005b), and has specifically focused on TiO_2 and ZnO nanoparticle inclusion in commercially available sunscreens (Lewicka *et al.*, 2013, Gulson *et al.*, 2012, Monteiro-Riviere *et al.*, 2011, Schilling *et al.*, 2010, (SCCP), 2007, Lademann *et al.*, 1999, Tan *et al.*, 1996). Despite the abundance of studies, controversy still persists to the extent and effects of these nanomaterials to penetrate the epidermal layers, especially when formulated alongside chemicals designed to impart surface and formulation stability of particulates (Monteiro-Riviere *et al.*, 2011, Nohynek *et al.*, 2010, Schulz *et al.*, 2002). The current consensus is that nanomaterial uptake remains limited to the outermost layers of healthy skin epithelium ((SCCP), 2007, Gulson *et al.*, 2010, Lademann *et al.*, 1999, Nohynek *et al.*, 2010, Weir *et al.*, 2012), and that their inclusion in cosmetics remains safer than the effects of UV damage (Schilling *et al.*, 2010). Extrapolation between their safe exposure at the epidermis may suggest an acceptable and low risk for keratinised areas of the oral mucosa, that share the similar protection of a tough stratum corneum at the membrane of apical cells. However, a typical oral healthcare formulation is unlikely to remain constrained to one region of the oral mucosa, and would be expected to interact with non-keratinised tissue areas also. These have long been identified as more permeable regions of the mouth as differences in structure have been discovered (Presland & Jurevic, 2002, Squier & Wertz, 1993, Wertz *et al.*, 1993), and alternate drug delivery sites have been explored (Campisi *et al.*, 2010, Gandhi & Robinson, 1994, Hao & Heng, 2003, Hoogstraate & Wertz, 1998, Nicolazzo *et al.*, 2005, Sudhakar *et al.*, 2006). Therefore, it was an important consideration within a comprehensive preliminary risk assessment of nanomaterial exposure in the oral mucosa, to investigate their potential for uptake.

The results from this investigation showed monolayer cell exposure to SiO_2 materials that contained nanoparticles (SigmaAldrich sourced 'bulk' and nanopowder), to contribute an increase in fluorescence using the SynaptoGreen™/FM1-43 assay. H376 cells were characterised demonstrating the same uptake mechanisms to those of the positive control Caco-2 cell model. Assay results were supported by similar observations from confocal microscopy. The use of these methods was associated with the transport of nanoparticles using the transcellular uptake pathways available in monolayer models, and this is put forward as the route for speculated internalised ZnO nanomaterial observed in TEM micrographs of both keratinised and non-keratinised tissue models. The factors and influences that cause these outcomes will now be discussed in detail.

Specifically, this will be aimed at the results reported here in the context of the wider study exploring nanoparticle uptake related to their risk on human health.

6.2.1 Nanomaterial uptake routes

The transport pathways available to nanomaterials in the human oral mucosa have previously been introduced in detail (within introduction section 1.2.6). Elucidating the exact uptake pathway taken by each different nanomaterial applied to the human oral mucosa was considered an ambitious initial aim, given the current level of established links between nanoparticles and internalisation mechanisms hindered by the complexities associated with cellular uptake pathways (Doherty & McMahon, 2009). Even within the confines of *in vitro* assessment, there exists a multitude of transcellular transport routes available to substances passing through a number of different membranes in stratified oral mucosal epithelia (Campisi *et al.*, 2010). Paracellular transport of nanomaterials is harder to model, as it can only be discerned from stratified models of the epithelium. These pathways have been demonstrated to a lesser extent, due to many common *in vitro* cell models limited in full representation the stratified *in vivo* structure (Ward *et al.*, 2000).

The uptake pathway and subsequent biodistribution of nanomaterials following exposures are linked to complex surface physio-chemical properties, which make them chemically more reactive upon interaction with biological systems (Gosens *et al.*, 2010). It has been well stated that the novel risk concerning nanotoxicity emanates from the small particle sizes conferring the ability to transport through tissues, across cell membranes and even into organelles (Besic Gyenge *et al.*, 2011, Geiser *et al.*, 2005, Lovric *et al.*, 2005). Considering the size range used to define nanomaterials (1 – 100nm), they correspond closely with the sizes of typical cellular components, viruses and even DNA ((FDA), 2009, Kim *et al.*, 2008). A wealth of evidence has demonstrated this, from alveolar macrophage (Ruge *et al.*, 2011, Takenaka *et al.*, 2001, Vranic *et al.*, 2013b), endothelial cells (Davda & Labhasetwar, 2002, Soenen *et al.*, 2010, Xia *et al.*, 2007), pulmonary epithelium (Nemmar *et al.*, 2002, Oberdorster *et al.*, 2005a, Pickrell *et al.*, 2010), gastrointestinal epithelium (Cavet *et al.*, 1996, Desai *et al.*, 1997, Finley *et al.*, 1995, Lin *et al.*, 2012, Moyes *et al.*, 2010), red blood cells (Antonelli *et al.*, 2011, Zhao *et al.*, 2011), platelets (Solomon *et al.*, 2013) and nerve cells (Bulcke *et al.*, 2013, Ceresa *et al.*, 2013, Hutter *et al.*, 2010). The nanomaterials of interest here for future healthcare formulations (hydroxyapatite, SiO_2, TiO_2 and ZnO) have all been reported to internalise

within a number of different cell types in the body (Bauer *et al.*, 2008, Besic Gyenge *et al.*, 2011, Hackenberg *et al.*, 2010, Kao *et al.*, 2012, Kasper *et al.*, 2013b, Schilling *et al.*, 2010, Tay *et al.*, 2013, Tedja *et al.*, 2012, Yu & et al., 2011), but not in oral epithelial cells, until now.

It is not solely nano-size that permits transport of metal oxide materials through biological membranes. Nano-characteristics also include unique surface properties resulting from the large volume to surface area ratio of a nanoparticle. These are thought to contribute an increased ability to permeate cell structures through high surface reactivity, specific charge properties and other related surface modifications (Elder *et al.*, 2009, Harush-Frenkel *et al.*, 2008, Massignani *et al.*, 2009, Schleh *et al.*, 2012, Verma & Stellacci, 2010). The increased surface reactivity of nanomaterials can be considered the initial catalyst for interactions leading to uptake of material upon exposure to an epithelial layer. These can occur through Van der Waals forces, electrostatic charges, steric interactions or interfacial tension effects, all dependent upon the characteristics of the nanomaterial (Buzea *et al.*, 2007). The type of interaction will then dictate what mechanism of uptake is initiated, dependent upon those available to the cells exposed.

Characterisation outcomes of the key properties exhibited by each nanomaterials under the *in vitro* conditions investigated here, were used to narrow the transport pathways available in each of the cell models. SiO_2, TiO_2 and ZnO nanoparticle sizes had all been observed below 100nm in starting nanomaterial form with hydroxyapatite nanomaterial only slightly larger (Figure 3.4 and Figure 3.8). All were expected to agglomerate upon delivery in media and through interactions with the cell surface proteins. The increase in nanomaterial size when agglomeration occurs would be expected to limit the amount of uptake via transport routes that require extreme small particle size. Therefore, significant incidental internalisation through facilitated diffusion would be less likely (Teeguarden *et al.*, 2007). When size is not the principle property governing uptake, other physiochemical properties must take precedent. It was already discussed how charge and surface coatings play a major role in nanomaterials used as targeted drug delivery penetration enhancers. However, the nanomaterials were delivered here in serum-free media with no surface coatings or deliberate modification applied to govern interactions targeting specific cell membrane receptors. This would seemingly rule out selective uptake activated through specific binding *e.g.* receptor-mediated endocytosis.

Additionally, binding to receptors has also been calculated as size specific, dependent upon cell surface-nanoparticle adhesion concentrations (Zhang *et al.*, 2009). Individual nanoparticles may still be internalised through incidental uptake, via other mediated transport mechanisms, and so receptor-mediated transport routes need to be investigated on a case by case basis. Studies have recently been carried out using pharmaceutical inhibitors of known uptake pathways, to elucidate the exact uptake mechanisms of polystyrene nanoparticles designed with different surface characteristics (Jiang *et al.*, 2011).

Carrier mediated transport mechanism have been relatively well established in studies involving oral drug delivery of macromolecules (*e.g.* glucose, amino acids, sodium and potassium ions) that correspond to much smaller sizes of molecule than any of the nanomaterials here. However, demonstration of carrier mediated transport capacity by Caco-2 cells has been observed *in vitro* (Grandvuinet *et al.,* 2013, Grès *et al.*, 1998, Hubatsch *et al.*, 2007, Neuhoff *et al.*, 2005), including incidents of unregulated access by cadmium and chromium nanomaterials internalised using this pathway (Wang *et al.*, 2008b, Zha *et al.*, 2008). Studies have linked nanomaterial surface reactivity with their ability to adsorb cell culture constituents, making them more biocompatiable (Merhi *et al.*, 2012). Incidentally, this has also been put forward as a mechanism of nanoparticle cytotoxicity (Casey *et al.*, 2008, Elder *et al.*, 2009, Guo *et al.*, 2008, Hussain, 2009), and works essentially through cell starvation by depletion of available nutrients in the media. The formation of a protein corona, coating the reactive surfaces available at the nano-scale, has been reported to increase their potential for both incidental and intentional uptake (Cedervall *et al.*, 2007a, Cedervall *et al.*, 2007b, Dominguez-Medina *et al.*, 2013, Lynch *et al.*, 2007, Tedja *et al.*, 2012). Subsequently, cell receptor molecules may recognise the structure from protein coatings on nanoparticles, affording them entry through specialised uptake pathways, such as the heparin sulfate proteoglycans membrane receptor (Huang *et al.*, 2010b). This has been observed for cationic nanoparticles (Tyagi *et al.*, 2001, Wadia & Dowdy, 2005), demonstrating the potential for exploiting these interactions for drug delivery applications (Kreuter *et al.*, 2003, Medina-Kauwe, 2007, Rahimnejad *et al.*, 2006). Conversely, protein coatings have also been demonstrated to reduce uptake of nanoparticles, shielding their foreign structure from the immune response, specifically macrophage engulfment (Xie *et al.*, 2007). Currently our knowledge about conformational changes of the proteins upon adsorption onto nanoparticle surfaces remains limited. It is a complex area, only

recently gaining attention through studies directed towards modelling nanoparticle-protein corona interactions (Cedervall *et al.*, 2007b, Faunce *et al.*, 2008, Lynch *et al.*, 2007).

Characterisation was carried out under simplified conditions relating to the *in vitro* environment for nanomaterial delivery, and not in the presence of FBS supplemented media. This was deliberate, due to the highly heterogeneous nature of FBS, constituted of numerous proteins, each with complex behaviour and properties relating to their ability to interact with nanomaterials in different ways. Furthermore, this correlated with cytotoxicity studies demonstrating serum-free delivery of nanomaterials to correspond with increased cytotoxic actions (Dominguez-Medina *et al.*, 2013, Landsiedel *et al.*, 2010, Merhi *et al.*, 2012, Prasad *et al.*, 2013b, Tedja *et al.*, 2012, Xia *et al.*, 2008). However, it cannot be ruled out that during *in vitro* exposure to cells, the high surface reactivity may have interacted with a variety of media constituent or cellular proteins constituting the apical membrane (Nel *et al.*, 2009). *In situ*, this situation would be further complicated through the abundance of different interactions that may occur between nanomaterials, when formulated in oral healthcare products, and the complex cocktail of constituents available in saliva and mucus in the oral mucosa (Fröhlich & Roblegg, 2012, Lendenmann *et al.*, 2000).

Styryl dyes have routinely been used to monitor membrane cycling of synaptic vesicles (Groemer & Klingauf, 2007, Harata *et al.*, 2001, Lebonvallet *et al.*, 2012, Orenbuch *et al.*, 2012, Winterer *et al.*, 2006, Yakovleva *et al.*, 2013). Here, the styrl dye FM 1-43 was identified as a marker for assessing the membrane invagination uptake mechanisms, and was developed into a novel assay for rapidly screening the potential for nanomaterial uptake in this way. Membrane invagination is a constituent process of endocytosis, carried out in most eukaryote cells, including human epithelium (Innes & Ogden, 1999). The non-specific nature of pinocytosis meant this mechanism of transport into cells was considered the most likely for nanoparticle transcellular transport in oral mucosal tissues (Harush-Frenkel *et al.*, 2008, Treuel *et al.*, 2013, Vranic *et al.*, 2013a), although others could not be ruled out.

FM®1-43FX has been reported for other confocal work, describing similar nanoparticle compounds suspected of uptake into cells via endocytosis (Gomes *et al.*, 2013, Grabrucker *et al.*, 2011, Hosokawa *et al.*, 2011, Kao *et al.*, 2012, Rhee & Davis, 2006, Thevenot *et al.*, 2008). However, to the best of our knowledge utilisation of its

SynaptoGreen™ derivative in assay form remains novel as a method for investigating nanoparticle uptake across the cell membrane. Development of the dye as an assay allows real time analysis of uptake kinetics to be carried out in live cells, using nanomaterials that do not exhibit traditional fluorescence properties. Any positive results indicated a capacity for increased uptake, and would subsequently warrant more in depth mechanistic investigation. This could be linked to increased risk of intracellular cytotoxicity or potential for translocation through tissues, in much the same way as the tiered strategy employed for nanotoxicology studies.

6.2.2 Endocytosis as a transcellular uptake pathway for nanomaterials putative of interest in future oral healthcare applications

Results demonstrated the increased internalisation of SynaptoGreen™/ FM®1-43FX in response to exposure with SiO_2 nanomaterials. The increased fluorescent intensity was consistent in both H376 and Caco-2 cell monolayer models in both assay assessment and verification by confocal microscopy. Caco-2 cells, therefore served as an effective control model (known for expressing several morphological and functional characteristics of the mature enterocyte, including a number of enzymes and transporter molecules to mimic processes such as transcellular transport, paracellular transport, and some aspects of efflux and active transport (Sambuy *et al.*, 2005)) for SiO_2 nanoparticle uptake potential into oral mucosal non-keratinised cells (represented by the H376 model). Similar fluorescent intensities were observed across both monolayer models, perhaps indicating the same mechanism was responsible for the increased rates of internalisation.

Endocytosis pathways were considered as the predominant mechanism of uptake for SiO_2 nanoparticles in epithelial cells, supported by the presence of fluorescent vesicles identified within the cells imaged using confocal microscopy. Various endocytotic pathways has been demonstrated to occur for the internalisation of SiO_2 in other cell models (Besic Gyenge *et al.*, 2011, Herd *et al.*, 2013, Kasper *et al.*, 2013a, Kasper *et al.*, 2013b, Tay *et al.*, 2013). Besic-Gyenge *et al.,* 2011, were the first to demonstrate the use of SiO_2 based nanoparticles as a novel therapeutic delivered to head and neck cell carcinomas, with fluorescent core SiO_2 nanoparticles seen as both agglomerated and free forms, localised in cytoplasmic membrane-bound vesicles. The exact endocytotic pathway was not fully deciphered, but speculated to involve clathrin-associated pathways. Herd *et al.,* 2013, used a series of chemical inhibitors of endocytosis, to

elucidate that different geometries of SiO_2 nanoparticles that exhibit different uptake profiles dependent upon their orientation when they interact at the cell surface. Kasper *et al.,* 2013, have demonstrated the importance of flotillins as indicators for clathrin- or caveolae-independent uptake mechanisms of amorphous SiO_2 nanoparticles, in both alveolar and microvascular cell lines. These are likely to have been internalised using CLIC-GEEC endocytosis mechanisms (Doherty & McMahon, 2009). Tay *et al.*, 2013 have even demonstrated the localisation of SiO_2 nanoparticles in cell nuclei of TR146 cells, similar to the cell line used as the basis for RHO 3-D tissue models. Internalisation was associated with increased oxidative stress in the cells, but only marginal nanotoxicity as assessed using apoptotic markers. These results provoke thought as to the cytotoxic effect of SiO_2 nanoparticle internalisation in non-keratinised oral tissue, which is measured as not being significant in this study using LDH and MTT assay assessment. As discussed within the introduction, the use of *in vivo* models that enable multiple dosing has demonstrated SiO_2 internalisation and subsequent translocation to bioaccumulate in the liver, causing hepatotoxicity (Hasezaki *et al.*, 2011, Liu *et al.*, 2012, Nishimori *et al.*, 2009). In each of the studies, SiO_2 nanoparticles had to be delivered intravenously for accumulation to occur in the liver. However, SiO_2 inclusion in future oral healthcare formulations may provide an entry route to systemic circulation, were uptake, as demonstrated here, is persistent enough to penetrate deeper through the tissue layers of the stratified epithelium, through the submucosa and into systemic circulation via numerous blood vessels connected to the lingual artery (Squier & Wertz, 1993). The risk cannot be accurately extrapolated from the simplified in vitro models here, which do not include the full thickness of the non-keratinised tissue, or replicate the permeability barriers of the sub-mucosa, stratified epithelial tissue (Nicolazzo *et al.*, 2003, Rossi *et al.*, 2005, Senel & Hincal, 2001, Wertz & Squier, 1991) or the physiological barriers of salivary flow and pellicle formation alongside mucus (Collins & Dawes, 1987, Lendenmann *et al.*, 2000, Slomiany *et al.*, 1996, Squier & Wertz, 1993). However, the risk requires further consideration, considering the routine application of oral healthcare products as part of a regimented oral hygiene treatment (Lagerweij & Ten Cate, 2010, Moore *et al.*, 2008) e.g. brushing teeth twice a day ((BDHF), 2013, O'Mullane *et al.*, 2004), and the potential for bioaccumulation over time.

Exposure to the original SiO_2 bulk material sourced from Sigma Aldrich (which was characterised containing individual nanoparticles similar in size to the distinct

nanomaterial product) was also observed to increase internalised fluorescence into H376 and Caco-2 cells, to a similar extent as the nanomaterial. These results demonstrated the importance of appropriate controls being utilised in studies investigating nano-specific effects (Borm *et al.*, 2006). For uptake, this was achieved through comparisons to an extra material: the ACROS Organics sourced SiO_2 bulk (Figure 9.2). Exposure of the larger SiO_2 particles to both H376 and Caco-2 cells did not correspond with increased SynaptoGreen™/FM®1-43FX fluorescent intensities above the negative control (Figure 6.2 and Figure 6.4). The investigation involving the larger particles of ACROS sourced SiO_2 material proved uptake was experienced solely by SiO_2 nanoparticles. Characterisation data had proved the materials that correlated with increased SynaptoGreen™/FM®1-43FX fluorescent-linked uptake, were amongst the smallest analysed from starting state as powders (Table 3.5). Combined, these results would suggest that the transcellular uptake mechanism experienced by both H376 and Caco-2 cells, was nano-size dependent.

Hydroxyapatite, TiO_2 and ZnO nanomaterial (45009 and 45408) exposure did not result in increased SynaptoGreen™/FM®1-43FX fluorescence for either monolayer cell model. Evidence in the literature has demonstrated internalisation of hydroxyapatite, TiO_2 and ZnO internalisation (Bacchetta *et al.*, 2013, Belade *et al.*, 2012, Jaeger *et al.*, 2012, Motskin *et al.*, 2009, Xia *et al.*, 2008, Yuan *et al.*, 2010). In each study, this uptake was observed alongside cytotoxic responses by the cell. Hydroxyapatite and TiO_2 nanomaterials were not observed as causing cytotoxicity in earlier assessment using the H376 cell model (Figure 4.1 and Figure 4.5), and considering the lack of SynaptoGreen™/FM®1-43FX fluorescence in these cell lines, this was taken to suggest that neither nanomaterial were internalised into epithelial cells using endocytosis. However, it is important in risk assessment to stress that unlike *in vitro* cell lines, there may be multiple uptake pathways within *in vivo* tissue structures comprised of multiple cell types (Elder *et al.*, 2009, Junginger *et al.*, 1999, Oberdorster *et al.*, 2005a). Therefore, the passage through cell membranes using other pathways cannot be ruled out, based on the results presented here for hydroxyapatite and TiO_2 nanoparticle exposure.

For ZnO nanomaterials, it was thought their cytotoxic action (observed across all *in vitro* oral mucosal models), may have interfered with the assessment of their uptake potential using SynaptoGreen™/FM®1-43FX. The mechanism of styrl dye fluorescence relies upon the existence of an electrochemical differential between intra and extracellular

environment (Betz *et al.*, 1996). This effects the electron transfer potential between the lipophilic tail inserted into a lipid bilayer (membrane or internalised vesicle) and the polar head that anchors the molecule from complete passage through cell membranes (Richards *et al.*, 2005). The fluorophore core of the molecule is redundant where no difference in pH or solvent environment exists between the polar head and lipophilic tail. Equilibrium would be anticipated between the intra- and extracellular environments, following cell lysis. ZnO materials were observed to cause cytotoxicity as measured using an assay to detect the extracellular release of LDH enzyme following cell lysis (Figure 4.1). In addition, apoptosis signals were observed during particle interactions at the surface of H376 cells, and through morphological observations of the confocal microscope images presented in this chapter (Figure 6.5). Cytotoxicity, particle uptake associated or not, would likely break down the mechanism that permits the dye molecule to fluoresce. The fact that SiO_2 nanomaterials were observed to be well tolerated by the H376 cell model during cytotoxic screening may account for the significant increases in SynaptoGreen™ or FM®1-43FX observed for this material over the others.

Extracellular ATP was similarly not found to have stimulated an increase in uptake of SynaptoGreen™/FM®1-43FX into the cell as vesicles. This was not anticipated, a result that deviated from studies reporting pinocytosis commonly observed alongside energy-dependent carrier mediated diffusion (Campisi *et al.*, 2010, Dobson & Kell, 2008, Sugano *et al.*, 2010). ATP was chosen as it had been successfully used to stimulate uptake in other epithelial cells (Benali *et al.*, 1994, Mason *et al.*, 1991, Schwiebert & Zsembery, 2003), including for FM 1-43 trafficking in human colonic epithelial goblet cells (Bertrand *et al.*, 2006). At excess levels, extracellular ATP has been implicated in the expression of anti-ATP and other markers of cell apoptosis (Schulze-Lohoff *et al.*, 1998). This study was used as a hypothesis that might help explain the difference in the results reported here to that of others observing increased uptake in other epithelium, with ATP induced cytotoxicity causing a similar break down in the mechanism of SynaptoGreen™/FM®1-43FX fluorescence, as experienced following ZnO material exposure. However, cell death reported in the Schulze-Lohoff study, was caused through ATP exposure to mesangial cells, at concentrations greater than 0.3mM for a 3 hour time period. The method employed in our study required only 5 minutes of exposure, at less than 0.3mM in all instances. The observations drawn from interpretation of the cell morphologies (stained by TRITC-labelled phalloidin) revealed

no obvious signs of cytotoxicity, following a 0.1mM dosage (Figure 6.5 and Figure 6.7). Instead, the lack of significant increase in uptake (for positive control) was considered to be indicative of the type of mechanism responsible for internalisation of SynaptoGreen™/FM®1-43FX. ATP plays a critical role in internal transport, and so the results observed would seemingly rule this out as the predominant mechanism of uptake in either H376 or Caco-2 epithelial cells. Endocytosis is a relatively low energy consumptive process in comparison (Lodish H, 2000). Sufficient stores of energy may have been available to both H376 and Caco-2 cells during their culture, thus permitting the uptake of SynaptoGreen™/FM®1-43FX containing vesicles into the cell (over the course of the experiments). Future work could follow the precedent of other studies, by using pharmaceutical inhibitors to deduce the mechanism of uptake for SiO_2 nanomaterials in each of the cell lines used (Herd *et al.*, 2013, Jiang *et al.*, 2011).

Future studies would also be focused on fully determining the link between nanomaterial uptake using SynaptoGreen™/FM®1-43FX fluorescence. It remains only an assumption that internalisation of dye captured in vesicles is accompanied by the nanoparticles themselves, and that SiO_2 nanoparticles did not just stimulate endocytosis (although no such evidence currently exists to suggest nanoparticle interactions stimulate uptake without becoming internalised themselves). Characterisation data (demonstrating the small starting size of SiO_2 nanomaterials over the others used) can be used to support this view, as individual nanoparticles remain small enough to fit inside endocytotic invaginations (Iversen *et al.*, 2011). In addition, SEM micrographs have previously demonstrated the abundance of close interactions between nanomaterials at the surface of H376 cells, an environment similar to known conditions that enable particle engulfment into vesicles (Innes & Ogden, 1999, Okamoto, 1998). Further experimentation could employ a fluorescent SiO_2 nanoparticle, engineered to similar specifications to those characteristics recorded for the SiO_2 materials investigated here, but with different excitation and emission wavelengths to the stryl dye. The aim would be to expose the fluorescent SiO_2 nanomaterial to the cell models in combination with FM®1-43FX, matching the study design reported here. Confocal microscopy would then be employed following a traditional application, as has been demonstrated in determining the localisation of various fluorescent nanoparticles internalised within different monolayer cells (Besic Gyenge *et al.*, 2011, Ceresa *et al.*, 2013, Gomes *et al.*, 2013, Jin *et al.*, 2007, Soenen *et al.*, 2013). The hypothesis would be that if SiO_2 nanoparticles were internalised, fluorescent nanoparticle signal would

overlay with regions of FM®1-43FX fluorescence. The limitation that would remain, concerns the modifications to the nanomaterial properties brought about by modified optical properties to enable fluorescence (Nel *et al.*, 2009).

6.2.3 Paracellular transport of nanoparticles

The development of 3-D tissue culture has enabled the study of paracellular transport pathways through stratified cell layers *in vitro*. Examples in the literature demonstrate the ability of extremely small, engineered nanoparticles, to penetrate across cell junctions, and through the permeability barrier of human epithelial tissue (Lin *et al.*, 2007, Nicolazzo *et al.*, 2003). However, it is important to consider, that under normal physiological conditions paracellular transport of nanoparticles is likely to be extremely limited due to the minute pore sizes (<1nm) measured at tight junctions between cells (des Rieux *et al.*, 2006). This is thought to be especially restrictive in the *gingiva* and hard *palate* tissues that make up the keratinised regions within the oral mucosa. Keratinised cells form a particularly tightly packed tissue structure, bound by multiple tight junctions and desmosome complexes, between protein and lipid rich squamous cells that lack much intercellular space for extraneous substances to travel through (Garrod & Chidgey, 2008, Presland & Jurevic, 2002, Wertz & Squier, 1991). The observations drawn from TEM micrographs of the EpiGingiva™ GIN-100 model exposed to ZnO nanomaterials support this, displaying no distinguishable barrier between the cells, and no electron dense regions (speculated to represent ZnO particles) observed (by TEM) within the extracellular spaces between cell membranes (Figure 6.13). Non-keratinised regions are more permeable areas of the oral mucosa, but not freely permeable to all substances (Hoogstraate & Wertz, 1998, Rossi *et al.*, 2005, Squier & Kremer, 2001, Wertz & Squier, 1991). They possess an array of morphological permeability barriers in to govern the transport of substances, as discussed within the introduction (section 1.3.1.2). The fact that no material was found within the extracellular spaces of SkinEthic RHO tissues maybe due to some, or all, of the effective barrier functions available. These were expected to mimic closely the inter-cellular lipid based bilayer (Wertz *et al.*, 1993), described in detail within section 1.3.1.2.

In the context of nanomaterials investigated for potential roles in future oral healthcare formulations, overall the risk of transcellular internalisation into systemic circulation remains limited. A major challenge in drug delivery is the internalisation through the apical plasma membrane of the polarised epithelial cells (Sandvig & van Deurs, 2005),

such as the oral mucosal tissue. The reduced permeation through this pathway is in part due to the mucosal barrier and low rate of endocytosis at these membranes, with only a few publications describing penetrative uptake of nanoparticles through the apical side of polarised tissues (Harush-Frenkel *et al.*, 2008). Substances looking to penetrate both keratinised and non-keratinised epithelial tissues in the oral mucosa *in situ*, have additionally to overcome the flowing obstruction provided by saliva and 40 to 300μm thick mucus layers that coat the mucosal surface (Sudhakar *et al.*, 2006). Mucus can be described as a viscous colloid, produced in the sublingual and minor salivary glands, that has evolved to encompass robust barrier mechanisms that trap and immobilise pathogens, (Cone, 2009). Alongside the salivary pellicle, both layers constitute numerous proteins, glycoproteins and mucins that will result in complex interactions with nanoparticle reactive surfaces (Lendenmann *et al.*, 2000). This is an area currently unexplored with relation to nanoparticle interaction with the human oral mucosa, and requires better characterisation with respect to the uptake of nanoparticles, and in order to understand the mechanisms of potential nanomaterial toxicity.

TEM micrographs of the pseudo-tissue sections showed morphological differences between the tissue models, following exposure of ZnO treatments. In RHO models, exposure to ZnO nanomaterials displayed incidents of clearer, more pronounced structural degradation than the keratinised model. But this was not observed alongside increased penetration of electron dense materials. The electron dense areas present within both nanomaterial treated tissue model samples, were suspected to constitute agglomerated ZnO nanomaterial. These observations are similar to reports of internalised ZnO nanoparticles seen in other cell types using TEM detection (Hackenberg *et al.*, 2011b, Monteiro-Riviere *et al.*, 2011, Sharma *et al.*, 2011). Despite the dark contrast of these areas on the micrograph, visual interpretation at increased magnification observed a textured appearance and distinctly non-organic morphology for each of the electron dense 'shapes'. Visualisation matched with other observations of internalised metal oxide nanoparticles (Jin *et al.*, 2008, Kreyling *et al.*, 2002, Kroll *et al.*, 2009, Mortensen *et al.*, 2008, Patri *et al.*, 2009, Shvedova *et al.*, 2003). Under the conditions of *in vitro* exposure, the ZnO nanomaterial was thought to agglomerate (Table 3.1), which may account for the approximate 1μm electron dense regions. At this size, ZnO agglomerates would have been too large to navigate the tightly packed paracellular transport pathways in keratinised tissue (des Rieux *et al.*, 2006). Locations of the suspected ZnO nanomaterial agglomerates were predominantly noted within

individual cells, supporting the view of localised uptake via a transcellular pathway, and not between the extracellular spaces of apical cells. In addition, incidents of electron dense regions remained confined to tissue model samples dosed with nanomaterial ZnO's, and not bulk particles. This observation would imply transcellular uptake to be nano-size specific.

With regards to their application in future oral healthcare formulations, internalised ZnO at the apical surface cells may not constitute an increased risk of cytotoxicity or potential for systemic translocation. This is despite the greater cytotoxic action of the ZnO nanomaterials observed here leading to more significant damage in the RHO models, and considered a consequence of the different keratinisation pathway followed by apical cells (Squier & Wertz, 1993, Wertz & Squier, 1991). Both keratinised and non-keratinised 3-D models displayed signs of desquamation, a protective mechanism exhibited by keratinised oral tissue *in situ*. Cell layers corresponding to signs of cytotoxicity, and even correlated with suspected nanomaterial internalisation (ZnO-45009 sample imaged in Figure 6.13) were observed 'sloughing off' away from the rest of the tissue. This protective mechanism, has been reported to absolve concerns of nanoparticle ZnO and TiO_2 penetration through all but the uppermost cell layers in human skin, when utilised in sunscreen products (Gulson *et al.*, 2010, Lademann *et al.*, 1999, Maynard, 2007a, Nohynek *et al.*, 2010, Park *et al.*, 2011). It is expected that this mechanism also protects the tissues of the oral mucosa from exogenous noxious or therapeutic substances (Dale *et al.*, 1990), such as oral healthcare constituents.

SDS, however, is a widely formulated surfactant agent in oral healthcare products that aids dispersion of other constituents during delivery (Newby *et al.*, 2011). It is also known to cause localised inflammation following exposure ((EU), 2013, di Nardo *et al.*, 1996) and increase the permeability of oral mucosal tissues (Healy *et al.*, 2000). Other detergents (adinol, Tego Betain and Pluronic) formulated in toothpastes have also been reported to reduce the cell viability of a keratinised cell line (OKF6) alongside SDS, and have been speculated to aggravate inflammation, weaken cell turnover and thus render the oral mucosa at risk of oral ulceration (Moore *et al.*, 2008). Nanomaterials formulated alongside other common constituents could profit from increased permeation thought a consequence of the loss of cell layers, or mucosal injury, in much the same way as hair follicles and injured skin pose a greater risk to the uptake of nanomaterials in sunscreens ((SCENIHR), 2006, Lademann *et al.*, 2006, Monteiro-Riviere *et al.*, 2011). However, the

complex interactions expected to occur between nanomaterials and other formulation constituents may also prove as unpredictable as their nano-scale properties.

Surface coatings such as PEGs, have been employed to improve stability in nanomaterial dispersions and are widely utilised in cosmetics (including toothpastes) for similar reasons (Fruijtier-Pölloth, 2005). Surface coatings have been demonstrated to reduce surface reactivity, and instances, cytotoxicity as a consequence (Ryman-Rasmussen *et al.*, 2007, Tsuji *et al.*, 2006). They have also been found to modify uptake characteristics, often manipulated to enhance drug delivery (Lipka *et al.*, 2010, Shah *et al.*, 2012). PEGs are used due to their low toxicity and do not readily penetrate the skin (Fruijtier-Pölloth, 2005). Their inclusion alongside nanomaterial constituents, may avoid the risks associated with nanomaterial uptake. Similarly, alcohols such as ethanol are common constituents in many commercially available mouthwashes (Koschier *et al.*, 2011) and have experienced safety concerns through regular exposure in their own right (Moharamzadeh *et al.*, 2009). During characterisation, ethanol was used here due to reports of its universal solvent properties aiding dispersion of nanoparticles, to stop mass agglomeration (Krebs *et al.*, 2008). In doing so, it can be expected to increase the proportion of individual nanoparticles and enhance nano-specific properties when formulated together. Yet contrary to fears, alcohol containing mouthwashes have not been demonstrated to increase cytotoxicity or permeability of exogenous substances, when tested using a similar *in vitro* oral buccal mucosal construct (Koschier *et al.*, 2011). Even SDS has been observed to lose its ability to increase the permeability of ventricle tongue mucosa in the presence of zinc and Triclosan (Healy *et al.*, 2000).

Nanomaterial interactions within the environment are now known to be important factors governing by there properties. There is no doubt that formulation constituents would form strong interactions at the nanoparticle surface, effecting their cytotoxic and uptake profiles when delivered to the oral mucosal tissues as a complete oral healthcare product. However, this is a complicated area of chemistry, which is in its infancy regarding investigations involving nanomaterials (Nel *et al.*, 2009). As a preliminary risk assessment, this study focused upon the interactions of unmodified nanomaterials within the *in vitro* environments.

6.2.4 Nanomaterial uptake potential summary

Results reported within this chapter show SiO_2 nanoparticles (SigmaAldrich bulk and nanomaterial products) to be the only materials linked to internalisation within oral epithelial monolayers. Hydroxyapatite and TiO_2 materials were not found to have increased styryl dye fluorescence, associated with increased endocytosis of materials into the cell. ZnO nanomaterial uptake potential remained inconclusive, due to no fluorescence-linked-internalisation being observed during uptake screening with SynaptoGreen™, but agglomerates of nanomaterial were speculated to have internalised within both keratinised and non-keratinised cells of the 3-D models. Transcellular pathways were considered the predominant mechanism of nanomaterial internalisation, as no evidence of paracellular transport was observed in the study (limited to investigating ZnO materials only). The result for each nanomaterial's uptake potential, taken in context alongside their cytotoxicity profiles, suggest hydroxyapatite and TiO_2 nanomaterials to constitute the lowest risk if moved forward in the research to exploit them in future oral healthcare formulations. However, due to the many uptake routes available in the oral mucosal tissues, especially non-keratinised regions, further investigation would be required to more fully evaluate their potential uptake. The assay developed within this chapter, may prove a useful screening tool, however it only explores one set of transport mechanisms that form the different endocytotic uptake routes for cellular internalisation. Crucially, it may prove limited with regard to risk assessment with the mechanism of fluorescent detection breaking down upon cell lysis: a pivotal mechanism of cytotoxicity.

SiO_2, despite proving non-cytotoxic under the *in vitro* conditions of exposure investigated here, would also constitute further investigation into the long term effects of exposure and speculated cellular internalisation. This is especially important for reputed potential inclusion in future oral healthcare formulations, where routine exposure would be expected through adoption of a daily oral hygiene regime ((BDHF), 2013).

Cytotoxicity combined with inconclusive uptake assessment would be cause enough for additional investigation into the effects of ZnO nanomaterial inclusion in oral healthcare formulations. It may be expected that additional constituents may limit the effects of their surface reactivity, speculated from their increased ability to generate ROS as nanoparticles (Bozym *et al.*, 2010, Cooper, 2008, Hackenberg *et al.*, 2011b,

Hsiao & Huang, 2011, Sharma *et al.*, 2012, Xia *et al.*, 2008). However, the surface interactions that govern the behaviour of nanomaterials and mechanism of internalisation, is a complex area that is only beginning to be explored in relation to biological environments (Nel *et al.*, 2009). To begin with, future work would have to fully elicit the potential for uptake into oral mucosal tissues, as speculated from the TEM micrographs reported here. TEM in combination with EDS would provide a simple answer, but it may take some time for studies to fully decipher the mechanism of uptake using simplified *in vitro* biological models and longer still in extrapolating the data from these studies to be able to predict with any degrees of certainty associated with the effects *in situ* (Stone *et al.*, 2010). Yet the results reported here do serve as a novel contribution to knowledge, as a preliminary risk assessment of nanomaterial interactions in the oral mucosa: an area of the body currently devoid of investigation from a nanotoxicology perspective.

7 GENERAL DISCUSSIONS AND CONCLUSIONS

This study set out to evaluate the risk of nanomaterial interactions with the human oral mucosae, based on wide-spread reporting of exposure to nanoparticles (<100nm) leading to toxic events not experienced by exposure to their non-nano (bulk) counterpart materials (Borm *et al.*, 2006, Kreyling *et al.*, 2006a, Nel *et al.*, 2006, Oberdorster *et al.*, 2005b). Establishing the risk of nanomaterials to this area of the body was important due to current gaps in knowledge related to their fate within the oral mucosa. With the increased development of nanotechnology, it is predicted that inclusion of nanoparticles within many products will only become even more wide-spread (Buzea *et al.*, 2007, Faunce, 2008, Oberdorster *et al.*, 2005b, Tsuji *et al.*, 2006, Whitesides, 2005). Cosmetics hold the most patents involving nanomaterial applications (Kimbrell, 2006, Raj *et al.*, 2012), linked to their novel properties and improved efficacy in comparison to existing bulk composites (Mihranyan *et al.*, 2012). Nano-hydroxyapatite, SiO_2, TiO_2 and ZnO nanomaterials are all reputedly of interest in future oral healthcare formulations and this would result in exposure to the oral mucosa. To ascertain the plausibility of their development, it was first important to apply a 'weight of evidence' approach through an integrated testing strategy to fully evaluate their risk. The experiments within the investigation here, contribute to address the absence of toxicity studies involving exposure at the human oral mucosa to nanomaterials. They were carried out specifically from the perspective of a preliminary risk assessment, to an area of the body hypothesised as being more susceptible to nanoparticle uptake (and related cytotoxicity) (Campisi *et al.*, 2010).

7.1 Study conclusions

Findings from this study have contributed the following conclusions.

(i) Hydroxyapatite and TiO_2 nanomaterials pose the lowest potential risk to the health of oral mucosal tissues, with an absence in cytotoxicity observed across all models. No internalisation of particles was detected using the FM1-43 assay developed.

(ii) SiO_2 nanomaterials are non-cytotoxic according to current cytotoxicity testing protocols, but evidence of particle internalisation was suggested, when assaying

endocytotic uptake using FM1-43 fluorescent dye. These results require further attention to fully extrapolate the risk of SiO_2 nanoparticle internalisation.

(iii) ZnO nanoparticles pose the greatest risk to oral mucosal tissues and may elicit a more severe inflammatory response. The status of their internalisation remains unknown, and until it is established, the nanomaterial forms of this material constitute a potential risk.

(iv) Consistent with literature, non-keratinised tissue was found to experience greater cytotoxicity at similar doses than the more robust keratinised epithelium. This was concluded following study using 3-D tissue models that demonstrated less sensitivity when compared to the H376 monolayer cell line, hypothesised as being more representative to the stratified nature of the oral mucosa *in situ*.

(v) Overall, nano-formulations were not though to pose a greater risk over bulk composites of the material purely through the basis of the reduction in particle size <100nm, as demonstrated by the cytotoxicity of ZnO-bulk. Nano-characteristics are therefore hypothesised as being highly complex, with dynamic physio-chemical factors governing the materials' properties, which may only remain consistent within a set environment.

These assessments are derived from the outcomes of experimental work carried out within this investigation. The study can be described as having been successful in answering the three main research questions stated within the aims. It was demonstrated that both SiO_2 and ZnO nanoparticles posed a greater risk to tissues of the oral mucosa than bulk counterpart materials. This was observed through the greater potential internalisation and cytotoxicity of SiO_2 and ZnO nanomaterials respectively. The study did not fully reveal the mechanistic details of *how* the nanomaterial forms affected the *in vitro* models differently to bulk materials. It was thought, however, that the smaller particle size enabled SiO_2 nanoparticles to fit inside membrane invaginations, likely to be linked to greater incidental internalisation of materials into monolayer cells. For ZnO materials risk, increased cytotoxicity was observed at the nano-scale and was likely a consequence of increased ease of free ion release related to greater surface reactivity. These resulting outcomes, especially when linked to the possible uptake potential, would warrant the investigation to be taken further, for full

evaluation as to the extent of related toxicity and dose determination of nanoparticle penetration.

Through attempts to answer the key research questions, the initial aims of the study were met with regards to fully characterising the nanomaterials in relation to bulk composites, and changes in behaviour associated with the type of media delivery *in vitro*. This enabled the successful screening of cytotoxicity, in identifying discreet differences between the effects of material interactions following exposure simulating single dose applications of an oral healthcare ingredient. Whilst only partially fulfilling the aim of linking nano-specific properties with the risk pathway, mechanisms of cytotoxic action could be hypothesised from the data. In doing so, cytotoxicity testing was carried out successfully without the use of animals, and 3-D models were demonstrated to have better represented native tissue robustness than the monolayer cells. Therefore, *in vitro* studies possess the potential to contribute to the risk assessment of substances coming into contact with the oral mucosa, in the same way fully validated skin models have for topical irritancy testing ((ECVAM), 2009, Spielmann *et al.*, 2007).

7.2 Experimental limitations of the study

Despite contributing to further the knowledge of nanomaterial interactions within the oral mucosa, difficulties associated with applied research were encountered, limiting some aspects of the investigation.

7.2.1 Difficulties associated with accurate nanoparticle characterisation

The nano-size range is used to confer the nanomaterial definition on a wide variety of different materials. Grouping such a diverse range of materials is always going to prove challenging when attempting to identify common themes or attributes that govern their behaviour. Arguably, this has proved more difficult due to unpredictable properties arising at the nano-scale. Furthermore, many characteristics are thought to contribute to nanomaterial properties but may only be specific under certain environmental conditions *i.e.* solvent, concentration or ionic composition *(Nel et al., 2006)*. This was demonstrated by the difficulty in even defining 'nano' status when measuring particle size here. No one measurement technique could accurately represent the true size characteristic of any of the nanomaterials studied (Linsinger *et al.*, 2012b). The extent of polydispersity or lack of homogeneity in particle morphology within each sample played

a role in size ranges measured, yet even reporting the average particle size was inappropriate for characterisation carried out in dynamic solutions more representative of the physiological environment. Using DLS and NTA to report particle size distributions was also fraught with problems, linked with the tendency for nanomaterial dispersions to agglomerate and flocculate in biological media (Allouni *et al.*, 2009, Murdock *et al.*, 2008, Oostingh *et al.*, 2011). These are not problems unique to the methods carried out within this study. Instead, these are problems experienced by the whole field of nanotoxicology, charged with accurate characterisation of complex physiochemical characteristics in even more complex and dynamic biological environments. Thus, currently there exists no identified nano-specific attributes that have firmly linked to specific cytotoxic actions across common exposure scenarios, and it is recommended that nanotoxicity must be carried out on a case by case basis ((SCENIHR), 2009). Key to these studies is accurate characterisation, and crucially the reporting of these in context, alongside the analysis conditions (Borm *et al.*, 2006). Collaborative initiatives are now underway, with the aim of reaching consensus on the priority of which key physiochemical characteristics to report with regards to nanotoxicology (Stone *et al.*, 2010). As yet, the most advanced report has evaluated the use of 8 separate techniques to measure the nanoparticle size characteristic alone, but failed to fully recommend the implementation of any one specific strategy (Linsinger *et al.*, 2012b).

Characterisation carried out here resulted in the surprising discovery that the SigmaAldrich sourced SiO_2 material, intended as the bulk control for SiO_2, contained nanoparticles as small in size as that of the distinct nano product. This result emphasises the importance of thorough characterisation, but also demonstrates the need for accurate nanoparticle standards that can be used as controls in nanotoxicology studies. A consensus was reached into the priority of candidates put forward for development, including TiO_2 (Aitken *et al.*, 2008), but the inherent difficulty in working at the nano-scale has meant their utilisation remains limited, through both the range available and their standardisation under different environments (Stefaniak *et al.*, 2013).

The use of suitable controls remains crucial to any scientific experiment, and in the lack of available *nano* reference materials, this study relied upon comparisons of nanomaterials to bulk-scale counterparts. SEM micrographs revealed potential problems with this approach, under the characterisation techniques used. Disparity between the

particle morphology of bulk and nano-hydroxyapatite was clearly observed relating to crystalline structure. This may have important consequences regarding nanotoxicology, with different forms of a chemical material having distinct toxicity profiles. An applicable example can be demonstrated between the respective differences in cytotoxicity of rutile and anatase TiO_2 particles (Hsiao & Huang, 2011, Park *et al.*, 2011, Yin *et al.*, 2012). Despite the employment of all nano-characterisation techniques available to the project, future work would have to include analysis into chemical composition and crystal structure, to determine that accurate comparisons were made between the bulk and nanomaterial varieties of each compound *e.g.* X-ray diffraction.

Related to accurate comparison between bulk and nanomaterial effects, the issue of dose has proved a complex parameter to measure in relation to nanotoxicology (Oberdorster *et al.*, 2007). The expression of dose as a weight per volume percent of material in solution remains the easiest comparison in relation to working with colloidal systems. However, in terms of particle number, there is obviously a disparity between the concentrations expressed as particles in a nanomaterial over their bulk material equivalents. Due to reports in the literature of nanoparticle characteristics affording them novel effects (*e.g.* large surface areas), other expressions of dose may prove more applicable under certain conditions (Borm *et al.*, 2006, Oberdorster *et al.*, 2007). For example, relative surface area may prove a more accurate comparison into the influence of nanoparticle size on the increased cytotoxicity observed between ZnO materials, with morphology and dispersion characteristics remaining constant between the bulk and nano-scale. A greater particle surface area has been linked to increased ion release implicated in ROS generation that has been linked to the cytotoxic action of ZnO nanoparticles (Jeong *et al.*, 2013, Sharma *et al.*, 2012, Xia *et al.*, 2008). Branauer-Emmett-Teller (BET) analysis should be considered for investigations into the specific surface area of the solid material's particles. This technique measures the precise molar volume of a gas (normally nitrogen) able to adsorb to the surface of the particles. Nitrogen intrusion porosimetry is an analytical technique expected to compliment other characterisation areas (Lewicka *et al.*, 2013).

7.2.2 In vitro models and the current limitations of toxicity testing

Overall the use of the models representative of the human oral mucosa proved pertinent to investigating the main research questions posed. Few oral epithelial human cell lines are currently available for such studies. Healthy non-keratinised primary tissue

is particularly difficult to obtain, requiring invasive punch biopsies subject to large variation between donors. *Gingiva*/keratinised primary tissue is more readily available (as surgical trimmings from non-invasive dental procedures) but were not considered for initial investigations. Development and characterisation of a suitable gingival model was beyond the focus of this work. In addition, gingival tissues undergo the process of keratinised differentiation resulting in the formation of a tough stratum corneum around the exterior of apical cells devoid of organelles (Presland & Jurevic, 2002, Wertz & Squier, 1991). This structure closely resembles keratinocytes of the skin, and similarly would be expected to offer superior protective capabilities over non-keratinised cell types. It was thought more logical to begin investigating cytotoxicity of nanoparticles using a model more representative of the non-keratinised mucosa, because this counts for approximately 60% of the total surface area of all epithelial lining in the oral mucosa (Rossi *et al.*, 2005).

The H376 cell model proved useful for preliminary screening but suffers limitations in representing the full function of differentiated, multi-layered tissues, crucial for studying paracellular transport pathways. Monolayer culturing of many *in vitro* models suffer intrinsic limitations that fail to fully replicate all the protective mechanisms from *in situ* ordered tissue and organ topography. These include reduced robustness, imbalance of metabolic competence, lack of cell–cell interactions, destruction of organ topology and absence of tissue communication (Eisenbrand *et al.*, 2002). Immortalised cell lines suffer greater limitation, differing further from normal cellular metabolism to an increased uniformity in geno- and phenotype after transformation, to make them pragmatic to handle in the laboratory (Pan *et al.*, 2009). Toxicology studies *in vitro* prove useful in isolating specific mechanisms of action by a substance, or cytotoxic pathways that may be experienced in different areas of the body (Eisenbrand *et al.*, 2002). Here, the exact mechanisms of cytotoxicity were deliberately not investigated in favour of the more pressing risk related to nanomaterial internalisation. Many studies have been performed elucidating the role of ROS generation related to large nanoparticle surface areas, using similar *in vitro* models of the exposure site investigated (Heinlaan *et al.*, 2008, Huang *et al.*, 2010a, Huang *et al.*, 2010b, Hussain *et al.*, 2005, Karlsson *et al.*, 2008, Nel *et al.*, 2006, Xiao *et al.*, 2003). Yet extrapolation of these relatively simple investigations to fully evaluate representative exposure conditions *in situ*, remains difficult. This is demonstrated by differing cytotoxicity thresholds calculated through *in vitro* studies in comparison to different assessments when using *in vivo* models (Johnston *et al.*, 2010a).

The use of three different *in vitro* models complied with current cosmetic ingredient testing guidelines ((EU), 2013), whilst simultaneously constituted a tiered strategy approach in the risk assessment of nanomaterials through the use of more comprehensive 3-D models of the oral mucosal tissues. However, the methods employed largely follow a toxicity testing strategy intended for assessment of traditional 'bulk-scale' chemicals. In addition, further restrictions in full representation include the lack of consideration given to the physiological barriers of saliva and mucous layers, in the substantial protective mechanisms they are speculated to afford the human oral mucosa (Cone, 2009, Lendenmann *et al.*, 2000, Rossi *et al.*, 2005). Yet because translocation of nanomaterials has been reported following passage both through cells and tissue structures, uptake remains the primary concern related to risk following exposure. Therefore, the stratified nature of both 3-D models utilised in this study, meant that they were considered more representative to study transport pathways, over monolayer cells lines that are restricted to the study of transcellular mechanisms of nanoparticle internalisation.

3-D cell culture models better simulate the composition of extracellular matrix by using collagen or hyaluronic acid based scaffolds (Chen *et al.*, 2012, Pescosolido *et al.*, 2011), with selective incorporation of signalling factors, adhesion factors, and proteins (Rimann & Graf-Hausner, 2012). These constitute the formation of representative stratified cell layers, which influences cell communication and subsequently tissue function, all of which is more sophisticated in comparison to monolayer models. Evidence of this can be shown through the support of closely-related skin epithelial models gaining accreditation by the European Centre for the Validation of Alternative Methods (ECVAM), to replace animal models in the assessment of potentially corrosive and irritant materials ((ECVAM), 2009). The capabilities of organotypic 3-D models in replacing *in vivo* study of toxicology are improving; however, their potential for assessing translocation of nanoparticles is currently at an early stage. To the best of the author's knowledge, this study is the first to expose RHO and GIN-100 tissue models to nanoparticles. It was hypothesised that the stratified structure of 3-D models (and consequently the increased sophistication that is brought about by the more natural cell-cell interactions) would enable transport pathways and permeability of the models to closely resemble that of non-keratinised and keratinised regions of the oral mucosa respectively. This was supported through their acceptance in other dental material toxicological studies (Klausner *et al.*, 2007), including retention and adsorption through

the tissues (Yang *et al.*, 2011), in addition to observations from micrographs reported in this thesis (Figure 6.14) showing evidence of ZnO nanomaterial internalisation in both non-keratinised and keratinised tissue models. Future work is required to definitively identify the electron dense regions as Zn material. However, the positioning of speculated ZnO nanomaterials within the structures of the tissue sections correlates closely to what may have been predicated based upon knowledge of keratinisation differentiation, and the implications this has on epithelial morphology. Thorough phenotypic characterisation of both tissue models has been carried out by the suppliers, who report fully representative differentiated morphology, expression of native proteins, lipid profiles and other small molecule signalling that contribute similarities to their respective, native tissue-type (Kamzi *et al.*, 2011, Klausner *et al.*, 2007 and Moharamzadeh *et al.*, 2007). However, the transport pathways available require comprehensive characterisation.

The full, elucidated risk of nanoparticle uptake is not easily represented *in vitro*. Many current models, including those utilised here, are limited through the lack of systemic modelling and links to multiple exposure sites (a limitation frustrating the whole area of nanotoxicology). The legislation implemented by the EU to ban the testing of cosmetic ingredients in animal models has increased the pressure on researchers to develop increasingly sophisticated *in vitro* models (Hartung, 2009). State of the art designs are under development, known as "organs-on-chip" technology, speculated to reduce the gap in predictive substance testing prior to human exposure (Sonntag *et al.*, 2010). Although some way off validation, these novel approaches will be crucial for the future safe application of nanomaterial technologies designed for use in the body (Chan *et al.*, 2013). Where they may still fall short however, is in the current necessity to investigate the effects of multiple or extended exposure periods. Within this study, SiO_2 nanoparticle demonstrated the capacity for cell internalisation, with no cytotoxic response observed. Yet their hepatotoxicity has been observed over multiple dosing in animal *in vivo* studies (Nishimori *et al.*, 2009). This suggests that acute toxicity may not be the only risk requiring assessment in nanomaterial exposure, with their small size linked to increased uptake and subsequent chronic exposure and toxicity through bioaccumulation ((SCENIHR), 2009). As all nanomaterials investigated here were metal oxides, they are unlikely to degrade and could accumulate within the cell where uptake pathways exist (Fröhlich & Roblegg, 2012, Kreyling *et al.*, 2002, Sharma *et al.*, 2011, Thubagere & Reinhard, 2010). Therefore, the stratified 3-D models may still be of use

in suggested future work (question 4, below), if their time in culture can maintain integrity of tissue strucure over a longer duration, to enable multiple dosing that would mimic a typical oral healthcare regime.

Other sources of extracellular nanotoxicity have again involved their characteristic large and reactive surface properties, in particular their high binding capacity. This has been linked to reports of cytotoxicity through media constituent depletion and essentially cell starvation (Casey *et al.*, 2008, Elder *et al.*, 2009, Guo *et al.*, 2008, Hussain, 2009, Oberdorster *et al.*, 2005a), observed for both TiO_2 and ZnO nanomaterials (Horie *et al.*, 2009, Kroll *et al.*, 2009, Xiong *et al.*, 2013). However, this property is thought unlikely to be responsible for loss in cell viability reported here, where just a 5 minute and 1 hour exposure was investigated in the monolayer and 3-D models respectively. In comparison most other studies suggesting this prominent property of nanoparticle propensity for cytotoxicity applied extended exposure periods in excess of 24 hours before results were assessed. However, this property has to be considered in study design investigating long term exposure, especially if doubling time is low for the cell line; meaning reactive surface area can certainly be thought of as nanotoxic characteristic, despite their links to affording protective effects through the formation of a protein corona (as mentioned previously).

Examples in the current literature provide insight into the possible mechanisms involved in nanoparticle cytotoxicity. However, they remain speculative and due in part to incomplete links to particle characteristic evaluations. Like the emerging science of nanotoxicology, we are still in the early stages of understanding how nanoparticle characteristics elucidate interactions with their environment. This remains complicated when the nanoparticle is subjected to the complex internal molecular mechanisms provided by an *in vitro* cellular model, able to express toxicity via a number of pathways. These include the relatively simple measurement of cell death, through the cell viability and toxicology assays mentioned. However, the more intricate processes of a cells inflammatory response; involving cascades of complex cell signalling that is thought to occur under the oxidative stresses of nanoparticle-cell interactions, unravelling this requires a far more specific and sensitive design towards cytotoxic measurements. Through increased understanding and skilled application of knowledge, different inflammatory responses can be measured and related to a network of indicators that will help explain the mechanisms of nanoparticle toxicity. The tools for this type of research

are available and growing commercially now. Therefore, there is hope that the increase in data reporting can be amalgamated within databases that, in the future, may offer some predictive modelling of nanomaterial interactions, with their effects becoming more familiar.

7.3 Future study

The outstanding questions that remain from the risk assessment of nanomaterial exposure to the oral mucosa require further investigation to definitively address the lack of knowledge. These can be formulated as new research questions to direct future research:

1) What are the characteristics attributed to increased cytotoxicity of ZnO nanoparticles, compared to both bulk material response and with other metal oxide nanomaterials?

From this investigation, it was hypothesised to be the greater availability of free ions, or alternatively, to the presence of elongated ZnO nanoparticle shapes that influenced cytotoxicity. Future work could employ more characterisation methods, specifically BET analysis to determine surface area disparities between the bulk and nanomaterial forms. In doing so, dose metrics may be more appropriately compared using similar surface areas in cytotoxicity assays (Borm *et al.*, 2006). Furthermore, fluorescent and more recently luminescent based detection systems are now available to quantify the intracellular levels of specific ROS (*e.g.* superoxide, hydrogen peroxide and nitric oxide) (Held, 2010). The levels can be used narrow down the likely redox signalling pathway activated (Burhans & Heintz, 2009), to determine the state of the cell and which mechanisms are activated at particular times or in the presence of different stimuli (Rada & Leto, 2008) *i.e.* nanomaterial exposure (Moos *et al.*, 2010, Park & Park, 2009, Sharma *et al.*, 2009b, Thubagere & Reinhard, 2010, Zhu *et al.*, 2011).

2) Internalisation of SiO_2 nanoparticles – what mechanism of uptake may be responsible in oral mucosal models?

It was hypothesised here that SiO_2 nanoparticle uptake is a result of endocytosis internalisation (either pinocytosis or receptor-mediated, depending upon the formation and influence of a protein corona), of SiO_2 nanoparticles within vesicles that fluoresced

during the capture of SynaptoGreen™/FM®1-43 dye. Future work could follow the approach adopted by other studies investigating the mechanistic uptake of materials by systematically inhibiting specific transport pathways with drugs to elucidate the preferential route into the cell (Doherty & McMahon, 2009, Herd *et al.*, 2013, Orenbuch *et al.*, 2012). As studies advance into modelling the protein corona thought likely to accumulate at the reactive surfaces of nanoparticles, these maybe used to predict which interactions predominate at the sites of surface reception in different cell types (Cedervall *et al.*, 2007a, Faunce *et al.*, 2008, Nel *et al.*, 2009).

3) Does SynaptoGreen™/FM®1-43 fluorescence correspond to locations of nanoparticle internalisation?

The hypothesis was affirmative, as only cell exposure to SiO_2 nanoparticles correlated to an increase in intracellular vesicles over that of the baseline endocytosis (negative control). SiO_2 was characterised to have the smallest particle sizes in starting form, within the encasing limits of membrane invagination (Iversen *et al.*, 2011). Further experimentation could employ existing confocal microscopy methods developed here, with a fluorescent SiO_2 nanoparticle similar in characteristics to those determined for SiO_2 nanomaterials. Using different fluorescence emission markers, any overlapping regions corresponding to the fluorescent dye and the stryl dye would validate the assay for evaluating particle uptale. This has the potential for application in exploring the kinetics involved in uptake, using real time imaging, and could be developed to provide analysis of penetration using the 3-D models.

4) Does repeated exposure and internalisation cause increased cytotoxicity, or pose a risk to deeper particle penetration in tissues?

The experimental data cannot be extrapolated to form an accurate hypothesis for this question. But it is an important question relating to the regular exposure that can be expected through application of a daily oral hygiene regime, in light of both SiO_2 nanoparticle internalisation, and ZnO cytotoxicity. From the literature, it could be hypothesised to have an increased cytotoxic effect were bioaccumulation to occur (Kreyling *et al.*, 2009), but alternatively, this has not been observed in studies where removal mechanisms exist within *in vivo* systems (Gulson *et al.*, 2012). Within the constraints of the EU cosmetic directive, the 3-D *in vitro* models could be explored with regards to characterisation of their morphological integrity and application towards

multiple or repeat dosing, as has been attempted using topical application of *o*-cymen-5-ol and zinc on reconstructed human gingival tissue (Yang *et al.*, 2011). With regards to the ZnO cytotoxicity observed here, other inflammatory markers could be investigated to determine the extent or pathway of cytokine response. Chasing the cytokine response would help identify the cellular processes that manifest the morphological symptoms of cytotoxicity, as was observed in the RHO model (Figure 6.12). Alternatively, investigation using other molecular biology techniques, (*e.g.* polymerase chain reaction (PCR), gel electrophoresis and blotting) would enable more detection of more subtle changes in cellular mechanisms to determine specific pathways that may manifest following low level cytotoxicity over longer exposure periods. Preliminary experiments already carried out using Western blotting have shown ZnO nanomaterial exposure to H376 cells causes translocation of NF-$\varkappa$B to the nucleus, and the subsequent activation of apoptosis signals (data not reported). Exploring these mechanisms further would help consolidate the hypothesis linking increased Zn^{2+} ion release from nanomaterial forms of ZnO (measured using ICP-OES (Figure 5.8)), to greater levels of ROS and heightened oxidative stress that has resulted in apoptosis, as reported in similar studies (Bozym *et al.*, 2010, Yeh *et al.*, 2011).

7.4 Original contribution to research

Despite the remaining questions that have emanated from this work, it is important to stress the lack of studies regarding nanomaterial exposure to the human oral mucosa, especially relating to the more relevant nanomaterials investigated here, and from a toxicology perspective. Therefore, the work carried out in this study can be described as novel in the following three ways:

(i) It reports for the first time, the effects of nanomaterial exposure to the oral mucosa, including both keratinised and non-keratinised tissues.

(ii) It is the first study to utilise commercial 3-D tissue models of the oral mucosa, to evaluate nanomaterial cytotoxicity.

(iii) The development of a screening assay for evaluating nanomaterial uptake into cells.

8 REFERENCES

(BDHF). (2013). *Caring For My Teeth* [Online]. British Dental Health Foundation. Available: http://www.dentalhealth.org/tell-me-about/topic/caring-for-teeth/caring-for-my-teeth [Accessed 21st October 2013 2013].

(CIR). (2008). *SLS (Sodium Lauryl Sulfate), Sodium Laureth Sulfate, and Ammonium Laureth Sulfate Ingredient Alerts* [Online]. Washington DC: US Cosmetic Ingredient Review. Available: http://www.cir-safety.org/alerts.shtml [Accessed 18th August 2011].

(CORDIS). (2009). *Welcome to the Nanotechnology Homepage of the European Commission* [Online]. Brussels, Belgium: European Commission. Available: http://cordis.europa.eu/nanotechnology/home.html [Accessed 11th May 2010].

(EC) (2006). EC, Regulation (EC) No. 1907/2006 of the European Parliament and of the Council of 18 December 2006 concerning the Registration, Evaluation, Authorisation and Restriction of Chemicals (REACH), establishing a European Chemicals Agency, amending Directive 1999/45/EC and repairing Council Regulation (EEC) No. 793/93 and Commission Regulation (EC) No. 1488/94 as well as Council Directive 76/769/EEC and Commission Directives 91/155/EEC, 93/67/EEC, 93/105/EC and 2000/21/EC. **REACH, European Commission,** Luxembourg. 1907/2006.

(ECVAM) (2009). Statement on the performance under un ghs of three in-vitro assays for skin irritation testing. April. **European Commission,** Ispra, Italy. Institute for Health and Consumer Protection In vitro methods Unit April 1-7.

(EPA) (2005). Nanotechnology White Paper. **U.S. Environmental Protection Agency,** Washington D.C. USA. External review draft 1-134.

(EU). (2010). *Enterprise and industry: cosmetic directives* [Online]. Brussels: European Commission. Available: http://ec.europa.eu/consumers/sectors/cosmetics/documents/directive/index_en.htm [Accessed 17th June 2010].

(EU) (2011). Commission recommendation on the definition of a nanomaterial (2011/696/EU). *Official Journal (OJ) of the European Union: L 275,* **L275,** 38-40.

(EU) (2013). Cosmetics Directive 76/768/EEC. *Official Journal (OJ) of the European Union,* **L 262,** p. 169.

(FDA). (2009). *FDA Readies for More 'Nanoscale' Challenges* [Online]. Washington D.C, USA: US Food & Drug Administration. Available: http://www.fda.gov/ScienceResearch/SpecialTopics/Nanotechnology/ucm153723.htm [Accessed 7th May 2012 2010].

(FoE). (2006). *Nanomaterials, sunscreens and cosmetics: small ingredients, big risks – report* [Online]. Brussels, EU: Friends of the Earth. Available: http://www.foeeurope.org/activities/nanotechnology/index.htm [Accessed 15th May 2010].

(HSE). (2010). *Nanotechnology* [Online]. London: Health & Saftey Executive. Available: http://www.hse.gov.uk/horizons/nanotech.htm [Accessed 4th May 2010].

(ISO) (2008). Nanotechnologies -Terminology and definitions for nano-objects - Nanoparticle, nanofibre and nanoplate. **International Organization for Standardization,** Geneva, Switzerland. 27687:2008 7.

(ISO) (2010). Dentistry - Dentifrices - Requirements, test methods and marking. **Futokukai Foundation,** Tokyo, Japan.

(NIEHS) (2001). Evaluation of In Vitro Cytotoxicity Test Methods. **National Institute of Environmental Health Services,** North Carolina, USA. NIH Publication No. 01-4499 1-370.

(SCCP) (2007). Safety of nanomaterials in cosmetic products. **Scientific Committee on Consumer Products,** Brussels. 1147 07 1-63.

(SCENIHR) (2006). The appropriateness of existing methodologies to assess the potential risks associated with engineered and adventitious products of nanotechnologies. 10th March. **European Commission: Scientific committee on emerging and newly identified health risks,** Brussels, Belgium. 002 C7 1-79.

(SCENIHR) (2009). Risk assessment of products of nanotechnologies. 19th January. **European Commission: Scientific Committee on Emerging and Newly Identified Health Risk,** Brussels, Belgium. Directorate - General for Health & Consumers 1-71.

Addy, M. (2002). Dentine hypersensitivity: new perspectives on an old problem. *International Dental Journal,* **52,** 367-375.

Addy, M. & Smith, S. (2010). Dentin hypersensitivity: an overview on which to base tubule occlusion as a management concept. *The Journal of clinical dentistry,* **21,** 25.

Agarwal, A., Lariya, N., Saraogi, G., Dubey, N., Agrawal, H. & Agrawal, G. (2009). Nanoparticles as novel carrier for brain delivery: a review. *Current pharmaceutical design,* **15,** 917-925.

Ahmad, J., Ahamed, M., Akhtar, M. J., Alrokayan, S. A., Siddiqui, M. A., Musarrat, J. & Al-Khedhairy, A. A. (2012). Apoptosis induction by silica nanoparticles mediated through reactive oxygen species in human liver cell line HepG2. *Toxicology and Applied Pharmacology,* **259,** 160-168.

Aitken, R. J., Chaudhry, M. Q., Boxall, A. B. A. & Hull, M. (2006). Manufacture and use of nanomaterials: current status in the UK and global trends. *Occupational Medicine,* **56,** 300-306.

Aitken, R. J., Hankin, S. M., Lang Tran, C., Donaldson, K., Stone, V., Cumpson, P., Johnstone, J., Chaudhry, Q., Cash, S. & Garrod, J. (2008). A multidisciplinary approach to the identification of reference materials for engineered nanoparticle toxicology. *Nanotoxicology,* **2,** 71-78.

Al-Dlaigan, Y. H., Shaw, L. & Smith, A. J. (2002). Dental erosion in a group of British 14-year-old, school children. Part III: Influence of oral hygiene practises. *Br Dent J,* **192,** 526-530.

Al-Otaibi, M. & Angmar-Månsson, B. (2004). Oral hygiene habits and oral health awareness among urban Saudi Arabians. *Oral health & preventive dentistry,* **2,** 389-396.

Albanese, A. & Chan, W. C. W. (2011). Effect of Gold Nanoparticle Aggregation on Cell Uptake and Toxicity. *ACS Nano,* **5,** 5478-5489.

Alberts, B. 2002. *Molecular Biology of the Cell,* New York, Garland Science.

Alépée, N., Bessou-Touya, S., Cotovio, J., De Smedt, A., De Wever, B., Faller, C., Jones, P., Le Varlet, B., Marrec-Fairley, M. & Pfannenbecker, U. (2013). Cosmetics Europe multi-laboratory pre-validation of the SkinEthic™ reconstituted human corneal epithelium test method for the prediction of eye irritation. *Toxicology in Vitro.*

AlfaAesar. (2012). *45009 Zinc oxide, NanoShield® ZN-3008C, 50% in H2O, colloidal dispersion with cationic dispersant* [Online]. Johnson Matthey Company. Available: http://www.alfa.com/en/GP100W.pgm?DSSTK=045009&rnd=961181463 [Accessed 23rd February 2010].

Alfano, R. R., Ni, X. & Zevallos, M. (2007). Changing skin-color perception using quantum and optical principles in cosmetic preparations. **Google Patents**.

Alissawi, N., Zaporojtchenko, V., Strunskus, T., Hrkac, T., Kocabas, I., Erkartal, B., Chakravadhanula, V. S. K., Kienle, L., Grundmeier, G., Garbe-Schönberg, D. & Faupel, F. (2012). Tuning of the ion release properties of silver nanoparticles buried under a hydrophobic polymer barrier. *Journal of Nanoparticle Research,* **14,** 1-12.

Alkilany, A. & Murphy, C. (2010). Toxicity and cellular uptake of gold nanoparticles: what we have learned so far? *Journal of Nanoparticle Research,* **12,** 2313-2333.

Allaker, R. (2010). The use of nanoparticles to control oral biofilm formation. *Journal of dental research,* **89,** 1175-1186.

Allaker, R. P. & Memarzadeh, K. (2013). Nanoparticles and the control of oral infections. *International Journal of Antimicrobial Agents,* **In Press**.

Allouni, Z. E., Cimpan, M. R., Høl, P. J., Skodvin, T. & Gjerdet, N. R. (2009). Agglomeration and sedimentation of TiO2 nanoparticles in cell culture medium. *Colloids and Surfaces B: Biointerfaces,* **68,** 83-87.

Alvarez-Román, R., Naik, A., Kalia, Y. N., Guy, R. H. & Fessi, H. (2004). Skin penetration and distribution of polymeric nanoparticles. *Journal of Controlled Release,* **99,** 53-62.

Amaral, E., Guatimosim, S. & Guatimosim, C. 2011. Using the Fluorescent Styryl Dye FM1-43 to Visualize Synaptic Vesicles Exocytosis and Endocytosis in Motor Nerve Terminals. *In:* Chiarini-Garcia, H. & Melo, R. C. N. (eds.) *Light Microscopy.* Humana Press.

Andrews, G. P., Laverty, T. P. & Jones, D. S. (2009). Mucoadhesive polymeric platforms for controlled drug delivery. *European Journal of Pharmaceutics and Biopharmaceutics,* **71,** 505-518.

Antonelli, A., Sfara, C., Manuali, E., Bruce, I. J. & Magnani, M. (2011). Encapsulation of superparamagnetic nanoparticles into red blood cells as new carriers of MRI contrast agents. *Nanomedicine,* **6,** 211-223.

Applerot, G., Lipovsky, A., Dror, R., Perkas, N., Nitzan, Y., Lubart, R. & Gedanken, A. (2009). Enhanced Antibacterial Activity of Nanocrystalline ZnO Due to Increased ROS-Mediated Cell Injury. *Advanced Functional Materials,* **19,** 842-852.

Araújo, G. C. L., Gonzalez, M. H., Ferreira, A. G., Nogueira, A. R. A. & Nóbrega, J. A. (2002). Effect of acid concentration on closed-vessel microwave-assisted digestion of plant materials. *Spectrochimica Acta Part B: Atomic Spectroscopy,* **57,** 2121-2132.

Armstrong, B. L., Sensat, M. L. & Stoltenberg, J. L. (2010). Halitosis: a review of current literature. *Journal of Dental Hygiene,* **84,** 65-74.

Asati, A., Santra, S., Kaittanis, C. & Perez, J. M. (2010). Surface-Charge-Dependent Cell Localization and Cytotoxicity of Cerium Oxide Nanoparticles. *ACS Nano,* **4,** 5321-5331.

AshaRani, P. V., Low Kah Mun, G., Hande, M. P. & Valiyaveettil, S. (2008). Cytotoxicity and Genotoxicity of Silver Nanoparticles in Human Cells. *ACS Nano,* **3,** 279-290.

Attin, T., Knöfel, S., Buchalla, W. & Tütüncü, R. (2001). In situ evaluation of different remineralization periods to decrease brushing abrasion of demineralized enamel. *Caries research,* **35,** 216-222.

Auffan, M., Rose, J., Wiesner, M. R. & Bottero, J.-Y. (2009). Chemical stability of metallic nanoparticles: A parameter controlling their potential cellular toxicity in vitro. *Environmental Pollution,* **157,** 1127-1133.

Axford, S. E., Ogden, G. R., Stewart, A. M., Saleh, H. A., Ross, P. E. & Hopwood, D. (1999). Fluid phase endocytosis within buccal mucosal cells of alcohol misusers. *Oral Oncology,* **35,** 86-92.

Ayehunie, S., Cannon, C., Lamore, S., Kubilus, J., Anderson, D. J., Pudney, J. & Klausner, M. (2006). Organotypic human vaginal-ectocervical tissue model for irritation studies of spermicides, microbicides, and feminine-care products. *Toxicology in Vitro,* **20,** 689-698.

Babson, A. L. & Phillips, G. E. (1965). A rapid colorimetric assay for serum lactic dehyurogenase. *Clinica Chimica Acta,* **12,** 210-215.

Bacchetta, R., Moschini, E., Santo, N., Fascio, U., Del Giacco, L., Freddi, S., Camatini, M. & Mantecca, P. (2013). Evidence and uptake routes for Zinc oxide nanoparticles through the gastrointestinal barrier in Xenopus laevis. *Nanotoxicology,* **7,** 1-17.

Balásházy, I., Hofmann, W., Farkas, Á. & Madas, B. G. (2008). Three-Dimensional Model for Aerosol Transport and Deposition in Expanding and Contracting Alveoli. *Inhalation Toxicology,* **20,** 611-621.

Balasubramanian, S. K., Jittiwat, J., Manikandan, J., Ong, C.-N., Yu, L. E. & Ong, W.-Y. (2010). Biodistribution of gold nanoparticles and gene expression changes in the liver and spleen after intravenous administration in rats. *Biomaterials,* **31,** 2034-2042.

Balharry, D., Sexton, K. & BéruBé, K. A. (2008). An in vitro approach to assess the toxicity of inhaled tobacco smoke components: Nicotine, cadmium, formaldehyde and urethane. *Toxicology,* **244,** 66-76.

Balkwill, F. R. & Burke, F. (1989). The cytokine network. *Immunology Today,* **10,** 299-304.

Barillet, S., Simon-Deckers, A., Herlin-Boime, N., Mayne-L'Hermite, M., Reynaud, C., Cassio, D., Gouget, B. & Carrière, M. (2010). Toxicological consequences of TiO₂, SiC nanoparticles and multi-walled carbon nanotubes exposure in several mammalian cell types: an in vitro study. *Journal of Nanoparticle Research,* **12,** 61-73.

Barkvoll, P. (1989). Should toothpastes foam? Sodium lauryl sulfate--a toothpaste detergent in focus. *Nor Tannlaegeforen Tid,* **99,** 82-4.

Barlow, P., Brown, D., Donaldson, K., MacCallum, J. & Stone, V. (2008). Reduced alveolar macrophage migration induced by acute ambient particle (PM₁₀) exposure. *Cell Biology and Toxicology,* **24,** 243-252.

Baroli, B., Ennas, M. G., Loffredo, F., Isola, M., Pinna, R. & Lopez-Quintela, M. A. (2007). Penetration of Metallic Nanoparticles in Human Full-Thickness Skin. *J Invest Dermatol,* **127,** 1701-1712.

Basketter, D. A., Angelini, G., Ingber, A., Kern, P. S. & Menné, T. (2003). Nickel, chromium and cobalt in consumer products: revisiting safe levels in the new millennium. *Contact Dermatitis,* **49,** 1-7.

Bauer, I., Li, S.-P., Han, Y.-C., Yuan, L. & Yin, M.-Z. (2008). Internalization of hydroxyapatite nanoparticles in liver cancer cells. *Journal of Materials Science: Materials in Medicine,* **19,** 1091-1095.

Belade, E., Armand, L., Martinon, L., Kheuang, L., Fleury-Feith, J., Baeza-Squiban, A., Lanone, S., Billon-Galland, M.-A., Pairon, J.-C. & Boczkowski, J. (2012). A comparative transmission electron microscopy study of titanium dioxide and carbon black nanoparticles uptake in human lung epithelial and fibroblast cell lines. *Toxicology in Vitro,* **26,** 57-66.

Ben-Dov, N. & Korenstein, R. (2012). Enhancement of Cell Membrane Invaginations, Vesiculation and Uptake of Macromolecules by Protonation of the Cell Surface. *PLoS ONE,* **7,** e35204.

Benali, R., Pierrot, D., Zahm, J., De Bentzmann, S. & Puchelle, E. (1994). Effect of extracellular ATP and UTP on fluid transport by human nasal epithelial cells in culture. *American journal of respiratory cell and molecular biology,* **10,** 363-368.

Bercu, J. P., Hoffman, W. P., Lee, C. & Ness, D. K. (2008). Quantitative assessment of cumulative carcinogenic risk for multiple genotoxic impurities in a new drug substance. *Regulatory Toxicology and Pharmacology,* **51,** 270-277.

Berg, J. M., Ho, S., Hwang, W., Zebda, R., Cummins, K., Soriaga, M. P., Taylor, R., Guo, B. & Sayes, C. M. (2010). Internalization of Carbon Black and Maghemite Iron Oxide Nanoparticle Mixtures Leads to Oxidant Production. *Chemical Research in Toxicology,* **23,** 1874-1882.

Berg, J. M., Romoser, A., Banerjee, N., Zebda, R. & Sayes, C. M. (2009). The relationship between pH and zeta potential of ~ 30 nm metal oxide nanoparticle suspensions relevant to in vitro toxicological evaluations. *Nanotoxicology,* **3,** 276-283.

Berg, M. J., Romoser, A. A., Figueroa, D. E., West, S. C. & Sayes, C. M. (2012). Comparative cytological responses of lung epithelial and pleural mesothelial cells following *in vitro* exposure to nanoscale SiO_2. *Toxicology in Vitro,* **27,** 24-33.

Berger, A. (2000). Th1 and Th2 responses: what are they? *BMJ,* **321,** 424.

Berger, M. (2006). *Nanotechnology - in my toothpaste...?* [Online]. Berlin: Nanowerk, LLC. Available: http://www.nanowerk.com/spotlight/spotid=1091.php [Accessed 18th November 2010].

Bernhofer, L. P., Seiberg, M. & Martin, K. M. (1999). The Influence of the Response of Skin Equivalent Systems to Topically Applied Consumer Products by Epithelial--Mesenchymal Interactions. *Toxicology in Vitro,* **13,** 219-229.

Berridge, M. V. & Tan, A. S. (1993). Characterization of the Cellular Reduction of 3-(4,5-dimethylthiazol-2-yl)-2,5-diphenyltetrazolium bromide (MTT): Subcellular Localization, Substrate Dependence, and Involvement of Mitochondrial Electron Transport in MTT Reduction. *Archives of Biochemistry and Biophysics,* **303,** 474-482.

Berthiaume, F., Maguire, T. J. & Yarmush, M. L. (2011). Tissue engineering and regenerative medicine: history, progress, and challenges. *Annu Rev Chem Biomol Eng,* **2,** 403-30.

Bertrand, C. A., Laboisse, C., Hopfer, U., Bridges, R. J. & Frizzell, R. A. (2006). Methods for detecting internalized, FM 1-43 stained particles in epithelial cells and monolayers. *Biophys J,* **91,** 3872-83.

BeruBe, K., Balharry, D., Sexton, K., Koshy, L. & Jones, T. (2007). Combustion-derived nanoparticles: mechansims of pulmonary toxicity. *Clinical and Experimental Pharmacology and Physiology,* **34,** 1044-1050.

Besic Gyenge, E., Darphin, X., Wirth, A., Pieles, U., Walt, H., Bredell, M. & Maake, C. (2011). Uptake and fate of surface modified silica nanoparticles in head and neck squamous cell carcinoma. *Journal of Nanobiotechnology,* **9,** 32.

Betha, R., Pavagadhi, S., Sethu, S., Hande, M. P. & Balasubramanian, R. (2012). Comparative *in vitro* cytotoxicity assessment of airborne particulate matter emitted from stationary engine fuelled with diesel and waste cooking oil-derived biodiesel. *Atmospheric Environment,* **61,** 23-29.

Bettinelli, M., Beone, G. M., Spezia, S. & Baffi, C. (2000). Determination of heavy metals in soils and sediments by microwave-assisted digestion and inductively

coupled plasma optical emission spectrometry analysis. *Analytica Chimica Acta,* **424,** 289-296.

Betz, W. & Bewick, G. (1992). Optical analysis of synaptic vesicle recycling at the frog neuromuscular junction. *Science,* **255,** 200-203.

Betz, W. J. & Angleson, J. K. (1998). The synaptic vesicle cycle. *Annual Review of Physiology,* **60,** 347-363.

Betz, W. J., Mao, F. & Smith, C. B. (1996). Imaging exocytosis and endocytosis. *Current Opinion in Neurobiology,* **6,** 365-371.

Bhanushali, M., Bagale, V., Shirode, A., Joshi, Y. a. & Kadam, V. (2010). An in-vitro toxicity testing - a reliable alternative to toxicity testing by reduction, replacement and refinement of animals. *International Journal of Advances in Pharamaceutical Sciences,* **1,** 15-31.

Bhattacharya, K., Davoren, M., Boertz, J., Schins, R. P., Hoffmann, E. & Dopp, E. (2009). Titanium dioxide nanoparticles induce oxidative stress and DNA-adduct formation but not DNA-breakage in human lung cells. *Part Fibre Toxicol,* **6,** 17.

Bihari, P., Vippola, M., Schultes, S., Praetner, M., Khandoga, A. G., Reichel, C. A., Coester, C., Tuomi, T., Rehberg, M. & Krombach, F. (2008). Optimized dispersion of nanoparticles for biological in vitro and in vivo studies. *Particle and Fibre Toxicology,* **5,** 14.

Bleeker, E. A. J., de Jong, W. H., Geertsma, R. E., Groenewold, M., Heugens, E. H. W., Koers-Jacquemijns, M., van de Meent, D., Popma, J. R., Rietveld, A. G., Wijnhoven, S. W. P., Cassee, F. R. & Oomen, A. G. (2013). Considerations on the EU definition of a nanomaterial: Science to support policy making. *Regulatory Toxicology and Pharmacology,* **65,** 119-125.

Blinkhorn, A. S. (1978). Influence of social norms on toothbrushing behavior of preschool children. *Community Dentistry and Oral Epidemiology,* **6,** 222-226.

Bootz, A., Vogel, V., Schubert, D. & Kreuter, J. (2004). Comparison of scanning electron microscopy, dynamic light scattering and analytical ultracentrifugation for the sizing of poly(butyl cyanoacrylate) nanoparticles. *European Journal of Pharmaceutics and Biopharmaceutics,* **57,** 369-375.

Borm, P. J., Robbins, D., Haubold, S., Kuhlbusch, T., Fissan, H., Donaldson, K., Schins, R., Stone, V., Kreyling, W., Lademann, J., Krutmann, J., Warheit, D. & Oberdorster, E. (2006). The potential risks of nanomaterials: a review carried out for ECETOC. *Part Fibre Toxicol,* **3,** 11.

Boron, W. F. & Boulpaep, E. L. 2008. *Medical Physiology*, Elsevier Health Sciences.

Boulanger, N. (2009). *Le marché mondial des parfums et cosmétiques* [Online]. Paris: Eurostaf. Available: http://www.eurostaf.fr/fr/catalogue/etudes/sectorielles/luxe-mode-beaute/parfum-cosmetique/resume.html [Accessed 18th November 2010].

Boulos, S., Davis, T., Yang, J. A., Lohse, S. E., Alkilany, A. M., Holland, L. A. & Murphy, C. J. (2013). Nanoparticle-Protein Interactions: A Thermodynamic and Kinetic Study of The Adsorption of Bovine Serum Albumin to Gold Nanoparticle Surfaces. *Langmuir.*

Bourke, J., Abel, K., Huxham, G., Cooper, V. & Manley, S. (1999). UTP-preferring P2 receptor mediates inhibition of sodium transport in porcine thyroid epithelial cells. *British Journal of Pharmacology,* **127,** 1787-1792.

Bours, M. J., Troost, F. J., Brummer, R.-J. M., Bast, A. & Dagnelie, P. C. (2007). Local effect of adenosine 5'-triphosphate on indomethacin-induced permeability changes in the human small intestine. *European Journal of Gastroenterology & Hepatology,* **19,** 245-250 10.1097/MEG.0b013e328011093c.

Boverhof, D. & David, R. (2010). Nanomaterial characterization: considerations and needs for hazard assessment and safety evaluation. *Analytical and Bioanalytical Chemistry,* **396,** 953-961.

Bozym, R. A., Chimienti, F., Giblin, L. J., Gross, G. W., Korichneva, I., Li, Y., Libert, S., Maret, W., Parviz, M., Frederickson, C. J. & Thompson, R. B. (2010). Free zinc ions outside a narrow concentration range are toxic to a variety of cells in vitro. *Exp Biol Med (Maywood),* **235,** 741-50.

Brager, D. H., Luther, P. W., Erdélyi, F., Szabó, G. & Alger, B. E. (2003). Regulation of Exocytosis from Single Visualized GABAergic Boutons in Hippocampal Slices. *The Journal of Neuroscience,* **23,** 10475-10486.

Brown, D. M., Kanase, N., Gaiser, B., Johnston, H. & Stone, V. (2013). Inflammation and gene expression in the rat lung after instillation of silica nanoparticles: effect of size, dispersion medium and particle surface charge. *Toxicology Letters.*

Brunk, U., Collins, V. P. & Arro, E. (1981). The fixation, dehydration, drying and coating of cultured cells for SEM. *Journal of Microscopy,* **123,** 121-131.

Brunner, T. J., Wick, P., Manser, P., Spohn, P., Grass, R. N., Limbach, L. K., Bruinink, A. & Stark, W. J. (2006). In Vitro Cytotoxicity of Oxide Nanoparticles: Comparison to Asbestos, Silica, and the Effect of Particle Solubility. *Environmental Science & Technology,* **40,** 4374-4381.

BSI (2009). Water quality - Determination of selected elements by inductively coupled plasma optical emission spectrometry (ICP-OES) (ISO 11885:2007). **British Standards Institution,** London. 11885 2009 1-38.

Bulcke, F., Thiel, K. & Dringen, R. (2013). Uptake and toxicity of copper oxide nanoparticles in cultured primary brain astrocytes. *Nanotoxicology***,** 1-11.

Buono, C., Anzinger, J. J., Amar, M. & Kruth, H. S. (2009). Fluorescent pegylated nanoparticles demonstrate fluid-phase pinocytosis by macrophages in mouse atherosclerotic lesions. *The Journal of clinical investigation,* **119,** 1373.

Burhans, W. C. & Heintz, N. H. (2009). The cell cycle is a redox cycle: linking phase-specific targets to cell fate. *Free Radical Biology and Medicine,* **47,** 1282-1293.

Burke, F. T., Murray, M. & Shortall, A. (2005). Trends in indirect dentistry: 6. Provisional restorations, more than just a temporary. *Dental update: London,* **32,** 443.

Buseck, P. R., Cowley, J. M. & Eyring, L. R. 1988. *High-Resolution Transmission Electron Microscopy: And Associated Techniques*, Oxford University Press.

Buzea, C., Pacheco, I. I. & Robbie, K. (2007). Nanomaterials and nanoparticles: Sources and toxicity. *Biointerphases,* **2,** MR17-MR71.

Cai, Y., Liu, Y., Yan, W., Hu, Q., Tao, J., Zhang, M., Shi, Z. & Tang, R. (2007). Role of hydroxyapatite nanoparticle size in bone cell proliferation. *Journal of Materials Chemistry,* **17,** 3780-3787.

Campisi, G., Paderni, C., Saccone, R., Di Fede, O., Wolff, A. & Giannola, L. I. (2010). Human buccal mucosa as an innovative site of drug delivery. *Curr Pharm Des,* **16,** 641-52.

Cancello, R. & Clément, K. (2006). Review article: Is obesity an inflammatory illness? Role of low-grade inflammation and macrophage infiltration in human white adipose tissue. *BJOG: An International Journal of Obstetrics & Gynaecology,* **113,** 1141-1147.

Cannon, J. G. (2000). Inflammatory Cytokines in Nonpathological States. *News Physiol Sci,* **15,** 298-303.

Card, J. W., Zeldin, D. C., Bonner, J. C. & Nestmann, E. R. (2008). Pulmonary applications and toxicity of engineered nanoparticles. *American Journal of Physiology - Lung Cellular and Molecular Physiology,* **295,** L400-L411.

Carlson, M. W., Alt-Holland, A., Egles, C. & Garlick, J. A. 2001. Three-Dimensional Tissue Models of Normal and Diseased Skin. *Current Protocols in Cell Biology*. John Wiley & Sons, Inc.

Carterson, A. J., Höner zu Bentrup, K., Ott, C. M., Clarke, M. S., Pierson, D. L., Vanderburg, C. R., Buchanan, K. L., Nickerson, C. A. & Schurr, M. J. (2005). A549 Lung Epithelial Cells Grown as Three-Dimensional Aggregates: Alternative Tissue Culture Model for Pseudomonas aeruginosa Pathogenesis. *Infection and Immunity,* **73,** 1129-1140.

Casey, A., Herzog, E., Lyng, F. M., Byrne, H. J., Chambers, G. & Davoren, M. (2008). Single walled carbon nanotubes induce indirect cytotoxicity by medium depletion in A549 lung cells. *Toxicology Letters,* **179,** 78-84.

Cavet, M. E., West, M. & Simmons, N. L. (1996). Transport and epithelial secretion of the cardiac glycoside, digoxin, by human intestinal epithelial (Caco-2) cells. *British Journal of Pharmacology,* **118,** 1389-1396.

Cedervall, T., Lynch, I., Foy, M., Berggård, T., Donnelly, S. C., Cagney, G., Linse, S. & Dawson, K. A. (2007a). Detailed Identification of Plasma Proteins Adsorbed on Copolymer Nanoparticles. *Angewandte Chemie International Edition,* **46,** 5754-5756.

Cedervall, T., Lynch, I., Lindman, S., Berggård, T., Thulin, E., Nilsson, H., Dawson, K. A. & Linse, S. (2007b). Understanding the nanoparticle–protein corona using methods to quantify exchange rates and affinities of proteins for nanoparticles. *Proceedings of the National Academy of Sciences,* **104,** 2050-2055.

Cencič, A. & Langerholc, T. (2010a). Functional cell models of the gut and their applications in food microbiology—A review. *International journal of food microbiology,* **141,** S4-S14.

Cencič, A. & Langerholc, T. (2010b). Functional cell models of the gut and their applications in food microbiology — A review. *International Journal of Food Microbiology,* **141, Supplement,** S4-S14.

Ceresa, C., Nicolini, G., Rigolio, R., Bossi, M., Pasqua, L. & Cavaletti, G. (2013). Functionalized Mesoporous Silica Nanoparticles: A Possible Strategy to Target Cancer Cells Reducing Peripheral Nervous System Uptake. *Current medicinal chemistry,* **20,** 2589-2600.

Chan, C. Y., Huang, P.-H., Guo, F., Ding, X., Kapur, V., Mai, J. D., Yuen, P. K. & Huang, T. J. (2013). Accelerating drug discovery via organs-on-chips. *Lab on a Chip,* **13,** 4697-4710.

Chang, M., Klausner, M., Hladik, F., Lockhart, D. W., Ayehunie, S., Nittayananta, W. & Coombs, R. W. (2007). A Human Oral Tissue Model to Evaluate Toxicity and anti-HIV Activity of the Spermicide-Microbicide, Nonoxynol-9. *14th Conference on Retroviruses and Opportunistic Infections,* **Los Angeles, CA, USA**.

Chen, H.-H., Chien, C.-C., Petibois, C., Wang, C.-L., Chu, Y., Lai, S.-F., Hua, T.-E., Chen, Y.-Y., Cai, X., Kempson, I., Hwu, Y. & Margaritondo, G. (2011). Quantitative analysis of nanoparticle internalization in mammalian cells by high resolution X-ray microscopy. *Journal of Nanobiotechnology,* **9,** 14.

Chen, L., Xiao, Z., Meng, Y., Zhao, Y., Han, J., Su, G., Chen, B. & Dai, J. (2012). The enhancement of cancer stem cell properties of MCF-7 cells in 3D collagen scaffolds for modeling of cancer and anti-cancer drugs. *Biomaterials,* **33,** 1437-1444.

Cheng, N., Conway, J. F., Watts, N. R., Hainfeld, J. F., Joshi, V., Powell, R. D., Stahl, S. J., Wingfield, P. E. & Steven, A. C. (1999). Tetrairidium, a Four-Atom Cluster, Is Readily Visible as a Density Label in Three-Dimensional Cryo-EM Maps of Proteins at 10–25 Å Resolution. *Journal of Structural Biology,* **127,** 169-176.

Chiang, Y.-C., Chen, H.-J., Liu, H.-C., Kang, S.-H., Lee, B.-S., Lin, F.-H., Lin, H.-P. & Lin, C.-P. (2010). A novel mesoporous biomaterial for treating dentin hypersensitivity. *Journal of dental research,* **89,** 236-240.

Chithrani, B. D., Ghazani, A. A. & Chan, W. C. (2006). Determining the size and shape dependence of gold nanoparticle uptake into mammalian cells. *Nano letters,* **6,** 662-668.

Cho, E. C., Au, L., Zhang, Q. & Xia, Y. (2010). The Effects of Size, Shape, and Surface Functional Group of Gold Nanostructures on Their Adsorption and Internalization by Cells. *Small,* **6,** 517-522.

Cho, E. C., Xie, J., Wurm, P. A. & Xia, Y. (2009). Understanding the Role of Surface Charges in Cellular Adsorption versus Internalization by Selectively Removing Gold Nanoparticles on the Cell Surface with a I2/KI Etchant. *Nano Letters,* **9,** 1080-1084.

Cho, K.-H., Park, J.-E., Osaka, T. & Park, S.-G. (2005). The study of antimicrobial activity and preservative effects of nanosilver ingredient. *Electrochimica Acta,* **51,** 956-960.

Choi, J.-Y., Ramachandran, G. & Kandlikar, M. (2009). The Impact of Toxicity Testing Costs on Nanomaterial Regulation. *Environmental Science & Technology,* **43,** 3030-3034.

Choi, J., Lee, S., Na, H., An, K., Hyeon, T. & Seo, T. (2010). In vitro cytotoxicity screening of water-dispersible metal oxide nanoparticles in human cell lines. *Bioprocess and Biosystems Engineering,* **33,** 21-30.

Choo, H. P., Liew, K. Y. & Liu, H. (2002). Factors affecting the size of polymer stabilized Pd nanoparticles. *Journal of Materials Chemistry,* **12,** 934-937.

Chowdhury, I., Hong, Y. & Walker, S. L. (2010). Container to characterization: Impacts of metal oxide handling, preparation, and solution chemistry on particle stability. *Colloids and Surfaces A: Physicochemical and Engineering Aspects,* **368,** 91-95.

Collins, L. M. & Dawes, C. (1987). The surface area of the adult human mouth and thickness of the salivary film covering the teeth and oral mucosa. *J Dent Res,* **66,** 1300-2.

Comfort, K. K., Maurer, E. I., Braydich-Stolle, L. K. & Hussain, S. M. (2011). Interference of Silver, Gold, and Iron Oxide Nanoparticles on Epidermal Growth Factor Signal Transduction in Epithelial Cells. *ACS Nano,* **5,** 10000-10008.

Cone, R. A. (2009). Barrier properties of mucus. *Advanced Drug Delivery Reviews,* **61,** 75-85.

Conrad, D. R. (2008). *Intracellular Calcium Signaling* [Online]. Gillingham, UK: Sigma-Aldrich. Available: http://www.sigmaaldrich.com/life-science/your-favorite-gene-search/pathway-overviews/intracellular-calcium-signaling.html [Accessed 2nd September 2010].

Cooper, G. M. 2000. *The cell: a molecular approach,* Sunderland, ASM Press.

Cooper, R. G. (2008). Zinc toxicology following particulate inhalation. *Indian J Occup Environ Med,* **12,** 10-3.

Coquette, A., Berna, N., Vandenbosch, A., Rosdy, M., De Wever, B. & Poumay, Y. (2003). Analysis of interleukin-1α (IL-1α) and interleukin-8 (IL-8) expression and release in in vitro reconstructed human epidermis for the prediction of in vivo skin irritation and/or sensitization. *Toxicology in Vitro,* **17,** 311-321.

Corsini, E., Bruccoleri, A., Marinovich, M. & Galli, C. L. (1996). Endogenous Interleukin-1α Is Associated with Skin Irritation Induced by Tributyltin. *Toxicology and Applied Pharmacology,* **138,** 268-274.

Cosgrove, T. 2010. *Colloid Science: Principles, Methods and Applications*, John Wiley & Sons.

Cotran, R. S., Kumar, V., Collins, T. & Robbins, S. L. 1999. *Robbins pathologic basis of disease,* Michigan, Saunders.

Cozzani, E., Cacciapuoti, M., Parodi, A., Ghohestani, R. & Rebora, A. (2000). Desmosomes and their autoimmune pathologies. *Eur J Dermatol,* **10,** 255-61.

Crane, M., Handy, R., Garrod, J. & Owen, R. (2008). Ecotoxicity test methods and environmental hazard assessment for engineered nanoparticles. *Ecotoxicology,* **17,** 421-437.

Creeth, J. E., Abraham, P. J., Barlow, J. A. & Cummins, D. (1993). Oral delivery and clearance of antiplaque agents from Triclosan-containing dentifrices. *Int Dent J,* **43,** 387-97.

Crowther, J. R. 2000. *The ELISA Guidebook*, Humana Press.

Cuesta, A. I., Jewtuchowicz, V., Brusca, M., Mujica, M. & Rosa, A. (2011). Antibiotic susceptibility of Staphylococcus aureus isolates in oral mucosa and pockets of patients with gingivitis-periodontitis. *Acta odontológica latinoamericana: AOL,* **24,** 35.

Cumberbatch, M., Dearman, R. J. & Kimber, I. (1996). Constitutive and inducible expression of interleukin-6 by Langerhans cells and lymph node dendritic cells. *Immunology,* **87,** 513-8.

Cummins, D. & Creeth, J. E. (1992). Delivery of Antiplaque Agents from Dentifrices, Gels, and Mouthwashes. *Journal of Dental Research,* **71,** 1439-1449.

Dale, B. A., Salonen, J. & Jones, A. H. (1990). New approaches and concepts in the study of differentiation of oral epithelia. *Crit Rev Oral Biol Med,* **1,** 167-90.

Daston, G. P. & McNamee, P. (2005). Alternatives to toxicity testing in animals: challenges and opportunities. *Essays on the Future of Environmental Health Research.*

Davda, J. & Labhasetwar, V. (2002). Characterization of nanoparticle uptake by endothelial cells. *International Journal of Pharmaceutics,* **233,** 51-59.

De Clement, W. W. & Wheater, M. (2009). Cytotoxicity of Calcium Aluminate and Portland Cements in Gingival Epithelium. *The 87th IADR General session,* **Poster presentation,** 1-4.

De Jong, W. H., Van Der Ven, L. T. M., Sleijffers, A., Park, M. V. D. Z., Jansen, E. H. J. M., Van Loveren, H. & Vandebriel, R. J. (2013). Systemic and immunotoxicity of silver nanoparticles in an intravenous 28 days repeated dose toxicity study in rats. *Biomaterials,* **34,** 8333-8343.

Debnath, J. & Brugge, J. S. (2005). Modelling glandular epithelial cancers in three-dimensional cultures. *Nat Rev Cancer,* **5,** 675-688.

Delgado, A. V., González-Caballero, F., Hunter, R. J., Koopal, L. K. & Lyklema, J. (2007). Measurement and interpretation of electrokinetic phenomena. *Journal of Colloid and Interface Science,* **309,** 194-224.

Demetrescu, I., Pirvu, C. & Mitran, V. (2010). Effect of nano-topographical features of Ti/TiO2 electrode surface on cell response and electrochemical stability in artificial saliva. *Bioelectrochemistry,* **79,** 122-129.

Deng, X. & et al. (2009). Nanosized zinc oxide particles induce neural stem cell apoptosis. *Nanotechnology,* **20,** 115101.

des Rieux, A., Fievez, V., Garinot, M., Schneider, Y.-J. & Préat, V. (2006). Nanoparticles as potential oral delivery systems of proteins and vaccines: A mechanistic approach. *Journal of Controlled Release,* **116,** 1-27.

Desai, M. P., Labhasetwar, V., Walter, E., Levy, R. J. & Amidon, G. L. (1997). The Mechanism of Uptake of Biodegradable Microparticles in Caco-2 Cells Is Size Dependent. *Pharmaceutical Research,* **14,** 1568-1573.

Dhawan, A. & Sharma, V. (2010). Toxicity assessment of nanomaterials: methods and challenges. *Analytical and Bioanalytical Chemistry,* **398,** 589-605.

Dhiman, H. K., Ray, A. R. & Panda, A. K. (2005). Three-dimensional chitosan scaffold-based MCF-7 cell culture for the determination of the cytotoxicity of tamoxifen. *Biomaterials,* **26,** 979-986.

di Nardo, A., Sugino, K., Wertz, P., Ademola, J. & Maibach, H. I. (1996). Sodium lauryl sulfate (SLS) induced irritant contact dermatitis: a correlation study between ceramides and in vivo parameters of irritation. *Contact Dermatitis,* **35,** 86-91.

Díaz, B., Sánchez-Espinel, C., Arruebo, M., Faro, J., de Miguel, E., Magadán, S., Yagüe, C., Fernández-Pacheco, R., Ibarra, M. R., Santamaría, J. & González-Fernández, Á. (2008). Assessing Methods for Blood Cell Cytotoxic Responses to Inorganic Nanoparticles and Nanoparticle Aggregates. *Small,* **4,** 2025-2034.

Dick, C. A., Brown, D. M., Donaldson, K. & Stone, V. (2003). The role of free radicals in the toxic and inflammatory effects of four different ultrafine particle types. *Inhal Toxicol,* **15,** 39-52.

Dinarello, C. A. (1998). Interleukin-1, Interleukin-1 Receptors and Interleukin-1 Receptor Antagonist. *International Reviews of Immunology,* **16,** 457-499.

Dingley, A. G., Fair, M. J., Glynn, J. R. & Sandstrom, G. A. (2008). Optical Blurring Pigment Composition Suitable for Use in Cosmetics. **Google Patents**.

Dixon, D., Mutreja, I., D'Sa, R., Meenan, B. J. & Kumar, D. (2012). Controlling the size and size distribution of gold nanoparticles: a design of experiment study. *International Journal of Nanoscience,* **11,** 1250023.

Dobson, P. D. & Kell, D. B. (2008). Carrier-mediated cellular uptake of pharmaceutical drugs: an exception or the rule? *Nat Rev Drug Discov,* **7,** 205-220.

Doherty, G. J. & McMahon, H. T. (2009). Mechanisms of endocytosis. *Annual review of biochemistry,* **78,** 857-902.

Domingos, R. F., Baalousha, M. A., Ju-Nam, Y., Reid, M. M., Tufenkji, N., Lead, J. R., Leppard, G. G. & Wilkinson, K. J. (2009). Characterizing manufactured nanoparticles in the environment: multimethod determination of particle sizes. *Environmental science & technology,* **43,** 7277-7284.

Dominguez-Medina, S., Blankenburg, J., Olson, J., Landes, C. F. & Link, S. (2013). Adsorption of a Protein Monolayer via Hydrophobic Interactions Prevents Nanoparticle Aggregation under Harsh Environmental Conditions. *ACS Sustainable Chemistry & Engineering*.

Donaldson, K. & Tran, C. L. (2002). Inflammation caused by particles and fibers. *Inhalation Toxicology,* **14,** 5-27.

Donaldson, K., Zhang, Q., Kusaka, Y., Sato, K., Nakakuki, K. & Kohyama, N. (1998). Differences in the extent of inflammation caused by intratracheal exposure to three ultrafine metals: role of free radicals. *Journal of Toxicology and Environmental Health, Part A: Current Issues,* **53,** 423 - 438.

Dover, R. & Wright, N. A. 1991. The cell proliferation kinetics of the epidermis. *In:* La, G. (ed.) *Physiology, biochemistry, and molecular biology of the skin* 2nd ed. Oxford: Oxford university press.

Duffin, R., Tran, L., Brown, D., Stone, V. & Donaldson, K. (2007). Proinflammogenic Effects of Low-Toxicity and Metal Nanoparticles In Vivo and In Vitro: Highlighting the Role of Particle Surface Area and Surface Reactivity. *Inhalation Toxicology,* **19,** 849-856.

Dunford, R., Salinaro, A., Cai, L., Serpone, N., Horikoshi, S., Hidaka, H. & Knowland, J. (1997). Chemical oxidation and DNA damage catalysed by inorganic sunscreen ingredients. *FEBS Letters,* **418,** 87-90.

Eby, G. A. (2008). Therapeutic Effectiveness of Ionic Zinc for Common Colds. *Clinical Infectious Diseases,* **46,** 483-484.

Einstein, A. (1905). Über die von der molekularkinetischen Theorie der Wärme geforderte Bewegung von in ruhenden Flüssigkeiten suspendierten Teilchen. *Annalen der Physik,* **322,** 549-560.

Eisenbrand, G., Pool-Zobel, B., Baker, V., Balls, M., Blaauboer, B. J., Boobis, A., Carere, A., Kevekordes, S., Lhuguenot, J. C., Pieters, R. & Kleiner, J. (2002). Methods of in vitro toxicology. *Food and Chemical Toxicology,* **40,** 193-236.

Elder, A., Gelein, R., Silva, V., Feikert, T., Opanashuk, L., Carter, J., Potter, R., Maynard, A., Ito, Y. & Finkelstein, J. (2006). Translocation of inhaled ultrafine manganese oxide particles to the central nervous system. *Environmental Health Perspectives,* **114,** 1172.

Elder, A., Vidyasagar, S. & DeLouise, L. (2009). Physicochemical factors that affect metal and metal oxide nanoparticle passage across epithelial barriers. *Wiley Interdisciplinary Reviews: Nanomedicine and Nanobiotechnology,* **1,** 434-450.

Elsom, J. (2004). *Development of a quartz crystal based biosensor for real-time monitoring of particulate cell interactions.* Doctor of Philosophy, The Uniersity of Brighton.

Eun, H. C., Chung, J. H., Jung, S. Y., Cho, K. H. & Kim, K. H. (1994). A comparative study of the cytotoxicity of skin irritants on cultured human oral and skin keratinocytes. *British Journal of Dermatology,* **130,** 24-28.

Everett, D. H. 2007. *Basic principles of colloid science,* Royal Society of Chemistry, Cambridge.

Eveson, J. W. (2008). Xerostomia. *Periodontology 2000,* **48,** 85-91.

Faunce, T. A. (2008). Toxicological and public good considerations for the regulation of nanomaterial-containing medical products. *Expert Opin Drug Saf,* **7,** 103-6.

Faunce, T. A., White, J. & Matthaei, K. I. (2008). Integrated research into the nanoparticle–protein corona: a new focus for safe, sustainable and equitable development of nanomedicines. *Nanomedicine,* **3,** 859-866.

Fesik, S. W. & Shi, Y. (2001). Structural biology. Controlling the caspases. *Science,* **294,** 1477-8.

Filipe, V., Hawe, A. & Jiskoot, W. (2010). Critical Evaluation of Nanoparticle Tracking Analysis (NTA) by NanoSight for the Measurement of Nanoparticles and Protein Aggregates. *Pharmaceutical Research,* **27,** 796-810.

Finley, J. W., Briske-Anderson, M., Reeves, P. G. & Johnson, L. K. (1995). Zinc uptake and transcellular movement by CACO-2 cells: Studies with media containing fetal bovine serum. *The Journal of Nutritional Biochemistry,* **6,** 137-144.

Flegler, S. L., John W. Heckman, J. & Klomparens, K. L. 1993. *Scanning and Transmission Electron Microscopy: An Introduction*, Oxford University Press.

Florence, A., Hillery, A., Hussain, N. & Jani, P. (1995). Factors affecting the oral uptake and translocation of polystyrene nanoparticles: histological and analytical evidence. *J Drug Target,* **3,** 65 - 70.

Forth, W., Henschler, D. & Rummel, W. (1987). Pharmacology and toxicology. For students of medicine, veterinary medicine, pharmacy, chemistry, biology as well as for physicians, veterinarians and pharmacists.

Fotakis, G. & Timbrell, J. A. (2006). In vitro cytotoxicity assays: Comparison of LDH, neutral red, MTT and protein assay in hepatoma cell lines following exposure to cadmium chloride. *Toxicology Letters,* **160,** 171-177.

Fredeen, C. B. B. a. K. J. 1997. *Concepts, Instrumentation and Techniques in Inductively Coupled Plasma Optical Emission Spectrometry,* U.S.A, Perkin-Elmer.

Freitas, C. & Müller, R. H. (1998). Effect of light and temperature on zeta potential and physical stability in solid lipid nanoparticle (SLN™) dispersions. *International Journal of Pharmaceutics,* **168,** 221-229.

Friedl, P. & Gilmour, D. (2009). Collective cell migration in morphogenesis, regeneration and cancer. *Nature Reviews Molecular Cell Biology,* **10,** 445-457.

Friis, M. B., Friborg, C. R., Schneider, L., Nielsen, M.-B., Lambert, I. H., Christensen, S. T. & Hoffmann, E. K. (2005). Cell shrinkage as a signal to apoptosis in NIH 3T3 fibroblasts. *The Journal of Physiology,* **567,** 427-443.

Fröhlich, E. & Roblegg, E. (2012). Models for oral uptake of nanoparticles in consumer products. *Toxicology,* **291,** 10-17.

Fruijtier-Pölloth, C. (2005). Safety assessment on polyethylene glycols (PEGs) and their derivatives as used in cosmetic products. *Toxicology,* **214,** 1-38.

Gaikwad, R. M. & Sokolov, I. (2008). Silica Nanoparticles to Polish Tooth Surfaces for Caries Prevention. *Journal of Dental Research,* **87,** 980-983.

Gaiser, B. K., Fernandes, T. F., Jepson, M. A., Lead, J. R., Tyler, C. R., Baalousha, M., Biswas, A., Britton, G. J., Cole, P. A. & Johnston, B. D. (2012). Interspecies comparisons on the uptake and toxicity of silver and cerium dioxide nanoparticles. *Environmental Toxicology and Chemistry,* **31,** 144-154.

Gallagher, A., Sowinski, J., Bowman, J., Barrett, K., Lowe, S., Patel, K., Bosma, M. L. & Creeth, J. E. (2009). The Effect of Brushing Time and Dentifrice on Dental Plaque Removal *in vivo*. *Journal of Dental Hygiene,* **83,** 111-116.

Gamer, A. O., Leibold, E. & van Ravenzwaay, B. (2006). The in vitro absorption of microfine zinc oxide and titanium dioxide through porcine skin. *Toxicology in Vitro,* **20,** 301-307.

Gandhi, R. B. & Robinson, J. R. (1994). Oral cavity as a site for bioadhesive drug delivery. *Advanced Drug Delivery Reviews,* **13,** 43-74.

Gardiner, C., Ferreira, Y. J., Dragovic, R. A., Redman, C. W. & Sargent, I. L. (2013). Extracellular vesicle sizing and enumeration by nanoparticle tracking analysis. *Journal of Extracellular Vesicles,* **2**.

Garrod, D. & Chidgey, M. (2008). Desmosome structure, composition and function. *Biochim Biophys Acta,* **1778,** 572-87.

Gaumet, M., Vargas, A., Gurny, R. & Delie, F. (2008). Nanoparticles for drug delivery: The need for precision in reporting particle size parameters. *European Journal of Pharmaceutics and Biopharmaceutics,* **69,** 1-9.

Geiser, M., Rothen-Rutishauser, B., Kapp, N., Schurch, S., Kreyling, W., Schulz, H., Semmler, M., Im Hof, V., Heyder, J. & Gehr, P. (2005). Ultrafine particles cross cellular membranes by nonphagocytic mechanisms in lungs and in cultured cells. *Environ Health Perspect,* **113,** 1555-60.

Gennari, A., Cortese, E., Boveri, M., Casado, J. & Prieto, P. (2003). Sensitive endpoints for evaluating cadmium-induced acute toxicity in LLC-PK1 cells. *Toxicology,* **183,** 211-220.

George, S., Pokhrel, S., Xia, T., Gilbert, B., Ji, Z., Schowalter, M., Rosenauer, A., Damoiseaux, R., Bradley, K. A., Madler, L. & Nel, A. E. (2010). Use of a rapid cytotoxicity screening approach to engineer a safer zinc oxide nanoparticle through iron doping. *ACS Nano,* **4,** 15-29.

Gerloff, K., Albrecht, C., Boots, A. W., Förster, I. & Schins, R. P. F. (2009). Cytotoxicity and oxidative DNA damage by nanoparticles in human intestinal Caco-2 cells. *Nanotoxicology,* **3,** 355-364.

Giertsen, E. (2004). Effects of mouthrinses with triclosan, zinc ions, copolymer, and sodium lauryl sulphate combined with fluoride on acid formation by dental plaque in vivo. *Caries research,* **38,** 430-435.

Gilbert, R. J. & Williams, P. E. (1987). The oral retention and antiplaque efficacy of triclosan in human volunteers. *Br J Clin Pharmacol,* **23,** 579-83.

Gleyzes, C., Tellier, S. & Astruc, M. (2002). Fractionation studies of trace elements in contaminated soils and sediments: a review of sequential extraction procedures. *TrAC Trends in Analytical Chemistry,* **21,** 451-467.

Goldstein, J. 2003. *Scanning electron microscopy and x-ray microanalysis*, Kluwer Academic/Plenum Publishers.

Gomes, M. C., Fernandes, R., Cunha, A., Tome, J. P. & Trindade, T. (2013). Fluorescence biolabeling using methylated silica nanoparticles containing a lanthanide complex. *Journal of Materials Chemistry B,* **1,** 5429-5435.

Gonzales, M., Mitsumori, L. M., Kushleika, J. V., Rosenfeld, M. E. & Krishnan, K. M. (2010). Cytotoxicity of iron oxide nanoparticles made from the thermal decomposition of organometallics and aqueous phase transfer with Pluronic F127. *Contrast Media & Molecular Imaging,* **5,** 286-293.

González, S., Sung, H., Sepúlveda, D., González, M. J. & Molina, C. (2013). Oral manifestations and their treatment in Sjögren' s syndrome. *Oral diseases*.

Goodman, L. S., Goodman Gilman, A. G., Hardman, J. G. & Limbird, L. E. 2001. *Goodman and Gilman's the pharmacological basis of therapeutics,* New York ; London McGraw-Hill.

Gosens, I., Post, J. A., de la Fonteyne, L., Jansen, E., Geus, J. W., Cassee, F. R. & de Jong, W. H. (2010). Impact of agglomeration state of nano-and submicron sized gold particles on pulmonary inflammation. *Part Fibre Toxicol,* **7,** 3-7.

Grabrucker, A. M., Garner, C. C., Boeckers, T. M., Bondioli, L., Ruozi, B., Forni, F., Vandelli, M. A. & Tosi, G. (2011). Development of novel Zn2+ loaded nanoparticles designed for cell-type targeted drug release in CNS neurons: in vitro evidences. *PloS one,* **6,** e17851.

Grandvuinet, A. S., Gustavsson, L. & Steffansen, B. (2013). New Insights into the Carrier-Mediated Transport of Estrone-3-sulfate in the Caco-2 Cell Model. *Molecular Pharmaceutics,* **10,** 3285-3295.

Grant, B. D. & Donaldson, J. G. (2009). Pathways and mechanisms of endocytic recycling. *Nat Rev Mol Cell Biol,* **10,** 597-608.

Green & John C. Reed, D. R. (1998). Mitochondria and Apoptosis. *Science,* **281,** 1309-1312.

Green, D. R. 2011. *Means to an End: Apoptosis and Other Cell Death Mechanisms*, Cold Spring Harbor Laboratory Press.

Grellier, M., Bordenave, L. & Amédée, J. (2009). Cell-to-cell communication between osteogenic and endothelial lineages: implications for tissue engineering. *Trends in Biotechnology,* **27,** 562-571.

Grès, M.-C., Julian, B., Bourrié, M., Meunier, V., Roques, C., Berger, M., Boulenc, X., Berger, Y. & Fabre, G. (1998). Correlation Between Oral Drug Absorption in Humans, and Apparent Drug Permeability in TC-7 Cells, A Human Epithelial Intestinal Cell Line: Comparison with the Parental Caco-2 Cell Line. *Pharmaceutical Research,* **15,** 726-733.

Griffith, L. G. & Swartz, M. A. (2006). Capturing complex 3D tissue physiology in vitro. *Nature Reviews Molecular Cell Biology,* **7,** 211-224.

Grindon, C., Combes, R., Cronin, M. T. D., and, R. D. W. & Garrod, J. F. (2007). Integrated Decision-tree Testing Strategies for Skin Corrosion and Irritation with Respect to the Requirements of the EU REACH Legislation. *Alternatives to Laboratory Animals,* **35,** 673-682.

Groeber, F., Holeiter, M., Hampel, M., Hinderer, S. & Schenke-Layland, K. (2011). Skin tissue engineering — In vivo and in vitro applications. *Advanced Drug Delivery Reviews,* **63,** 352-366.

Groemer, T. W. & Klingauf, J. (2007). Synaptic vesicles recycling spontaneously and during activity belong to the same vesicle pool. *Nature neuroscience,* **10,** 145-147.

Group, N. P. (1999). Tissue engineering. *Nat Biotech,* **17,** 508-510.

Gui, S., Li, B., Zhao, X., Sheng, L., Hong, J., Yu, X., Sang, X., Sun, Q., Ze, Y. & Wang, L. (2013). Renal Injury and Nrf2 Modulation in Mouse Kidney Following Chronic Exposure to TiO2 Nanoparticles. *Journal of Agricultural and Food Chemistry,* **61,** 8959-8968.

Gulson, B., McCall, M., Korsch, M., Gomez, L., Casey, P., Oytam, Y., Taylor, A., McCulloch, M., Trotter, J., Kinsley, L. & Greenoak, G. (2010). Small Amounts of Zinc from Zinc Oxide Particles in Sunscreens Applied Outdoors Are Absorbed through Human Skin. *Toxicological Sciences,* **118,** 140-149.

Gulson, B., Wong, H., Korsch, M., Gomez, L., Casey, P., McCall, M., McCulloch, M., Trotter, J., Stauber, J. & Greenoak, G. (2012). Comparison of dermal absorption of zinc from different sunscreen formulations and differing UV exposure based on stable isotope tracing. *Science of The Total Environment,* **420,** 313-318.

Gunness, P., Mueller, D., Shevchenko, V., Heinzle, E., Ingelman-Sundberg, M. & Noor, F. (2013). 3D Organotypic Cultures of Human HepaRG Cells: A Tool for In Vitro Toxicity Studies. *Toxicological Sciences,* **133,** 67-78.

Gunstone, F. D. 1996. *Fatty acid and lipid chemistry,* Glasgow, Blackie academic and professional.

Guo, L., Von Dem Bussche, A., Buechner, M., Yan, A., Kane, A. B. & Hurt, R. H. (2008). Adsorption of Essential Micronutrients by Carbon Nanotubes and the Implications for Nanotoxicity Testing. *Small,* **4,** 721-727.

Gupta, A. K., Gupta, M., Yarwood, S. J. & Curtis, A. S. G. (2004). Effect of cellular uptake of gelatin nanoparticles on adhesion, morphology and cytoskeleton organisation of human fibroblasts. *Journal of Controlled Release,* **95,** 197-207.

Gupta, J. (2011). Nanotechnology applications in medicine and dentistry. *Journal of Investigative and Clinical Dentistry,* **2,** 81-88.

Hackenberg, S., Friehs, G., Froelich, K., Ginzkey, C., Koehler, C., Scherzed, A., Burghartz, M., Hagen, R. & Kleinsasser, N. (2010). Intracellular distribution, geno- and cytotoxic effects of nanosized titanium dioxide particles in the anatase crystal phase on human nasal mucosa cells. *Toxicology Letters,* **195,** 9-14.

Hackenberg, S., Scherzed, A., Kessler, M., Hummel, S., Technau, A., Froelich, K., Ginzkey, C., Koehler, C., Hagen, R. & Kleinsasser, N. (2011a). Silver nanoparticles: Evaluation of DNA damage, toxicity and functional impairment in human mesenchymal stem cells. *Toxicology Letters,* **201,** 27-33.

Hackenberg, S., Scherzed, A., Technau, A., Kessler, M., Froelich, K., Ginzkey, C., Koehler, C., Burghartz, M., Hagen, R. & Kleinsasser, N. (2011b). Cytotoxic, genotoxic and pro-inflammatory effects of zinc oxide nanoparticles in human nasal mucosa cells in vitro. *Toxicology in Vitro,* **25,** 657-663.

Hainfeld, J. F. & Powell, R. D. (2000). New Frontiers in Gold Labeling. *Journal of Histochemistry & Cytochemistry,* **48,** 471-480.

Han, S. G., Newsome, B. & Hennig, B. (2013). Titanium dioxide nanoparticles increase inflammatory responses in vascular endothelial cells. *Toxicology,* **306,** 1-8.

Han, X., Gelein, R., Corson, N., Wade-Mercer, P., Jiang, J., Biswas, P., Finkelstein, J. N., Elder, A. & Oberdörster, G. (2011). Validation of an LDH assay for assessing nanoparticle toxicity. *Toxicology,* **287,** 99-104.

Handy, R., Owen, R. & Valsami-Jones, E. (2008). The ecotoxicology of nanoparticles and nanomaterials: current status, knowledge gaps, challenges, and future needs. *Ecotoxicology,* **17,** 315-325.

Hannig, M. & Hannig, C. (2010). Nanomaterials in preventive dentistry. *Nat Nano,* **5,** 565-569.
Hansen, S., Michelson, E., Kamper, A., Borling, P., Stuer-Lauridsen, F. & Baun, A. (2008). Categorization framework to aid exposure assessment of nanomaterials in consumer products. *Ecotoxicology,* **17,** 438-447.
Hansson, S. O. & Rudén, C. (2007). Towards a theory of tiered testing. *Regulatory Toxicology and Pharmacology,* **48,** 35-44.
Hao, J. & Heng, P. W. (2003). Buccal delivery systems. *Drug Dev Ind Pharm,* **29,** 821-32.
Harata, N., Ryan, T. A., Smith, S. J., Buchanan, J. & Tsien, R. W. (2001). Visualizing recycling synaptic vesicles in hippocampal neurons by FM 1-43 photoconversion. *Proceedings of the National Academy of Sciences,* **98,** 12748-12753.
Hardman, R. (2006). A toxicologic review of quantum dots: toxicity depends on physicochemical and environmental factors. *Environ Health Perspect,* **114,** 165-72.
Härmä, V., Virtanen, J., Mäkelä, R., Happonen, A., Mpindi, J.-P., Knuuttila, M., Kohonen, P., Lötjönen, J., Kallioniemi, O. & Nees, M. (2010). A comprehensive panel of three-dimensional models for studies of prostate cancer growth, invasion and drug responses. *PLoS One,* **5,** e10431.
Harris, D. & Robinson, J. R. (1992). Drug delivery via the mucous membranes of the oral cavity. *Journal of Pharmaceutical Sciences,* **81,** 1-10.
Hartung, T. (2009). Toxicology for the twenty-first century. *Nature,* **460,** 208-212.
Harush-Frenkel, O., Rozentur, E., Benita, S. & Altschuler, Y. (2008). Surface Charge of Nanoparticles Determines Their Endocytic and Transcytotic Pathway in Polarized MDCK Cells. *Biomacromolecules,* **9,** 435-443.
Hasezaki, T., Isoda, K., Kondoh, M., Tsutsumi, Y. & Yagi, K. (2011). Hepatotoxicity of silica nanoparticles with a diameter of 100 nm. *Die Pharmazie-An International Journal of Pharmaceutical Sciences,* **66,** 698-703.
He, C., Hu, Y., Yin, L., Tang, C. & Yin, C. (2010). Effects of particle size and surface charge on cellular uptake and biodistribution of polymeric nanoparticles. *Biomaterials,* **31,** 3657-3666.
Healy, C. M., Cruchley, A. T., Thornhill, M. H. & Williams, D. M. (2000). The effect of sodium lauryl sulphate, triclosan and zinc on the permeability of normal oral mucosa. *Oral Diseases,* **6,** 118-123.
Hearnden, V., Sankar, V., Hull, K., Juras, D. V., Greenberg, M., Kerr, A. R., Lockhart, P. B., Patton, L. L., Porter, S. & Thornhill, M. H. (2012). New developments and opportunities in oral mucosal drug delivery for local and systemic disease. *Advanced drug delivery reviews,* **64,** 16-28.
Heinlaan, M., Ivask, A., Blinova, I., Dubourguier, H. C. & Kahru, A. (2008). Toxicity of nanosized and bulk ZnO, CuO and TiO2 to bacteria Vibrio fischeri and crustaceans Daphnia magna and Thamnocephalus platyurus. *Chemosphere,* **71,** 1308-16.
Held, P. (2010). *An Introduction to Reactive Oxygen Species-Measurement of ROS in Cells* [Online]. Tech resources - App guides: Biotech instruments. Available: http://www.biotek.com/resources/articles/reactive-oxygen-species.html [Accessed 9th December 2013].
Herd, H., Daum, N., Jones, A. T., Huwer, H., Ghandehari, H. & Lehr, C.-M. (2013). Nanoparticle Geometry and Surface Orientation Influence Mode of Cellular Uptake. *ACS Nano,* **7,** 1961-1973.
Heylings, J. R., Diot, S., Esdaile, D. J., Fasano, W. J., Manning, L. A. & Owen, H. M. (2003). A prevalidation study on the in vitro skin irritation function test (SIFT) for prediction of acute skin irritation in vivo: results and evaluation of ECVAM Phase III. *Toxicology in Vitro,* **17,** 123-138.

Hillegass, J. M., Shukla, A., Lathrop, S. A., MacPherson, M. B., Fukagawa, N. K. & Mossman, B. T. (2010). Assessing nanotoxicity in cells in vitro. *Wiley Interdisciplinary Reviews: Nanomedicine and Nanobiotechnology,* **2,** 219-231.

Hiroshima, Y., Bando, M., Kataoka, M., Inagaki, Y., Herzberg, M. C., Ross, K. F., Hosoi, K., Nagata, T. & Kido, J.-i. (2011). Regulation of antimicrobial peptide expression in human gingival keratinocytes by interleukin-1α. *Archives of Oral Biology,* **56,** 761-767.

Ho, E. & Ames, B. N. (2002). Low intracellular zinc induces oxidative DNA damage, disrupts p53, NFkappa B, and AP1 DNA binding, and affects DNA repair in a rat glioma cell line. *Proc Natl Acad Sci U S A,* **99,** 16770-5.

Hoet, P., Bruske-Hohlfeld, I. & Salata, O. (2004). Nanoparticles - known and unknown health risks. *Journal of Nanobiotechnology,* **2,** 12.

Holpuch, A., Hummel, G., Tong, M., Seghi, G., Pei, P., Ma, P., Mumper, R. & Mallery, S. (2010). Nanoparticles for Local Drug Delivery to the Oral Mucosa: Proof of Principle Studies. *Pharmaceutical Research,* **27,** 1224-1236.

Holsapple, M. P., Farland, W. H., Landry, T. D., Monteiro-Riviere, N. A., Carter, J. M., Walker, N. J. & Thomas, K. V. (2005). Research strategies for safety evaluation of nanomaterials, part II: toxicological and safety evaluation of nanomaterials, current challenges and data needs. *Toxicological Sciences,* **88,** 12-17.

Hoogstraate, J. A. J. & Wertz, P. W. (1998). Drug delivery via the buccal mucosa. *Pharmaceutical Science & Technology Today,* **1,** 309-316.

Horie, M., Nishio, K., Fujita, K., Endoh, S., Miyauchi, A., Saito, Y., Iwahashi, H., Yamamoto, K., Murayama, H., Nakano, H., Nanashima, N., Niki, E. & Yoshida, Y. (2009). Protein Adsorption of Ultrafine Metal Oxide and Its Influence on Cytotoxicity toward Cultured Cells. *Chemical Research in Toxicology,* **22,** 543-553.

Hoshino, A., Hanaki, K., Suzuki, K. & Yamamoto, K. (2004). Applications of T-lymphoma labeled with fluorescent quantum dots to cell tracing markers in mouse body. *Biochem Biophys Res Commun,* **314,** 46 - 53.

Hosokawa, C., Kudoh, S. N., Kiyohara, A. & Taguchi, T. (2011). Optical trapping of synaptic vesicles in neurons. *Applied Physics Letters,* **98,** 163705-163705-3.

Hsiao, I. L. & Huang, Y.-J. (2011). Effects of various physicochemical characteristics on the toxicities of ZnO and TiO2 nanoparticles toward human lung epithelial cells. *Science of The Total Environment,* **409,** 1219-1228.

Huang, C.-C., Aronstam, R. S., Chen, D.-R. & Huang, Y.-W. (2010a). Oxidative stress, calcium homeostasis, and altered gene expression in human lung epithelial cells exposed to ZnO nanoparticles. *Toxicology in Vitro,* **24,** 45-55.

Huang, Y.-W., Wu, C.-h. & Aronstam, R. S. (2010b). Toxicity of Transition Metal Oxide Nanoparticles: Recent Insights from in vitro Studies. *Materials Letters,* **3,** 4842-4859.

Hubatsch, I., Ragnarsson, E. G. E. & Artursson, P. (2007). Determination of drug permeability and prediction of drug absorption in Caco-2 monolayers. *Nat. Protocols,* **2,** 2111-2119.

Hugh J. Byrne, I. L., Wim H.de Jong, Wolfgang G.Kreyling, Steffen Loft, Margriet V.D.Z.Park, Michael Riediker and David Warheit (2010). Protocols for assessment of biological hazards of engineered nanomaterials. *The European Network on the Health and Environmental Impact of Nanomaterials,* **NanoImpactNet,** 1-30.

Hume, W. (1985). Keratinocyte proliferative hierarchies confer protective mechanisms in surface epithelia. *British Journal of Dermatology,* **112,** 493-502.

Hunter, R. J. 1993. *Introduction to Modern Colloid Science,* Oxford, UK, Oxford Science Publications.

Hussain, M. A. K., M. A. ; Sood, A. K (2009). On the cytotoxicity of carbon nanotubes. *Current Science,* **96,** 664-673.

Hussain, S. M., Hess, K. L., Gearhart, J. M., Geiss, K. T. & Schlager, J. J. (2005). In vitro toxicity of nanoparticles in BRL 3A rat liver cells. *Toxicology in Vitro,* **19,** 975-983.

Hutter, E., Boridy, S., Labrecque, S., Lalancette-Hébert, M., Kriz, J., Winnik, F. M. & Maysinger, D. (2010). Microglial response to gold nanoparticles. *ACS nano,* **4,** 2595-2606.

Illum, L. (2003). Nasal drug delivery—possibilities, problems and solutions. *Journal of Controlled Release,* **87,** 187-198.

Innes, N. P. T. & Ogden, G. R. (1999). A technique for the study of endocytosis in human oral epithelial cells. *Archives of Oral Biology,* **44,** 519-523.

Iriyama, S., Ono, T., Aoki, H. & Amano, S. (2011). Hyperpigmentation in human solar lentigo is promoted by heparanase-induced loss of heparan sulfate chains at the dermal–epidermal junction. *Journal of dermatological science,* **64,** 223-228.

Itthagarun, A., King, N. M. & Cheung, Y.-M. (2010). The effect of nano-hydroxyapatite toothpaste on artificial enamel carious lesion progression: an in-vitro pH-cycling study. *Hong Kong Dent J,* **7,** 61-66.

Iversen, T.-G., Skotland, T. & Sandvig, K. (2011). Endocytosis and intracellular transport of nanoparticles: Present knowledge and need for future studies. *Nano Today,* **6,** 176-185.

Jaeger, A., Weiss, D. G., Jonas, L. & Kriehuber, R. (2012). Oxidative stress-induced cytotoxic and genotoxic effects of nano-sized titanium dioxide particles in human HaCaT keratinocytes. *Toxicology,* **296,** 27-36.

Jahn, M. R., Nawroth, T., Futterer, S. r., Wolfrum, U., Kolb, U. & Langguth, P. (2012). Iron oxide/hydroxide nanoparticles with negatively charged shells show increased uptake in Caco-2 cells. *Molecular Pharmaceutics,* **9,** 1628-1637.

James-Smith, M., Hellner, B., Annunziato, N. & Mitragotri, S. (2011). Effect of Surfactant Mixtures on Skin Structure and Barrier Properties. *Annals of Biomedical Engineering,* **39,** 1215-1223.

Jani, P. U., McCarthy, D. E. & Florence, A. T. (1994). Titanium dioxide (rutile) particle uptake from the rat GI tract and translocation to systemic organs after oral administration. *International Journal of Pharmaceutics,* **105,** 157-168.

Jans, H., Liu, X., Austin, L., Maes, G. & Huo, Q. (2009). Dynamic Light Scattering as a Powerful Tool for Gold Nanoparticle Bioconjugation and Biomolecular Binding Studies. *Analytical Chemistry,* **81,** 9425-9432.

Jaworska, J., Gabbert, S. & Aldenberg, T. (2010). Towards optimization of chemical testing under REACH: A Bayesian network approach to Integrated Testing Strategies. *Regulatory Toxicology and Pharmacology,* **57,** 157-167.

Jeng, H. A. & Swanson, J. (2006). Toxicity of Metal Oxide Nanoparticles in Mammalian Cells. *Journal of Environmental Science and Health, Part A,* **41,** 2699-2711.

Jennifer, M. a. M., W. (2013). Nanoparticle Technology as a Double-Edged Sword: Cytotoxic, Genotoxic and Epigenetic Effects on Living Cells. *Journal of Biomaterials and Nanobiotechnology,* **4,** 53-63.

Jeong, G.-H., Suzuki, S., Kobayashi, Y., Yamazaki, A., Yoshimura, H. & Homma, Y. (2005). Effect of nanoparticle density on narrow diameter distribution of carbon nanotubes and particle evolution during chemical vapor deposition growth. *Journal of applied physics,* **98,** 124311-124311-6.

Jeong, S. H., Kim, H. J., Ryu, H. J., Ryu, W. I., Park, Y.-H., Bae, H. C., Jang, Y. S. & Son, S. W. (2013). ZnO nanoparticles induce TNF-α expression via ROS-ERK-

Egr-1 pathway in human keratinocytes. *Journal of Dermatological Science,* **72,** 263-273.

Jeong, S. H., Park, J. H., Kim, J. N., Park, Y.-H., Shin, S. Y., Lee, Y. H., Kye, Y. C. & Son, S. W. (2010). Up-regulation of TNF-alpha secretion by cigarette smoke is mediated by Egr-1 in HaCaT human keratinocytes. *Experimental Dermatology,* **19,** e206-e212.

Jevnikar, P., Krnel, K., Kocjan, A., Funduk, N. & Kosmač, T. (2010). The effect of nano-structured alumina coating on resin-bond strength to zirconia ceramics. *dental materials,* **26,** 688-696.

Jiang, X., Musyanovych, A., Rocker, C., Landfester, K., Mailander, V. & Nienhaus, G. U. (2011). Specific effects of surface carboxyl groups on anionic polystyrene particles in their interactions with mesenchymal stem cells. *Nanoscale,* **3,** 2028-2035.

Jin, H., Heller, D. A. & Strano, M. S. (2008). Single-Particle Tracking of Endocytosis and Exocytosis of Single-Walled Carbon Nanotubes in NIH-3T3 Cells. *Nano Letters,* **8,** 1577-1585.

Jin, Y., Kannan, S., Wu, M. & Zhao, J. X. (2007). Toxicity of Luminescent Silica Nanoparticles to Living Cells. *Chemical Research in Toxicology,* **20,** 1126-1133.

Johnston, H. J., Hutchison, G., Christensen, F. M., Peters, S., Hankin, S. & Stone, V. (2010a). A review of the in vivo and in vitro toxicity of silver and gold particulates: particle attributes and biological mechanisms responsible for the observed toxicity. *Critical reviews in toxicology,* **40,** 328-346.

Johnston, H. J., Semmler-Behnke, M., Brown, D. M., Kreyling, W., Tran, L. & Stone, V. (2010b). Evaluating the uptake and intracellular fate of polystyrene nanoparticles by primary and hepatocyte cell lines in vitro. *Toxicology and Applied Pharmacology,* **242,** 66-78.

Jones, C. G. (1997). Chlorhexidine: is it still the gold standard? *Periodontology 2000,* **15,** 55-62.

Jones, M. N. (1999). Surfactants in membrane solubilisation. *International Journal of Pharmaceutics,* **177,** 137-159.

Jung, T., Kamm, W., Breitenbach, A., Kaiserling, E., Xiao, J. X. & Kissel, T. (2000). Biodegradable nanoparticles for oral delivery of peptides: is there a role for polymers to affect mucosal uptake? *European Journal of Pharmaceutics and Biopharmaceutics,* **50,** 147-160.

Junginger, H. E., Hoogstraate, J. A. & Verhoef, J. C. (1999). Recent advances in buccal drug delivery and absorption -- in vitro and in vivo studies. *Journal of Controlled Release,* **62,** 149-159.

Kambhu, P. P. & Levy, S. M. (1993). Oral hygiene care levels in Iowa intermediate care facilities. *Special Care in Dentistry,* **13,** 209-214.

Kao, Y.-Y., Cheng, T.-J., Yang, D.-M., Wang, C.-T., Chiung, Y.-M. & Liu, P.-S. (2012). Demonstration of an Olfactory Bulb–Brain Translocation Pathway for ZnO Nanoparticles in Rodent Cells In Vitro and In Vivo. *Journal of Molecular Neuroscience,* **48,** 464-471.

Karlsson, H. L., Cronholm, P., Gustafsson, J. & Moller, L. (2008). Copper Oxide Nanoparticles Are Highly Toxic: A Comparison between Metal Oxide Nanoparticles and Carbon Nanotubes. *Chemical Research in Toxicology,* **21,** 1726-1732.

Kasper, J., Hermanns, M. I., Bantz, C., Koshkina, O., Lang, T., Maskos, M., Pohl, C., Unger, R. E. & Kirkpatrick, C. J. (2013a). Interactions of silica nanoparticles with lung epithelial cells and the association to flotillins. *Arch Toxicol,* **87,** 1053-65.

Kasper, J., Hermanns, M. I., Bantz, C., Utech, S., Koshkina, O., Maskos, M., Brochhausen, C., Pohl, C., Fuchs, S., Unger, R. E. & James Kirkpatrick, C. (2013b). Flotillin-involved uptake of silica nanoparticles and responses of an alveolar-capillary barrier in vitro. *European Journal of Pharmaceutics and Biopharmaceutics,* **84,** 275-287.

Kaszuba, M., Corbett, J., Watson, F. M. & Jones, A. (2010). High-concentration zeta potential measurements using light-scattering techniques. *Philosophical Transactions of the Royal Society A: Mathematical, Physical and Engineering Sciences,* **368,** 4439-4451.

Kato, H., Suzuki, M., Fujita, K., Horie, M., Endoh, S., Yoshida, Y., Iwahashi, H., Takahashi, K., Nakamura, A. & Kinugasa, S. (2009). Reliable size determination of nanoparticles using dynamic light scattering method for in vitro toxicology assessment. *Toxicology in Vitro,* **23,** 927-934.

Kazmi , R., Alonso , B., A., d. B. d. F., Raabe , B., Wurzburger , H. & Wilt , S. (2011). Evaluation of an Oral Care Product Safety Screening Program Utilizing the In Vitro SkinEthic Human Gingival Epithelium (RHG) and Oral Buccal (RHO) Models. SkinEthic labortories. **The Toxicologist: Conference proceedings of the 50th Annual SOT Meeting,** Washington D.C, USA. March 2011 10-14th.

Kendall, K. 2004. Adhesion of Colloids: Dispersion, Aggregation, and Flocculation. *Molecular Adhesion and Its Applications.* Springer US.

Kenzaoui, B. H., Vilà, M. R., Miquel, J. M., Cengelli, F. & Juillerat-Jeanneret, L. (2012). Evaluation of uptake and transport of cationic and anionic ultrasmall iron oxide nanoparticles by human colon cells. *International journal of nanomedicine,* **7,** 1275.

Kessler, R. (2011). Engineered nanoparticles in consumer products: understanding a new ingredient. *Environmental health perspectives,* **119,** A120.

Khataee, A. R. & Kasiri, M. B. (2010). Photocatalytic degradation of organic dyes in the presence of nanostructured titanium dioxide: Influence of the chemical structure of dyes. *Journal of Molecular Catalysis A: Chemical,* **328,** 8-26.

Kidd, D. A., Johnson, M. & Clements, J. (2007). Development of an in vitro corrosion/irritation prediction assay using the EpiDerm™ skin model. *Toxicology in Vitro,* **21,** 1292-1297.

Kim, A. H., Sheline, C. T., Tian, M., Higashi, T., McMahon, R. J., Cousins, R. J. & Choi, D. W. (2000). L-type Ca2+ channel-mediated Zn2+ toxicity and modulation by ZnT-1 in PC12 cells. *Brain Research,* **886,** 99-107.

Kim, B.-S. & Mooney, D. J. (1998). Development of biocompatible synthetic extracellular matrices for tissue engineering. *Trends in Biotechnology,* **16,** 224-230.

Kim, J., Grate, J. W. & Wang, P. (2008). Nanobiocatalysis and its potential applications. *Trends in biotechnology,* **26,** 639-646.

Kimbrell, G. A. (2006). Nanomaterial Consumer Products and FDA Regulation: Regulatory Challenges and Necessary Amendments. *Nanotechnology Law & Business,* **3,** 329-338.

Kipp, J. E. (2004). The role of solid nanoparticle technology in the parenteral delivery of poorly water-soluble drugs. *International Journal of Pharmaceutics,* **284,** 109-122.

Kirby, B. 2010. *Micro- And Nanoscale Fluid Mechanics: Transport in Microfluidic Devices*, Cambridge University Press.

Klaine, S. J., Alvarez, P. J. J., Batley, G. E., Fernandes, T. F., Handy, R. D., Lyon, D. Y., Mahendra, S., McLaughlin, M. J. & Lead, J. R. (2008). Nanomaterials in the environment: Behavior, fate, bioavailability, and effects. *Environmental Toxicology and Chemistry,* **27,** 1825-1851.

Klausner, M., Ayehunie, S., Breyfogle, B. A., Wertz, P. W., Bacca, L. & Kubilus, J. (2007). Organotypic human oral tissue models for toxicological studies. *Toxicology in Vitro,* **21,** 938-949.

Klein, J. (2007). Probing the interactions of proteins and nanoparticles. *Proceedings of the National Academy of Sciences,* **104,** 2029-2030.

Köck, A., Schwarz, T., Kirnbauer, R., Urbanski, A., Perry, P., Ansel, J. C. & Luger, T. A. (1990). Human keratinocytes are a source for tumor necrosis factor alpha: evidence for synthesis and release upon stimulation with endotoxin or ultraviolet light. *The Journal of Experimental Medicine,* **172,** 1609-1614.

Kodali, V., Littke, M. H., Tilton, S. C., Teeguarden, J. G., Shi, L., Frevert, C. W., Wang, W., Pounds, J. G. & Thrall, B. D. (2013). Dysregulation of Macrophage Activation Profiles by Engineered Nanoparticles. *ACS Nano,* **7,** 6997-7010.

Koffie, R. M., Farrar, C. T., Saidi, L.-J., William, C. M., Hyman, B. T. & Spires-Jones, T. L. (2011). Nanoparticles enhance brain delivery of blood–brain barrier-impermeable probes for in vivo optical and magnetic resonance imaging. *Proceedings of the National Academy of Sciences,* **108,** 18837-18842.

Koizumi, T., Shirakura, H., Kumagai, H., Tatsumoto, H. & Suzuki, K. T. (1996). Mechanism of cadmium-induced cytotoxicity in rat hepatocytes: cadmium-induced active oxygen-related permeability changes of the plasma membrane. *Toxicology,* **114,** 125-134.

Kolb, H. & Mandrup-Poulsen, T. (2010). The global diabetes epidemic as a consequence of lifestyle-induced low-grade inflammation. *Diabetologia,* **53,** 10-20.

Koppel, D. E. (1972). Analysis of macromolecular polydispersity in intensity correlation spectroscopy: the method of cumulants. *The Journal of Chemical Physics,* **57,** 4814.

Koschier, F., Kostrubsky, V., Toole, C. & Gallo, M. A. (2011). In vitro effects of ethanol and mouthrinse on permeability in an oral buccal mucosal tissue construct. *Food and Chemical Toxicology,* **49,** 2524-2529.

Koziara, J. M., Lockman, P. R., Allen, D. D. & Mumper, R. J. (2003). In Situ Blood-Brain Barrier Transport of Nanoparticles. *Pharmaceutical Research,* **20,** 1772-1778.

Krause, B., Mende, M., Pötschke, P. & Petzold, G. (2010). Dispersability and particle size distribution of CNTs in an aqueous surfactant dispersion as a function of ultrasonic treatment time. *Carbon,* **48,** 2746-2754.

Krebs, F. C., Thomann, Y., Thomann, R. a. & Andreasen, J. W. (2008). A simple nanostructured polymer/ZnO hybrid solar cell—preparation and operation in air. *Nanotechnology,* **19,** 424013.

Kreuter, J. (2001). Nanoparticulate systems for brain delivery of drugs. *Advanced Drug Delivery Reviews,* **47,** 65-81.

Kreuter, J. (2012). Nanoparticulate systems for brain delivery of drugs. *Advanced drug delivery reviews*.

Kreuter, J. (2013). Mechanism of polymeric nanoparticle-based drug transport across the blood-brain barrier (BBB). *Journal of Microencapsulation,* **30,** 49-54.

Kreuter, J., Ramge, P., Petrov, V., Hamm, S., Gelperina, S. E., Engelhardt, B., Alyautdin, R., von Briesen, H. & Begley, D. J. (2003). Direct Evidence That Polysorbate-80-Coated Poly(Butylcyanoacrylate) Nanoparticles Deliver Drugs to the CNS via Specific Mechanisms Requiring Prior Binding of Drug to the Nanoparticles. *Pharmaceutical Research,* **20,** 409-416.

Kreyling, W., Semmler-Behnke, M. & Möller, W. (2006a). Health implications of nanoparticles. *Journal of Nanoparticle Research,* **8,** 543-562.

Kreyling, W. G. (2013). 1.3 Toxicokinetics of Inhaled Nanoparticles. *Commission for the Investigation of Health Hazards of Chemical Compounds in the Work Area,* **Chapter,** 32.

Kreyling, W. G., Semmler-Behnke, M. & Moller, W. (2006b). Ultrafine Particle-Lung Interactions: Does Size Matter? *Journal of Aerosol Medicine,* **19,** 74-83.

Kreyling, W. G., Semmler-Behnke, M., Seitz, J., Scymczak, W., Wenk, A., Mayer, P., Takenaka, S. & Oberdörster, G. (2009). Size dependence of the translocation of inhaled iridium and carbon nanoparticle aggregates from the lung of rats to the blood and secondary target organs. *Inhalation Toxicology,* **21,** 55-60.

Kreyling, W. G., Semmler, M., Erbe, F., Mayer, P., Takenaka, S., Schulz, H., Oberdorster, G. & Ziesenis, A. (2002). Translocation of ultrafine insoluble iridium particles from lung epithelium to extrapulmonary organs is size dependent but very low. *J Toxicol Environ Health A,* **65,** 1513-30.

Kroll, A., Pillukat, M., Hahn, D. & Schnekenburger, J. (2012). Interference of engineered nanoparticles with in vitro toxicity assays. *Archives of Toxicology,* **86,** 1123-1136.

Kroll, A., Pillukat, M. H., Hahn, D. & Schnekenburger, J. (2009). Current in vitro methods in nanoparticle risk assessment: Limitations and challenges. *European Journal of Pharmaceutics and Biopharmaceutics,* **72,** 370-377.

Kulkarni, U., Mahalingam, R., Pather, S. I., Li, X. & Jasti, B. (2009). Porcine buccal mucosa as an in vitro model: Relative contribution of epithelium and connective tissue as permeability barriers. *Journal of Pharmaceutical Sciences,* **98,** 471-483.

Kuriakose, T. A., Kalkura, S. N., Palanichamy, M., Arivuoli, D., Dierks, K., Bocelli, G. & Betzel, C. (2004). Synthesis of stoichiometric nano crystalline hydroxyapatite by ethanol-based sol–gel technique at low temperature. *Journal of Crystal Growth,* **263,** 517-523.

Kuypers, S. (2002). Soft X-Rays and Low-Voltage SEM in Practice. *Microchimica Acta,* **138,** 235-247.

Lademann, J., Richter, H., Schaefer, U. F., Blume-Peytavi, U., Teichmann, A., Otberg, N. & Sterry, W. (2006). Hair follicles - a long-term reservoir for drug delivery. *Skin Pharmacol Physiol,* **19,** 232-6.

Lademann, J., Weigmann, H., Rickmeyer, C., Barthelmes, H., Schaefer, H., Mueller, G. & Sterry, W. (1999). Penetration of titanium dioxide microparticles in a sunscreen formulation into the horny layer and the follicular orifice. *Skin Pharmacol Appl Skin Physiol,* **12,** 247-56.

Lagerweij, M. & Ten Cate, J. (2010). Remineralisation of enamel lesions with daily applications of a high-concentration fluoride gel and a fluoridated toothpaste: an in situ study. *Caries research,* **36,** 270-274.

Lalor, P., Revell, P., Gray, A., Wright, S., Railton, G. & Freeman, M. (1991). Sensitivity to titanium. A cause of implant failure? *Journal of Bone & Joint Surgery, British Volume,* **73,** 25-28.

Landsiedel, R., Ma-Hock, L., Kroll, A., Hahn, D., Schnekenburger, J., Wiench, K. & Wohlleben, W. (2010). Testing Metal-Oxide Nanomaterials for Human Safety. *Advanced Materials,* **22,** 2601-2627.

Lebonvallet, N., Boulais, N., Le Gall, C., Chéret, J., Pereira, U., Mignen, O., Bardey, V., Jeanmaire, C., Danoux, L. & Pauly, G. (2012). Characterization of neurons from adult human skin-derived precursors in serum-free medium: a PCR array and immunocytological analysis. *Experimental dermatology,* **21,** 195-200.

Lendenmann, U., Grogan, J. & Oppenheim, F. (2000). Saliva and dental pellicle-a review. *Advances in dental research,* **14,** 22-28.

Leroueil, P. R., Berry, S. A., Duthie, K., Han, G., Rotello, V. M., McNerny, D. Q., Baker, J. R., Orr, B. G. & Banaszak Holl, M. M. (2008). Wide varieties of cationic nanoparticles induce defects in supported lipid bilayers. *Nano letters,* **8,** 420-424.

Lewicka, Z. A., Yu, W. W., Oliva, B. L., Contreras, E. Q. & Colvin, V. L. (2013). Photochemical behavior of nanoscale TiO2 and ZnO sunscreen ingredients. *Journal of Photochemistry and Photobiology A: Chemistry,* **263,** 24-33.

Lewinski, N., Colvin, V. & Drezek, R. (2008). Cytotoxicity of nanoparticles. *Small,* **4,** 26-49.

Li, Q., Mahendra, S., Lyon, D. Y., Brunet, L., Liga, M. V., Li, D. & Alvarez, P. J. J. (2008). Antimicrobial nanomaterials for water disinfection and microbial control: Potential applications and implications. *Water Research,* **42,** 4591-4602.

Li, W. & Kong, A. N. (2009). Molecular mechanisms of Nrf2-mediated antioxidant response. *Mol Carcinog,* **48,** 91-104.

Li, X. Y., Brown, D., Smith, S., MacNee, W. & Donaldson, K. (1999). Short-term inflammatory responses following intratracheal instillation of fine and ultrafine carbon black in rats. *Inhal Toxicol,* **11,** 709-31.

Limbach, L. K., Wick, P., Manser, P., Grass, R. N., Bruinink, A. & Stark, W. J. (2007). Exposure of engineered nanoparticles to human lung epithelial cells:influence of chemical composition and catalytic activity on oxidative stress. *Environmental Science & Technology,* **41,** 4158-4163.

Lin, I. C., Liang, M., Liu, T.-Y., Monteiro, M. J. & Toth, I. (2012). Cellular transport pathways of polymer coated gold nanoparticles. *Nanomedicine : nanotechnology, biology, and medicine,* **8,** 8-11.

Lin, J., Zhang, H., Chen, Z. & Zheng, Y. (2010). Penetration of Lipid Membranes by Gold Nanoparticles: Insights into Cellular Uptake, Cytotoxicity, and Their Relationship. *ACS Nano,* **4,** 5421-5429.

Lin, L., Grice, J., Butler, M., Zvyagin, A., Becker, W., Robertson, T., Soyer, H. P., Roberts, M. & Prow, T. (2011). Time-Correlated Single Photon Counting For Simultaneous Monitoring Of Zinc Oxide Nanoparticles And NAD(P)H In Intact And Barrier-Disrupted Volunteer Skin. *Pharmaceutical Research,* **28,** 2920-2930.

Lin, W., Xu, Y., Huang, C.-C., Ma, Y., Shannon, K., Chen, D.-R. & Huang, Y.-W. (2009). Toxicity of nano- and micro-sized ZnO particles in human lung epithelial cells. *Journal of Nanoparticle Research,* **11,** 25-39.

Lin, Y.-H., Chen, C.-T., Liang, H.-F., Kulkarni, A. R., Lee, P.-W., Chen, C.-H. & Sung, H.-W. (2007). Novel nanoparticles for oral insulin delivery via the paracellular pathway. *Nanotechnology,* **18,** 105102.

Linsinger, T., Roebben, G., Gilliland, D., Calzolai, L., Rossi, F., Gibson, P. & Klein, C. (2012a). Requirements on measurements for the implementation of the European Commission definition of the term 'nanomaterial'. **European Commission: Institute for Reference Materials and Measurements,** Luxemburg. JRC73260 EUR 25404 EN 1-56.

Linsinger, T., Roebben, G., Gilliland, D., Calzolai, L., Rossi, F., Gibson, P. & Klein, C. (2012b). Requirements on measurements for the implementation of the European Commission definition of the term 'nanomaterial'. *EUR Report,* **25404**.

Lipka, J., Semmler-Behnke, M., Sperling, R. A., Wenk, A., Takenaka, S., Schleh, C., Kissel, T., Parak, W. J. & Kreyling, W. G. (2010). Biodistribution of PEG-modified gold nanoparticles following intratracheal instillation and intravenous injection. *Biomaterials,* **31,** 6574-6581.

Lison, D., Thomassen, L. C. J., Rabolli, V., Gonzalez, L., Napierska, D., Seo, J. W., Kirsch-Volders, M., Hoet, P., Kirschhock, C. E. A. & Martens, J. A. (2008). Nominal and Effective Dosimetry of Silica Nanoparticles in Cytotoxicity Assays. *Toxicological Sciences,* **104,** 155-162.

Liu, J. & Hurt, R. H. (2010). Ion release kinetics and particle persistence in aqueous nano-silver colloids. *Environmental science & technology,* **44,** 2169-2175.

Liu, T., Li, L., Fu, C., Liu, H., Chen, D. & Tang, F. (2012). Pathological mechanisms of liver injury caused by continuous intraperitoneal injection of silica nanoparticles. *Biomaterials,* **33,** 2399-2407.

Liu, X. & Sun, J. (2010). Endothelial cells dysfunction induced by silica nanoparticles through oxidative stress via JNK/P53 and NF-[kappa]B pathways. *Biomaterials,* **31,** 8198-8209.

Liu, Y., He, L., Mustapha, A., Li, H., Hu, Z. Q. & Lin, M. (2009). Antibacterial activities of zinc oxide nanoparticles against Escherichia coli O157:H7. *J Appl Microbiol,* **107,** 1193-201.

Lockman, P. R., Koziara, J., Roder, K. E., Paulson, J., Abbruscato, T. J., Mumper, R. J. & Allen, D. D. (2003). In vivo and in vitro assessment of baseline blood-brain barrier parameters in the presence of novel nanoparticles. *Pharm Res,* **20,** 705-13.

Lockman, P. R., Mumper, R. J., Khan, M. A. & Allen, D. D. (2002). Nanoparticle Technology for Drug Delivery Across the Blood-Brain Barrier. *Drug Development and Industrial Pharmacy,* **28,** 1 - 13.

Lodish H, B. A., Zipursky SL, Matsudaira P, Baltimore D and Darnell J 2000. Active Transport by ATP-Powered Pumps. *In:* Freeman, W. H. (ed.) *Molecular Cell Biology 4th edition.* New York: W. H. Freeman and Company.

Loessner, D., Stok, K. S., Lutolf, M. P., Hutmacher, D. W., Clements, J. A. & Rizzi, S. C. (2010). Bioengineered 3D platform to explore cell–ECM interactions and drug resistance of epithelial ovarian cancer cells. *Biomaterials,* **31,** 8494-8506.

Lomer, M. C. E., Thompson, R. P. H. & Powell, J. J. (2002). Fine and ultrafine particles of the diet: influence on the mucosal immune response and association with Crohn?s disease. *Proceedings of the Nutrition Society,* **61,** 123-130.

Lorenz, C., Von Goetz, N., Scheringer, M., Wormuth, M. & Hungerbühler, K. (2011). Potential exposure of German consumers to engineered nanoparticles in cosmetics and personal care products. *Nanotoxicology,* **5,** 12-29.

Lovric, J., Cho, S., Winnik, F. & Maysinger, D. (2005). Unmodified cadmium telluride quantum dots induce reactive oxygen species formation leading to multiple organelle damage and cell death. *Chem Biol,* **12,** 1227 - 1234.

Lu, Y., Zhang, G., Shen, C., Uygun, K., Yarmush, M. L. & Meng, Q. (2012). A novel 3D liver organoid system for elucidation of hepatic glucose metabolism. *Biotechnology and Bioengineering,* **109,** 595-604.

Lund, T., Callaghan, M. F., Williams, P., Turmaine, M., Bachmann, C., Rademacher, T., Roitt, I. M. & Bayford, R. (2011). The influence of ligand organization on the rate of uptake of gold nanoparticles by colorectal cancer cells. *Biomaterials,* **32,** 9776-9784.

Lundborg, M., Dahlén, S.-E., Johard, U., Gerde, P., Jarstrand, C., Camner, P. & Låstbom, L. (2006). Aggregates of ultrafine particles impair phagocytosis of microorganisms by human alveolar macrophages. *Environmental research,* **100,** 197-204.

Lundqvist, M., Stigler, J., Elia, G., Lynch, I., Cedervall, T. & Dawson, K. A. (2008). Nanoparticle size and surface properties determine the protein corona with possible implications for biological impacts. *Proceedings of the National Academy of Sciences,* **105,** 14265-14270.

Lussi, A., Hellwig, E., Zero, D. & Jaeggi, T. (2006). Erosive tooth wear: diagnosis, risk factors and prevention. *American journal of dentistry,* **19,** 319.

Lussi, A., Schlueter, N., Rakhmatullina, E. & Ganss, C. (2011). Dental erosion–an overview with emphasis on chemical and histopathological aspects. *Caries research,* **45,** 2-12.

Lyklema, J. 2005. *Fundamentals of Interface and Colloid Science: Soft Colloids*, Elsevier Science.

Lynch, I., Cedervall, T., Lundqvist, M., Cabaleiro-Lago, C., Linse, S. & Dawson, K. A. (2007). The nanoparticle-protein complex as a biological entity; a complex fluids and surface science challenge for the 21st century. *Advances in Colloid and Interface Science,* **134-135,** 167-174.

Macfarlane, M., Jones, P., Goebel, C., Dufour, E., Rowland, J., Araki, D., Costabel-Farkas, M., Hewitt, N. J., Hibatallah, J., Kirst, A., McNamee, P., Schellauf, F. & Scheel, J. (2009). A tiered approach to the use of alternatives to animal testing for the safety assessment of cosmetics: Skin irritation. *Regulatory Toxicology and Pharmacology,* **54,** 188-196.

Maitra, P., Brown, S. E., Glynn, J. R., Rothouse, J., Brahms, J. C. & Fair, M. J. (2008). Gel Technology Suitable for Use in Cosmetic Compositions. **Google Patents**.

Malloy, A. & Carr, B. (2006). NanoParticle Tracking Analysis – The Halo™ System. *Particle & Particle Systems Characterization,* **23,** 197-204.

Malvern (1996). Sample dispersion and refractive index guide. **Malvern Instruments Ltd.,,** Malvern. MRK 0172-01 1-1 to 2-1.

Malvern (2001). Zeta Potential An Introduction in 30 Minutes **Malvern Instruments Ltd.,** Malvern Website. Zetasizer Nano series technical note MRK654-01 1-6.

Malvern. (2011). *Zetasizer Nano ZS90* [Online]. Malvern, Worcestershire: Instruments Ltd. Available: http://www.malvern.com/labeng/products/zetasizer/zetasizer_nano/zetasizer_nano_zs90.htm?gclid=CN_Cl_3Nn6sCFeILtAodZHbokQ [Accessed 15th Septemeber 2011].

Mao, J., Wang, L., Qian, Z. & Tu, M. (2010). Uptake and cytotoxicity of Ce(IV) doped TiO_2 nanoparticles in human hepatocyte cell line L02. *J. Nanomaterials,* **2010,** 1-8.

Marchiando, A. M., Graham, W. V. & Turner, J. R. (2010). Epithelial barriers in homeostasis and disease. *Annual Review of Pathological Mechanical Disease,* **5,** 119-144.

Maret, W. & Moulis, J.-M. 2013. The Bioinorganic Chemistry of Cadmium in the Context of Its Toxicity. *In:* Sigel, A., Sigel, H. & Sigel, R. K. O. (eds.) *Cadmium: From Toxicity to Essentiality*. Springer Netherlands.

Marin, F., Luquet, G., Marie, B. & Medakovic, D. (2008). Molluscan shell proteins: primary structure, origin, and evolution. *Curr Top Dev Biol,* **80,** 209-76.

Markowitz, K. (2012). A new treatment alternative for sensitive teeth: A desensitizing oral rinse. *Journal of Dentistry*.

Márquez-Ramírez, S. G., Delgado-Buenrostro, N. L., Chirino, Y. I., Iglesias, G. G. & López-Marure, R. (2012). Titanium dioxide nanoparticles inhibit proliferation and induce morphological changes and apoptosis in glial cells. *Toxicology,* **302,** 146-156.

Martin, K. (2007). The chemistry of silica and its potential health benefits. *The Journal of nutrition, health & aging,* **11,** 94-98.

Marvin, H. J., Bouwmeester, H., Bakker, M., Kroese, E. D., van de Meent, D., Bourgeois, F., Lokers, R., van der Ham, H. & Verhelst, L. (2013). Exploring the development of a decision support system (DSS) to prioritize engineered nanoparticles for risk assessment. *Journal of nanoparticle research,* **15,** 1-13.

Mason, S., Paradiso, A. & Boucher, R. (1991). Regulation of transepithelial ion transport and intracellular calcium by extracellular ATP in human normal and cystic fibrosis airway epithelium. *British journal of pharmacology,* **103,** 1649-1656.

Massignani, M., LoPresti, C., Blanazs, A., Madsen, J., Armes, S. P., Lewis, A. L. & Battaglia, G. (2009). Controlling Cellular Uptake by Surface Chemistry, Size, and Surface Topology at the Nanoscale. *Small,* **5,** 2424-2432.

Masuoka, J. & Saltman, P. (1994). Zinc(II) and copper(II) binding to serum albumin. A comparative study of dog, bovine, and human albumin. *J Biol Chem,* **269,** 25557-61.

Mathaes, R., Winter, G., Engert, J. & Besheer, A. (2013). Application of different analytical methods for the characterization of non-spherical micro- and nanoparticles. *International Journal of Pharmaceutics,* **453,** 620-629.

Mathes, S. H., Wohlwend, L., Uebersax, L., von Mentlen, R., Thoma, D. S., Jung, R. E., Görlach, C. & Graf-Hausner, U. (2010). A bioreactor test system to mimic the biological and mechanical environment of oral soft tissues and to evaluate substitutes for connective tissue grafts. *Biotechnology and Bioengineering,* **107,** 1029-1039.

MatTek. (2010). *EpiOral™ and EpiGingival™ Technical Specifications* [Online]. Ashland, MA: Corperation. Available: http://www.mattek.com/pages/products/epioral/specification [Accessed 24th August 2010].

Mattes, R. D. (1997). Physiologic Responses to Sensory Stimulation by Food: Nutritional Implications. *Journal of the American Dietetic Association,* **97,** 406-413.

Mattson, M. P. & Chan, S. L. (2003). Calcium orchestrates apoptosis. *Nat Cell Biol,* **5,** 1041-1043.

Maurer-Jones, M. A., Lin, Y.-S. & Haynes, C. L. (2010). Functional Assessment of Metal Oxide Nanoparticle Toxicity in Immune Cells. *ACS Nano,* **4,** 3363-3373.

Maynard, A. (2007a). *Industry critics give nanotechnology sunscreens the thumbs up* [Online]. Edinburgh: Safe Nano organistation. Available: http://community.safenano.org/blogs/andrew_maynard/archive/2009/07/05/industry-critics-give-nanotechnology-sunscreens-the-thumbs-up.aspx [Accessed 8th August 2010].

Maynard, A. D. (2007b). Nanotechnology: The Next Big Thing, or Much Ado about Nothing? *Annals of Occupational Hygiene,* **51,** 1-12.

Maynard, A. D. (2011). Don't define nanomaterials. *Nature,* **475,** 31-31.

Maynard, A. D., Aitken, R. J., Butz, T., Colvin, V., Donaldson, K., Oberdorster, G., Philbert, M. A., Ryan, J., Seaton, A., Stone, V., Tinkle, S. S., Tran, L., Walker, N. J. & Warheit, D. B. (2006). Safe handling of nanotechnology. *Nature,* **444,** 267-269.

Mazzoleni, G., Di Lorenzo, D. & Steimberg, N. (2009). Modelling tissues in 3D: the next future of pharmaco-toxicology and food research? *Genes & nutrition,* **4,** 13-22.

Mazzone, S. B., Reynolds, S. M., Mori, N., Kollarik, M., Farmer, D. G., Myers, A. C. & Canning, B. J. (2009). Selective Expression of a Sodium Pump Isozyme by Cough Receptors and Evidence for Its Essential Role in Regulating Cough. *The Journal of Neuroscience,* **29,** 13662-13671.

McCall, M. J., Coleman, V. A., Herrmann, J., Kirby, J. K., Gardner, I. R., Brent, P. J. & Johnson, C. M. (2013). A tiered approach. *Nature nanotechnology,* **8,** 307-308.

McKelvey-Martin, V., Green, M., Schmezer, P., Pool-Zobel, B., De Meo, M. & Collins, A. (1993). The single cell gel electrophoresis assay (comet assay): a European review. *Mutation Research/Fundamental and Molecular Mechanisms of Mutagenesis,* **288,** 47-63.

McNeilly, C., Banes, A., Benjamin, M. & Ralphs, J. (1996). Tendon cells in vivo form a three dimensional network of cell processes linked by gap junctions. *Journal of anatomy,* **189,** 593.

Medina-Kauwe, L. K. (2007). "Alternative" endocytic mechanisms exploited by pathogens: New avenues for therapeutic delivery? *Advanced Drug Delivery Reviews,* **59,** 798-809.

Meidan, V. M., Bonner, M. C. & Michniak, B. B. (2005). Transfollicular drug delivery--Is it a reality? *International Journal of Pharmaceutics,* **306,** 1-14.

Meißner, T., Potthoff, A. & Richter, V. Suspension characterization as important key for toxicological investigations. Journal of Physics: Conference Series, 2009. IOP Publishing, 012012.

Merhi, M., Dombu, C. Y., Brient, A., Chang, J., Platel, A., Le Curieux, F., Marzin, D., Nesslany, F. & Betbeder, D. (2012). Study of serum interaction with a cationic nanoparticle: Implications for in vitro endocytosis, cytotoxicity and genotoxicity. *International Journal of Pharmaceutics,* **423,** 37-44.

Merry, R., Belfield, L., McArdle, P., McLennan, A., Crean, S. & Foey, A. (2012). Oral health and pathology: a macrophage account. *British Journal of Oral and Maxillofacial Surgery,* **50,** 2-7.

Meyer, U., Handschel, J. & Wiesmann, H. P. 2009. *Fundamentals of Tissue Engineering and Regenerative Medicine*, Springer Berlin Heidelberg.

Mihranyan, A., Ferraz, N. & Strømme, M. (2012). Current status and future prospects of nanotechnology in cosmetics. *Progress in Materials Science,* **57,** 875-910.

Minang, J. T., Areström, I., Troye-Blomberg, M., Lundeberg, L. & Ahlborg, N. (2006). Nickel, cobalt, chromium, palladium and gold induce a mixed Th1- and Th2-type cytokine response in vitro in subjects with contact allergy to the respective metals. *Clinical & Experimental Immunology,* **146,** 417-426.

Moharamzadeh, K., Brook, I. M., Van Noort, R., Scutt, A. M. & Thornhill, M. H. (2007). Tissue-engineered oral mucosa: a review of the scientific literature. *J Dent Res,* **86,** 115-24.

Moharamzadeh, K., Colley, H., Murdoch, C., Hearnden, V., Chai, W. L., Brook, I. M., Thornhill, M. H. & MacNeil, S. (2012). Tissue-engineered Oral Mucosa. *Journal of Dental Research.*

Moharamzadeh, K., Franklin, K. L., Brook, I. M. & van Noort, R. (2009). Biologic Assessment of Antiseptic Mouthwashes Using a Three-Dimensional Human Oral Mucosal Model. *Journal of Periodontology,* **80,** 769-775.

Monteiro-Riviere, N. A., Inman, A. O. & Zhang, L. W. (2009). Limitations and relative utility of screening assays to assess engineered nanoparticle toxicity in a human cell line. *Toxicology and Applied Pharmacology,* **234,** 222-235.

Monteiro-Riviere, N. A., Wiench, K., Landsiedel, R., Schulte, S., Inman, A. O. & Riviere, J. E. (2011). Safety evaluation of sunscreen formulations containing titanium dioxide and zinc oxide nanoparticles in UVB sunburned skin: an in vitro and in vivo study. *Toxicological Sciences,* **123,** 264-280.

Monteleone, G., Caruso, R. & Pallone, F. (2014). Targets for new immunomodulation strategies in inflammatory bowel disease. *Autoimmunity Reviews,* **13,** 11-14.

Montes-Burgos, I., Walczyk, D., Hole, P., Smith, J., Lynch, I. & Dawson, K. (2010). Characterisation of nanoparticle size and state prior to nanotoxicological studies. *Journal of Nanoparticle Research,* **12,** 47-53.

Moore, C., Addy, M. & Moran, J. (2008). Toothpaste detergents: a potential source of oral soft tissue damage? *International Journal of Dental Hygiene,* **6,** 193-198.

Moos, P. J., Chung, K., Woessner, D., Honeggar, M., Cutler, N. S. & Veranth, J. M. (2010). ZnO Particulate Matter Requires Cell Contact for Toxicity in Human Colon Cancer Cells. *Chemical Research in Toxicology,* **23,** 733-739.

Morabito, K., Shapley, N. C., Steeley, K. G. & Tripathi, A. (2011). Review of sunscreen and the emergence of non-conventional absorbers and their applications in ultraviolet protection. *International Journal of Cosmetic Science,* **33,** 385-390.

Moran, C. A., Mullick, F. G., Ishak, K. G., Johnson, F. B. & Hummer, W. B. (1991). Identification of titanium in human tissues: Probable role in pathologic processes. *Human Pathology,* **22,** 450-454.

Mortensen, L. J., OberdoÌˆrster, G., Pentland, A. P. & DeLouise, L. A. (2008). In Vivo Skin Penetration of Quantum Dot Nanoparticles in the Murine Model: The Effect of UVR. *Nano Letters,* **8,** 2779-2787.

Mosmann, T. (1983). Rapid colorimetric assay for cellular growth and survival: Application to proliferation and cytotoxicity assays. *Journal of Immunological Methods,* **65,** 55-63.

Mossman, B., Light, W. & Wei, E. (1983). Asbestos: Mechanisms of Toxicity and Carcinogenicity in the Respiratory Tract. *Annual Review of Pharmacology and Toxicology,* **23,** 595-615.

Mostefaoui, Y., Claveau, I. & Rouabhia, M. (2004). In vitro analyses of tissue structure and interleukin-1β expression and production by human oral mucosa in response to *Candida albicans* infections. *Cytokine,* **25,** 162-171.

Motskin, M., Wright, D. M., Muller, K., Kyle, N., Gard, T. G., Porter, A. E. & Skepper, J. N. (2009). Hydroxyapatite nano and microparticles: Correlation of particle properties with cytotoxicity and biostability. *Biomaterials,* **30,** 3307-3317.

Moutsopoulos, N. M. & Madianos, P. N. (2006). Low-Grade Inflammation in Chronic Infectious Diseases. *Annals of the New York Academy of Sciences,* **1088,** 251-264.

Moyes, S. M., Morris, J. F. & Carr, K. E. (2010). Culture conditions and treatments affect Caco-2 characteristics and particle uptake. *International Journal of Pharmaceutics,* **387,** 7-18.

Mroz, R. M., Schins, R. P., Li, H., Jimenez, L. A., Drost, E. M., Holownia, A., MacNee, W. & Donaldson, K. (2008). Nanoparticle-driven DNA damage mimics irradiation-related carcinogenesis pathways. *Eur Respir J,* **31,** 241-51.

Mueller, D., Krämer, L., Hoffmann, E., Klein, S. & Noor, F. (2013). 3D organotypic HepaRG cultures as in vitro model for acute and repeated dose toxicity studies. *Toxicology in Vitro,* **In Press,** Available online 9 July 2013.

Muller, L., Riediker, M., Wick, P., Mohr, M., Gehr, P. & Rothen-Rutishauser, B. (2010). Oxidative stress and inflammation response after nanoparticle exposure: differences between human lung cell monocultures and an advanced three-dimensional model of the human epithelial airways. *J R Soc Interface,* **7 Suppl 1,** S27-40.

Murdock, R. C., Braydich-Stolle, L., Schrand, A. M., Schlager, J. J. & Hussain, S. M. (2008). Characterization of Nanomaterial Dispersion in Solution Prior to In Vitro Exposure Using Dynamic Light Scattering Technique. *Toxicological Sciences,* **101,** 239-253.

Murthy, V. N. & Stevens, C. F. (1998). Synaptic vesicles retain their identity through the endocytic cycle. *Nature,* **392,** 497-501.

Musa, M., Kannan, T. P. & Ab Rahman, I. (2012). Assessment of DNA damage caused by locally produced hydroxyapatite-silica nanocomposite using Comet assay on human lung fibroblast cell line. *Molecular & Cellular Toxicology,* **8,** 53-60.

Nachlas, M. M., Margulies, S. I., Goldberg, J. D. & Seligman, A. M. (1960). The determination of lactic dehydrogenase with a tetrazolium salt. *Analytical Biochemistry,* **1,** 317-326.

Nagarajan, P. & Rajagopalan, V. (2008). Enhanced bioactivity of ZnO nanoparticles - an antimicrobial study. *Science and Technology of Advanced Materials,* **9,** 035004.

Nair, S., Sasidharan, A., Divya Rani, V. V., Menon, D., Nair, S., Manzoor, K. & Raina, S. (2009). Role of size scale of ZnO nanoparticles and microparticles on toxicity toward bacteria and osteoblast cancer cells. *Journal of Materials Science: Materials in Medicine,* **20,** 235-241.

NanoSight. (2009). *Applications of Nanoparticle Tracking Analysis (NTA) in Nanoparticle Research* [Online]. Amesbury, Wiltshire: Ltd. Available: http://www.nanosight.com/appnotes/M110B%20Application%20Review%20NTA%20April%202009.pdf [Accessed 16th September 2011].

Navrotsky, A., Mazeina, L. & Majzlan, J. (2008). Size-driven structural and thermodynamic complexity in iron oxides. *Science,* **319,** 1635-1638.

Nel, A., Xia, T., Madler, L. & Li, N. (2006). Toxic Potential of Materials at the Nanolevel. *Science,* **311,** 622-627.

Nel, A. E., Madler, L., Velegol, D., Xia, T., Hoek, E. M. V., Somasundaran, P., Klaessig, F., Castranova, V. & Thompson, M. (2009). Understanding biophysicochemical interactions at the nano-bio interface. *Nat Mater,* **8,** 543-557.

Nel, A. E., Nasser, E., Godwin, H., Avery, D., Bahadori, T., Bergeson, L., Beryt, E., Bonner, J. C., Boverhof, D. & Carter, J. (2013). A Multi-Stakeholder Perspective on the Use of Alternative Test Strategies for Nanomaterial Safety Assessment. *ACS nano,* **7,** 6422-6433.

Nelson, B. C., Peterson, E. J., Marquis, B. J., Atha, D. H., Elliott, J. T., Cleveland, D., Watson, S. S., Tseng, I.-H., Dillon, A., Theodore, M. & Jackman, J. (2013). NIST gold nanoparticle reference materials do not induce oxidative DNA damage. *Nanotoxicology,* **7,** 21-29.

Nemmar, A., Hoet, P. H., Vanquickenborne, B., Dinsdale, D., Thomeer, M., Hoylaerts, M. F., Vanbilloen, H., Mortelmans, L. & Nemery, B. (2002). Passage of inhaled particles into the blood circulation in humans. *Circulation,* **105,** 411-4.

Neuhoff, S., Ungell, A.-L., Zamora, I. & Artursson, P. (2005). pH-Dependent passive and active transport of acidic drugs across Caco-2 cell monolayers. *European Journal of Pharmaceutical Sciences,* **25,** 211-220.

Newby, C. S., Rowland, J. L., Lynch, R. J. M., Bradshaw, D. J., Whitworth, D. & Bosma, M. L. (2011). Benefits of a silica-based fluoride toothpaste containing o-cymen-5-ol, zinc chloride and sodium fluoride. *International Dental Journal,* **61,** 74-80.

NHS. (2013). *How to keep your teeth clean* [Online]. NHS Choices: UK government. Available: http://www.nhs.uk/Livewell/dentalhealth/Pages/Teethcleaningguide.aspx [Accessed 21st October 2013].

Nicolazzo, J. A., Reed, B. L. & Finnin, B. C. (2003). The effect of various in vitro conditions on the permeability characteristics of the buccal mucosa. *Journal of Pharmaceutical Sciences,* **92,** 2399-2410.

Nicolazzo, J. A., Reed, B. L. & Finnin, B. C. (2005). Buccal penetration enhancers—How do they really work? *Journal of Controlled Release,* **105,** 1-15.

Nishikawa, S. (2011). Fluorescent AM1-43 and FM1-43 probes for dental sensory nerves and cells: Their labeling mechanisms and applications. *Japanese Dental Science Review,* **47,** 150-156.

Nishimori, H., Kondoh, M., Isoda, K., Tsunoda, S.-i., Tsutsumi, Y. & Yagi, K. (2009). Silica nanoparticles as hepatotoxicants. *European Journal of Pharmaceutics and Biopharmaceutics,* **72,** 496-501.

Nohynek, G. J., Antignac, E., Re, T. & Toutain, H. (2010). Safety assessment of personal care products/cosmetics and their ingredients. *Toxicology and Applied Pharmacology,* **243,** 239-259.

Nohynek, G. J., Lademann, J., Ribaud, C. & Roberts, M. S. (2007). Grey Goo on the Skin? Nanotechnology, Cosmetic and Sunscreen Safety. *Critical Reviews in Toxicology,* **37,** 251 - 277.

Nyström, A. M. & Fadeel, B. (2012). Safety assessment of nanomaterials: Implications for nanomedicine. *Journal of Controlled Release,* **161,** 403-408.

O'Mullane, D. M., Cochran, J. A. & Whelton, H. P. (2004). Fluoride ingestion from toothpaste: background to European Union-funded multicentre project. *Community Dentistry and Oral Epidemiology,* **32,** 5-8.

O'Neill, L. A. & Greene, C. (1998). Signal transduction pathways activated by the IL-1 receptor family: ancient signaling machinery in mammals, insects, and plants. *Journal of Leukocyte Biology,* **63,** 650-7.

Oberdörster, G. (2010). Safety assessment for nanotechnology and nanomedicine: concepts of nanotoxicology. *Journal of Internal Medicine,* **267,** 89-105.

Oberdorster, G., Finkelstein, J. N., Johnston, C., Gelein, R., Cox, C., Baggs, R. & Elder, A. C. (2000). Acute pulmonary effects of ultrafine particles in rats and mice. *Res Rep Health Eff Inst***,** 5-74; disc 75-86.

Oberdorster, G., Maynard, A., Donaldson, K., Castranova, V., Fitzpatrick, J., Ausman, K., Carter, J., Karn, B., Kreyling, W., Lai, D., Olin, S., Monteiro-Riviere, N., Warheit, D. & Yang, H. (2005a). A report from the ILSI Research Foundation/Risk Science Institute Nanomaterial Toxicity Screening Working Group: **Principles for characterizing the potential human health effects from exposure to nanomaterials: elements of a screening strategy**. *Particle and Fibre Toxicology,* **2,** 8.

Oberdorster, G., Oberdorster, E. & Oberdorster, J. (2005b). Nanotoxicology: An Emerging Discipline Evolving from Studies of Ultrafine Particles. *Environ Health Perspect,* **113**.

Oberdorster, G., Oberdorster, E. & Oberdorster, J. (2007). Concepts of nanoparticle dose metric and response metric. *Environ Health Perspect,* **115,** A290.

Okamoto, C. T. (1998). Endocytosis and transcytosis. *Advanced Drug Delivery Reviews,* **29,** 215-228.

Okeson, C. D., Riley, M. R. & Riley-Saxton, E. (2004). In vitro alveolar cytotoxicity of soluble components of airborne particulate matter: effects of serum on toxicity of transition metals. *Toxicology in Vitro,* **18,** 673-680.

Olivier, J.-C., Fenart, L., Chauvet, R., Pariat, C., Cecchelli, R. & Couet, W. (1999). Indirect Evidence that Drug Brain Targeting Using Polysorbate 80-Coated Polybutylcyanoacrylate Nanoparticles Is Related to Toxicity. *Pharmaceutical Research,* **16,** 1836-1842.

Ong, G. (1990). The effectiveness of 3 types of dental floss for interdental plaque removal. *Journal of clinical periodontology,* **17,** 463-466.

Oostingh, G., Casals, E., Italiani, P., Colognato, R., Stritzinger, R., Ponti, J., Pfaller, T., Kohl, Y., Ooms, D., Favilli, F., Leppens, H., Lucchesi, D., Rossi, F., Nelissen, I., Thielecke, H., Puntes, V., Duschl, A. & Boraschi, D. (2011). Problems and challenges in the development and validation of human cell-based assays to determine nanoparticle-induced immunomodulatory effects. *Particle and Fibre Toxicology,* **8,** 8.

Orenbuch, A., Shulman, Y., Lipstein, N., Bechar, A., Lavy, Y., Brumer, E., Vasileva, M., Kahn, J., Barki-Harrington, L. & Kuner, T. (2012). Inhibition of exocytosis or endocytosis blocks activity-dependent redistribution of synapsin. *Journal of neurochemistry,* **120,** 248-258.

Ostuni, E., Chapman, R. G., Holmlin, R. E., Takayama, S. & Whitesides, G. M. (2001). A Survey of Structure−Property Relationships of Surfaces that Resist the Adsorption of Protein. *Langmuir,* **17,** 5605-5620.

Pabst, W. & Gregorová, E. (2007). Characterization of particles and particle systems. **Institute of Chemical Technology,** Prague, Czech Republic.

Pal, S., Tak, Y. K. & Song, J. M. (2007). Does the Antibacterial Activity of Silver Nanoparticles Depend on the Shape of the Nanoparticle? A Study of the Gram-Negative Bacterium Escherichia coli. *Applied and Environmental Microbiology,* **73,** 1712-1720.

Pampaloni, F., Reynaud, E. G. & Stelzer, E. H. K. (2007). The third dimension bridges the gap between cell culture and live tissue. *Nat Rev Mol Cell Biol,* **8,** 839-845.

Pan, C., Kumar, C., Bohl, S., Klingmueller, U. & Mann, M. (2009). Comparative Proteomic Phenotyping of Cell Lines and Primary Cells to Assess Preservation of Cell Type-specific Functions. *Molecular & Cellular Proteomics,* **8,** 443-450.

Papageorgiou, I., Brown, C., Schins, R., Singh, S., Newson, R., Davis, S., Fisher, J., Ingham, E. & Case, C. P. (2007). The effect of nano- and micron-sized particles of cobalt-chromium alloy on human fibroblasts in vitro. *Biomaterials,* **28,** 2946-2958.

Park, E.-J. & Park, K. (2009). Oxidative stress and pro-inflammatory responses induced by silica nanoparticles in vivo and in vitro. *Toxicology Letters,* **184,** 18-25.

Park, E.-J., Yoon, J., Choi, K., Yi, J. & Park, K. (2009). Induction of chronic inflammation in mice treated with titanium dioxide nanoparticles by intratracheal instillation. *Toxicology,* **260,** 37-46.

Park, H.-O., Yu, M., Kang, S., Yang, S. & Kim, Y.-J. (2011). Comparison of cellular effects of titanium dioxide nanoparticles with different photocatalytic potential in human keratinocyte, HaCaT cells. *Molecular & Cellular Toxicology,* **7,** 67-75.

Park, Y.-H., Bae, H., Jang, Y., Jeong, S., Lee, H., Ryu, W.-I., Yoo, M., Kim, Y.-R., Kim, M.-K., Lee, J., Jeong, J. & Son, S. (2013). Effect of the size and surface charge of silica nanoparticles on cutaneous toxicity. *Molecular & Cellular Toxicology,* **9,** 67-74.

Patel, R. (2012). The state of oral health in Europe. **Report commissioned by The Platform for Better Oral Health in Europe,** European Union. September 2012.

Patel, V., Yeudall, W. A., Gardner, A., Mutlu, S., Scully, C. & Prime, S. S. (1993). Consistent chromosomal anomalies in keratinocyte cell lines derived from untreated malignant lesions of the oral cavity. *Genes, Chromosomes and Cancer,* **7,** 109-115.

Patlolla, A., Patlolla, B. & Tchounwou, P. (2010). Evaluation of cell viability, DNA damage, and cell death in normal human dermal fibroblast cells induced by functionalized multiwalled carbon nanotube. *Molecular and Cellular Biochemistry,* **338,** 225-232.

Patnode, W. & Scheiber, W. J. (1939). The Density, Thermal Expansion, Vapor Pressure, and Refractive Index of Styrene, and the Density and Thermal Expansion of Polystyrene. *Journal of the American Chemical Society,* **61,** 3449-3451.

Patri, A., Umbreit, T., Zheng, J., Nagashima, K., Goering, P., Francke-Carroll, S., Gordon, E., Weaver, J., Miller, T., Sadrieh, N., McNeil, S. & Stratmeyer, M. (2009). Energy dispersive X-ray analysis of titanium dioxide nanoparticle

distribution after intravenous and subcutaneous injection in mice. *Journal of Applied Toxicology,* **29,** 662-672.

Pedersen, De Bruijn, F. J., Munn, S. J. & Van Leeuwen, K. (2003). Assessment of additional testing needs under REACH. Effects of (Q)SARs, risk based testing and voluntary industry initiatives. September 2003. **European Commission,** Brussels, Belgium. EUR 20863 EN.

Penn, A., Murphy, G., Barker, S., Henk, W. & Penn, L. (2005). Combustion-Derived Ultrafine Particles Transport Organic Toxicants to Target Respiratory Cells. *Environ Health Perspect,* **113**.

Penn, S. G., He, L. & Natan, M. J. (2003). Nanoparticles for bioanalysis. *Current Opinion in Chemical Biology,* **7,** 609-615.

Pescosolido, L., Schuurman, W., Malda, J., Matricardi, P., Alhaique, F., Coviello, T., van Weeren, P. R., Dhert, W. J. A., Hennink, W. E. & Vermonden, T. (2011). Hyaluronic Acid and Dextran-Based Semi-IPN Hydrogels as Biomaterials for Bioprinting. *Biomacromolecules,* **12,** 1831-1838.

Petersen, P. E. (2003). The World Oral Health Report 2003: continuous improvement of oral health in the 21st century – the approach of the WHO Global Oral Health Programme. *Community Dentistry and Oral Epidemiology,* **31,** 3-24.

Pickrell, J. A., van der Merwe, D., Erickson, L. E., Dhakal, K., Dhakal, M., Klabunde, K. J. & Sorensen, C. 2010. Comparative Pulmonary Toxicity of Metal Oxide Nanoparticles. *Nanoscale Materials in Chemistry: Environmental Applications.* American Chemical Society.

Piersma, A. H. (2006). Alternative Methods for Developmental Toxicity Testing. *Basic & Clinical Pharmacology & Toxicology,* **98,** 427-431.

Pihlstrom, B. L., Michalowicz, B. S. & Johnson, N. W. (2005). Periodontal diseases. *The Lancet,* **366,** 1809-1820.

Ponec, M. & Kempenaar, J. (1995). Use of Human Skin Recombinants as an in vitro Model for Testing the Irritation Potential of Cutaneous Irritants. *Skin Pharmacology and Physiology,* **8,** 49-59.

Popat, K. (2010). Nanotechnology in Tissue Engineering and Regenerative Medicine. **Taylor & Francis,** Boca Raton, FL, USA. 1st edition 302.

Porter, S., Scully, C. & Hegarty, A. (2004). An update of the etiology and management of xerostomia. *Oral Surgery, Oral Medicine, Oral Pathology, Oral Radiology, and Endodontology,* **97,** 28-46.

Powell, J. J., Faria, N., Thomas-McKay, E. & Pele, L. C. (2010). Origin and fate of dietary nanoparticles and microparticles in the gastrointestinal tract. *Journal of autoimmunity,* **34,** J226-J233.

Powers, K. W., Brown, S. C., Krishna, V. B., Wasdo, S. C., Moudgil, B. M. & Roberts, S. M. (2006). Research Strategies for Safety Evaluation of Nanomaterials. Part VI. Characterization of Nanoscale Particles for Toxicological Evaluation. *Toxicological Sciences,* **90,** 296-303.

Prasad, R. Y., McGee, J. K., Killius, M. G., Suarez, D. A., Blackman, C. F., DeMarini, D. M. & Simmons, S. O. (2013a). Investigating oxidative stress and inflammatory responses elicited by silver nanoparticles using high-throughput reporter genes in HepG2 cells: Effect of size, surface coating, and intracellular uptake. *Toxicology in Vitro,* **27,** 2013-2021.

Prasad, R. Y., Wallace, K., Daniel, K. M., Tennant, A. H., Zucker, R. M., Strickland, J., Dreher, K., Kligerman, A. D., Blackman, C. F. & DeMarini, D. M. (2013b). Effect of Treatment Media on the Agglomeration of Titanium Dioxide Nanoparticles: Impact on Genotoxicity, Cellular Interaction, and Cell Cycle. *ACS Nano,* **7,** 1929-1942.

Presland, R. B. & Dale, B. A. (2000). Epithelial structural proteins of the skin and oral cavity: function in health and disease. *Crit Rev Oral Biol Med,* **11,** 383-408.
Presland, R. B. & Jurevic, R. J. (2002). Making sense of the epithelial barrier: what molecular biology and genetics tell us about the functions of oral mucosal and epidermal tissues. *J Dent Educ,* **66,** 564-74.
Proctor, P. H. & Reynolds, E. S. (1984). Free radicals and disease in man. *Physiol Chem Phys Med NMR,* **16,** 175-95.
Promega. (2010). *CellTiter 96 Non-Radioactive Cell Proliferation Assay Technical Bulletin #TB169* [Online]. Madison, WI: Promega Corperation. Available: http://www.promega.com/tbs/tb169/tb169.html.
Provder, T. (1997). Challenges in particle size distribution measurement past, present and for the 21st century. *Progress in Organic Coatings,* **32,** 143-153.
Puckett, C. A., Ernst, R. J. & Barton, J. K. (2010). Exploring the cellular accumulation of metal complexes. *Dalton Transactions,* **39,** 1159-1170.
Rabani, E. (2001). Structure and electrostatic properties of passivated CdSe nanocrystals. *J Chem Phys,* **115,** 1493 - 1497.
Rabolli, V., Thomassen, L. C. J., Princen, C., Napierska, D., Gonzalez, L., Kirsch-Volders, M., Hoet, P. H., Huaux, F., Kirschhock, C. E. A., Martens, J. A. & Lison, D. (2010). Influence of size, surface area and microporosity on the in vitro cytotoxic activity of amorphous silica nanoparticles in different cell types. *Nanotoxicology,* **4,** 307-318.
Rada, B. & Leto, T. L. (2008). Oxidative innate immune defenses by Nox/Duox family NADPH oxidases. *Contrib Microbiol,* **15,** 164-87.
Radisic, M., Park, H., Shing, H., Consi, T., Schoen, F. J., Langer, R., Freed, L. E. & Vunjak-Novakovic, G. (2004). Functional assembly of engineered myocardium by electrical stimulation of cardiac myocytes cultured on scaffolds. *Proceedings of the National Academy of Sciences,* **101,** 18129-18134.
Rahimnejad, M. M., Jahanshahi, M. & Najafpour, G. D. (2006). Production of biological nanoparticles from bovine serum albumin for drug delivery. *African Journal of Biotechnology,* **5,** 1918-1923.
Rahman, I. (2002). Oxidative Stress and Gene Transcription in Asthma and Chronic Obstructive Pulmonary Disease: Antioxidant Therapeutic Targets. *Current Drug Targets - Inflammation & Allergy,* **1,** 291-315.
Raj, S., Jose, S., Sumod, U. & Sabitha, M. (2012). Nanotechnology in cosmetics: Opportunities and challenges. *Journal of pharmacy & bioallied sciences,* **4,** 186.
Rea, R., Li, J., Dharia, A., Levitan, E. S., Sterling, P. & Kramer, R. H. (2004). Streamlined Synaptic Vesicle Cycle in Cone Photoreceptor Terminals. *Neuron,* **41,** 755-766.
Reed, S. J. B. 2005. *Electron microprobe analysis and scanning electron microscopy in geology*, Cambridge University Press Cambridge.
Ren, D. & Daines, D. A. (2011). Use of the EpiAirway model for characterizing long-term host-pathogen interactions. *Journal of visualized experiments: JoVE.*
Renwick, L. C., Donaldson, K. & Clouter, A. (2001). Impairment of Alveolar Macrophage Phagocytosis by Ultrafine Particles. *Toxicology and Applied Pharmacology,* **172,** 119-127.
Rhee, M. & Davis, P. (2006). Mechanism of Uptake of C105Y, a Novel Cell-penetrating Peptide. *Journal of Biological Chemistry,* **281,** 1233-1240.
Rhodus, N. L., Cheng, B., Myers, S., Bowles, W., Ho, V. & Ondrey, F. (2005). A comparison of the pro-inflammatory, NF-κB-dependent cytokines: TNF-alpha, IL-1-alpha, IL-6, and IL-8 in different oral fluids from oral lichen planus patients. *Clinical Immunology,* **114,** 278-283.

Richards, D. A., Bai, J. & Chapman, E. R. (2005). Two modes of exocytosis at hippocampal synapses revealed by rate of FM1-43 efflux from individual vesicles. *The Journal of cell biology,* **168,** 929-939.

Rimann, M. & Graf-Hausner, U. (2012). Synthetic 3D multicellular systems for drug development. *Current Opinion in Biotechnology,* **23,** 803-809.

Robinson, V. C., Bergfeld, W. F., Belsito, D. V., Hill, R. A., Klaassen, C. D., Marks, J. G., Jr., Shank, R. C., Slaga, T. J., Snyder, P. W. & Alan Andersen, F. (2010). Final report of the amended safety assessment of sodium laureth sulfate and related salts of sulfated ethoxylated alcohols. *Int J Toxicol,* **29,** 151S-61S.

Roebben, G., Ramirez-Garcia, S., Hackley, V., Roesslein, M., Klaessig, F., Kestens, V., Lynch, I., Garner, C., Rawle, A. & Elder, A. (2011). Interlaboratory comparison of size and surface charge measurements on nanoparticles prior to biological impact assessment. *Journal of Nanoparticle Research,* **13,** 2675-2687.

Romoser, A. A., Figueroa, D. E., Sooresh, A., Scribner, K., Chen, P. L., Porter, W., Criscitiello, M. F. & Sayes, C. M. (2012). Distinct immunomodulatory effects of a panel of nanomaterials in human dermal fibroblasts. *Toxicology Letters,* **210,** 293-301.

Ross, G. M., Shamovsky, I. L., Lawrance, G., Solc, M., Dostaler, S. M., Jimmo, S. L., Weaver, D. F. & Riopelle, R. J. (1997). Zinc alters conformation and inhibits biological activities of nerve growth factor and related neurotrophins. *Nat Med,* **3,** 872-878.

Rossi, S., Sandri, G. & Caramella, C. M. (2005). Buccal drug delivery: A challenge already won? *Drug Discovery Today: Technologies,* **2,** 59-65.

Rothen-Rutishauser, B., Blank, F., Mühlfeld, C. & Gehr, P. (2008). In vitro models of the human epithelial airway barrier to study the toxic potential of particulate matter. *Expert Opinion on Drug Metabolism & Toxicology,* **4,** 1075-1089.

Rovida, C. & Hartung, T. (2009). Re-evaluation of animal numbers and costs for in vivo tests to accomplish REACH legislation requirements for chemicals-a report by the transatlantic think tank for toxicology (t (4)). *Altex,* **26,** 187.

Ruge, C. A., Kirch, J., Cañadas, O., Schneider, M., Perez-Gil, J., Schaefer, U. F., Casals, C. & Lehr, C.-M. (2011). Uptake of nanoparticles by alveolar macrophages is triggered by surfactant protein A. *Nanomedicine: Nanotechnology, Biology and Medicine,* **7,** 690-693.

Rupniak, H. T., Rowlatt, C., Lane, E. B., Steele, J. G., Trejdosiewicz, L. K., Laskiewicz, B., Povey, S. & Hill, B. T. (1985). Characteristics of four new human cell lines derived from squamous cell carcinomas of the head and neck. *Journal of the National Cancer Institute,* **75,** 621-635.

Russell, W. M. S., Burch, R. L. & Hume, C. W. (1959). The principles of humane experimental technique.

Rybachuk, A. V., Chekman, I. S. & Nebesna, T. Y. (2009). Nanotechnology and nanoparticles in dentistry. *Pharmacol Pharm,* **1,** 18-20.

Ryman-Rasmussen, J., Riviere, J. & Monteiro-Riviere, N. (2007). Surface coatings determine cytotoxicity and irritation potential of quantum dot nanoparticles in epidermal keratinocytes. *J Invest Dermatol,* **127,** 143 - 153.

Sackmann, E. & Tanaka, M. (2000). Supported membranes on soft polymer cushions: fabrication, characterization and applications. *Trends in Biotechnology,* **18,** 58-64.

Sacks, P., Parnes, S., Price, J., Risemberg, H., Goldstein, J., Marko, M. & Parsons, D. (1985). In vitro modulation of differentiation by calcium in organ cultures of human and murine epithelial tissue. *In Vitro Cellular & Developmental Biology - Plant,* **21,** 99-107.

Sacks, P. G. (1996). Cell, tissue and organ culture as in vitro models to study the biology of squamous cell carcinomas of the head and neck. *Cancer and Metastasis Reviews,* **15,** 27-51.

Saha, K., Kim, S. T., Yan, B., Miranda, O. R., Alfonso, F. S., Shlosman, D. & Rotello, V. M. (2013). Surface Functionality of Nanoparticles Determines Cellular Uptake Mechanisms in Mammalian Cells. *Small,* **9,** 300-305.

Salido, G. M., Rosado, J. A. & Salido, G. M. 2009. Oxidative Stress, Intracellular Calcium Signals and Apoptotic Processes. *Apoptosis: Involvement of Oxidative Stress and Intracellular Ca2+ Homeostasi.* Springer Netherlands.

Samberg, M. E., Oldenburg, S. J. & Monteiro-Riviere, N. A. (2009). Evaluation of Silver Nanoparticle Toxicity in Skin *in Vivo* and Keratinocytes *in Vitro. Environ Health Perspect,* **118**.

Sambuy, Y., Angelis, I., Ranaldi, G., Scarino, M. L., Stammati, A. & Zucco, F. (2005). The Caco-2 cell line as a model of the intestinal barrier: influence of cell and culture-related factors on Caco-2 cell functional characteristics. *Cell Biology and Toxicology,* **21,** 1-26.

Sanches, G., Alencar, L. S. d. & Ventura, A. L. M. (2002). ATP induces proliferation of retinal cells in culture via activation of PKC and extracellular signal-regulated kinase cascade. *International Journal of Developmental Neuroscience,* **20,** 21-27.

Sandjeu, Y. & Haftek, M. (2009). Desmosealin and other components of the epidermal extracellular matrix. *J Physiol Pharmacol,* **60 Suppl 4,** 23-30.

Sandvig, K. & van Deurs, B. (2005). Delivery into cells: lessons learned from plant and bacterial toxins. *Gene Ther,* **12,** 865-872.

Sang, X., Zheng, L., Sun, Q., Li, N., Cui, Y., Hu, R., Gao, G., Cheng, Z., Cheng, J., Gui, S., Liu, H., Zhang, Z. & Hong, F. (2012). The chronic spleen injury of mice following long-term exposure to titanium dioxide nanoparticles. *Journal of Biomedical Materials Research Part A,* **100A,** 894-902.

Sarin, H., Kanevsky, A., Wu, H., Brimacombe, K., Fung, S., Sousa, A., Auh, S., Wilson, C., Sharma, K., Aronova, M., Leapman, R., Griffiths, G. & Hall, M. (2008). Effective transvascular delivery of nanoparticles across the blood-brain tumor barrier into malignant glioma cells. *Journal of Translational Medicine,* **6,** 80.

Sasaki, R., Yamato, M., Takagi, R., Ohki, T., Matsumine, H., Okano, T. & Ando, T. (2012). Punch and spindle-shaped biopsies for collecting oral mucosal tissue for the fabrication of transplantable autologous epithelial cell sheets. *Journal of Biomedical Materials Research Part A,* **100A,** 2849-2854.

Sawai, J., Igarashi, H., Hashimoto, A., Kokugan, T. & Shimizu, M. (1996). Effect of Particle Size and Heating Temperature of Ceramic Powders on Antibacterial Activity of Their Slurries. *Journal of chemical engineering of japan,* **29,** 251-256.

Saxton, C. A., Harrap, G. J. & Lloyd, A. M. (1986). The effect of dentifrices containing zinc citrate on plaque growth and oral zinc levels. *Journal of Clinical Periodontology,* **13,** 301-306.

Schaeublin, N. M., Braydich-Stolle, L. K., Schrand, A. M., Miller, J. M., Hutchison, J., Schlager, J. J. & Hussain, S. M. (2011). Surface charge of gold nanoparticles mediates mechanism of toxicity. *Nanoscale,* **3,** 410-420.

Schaller, M., Boeld, U., Oberbauer, S., Hamm, G., Hube, B. & Korting, H. C. (2004). Polymorphonuclear leukocytes (PMNs) induce protective Th1-type cytokine epithelial responses in an in vitro model of oral candidosis. *Microbiology,* **150,** 2807-2813.

Scheel, J. & Hermann, M. (2011). Integrated risk assessment of a hydroxyapatite-protein-composite for use in oral care products: A weight-of-evidence case study. *Regulatory Toxicology and Pharmacology,* **59,** 310-323.

Schemehorn, B., Orban, J., Wood, G., Fischer, G. & Winston, A. (1999). Remineralization by fluoride enhanced with calcium and phosphate ingredients. *The Journal of clinical dentistry,* **10,** 13.

Schilling, K., Bradford, B., Castelli, D., Dufour, E., Nash, J. F., Pape, W., Schulte, S., Tooley, I., van den Bosch, J. & Schellauf, F. (2010). Human safety review of "nano" titanium dioxide and zinc oxide. *Photochemical & Photobiological Sciences,* **9,** 495-509.

Schins, R. P. F., Lightbody, J. H., Borm, P. J. A., Shi, T., Donaldson, K. & Stone, V. (2004). Inflammatory effects of coarse and fine particulate matter in relation to chemical and biological constituents. *Toxicology and Applied Pharmacology,* **195,** 1-11.

Schleh, C., Semmler-Behnke, M., Lipka, J., Wenk, A., Hirn, S., Schäffler, M., Schmid, G., Simon, U. & Kreyling, W. G. (2012). Size and surface charge of gold nanoparticles determine absorption across intestinal barriers and accumulation in secondary target organs after oral administration. *Nanotoxicology,* **6,** 36-46.

Schlesinger, L., Arevalo, M., Arredondo, S., Lönnerdal, B. & Stekel, A. (1993). Zinc supplementation impairs monocyte function. *Acta Paediatrica,* **82,** 734-738.

Schmalz, G., Schweikl, H. & Hiller, K.-A. (2000). Release of prostaglandin E2, IL-6 and IL-8 from human oral epithelial culturemodels after exposure to compounds of dental materials. *European Journal of Oral Sciences,* **108,** 442-448.

Schrand, A. M., Rahman, M. F., Hussain, S. M., Schlager, J. J., Smith, D. A. & Syed, A. F. (2010). Metal-based nanoparticles and their toxicity assessment. *Wiley Interdisciplinary Reviews: Nanomedicine and Nanobiotechnology,* **2,** 544-568.

Schroder, J. M. (1995). Cytokine networks in the skin. *J Invest Dermatol,* **105,** 20S-24S.

Schug, T. T., Johnson, A. F., Balshaw, D. M., Garantziotis, S., Walker, N. J., Weis, C., Nadadur, S. S. & Birnbaum, L. S. (2013). ONE Nano: NIEHS's Strategic Initiative on the Health and Safety Effects of Engineered Nanomaterials. *Environmental health perspectives,* **121,** 410.

Schulz, J., Hohenberg, H., Pflücker, F., Gärtner, E., Will, T., Pfeiffer, S., Wepf, R., Wendel, V., Gers-Barlag, H. & Wittern, K. P. (2002). Distribution of sunscreens on skin. *Advanced Drug Delivery Reviews,* **54,** S157-S163.

Schulze-Lohoff, E., Hugo, C., Rost, S., Arnold, S., Gruber, A., Brüne, B. & Sterzel, R. B. (1998). Extracellular ATP causes apoptosis and necrosis of cultured mesangial cells via P2Z/P2X7receptors. *American Journal of Physiology - Renal Physiology,* **275,** F962-F971.

Schulze, C., Kroll, A., Lehr, C.-M., Schaefer, U. F., Becker, K., Schnekenburger, J., Schulze Isfort, C., Landsiedel, R. & Wohlleben, W. (2008). Not ready to use – overcoming pitfalls when dispersing nanoparticles in physiological media. *Nanotoxicology,* **2,** 51-61.

Schwiebert, E. M. & Zsembery, A. (2003). Extracellular ATP as a signaling molecule for epithelial cells. *Biochimica et Biophysica Acta (BBA) - Biomembranes,* **1615,** 7-32.

Scully, C. & Felix, D. H. (2005). Oral Medicine [mdash] Update for the dental practitioner Oral malodour. *Br Dent J,* **199,** 498-500.

Seaton, A., Tran, L., Aitken, R. & Donaldson, K. (2010). Nanoparticles, human health hazard and regulation. *Journal of The Royal Society Interface,* **7,** S119-S129.

Senel, S. & Hincal, A. A. (2001). Drug permeation enhancement via buccal route: possibilities and limitations. *Journal of Controlled Release,* **72,** 133-144.

Senel, S., Kremer, M. J., Kas, S., Wertz, P. W., Hincal, A. A. & Squier, C. A. (2000). Enhancing effect of chitosan on peptide drug delivery across buccal mucosa. *Biomaterials,* **21,** 2067-2071.

Shah, N. B., Vercellotti, G. M., White, J. G., Fegan, A., Wagner, C. R. & Bischof, J. C. (2012). Blood–nanoparticle interactions and in vivo biodistribution: impact of surface PEG and ligand properties. *Molecular Pharmaceutics,* **9,** 2146-2155.

Sharma, H. S., Ali, S. F., Hussain, S. M., Schlager, J. J. & Sharma, A. (2009a). Influence of engineered nanoparticles from metals on the blood-brain barrier permeability, cerebral blood flow, brain edema and neurotoxicity. An experimental study in the rat and mice using biochemical and morphological approaches. *Journal of nanoscience and nanotechnology,* **9,** 5055-5072.

Sharma, V., Anderson, D. & Dhawan, A. (2012). Zinc oxide nanoparticles induce oxidative DNA damage and ROS-triggered mitochondria mediated apoptosis in human liver cells (HepG2). *Apoptosis,* **17,** 852-870.

Sharma, V., Shukla, R. K., Saxena, N., Parmar, D., Das, M. & Dhawan, A. (2009b). DNA damaging potential of zinc oxide nanoparticles in human epidermal cells. *Toxicology Letters,* **185,** 211-218.

Sharma, V., Singh, S. K., Anderson, D., Tobin, D. J. & Dhawan, A. (2011). Zinc Oxide Nanoparticle Induced Genotoxicity in Primary Human Epidermal Keratinocytes. *Journal of Nanoscience and Nanotechnology,* **11,** 3782-3788.

Shojaei, A. H. (1998). Buccal mucosa as a route for systemic drug delivery: a review. *Journal of pharmaceutical and pharmacology sciences,* **1,** 15-30.

Shukla, R., Bansal, V., Chaudhary, M., Basu, A., Bhonde, R. R. & Sastry, M. (2005). Biocompatibility of gold nanoparticles and their endocytotic fate inside the cellular compartment: a microscopic overview. *Langmuir,* **21,** 10644-10654.

Shukla, R. K., Sharma, V., Pandey, A. K., Singh, S., Sultana, S. & Dhawan, A. (2011). ROS-mediated genotoxicity induced by titanium dioxide nanoparticles in human epidermal cells. *Toxicology in Vitro,* **25,** 231-241.

Shvedova, A., Castranova, V., Kisin, E., Schwegler-Berry, D., Murray, A., Gandelsman, V., Maynard, A. & Baron, P. (2003). Exposure to Carbon Nanotube Material: Assessment of Nanotube Cytotoxicity using Human Keratinocyte Cells. *Journal of Toxicology and Environmental Health, Part A: Current Issues,* **66,** 1909 - 1926.

Siddiqui, S. W., Unwin, P. J., Xu, Z. & Kresta, S. M. (2009). The effect of stabilizer addition and sonication on nanoparticle agglomeration in a confined impinging jet reactor. *Colloids and Surfaces A: Physicochemical and Engineering Aspects,* **350,** 38-50.

Silva, M. F., Cerutti, E. S. & Martinez, L. D. (2006). Coupling Cloud Point Extraction to Instrumental Detection Systems for Metal Analysis. *Microchimica Acta,* **155,** 349-364.

Silvers, A. R. & Som, P. M. (1998). Salivary Glands. *Radiologic Clinics of North America,* **36,** 941-966.

Simon-Deckers, A., Gouget, B., Mayne-L'Hermite, M., Herlin-Boime, N., Reynaud, C. & Carrière, M. (2008). In vitro investigation of oxide nanoparticle and carbon nanotube toxicity and intracellular accumulation in A549 human pneumocytes. *Toxicology,* **253,** 137-146.

Simon, M. I., Thorner, J., Emr, S. D. & Abelson, J. N. 2000. *Applications of Chimeric Genes and Hybrid Proteins, Part B: Cell Biology and Physiology: Cell Biology and Physiology*, Elsevier Science.

Sims, J. E., Gayle, M. A., Slack, J. L., Alderson, M. R., Bird, T. A., Giri, J. G., Colotta, F., Re, F., Mantovani, A. & Shanebeck, K. (1993). Interleukin 1 signaling occurs exclusively via the type I receptor. *Proceedings of the National Academy of Sciences,* **90,** 6155-6159.

Skapin, S. D., Drazic, G. & Orel, Z. C. (2007). Microstructure of nanoscale zinc oxide crystallites. *Materials Letters,* **61,** 2783-2788.

Slomiany, B. L., Murty, V. L. N., Piotrowski, J. & Slomiany, A. (1996). Salivary mucins in oral mucosal defense. *General Pharmacology: The Vascular System,* **27,** 761-771.

Soenen, S. J. & De Cuyper, M. (2010). Assessing iron oxide nanoparticle toxicity in vitro: current status and future prospects. *Nanomedicine,* **5,** 1261-1275.

Soenen, S. J., Manshian, B., Doak, S. H., De Smedt, S. C. & Braeckmans, K. (2013). Fluorescent non-porous silica nanoparticles for long-term cell monitoring: Cytotoxicity and particle functionality. *Acta Biomaterialia,* **9,** 9183-9193.

Soenen, S. J. H., Illyes, E., Vercauteren, D., Braeckmans, K., Majer, Z., De Smedt, S. C. & De Cuyper, M. (2009). The role of nanoparticle concentration-dependent induction of cellular stress in the internalization of non-toxic cationic magnetoliposomes. *Biomaterials,* **30,** 6803-6813.

Soenen, S. J. H., Nuytten, N., De Meyer, S. F., De Smedt, S. C. & De Cuyper, M. (2010). High Intracellular Iron Oxide Nanoparticle Concentrations Affect Cellular Cytoskeleton and Focal Adhesion Kinase-Mediated Signaling. *Small,* **6,** 832-842.

Solomon, A., Smyth, E., Mitha, N., Pitchford, S., Vydyanath, A., Luther, P., Thorley, A., Tetley, T. & Emerson, M. (2013). Induction of platelet aggregation after a direct physical interaction with diesel exhaust particles. *Journal of Thrombosis and Haemostasis,* **11,** 325-334.

Sonntag, F., Schilling, N., Mader, K., Gruchow, M., Klotzbach, U., Lindner, G., Horland, R., Wagner, I., Lauster, R., Howitz, S., Hoffmann, S. & Marx, U. (2010). Design and prototyping of a chip-based multi-micro-organoid culture system for substance testing, predictive to human (substance) exposure. *Journal of Biotechnology,* **148,** 70-75.

Soppimath, K. S., Aminabhavi, T. M., Kulkarni, A. R. & Rudzinski, W. E. (2001). Biodegradable polymeric nanoparticles as drug delivery devices. *Journal of Controlled Release,* **70,** 1-20.

Sotiriou, G. A. & Pratsinis, S. E. (2010). Antibacterial activity of nanosilver ions and particles. *Environmental science & technology,* **44,** 5649-5654.

Soto, K., Garza, K. M. & Murr, L. E. (2007). Cytotoxic effects of aggregated nanomaterials. *Acta Biomaterialia,* **3,** 351-358.

Spielmann, H., Hoffmann, S., Liebsch, M., Botham, P., Fentem, J. H., Eskes, C., Roguet, R., Cotovio, J., Cole, T., Worth, A., Heylings, J., Jones, P., Robles, C., Kandarova, H., Gamer, A., Remmele, M., Curren, R., Raabe, H., Cockshott, A., Gerner, I. & Zuang, V. (2007). The ECVAM international validation study on in vitro tests for acute skin irritation: report on the validity of the EPISKIN and EpiDerm assays and on the Skin Integrity Function Test. *Altern Lab Anim,* **35,** 559-601.

Squier, C. A. (1977). Membrane coating granules in nonkeratinizing oral epithelium. *Journal of Ultrastructure Research,* **60,** 212-220.

Squier, C. A., Cox, P. & Wertz, P. W. (1991). Lipid Content and Water Permeability of Skin and Oral Mucosa. *J Investig Dermatol,* **96,** 123-126.

Squier, C. A. & Hall, B. K. (1985). The Permeability of Skin and Oral Mucosa to Water and Horseradish Peroxidase as Related to the Thickness of the Permeability Barrier. *J Investig Dermatol,* **84,** 176-179.

Squier, C. A. & Kremer, M. J. (2001). Biology of oral mucosa and esophagus. *J Natl Cancer Inst Monogr,* 7-15.

Squier, C. A. & Wertz, P. W. (1993). Permeability and the pathophysiology of oral mucosa. *Advanced Drug Delivery Reviews,* **12,** 13-24.

Srivastava, B. I., Srivastava, A. & Srivastava, M. D. (1994). Phenotype, genotype and cytokine production in acute leukemia involving progenitors of dendritic Langerhans' cells. *Leuk Res,* **18,** 499-511.

Stefaniak, A. B., Hackley, V. A., Roebben, G., Ehara, K., Hankin, S., Postek, M. T., Lynch, I., Fu, W.-E., Linsinger, T. P. J. & Thünemann, A. F. (2013). Nanoscale reference materials for environmental, health and safety measurements: needs, gaps and opportunities. *Nanotoxicology,* **7,** 1325-1337.

Stefanidou, M., Maravelias, C., Dona, A. & Spiliopoulou, C. (2006). Zinc: a multipurpose trace element. *Archives of Toxicology,* **80,** 1-9.

Stone, V., Nowack, B., Baun, A., van den Brink, N., von der Kammer, F., Dusinska, M., Handy, R., Hankin, S., Hassellöv, M., Joner, E. & Fernandes, T. F. (2010). Nanomaterials for environmental studies: Classification, reference material issues, and strategies for physico-chemical characterisation. *Science of The Total Environment,* **408,** 1745-1754.

Stranding, S. 2008. *Gray's Anatomy: The Anatomical Basis of Clinical Practice*, Churchill Livingstone, Elsevier.

Strasser, A., O'Connor, L. & Dixit, V. M. (2000). Apoptosis signaling. *Annual Review of Biochemistry,* **69,** 217-245.

Stylianou, E. & Saklatvala, J. (1998). Interleukin-1. *The International Journal of Biochemistry & Cell Biology,* **30,** 1075-1079.

Subramani, K., Jung, R. E., Molenberg, A. & Hammerle, C. (2009). Biofilm on dental implants: a review of the literature. *The International journal of oral & maxillofacial implants,* **24,** 616.

Subramanian, B., Rudym, D., Cannizzaro, C., Perrone, R., Zhou, J. & Kaplan, D. L. (2010). Tissue-engineered three-dimensional in vitro models for normal and diseased kidney. *Tissue Engineering Part A,* **16,** 2821-2831.

Sudhakar, Y., Kuotsu, K. & Bandyopadhyay, A. K. (2006). Buccal bioadhesive drug delivery -- A promising option for orally less efficient drugs. *Journal of Controlled Release,* **114,** 15-40.

Sugano, K., Kansy, M., Artursson, P., Avdeef, A., Bendels, S., Di, L., Ecker, G. F., Faller, B., Fischer, H., Gerebtzoff, G., Lennernaes, H. & Senner, F. (2010). Coexistence of passive and carrier-mediated processes in drug transport. *Nat Rev Drug Discov,* **9,** 597-614.

Sullivan, R., Santarpia, P., Lavender, S., Gittins, E., Liu, Z., Anderson, M., He, J., Shi, W. & Eckert, R. (2011). Clinical efficacy of a specifically targeted antimicrobial peptide mouth rinse: targeted elimination of Streptococcus mutans and prevention of demineralization. *Caries research,* **45,** 415-428.

Sun, C., Lee, J. S. H. & Zhang, M. (2008a). Magnetic nanoparticles in MR imaging and drug delivery. *Advanced Drug Delivery Reviews,* **60,** 1252-1265.

Sun, H., Chow, E. C., Liu, S., Du, Y. & Pang, K. S. (2008b). The Caco-2 cell monolayer: usefulness and limitations. *Expert Opinion on Drug Metabolism & Toxicology,* **4,** 395-411.

Sun, T., Jackson, S., Haycock, J. W. & MacNeil, S. (2006). Culture of skin cells in 3D rather than 2D improves their ability to survive exposure to cytotoxic agents. *Journal of Biotechnology,* **122,** 372-381.

Sun, T. T., Tseng, S. C. G., Huang, A. J. W., Cooper, D., Schermer, A., Lynch, M. H., Weiss, R. & Eichner, R. (1985). Monoclonal Antibody Studies of Mammalian Epithelial Keratins: A Review a. *Annals of the New York Academy of Sciences,* **455,** 307-329.

Suska, F., Gretzer, C., Esposito, M., Tengvall, P. & Thomsen, P. (2005). Monocyte viability on titanium and copper coated titanium. *Biomaterials,* **26,** 5942-5950.

Svensson, C. R., Messing, M. E., Lundqvist, M., Schollin, A., Deppert, K., Pagels, J. H., Rissler, J. & Cedervall, T. (2013). Direct Deposition of Gas Phase Generated Aerosol Gold Nanoparticles into Biological Fluids-Corona Formation and Particle Size Shifts. *PloS one,* **8,** e74702.

Sze, A., Erickson, D., Ren, L. & Li, D. (2003). Zeta-potential measurement using the Smoluchowski equation and the slope of the current–time relationship in electroosmotic flow. *Journal of Colloid and Interface Science,* **261,** 402-410.

Taatjes, D., Sobel, B. & Budd, R. (2008). Morphological and cytochemical determination of cell death by apoptosis. *Histochemistry and Cell Biology,* **129,** 33-43.

Takenaka, S., Karg, E., Roth, C., Schulz, H., Ziesenis, A., Heinzmann, U., Schramel, P. & Heyder, J. (2001). Pulmonary and systemic distribution of inhaled ultrafine silver particles in rats. *Environ Health Perspect,* **109 Suppl 4,** 547-51.

Tan, M. H., Commens, C. A., Burnett, L. & Snitch, P. J. (1996). A pilot study on the percutaneous absorption of microfine titanium dioxide from sunscreens. *Australas J Dermatol,* **37,** 185-7.

Tay, C. Y., Fang, W., Setyawati, M. I., Sum, C. P., Xie, J., Ng, K. W., Chen, X., Hong, C. H. L. & Leong, D. T. (2013). Reciprocal Response of Human Oral Epithelial Cells to Internalized Silica Nanoparticles. *Particle & Particle Systems Characterization,* **30,** 784-793.

Tedja, R., Lim, M., Amal, R. & Marquis, C. (2012). Effects of Serum Adsorption on Cellular Uptake Profile and Consequent Impact of Titanium Dioxide Nanoparticles on Human Lung Cell Lines. *ACS Nano,* **6,** 4083-4093.

Teeguarden, J. G., Hinderliter, P. M., Orr, G., Thrall, B. D. & Pounds, J. G. (2007). Particokinetics In Vitro: Dosimetry Considerations for In Vitro Nanoparticle Toxicity Assessments. *Toxicological Sciences,* **95,** 300-312.

Tenzer, S., Docter, D., Kuharev, J., Musyanovych, A., Fetz, V., Hecht, R., Schlenk, F., Fischer, D., Kiouptsi, K. & Reinhardt, C. (2013). Rapid formation of plasma protein corona critically affects nanoparticle pathophysiology. *Nature nanotechnology,* **8,** 772-781.

Thevenot, P., Cho, J., Wavhal, D., Timmons, R. B. & Tang, L. (2008). Surface chemistry influences cancer killing effect of TiO2 nanoparticles. *Nanomedicine: Nanotechnology, Biology and Medicine,* **4,** 226-236.

Thomas, J. C. (1987). The determination of log normal particle size distributions by dynamic light scattering. *Journal of colloid and interface science,* **117,** 187-192.

Thomas, T., Thomas, K., Sadrieh, N., Savage, N., Adair, P. & Bronaugh, R. (2006). Research Strategies for Safety Evaluation of Nanomaterials, Part VII: Evaluating Consumer Exposure to Nanoscale Materials. *Toxicological Sciences,* **91,** 14-19.

Thubagere, A. & Reinhard, B. r. M. (2010). Nanoparticle-Induced Apoptosis Propagates through Hydrogen-Peroxide-Mediated Bystander Killing: Insights from a Human Intestinal Epithelium In Vitro Model. *ACS Nano,* **4,** 3611-3622.

Tinkle, S. S., Antonini, J. M., Rich, B. A., Roberts, J. R., Salmen, R., DePree, K. & Adkins, E. J. (2003). Skin as a Route of Exposure and Sensitization in Chronic Beryllium Disease. *Environ Health Perspect,* **111**.

Toll, R., Jacobi, U., Richter, H., Lademann, J., Schaefer, H. & Blume-Peytavi, U. (2003). Penetration Profile of Microspheres in Follicular Targeting of Terminal Hair Follicles. *J Investig Dermatol,* **123,** 168-176.

Treuel, L., Jiang, X. & Nienhaus, G. U. (2013). New views on cellular uptake and trafficking of manufactured nanoparticles. *Journal of The Royal Society Interface,* **10**.

Trung, T., Cho, W.-J. & Ha, C.-S. (2003). Preparation of TiO2 nanoparticles in glycerol-containing solutions. *Materials Letters,* **57,** 2746-2750.

Tschoppe, P., Zandim, D. L., Martus, P. & Kielbassa, A. M. (2011). Enamel and dentine remineralization by nano-hydroxyapatite toothpastes. *Journal of Dentistry,* **39,** 430-437.

Tsuji, J. S., Maynard, A. D., Howard, P. C., James, J. T., Lam, C. W., Warheit, D. B. & Santamaria, A. B. (2006). Research strategies for safety evaluation of nanomaterials, part IV: risk assessment of nanoparticles. *Toxicol Sci,* **89,** 42-50.

Tyagi, M., Rusnati, M., Presta, M. & Giacca, M. (2001). Internalization of HIV-1 tat requires cell surface heparan sulfate proteoglycans. *Journal of Biological Chemistry,* **276,** 3254-3261.

Valant, J., Iavicoli, I. & Drobne, D. (2012). The importance of a validated standard methodology to define in vitro toxicity of nano-TiO2. *Protoplasma,* **249,** 493-502.

Vallar, S., Houivet, D., El Fallah, J., Kervadec, D. & Haussonne, J. M. (1999). Oxide slurries stability and powders dispersion: optimization with zeta potential and rheological measurements. *Journal of the European Ceramic Society,* **19,** 1017-1021.

van der Lubben, I. M., Verhoef, J. C., Borchard, G. & Junginger, H. E. (2001). Chitosan and its derivatives in mucosal drug and vaccine delivery. *European Journal of Pharmaceutical Sciences,* **14,** 201-207.

van der Valk, J., Brunner, D., De Smet, K., Fex Svenningsen, Å., Honegger, P., Knudsen, L. E., Lindl, T., Noraberg, J., Price, A., Scarino, M. L. & Gstraunthaler, G. (2010). Optimization of chemically defined cell culture media – Replacing fetal bovine serum in mammalian in vitro methods. *Toxicology in Vitro,* **24,** 1053-1063.

Van Itallie, C. M. & Anderson, J. M. (2006). Claudins and epithelial paracellular transport. *Annu. Rev. Physiol.,* **68,** 403-429.

Vande Vannet, B., Hanssens, J.-L. & Wehrbein, H. (2007). The use of three-dimensional oral mucosa cell cultures to assess the toxicity of soldered and welded wires. *The European Journal of Orthodontics,* **29,** 60-66.

Vane, L. M. & Zang, G. M. (1997). Effect of aqueous phase properties on clay particle zeta potential and electro-osmotic permeability: Implications for electro-kinetic soil remediation processes. *Journal of Hazardous Materials,* **55,** 1-22.

Veerapandian, M., Marimuthu, M., KS, K. Y. & Kim, S. (2009). Biomaterial as nanobiopharmaceuticals. *Thai journal of pharmaceutical sciences,* **33,** 1-21.

Verma, A. & Stellacci, F. (2010). Effect of Surface Properties on Nanoparticle–Cell Interactions. *Small,* **6,** 12-21.

Vinardell, M. P. & Mitjans, M. (2008). Alternative methods for eye and skin irritation tests: An overview. *Journal of Pharmaceutical Sciences,* **97,** 46-59.

Vogt, A., Combadiere, B., Hadam, S., Stieler, K. M., Lademann, J., Schaefer, H., Autran, B., Sterry, W. & Blume-Peytavi, U. (2006). 40[thinsp]nm, but not 750 or 1,500[thinsp]nm, Nanoparticles Enter Epidermal CD1a+ Cells after Transcutaneous Application on Human Skin. *J Invest Dermatol,* **126,** 1316-1322.

Vranic, S., Boggetto, N., Contremoulins, V., Mornet, S., Reinhardt, N., Marano, F., Baeza-Squiban, A. & Boland, S. (2013a). Deciphering the mechanisms of cellular uptake of engineered nanoparticles by accurate evaluation of internalization using imaging flow cytometry. *Particle and Fibre Toxicology,* **10,** 2.

Vranic, S., Garcia-Verdugo, I., Darnis, C., Sallenave, J.-M., Boggetto, N., Marano, F., Boland, S. & Baeza-Squiban, A. (2013b). Internalization of SiO2 nanoparticles by alveolar macrophages and lung epithelial cells and its modulation by the lung surfactant substitute Curosurf®. *Environmental Science and Pollution Research***,** 1-10.

Wacker, W. E. C., Ulmer, D. D. & Vallee, B. L. (1956). Metalloenzymes and Myocardial Infarction. *New England Journal of Medicine,* **255,** 449-456.

Wadia, J. S. & Dowdy, S. F. (2005). Transmembrane delivery of protein and peptide drugs by TAT-mediated transduction in the treatment of cancer. *Advanced Drug Delivery Reviews,* **57,** 579-596.

Walker, D. M., Dolby, A. E., Joynson, D. M. & Jacobs, A. (1973). Mitotic index and migration inhibition factor: Effect of two different culture media. *Journal of Immunological Methods,* **3,** 315-317.

Walkey, C. D., Olsen, J. B., Guo, H., Emili, A. & Chan, W. C. W. (2011). Nanoparticle Size and Surface Chemistry Determine Serum Protein Adsorption and Macrophage Uptake. *Journal of the American Chemical Society,* **134,** 2139-2147.

Wallace, W., Keane, M., Murray, D., Chisholm, W., Maynard, A. & Ong, T.-m. (2007). Phospholipid lung surfactant and nanoparticle surface toxicity: Lessons from diesel soots and silicate dusts. *Journal of Nanoparticle Research,* **9,** 23-38.

Waltimo, T., Brunner, T., Vollenweider, M., Stark, W. & Zehnder, M. (2007). Antimicrobial effect of nanometric bioactive glass 45S5. *Journal of dental research,* **86,** 754-757.

Wang, G., Zhang, J., Dewilde, A. H., Pal, A. K., Bello, D., Therrien, J. M., Braunhut, S. J. & Marx, K. A. (2012a). Understanding and correcting for carbon nanotube interferences with a commercial LDH cytotoxicity assay. *Toxicology,* **299,** 99-111.

Wang, J., Liu, Y., Jiao, F., Lao, F., Li, W., Gu, Y., Li, Y., Ge, C., Zhou, G. & Li, B. (2008a). Time-dependent translocation and potential impairment on central nervous system by intranasally instilled TiO_2 nanoparticles. *Toxicology,* **254,** 82-90.

Wang, L., Nagesha, D., Selvarasah, S., Dokmeci, M. & Carrier, R. (2008b). Toxicity of CdSe Nanoparticles in Caco-2 Cell Cultures. *Journal of Nanobiotechnology,* **6,** 11.

Wang, P., Li, C., Gong, H., Jiang, X., Wang, H. & Li, K. (2010). Effects of synthesis conditions on the morphology of hydroxyapatite nanoparticles produced by wet chemical process. *Powder Technology,* **203,** 315-321.

Wang, S., Yu, H. & Wickliffe, J. K. (2011). Limitation of the MTT and XTT assays for measuring cell viability due to superoxide formation induced by nano-scale TiO2. *Toxicology in Vitro,* **25,** 2147-2151.

Wang, T. T., Bai, J., Jiang, X. & Nienhaus, G. U. (2012b). Cellular Uptake of Nanoparticles by Membrane Penetration: A Study Combining Confocal Microscopy with FTIR Spectroelectrochemistry. *Acs Nano,* **6,** 1251-1259.

Ward, P. D., Tippin, T. K. & Thakker, D. R. (2000). Enhancing paracellular permeability by modulating epithelial tight junctions. *Pharmaceutical Science & Technology Today,* **3,** 346-358.

Ware, L. B. (2008). Modeling human lung disease in animals. *Am J Physiol Lung Cell Mol Physiol,* **294,** L149-50.

Warheit, D. B., Borm, P. J., Hennes, C. & Lademann, J. (2007). Testing strategies to establish the safety of nanomaterials: conclusions of an ECETOC workshop. *Inhalation toxicology,* **19,** 631-643.

Watt, F. M. (1998). Epidermal stem cells: markers, patterning and the control of stem cell fate. *Philos Trans R Soc Lond B Biol Sci,* **353,** 831-7.

Watts, C. & Marsh, M. (1992). Endocytosis: what goes in and how. *J. Cell Sci,* **103,** 8.

Wei, X.-L., Mo, Z.-H., Li, B. & Wei, J.-M. (2007). Disruption of HepG2 cell adhesion by gold nanoparticle and Paclitaxel disclosed by in situ QCM measurement. *Colloids and Surfaces B: Biointerfaces,* **59,** 100-104.

Weir, A., Westerhoff, P., Fabricius, L., Hristovski, K. & von Goetz, N. (2012). Titanium Dioxide Nanoparticles in Food and Personal Care Products. *Environmental Science & Technology,* **46,** 2242-2250.

Welss, T., Basketter, D. A. & Schröder, K. R. (2004). In vitro skin irritation: facts and future. State of the art review of mechanisms and models. *Toxicology in Vitro,* **18,** 231-243.
Wertz, P. W. & Squier, C. A. (1991). Cellular and molecular basis of barrier function in oral epithelium. *Crit Rev Ther Drug Carrier Syst,* **8,** 237-69.
Wertz, P. W., Swartzendruber, D. C. & Squier, C. A. (1993). Regional variation in the structure and permeability of oral mucosa and skin. *Advanced Drug Delivery Reviews,* **12,** 1-12.
Weyermann, J., Lochmann, D. & Zimmer, A. (2005). A practical note on the use of cytotoxicity assays. *International Journal of Pharmaceutics,* **288,** 369-376.
Whitesides, G. (2005). Nanoscience, nanotechnology, and chemistry. *Small,* **1,** 172 - 179.
Williams, D. & Carter, C. B. 2009a. Scattering and Diffraction. *Transmission Electron Microscopy*. Springer US.
Williams, D. B. & Carter, C. B. 2009b. *Transmission Electron Microscopy: A Textbook for Materials Science*, Springer.
Williams, E. S., Panko, J. & Paustenbach, D. J. (2009). The European Union's REACH regulation: a review of its history and requirements. *Critical Reviews in Toxicology,* **39,** 553-575.
Williams, I. R. & Kupper, T. S. (1996). Immunity at the surface: Homeostatic mechanisms of the skin immune system. *Life Sciences,* **58,** 1485-1507.
Wilson, M. R., Foucaud, L., Barlow, P. G., Hutchison, G. R., Sales, J., Simpson, R. J. & Stone, V. (2007). Nanoparticle interactions with zinc and iron: implications for toxicology and inflammation. *Toxicology and applied pharmacology,* **225,** 80-89.
Winning, T. A. & Townsend, G. C. (2000). Oral mucosal embryology and histology. *Clinics in Dermatology,* **18,** 499-511.
Winterer, J., Stanton, P. K. & Muller, W. (2006). Direct monitoring of vesicular release and uptake in brain slices by multiphoton excitation of styryl FM® 1-43. *Biotechniques,* **40,** 343.
Wohlfart, S., Gelperina, S. & Kreuter, J. (2012). Transport of drugs across the blood–brain barrier by nanoparticles. *Journal of Controlled Release,* **161,** 264-273.
Wong, S., Leung, P., Djurišić, A. & Leung, K. (2010). Toxicities of nano zinc oxide to five marine organisms: influences of aggregate size and ion solubility. *Analytical and Bioanalytical Chemistry,* **396,** 609-618.
Woodrow-Wilson. (2010). *The Project on Emerging Nanotechnologies (PEN)* [Online]. Washington D.C. USA: Processwire: International centre for scholars and Pew charitable trusts. Available: http://www.nanotechproject.org [Accessed 4th May 2010].
Wörle-Knirsch, J. M., Pulskamp, K. & Krug, H. F. (2006). Oops They Did It Again! Carbon Nanotubes Hoax Scientists in Viability Assays. *Nano Letters,* **6,** 1261-1268.
Wu, H., Liu, G., Zhuang, Y., Wu, D., Zhang, H., Yang, H., Hu, H. & Yang, S. (2011). The behavior after intravenous injection in mice of multiwalled carbon nanotube / Fe3O4 hybrid MRI contrast agents. *Biomaterials,* **32,** 4867-4876.
Wu, J., Wang, L., He, J. & Zhu, C. (2012). In vitro cytotoxicity of Cu2+, Zn2+, Ag+ and their mixtures on primary human endometrial epithelial cells. *Contraception,* **85,** 509-518.
Wu, X. & Guy, R. (2009). Applications of nanoparticles in topical drug delivery and in cosmetics. *Journal of drug delivery science and technology,* **19,** 371-384.
Wyllie, A., Kerr, J. & Currie, A. (1980). Cell death: the significance of apoptosis. *Int Rev Cytol,* **68,** 251 - 306.

Xia, L., Stoll, S. W., Liebert, M., Ethier, S. P., Carey, T., Esclamado, R., Carroll, W., Johnson, T. M. & Elder, J. T. (1997). CaN19 expression in benign and malignant hyperplasias of the skin and oral mucosa: evidence for a role in regenerative differentiation. *Cancer Res,* **57,** 3055-62.

Xia, T., Korge, P., Weiss, J. N., Li, N., Venkatesen, M. I., Sioutas, C. & Nel, A. (2004). Quinones and aromatic chemical compounds in particulate matter induce mitochondrial dysfunction: implications for ultrafine particle toxicity. *Environ Health Perspect,* **112,** 1347-58.

Xia, T., Kovochich, M., Brant, J., Hotze, M., Sempf, J., Oberley, T., Sioutas, C., Yeh, J. I., Wiesner, M. R. & Nel, A. E. (2006). Comparison of the abilities of ambient and manufactured nanoparticles to induce cellular toxicity according to an oxidative stress paradigm. *Nano Lett,* **6,** 1794-807.

Xia, T., Kovochich, M., Liong, M., MaÌdler, L., Gilbert, B., Shi, H., Yeh, J. I., Zink, J. I. & Nel, A. E. (2008). Comparison of the Mechanism of Toxicity of Zinc Oxide and Cerium Oxide Nanoparticles Based on Dissolution and Oxidative Stress Properties. *ACS Nano,* **2,** 2121-2134.

Xia, T., Kovochich, M., Liong, M., Zink, J. I. & Nel, A. E. (2007). Cationic Polystyrene Nanosphere Toxicity Depends on Cell-Specific Endocytic and Mitochondrial Injury Pathways. *ACS Nano,* **2,** 85-96.

Xiao, G. G., Wang, M., Li, N., Loo, J. A. & Nel, A. E. (2003). Use of proteomics to demonstrate a hierarchical oxidative stress response to diesel exhaust particle chemicals in a macrophage cell line. *J Biol Chem,* **278,** 50781-90.

Xie, J., Xu, C., Kohler, N., Hou, Y. & Sun, S. (2007). Controlled PEGylation of Monodisperse Fe3O4 Nanoparticles for Reduced Non-Specific Uptake by Macrophage Cells. *Advanced Materials,* **19,** 3163-3166.

Xiong, S., George, S., Yu, H., Damoiseaux, R., France, B., Ng, K. & Loo, J.-C. (2013). Size influences the cytotoxicity of poly (lactic-co-glycolic acid) (PLGA) and titanium dioxide (TiO2) nanoparticles. *Archives of Toxicology,* **87,** 1075-1086.

Yadev, N. P., Murdoch, C., Saville, S. P. & Thornhill, M. H. (2011). Evaluation of tissue engineered models of the oral mucosa to investigate oral candidiasis. *Microbial Pathogenesis,* **50,** 278-285.

Yakovleva, O., Shafigullin, M. & Sitdikova, G. (2013). The role of nitric oxide in the regulation of neurotransmitter release and processes of exo-and endocytosis of synaptic vesicles in mouse motor nerve endings. *Neurochemical Journal,* **7,** 103-110.

Yan, H. N., Mruk, D., Lee, W. & Cheng, C. Y. 2009. Cross-Talk between Tight and Anchoring Junctions—Lesson from the Testis. *In:* Cheng, C. Y. (ed.) *Molecular Mechanisms in Spermatogenesis.* Springer New York.

Yang, H., Liu, C., Yang, D., Zhang, H. & Xi, Z. (2009). Comparative study of cytotoxicity, oxidative stress and genotoxicity induced by four typical nanomaterials: the role of particle size, shape and composition. *Journal of Applied Toxicology,* **29,** 69-78.

Yang, J., Deol, G. & Myangar, N. (2011). Retention of o-cymen-5-ol and zinc on reconstructed human gingival tissue from a toothpaste formulation. *Int Dent J,* **61 Suppl 3,** 41-5.

Yang, R. S., Chang, L. W., Wu, J. P., Tsai, M. H., Wang, H. J., Kuo, Y. C., Yeh, T. K., Yang, C. S. & Lin, P. (2007). Persistent tissue kinetics and redistribution of nanoparticles, quantum dot 705, in mice: ICP-MS quantitative assessment. *Environ Health Perspect,* **115,** 1339-43.

Yang, S.-T., Wang, X., Jia, G., Gu, Y., Wang, T., Nie, H., Ge, C., Wang, H. & Liu, Y. (2008). Long-term accumulation and low toxicity of single-walled carbon nanotubes in intravenously exposed mice. *Toxicology Letters,* **181,** 182-189.

Yang, Y., Chen, H., Zhao, B. & Bao, X. (2004). Size control of ZnO nanoparticles via thermal decomposition of zinc acetate coated on organic additives. *Journal of Crystal Growth,* **263,** 447-453.

Yao, N. & Wang, Z. L. 2006. *Handbook of Microscopy for Nanotechnology*, Kluwer Academic Publishers.

Ye, Y., Liu, J., Xu, J., Sun, L., Chen, M. & Lan, M. (2010). Nano-SiO2 induces apoptosis via activation of p53 and Bax mediated by oxidative stress in human hepatic cell line. *Toxicology in Vitro,* **24,** 751-758.

Yeh, S.-C., Tsai, F.-Y., Chao, H.-R. & Tsou, T.-C. (2011). Zinc Ions Induce Inflammatory Responses in Vascular Endothelial Cells. *Bulletin of Environmental Contamination and Toxicology,* **87,** 113-116.

Yin, J.-J., Liu, J., Ehrenshaft, M., Roberts, J. E., Fu, P. P., Mason, R. P. & Zhao, B. (2012). Phototoxicity of nano titanium dioxides in HaCaT keratinocytes—Generation of reactive oxygen species and cell damage. *Toxicology and Applied Pharmacology,* **263,** 81-88.

Yin Win, K. & Feng, S.-S. (2005). Effects of particle size and surface coating on cellular uptake of polymeric nanoparticles for oral delivery of anticancer drugs. *Biomaterials,* **26,** 2713-2722.

Yip, D. & Cho, C. H. (2013). A multicellular 3D heterospheroid model of liver tumor and stromal cells in collagen gel for anti-cancer drug testing. *Biochemical and biophysical research communications*.

Young, C. N., Koepke, J. I., Terlecky, L. J., Borkin, M. S., Boyd, S. L. & Terlecky, S. R. (2008). Reactive Oxygen Species in Tumor Necrosis Factor-[alpha]-Activated Primary Human Keratinocytes: Implications for Psoriasis and Inflammatory Skin Disease. *J Invest Dermatol,* **128,** 2606-2614.

Yu, J. & et al. (2011). Effects of physicochemical properties of zinc oxide nanoparticles on cellular uptake. *Journal of Physics: Conference Series,* **304,** 012007.

Yu, K., Grabinski, C., Schrand, A., Murdock, R., Wang, W., Gu, B., Schlager, J. & Hussain, S. (2009). Toxicity of amorphous silica nanoparticles in mouse keratinocytes. *Journal of Nanoparticle Research,* **11,** 15-24.

Yuan, Y., Liu, C., Qian, J., Wang, J. & Zhang, Y. (2010). Size-mediated cytotoxicity and apoptosis of hydroxyapatite nanoparticles in human hepatoma HepG2 cells. *Biomaterials,* **31,** 730-740.

Yun, Y., Cho, Y. W. & Park, K. (2012). Nanoparticles for oral delivery: Targeted nanoparticles with peptidic ligands for oral protein delivery. *Advanced drug delivery reviews*.

Zbinden, G. & Flury-Roversi, M. (1981). Significance of the LD50-test for the toxicological evaluation of chemical substances. *Archives of Toxicology,* **47,** 77-99.

Zensi, A., Begley, D., Pontikis, C., Legros, C., Mihoreanu, L., Büchel, C. & Kreuter, J. (2010). Human serum albumin nanoparticles modified with apolipoprotein AI cross the blood-brain barrier and enter the rodent brain. *Journal of drug targeting,* **18,** 842-848.

Zepter, K., Häffner, A., Soohoo, L. F., De Luca, D., Tang, H. P., Fisher, P., Chavinson, J. & Elmets, C. A. (1997). Induction of biologically active IL-1 beta-converting enzyme and mature IL-1 beta in human keratinocytes by inflammatory and immunologic stimuli. *The Journal of Immunology,* **159,** 6203-8.

Zero, D. T., Raubertas, R. F., Pedersen, A. M., Fu, J., Hayes, A. L. & Featherstone, J. D. B. (1992). Studies of Fluoride Retention by Oral Soft Tissues after the

Application of Home-use Topical Fluorides. *Journal of Dental Research,* **71,** 1546-1552.

Zha, L. Y., Xu, Z. R., Wang, M. Q. & Gu, L. Y. (2008). Chromium nanoparticle exhibits higher absorption efficiency than chromium picolinate and chromium chloride in Caco-2 cell monolayers. *Journal of animal physiology and animal nutrition,* **92,** 131-140.

Zhang, L., Jiang, Y., Ding, Y., Daskalakis, N., Jeuken, L., Povey, M., O'Neill, A. & York, D. (2010). Mechanistic investigation into antibacterial behaviour of suspensions of ZnO nanoparticles against *E. coli*. *Journal of Nanoparticle Research,* **12,** 1625-1636.

Zhang, L., Jiang, Y., Ding, Y., Povey, M. & York, D. (2007). Investigation into the antibacterial behaviour of suspensions of ZnO nanoparticles (ZnO nanofluids). *Journal of Nanoparticle Research,* **9,** 479-489.

Zhang, L. W., Bäumer, W. & Monteiro-Riviere, N. A. (2011a). Cellular uptake mechanisms and toxicity of quantum dots in dendritic cells. *Nanomedicine,* **6,** 777-791.

Zhang, Q., Kusaka, Y., Zhu, X., Sato, K., Mo, Y., Kluz, T. & Donaldson, K. (2003). Comparative toxicity of standard nickel and ultrafine nickel in lung after intratracheal instillation. *J Occup Health,* **45,** 23-30.

Zhang, S., Li, J., Lykotrafitis, G., Bao, G. & Suresh, S. (2009). Size-Dependent Endocytosis of Nanoparticles. *Advanced Materials,* **21,** 419-424.

Zhang, W., Yao, Y., Sullivan, N. & Chen, Y. (2011b). Modeling the primary size effects of citrate-coated silver nanoparticles on their ion release kinetics. *Environmental science & technology,* **45,** 4422-4428.

Zhao, P., Zhang, L., Grillo, J., Liu, Q., Bullock, J., Moon, Y., Song, P., Brar, S., Madabushi, R. & Wu, T. (2010). Applications of physiologically based pharmacokinetic (PBPK) modeling and simulation during regulatory review. *Clinical Pharmacology & Therapeutics,* **89,** 259-267.

Zhao, X. D., Yao, J. B. & Yi, D. (2005). Studies on the antibacterial properties of ZnO. *Dyeing technology,* **1,** 13-15.

Zhao, Y., Sun, X., Zhang, G., Trewyn, B. G., Slowing, I. I. & Lin, V. S.-Y. (2011). Interaction of mesoporous silica nanoparticles with human red blood cell membranes: size and surface effects. *ACS nano,* **5,** 1366-1375.

Zhu, M.-T., Wang, B., Wang, Y., Yuan, L., Wang, H.-J., Wang, M., Ouyang, H., Chai, Z.-F., Feng, W.-Y. & Zhao, Y.-L. (2011). Endothelial dysfunction and inflammation induced by iron oxide nanoparticle exposure: Risk factors for early atherosclerosis. *Toxicology Letters,* **203,** 162-171.

Ziegler, U. & Groscurth, P. (2004). Morphological Features of Cell Death. *Physiology,* **19,** 124-128.

Zolnik, B. S., Gonzalez-Fernandez, A., Sadrieh, N. & Dobrovolskaia, M. A. (2010). Nanoparticles and the immune system. *Endocrinology,* **151,** 458-65.

9 APPENDICIES

The following figures serve as supplementary evidence, to support fundamental hypothesis and statements included within the investigation.

9.1 H376 cell loss of cell adhesion in response to SDS cytotoxicity

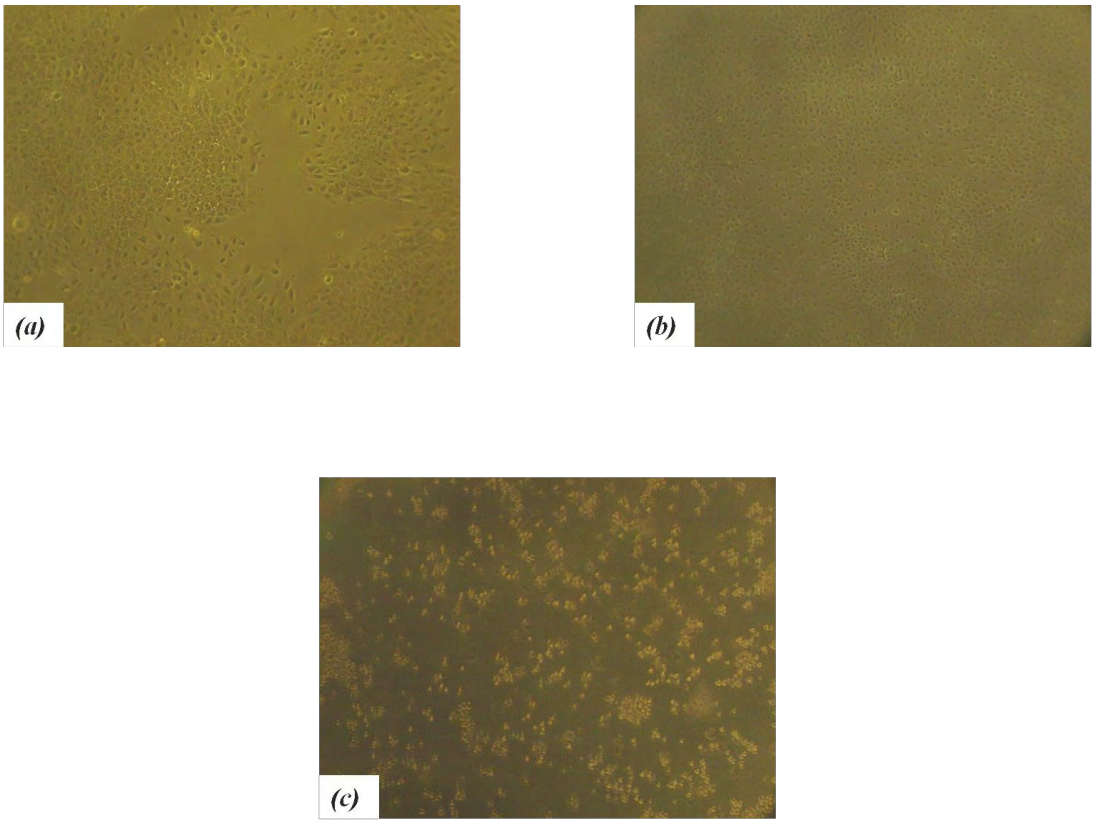

Figure 9.1. Light microscopy images taken of H376 cells using a Nikon Eclipse TE2000-U Light-Fluorescence Microscope with Digital SLR Camera, at 40X magnification. Cells were photographed following exposure to **(a)** serum free media for 5 minutes, **(b)** 1% Triton-X100 positive control for 45 minutes and **(c)** 0.125% w/v SDS for 5 minutes. These images support the hypothesis that high levels of SDS cytotoxicity result in loss of cellular adhesion and consequently affect the sensitivity of LDH release in supernatent leading to a false negative assessment of cytotoxicity.

9.2 SiO_2-ACROS-Bulk material characterisation

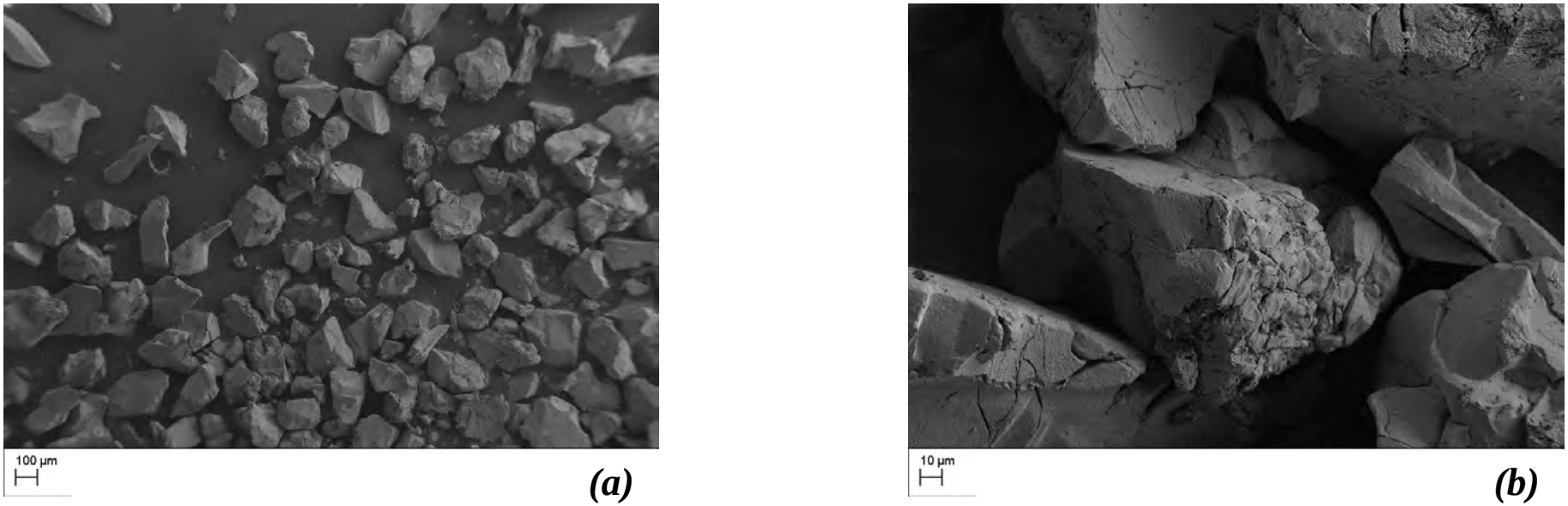

Figure 9.2. SEM micrographs demonstrating the micron size of SiO_2 –ACROS-Bulk material. (a) 100X magnification and **(b)** 1,000X magnification with scale bar shown respectively.